

# **Heterometallic Ruthenium(II)-Platinum(II) Complexes- A New Paradigm**

*A Kinetic, Mechanistic and Computational Investigation into Substitution  
Behaviour*

**AISHATH SHAIRA**

**School of Chemistry and Physics  
University of KwaZulu-Natal  
Pietermaritzburg  
September 2013**

# Heterometallic Ruthenium(II) Platinum(II) Complexes- A New Paradigm

*A Kinetic, Mechanistic and Computational Investigation into Substitution  
Behaviour*



By

**AISHATH SHAIRA**

**B.Ed, B.Sc (Hons), MSc, (UKZN)**

Submitted in partial fulfilment of the academic requirements for the degree of

**Doctor of Philosophy**

in the College of Agriculture, Engineering and Science

School of Chemistry and Physics

University of KwaZulu-Natal

Pietermaritzburg

September 2013

## DECLARATION

I, A. Shaira declare that:

1. The research reported in this thesis, except where otherwise indicated, is my original research.
2. This thesis has not been submitted for any degree or examination at any other university.
3. This thesis does not contain other persons' data, pictures, graphs or other information, unless specifically acknowledged as being sourced from other persons.
4. This thesis does not contain other persons' writing, unless specifically acknowledged as being sourced from other researchers. Where other written sources have been quoted, then:
  - a. Their words have been re-written but the general information attributed to them has been referenced
  - b. Where their exact words have been used, then their writing has been placed in italics and inside quotation marks, and referenced.
5. This thesis does not contain text, graphics or tables copied and pasted from the Internet, unless specifically acknowledged, and the source being detailed in the thesis and in the References sections.

Signed: ..... **A. Shaira)**

Date: .....

I hereby certify that this is correct, and as the candidates' supervisor I have approved this thesis for submission

Signed: ..... **Professor D. Jaganyi (supervisor)**

Date: .....

Pietermaritzburg

September 2013

***To My Loving Mom, Dad and Family, With Lots of Love***



***A handful of patience is worth more than a bushel of brains.***

***~Dutch Proverb~***

## Contents

Abstract	i
Acknowledgements	iii
Publications and Conference Contributions	vi
List of Abbreviations and Symbols	viii
List of Figures	xii
List of Tables	xviii
List of Schemes	xx

### Chapter One

<b>Role of Platinum and Ruthenium Complexes as Anticancer Agents</b>	<b>1</b>
1.1 Introduction	1
The General Chemistry of Platinum(II) Complexes	2
1.3 Development of Platinum-based Anticancer Drugs and Structure Activity Relationship	3
1.3.1 Cisplatin	4
1.3.1.1 Mechanism of Action of Cisplatin	4
1.3.1.2 Reactivity of Cisplatin with DNA	5
1.3.1.3 Cisplatin Resistance	8
1.3.2 Development of Second Generation Cisplatin Analogues	8
1.4 Current Findings on Anticancer Platinum(II) Drugs	9
1.4.1 Multinuclear Platinum(II) Complexes	9
1.4.2 Polynuclear Platinum(II) Complexes with Flexible Linkers	9
1.4.3 Polynuclear Platinum(II) Complexes with Rigid Linkers	11
1.5 Platinum(II) Polypyridyl Complexes	13
1.5.1 DNA Intercalation	13
1.5.2 Substitution of Platinum(II) terpyridine Complexes with Biologically Active Nucleophiles	14
1.5.3 Previous Kinetics and Mechanistic Studies on Platinum(II) terpyridine Complexes with Thiourea and Ionic nucleophiles	16
1.6 Therapeutic Ruthenium Complexes: A Possible Alternative to Platinum	17
1.6.1 The General Chemistry of Ruthenium(II) Complexes	18
1.6.2 The Biological Importance of Ruthenium(II) Complexes	19
1.6.3 Ruthenium Complexes as Biological Probes	21
1.6.4 Intercalation of Ruthenium Complexes in Two DNA Bases	23

1.6.5	Photodynamic Therapy .....	25
1.6.6	Postulated Mechanisms of Action of Anticancer Ruthenium Complexes .....	25
1.6.7	Substitution Reactions of Ruthenium(II) Complexes .....	26
1.6.8	Polynuclear Ruthenium Complexes .....	27
1.7	Heteronuclear Ruthenium(II)-Platinum(II) Polypyridyl Complexes .....	29
1.8	Aims of this Study.....	32
1.9	References.....	35

## Chapter Two

<b>Substitution Reaction Kinetics .....</b>	<b>1</b>
2.1 General Considerations .....	1
2.2 Mechanistic Classification of Inorganic Substitution Reactions.....	2
2.2.1 Limiting Associative Mechanism .....	3
2.2.2 Dissociative Mechanism .....	4
2.2.3 Interchange Mechanism.....	5
2.3 Substitution Reactions of Square Planar Platinum(II) Complexes .....	5
2.3.1 Kinetics and Mechanism of Substitution Reactions .....	7
2.4 Determining the Rates of Ligand Substitution Reactions .....	7
2.4.1 Reversible Second-Order Reactions .....	7
2.4.2 Activation Parameters.....	11
2.4.2.1 Measurement of enthalpy of activation ( $\Delta H^\ddagger$ ) and entropy of activation ( $\Delta S^\ddagger$ ) .....	11
2.4.2.2 Volume of Activation ( $\Delta V^\ddagger$ ) .....	13
2.4.3 Instrumental Techniques Used in Chemical Kinetics.....	14
2.4.3.1 UV/visible Spectrophotometry.....	15
2.4.4 Flow methods.....	19
2.4.4.1 Continuous flow method.....	20
2.4.4.2 Stopped-Flow Technique .....	20
2.5 Factors Influencing the Reactivity of Square Planar Platinum(II) Complexes .....	22
2.5.1 Effect of the Entering Group.....	22
2.5.2 The Effect of Leaving Group .....	26
2.5.3 Effect of Steric Hindrance .....	27
2.5.4 Effect of Solvent.....	29
2.5.5 Non-Participating Ligand.....	30
2.5.5.1 The <i>trans</i> Effect.....	30

i $\sigma$ - <i>trans</i> effect.....	33
ii $\pi$ - <i>trans</i> effect .....	36
2.5.5.2 <i>Cis</i> - Effect.....	36
2.6 References.....	38

## Chapter Three

### **Mixed-metal Ruthenium(II)-Platinum(II) and Cobalt(II)-Platinum(II) Complexes of Tetra-2-pyridyl-1,4-pyrazine Bridging Ligand. A Kinetic, Mechanistic and Computational Investigation .....**

3.0 Abstract.....	1
3.1 Introduction.....	2
3.2 Experimental .....	5
3.2.1 Chemicals.....	5
3.2.2 Characterizations and Instrumentations .....	5
3.2.3 Synthesis of Ruthenium Precursors and Intermediate Complexes.....	5
3.2.4 Synthesis of Platinum(II) Complexes.....	6
3.2.5 Preparation of Nucleophile Solutions for Kinetic Measurements.....	8
3.2.6 Kinetic Measurements.....	9
3.2.7 Computational Modelling .....	9
3.3 Results and Discussion .....	12
3.3.1 Synthesis and Characterization.....	12
3.3.2 Computation Calculations .....	12
3.3.3 Kinetic Analyses .....	13
3.4 Conclusion .....	31
3.5 References .....	33
3.6 Supporting Information .....	39

## Chapter Four

### **The Effect of Ruthenium(II) Terpyridine Fragment on the Reactivity of Platinum(II) centre. A Kinetic and Computational Approach.....**

4.0 Abstract.....	1
4.1 Introduction.....	2
4.2 Experimental .....	4
4.2.1 Materials .....	4
4.2.2 Synthesis of Ligand and Ruthenium Moieties .....	5

4.2.3	Synthesis of Platinum(II) Complexes.....	6
4.2.4	Preparation of Aqua Complexes .....	7
4.2.5	Instrumentation and Measurements .....	8
4.2.6	Determination of $pK_a$ of Aqua Complexes.....	8
4.2.7	Kinetic Measurements.....	9
4.2.8	Computational Modelling .....	10
4.3	Results and Discussion .....	10
4.3.1	Synthesis and Characterization.....	10
4.3.2	Acid-base Equilibria of the Aqua Platinum(II) Complexes .....	11
4.3.3	Computational Calculations .....	13
4.3.4	Kinetics Analyses .....	17
4.4	Conclusion .....	26
4.5	References .....	27
4.6	Supporting Information .....	33

## Chapter Five

### **Understanding the Role of Flexible 4'-Functionalised Polyethylene glycoxy Chains on the Behaviour of Platinum(II) (4'-(ethylene glycoxy)-2,2':6',2''-terpyridine- A kinetic and a Mechanistic Study.....**

5.0	Abstract .....	1
5.1	Introduction.....	1
5.2	Experimental.....	4
5.2.1	Materials.....	4
5.2.2	Synthesis of Ligands .....	4
5.2.3	Synthesis of Platinum(II) Complexes .....	5
5.2.4	Physical Measurements.....	7
5.2.5	Computational Modelling.....	7
5.2.6	Kinetic Analyses .....	7
5.3	Results and Discussion.....	10
5.3.1	Synthesis and Characterization .....	10
5.3.2	DFT Calculations .....	11
5.3.3	Kinetics.....	14
5.4	Conclusions.....	19
5.5	References .....	20
5.6	Supporting Information.....	24

## Chapter Six

### A Kinetic and Mechanistic Investigation of Polyethyleneglycol Ether Bridged Dinuclear Platinum(II) 2,2':6',2''-Tpyridine Complexes.....1

6.0	Abstract .....	1
6.1	Introduction.....	1
6.2	Experimental.....	4
6.2.1	Materials.....	4
6.2.2	Synthesis of Ligands .....	5
6.2.3	Synthesis of Platinum(II) Complexes .....	6
6.2.4	Instrumentation and Physical Measurements.....	8
6.2.5	Computational Modelling.....	8
6.2.6	Kinetic Analyses .....	9
6.3	Results.....	9
6.3.1	Computational Modelling.....	13
6.4	Discussion.....	18
6.5	Conclusions.....	23
6.6	References.....	24
6.7	Supporting Information.....	28

## Chapter Seven

### Role of Bridging Polyethyleneglycol Ether Linkers on the Rate of Ligand Substitution of Heterometallic Ruthenium(II)-Platinum(II) Complexes ..... 1

7.0	Abstract.....	1
7.1	Introduction.....	1
7.2	Experimental .....	4
7.2.1	Materials .....	4
7.2.2	Synthesis.....	5
7.2.3	Synthesis of [(tpy)Ru(polyethyleneglycol ether)]Cl <sub>2</sub> Moieties.....	5
7.2.4	Synthesis of Platinum(II) Complexes.....	7
7.2.5	Instrumentation and Physical Measurements .....	8
7.2.6	Preparation of Solution for Kinetic Analysis .....	9
7.2.7	Computational Modelling .....	9
7.3	Results .....	12
7.3.1	Kinetic Studies on Substitution Reactions of Chloro Complexes .....	12
7.3.2	Discussion.....	16
7.4	Conclusions .....	20

7.5	References .....	21
7.6	Supporting Information .....	25

## **Chapter Eight**

<b>Summary and Future Prospcts .....</b>	<b>1</b>
8.1 Summary.....	1
8.2 Work Completed but Not Included in This Thesis.....	7
8.3 Future Prospects.....	10
8.4 References.....	12

## Abstract

Thermodynamic and kinetic analysis of the ligand substitution reactions of different heterometallic Ru(II)-Pt(II) complexes with a series of bio-relevant thiourea nucleophiles of different steric demands and ionic nucleophiles have been investigated as a function of concentration and temperature using UV/visible and stopped-flow spectrophotometric techniques. To achieve this, five different sets of complexes involving mono di and multinuclear homo and heterometallic complexes with tridentate N-donor ligands of different linker ligands were synthesized and characterized by various spectroscopic methods. The substitution reactions of the chloride complexes were studied in methanol in the presence of 0.02 M LiCf<sub>3</sub>SO<sub>3</sub> adjusted with LiCl to prevent possible solvolysis. The aqua complexes were studied in acidic aqueous medium at pH 2.0. All reactions were investigated under *pseudo* first-order conditions. Density functional theory (DFT) calculations were used to aid further interpretations and understandings of the experimental results.

Substitution reactivity of heterometallic Ru(II)-Pt(II) and Co(II)-Pt(II) complexes bridged by tetra-2-pyridyl-1,4-pyrazine (tppz) ligand was investigated for the first time. The reactions proceeded *via* two steps. The *pseudo* first-order rate constants,  $k_{\text{obs}}(1^{\text{st}}, 2^{\text{nd}})$  for the substitution of the chloride ligand(s) from the Pt(II) complexes and subsequent displacement of the linker. The dechelation step was confirmed by <sup>1</sup>H NMR and <sup>195</sup>Pt NMR studies. Incorporation of Ru(tppz) moiety increases the substitution reactivity and is ascribed to the increased  $\pi$ -back donation from the tppz ligand which increases the electrophilicity of the metal centre, overall charge and the global electrophilicity index of the complex. However, when changed the second metal centre from a Ru(II) to a Co(II), the rate of substitution decreased by a factor of four due to the weaker  $\pi$ -backbonding from Co(II).

The substitution reactivity of another set of heterometallic Ru(II)-Pt(II) complexes with a semi-rigid linker, 4'-pyridyl-2,2':6',2''-terpyridine (qpy) showed that replacing the *cis* pyridyl group by a (tpy)Ru(qpy) moiety lowers the energy of anti-bonding LUMO ( $\pi^*$ ) orbitals and increases the metal-metal interactions and electronic transition within the complex whereby enhancing the reactivity of Pt(II) centre. However, when two Pt(II) moieties are linked to a (qpy)Ru(qpy), the orthogonal geometry at the Ru(II) metal centre prevents the extended  $\pi$ -electron density to flow through the three metal centres. The kinetic results obtained were supported by pK<sub>a</sub> and <sup>195</sup>Pt NMR studies.



Substitution reactions of the mononuclear Pt(II) complexes revealed that the polyethylene glycoxy pendent units act as a  $\sigma$ -donors including the lone pair electrons on the first oxygen atom thereby decreasing the reactivity of the parent Pt(II) terpyridine complex. However, this  $\sigma$ -donation towards the terpyridine moiety was found to be effective only up to one unit of the ethylene glycoxy pendant, beyond which the reactivity was sterically controlled. The dinuclear Pt(II) complexes bridged by polyethyleneglycol ether units show that the reactivity of the complexes depend on the Pt...Pt distance and the steric hindrance at the Pt(II) centre. The substitution reactivity of heterometallic Ru(II)-Pt(II) complexes bridged by the same polyethyleneglycol ether units indicate that the presence of Ru(tpy)<sub>2</sub> moiety influences the structural geometry of the complex system which in turn controls the reactivity of the Pt(II) centre. This is further driven by the entrapment effect of the nucleophile due to the V-shape geometry adopted by the heterometallic complexes. In all cases the reactivity was also controlled by steric and electronic effects. However, when two metal centres are bridged by a flexible non-aromatic linker, the electronic transitions and the metal-metal interactions were found to be minor, especially for the longer linkers.

The <sup>1</sup>H and <sup>195</sup>Pt NMR spectroscopic techniques were used to further understand the observed substitution kinetics and to confirm the degradation of the bridging ligand from the metal centre(s). In all cases, the negative activation entropies obtained support the associative mode of substitution. This investigation reveals that the length and the nature of the bridging linker plays an important role in controlling the reactivity of the heterometallic complexes. It is envisaged that the findings of this project would offer a significant contribution to the pharmacological design of effective anticancer drugs.

## Acknowledgements

*This research accomplishment was made possible with the support and inspiration of many kind people around me. I owe a debt of gratitude to all of them. I would like to express my sincere gratitude to my supervisor, who is also my advisor, **Professor Deogratius Jaganyi** for his patience, guidance, enthusiasm and feedback for my advancement in this field. I thank him for finding time to read my work despite his busy schedule. I also gratefully acknowledge his trust in me on carrying out this remarkable new idea of heterometallic reaction kinetics and more importantly allowing me to work independently. Thank you Prof., for your words of encouragement, support on both an academic and a personal level. I absolutely enjoyed the work!*

*I wish to extend my sincere gratitude to:*

- ✓ *Dr. D. Reddy, for his help to accomplish this work and untiring support and guidance especially, during initial stages of the work. Thank you Dr. Reddy. I wouldn't have been able to move faster with the work if it was not your help.*
- ✓ *Dr. A. Mambanda, for his readily offered and unreserved help in reading my work, the constructive feedback and willingness to share his ideas. The discussions were very fruitful and encouraging.*
- ✓ *Mr. C. Grimmer for his expertise and untiring technical support in NMR spectra acquisitions, especially running all the kinetic and temperature dependence NMR spectra and his assistance and advice thereafter. Dr. M. P. Akerman and Prof. O. Q. Munro for their contribution in X-ray crystal structure determinations and fruitful discussions. Dr. M. P. Akerman for his guidance and help on my computational work. Mrs. Caryl J. van Rensburg for her help in acquisition of mass spectra and elemental analysis.*
- ✓ *Prof. J. S. Field for the fruitful discussions during early stages of my work and Prof. R. Robinson for his willingness to help with a microwave reaction.*
- ✓ *University of KwaZulu-Natal, South Africa for financial support. Special thanks to all the academic and technical staff in the School of Chemistry who readily offered help, support and assistance at all times. Technical staff: H. Desai and S. Ball for procuments. P. Forder and C. Mortlock for making my glassware and fixing of broken glassware. Fayzil, Prenesha, Bheki, Mrs. Ngubane (Mama Ireen), Prudence*

*(Pru), Marvin and Siya for technical assistance. Muvhango for the social Braaies. I feel grateful to have been able to study at the Chemistry Department. I will always cherish the memories of the Department and its people.*

- ✓ *My past and present colleagues in the kinetics research group: Especially, Dr. Ongoma, Isaac Wekesa and Grace Kinunda for their fruitful discussions and moral support. Thanks Dr. Ongoma for your unreserved help. Thanks Grace for your kindness especially your support during early days of my doctoral studies. Thanks Isaac for all your help, your brotherly kindness, your timeous constructive feedback on my work. Dr. Altaf, Tshephiso (Terpy), Slindokuhle (Sli), Musawenkosi (Msaa) and Panyako (Panyi), Meshack for all your help and friendly atmosphere in the laboratory. Thanks Kevoulee (Kev), for all your help. You all were like my family. Thank you all!*
- ✓ *All my friends and colleagues at the School of Chemistry in Pietermaritzburg Campus for all their support and inspiration for making my work a pleasant experience. Especially, Kate for her readily offered help whenever I asked for, Mzozo for the column with which I managed to separate my samples, Bongiwe, Elizabeth and Ashawin for the friendly platform and Dr. M. Ndoile, my flat mate for all her support especially, when I fell sick. My colleagues in the postgraduate students' office; Abimbola, Nancy and Dr. Alam for their friendly work platform. Aloice and George, for helping me to proof read my work. Special thanks to Bilaal (including his supervisor, Dr. Booysen) for allowing me to use his computer for Gaussian computational work.*
- ✓ *Student Housing of University of KwaZulu-Natal, Pietermaritzburg Campus, especially the Director of Student Housing, Ms. R. Yender and Matron S. Amod for their support and kind considerations in providing me a safe and a convenient accommodation during my stay for doctoral studies. S. Amod for all her care and willingness to help me on whatever I asked for. All my South African friends who made me feel home especially, Shaeda aunty, Fareeda aunty, Shenehaz, Shanoon and their families. My Kenyan sister, Dr. H. Abdillahi for accommodating me on my arrival to South Africa for doctoral studies. My Tanzanian friend Mushi for her support. I also thank my other good friends in South Africa and back at home country for their support and prayers.*

- ✓ *Finally, I am indebted to my mom, dad and family for their endless love, encouragement, unequivocal support and prayers for which my mere expression of thanks does not suffice. You are the secret of my success. This work would not have been possible if it was not for you all. Thank you for believing in me.*
- ✓ *Above all, I would like to thank the Almighty God for his love, grace and watching over me throughout my life.*

## Publications and Conference Contributions

### Previous Publications

- 1- J. Field, J. A. Gertenbach, D. Jaganyi, D. R. McMillin, A. Shaira and D. J. Stewart, Z. Naturforsch., B: Chem. Sci., 2010, 65, 1318–1326.
- 2- A. Shaira, D. Reddy, D. Jaganyi, Dalton Trans., 2013, 42, 8426-8436

### Publications of This Work

1. **A. Shaira** and D. Jaganyi, Understanding the Role of Flexible 4'-functionalised Polyethylene Glycoxy Chains on the Behaviour of Platinum(II) (4'-(ethylene glycoxy)-2,2':6',2''-Terpyridine- A Kinetic and a Mechanistic Study.  
This work has been submitted to Dalton Transactions for publication.  
Manuscript ID is DT-ART-08-2013-052241.

Other works reported in this thesis are ready for submission for publication.

2. **A. Shaira** and D. Jaganyi, Mixed-metal Ruthenium(II)-Platinum(II) and Cobalt(II)-Platinum(II) complexes of Tetra-2-pyridyl-1,4-pyrazine Bridging Ligand. A Kinetic, Mechanistic and Computational Investigation.
3. **A. Shaira** and D. Jaganyi, The Effect of Ruthenium(II) Terpyridine Fragment on the Reactivity of Platinum(II) centre. A Kinetic and Computational Approach.
4. **A. Shaira** and D. Jaganyi, A Kinetic and Mechanistic Study of Dinuclear Platinum(II) 2,2':6',2''-Tpyridine Compounds Bridged with Polyethylethylene glycol Ether Flexible Linkers.
5. **A. Shaira** and D. Jaganyi, Role of Bridging Polyethyleneglycol Ether Linkers on the Rate of Ligand Substitution of Heterometallic Ruthenium(II)-Platinum(II) Complexes.

## Poster Presentation

16<sup>th</sup> Biennial SACI Inorganic Chemistry Conference (SACI2013). Incorporating the Carman Physical Chemistry Symposium, Durban, South Africa, 30<sup>th</sup> June to 4<sup>th</sup> July 2013, entitled: *Kinetic and Mechanistic Studies of Heteropolynuclear Ru(II)-Pt(II) Complexes with Short and Semi-rigid Linkers*, by **Aishath Shaira**, Desigan Reddy and Deogratias Jaganyi.

## List of Abbreviations and Symbols

A2780cis	cisplatin-sensitive human ovarian carcinoma cell line
A2780R	cisplatin-resistant human ovarian carcinoma cell line
A549	human lung tumour cells (lung carcinoma, epithelial cells)
Å	Angstrom (10 <sup>-10</sup> m)
A	Associative mechanism/Adenine
<b>aaa</b>	[Pt(diethylenetriamine)OH <sub>2</sub> ] <sup>2+</sup>
<b>aap</b>	[Pt(N-(pyridyl-2-methyl)-1,2diamino-ethane)OH <sub>2</sub> ] <sup>2+</sup>
<b>apa</b>	[Pt(2,6-bis-aminomethylpyridine)OH <sub>2</sub> ] <sup>2+</sup>
AET	aminoethanethiol
AgSO <sub>3</sub> CF <sub>3</sub>	Silver trifluoromethanesulfonate
SO <sub>3</sub> CF <sub>3</sub> H	Trifluoromethanesulfonic acid
AgCl	Silver chloride
AgSbF <sub>6</sub>	Silver hexafluoroantimonate
<b>app</b>	[Pt(2,2'-bipyridine)(NH <sub>3</sub> )(OH <sub>2</sub> )] <sup>2+</sup>
apy	2,2'-azobispyridine
azpy	2-phenylazopyridine
B3LYP	Becke-Perdev-Parr model. A local density functional model which improves on the local density by accounting explicitly for the non-uniformity in the electron density.
BBR3464	[{ <i>trans</i> -PtCl(NH <sub>3</sub> ) <sub>2</sub> ] <sub>2</sub> {μ- <i>trans</i> -Pt(NH <sub>3</sub> ) <sub>2</sub> -(HN <sub>2</sub> (CH <sub>2</sub> ) <sub>6</sub> NH <sub>2</sub> ) <sub>2</sub> }] <sup>4+</sup>
<sup>t</sup> Bu	<i>tert</i> -butyl
bpy	2,2'-bipyridine
bp	base pair
bn	binuclear
C	Cystosine or Celsius
CH <sub>3</sub> CN	acetonitrile
C-PCM	Conductor Polarizable Continuum Model
cisplatin	<i>cis</i> -diaminedichloroplatinum(II)
CT	Calf Thymas
CTR1	Constructive triple response 1
Cys	cysteine
D	dissociative
δ/ ppm	chemical shift in parts per million

DFT	Density functional theory
dmso	Dimethyl sulfoxide
DMF	dimethylformamide
DMTU	dimethylthourea
dmp	2,9-dimethyl-1,10-phenanthroline
DNA	Deoxyribonucleic acid
dpb	2,3-bis(2-pyridyl)benzoquinoxaline
dpq	dipyrido[3,2- <i>d</i> :2',3'- <i>f</i> ]-quinoxaline
dteg	bis[4'-(2,2':6',2''-terpyridyl)]-ethyleneglycol ether
dtdeg	bis[4'-(2,2':6',2''-terpyridyl)]-diethyleneglycol ether
dtteg	bis[4'-(2,2':6',2''-terpyridyl)]-triethyleneglycol ether
dtteg	bis[4'-(2,2':6',2''-terpyridyl)]-tetraethyleneglycol ether
$E_a$	Activation energy
$\epsilon$	Molar absorptivity coefficient
$e$	exponential
en	ethylene diamine
eqm	Equilibrium
eqv	Equivalence
g	gram
G	Guanine
$\Delta G^\ddagger/\Delta G^\circ$	Gibbs free energy of activation
5'-GMP	guanine-5'-monophosphate
GSH	glutathione
Etg	9-ethylguanine
$h$	Planck constant ( $6.626 \times 10^{-34} \text{ J s}^{-1}$ )
$\Delta H^\ddagger$	Activation enthalpy
HCC827	human lung tumour cells
HCF <sub>3</sub> SO <sub>3</sub>	Triflic acid
HET	2-hydroxyethanethiol
His	histidine
HMG	high-mobility group proteins
Hmcyt	1-methylcytosine
HOMO	Highest occupied molecular orbital
$I$	Ionic strength
I	interchange



I <sub>A</sub>	Associatively activated
IC <sub>50</sub>	concentration of a compound that induces 50 % of growth inhibition of cells compared to untreated cells
I <sub>D</sub>	Dissociatively activated
5'IMP	inosine-5'-monophosphate
INO	inosine
impy	2-phenylpyridinylmethylene amine
IR	infrared
K	Kelvin
$k_1, k_{-1}, k_2, k_{-2}$	rate constants
$k_b$	Boltzmann constant ( $1.3807 \times 10^{-23} \text{ J K}^{-1}$ )
$k_{\text{obs}}$	observed pseudo first-order constant
kcal	Kilocalorie
kJ	kilojoules
$\lambda$	wavelength
L	ligand
L1210	murine leukemia cell-line
LACVP	Los Alamos Core Valence Potential
LFER	Linear free energy relationship
LiCF <sub>3</sub> SO <sub>3</sub>	Lithium triflate
LUMO	Lowest unoccupied molecular orbital
M	Molarity (mol dm <sup>-3</sup> ) or metal
mL	millilitre
MLCT	Metal to ligand charge transition
TOF MS-ES <sup>+</sup>	A time-of-flight mass spectrometer with an electron spray source operated in the positive ion mode
MO	Molecular orbital
NAMI	Na{ <i>trans</i> -[Ru(III)Cl <sub>4</sub> (dmso)(Him)]}
NAMI-A	[H <sub>2</sub> im][ <i>trans</i> -Ru(III)Cl <sub>4</sub> (dmso)(Him)]
NBO	Natural bond orbital
NER	Nucleotide excision repair
nm	nanometer
NMR	nuclear magnetic resonance
OH•	Hydroxide radical
Nu	nucleophile

<i>o</i> -tolyl	ortho toluene
Pa	Pascal
Paa	2-pyridinealdazine
<b>pap</b>	[Pt(bis(2-pyridylmethyl)amine) OH <sub>2</sub> ] <sup>2+</sup>
PDT	Photodynamic therapy
phen	1,10-phenanthraline
PMIP	2-(4-methylphenyl)imidazo[4,5- <i>f</i> ]1,10-phenanthroline
PPh <sub>3</sub>	triphenylphosphine
ppm	Parts per million
<b>ppp</b>	[Pt(terpy)OH <sub>2</sub> ] <sup>2+</sup>
Pt(cod)Cl <sub>2</sub>	Dichloro(1,5-cyclooctadiene)Platinum(II)
<b>Pttpy</b>	[Pt(2,2':6',2''-terpyridine)Cl]Cl·2H <sub>2</sub> O
py	Pyridine/pyridyl
qpy	4'-pyridyl-2,2':6',2''-terpyridine
R	universal gas constant (8.3145 JK <sup>-1</sup> mol <sup>-1</sup> )
RNA	ribonucleic acid
<b>s</b>	nucleophilic discrimination factor
s	singlet or strong
$\Delta S^\ddagger$	Activation entropy
SAR	structure activity relationship
Si(CH <sub>3</sub> ) <sub>4</sub>	trimethylsilane
T	Temperature, Thymine
tppz	2,3,5,6-tetrakis(2-pyridyl)pyrazine
tpy	2,2':6',2''-terpyridine
tmem	<i>N,N,N',N'</i> -tetramethylenediamine
TMTU	1,1,3,3-tetramethyl-2-thiourea
TU	thiourea
UV/vis	Ultraviolet/visible
$\Delta V^\ddagger$	activation volume
X	Leaving group (unless otherwise mentioned)
Y	Incoming group ( unless otherwise mentioned)
<i>v</i>	frequency
<i>n<sub>pt</sub></i>	nucleophilicity

## List of Figures

Figure 1.1	Platinum complexes in worldwide clinical use and as well as those with regionally limited approval: nedaplatin, lobaplatin.....	3
Figure 1.2	Suggested reaction pathway for cisplatin in the cell and binding to DNA. Extracted from references. ....	5
Figure 1.3	Some possible cisplatin-DNA binding modes. ....	7
Figure 1.4	Some polynuclear Pt(II) complexes which have shown potential anticancer activity. ....	10
Figure 1.5	Multinuclear platinum (II) complexes with rigid linkers which have shown anticancer activity. ....	12
Figure 1.6	Multinuclear Pt(II) complexes with rigid linkers which are used for kinetic and mechanistic study. ....	13
Figure 1.7	Pt(II) complexes studied by van Eldik et al. (33-38). Pt(II)terpyridine complexes studied by Jaganyi et al. (38,39) and (40). ....	17
Figure 1.8	Structure of some of the ruthenium complexes which were found to have antitumour activity. ....	20
Figure 1.9	Some dinuclear cationic Ru(II) complexes linked by flexible and rigid linkers. ....	29
Figure 1.10	The Ru(II)-Pt(II) with a long and flexible linkers (58) and (59) along with the heterodinuclear Ru(II)-Pt(II) complexes with different linkers. Anions omitted for simplicity. ....	31
Figure 2.1	Reaction profiles for (a) associative A, (b) associative interchange, $I_a$ , (c) dissociative interchange $I_d$ and (d) dissociative D. ....	3
Figure 2.2	Schematic representation of the energy profile and possible steric changes during an associative substitution of leaving group, X by the entering group, Y of a square planar complex: energies at 2, 4, 6, and 8 represent the transition states and the reaction intermediates would have energies shown at 3, 5 and 7. ....	6
Figure 2.3	Schematic representation for substitution in $d^8$ four coordinate square planar complexes showing the alternative D and A or $I_a$ solvolysis. ....	7
Figure 2.4	Dependence of the <i>pseudo</i> first-order rate constant ( $k_{obs}$ ) on the concentration of the nucleophiles for the chloride substitution from Pt(ppy)tegg in methanol solution ( $I = 0.02$ M $LiCF_3SO_3$ , adjusted with LiCl) at 298 K. ....	10

Figure 2.5	Schematic diagram of a UV/visible spectrophotometry setup.....	16
Figure 2.6	Photograph of a double-beam-in-space Varian Cary 100 Bio UV/visible spectrophotometer used by the University of KwaZulu Natal, Pietermaritzburg campus kinetics research group.....	17
Figure 2.7	Spectrum obtained from Cary UV/visible spectrophotometer for the substitution of $\text{Cl}^-$ from $[\text{ClPt}(\text{tppz})\text{Ru}(\text{tppz})\text{PtCl}](\text{PF}_6)_4$ ( $2.0 \times 10^{-5}$ M) by thiourea (0.0004 M) in methanol solution ( $I = 0.02$ M (adjusted with $\text{LiCF}_3\text{SO}_3$ and $\text{LiCl}$ ) at 383 nm and 298 K. ....	19
Figure 2.8	Diagrammatic representation of a continuous flow kinetic system. The letter $d$ represents the distance from the mixture to the point of observation.....	20
Figure 2.9	Diagrammatic representation of stopped-flow apparatus.....	21
Figure 2.10	Photograph of the Applied Photophysics SX 20 stopped-flow system coupled to an online data acquisition system setup used by the University of KwaZulu Natal, Pietermaritzburg campus kinetics research group.....	22
Figure 2.11	Correlation of the rates of reaction of Pt(II) complexes with the standard <i>trans</i> - $\text{Pt}(\text{py})_2\text{Cl}_2$ for different nucleophiles: •, <i>trans</i> - $\text{Pt}(\text{PEt}_3)_2\text{Cl}_2$ in methanol at 30 °C; ■, $\text{Pt}(\text{en})\text{Cl}_2$ in water at 35 °C, produced from references. ....	26
Figure 2.12	The steric effect of the aryl square planar complex showing the steric bulk for the <i>cis</i> isomer blocking the attacking site.....	29
Figure 2.13	$\pi$ -back donation of the electrons from the filled $d$ orbital to the vacant orbitals of the trans ligand in $\text{PtA}_2\text{LXY}$ . ....	32
Figure 2.14	Distribution of Charge induced dipoles in the $\text{L}-\text{Pt}-\text{X}$ coordinate of <i>trans</i> - $\text{PtA}_2\text{LX}$ .....	33
Figure 2.15	Molecular orbital representation showing the relative orbital energies in $\text{PtCl}_4^{2-}$ . ....	34
Figure 2.16	Representation of $\text{L}-\text{Pt}-\text{X}$ bonding using $\sigma$ x MO (a) The $\sigma$ -bond strength of L and X are almost equal. (b) Strong $\sigma$ -donor ligand L, the $\sigma$ -bond strength of L is much greater than that of X.....	35
Figure 2.17	The $\sigma$ - <i>trans</i> effect due to the stabilization of the trigonal bipyramidal intermediate. (a) Only one $p$ orbital is available for $\sigma$ -bond formation of L and X. (b) Two $p$ orbitals are available for the $\sigma$ -bonding of L, X and Y. ....	35

Figure 3.1	Optimized molecular structure of CoPt, showing the torsion angles of the pyridyl groups. ....	13
Figure 3.2	$^1\text{H}$ NMR spectra of PtRuPt (6.48 mM) with TU in acetonitrile at 298 K showing the dechelation of the coordinated platinum complex to form the $(\text{Ru}(\text{tppz})_2)$ unit. The spectra also indicates the formation of other intermediate products, in which some of their chemical shifts merges making it difficult to assign them exactly. The numbering system used to monitor the reaction progress is shown on the structure of PtRuPt (inset). ....	15
Figure 3.3	$^{195}\text{Pt}$ NMR spectra for the reaction of RuPt (6.28 mM) with TU, showing the changes in the chemical shift of the Pt before adding the TU nucleophile and the degradation after addition of TU for the new complex $[\text{Pt}(\text{TU})_4]^{2+}$ .....	16
Figure 3.4	(a) Typical two well-resolved kinetic traces at 382 nm for the two-steps reaction between RuPt ( $2.0 \times 10^{-5}$ M) by TU ( $6.00 \times 10^{-4}$ M) followed on stopped-flow spectrophotometer at 298 K. (b) A typical plot showing the changes in absorbance between 250 – 750 nm wavelength range for the degradation of the chelate ligand in RuPt ( $2.00 \times 10^{-5}$ M) by TU ( $6.00 \times 10^{-4}$ M) at 298 K. Inset is the kinetic trace followed at 382 nm. $I = 0.02$ M (adjusted with $\text{LiCF}_3\text{SO}_3$ and $\text{LiCl}$ ). ....	18
Figure 3.5	Dependence of the <i>pseudo</i> first-order rate constants ( $k_{\text{obs}}$ ) on the concentrations of the nucleophiles (a) for the simultaneous displacement of chloride ligands in $k_{\text{obs.}(1^{\text{st}})}$ , $\text{s}^{-1}$ , (b) for the dechelation of the ligands in $k_{\text{obs.}(2^{\text{nd}})}$ , $\text{s}^{-1}$ , from PtRuPt in methanol solution at 298 K and $I = 0.02$ M (adjusted with $\text{LiCF}_3\text{SO}_3$ and $\text{LiCl}$ ). ....	20
Figure 3.6	Eyring plots obtained for (a) RuPt with the nucleophiles for the substitution of chloride ligand, (b) Plots of $\ln(k_2/T)$ against $1/T$ for the reactions of RuPt with the nucleophiles for the dechelation of the linker at various temperatures in the range 15 - 35 °C. ....	22
Figure 3.7	(a) UV/visible spectra of Ptpy, RuPt, PtRuPt, PtRuRuPt and CoPt in methanol (0.01 mM). (b) Energy of highest absorption wavelength peak of band against the number of tppz units in the complexes. CoPt deviates from the straight line.....	26

Figure 4.1	Structural formulae of the mono, di and tri- nuclear complexes investigated. .....	4
Figure 4.2	UV/visible spectrum recorded for the titration of 0.019 mM Pt1 with NaOH, in the pH range 2 - 9 at 298 K. Inset is the plot of absorbance against pH at 275 nm. ....	12
Figure 4.3	Optimized structure of Pt1 (obtained using Gaussian09 software package) showing the steric interactions of the protons on the 4'-pyridyl ring owing to the NH <sub>2</sub> <i>trans</i> protons. Due to the longer distance between the NH <sub>2</sub> <i>cis</i> protons and the aqua ligand, no hydrogen binding is possible.....	15
Figure 4.4	Kinetic trace obtained at 291 nm for the reaction between Pt2 (2.86 x 10 <sup>-5</sup> M) and DMTU (8.58 x 10 <sup>-4</sup> M) on stopped-flow at 298 K, I = 0.02 M LiCF <sub>3</sub> SO <sub>3</sub> , adjusted with LiCl.....	17
Figure 4.5	<sup>195</sup> Pt NMR arrays showing the Pt3-Cl with 2 to 6 equivalents of TU, as a function of time. t = 0 spectrum of pure Pt3 (δ = -2506 ppm) and the subsequent spectra at t = 3, 6 and 15 hours. ....	18
Figure 4.6	Concentration dependence of the <i>pseudo</i> first-order rate constant, <i>k</i> <sub>obs</sub> for the substitution of aqua ligand in Pt2 with the thiourea nucleophiles at pH = 2, T = 298 K, I = 0.02 M HCF <sub>3</sub> SO <sub>3</sub> , adjusted with LiCF <sub>3</sub> SO <sub>3</sub> .....	19
Figure 4.7	Eyring plots for the reaction of Pt2 with the nucleophiles for the substitution reactions over the temperature range 15 - 40 °C at pH = 2, T = 298 K, I = 0.02 M HCF <sub>3</sub> SO <sub>3</sub> , adjusted with LiCF <sub>3</sub> SO <sub>3</sub> .....	21
Figure 4.8	Schematic representation of the aerial steric effect due to the <i>ortho</i> -H atoms on the <i>cis</i> pyridyl moiety. Optimized structure obtained for Pt1 from computational calculations using Gaussian09 software package.....	23
Figure 4.9	UV/visible spectra of Pt1-Cl, Pt2-Cl and Pt3-Cl in methanol (0.008 mM). .....	25
Figure 5.1	Structures of polyethylene glycoxy appended Pt(II) complexes studied. Shown on the diagram is the numbering scheme used. Ptppy is included for reference.....	3
Figure 5.2	Kinetic trace for the reaction of Ptppydeg (4.0 x 10 <sup>-5</sup> M) with TU (6.0 x 10 <sup>-4</sup> M) in methanol solution (I = 0.02 M) at 330 nm at 298 K.....	8
Figure 5.3	Dependence of the pseudo first-order rate constants ( <i>k</i> <sub>obs</sub> ) on the concentrations of the nucleophiles for the chloride substitution from Ptppydeg (4.0 x 10 <sup>-5</sup> M) in methanol solution (I = 0.02 M) at 298 K.....	9

Figure 5.4	Eyring plots obtained for Pttpydeg with the nucleophiles for the forward reactions over the temperature range 15 - 35 °C.....	10
Figure 5.5	DFT calculated minimum energy structures, frontier molecular orbitals (HOMO and LUMO) and the planarity of the complexes investigated. Included is the data obtained for the DFT calculated Pttpy complex for comparisons.....	13
Figure 5.6	Aerial view showing the angles of inclination, $\alpha$ , of the pendant units in the DFT calculated structures of Pttpyeg and Pttpytdeg.....	18
Figure 6.1	Structures of polyethyleneglycol ether linked dinuclear Pt(II) complexes studied. Shown on the diagram is the numbering scheme used. Pttpy is included for comparisons. ....	4
Figure 6.2	Kinetic trace at 301 nm for the reaction of Ptdtdeg ( $3.0 \times 10^{-5} \text{ mol dm}^{-3}$ ) with DMTU ( $8.99 \times 10^{-4} \text{ mol dm}^{-3}$ ) at 298 K, $I = 0.02 \text{ M LiCF}_3\text{SO}_3$ , adjusted with LiCl.....	10
Figure 6.3	Dependence of the pseudo first-order rate constants ( $k_{\text{obs}}$ ) on the concentrations of the nucleophiles for the chloride substitution from Ptdteg ( $2.65 \times 10^{-5} \text{ M}$ ) in methanol solution ( $I = 0.02 \text{ M}$ ) at 298 K. ....	11
Figure 6.4	Eyring plots obtained for Ptdteg with the nucleophiles for the forward reactions over the temperature range 15 - 35 °C.....	13
Figure 6.5	Aerial view showing the angles of inclination, $\alpha$ , in the DFT calculated distorted slip-up stair case like linkers and the angle of twisting ( $\delta$ ) of the tpy moieties from each other.....	15
Figure 6.6	DFT calculated minimum energy structures, frontier molecular orbitals (HOMO and LUMO) of Pttpy, Ptdt and Ptdteg. Data for Pttpy is included for comparisons. Data for Ptdtdeg, Ptdtdeg and Ptdttdeg are included in Figure S1 (Supporting Information).....	17
Figure 6.7	$^{195}\text{Pt}$ NMR the reaction mixture of Ptdtdeg ( $2 \times 10^{-2} \text{ M}$ ) with six equivalents of TU ( $2.0 \text{ M}$ ), showing a peak for pure dinuclear Pt(II) complex at $\delta = -2687 \text{ ppm}$ before the reaction ( $t = 0$ ) and the final substituted product (B, $\delta = -3099 \text{ ppm}$ ) corresponding to $[(\text{TU})\text{Pt}(\text{dtteg})\text{Pt}(\text{TU})]^{4+}$ , over a period of 4.5 hours after the reaction begins.....	19
Figure 6.8	$^1\text{H}$ spectra of Ptdttdeg ( $0.02 \text{ M}$ ) in DMSO- $d_6$ at temperatures, 30 °C to 80 °C.....	22

Figure 7.1	Structure of heterometallic complexes investigated. Shown on the structure, RuPtddtdeg is the numbering scheme employed for characterizations and DFT data. Rectangular inset shows the structures of additional mononuclear complexes, without the linker (Ptpty) and with the linker (Ptptyeg) for comparisons. The kinetic data for Ptpty is obtained from reference and Ptptyeg from our previous work ( <i>Chapter 5</i> ). ..... 4
Figure 7.2	DFT calculated minimum energy structures, frontier molecular orbitals (HOMO and LUMO) of RuPtddtdeg showing the V-shape geometry. Included is the data obtained for the DFT calculated complexes, Ptpty and Ptptyeg for comparisons. Calculations were performed at B3LYP/LanL2DZ level of theory in all the systems. Data for Ptddtdeg, Ptddtdeg and Ptddtdeg are included in Figure S7.1 (Supporting Information)..... 11
Figure 7.3	Kinetic trace for the substitution reaction of RuPtddtdeg ( $1.0 \times 10^{-5}$ M) with TU ( $3.0 \times 10^{-5}$ M) in methanol solution ( $I = 0.02$ M) at 330 nm at 298 K. 12
Figure 7.4	Dependence of the <i>pseudo</i> first-order rate constants ( $k_{\text{obs}}$ ) on the concentrations of the nucleophiles for the chloride substitution from RuPtddtdeg ( $1.0 \times 10^{-5}$ M) in methanol solution ( $I = 0.02$ M) at 298 K. .... 15
Figure 7.5	Eyring plots obtained for RuPtddtdeg with the nucleophiles for the forward reactions over the temperature range 15 - 35 °C. .... 16
Figure 7.6	Aerial view showing the steric disposition of the pendant group on the 4'-position of the chelate ligand (tpy) bonded to the Pt(II) metal centre obtained from DFT calculations. .... 18
Figure 8.1	Structure of complexes reported in Chapter 3. .... 3
Figure 8.2	Structure of complexes reported in Chapter 4. .... 4
Figure 8.3	Structure of complexes reported in Chapter 5. .... 5
Figure 8.4	Structure of complexes reported in Chapter 6. .... 6
Figure 8.5	Structure of complexes reported in Chapter 7. .... 7
Figure 8.6	Structure of the two heterometallic complexes; Ru(Ptdeg) <sub>2</sub> and (RuPt) <sub>2</sub> (deg) <sub>3</sub> investigated. Complexes, Ptptydeg and RuPtdeg are already reported in this thesis and Ptpty reported from literature are included for comparisons. .... 8
Figure 8.7	Structure of complexes synthesized and characterized. .... 10



## List of Tables

Table 1.1	Binding constants of Pt(II) terpyridine complexes reported.....	14
Table 1.2	Concentration that inhibits 50% growth inhibition of cells ( $\mu\text{M}$ ) of mononuclear ruthenium complexes and the dinuclear ruthenium complex, $[\text{Ru}(\text{apy})(\text{tpy})]_2[\mu\text{-H}_2\text{N}(\text{CH}_2)_6\text{NH}_2](\text{ClO}_4)_4$ after 48 hours treatment in some selected cell-lines.....	24
Table 2.1	Some nucleophilic constants given for $\text{Pt}(\text{py})_2\text{Cl}_2$ with different nucleophiles of donor atoms.....	25
Table 2.2	Effects of leaving group on the rates of reaction of $\text{Pt}(\text{dien})$ complexes in water at 25 °C.....	27
Table 2.3	Rate constants and activation parameters for the substitution of $\text{Cl}^-$ by $\text{I}^-$ in $[\text{Pd}(\text{R}_n\text{dien})\text{Cl}]^+$ ( $n = 0, 3-5$ ) in aqueous solution at 25 °C.....	28
Table 2.4	Effect of solvent on the chloride exchange reaction ( <i>Equation 2.39</i> ) at 25 °C.....	30
Table 3.1	Selected bond lengths ( $\text{\AA}$ ), bond angles ( $^\circ$ ), natural bond orbital (NBO) charges, HOMO and LUMO energies and other computational data obtained for the complexes $\text{Pttpy}$ , $\text{RuPt}$ , $\text{PtRuPt}$ , $\text{PtRuRuPt}$ and $\text{CoPt}$ obtained from the computational studies. Data for $\text{Pttpy}$ is included for reference.....	10
Table 3.2	Density functional theoretical (DFT) calculated minimum energy structures, HOMO and LUMO frontier molecular orbitals for the complexes investigated. The planarity of the molecules is viewed along the propagation axis showing the different planes.....	11
Table 3.3	Summary of the rate constants and activation parameters for the displacement of the chloride ligand(s) by the nucleophiles studied and the kinetic data for the dechelation of the $\text{tpyz}$ units by thiourea nucleophiles. Data for $\text{Pttpy}$ except with MTU is obtained from references and is included for comparisons.....	23
Table 4.1	The $\text{pK}_a$ values of the deprotonation of the coordinated aqua ligand in mono-, di- and tri-nuclear complexes studied.....	11
Table 4.2	Summary of DFT calculated data for the complexes using Gaussian09 software package based on B3LYP and LanL2DZ basis set.....	14
Table 4.3	DFT calculated minimum energy structures and frontier molecular orbitals (HOMO and LUMO) of the complexes investigated. Calculations were done using Gaussian09 software package based on B3LYP and LanL2DZ basis set.....	16

Table 4.4	Summary of the second-order rate constants, $k_2$ and activation parameters, with the corresponding standard deviations for the substitution of the aqua ligand(s) by a series of thiourea nucleophiles at pH = 2, $I = 0.02$ M $\text{HCF}_3\text{SO}_3$ , adjusted with $\text{LiCF}_3\text{SO}_3$ .....	20
Table 5.1	Summary of DFT calculated data for the complexes investigated. Included is the data obtained for the DFT calculated Ptpty complex for comparisons..	12
Table 5.2	Summary of second-order rate constants, $k_2$ and activation parameters, with the corresponding standard deviations for the substitution of the chloro ligand by a series of thiourea nucleophiles and iodide at $I = 0.02$ M $\text{LiCF}_3\text{SO}_3$ , adjusted with $\text{LiCl}$ . Given in brackets for TU is the data for Ptpty taken from literature and included for comparison.....	16
Table 6.1	Summary of the second-order rate constants, $k_2$ and activation parameters, with the corresponding standard deviations for the substitution of the chloro ligands by a series of thiourea nucleophiles at $I = 0.02$ M $\text{LiCF}_3\text{SO}_3$ , adjusted with $\text{LiCl}$ . Data for Ptpty is taken from literature and included for comparison.....	12
Table 6.2	Geometry optimised structures of the complexes investigated.....	16
Table 6.3	Summary of DFT calculated data for the complexes investigated. Included is the data obtained for the DFT calculated Ptpty complex for comparisons.	18
Table 7.1	Summary of DFT calculated data for the complexes investigated. Included for comparison purposes is the data for Ptpty and Ptptyeg. Calculations were performed at B3LYP/LanL2DZ level of theory in all the systems.....	10
Table 7.2	Summary of second-order rate constants, $k_2$ and activation parameters, with the corresponding standard deviations for the substitution of the chloro ligand by a series of thiourea nucleophiles and iodide at $I = 0.02$ M $\text{LiCF}_3\text{SO}_3$ , adjusted with $\text{LiCl}$ . Data for Ptpty is taken from literature and data on mononuclear complexes are from <i>Chapter 5</i> and are included for comparison.....	14
Table 8.1	Summary of second-order rate constants, $k_2$ and activation parameters, with the corresponding standard deviations for the substitution of the chloro ligands by a series of thiourea nucleophiles and iodide ion at $I = 0.02$ M $\text{LiCF}_3\text{SO}_3$ , adjusted with $\text{LiCl}$ . Data for Ptptydeg and RuPtdtdeg are taken from <i>Chapter 5</i> and <i>Chapter 6</i> and data for Ptpty are included for comparison.....	9

## List of Schemes

Scheme 1.1	The sequence of cisplatin binding to DNA and the structurally different adducts formed. The $k$ values and $t_{1/2}$ values were obtained from a kinetic study of hydrolysis of cisplatin by short lengths of single- or double-strand DNA containing adjacent guanosines using $^{15}\text{N}$ NMR at pH 7.1 in water containing $10 \text{ mol dm}^{-3}$ sodium phosphate. ....	6
Scheme 1.2	Reaction of Pt(II) (tpy) with guanosine (1:1) showing the N7 binding of guanosine with Pt(II) (tpy) (32). ....	15
Scheme 1.3	Schematic representation of catalytic electrolysis reaction for the cleavage of DNA by $[\text{Ru}(\text{tpy})(\text{bpy})\text{O}]^{2+}$ . ....	21
Scheme 1.4	Schematic representation of suggested mode of action of ruthenium based anticancer drugs. ....	26
Scheme 2.1	Associative mode of substitution at the metal centre. ....	3
Scheme 3.1	Structural formulae of investigated complexes. The numbering schemes used for DFT calculations and the other references are shown on the structure of PtRuRuPt. ....	4
Scheme 3.2	Proposed reaction mechanism for the reactions between the complexes, RuPt, PtRuPt, PtRuRuPt and CoPt with thiourea nucleophiles. The full reaction mechanism holds for RuPt, PtRuPt, PtRuRuPt and CoPt with thiourea nucleophiles only. For the ionic nucleophiles studied, $\text{I}^-$ and $\text{SCN}^-$ , the reaction mechanism holds only for the first step. The charges on the complexes are omitted for clarity. ....	17
Scheme 4.1	Schematic representation of preparation of aqua complexes. ....	7
Scheme 4.2	The $\text{p}K_{\text{a}}$ titration reactions of the aqua complexes with $\text{OH}^-$ . ....	9
Scheme 4.3	Proposed reaction mechanism for the substitution of aqua ligand(s) by thiourea nucleophiles studied. ....	20
Scheme 5.1	Proposed mechanism for the substitution of chloride ligand from the Pt(II) complexes. ....	14
Scheme 6.1	Proposed substitution mechanism for the dinuclear Pt(II) complex system with thiourea nucleophiles. ....	11
Scheme 7.1	The general reaction scheme for the reactions between the complexes and the nucleophiles studied. ....	17

**Table of Contents- 1**

List of Figures.....	ii
List of Tables.....	iii
List of Schemes .....	iii
Chapter One .....	1
<b>Role of Platinum and Ruthenium Complexes as Anticancer Agents .....</b>	<b>1</b>
1.1    Introduction.....	1
1.2    The General Chemistry of Platinum(II) Complexes .....	2
1.3    Development of Platinum-based Anticancer Drugs and Structure Activity Relationship.....	3
1.3.1    Cisplatin.....	4
1.3.1.1 Mechanism of Action of Cisplatin.....	4
1.3.1.2 Reactivity of Cisplatin with DNA.....	5
1.3.1.3 Cisplatin Resistance.....	8
1.3.2    Development of Second Generation Cisplatin Analogues.....	8
1.4    Current Findings on Anticancer Platinum(II) Drugs .....	9
1.4.1    Multinuclear Platinum(II) Complexes.....	9
1.4.2    Polynuclear Platinum(II) Complexes with Flexible Linkers .....	9
1.4.3    Polynuclear Platinum(II) Complexes with Rigid Linkers.....	11
1.5    Platinum(II) Polypyridyl Complexes.....	13
1.5.1    DNA Intercalation.....	13
1.5.2    Substitution of Platinum(II) terpyridine Complexes with Biologically Active Nucleophiles .....	14
1.5.3    Previous Kinetics and Mechanistic Studies on Platinum(II) terpyridine Complexes with Thiourea and Ionic nucleophiles .....	16
1.6    Therapeutic Ruthenium Complexes: A Possible Alternative to Platinum .....	17
1.6.1    The General Chemistry of Ruthenium(II) Complexes .....	18
1.6.2    The Biological Importance of Ruthenium(II) Complexes .....	19
1.6.3    Ruthenium Complexes as Biological Probes .....	21
1.6.4    Intercalation of Ruthenium Complexes in Two DNA Bases .....	23
1.6.5    Photodynamic Therapy.....	25
1.6.6    Postulated Mechanisms of Action of Anticancer Ruthenium Complexes.....	25
1.6.7    Substitution Reactions of Ruthenium(II) Complexes .....	26
1.6.8    Polynuclear Ruthenium Complexes .....	27
1.7    Heteronuclear Ruthenium(II)-Platinum(II) Polypyridyl Complexes .....	29
1.8    Aims of this Study.....	32

1.9	References.....	35
-----	-----------------	----

**List of Figures**

Figure 1.1	Platinum complexes in worldwide clinical use and as well as those with regionally limited approval: nedaplatin, lobaplatin.....	3
Figure 1.2	Suggested reaction pathway for cisplatin in the cell and binding to DNA. Extracted from references. ....	5
Figure 1.3	Some possible cisplatin-DNA binding modes. ....	7
Figure 1.4	Some polynuclear Pt(II) complexes which have shown potential anticancer activity. ....	10
Figure 1.5	Multinuclear platinum (II) complexes with rigid linkers which have shown anticancer activity. ....	12
Figure 1.6	Multinuclear Pt(II) complexes with rigid linkers which are used for kinetic and mechanistic study. ....	13
Figure 1.7	Pt(II) complexes studied by van Eldik <i>et al.</i> (33-38). Pt(II)terpyridine complexes studied by Jaganyi <i>et al.</i> (38,39) and (40).....	17
Figure 1.8	Structure of some of the ruthenium complexes which were found to have antitumour activity. ....	20
Figure 1.9	Some dinuclear cationic Ru(II) complexes linked by flexible and rigid linkers.....	29
Figure 1.10	The Ru(II)-Pt(II) with a long and flexible linkers (58) and (59) along with the heterodinuclear Ru(II)-Pt(II) complexes with different linkers. Anions omitted for simplicity. ....	31

**List of Tables**

Table 1.1	Binding constants of Pt(II) terpyridine complexes reported.....	14
Table 1.2	Concentration that inhibits 50% growth inhibition of cells ( $\mu\text{M}$ ) of mononuclear ruthenium complexes and the dinuclear ruthenium complex, $[\text{Ru}(\text{apy})(\text{tpy})]_2[\mu\text{-H}_2\text{N}(\text{CH}_2)_6\text{NH}_2](\text{ClO}_4)_4$ after 48 hours treatment in some selected cell-lines.....	24

**List of Schemes**

Scheme 1.1	The sequence of cisplatin binding to DNA and the structurally different adducts formed. The $k$ values and $t_{1/2}$ values were obtained from a kinetic study of hydrolysis of cisplatin by short lengths of single- or double-strand DNA containing adjacent guanosines using $^{15}\text{N}$ NMR at pH 7.1 in water containing $10 \text{ mol dm}^{-3}$ sodium phosphate.....	6
Scheme 1.2	Reaction of Pt(II) (tpy) with guanosine (1:1) showing the N7 binding of guanosine with Pt(II) (tpy) (32).....	15
Scheme 1.3	Schematic representation of catalytic electrolysis reaction for the cleavage of DNA by $[\text{Ru}(\text{tpy})(\text{bpy})\text{O}]^{2+}$ . ....	21
Scheme 1.4	Schematic representation of suggested mode of action of ruthenium based anticancer drugs. ....	26

# Chapter One

## Role of Platinum and Ruthenium Complexes as Anticancer Agents

### 1.1 Introduction

Cancer is one of the most deadly diseases in the world that is caused mainly by abnormalities in the genetic material of cell transformation.<sup>1</sup> Such abnormalities are caused due to the effect of environmental factors such as exposure to carcinogens; chemicals, certain type of radiation, tobacco smoke. Depending on the type and location, this disease is treated by surgery, chemotherapy, radiation and immunotherapy.<sup>2</sup> However, to date, effective treatment of cancer has become one of the challenging tasks since certain cancer cell-lines are resistant to the available anticancer treatments.<sup>3</sup> Therefore, current anticancer research focuses on synthesizing new drugs which are of improved cytotoxicity.<sup>4</sup>

Even though metals are considered toxic for human body, many precious metal ions still play a vital role in many biological processes.<sup>5</sup> The positively charged metal centers interact with the negatively charged groups of proteins and nucleic acids. The number of metal based anticancer drugs which are in current clinical use is still low. The majority of the drugs are platinum compounds. Examples include; **cisplatin** (*cis*-diamminedichloridoplatinum(II)) **(1)**, **carboplatin** (*cis*-diammine(1,1-cyclobutanedicarboxylato) platinum(II)), and **oxaliplatin** (*Figure 1.1*).<sup>6</sup> However, due to the severe side effects and acquired resistance to certain cancer cells, a large number of other metal complexes have been synthesized and screened for anticancer activity.<sup>5</sup> Amongst them, ruthenium complexes are the most well documented. The two most promising ruthenium based anticancer compounds known to date are NAMI-A<sup>7</sup> and KP1019.<sup>8</sup> They have shown unique antitumour activity. The complexes were found to be active against most cisplatin- resistant tumour cells. This chapter reviews the chemistry of Pt(II) and Ru(II) and their compounds as metalotherapeutic agents in the medicinal chemistry.

## 1.2 The General Chemistry of Platinum(II) Complexes

Platinum is one of the most well studied transition metals due to its biological activity.<sup>9</sup> The most well known oxidation states are 0, +2, +4.<sup>10</sup> The +2 and +4 states are the most important because they comprise the majority of the platinum complexes. These complexes are kinetically and thermodynamically stable. Research on biological applications of Pt(II) complexes started in the 1950s with the systematic investigations of inorganic reaction mechanisms. Of all the oxidation states of platinum, the +2 species is the most versatile and well studied in the reaction mechanisms due its moderately slow reactivity and high redox stability.<sup>10b,11</sup> Moreover other distinctive features of Pt(II) species include the presence of a vacant  $p_z$  orbital for nucleophilic attack, formation of  $\sigma$  and  $\pi$ -bonds with complexes and the ability to undergo oxidative addition and reductive elimination.<sup>10b</sup>

Since Pt(II) is a soft acid, it prefers to bind with soft bases. Pt(II) forms a range of stable mono and multinuclear complexes with neutral ligands such as  $C_2H_4$ , CO, tertiary phosphines and anionic monodentate ligands such as halides, sulphides and nitrites.<sup>10b,12</sup> With tridentate N—N—N donor ligands such as 2,2':6',2''-terpyridine (tpy), four-coordinate mononuclear complexes are more common. Furthermore, apart from mono and multinuclear complexes, with bidentate ligands such as N—N, P—P, S—S, N—O, N—P and N—S, Pt(II) often forms bridged dinuclear chelated complexes.<sup>13</sup>

Compared to other square planar complexes of platinum group elements, Pt(II) complexes are relatively inert. This kinetic property of Pt(II) complexes is thought to be the key to the activity of most Pt(II) coordinated compounds. It is also often used for studying the mechanism of their reactions. In the past, several studies<sup>13-14</sup> have been reported on understanding the substitution and kinetic behaviour of Pt(II) complexes. Data from these studies resulted in the development of the *trans* effect.<sup>15</sup>

Apart from medicinal applications, other major applications of platinum compounds include catalysis, electrical and electronic applications, photoluminescence, usage in high sensitive optical sensors.<sup>16</sup> However, the greatest accomplishment of platinum chemistry was the discovery of the biologically active platinum antitumour complex, cisplatin.<sup>9</sup>



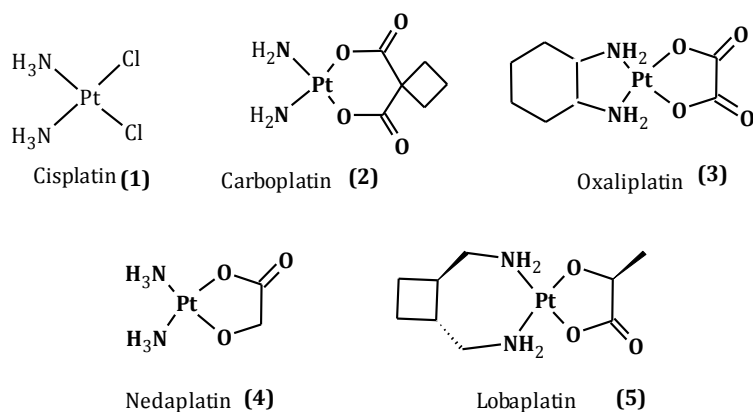
### 1.3 Development of Platinum-based Anticancer Drugs and Structure Activity Relationship

The antitumour activity of cisplatin, first synthesized by Peyrone in 1845 was serendipitously discovered in 1969 by Barnett Rosenberg<sup>9,17</sup> during an investigation of the effects of electric field on *Escherichia coli* (*E. coli*) bacteria growth in ammonium chloride solution using a platinum electrode.<sup>18</sup> The drug was first approved for clinical uses in 1978.<sup>19</sup> Cisplatin forms DNA adducts and interferes with DNA transcription and replication, causing cell apoptosis.<sup>20</sup>

Following the success of cisplatin, a number of platinum based compounds were synthesized and tested for anticancer activity. Based on the results obtained by screening a large number of cisplatin related complexes, Cleare and Hoeschele, proposed some early structural-activity relationships, (SAR), governing the activity.<sup>21</sup> They proposed that:<sup>21-22</sup>

- ✓ the platinum complexes must have anionic leaving groups with moderate binding strength to platinum and should possess a weak *trans effect* to avoid labilisation of the amine moiety.
- ✓ the platinum complexes must have a *cis* geometry. The *cis* geometry is preferred because the complexes of *trans* geometry were found to be inactive.
- ✓ the amine group(s) must possess at least one N—H group, which is thought to play a role in the hydrogen bond formation with the DNA.<sup>22a</sup>
- ✓ the complex must be neutral.<sup>23</sup> It was thought that neutral complexes would lead higher activity through and facilitate the entry of the drug through the cell membrane.

In recent years complexes with several modifications have been synthesized.<sup>24</sup>



**Figure 1.1** Platinum complexes in worldwide clinical use and as well as those with regionally limited approval: nedaplatin, lobaplatin.<sup>6</sup>

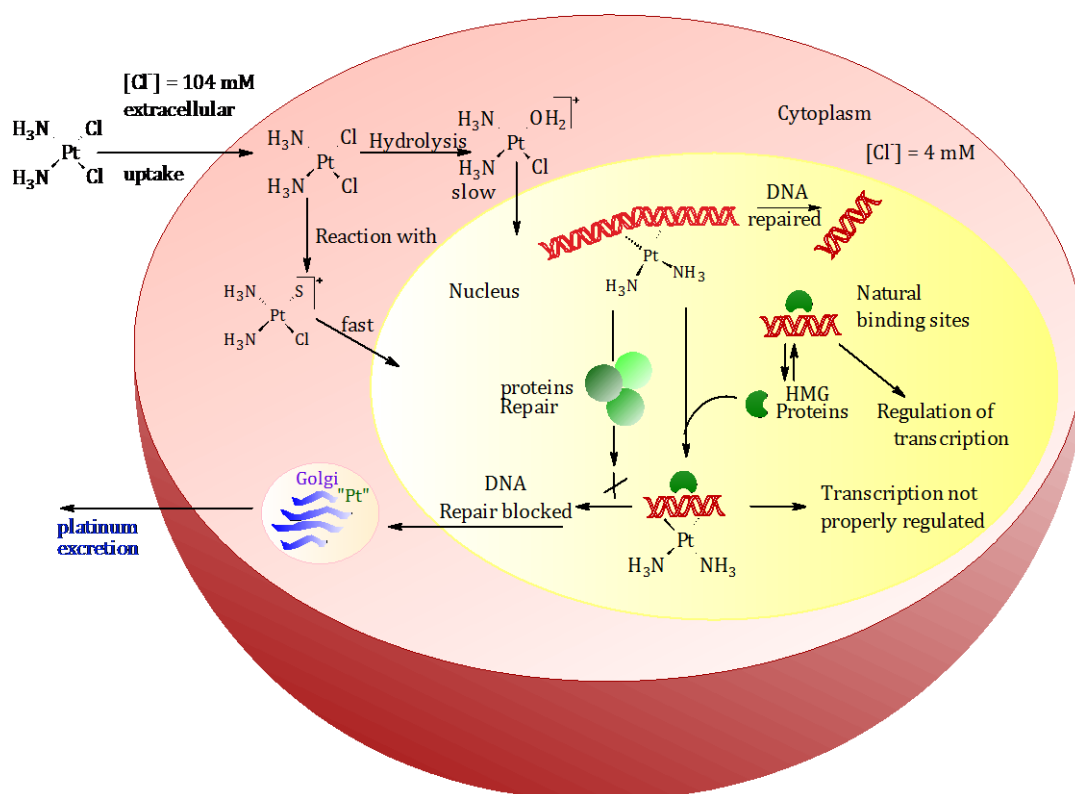
### 1.3.1 Cisplatin

Despite its simplicity in structure, cisplatin is one of the most potent anticancer drugs developed for chemotherapy in the last three decades.<sup>17c,23,25</sup> Since the beginning of its clinical trials in 1971,<sup>9,26</sup> the drug has been used as an effective treatment against a wide range of cancerous cells such as cancers of the bladder, head, testicular, neck and ovarian.<sup>9,17c,27</sup> However, due to the severe side effects, such as vomiting/nausea,<sup>28</sup> nephrotoxicity and neurotoxicity,<sup>6b,29</sup> frequent development of drug resistance in certain tumour cells<sup>29j,30</sup> and limited water solubility,<sup>17c</sup> the effectiveness of the drug is limited. Even though, the actual cell distribution of cisplatin and its mechanism of action with cellular material are not fully understood,<sup>31</sup> a large body of research in the past three decades have revealed considerable information about how the drug kills certain tumour cells and becomes resistant to others.<sup>32</sup>

#### 1.3.1.1 Mechanism of Action of Cisplatin

Further studies on cisplatin unravelled the mechanism of Pt(II) compounds and how it destroys cancer cells in the human body. It is widely accepted that the main binding target of cisplatin is DNA.<sup>17c,33</sup> In the blood plasma the chloride concentration is high enough (~100 mM) to suppress the hydrolysis of the complex thus, most of it remains unchanged.<sup>22a,27d</sup> The neutral compound enters into the cell either by passive diffusion or active uptake which have been now reported to involve copper transporter proteins so-called constitutive triple response 1 (CTR1) sites.<sup>34</sup> However, on crossing the cell membrane, the neutral cisplatin molecule undergoes hydrolysis of one or both the chloride ligands producing charged species (*Figure 1.2*).<sup>17c,18,22a</sup> The first aquation process is rapid due to the low chloride concentration inside the cell (*ca.* 2 - 4 mM)<sup>35</sup> onto which the rate of reaction of cisplatin with DNA depends on.<sup>36</sup> Since water is a better leaving group than chloride, the resulting charged species are more reactive towards biomolecules.<sup>37</sup> The antitumour activity of cisplatin is intervened by recognition of platinated DNA adducts<sup>17c</sup> by the proteins (for example high-mobility group proteins (HMG)) which prevent cisplatin adducts from interfering with DNA transcription (*Figure 1.2*). Inside the cell some of the drug may interact with sulfur donors in the blood since they have a high affinity for platinum centres,<sup>38</sup> yielding to stable or kinetically inert<sup>39</sup> Pt—S bonded products. Accumulation of coordinated sulfur containing proteins and amino acids<sup>40</sup> to the platinum drug may lead to potential deactivation of the drug and some toxic side effects<sup>41,37</sup> which affects the biodistribution of the drug and its pharmacokinetics. This reduces the formation of the

required Pt—DNA adducts and drug accumulation.<sup>40a,42</sup> Due to the *trans* influence of certain sulfur containing compounds of thioethers<sup>40a</sup> or methionine derivatives<sup>43</sup> to the Pt(II) centre results in the removal of the *trans* amine ligand by the incoming sulfur ligand before DNA binds with the drug<sup>40a,43</sup> thereby hindering the actual mechanism of the action of the drug and its cytotoxicity.<sup>40a</sup>



**Figure 1.2** Suggested reaction pathway for cisplatin in the cell and binding to DNA. Extracted from references.<sup>17c,18,24,38</sup>

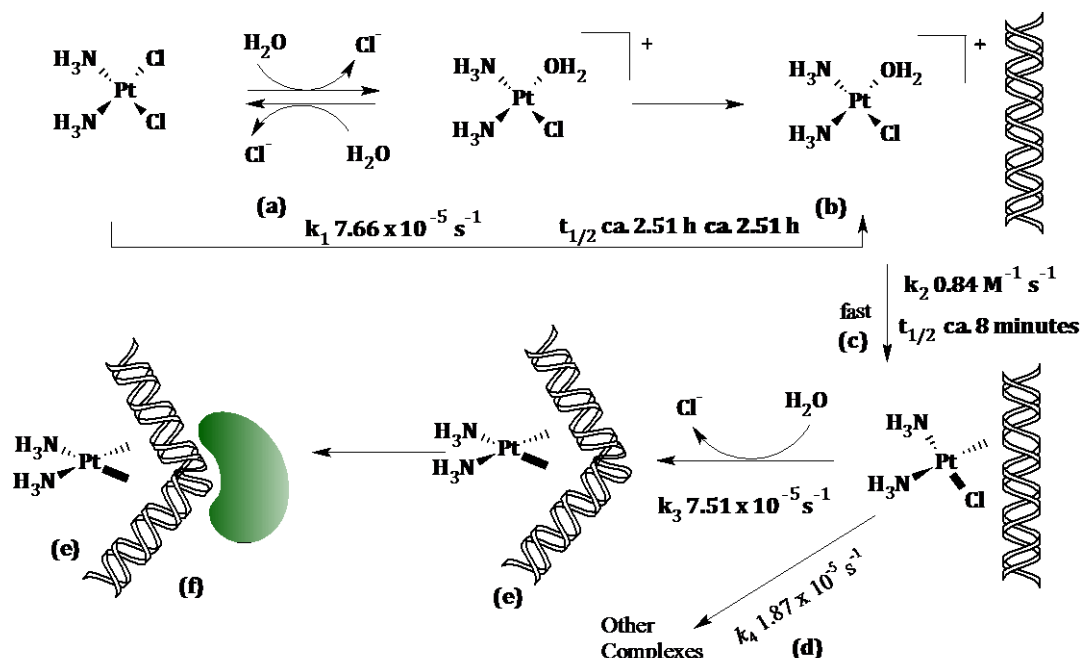
### 1.3.1.2 Reactivity of Cisplatin with DNA

Due to poor solubility, cisplatin is administered into the human body intravenously as a sterile saline solution at a dose of about 50 - 120 mg/m<sup>2</sup> (m<sup>2</sup> = body surface area) per course over 0.5 to 2 hours<sup>9,27d</sup> for five consecutive days in every 21 days. To minimise the side effects, the drug is often given in combination therapy with other antitumour adjuvants such as bleomycin,<sup>44</sup> arabinofurascylcytosine,<sup>45</sup> 5-fluorouracil<sup>46</sup> and paclitaxel.<sup>44</sup> Once it is entered into the cell, the hydrolysed form of cisplatin lowers the  $pK_a$  of the complex. However, under physiological pH,<sup>47</sup> some of the aqua drug complexes may get changed to hydroxo species. The hydrated species may bind to DNA in multiple steps (*Scheme 1.1*), which include:<sup>48</sup>

- Aquation:** Binding of cisplatin to DNA proceeds *via* formation of the mono aquated species which follows a first-order kinetics and is thought to be the rate

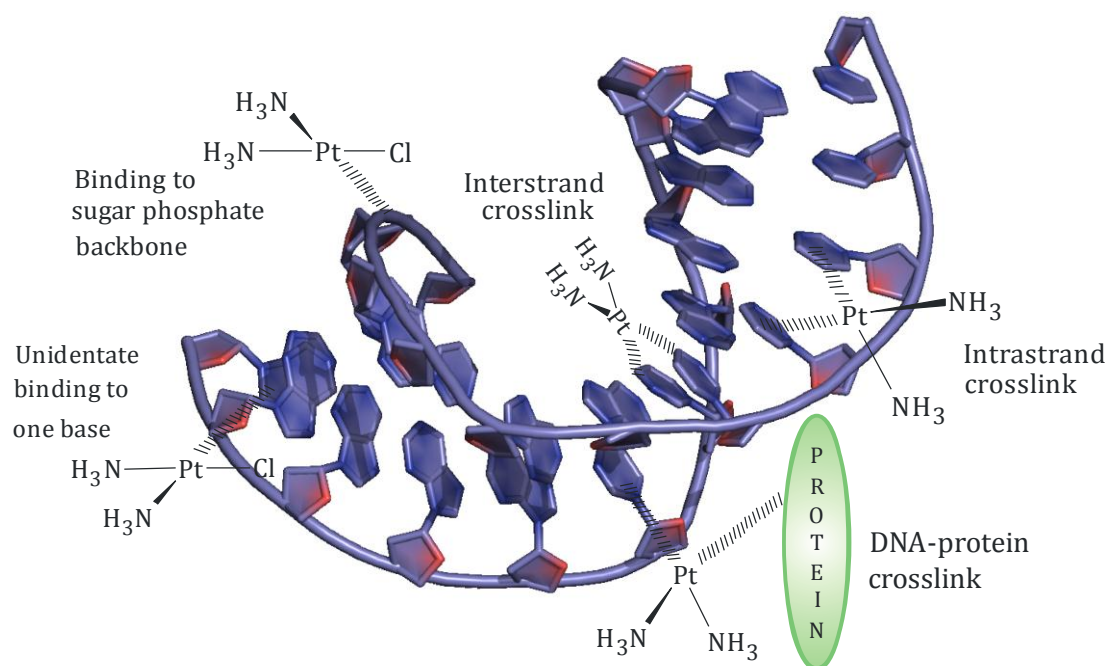
determining step.<sup>42,49</sup> This step also depends on the nature of the *trans* amine group.<sup>50</sup>

- b. **Preassociation:** This involves formation of hydrogen bonding and insertion by intercalation with DNA.
- c. **Monofunctional adduct formation:** Approximately 90% of the Pt-DNA adducts formed here are mainly between 1,2 adjacent N7 guanine sites (60-65%)<sup>36</sup> which causes the double strand DNA to form a kink<sup>51</sup> of 45° - 70° at the platinations site, resulting in partial unwinding and loss of helical stability while the cross-links between adjacent N7 adenine- N7 guanine are 20 - 25%<sup>52</sup> which unwinds DNA by 13° at the platination site.
- d. **Second aquation:** Hydrolysis of the second chloride ligand produces diaqua species which are twice reactive towards DNA compared to the mono aqua species.
- e. **Ring closure and formation of bifunctional adduct:** Formation of interstrand or intrastrand bifunctional adduct is thought to be essential for effective anticancer activity. However, it is not yet known whether the bifunctional adduct is formed directly from the monochloro complex or whether it is *via* aquation.
- f. **DNA distortion :** DNA gets distorted by various proteins.



**Scheme 1.1** The sequence of cisplatin binding to DNA and the structurally different adducts formed.<sup>48</sup> The  $k$  values and  $t_{1/2}$  values were obtained from a kinetic study of hydrolysis of cisplatin by short lengths of single- or double-strand DNA containing adjacent guanosines using  $^{15}\text{N}$  NMR at pH 7.1 in water containing 10 mol  $\text{dm}^{-3}$  sodium phosphate.<sup>22a</sup>

Even though, inside the cell cisplatin can also react with many other cellular components, a number of reasearch has shown that the major bindings involve the coordination of cisplatin with the DNA bases viz. adenine (A), cytosine (C), guanine (G) and thymine (T) especially, the N7-position of guanine.<sup>9,18,22a,26,40a,52-53</sup> The possible modes of cisplatin binding to DNA are shown in *Figure 1.3*. The monofunctional adducts often form either interstrand or intrastrand adducts which can then stop DNA multiplication.<sup>54</sup> However, the major contributor to the cisplatin anticancer activity are the di-Pt-DNA adducts.<sup>53b</sup>



**Figure 1.3** Some possible cisplatin-DNA binding modes.<sup>22a,55</sup>

The binding of cisplatin to DNA alters the DNA conformation and brings distortion to the structure. This results in DNA unwinding, bending<sup>56</sup> and flattening of the minor grooves in the DNA helix.<sup>9,53d</sup> These changes result in the inhibition of DNA transcription which is an important step for protein synthesis and cell division. The target of cisplatin inside the DNA is the telomeric regions of chromosomes<sup>27d,57</sup> which protect the ends of chromosomes from degradation during cell division.<sup>27d,58</sup> Degradation of the telomeric regions in the chromosomes by cisplatin suppresses cell division causing significant damages in the DNA and DNA replication leading to apoptosis.<sup>27d,59</sup>

### 1.3.1.3 Cisplatin Resistance

Resistance of certain tumour cells to cisplatin is due to failure of cancerous cells to respond to the inhibitory effects of the drug. Experimental evidence suggests that the development of resistance to cisplatin is thought to be due to a number of reasons. Any or all of the following factors may play a role in resistance of the drug to the tumour cells;<sup>22a,27d,52,60</sup>

- ✓ low intracellular accumulation due to either by decreased influx (intake) or enhanced efflux (expelling) in the plasma membrane,
- ✓ Increased detoxification by binding with S-donor molecules such as glutathione and methallothioneins.
- ✓ Increased tolerance to Pt-DNA adducts,
- ✓ Increased nucleotide excision repair (NER) mechanism which confer the resistance on the cell line. To circumvent this problem, various agents are given in conjunction with cisplatin.

### 1.3.2 Development of Second Generation Cisplatin Analogues

Since cisplatin's therapeutic efficacy is limited due to its severe side effects and resistance to certain tumour cells, a number of Pt(II) complexes have been developed in order to improve the clinical limitations with less tumour resistance and toxicity.<sup>9,29a-c,30g,61</sup> Out of a large pool of platinum complexes that have been synthesised and clinically screened for anticancer activity, only a few are currently registered for clinical administration. These include; carboplatin, [cis-diamine(1,1-cyclobutanedicarboxylato)platinum(II)] **(2)**, *trans*-L-1,2-diaminocyclohexaneoxalato platinum(II) oxaliplatin **(3)**, *cis*-diammineglycolatoplatinum(II), nedaplatin **(4)**, [cis-diammineglycolatoplatinum(II)] and lobaplatin **(5)**<sup>17c,52,61</sup> (*Figure 1.1*).<sup>6</sup>

Of the five platinum complexes in *Figure 1.1*; carboplatin was reported to be less toxic<sup>9,17c,62</sup> and hence, the drug is administered at higher doses (2000 mg/dose)<sup>63</sup> than standard regimens (900 mg/m<sup>2</sup>)<sup>9,64</sup> due to its slower aquation<sup>62,65</sup> owing the less labile cyclobutanedicarboxylato ligand<sup>42,53f</sup> compared to the chloride ligands in cisplatin.<sup>9,17c,42</sup> The drug is now widely used for the treatment of ovarian cancer<sup>66</sup> and is remarkably less toxic towards kidney and nervous system. This led to the synthesis of 1,2-diaminocyclohexaneplatinum(II), oxaliplatin which contains a bidentate leaving group<sup>22a</sup> with enhanced water solubility and slower hydrolysis process resulting in a high cellular uptake.<sup>67</sup> The drug was effective for treatment of colorectal cancer, a type

of cancer which is resistant to cisplatin and carboplatin.<sup>9,17c,68</sup> It is currently approved for clinical use in France<sup>27c</sup> Europe, China and United States.<sup>17c,69</sup> The carboplatin analogue, nedaplatin, is registered in Japan for the treatment of head, neck, lung and oesophageal cancer<sup>27c</sup> while lobaplatin has been clinically approved in China.<sup>27c</sup> However, these complexes which are structural analogues of cisplatin, suffer from a similar kind of cross-resistance.<sup>30f,70</sup> and hence the search for effective anticancer drugs is ongoing.

## **1.4 Current Findings on Anticancer Platinum(II) Drugs**

Current research on anticancer drugs focuses on the synthesis of structurally different complexes of cisplatin which can exhibit effective antitumour activity with less side effects and tumour resistance. Thus, a number of active mono- and multi-nuclear Pt(II) and other transition metal complexes have been discovered with various structural modifications. This includes complexes with *trans* configuration, non- H-amine neutral ligands of homometallic and heterometallic supramolecular complexes.<sup>23</sup> However, focus here will be only on multinuclear platinum complexes.

### **1.4.1 Multinuclear Platinum(II) Complexes**

Multinuclear platinum complexes contain two or more platinum atoms linked together by a bridging linker. The new approach of designing Pt(II) anticancer drugs allowed the synthesis of various multinuclear Pt(II) compounds having different binding modes with DNA. The complexes vary from *cis* to *trans* and from bifunctional to polyfunctional, with varying flexible linkers<sup>71</sup> as well as rigid bridges<sup>72</sup> (*Figure 1.4*). Mechanistically, these complexes are expected to interact with DNA in a unique way. Results obtained showed some of these complexes display a very good antitumour activity where some complexes overcome the cisplatin resistance.

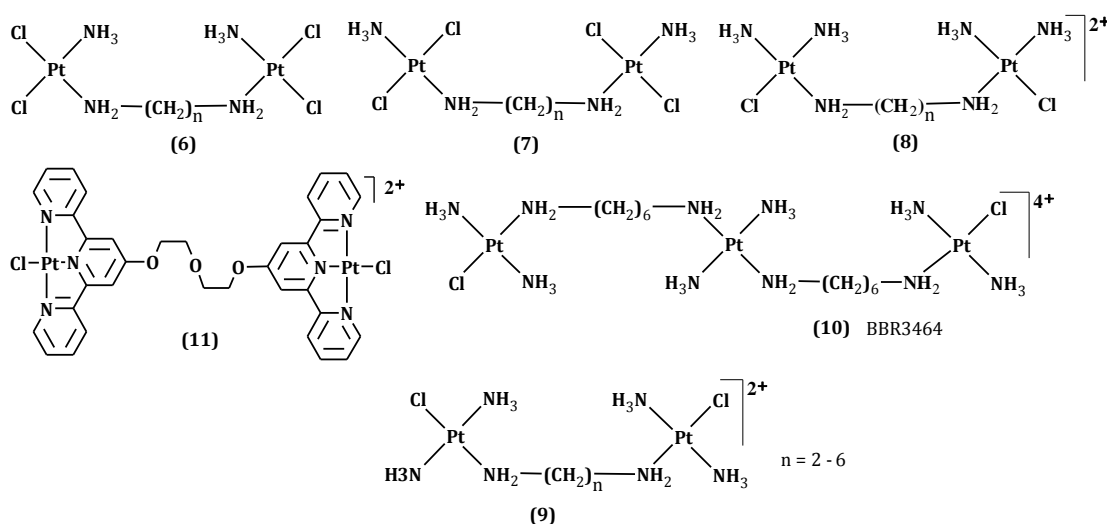
### **1.4.2 Polynuclear Platinum(II) Complexes with Flexible Linkers**

The first reported multinuclear platinum complexes were based on cisplatin like (2,2-*cis,cis*) (**6**)<sup>73</sup> and transplatin like (2,2-*trans,trans*) (**7**)<sup>73</sup> terminal structures linked by flexible alkyldiamine bridging groups of variable lengths.<sup>73-74</sup> The complexes were bifunctional at each metal centre. The complexes were found to cross-link with DNA upon reacting. When tested for anticancer activity, the 2,2-*cis,cis* complex was reported to be active in cells resistant to cisplatin. Furthermore, DNA binding functions of their monofunctional complexes showed that DNA 1,1/t,t complex cross-links with DNA more efficiently than 2,2/*cis,cis* complex.<sup>75</sup> Furthermore, for the straight chain enjoined

complexes, it was reported that 1,6-hexanediamine ( $n = 6 \text{ CH}_2$ ) was ideal for their optimum activity.<sup>73-74,76</sup>

However, the most promising within this new class of anticancer compounds is the trinuclear complex,  $[\{trans\text{-PtCl}(\text{NH}_3)_2\}_2\{\mu\text{-trans-Pt}(\text{NH}_3)_2(\text{H}_2\text{N}(\text{CH}_2)_6\text{NH}_2)_2\}]^{4+}$  (1,0,1/t,t,t), or **BBR3464**. This complex was found to exhibit cytotoxicity at ten to thousand times lower dose limits<sup>77</sup> than cisplatin and has successfully passed through the phase II clinical trials and is currently undergoing some other clinical trials.<sup>78</sup> The complex was found to be a very potent cytotoxic agent and is effective against melanoma, pancreatic cancer, lung cancer<sup>27c,72,75</sup> and has less neuro and nephro toxicity and less side effects such as nausea and vomiting. This compound can monofunctionally bind to DNA to form long-range interstrand and intrastrand DNA cross-links.<sup>72,79</sup> It has a higher cellular uptake due to its high effective positive charge and no cross-resistance to cisplatin resistance cells.<sup>27c</sup> The cationic inert tetraamine platinum linker enhances water solubility and high DNA affinity.

Meanwhile, a number of other linking ligands have also been used to develop related dinuclear platinum complexes.<sup>80</sup> The dinuclear Pt(II) complex, **(11)**  $[\text{ClPt}(\text{dtdeg})\text{PtCl}]$  (where dtdeg = bis[4'-(2,2':6',2''-tpyridyl)]-diethyleneglycolether), was synthesized and characterized.<sup>81</sup> DNA interaction study using calf thymus (CT) DNA as a substrate showed a very high activity against all the cancer cell-lines tested, in some cases with a better activity than the well known anticancer drug, cisplatin.<sup>81</sup>



**Figure 1.4** Some polynuclear Pt(II) complexes which have shown potential anticancer activity.<sup>75,78-79,81-82</sup>



### 1.4.3 Polynuclear Platinum(II) Complexes with Rigid Linkers

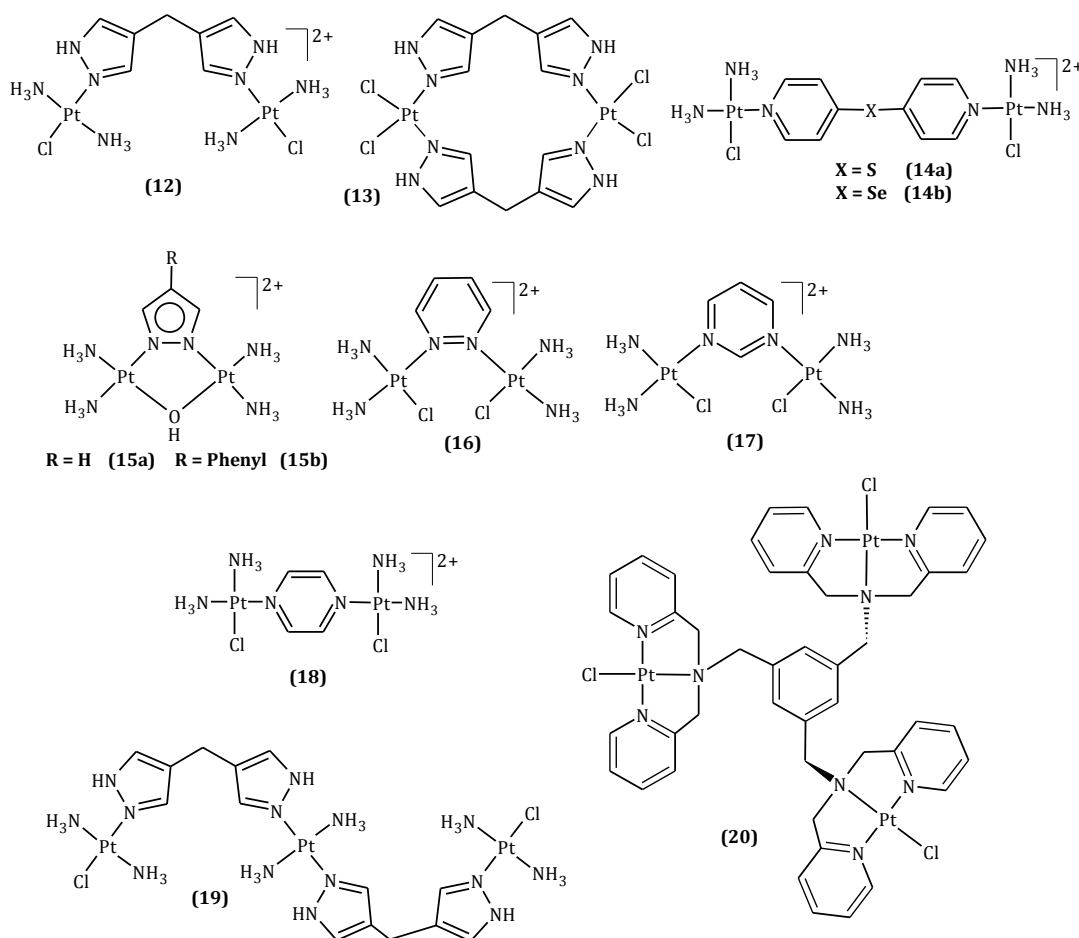
A number of other multinuclear platinum complexes, with rigid bridging linkers which include; 4,4'-dipyridyl(sulfide or selenide),<sup>83</sup> 4,4'-dipyrazolylmethane,<sup>84</sup> mesitylene,<sup>85</sup> phenyldiamine, azines,<sup>14a,25a</sup> azoles<sup>29b,86</sup> and hydrazines<sup>87</sup> have been synthesized and tested for cytotoxicity.

A rigid bridged dinuclear platinum complex **(12)** (*Figure 1.5*) with square planar geometries has been reported by linking two cisplatin like platinum centres through 4,4'-dipyrazolylmethane (dpzm) ligand.<sup>84b,c</sup> Another dinuclear transplatin like platinum complex,  $[\{trans\text{-Pt}(\text{NH}_3)_2\text{Cl}\}_2(\mu\text{-dpzm})]\text{Cl}_2$  (**13**) along with complex **(12)** were found to have high levels of DNA intrastand cross-linking which was thought to be due to the rigidity of the linker especially, the bifunctional complex, **(13)** was found to bind preferentially with adenine residues.<sup>88</sup> Furthermore, since selenium and sulphur compounds are known to have chemoprotective activity, the dinuclear complexes bridged by either 4,4'-dipyridylselenide or sulfur<sup>89</sup> **(14a)** and **(14b)** were found to diminish the known toxic side effects of anticancer drugs.<sup>90</sup>

A series of short pyrazole and hydroxo bridged dinuclear platinum complexes (*Figure 1.5*) were synthesized **(15a)** and **(15b)** and expected to form 1,2-intrastand adducts without major distortions of the DNA.<sup>29b</sup> In these complexes the hydroxo group was incorporated both as a linker as well as a leaving group. From the crystal structure obtained for  $[\{cis\text{-Pt}(9\text{-EtG}_2)_2(\mu\text{-OH})(\mu\text{-pyrazolate})\}](\text{NO}_3)_2$ , (where EtG = 9-ethylguanine which is a model nucleobase)<sup>86a</sup> it was reported that the average distance between the platinum atoms is comparable with the distance separating a normal sequential nucleobase in a B- type DNA strand to form stable DNA adducts. The rate of reaction of these complexes with DNA was found to be relatively slower for the first step.<sup>91</sup> However, the rate of second step, once the five membered ring is opened, was found to be faster.<sup>91</sup>

In a related effort, Wheat *et al.*<sup>84a</sup> reported an extension of the work on complex **(12)** to yield a trinuclear Pt(II) complex **(19)**. The dpzm moiety offers moderate rigidity due to the incorporation of the CH<sub>2</sub> spacers in the linker. The complex shows anticancer activity in the murine leukaemia cell line L1210.<sup>84a</sup> This complex is a structural analogue of the well known trinuclear anticancer complex, **BBR3464**.

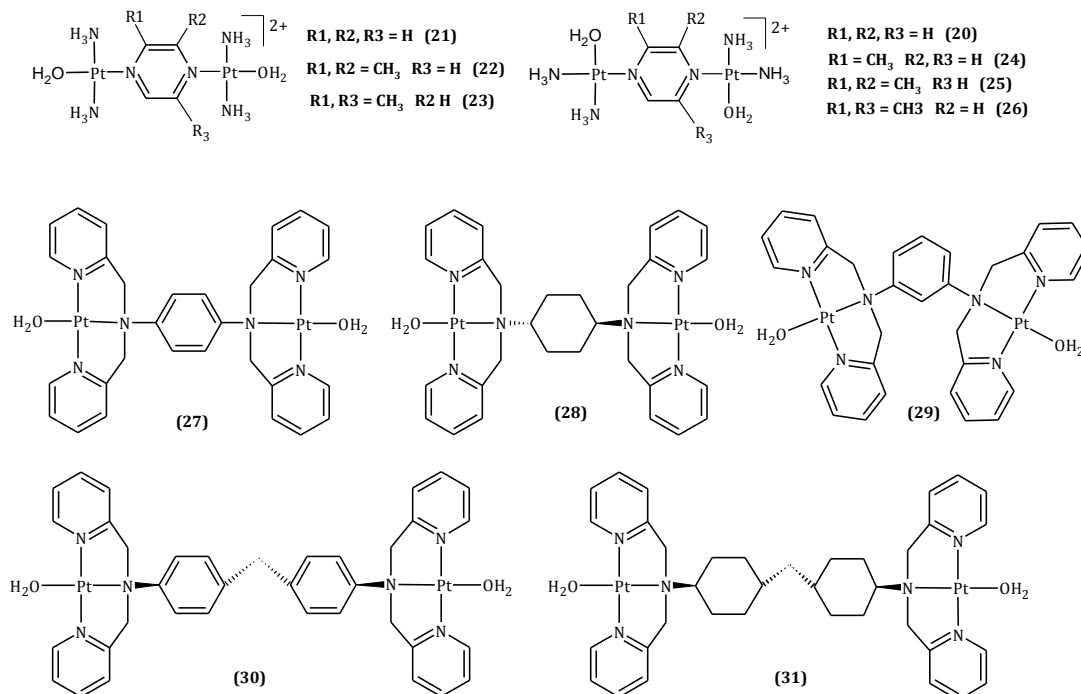
An interesting design of another trinuclear Pt(II) complex with moderate rigidity comes from the mesitylene ligand with three terminus Pt(II) centres linked by three *N,N'*-bis(2-pyridylmethyl)amine **(20)**.<sup>85</sup> This complex shows promising cytotoxicity in human and mouse tumour cells including those which are cisplatin resistant.<sup>92</sup> Molecular pharmacology studies on the underlying mechanisms of its antitumour effects revealed that the complex has a unique DNA binding mode thereby forming trifunctional intrastrand DNA adducts.<sup>93</sup> All three Pt(II) centres of the complex were found to coordinate to DNA base pairs leading to broad conformational modifications.<sup>92</sup>



**Figure 1.5** Multinuclear platinum (II) complexes with rigid linkers which have shown anticancer activity.<sup>25a,84a,85,93-94</sup>

Often, azine bridged dinuclear complexes (*Figure 1.6*), **(21)**, **(22)**, **(23)**, **(24)**, **(25)** and **(26)** compared to cisplatin, were found to show lower cytotoxicity in several human cell-lines. However, their activity (as chloride complexes) against mouse leukemia cells, which is cisplatin resistant, was found to be comparably higher.<sup>25a</sup> Furthermore, the complexes undergo substitution reactions with thiourea and biologically active nucleophiles. Another group of polynuclear complexes bridged by phenyldiamine and

cyclohexanediamine rigid linkers (27), (28), (29), (30) and (31) have been reported in a kinetic and mechanistic study by Jaganyi *et al.*<sup>14a,14d,14f</sup> and van Rudi *et al.*<sup>95</sup> However, their DNA binding affinity and cytotoxic activity have not been studied.



**Figure 1.6** Multinuclear Pt(II) complexes with rigid linkers which are used for kinetic and mechanistic study,<sup>14a,14d</sup>

## 1.5 Platinum(II) Polypyridyl Complexes

Platinum complexes of 2,2':6',2''-terpyridine (tpy) have the basic form  $[\text{Pt}(\text{Ytpy})\text{X}]^{n+}$ , where Y is the substituent on the terpyridine ligand and X is the ligand in the fourth coordination site.<sup>17d</sup> Pt(II) terpyridine chromophores are known as potential anticancer agents due to their tendency to selectively bind to DNA.<sup>59b,96</sup> Cationic, Pt(II) terpyridine and its derivatives have been proven to inhibit the telomerase activity by binding with the G-quadruplex of DNA.<sup>59b</sup> Polypyridyl complexes with extended  $\pi$ -conjugated ligand systems enhance the strength of  $\sigma$ -bonding framework within the ligand system and the  $\pi$ -stacking with DNA.<sup>97</sup> They can interact with DNA either by covalent binding or by intercalating with the base pairs.<sup>17d,96c</sup>

### 1.5.1 DNA Intercalation

DNA intercalation is a non-covalent association between DNA base pairs and platinum molecules.<sup>17d,98</sup> Intercalation of Pt(II) terpyridine with DNA was reported in 1974 by Lippard and co workers<sup>96a</sup> during an investigation of  $[\text{Pt}(\text{tpy})(\text{HET})]^+$  (HET = 2-

hydroxyethanethiol) and CT DNA, which showed interactions of the compound with DNA with a binding constant of  $1.2 \pm 0.2 \times 10^6 \text{ M}^{-1}$  at a pH of 6.8 in 0.003 M sodium chloride solution.<sup>17d</sup> The complex was shown to add between the DNA base pairs where it is bound to every other base-pair space in DNA.<sup>99</sup>

Lippard and co-workers<sup>17d,96a</sup> further investigated the intercalative property of a variety of Pt(II) terpyridine complexes of the type  $[\text{Pt}(\text{tpy})\text{X}]^{n+}$  (for  $n = 1$ ,  $\text{X} = \text{HO}^-$ ,  $\text{Cl}^-$ , HET, Cysteine (Cys) and  $n = 2$ ,  $\text{X} = \text{aminoethanethiol (AET)}$ ). Each of these complexes was found to unwind circular DNA. The observed high binding constant for the AET complex was believed to be due to its high charge (*Table 1.1*).<sup>17d</sup> Further investigations reported<sup>100</sup> for two complexes,  $[\text{Pt}(\text{tpy})(2\text{-CH}_3\text{py})]^{2+}$  (py = pyridine) and  $[\text{Pt}(\text{tpy})(\text{py})]^{2+}$  with similar aromatic surfaces when subjected to DNA binding, showed a higher binding constant for the latter complex. The methyl group on the second position of  $[\text{Pt}(\text{tpy})(2\text{-CH}_3\text{py})]^{2+}$  reduces the stacking surface which causes more destabilization of the resulting complex thereby reducing the binding constant. Thus, it has been established<sup>17d</sup> structural features such as, the planarity and size of the molecule, aromaticity and surface extension of the  $\pi$  system, the charge and the ability of the group on the fourth coordination centre to form hydrogen bonding with DNA base pairs<sup>17d,100</sup> influences the DNA binding ability.

**Table 1.1** Binding constants of Pt(II) terpyridine complexes reported.<sup>17d,101, 102, 103</sup>

Complex	DNA medium	Binding constant, $K (\text{M}^{-1})$
$[\text{Pt}(\text{tpy})\text{Cl}]^+$	ct-DNA; Tris buffer	$3.9 \times 10^5$
$[\text{Pt}(\text{tpy})(\text{HET})]^+$	ct-DNA; pH 7.5, 0.2 M NaCl	$1.2 \times 10^5$
$[\text{Py}(\text{tpy})(\text{AET})]^{2+}$	ct-DNA; pH 7.5, 0.2 M NaCl	$4.3 \times 10^5$
$[\text{Pt}(\text{tpy})\text{Cys}]^+$	ct-DNA; pH 7.5, 0.2 M NaCl	$1.0 \times 10^5$
$[\text{Pt}(\text{tpy})(\text{OH})]^+$	st-DNA; pH 9.0, 0.5 M EPSS buffer	$7 \times 10^4$

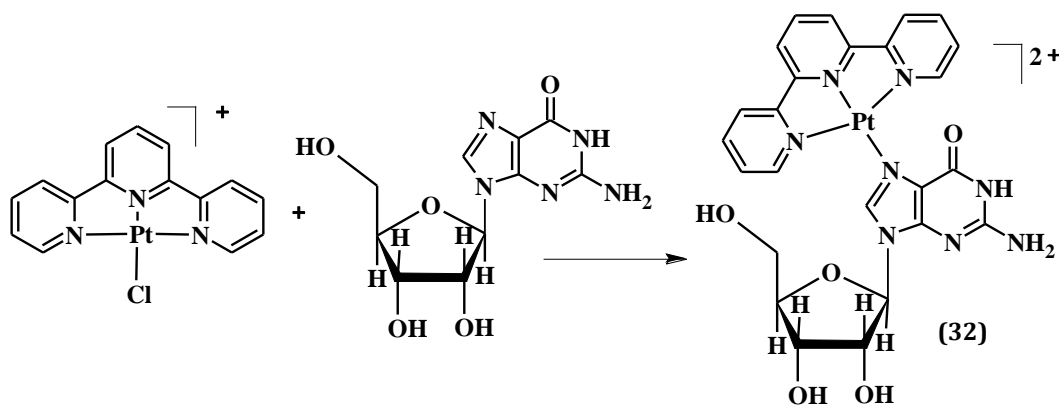
### 1.5.2 Substitution of Platinum(II) terpyridine Complexes with Biologically Active Nucleophiles

Apart from non-covalent binding,  $[\text{Pt}(\text{Ytpy})\text{X}]^{n+}$  (where  $\text{X} =$  a labile group such as chloride, hydroxide, water or pyridine derivatives and  $\text{Y} = \text{H}$ ,  $\text{Cl}$ ,  $\text{OCH}_3$ ,  $\text{CH}_3$  and 2- $\text{C}_5\text{H}_5\text{N}$ ), is also capable of undergoing ligand substitution reactions with biological molecules.<sup>17d,104</sup> An example of such a reaction is shown in *Scheme 1.2* for the reaction of terpyridine with guanosine. Information obtained from such kinetic studies is

important for understanding the mechanism of action of platinum anticancer drugs with DNA. (Scheme 1.2).

An equilibrium kinetic study reported by Bugarčić *et al.*<sup>14j,105</sup> on  $[\text{Pt}(\text{tpy})\text{Cl}]^+$  at pH 6, and van Eldik and co-workers<sup>14j</sup> on  $[\text{Pt}(\text{tpy})(\text{OH}_2)]^{2+}$  at pH of 2.5, with some biologically active nucleophiles, glutathione (GSH), inosine (INO), inosine-5'-monophosphate (5'-IMP) and guanine-5'-monophosphate(5'-GMP) has shown a high reactivity towards all the selected nucleophiles, particularly 5'-GMP and GSH.<sup>105,14j</sup> In addition, reactions of Pt(II)terpyridine complexes with other DNA bases such as adenosine and 1-methylcytosine (Hmcyt) were found to form di- and tri-cationic complexes depending on the reaction stoichiometry.<sup>17d</sup> Further kinetic studies of  $[\text{Pt}(\text{tpy})\text{Cl}]^+$  with other bionucleophiles, viz. histidine (His) and cysteine (Cys) at pH 3 under *pseudo* first-order conditions showed a higher reactivity for Cys ( $k_{\text{obs}} = 1.3 \times 10^{-2} \text{ s}^{-1}$ ) compared to His ( $k_{\text{obs}} = 8.5 \times 10^{-5} \text{ s}^{-1}$ ),<sup>106</sup> which was attributed to the stability of the  $[\text{Pt}(\text{tpy})(\text{His})]^+$  cation in aqueous medium compared to the Cys coordinated cation.<sup>17d</sup>

The driving force for such reactions depends on both thermodynamic factors such as the stability of the Pt–N bond formed relative to the Pt–X bond, and kinetic factors such as the rate of replacement of X by the incoming ligand.<sup>17d</sup> In such instances, investigating the reactions under *pseudo* conditions can force the reaction to go to completion. Studies reported by Lowe *et al.*<sup>104</sup> support the binding of Pt(II) (tpy) to N7 position of guanosine (32).



**Scheme 1.2** Reaction of Pt(II) (tpy) with guanosine (1:1) showing the N7 binding of guanosine with Pt(II) (tpy) (32).<sup>17d,104</sup>

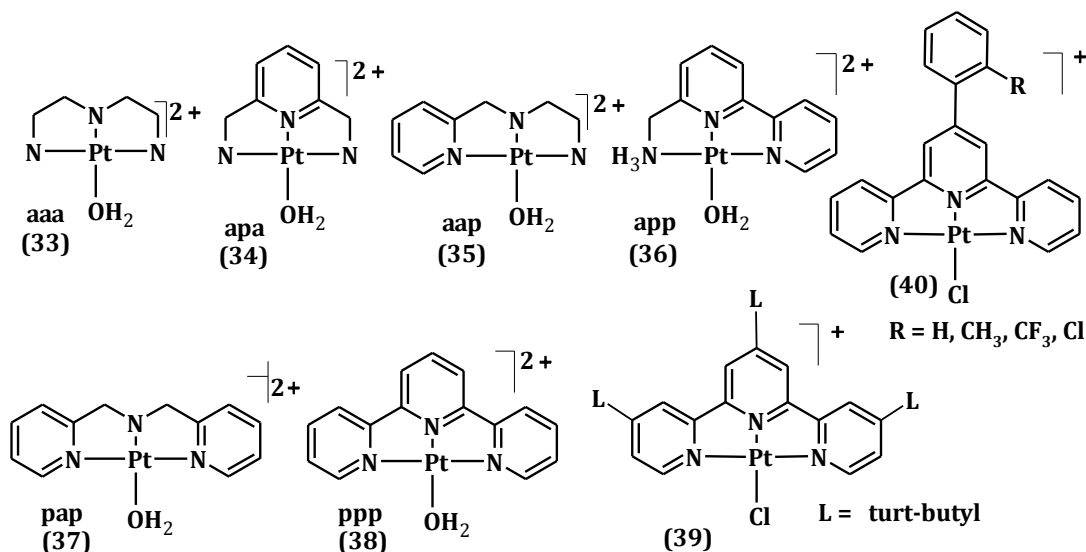
### 1.5.3 Previous Kinetics and Mechanistic Studies on Platinum(II) terpyridine Complexes with Thiourea and Ionic nucleophiles

Pt(II) terpyridine and its analogues are good anticancer probes and have gained a considerable research interest in the past few decades. To design more effective anticancer Pt(II) drugs, a clear understanding of kinetic and mechanistic substitution behaviour of such complexes is important in order to elucidate the mechanism of action of the drug in the body.<sup>107</sup>

van Eldik *et al.*<sup>14k</sup> investigated the effect of increasing the  $\pi$ -acceptor of pyridine ligands on the substitution kinetics of aqua Pt(II) with tri(N-donor) non-leaving ligands *viz.* [Pt(diethylenetriamine)OH<sub>2</sub>]<sup>2+</sup> (**aaa**), [Pt(2,6-bis-aminomethylpyridine)OH<sub>2</sub>]<sup>2+</sup> (**apa**), [Pt(N-(pyridyl-2-methyl)-1,2diamino-ethane)OH<sub>2</sub>]<sup>2+</sup> (**aap**), [Pt(bis(2-pyridylmethyl)amine) OH<sub>2</sub>]<sup>2+</sup> (**pap**), [Pt(2,2'-bipyridine)(NH<sub>3</sub>)(OH<sub>2</sub>)]<sup>2+</sup> (**app**) and [Pt(tpy)OH<sub>2</sub>]<sup>2+</sup> (**ppp**) (Figure 1.7) with thiourea (**TU**), dimethylthiourea (**DMTU**), trimethylthiourea (**TMTU**). The rate of substitution reactions showed a general increase by a factor of four orders of magnitude simply by adding pyridine rings within the non-leaving chelate ligand of the complexes. The aqua ligands were substituted in the order **aaa** < **apa** < **aap** < **pap** < **app** < **ppp**. The increase in reactivity was attributed to an increased electronic communication within the chelate ligand due to the increase in the  $\pi$ -acceptance of the pyridine rings.<sup>14k</sup> It is known that increasing the  $\pi$ -backbonding ability of the ligand system around the platinum centre helps to stabilise the five coordinate transition state through back donation of the electron density onto the aromatic system resulting in an increase in the substitution reaction.<sup>14k</sup>

Jaganyi *et al.*<sup>14b</sup> further extended the investigation to include an understanding of how groups that are attached to the terpyridine ligand (ancillary group) affects its capacity to receive electron density from the platinum metal centre and ultimately the reactivity of the metal centre.<sup>107-108</sup> For example, when the ancillary substituent at the 4'-position is an *ortho* substituted phenyl ring (**39**), the reactivity of the complexes depended on the electron donating or electron withdrawing capacity of the substituent groups.<sup>108</sup> When electron donating groups (as in **39**) are attached, the reactivity is smaller than that of **Ptppy** and vice versa when electron accepting groups (Cl, CF<sub>3</sub> as in **40**) are attached. Furthermore, when the ancillary is a phenyl ring, extension of  $\pi$ -backbonding towards the ancillary ring is absent.<sup>14b</sup> They also studied the *cis*  $\sigma$ -effect<sup>108</sup> by replacing one of the *cis* pyridine ring on the terpyridine with a phenyl ring. Results obtained further

support previous studies on *cis* and *trans*  $\sigma$ -effect of terpyridine type chelate backbone.<sup>109,110</sup>



**Figure 1.7** Pt(II) complexes studied by van Eldik *et al.*<sup>14k</sup> (33-38). Pt(II)terpyridine complexes studied by Jaganyi *et al.* (38,39) and (40).<sup>86-87,90-91</sup>

Additionally, the type of substituents on the *ortho* position of the ancilliary phenyl ring influences the reactivity either by enhancing or reducing the  $\pi$ -backbonding ability of the terpyridine moiety. The presence of electron withdrawing groups such as CF<sub>3</sub> group on the 4'-position of terpyridine (40, when R = CF<sub>3</sub>), the substitution reactivity was moderately enhanced due to the electron withdrawal property of terpyridine which increases the  $\pi$ -backbonding ability of the chelated terpyridine ring. The opposite was observed for the electron donating CH<sub>3</sub> group present on the *ortho* position of the 4'-phenyl ring, which reduces the  $\pi$ -backbonding ability of the terpyridine system.

## 1.6 Therapeutic Ruthenium Complexes: A Possible Alternative to Platinum

To widen the search of clinically improved anticancer drugs, with broader spectrum of activity, other metals such as ruthenium<sup>34b,111</sup> and cobalt<sup>112</sup> have to be considered. Such metal complexes are expected to have the same or different mechanism of action but certainly different biodistribution and toxicity profiles to that of Pt(II) compounds.<sup>111g,113</sup> Of the metal complexes studied so far, Ru(II) complexes offer the most potential alternatives to cisplatin resistant tumour cells with reduced toxicity.<sup>5,113</sup> This section will focus mainly on terpyridine and polypyridine type Ru(II) complexes.

Applications of ruthenium complexes are wide. The complexes are used as immunosuppressants, antimicrobial agents, antibiotics, radiophysical therapeutic agents and antimicrobial agents. For example, ruthenium compounds such as  $[\text{Ru(II)Cl}_2(\text{chloroquine})_2]$  is active against malaria vectors and other antibiotics such as Ru(III) derivatives of thiosemicarbazone are active against *salmonella typhi*.<sup>7</sup> Properties of ruthenium complexes or compounds which make them suitable in various applications include their low redox potential, greater potential to transfer of electrons, coordination ability to heteroatoms, their Lewis acid property and their unique reactivity towards metallic species.<sup>114</sup> Ruthenium is also important due to its excellent catalytic properties.<sup>114-115</sup> Compounds such as  $[\text{RuH}_2(\text{PPh}_3)_2(\text{PPh}_2)\text{C}_6\text{H}_4\text{F}]$  (where  $\text{PPh}_3$  = triphenylphosphine) are used in the catalytic hydrogenation of anthracene.<sup>116</sup>

### 1.6.1 The General Chemistry of Ruthenium(II) Complexes

Ruthenium was discovered in 1844 in Russia by Karl Klaus from *Ruthenia* ores, the Latin name for Russia.<sup>117</sup> It is a silvery metal which crystallizes in hexagonal close packing arrangement and have a high melting point of 2334 °C.<sup>118</sup> Ruthenium belongs to group 8 in the periodic table and has a  $[\text{Kr}] 4d^7 5s^1$  electronic configuration. Properties of ruthenium are more similar to osmium than iron.<sup>119</sup> Ruthenium forms various compounds in different ligand systems containing carbon, nitrogen, oxygen and sulfur donors. It also forms bridged binuclear, trinuclear and poly nuclear complexes with different oxidation states.<sup>120</sup> Of the most common oxidation states, Ru(III) and Ru(II) are the most inert, the latter is much less inert.<sup>11b</sup> This inertness of oxidation states is a great advantage for the study of substitution reactions of ruthenium complexes. Some examples of common ruthenium complexes include  $[\text{RuHCl}(\text{PPh}_3)_2]$ ,  $[\text{Ru}(\text{NH}_3)_5\text{H}_2\text{O}]^{2+}$  and  $[\text{Ru}(\text{tpy})\text{Cl}_3]$ .<sup>119</sup>

In solution, Ru(II) and Ru(III) complexes form very stable complexes specially with nitrogen donor ligands.<sup>121</sup> Due to the stability of ruthenium complexes bearing nitrogen donor ligands, coordination chemistry of ruthenium with ligands such as terpyridine and bipyridine have gained a considerable research interest.<sup>120,122</sup> Complexes formed with those ligands are often used in photochemistry,<sup>123</sup> pharmaceutical applications and in electrochemistry.<sup>124</sup> Ruthenium compounds of terpyridine and bipyridine show strong metal to ligand charge transfer (MLCT) absorptions.<sup>124b,125</sup> As a result, they are often used in photophysical applications.<sup>125</sup>



### 1.6.2 The Biological Importance of Ruthenium(II) Complexes

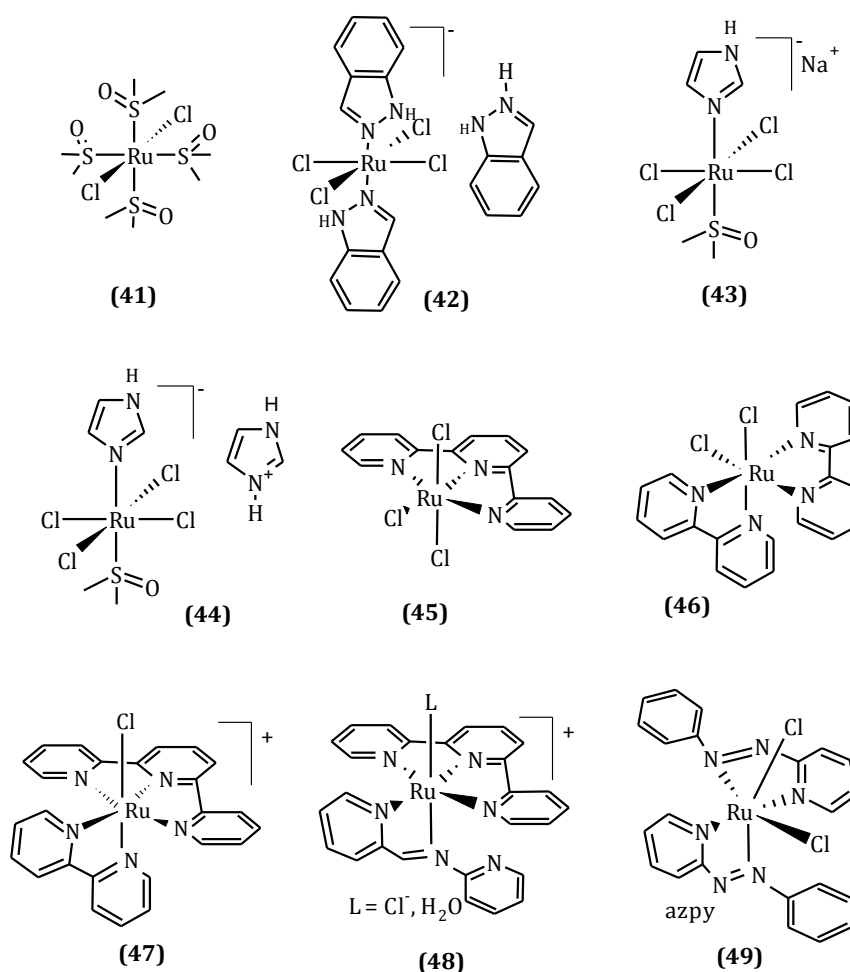
The exploration of ruthenium complexes as potential anticancer agents dates back to the 1970's when Clarke *et al.*<sup>126</sup> reported the anticancer activity of pentaammine(purine)ruthenium(III) complexes capable of inhibiting DNA and protein synthesis.<sup>5</sup> Complexes of *cis*-[Ru(III)(NH<sub>3</sub>)<sub>4</sub>Cl<sub>2</sub>]<sup>+</sup> and *fac*-[Ru(III)(NH<sub>3</sub>)<sub>3</sub>Cl<sub>3</sub>] also exhibited a very promising cytotoxicity. However, due to the low water solubility of most of the complexes, further clinical trials were hindered. At a later time, Mestroni *et al.*<sup>127</sup> reported *cis* and *trans*- RuCl<sub>2</sub>(dimethylsulfoxide)<sub>4</sub> complexes (**41**) (Figure 1.8) which bind to DNA and exhibit anticancer activity. The complexes had better aqueous solubility. The complexes were found to bind at the N7 position of guanine residues and have less severe side effects. They also prolongs host survival.<sup>128</sup> Interestingly, the *trans* compound was found to show a better antimetastatic activity. This compound may be a possible replacement for cisplatin therapy which could exhibit a different mechanism.<sup>113,129</sup>

Apart from the ruthenium ammine-chloro derivatives, ruthenium complexes with dimethylsulfoxide (dmsO) ligands have been reported. Of the ruthenium heterocyclic compounds known, the complexes reported by Keppler *et al.*,<sup>5</sup> showed the best anticancer activity. They possess the formula *trans*-[RuCl<sub>4</sub>(L)<sub>2</sub>]<sup>-</sup>, where L is imidazole (KP418) or indazole (KP1019 (**42**)).<sup>5</sup> More improved compounds of dmsO of the form Na{*trans*-[Ru(III)Cl<sub>4</sub>(dmsO)(Him)]}, (Him = imidazole), nicknamed NAMI (**43**), and [H<sub>2</sub>Im][*trans*-Ru(III)Cl<sub>4</sub>(dmsO)(HIm)], also known as NAMI-A (**44**) were later synthesized. The compounds were found to bind DNA *via* the sulfur atoms on the compound.<sup>113,130</sup> The most promising ruthenium complexes to enter clinical trials are, NAMI-A<sup>7</sup> and KP1019, developed by Keppler *et al.*<sup>8</sup> NAMI-A and KP1019 were found to be less toxic with mild side effects.<sup>131</sup> They were found to be effective on solid tumours.<sup>132</sup> These complexes are thought to be more effective against metastatic cancers since the mechanism of action of these complexes is expected to be *via* transferrin-mediated transport to the cells.<sup>131</sup>

Recent studies have explored potential Ru(II) antitumour complexes of the form [(η<sup>6</sup>-arene)Ru(XY)(Z)] where XY is a chelating ligand and Z is monoanionic.<sup>133</sup> The arene ligand binds as a 16-electron donor and a π-acceptor. It is thought to stabilize the +2 oxidation state. The XY chelate ligand provides additional stability to the whole structure.<sup>133</sup> The anionic ligand, Z, is a leaving group and if it is a labile group such as

halide, that can provide a coordination site for the biomolecules. Small variations of the ligands possibly can fine-tune their pharmacological properties.<sup>133</sup>

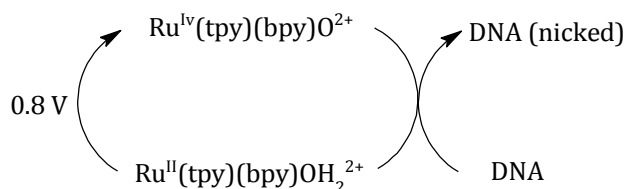
Another group of ruthenium compounds which exhibits antitumour activity are Ru(II) polypyridyl complexes. Complexes such as  $[\text{Ru}(\text{tpy})\text{Cl}_3]$  (**45**) were found to have strong cytotoxicity and antitumour activity which are expected to be due to the binding of two guanines of DNA.<sup>134</sup> Some of these complexes exist as enantiomers, hence are able to enantioselectively recognize DNA.<sup>113</sup> For example, the *cis*- $[\text{Ru}(\text{bpy})_2]^{2+}$  fragment was found to bind with DNA<sup>135</sup> while *cis*- $[\text{Ru}(\text{bpy})_2\text{Cl}_2]$  (**46**) was found to be inactive. Polypyridyl ruthenium complexes are also found to be useful probes for DNA cleavage and DNA conformation.<sup>111g,136</sup> Ru(II) polypyridyl complexes can interact with DNA through noncovalent interactions such as groove binding, electrostatic binding<sup>137</sup> and intercalative binding.<sup>138</sup>



**Figure 1.8** Structure of some of the ruthenium complexes which were found to have antitumour activity.<sup>5,8</sup>

In vitro studies for complexes **(48)** showed cytotoxicity against certain cancer cell-lines and the effect was dependent on the concentration of ruthenium complex. This behaviour was reported to be fairly comparable to that of NAMI-A.<sup>139</sup> Another related mononuclear Ru(II) complex, *cis*-[Ru(azpy)<sub>2</sub>Cl<sub>2</sub>] **(49)** where azpy = 2-phenylazopyridine was found to show high cytotoxicity against some fast growing cell-lines.<sup>140</sup> The higher reactivity of this compound was assumed to be due to the flexibility of the azpy ligands which enhances the substitution of the chloride ligands thereby allowing it to bind with two DNA bases.<sup>5</sup>

Thorp and co-workers<sup>141</sup> have reported the DNA cleavage due to Ru(II) complex of the form [Ru(tpy)(L)OH<sub>2</sub>]<sup>2+</sup> (where L = bpy, phen (1,10-phenanthroline) and tmen (*N,N,N',N'*-tetramethylethylenediamine)) by cyclic voltammetry. The aqua complexes were first converted to oxo form by electrolysis at pH 7. Addition of these complexes to DNA solution was found to decrease the current, which indicates the binding of the charged complexes to DNA. Apart from the direct addition of the oxo activated complexes, the authors also reported that the DNA cleavage reactions can also be performed *via* electrolysis at a specific potential and pH. The electrochemical process was found to be catalytic. *Scheme 1.3* summarizes the catalytic cleavage of DNA due to [Ru(tpy)(bpy)O]<sup>2+</sup>.<sup>141</sup>



**Scheme 1.3** Schematic representation of catalytic electrolysis reaction for the cleavage of DNA by [Ru(tpy)(bpy)O]<sup>2+</sup>.<sup>141</sup>

### 1.6.3 Ruthenium Complexes as Biological Probes

After the success of cisplatin and its related complexes as anticancer agents, the search for other active metal based anticancer complexes has been extended.<sup>142</sup> Since Ru(II) and Ru(III) complexes have similar ligand exchange kinetics as Pt(II) complexes, this property of ruthenium gained research interest in the search for the development of better anticancer drugs.<sup>133,142c,143</sup> Of the number of complexes synthesized, only very few metal based drugs reach the biological target without the molecule being modified. In a biological environment such as the human body, most metal based drugs interact with macromolecules, proteins, as well as some sulfur and oxygen donor compounds,

some of which are vital for the desired therapeutic properties.<sup>5,7</sup> Ability to have variable coordinating sites, oxidation states, alterations to ligand affinity and substitution kinetics and photodynamic property makes ruthenium a suitable metal for synthesizing future therapeutic agents.<sup>113,122</sup>

There are three main properties of ruthenium complexes which makes them suitable for therapeutic applications:<sup>7-8,113</sup>

➤ **rate of ligand exchange**

Many ruthenium complexes have been clinically tested especially for treating cancer since Ru(II) and Ru(III) complexes exhibit similar kinetic ligand exchange behaviour to those of Pt(II) complexes.<sup>72</sup> Their ligand exchange reactions are kinetically stable and this prevents them from rapid equilibrations.<sup>144</sup> Their ligand exchange reactions are moderate enough to be monitored. For example, the time frame that Pt(II), Ru(II), Ru(III) and Co(III) along with some other few metals take for ligand exchange reactions is within the time scale for many cell division processes.<sup>145</sup>

➤ **variable oxidation states**

Availability of Ru(II), Ru(III) and Ru(IV) under physiological conditions makes ruthenium unique among the platinum group. Ru(II) and Ru(IV) complexes are more biologically active than Ru(III) complexes. In biological systems, single electron transfer proteins reduce Ru(III) and Ru(IV) while molecular oxygen and cytochrome oxidase oxidizes Ru(II). This redox property of ruthenium increases the effectiveness of ruthenium drugs in biological environments.<sup>8</sup> For example, the drug can be administered into the body as an inert Ru(III) complex, which then gets activated in the diseased tissues. Compared to healthy tissues, most cancer cells have high concentration of glutathione and low pH, which creates a reducing environment. In this environment, Ru(II) complexes can get oxidized to Ru(III) by biological oxidants.<sup>146</sup>

➤ **the ability of ruthenium to mimic iron when binding to certain biological molecules**

The low toxicity of ruthenium drugs make it suitable for ruthenium to mimic iron<sup>147</sup> in many biological molecules including serum transferrin and albumin which are used to solubilise and transport iron in mammals.<sup>148</sup> Since rapidly dividing cancer cells have a greater necessity for iron, it increases the number

of transferrin receptors on the surface of the cell whereby increasing the radio-labelled ruthenium compounds in cancer cells from 2 - 12 fold compared to the healthy cells.<sup>149</sup>

The above mentioned properties along with the unique DNA binding pattern of ruthenium due to its different geometries compared to platinum, offer ruthenium a relatively low resistance amongst its active compounds. Since ruthenium selectively accumulate in cancer cell,<sup>149</sup> its toxicity is expected to be reduced. Additionally, ruthenium is transported into the cells by tranfering dependent and transferring independent mechanisms; transferring mediated uptake is assumed to be more efficient. The pharmacological target and the underlying molecular mechanism of anticancer activity of ruthenium complexes has not yet been clearly understood. However, it was found that the cytotoxicity of ruthenium complex is due to their ability to bind with DNA helix.<sup>113</sup>

#### 1.6.4 Intercalation of Ruthenium Complexes in Two DNA Bases

Polypyridyl complexes of Ru(II) can interact with DNA by intercalation.<sup>150</sup> This involves DNA mediated electron transfer interactions which play an important role in understanding the mechanism of action of anticancer ruthenium drugs. Complexes such as  $[\text{Ru}(\text{phen})_3]^{2+}$ ,  $[\text{Ru}(\text{bpy})_3]^{2+}$ ,  $[\text{Ru}(\text{phen})_2\text{PMIP}]^{2+}$ , PMIP = 2-(4-methylphenyl)imidazo[4,5-*f*]1,10-phenanthroline,  $[\text{Ru}(\text{dmp})_2\text{PMIP}]^{2+}$ <sup>[57f]</sup> where dmp = 2,9-dimethyl-1,10-phenanthroline and isomers of  $\alpha, \beta, \gamma$ - $[\text{Ru}(\text{azpy})_2\text{Cl}_2]$  were found to be useful probes.<sup>113,151</sup> Those complexes were found to have very high cytotoxicity as well.<sup>113</sup> The complex  $\alpha$ - $[\text{Ru}(\text{azpy})_2\text{Cl}_2]$  was found to have even higher cytotoxicity than cisplatin and possess more orientations to interact with DNA.<sup>152</sup> The complexes were found to bind with DNA by surface interactions as well as by DNA intercalations. When human lung tumour cells, A549 were treated with  $[\text{Ru}(\text{dmp})_2\text{PMIP}]^{2+}$  at  $\text{IC}_{50}$  concentration (80  $\mu\text{M}$ ), an increase in apoptotic cells of 11.8% was reported.<sup>111e</sup> This compound was found to bind to DNA enantiospecifically. From this study, it was found that the Ru(II) polypyridyl complexes showed a significant dose dependent cytotoxicity towards human lung cancer cells, A549. Further flow cytometry experiments showed that the polypyridyl complexes strongly intercalate with CT DNA with a binding constant of  $10^6 \text{ M}^{-1}$ , suggesting that the antitumour activity of Ru(II) complexes may be due to their ability to intercalate with DNA.<sup>111e</sup> Another study by Zhang *et al.*<sup>111f</sup> reported that Ru(II)-arene complexes induced significant apoptosis in human lung cancer HCC827 cell-line at the concentration range of 5 – 100  $\mu\text{M}$  with  $\text{IC}_{50}$  values

ranging from  $19.6 \pm 5.3 \mu\text{M}$ . Ru(II) complex with planar aromatic ligands such as terpyridine and phenanthroline have advantages over the other ruthenium complexes. Some of these advantages include:<sup>122</sup>

- ✓ the ease of controlling the metalation and substitution reactions
- ✓ strong absorption due to MLCT
- ✓ strong luminescent characteristics
- ✓ lengthening of DNA double helix on binding to DNA
- ✓ aromaticity of the ligand moiety which allows overlapping of the  $\pi$  system with DNA base pairs

A study on the effect of leaving group and the internal functional groups of Ru(II) polypyridyl complexes on the cytotoxicity was reported by Corral *et al.*<sup>111g</sup> No correlation was found between the lability of the leaving group and the cytotoxicity. However, the complexes were found to be cytotoxic against certain cancer cell-lines (Table 1.2)<sup>111g</sup> and bind with DNA in a non-cisplatin mode.<sup>111g</sup>

**Table 1.2** Concentration that inhibits 50% growth inhibition of cells ( $\mu\text{M}$ ) of mononuclear ruthenium complexes and the dinuclear ruthenium complex,  $[\text{Ru}(\text{apy})(\text{tpy})]_2[\mu\text{-H}_2\text{N}(\text{CH}_2)_6\text{NH}_2](\text{ClO}_4)_4$  after 48 hours treatment in some selected cell-lines.<sup>111g</sup>

Compound tested	A2780	A2780R	L1210/0	L1212/2
$[\text{Ru}(\text{apy})(\text{tpy})\text{Cl}](\text{ClO}_4)$	23	25	100	56
$[\text{Ru}(\text{apy})(\text{tpy})(\text{H}_2\text{O})](\text{ClO}_4)_2 \cdot 2\text{H}_2\text{O}$	11	30	80	97
$[\text{Ru}(\text{apy})(\text{tpy})(\text{CH}_3\text{CN})](\text{ClO}_4)_2$	31	28	70	40
$[\text{Ru}(\text{azpy})(\text{tpy})\text{Cl}]\text{Cl} \cdot 5\text{H}_2\text{O}$	19	42	42	26
$[\text{Ru}(\text{impy})(\text{tpy})\text{Cl}](\text{ClO}_4)$	>100	62	>100	>100
$[\text{Ru}(\text{apy})(\text{tpy})]_2[\mu\text{-H}_2\text{N}(\text{CH}_2)_6\text{NH}_2](\text{ClO}_4)_4$	33	28	>100	>100
$x\text{-}[\text{Ru}(\text{azpy})_2\text{Cl}_2]$	0.1	0.2	0.1	0.2
cisplatin	6	25	2	24

$x\text{-}[\text{Ru}(\text{azpy})_2\text{Cl}_2]$  and cisplatin are included as references, apy= 2,2'-azobispyridine, azpy= 2-phenylazopyridine or 2-phenylpyridinylmethylene amine, impy= 2-phenylpyridinylmethylene amine.

Most mononuclear polypyridyl complexes of Ru(II) complexes that bind with DNA non-intercalatively were found in the minor grooves of DNA with particular preference for A/T (adenine/ thymine) centres<sup>153</sup> mainly due to electrostatic interaction and van der Waals forces.<sup>154</sup> The  $^1\text{H}$  NMR study on DNA binding of Ru(II) complexes,  $\Delta\Delta\text{-}[\{\text{Ru}(\text{Me}_2\text{bpy})_2\}_2(\mu\text{-bpm})]^{4+}$  and  $\Delta\Delta\text{-}[\{\text{Ru}(\text{Me}_2\text{bpy})_2\}_2(\mu\text{-bpm})]^{4+}$  with free

$d(\text{CAATCGCGATTG})_2$  where  $\text{Me}_2\text{bpy} = 4,4'$ -dimethyl-2,2'-bipyridine;  $\text{bpm} = 2,2'$ -bipyrimidine, were found to be of *ca.*  $1 \times 10^4 \text{ M}^{-1}$ .<sup>154</sup> This binding was further enhanced by the van der Waal forces and hydrogen bonding. Dinuclear ruthenium complexes were found to have advantages over other platinum complexes due to their photochemical and stereochemical activities with the nucleic acids such as variations in their size and shapes.<sup>154</sup>

### 1.6.5 Photodynamic Therapy

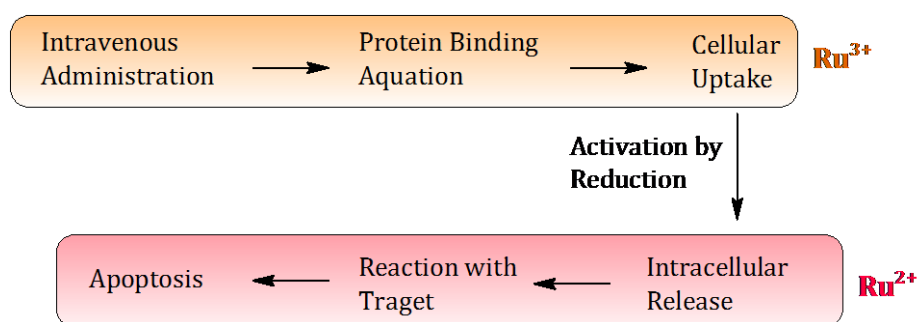
Photodynamic therapy (PDT) is a technique that uses a photosensitizer drug, and a light of particular wavelength to kill the cells.<sup>118</sup> In this technique, the photosensitizing agent is injected into the bloodstream, which is then absorbed by the cells in the body.<sup>118</sup> Some agents get retained with the cancer cells and during which the drug is photoactivated by the light.<sup>155</sup> The use of ruthenium complexes as PDT agents is promising as they are expected to react with double stranded DNA either from their excited state or *via* the formation of free radicals such as  $\text{OH}^\bullet$ .<sup>156</sup> Complexes such as  $[\text{Ru}(\text{bpy})_3]^{2+}$  and  $\text{Ru}(\text{phen})_3^{2+}$  have intense absorption in the visible region due to MLCT transitions. Generally,  $\text{Ru(II)}$  polypyridyl and related complexes have intense MLCT and exhibit long-lived triplet  $^3\text{MLCT}$  excited states due to absorption of photons, to transfer energy to another molecule either by electron transfer to energy transfer.<sup>118,157</sup>

### 1.6.6 Postulated Mechanisms of Action of Anticancer Ruthenium Complexes

Anticancer therapy of ruthenium is generally based on the ability of ruthenium to coordinate to DNA base pairs *via* the nitrogen atoms of the nucleic bases, in particular N7 of guanine. The interactions of ruthenium complexes with DNA is thought to be enhanced by non-covalent interactions such as H-bonding interactions with the DNA base pairs.<sup>158</sup> However, these drugs are thought to be inactive until  $\text{Ru(III)}$  gets reduced in the cell.<sup>159</sup>

The mechanism of action of ruthenium anticancer compounds with DNA is hardly known.<sup>34b</sup> In biological environments, ruthenium mimics iron when binding with certain proteins such as transferrins and albumins.<sup>7</sup> The serum transferrins recognize  $\text{Fe(III)}$  not  $\text{Fe(II)}$ . Transferrin bound to  $\text{Fe(III)}$  bind strongly to its receptor thereby internalizing into the cells. Low pH induces the release of  $\text{Fe(III)}$  from transferrin. Since many solid tumour cells express higher level of transferrin receptors, this transport

mechanism is thought to be useful for cancer therapy. Apart from the redox transformations, interaction of the ruthenium complexes with different biomolecules such as serum transport proteins<sup>160</sup> and DNA nucleotides<sup>161</sup> is expected to play an important role in the compounds' mode of action.<sup>162</sup> NMR studies reported for the well-known two ruthenium complexes, KP1019<sup>163</sup> and NAMI-A<sup>132a</sup> shows that in the presence of certain biological reducing agents such as ascorbic acid and glutathione, the Ru(III) centres in those molecules are likely to undergo reduction<sup>162</sup> which then can bind to DNA causing apoptosis as represented in *Scheme 1.4*.



**Scheme 1.4** Schematic representation of suggested mode of action of ruthenium based anticancer drugs.<sup>162</sup>

Insertion to DNA is also achieved when the intercalating polypyridyl ligands are coordinated or attached on the non-leaving group to the ruthenium complex.<sup>5</sup> Furthermore, presence of polypyridyl ligands enhance their photoluminescence property as well as the stability of ruthenium complexes.<sup>164</sup> In addition, it was found that the presence of large aromatic ring systems, promoted binding of the complex with DNA by hydrophobic arene-purine base  $\pi$ - $\pi$  stacking interactions.<sup>5,165</sup>

### 1.6.7 Substitution Reactions of Ruthenium(II) Complexes

Substitution kinetics of Ru(II) complexes have not been extensively studied. Most substitution reactions of ruthenium involve complexes of Ru(III) and Ru(II), in particular Ru(II).<sup>154,166</sup> Substitution reactions of Ru(II) complexes are generally slow and follow a dissociative<sup>167</sup> or dissociative interchange<sup>168</sup> mechanism whereas Ru(III) complexes have shown some associative mechanism.<sup>167a,169</sup> Most reported substitution kinetics of Ru(II) complexes are in the form  $[\text{Ru}(\text{NH}_3)_5\text{X}]^{2+}$  where X is a halide or water. The specific rates of substitution of  $[\text{Ru}(\text{NH}_3)_5\text{H}_2\text{O}]^{2+}$  form at 25 °C with neutral ligands vary in the range 0.02 - 0.3  $\text{M}^{-1} \text{s}^{-1}$ .<sup>170</sup> The activation parameter for the reaction over the range of temperature from 15 to 35 °C were  $\Delta H$  ( $+22.9 \pm 1$  kcal) and  $\Delta S$  ( $-2.5 \pm 3$  cal  $\text{mol}^{-1} \text{K}^{-1}$ ), which are within the range of an interchange dissociative mechanism.<sup>170</sup>



Creutz *et al.*<sup>171</sup> reported hydride substitution from Ru(II) complexes *viz.*, Ru(tpy)(bpy)H<sup>+</sup> and Ru(tpy)(dmb)H<sup>+</sup> (dmb = 4,4'-dimethyl-2,2'-bipyridine) in aqueous media at 25 °C using CO<sub>2</sub>, CO, CH<sub>2</sub>O, and H<sub>3</sub>O<sup>+</sup>. The substitution of Ru(tpy)(dmb)H<sup>+</sup> with CO was about 10<sup>5</sup> times lower than that of Ru(tpy)(bpy)H<sup>+</sup> using CH<sub>2</sub>O nucleophile. However, in the case of Ru(tpy)(bpy)H<sup>+</sup>, the protonation step was very fast, and only the formation of the product Ru(tpy)(bpy)(H<sub>2</sub>O)<sup>2+</sup> was observed. Substitution kinetics of another ruthenium complex of terpyridine, [Ru(tpy)(tmen)O]<sup>2+</sup> with (CH<sub>3</sub>)<sub>3</sub>CHOH at 25 °C gave the second order rate constant, (4.3 ± 0.4) M<sup>-1</sup> s<sup>-1</sup>.<sup>172</sup>

In a different study based on investigation of substitution kinetics of [Ru(tpy)(bpy)(OH<sub>2</sub>)]<sup>2+</sup> and [Ru(tpy)(tmen)(OH<sub>2</sub>)]<sup>2+</sup> with thiourea and acetonitrile nucleophiles,<sup>173</sup> the reactions pathway was reported to follow the first order kinetics. The substitution rate of the *cis* coordinated bidentate ligands was found to depend on the steric and the electronic properties of the bidentate ligand. The meridionally coordinated terpyridine ligand was found to ratify the stereoelectronic rigidity on metal centre. The rate of substitution was found to be in the order of 10<sup>-4</sup> M<sup>-1</sup> s<sup>-1</sup>.

### 1.6.8 Polynuclear Ruthenium Complexes

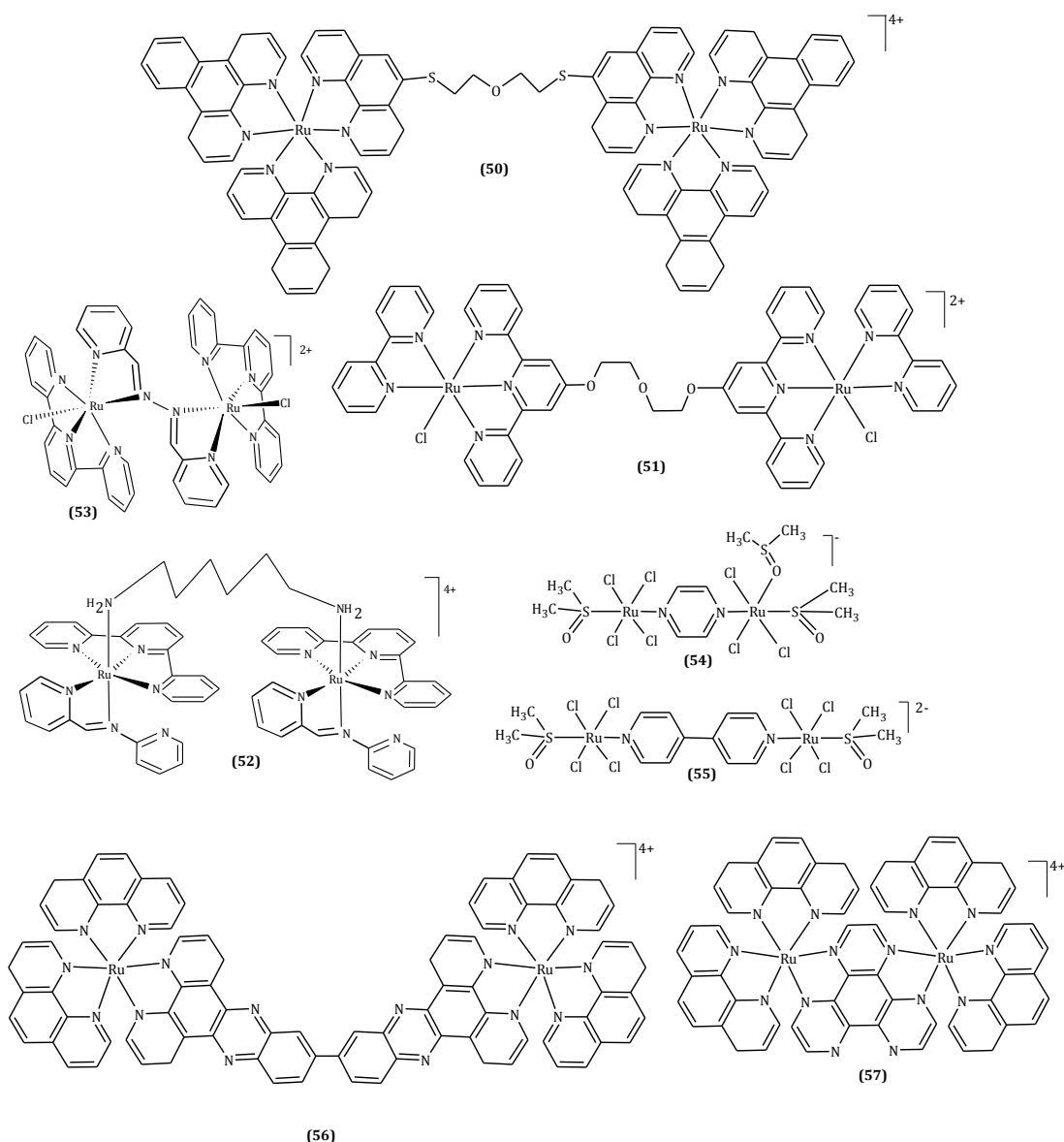
A number of polynuclear ruthenium complexes have been synthesized and tested for DNA interactions since ruthenium complexes are considered as anticipated probes for DNA conformation<sup>174</sup> or cleavage agents.<sup>136</sup> Some of these complexes exhibit chirality and thus, are capable of enantioselectively bind to DNA.<sup>161</sup> The interactions of these complexes with DNA are expected to be unique and would involve long range intrastrand cross-links.<sup>5</sup> The bulkiness, charge and the variability in geometry of multinuclear Ru(II) complexes is expected to increase their DNA binding affinity, which can be useful in the development of new photoprobes in the nucleic acid.<sup>111d</sup>

Dinuclear Ru(II) complexes of [Ru(bpy)<sub>3</sub>]<sup>2+</sup> and [Ru(phen)<sub>3</sub>]<sup>2+</sup> moieties bridged by flexible alkanes have been synthesized and studies on their DNA binding affinity have shown promising electrostatic interactions with DNA and photocleavage activity.<sup>175</sup> In those complexes, the length and the nature of the bridging linker play a crucial role on the binding efficacy.<sup>120</sup> A dinuclear Ru(II) complex [Ru(dpq)<sub>2</sub>(phen)]<sup>2+</sup> (dpq = dipyrido[3,2-*d*:2',3'-*f*]-quinoxaline) (**50**) (Figure 1.9) was found to have a high affinity for DNA intercalation.<sup>176</sup> The long flexible mercaptoethyl ether linker was found to influence DNA binding size. Another dinuclear Ru(II) complex,

[Cl(bpy)Ru(dtdeg)Ru(bpy)Cl]Cl<sub>2</sub> (**51**) was synthesized and its interaction with a guanine derivative, EtG was found to exhibit good cytotoxic activity.<sup>120</sup>

The dinuclear Ru(II) complex, ([{Ru(apy)(tpy)}<sub>2</sub>{μ-H<sub>2</sub>N(CH<sub>2</sub>)<sub>6</sub>NH<sub>2</sub>}])<sup>4+</sup> (**52**) has no labile leaving group attached to the metal centre for coordination. However, when cytotoxic tests were carried out using different cancerous cell-lines, the coordinative mechanism was found to be comparable to that of cisplatin.<sup>5</sup> Furthermore, the results suggest that the mechanism of action is different from that of cisplatin. Cytotoxicity occurs presumably *via* electrostatic and groove binding.<sup>5</sup> A similar dinuclear Ru(II) complex, [{Ru(tpy)Cl}<sub>2</sub>(μ-paa)](BF<sub>4</sub>)<sub>2</sub> (where paa = 2-pyridinealdazine) (**53**), possessing two chloride leaving groups was found to coordinatively interact with DNA by forming intra and interstrand DNA adducts.<sup>5</sup> Two structurally similar multinuclear ruthenium complexes formed by a pyrazine (pz) (**54**) and 4,4'-bipyridine (**55**) have been shown to modify human and murine carcinoma cells.<sup>139</sup>

Variations of the linker or the terminal ligand significantly influences the cytotoxicity of the complex. Semi-rigid dinuclear complex, (**56**) was found to show even higher DNA affinity<sup>177</sup> compared to its related complex (**57**). It was found that the increase in planarity of the bridging ligand increases the hydrophobicity, resulting in a stronger binding to DNA.<sup>178</sup> The rigid dinuclear phenanthroline complex, bridged by a rigid ligand HAT (HAT = 1,4,5,8,9,12 -hezaazatriphenylene) ligand has shown to bind DNA weakly compared to (**56**).<sup>179</sup>



**Figure 1.9** Some dinuclear cationic Ru(II) complexes linked by flexible and rigid linkers.<sup>5,120</sup>

## 1.7 Heteronuclear Ruthenium(II)-Platinum(II) Polypyridyl Complexes

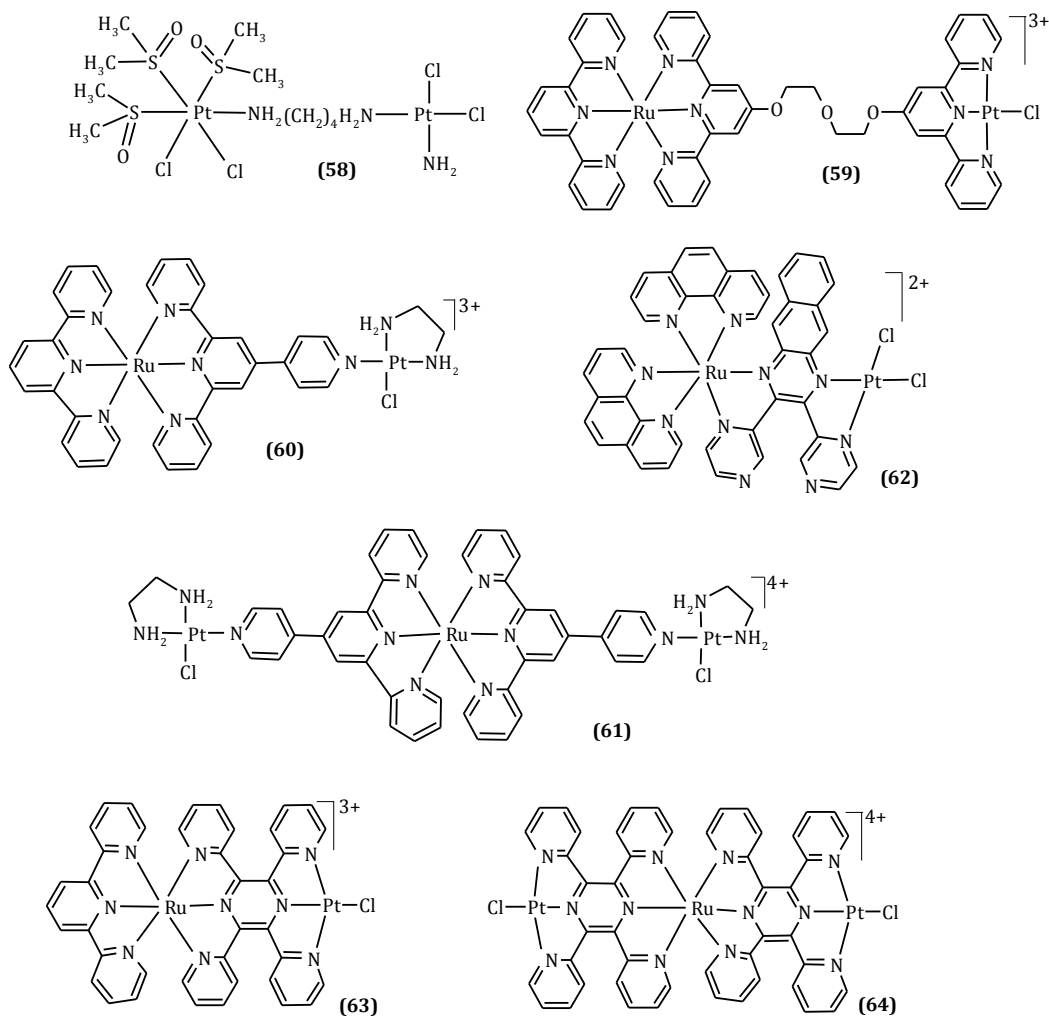
The continuous search for better anticancer drugs has gained interest in heteropolynuclear platinum and ruthenium complexes.<sup>34b,180</sup> Since the mechanisms of action of ruthenium and platinum anticancer complexes are different, it was thought that the combination of the two metals may result into anticancer drugs of improved efficacy. To date, only few heteropolynuclear ruthenium-platinum complexes have been synthesised and reported as potential anticancer agents.<sup>113,120,180-181</sup>

The first heteronuclear ruthenium-platinum complex reported was  $[\{cis-RuCl_2(dmsO)_3\}(H_2N(CH_2)_4NH_2)\{cis-PtCl_2(NH_3)\}]$  **(58)** (Figure 1.10) where the two metal

centres were linked by a long flexible  $\alpha,\omega$ -diaminoalkane group.<sup>180,182</sup> The compound was found to bind with DNA probably by forming DNA-DNA interstrand cross-link where each metal centre binds to one strand of DNA helix. Another heterometallic Ru(II)-Pt(II) complex having a flexible linker of the form  $[\text{Cl}(\text{tpy})\text{Ru}(\text{dtdeg})\text{Ru}(\text{tpy})\text{Cl}]\text{Cl}_3$  (**59**) has been reported.<sup>120</sup> Reactivity of this complex with DNA using EtG was studied using NMR study. The complex was found to coordinate with EtG *via* its N7 position.<sup>120</sup>

Heterometallic Ru(II)-Pt(II) complexes with a short semi-rigid linker, 4'-pyridyl-2,2':6',2''-terpyridine (qpy) has been synthesized and characterized.<sup>120</sup> The qpy linking ligand possess two different coordination sites; a tridentate coordination site at the parent terpyridine moiety as well as a monodentate coordination site at the pyridine which is appended at the 4'-position of the terpyridine backbone. Multinuclear Ru(II)-Pt(II) complexes of qpy,  $[(\text{tpy})\text{Ru}(\text{qpy})\text{Pt}(\text{en})\text{Cl}](\text{NO}_3)_3$  (**60**) and  $[\text{Cl}(\text{en})\text{Pt}(\text{qpy})\text{Ru}(\text{qpy})\text{Pt}(\text{en})\text{Cl}](\text{NO}_3)_4$  (**61**) (en = 1,2-ethylenediamine) have been reported. The complexes possess a bis(terpyridyl)-Ru(II) moiety and one or two ethylenediamine centres coordinated to a Pt(II) centre. The complexes were found to react with DNA model base, EtG *via* the platinum unit which substitutes the labile ligands on the terminal Pt(II) centre(s). Presence of ruthenium was found to increase the water solubility and electrostatic interactions with the DNA base by its high charge.<sup>120</sup>

Another heterometallic Ru(II)-Pt(II) complex,  $[(\text{bpy})_2\text{Ru}(\text{dpb})\text{PtCl}_2]\text{Cl}_2$  (**62**) was found to react with DNA at its platinum centre as well as *via* its planar ligands on the Ru(II) centre.<sup>183</sup> Cross-linking interactions of the complex with DNA were found to be higher than that of cisplatin.<sup>183</sup> The compounds were also found to have DNA intercalation when different bridging ligands such as 2,3-bis(2-pyridyl)pyrazine and 2,2'-bipyrimidine have been used.



**Figure 1.10** The Ru(II)-Pt(II) with a long and flexible linkers (58) and (59) along with the heterodinuclear Ru(II)-Pt(II) complexes with different linkers.<sup>5,113,120,180,172,181b</sup> Anions omitted for simplicity.

DNA intercalation of Ru(II)-Pt(II) complexes bridged by back to back planar tridentate ligands such as  $[(\text{tpy})\text{Ru}(\text{tppz})\text{PtPtCl}](\text{PF}_6)_3$  (**63**) and  $[\text{ClPt}(\text{tppz})\text{Ru}(\text{tppz})\text{PtPtCl}](\text{PF}_6)_4$  (**64**) where  $\text{tppz}$  = 2,3,5,6-tetrakis(2-pyridyl)pyrazine have been reported by Prussin *et al.*<sup>184</sup> The metal complexes (**63**) and (**64**) when incubated at different ratios of DNA base pair to metal concentrations at room temperature, results obtained show binding of the complexes to DNA base pairs and the effect was reported to be even greater than the well-known Pt(II) anticancer drug, cisplatin.<sup>184</sup> The binding of the complexes with DNA base pairs was also found to be temperature dependent and different from that of cisplatin. This was assumed to be due to the high molecular mass of the complexes and the formal charge of the complexes compared to that of cisplatin.<sup>184</sup> Furthermore, photochemical analysis of the complexes showed strong MLCT.<sup>185</sup> The planar ligands

were found to be excellent bridges which enhance the electronic communication between the hetero metal centres.<sup>124b,185a</sup> Since the complexes are currently under further studies of mechanism of action with DNA<sup>184</sup>, investigation of their substitution kinetics would bring useful data towards the development of these promising complexes as anticancer drugs.

In the mentioned heterometallic complexes, ruthenium was chosen as the second element<sup>180</sup> firstly, due to its antitumour activity<sup>186</sup> and secondly, because the octahedral Ru(II) coordination sphere is more sterically demanding compared to that of square planar Pt(II). These properties are thought to improve the kinetic control and the sequence specificity of the types of DNA adducts formed.<sup>180</sup> Furthermore, attaching a platinum ion can be useful for imparting the reactivity at the less reactive ruthenium centre in order to facilitate unique cross-linking with specific DNA sequences.<sup>180</sup>

Heterometallic Ru(II)-Pt(II) complexes are important models for introducing photoinduction of Pt(II) centres with DNA.<sup>111g,187</sup> In such complexes, photo reactive light absorbing ruthenium unit is linked with a reactive platinum centre. The molecule can be photoactivated by the light absorbing ruthenium unit which will improve the reactivity of the platinum centre which then coordinates to DNA.<sup>120</sup> The positively charged ruthenium centre is thought to increase the solubility of the complexes as well as electrostatic interactions with DNA.<sup>120</sup>

## **1.8 Aims of this Study**

Multinuclear platinum complexes have been found to exhibit remarkable anticancer activity towards many different cancer cell-lines. Some multinuclear complexes are endowed with superior cytotoxicity compared to clinical Pt(II) based drugs. The search for finding other effective anticancer drugs is ongoing. One attractive route is the development of heterometallic complexes where a Pt(II) moiety is combined with another metal possess cytotoxicity. One area of such complexes include heterometallic Ru(II)-Pt(II) complexes. The anticancer activity of heterometallic Ru(II)-Pt(II) complexes have not yet been studied extensively. An important aspect to the success of this approach is to investigate the mechanistic and kinetic substitution behaviour of such complexes.

Therefore, the main aim of this study is to investigate the ligand substitution kinetics of heterometallic Ru(II)-Pt(II) complexes. In this study mononuclear and dinuclear Pt(II)

complexes alongside heterometallic complexes were investigated with neutral thiourea ligands: thiourea, 1-methyl-2-thiourea, 1,3-dimethyl-2-thiourea, 1,1,3,3-tetramethyl-2-thiourea and/or anions, iodide and/or thiocyanate. The chosen thiourea nucleophiles vary according to their steric size. Sulfur donor thiourea nucleophiles are good models to represent the reaction of the sulphur containing biomolecules in the body with platinum based drugs. In order to understand how the structural arrangement of the complex influences the kinetic behaviour of the molecules, quantum calculations were performed at the B3LYP/LACVP level of theory using density functional theory technique.

The work reported in this thesis is based on an investigation of kinetics and thermodynamic properties of five different sets of complexes, three of which are designed to deliver an in-depth understanding of the role of flexible polyethyleneglycolether linker on the reactivity of mononuclear, dinuclear platinum complexes and heterometallic Ru(II)-Pt(II) complexes.

The specific objectives of this work were:

1. To investigate the kinetic and mechanistic behaviour of mixed-metal Ru(II)-Pt(II) and Co(II)-Pt(II) complexes of the form  $[(\text{tpy})\text{Ru}(\text{tppz})\text{PtCl}](\text{PF}_6)_3$ ,  $[\text{ClPt}(\text{tppz})\text{Ru}(\text{tppz})\text{PtCl}](\text{PF}_6)_4$  and  $[\text{ClPtRu}_2(\text{tppz})_3\text{PtCl}](\text{PF}_6)_6$  (where tppz = tetra-2-pyridyl-1,4-pyrazine). In this section a cobalt complex,  $[(\text{tpy})\text{Co}(\text{tppz})\text{PtCl}](\text{PF}_6)_3$  is used to understand the effect of the Ru(II) on the reactivity of the complexes. This is presented in **Chapter 3**.
2. To investigate the substitution kinetics of heterometallic Ru(II)-Pt(II) complexes, where the two metal centers are linked by a short semi-rigid linker, qpy. The ligand, qpy binds to Ru(II) tridentately *via* its terpyridine ligand backbone while the pyridine group on the 4'-position monodentately binds to the second metal center, Pt(II). This ligand has very versatile coordination chemistry; forming mononuclear compounds with pendant groups, metal coordinated polygons and polymers. This is presented in **Chapter 4**.
3. To gain an understanding on the effect of increasing the length of the flexible polyethylene glycoxy pendant on the rate of substitution kinetics of parent **Ptttpy** moiety. This work is covered in **Chapter 5**.

4. To gain further understanding of the role of flexible polyethyleneglycolether linkers on the reactivity of the dinuclear Pt(II) terpyridine complexes when a second Pt(II) terpyridine group is coupled through the polyethyleneglycoxy linker whose kinetics will be reported in **Chapter 6**.
5. To understand the role of Ru(tpy)<sub>2</sub> moiety on the substitution kinetics of heterometallic Ru(II)-Pt(II) complexes bridged by flexible polyethyleneglycol ether linkers of different chain lengths. This gives further understanding on the role of polyethyleneglycol ether linkers have on the reactivity of the mixed-metal Ru(II)-Pt(II) complexes, when one end of the ligand is capped with Ru(II) terpyridine. No kinetic data has been reported on multinuclear complexes linked by flexible linkers with mixed-metal complexes. In this study, different chain lengths of polyethyleneglycol ether ligand system is used for synthesis of heterometallic Ru(II)-Pt(II) polypyridyl complexes. The complexes consist of substitutionally inert Ru(II) terpyridine capped moieties linked with polyethyleneglycol ether linkers which are coordinated to a Pt(II) centre. This work will be presented in **Chapter 7**.



## 1.9 References

- (1) (a) Pan, M.; Ho, C. *Chem. Soc. Rev.* **2008**, 37, 2558(b) Walker, E. M.; Walker, S. M. *Ann Clin Lab Sci.* **1999**, 29, 263.
- (2) (a) Blattman, J. N.; Greenberg, P. D. *Science.* **2004**, 305, 200(b) Glanski, M.; Jakupec, M. A.; Keppler, B. K. *Curr. Med. Chem.* **2005**, 12, 225.
- (3) Panda, V.; Khambhat, P.; Patil, S. *Int. J. Clin. Med.* **2011**, 2, 515.
- (4) Kostava, I. *Recent Patents on Anti-Cancer Drug Discovery.* **2006**, 1, 1.
- (5) Simon, E. C., PhD Thesis, Ruthenium polypyridyl complexes with anticancer properties- Synthesis, characterization and mechanistic studies in search for structure-activity relationships, University of Laiden, 1979, pp: 12- 38, 83- 101, 105- 116.
- (6) (a) Galanski, M.; Keppler, B. K. *Anti-Cancer Agents Med. Chem.* **2007**, 7, 55(b) Yu, Y.; Lou, L.-G.; Liu, W.-P.; Zhu, H.-J.; Ye, Q.-S.; Chen, X.-Z.; Gao, W.-G.; Hou, S.-Q. *Eur. J. Med. Chem.* **2008**, 43, 1438.
- (7) Allardyce, C. S.; Dyson, P. J. *Platinum Metals Rev.* **2001**, 45, 62.
- (8) Antonarakis, E. S.; Emadi, A. *Cancer Chemother. Pharmacol.* **2010**, 66, 1.
- (9) Lippert, B. *Cisplatin: Chemistry and Biochemistry of a Leading Anticancer Drug*; Wiley-VCH: New York, 1999, 1-90, 184-221.
- (10) (a) Heslop, R. B.; Robinson, P. L. *Inorganic Chemistry: A Guide to Advance Study*; 2<sup>nd</sup> ed.; Elsevier Publishing Company: New York, 1963, 501-511(b) Belluco, U. *Organometalic Coordination Chemistry of Platinum*; Academic Pressd: London, 1974, 1, 19-50, 220-221.
- (11) (a) Henderson, R. A. *The Mechanisms of Reactions at Transition Metal Sites*; Oxford University Press: Oxford, 1993, 1-22(b) Tobe, M. L.; Burgess, J. *Inorganic Reaction Mechanisms*; Addison Wesley: London, 1999, 30- 43, 70-112
- (12) Housecroft, C. E.; Sharpe, A. G. *Inorganic Chemistry*; 2<sup>nd</sup> ed.; Pearson Prentice Hall: London, 2005, 684-689.
- (13) (a) Hochreuther, S.; Nandibewoor, S. T.; Puchta, R.; van Eldik, R. *Dalton Trans.* **2012**, 41, 52(b) Hochreuther, S.; Puchta, R.; van Eldik, R. *Inorg. Chem.* **2012**, 51, 3025.
- (14) (a) Reddy, D.; Jaganyi, D. *Int. J. Chem. kinet.* **2011**, 43, 161(b) Reddy, D.; Jaganyi, D. *Dalton Trans.* **2008**, 6724(c) Reddy, D.; Akerman, K. J.; Akerman, M. P.; Jaganyi, D. *Transition Met. Chem.* **2011**, 36, 593(d) Ongoma, P. O.; Jaganyi, D. *Dalton Trans.*, **2013**, 42, 2724(e) Ongoma, P. O.; Jaganyi, D. *Dalton Trans.* **2012**, 41, 10724(f) Mambanda, A.; Jaganyi, D. *Dalton Trans.* **2012**, 41, 908(g) Mambanda, A.; Jaganyi, D. *Dalton Trans* **2011**, 40, 79 (h) Ertürk, H.; Maigut, J.;

- Puchta, R.; van Eldik, R. *J. Chem. Soc. Dalton Trans.* **2008**, 2759(i) Ertürk, H.; Hofmann, A.; Puchta, R.; van Eldik, R. *Dalton Trans.* **2007**, 2295(j) Bugarcic, Z. D.; Heinemann, F. W.; van Eldik, R. *Dalton Trans.* **2004**, 279(k) Hofmann, A.; Jaganyi, D.; Munro, O. Q.; Liehr, G.; van Eldik, R. *Inorg. Chem.* **2003**, 42, 1688(l) Shaira, A.; Reddy, D.; Jaganyi, D. *Dalton Trans.* **2013**, 42, 8426.
- (15) Reedijk, J.; Fichtinger-Schepman, A. M.; Van Oosterom, A. T.; van de Putte, P. *Structure and Bonding, Platinum Ammine Coordination Compounds as Anti-Tumour Drugs, Molecular Aspects of the Mechanism of Action.*, 1987, 67, 53.
- (16) Seymour, R. J.; O'Farrelly, J. I. In *Kirk Othmer Encyclopedia of Chemical Technology*; Wiley, 2001.
- (17) (a) Rosenberg, B.; VanCamp, L.; Trosko, J. E.; Mansour, V. H. *Nature.* **1969**, 222, 385(b) Rosenberg, B.; van Camp, L.; Krigass, T. *Nature.* **1965**, 205, 698(c) Gieleng, M.; Tiekink, E. R. T. *Metallotherapeutic Drugs and Metal-Based Diagnostic Agents: The Use of Metals in Medicine*; John Wiley and Sons, Ltd: Canada, 2005, 489-502(d) Cummings, S. D. *Coor. Chem. Rev.* **2009**, 253, 1495.
- (18) Crichton, R. R. *Biological Inorganic Chemistry: An Introduction*; Elsevier: New York, 2008, 1, 341-344.
- (19) Jameison, E. R.; Lippard, S. J. *Chem. Rev.* **1999**, 2467.
- (20) Jamieson, E. R.; Lippard, S. J. *Chem. Rev.* **1999**, 99, 2467.
- (21) (a) Cleare, M. J.; Hoeschele, J. D. *Plat. Met. Rev.* **1973**, 17, 3(b) Cleare, M. J.; Hoeschele, J. D. *Bioinorg. Chem.* **1973**, 2, 187.
- (22) (a) Jones, C. J.; Thornback, J. R. *Medicinal Applications of Coordination Chemistry*; Royal Society of Chemistry: Cambridge, 2007, 1, 218-257(b) Sengupta, P. S.; Sinha, R.; Bera, S. K.; De, G. S. *Ind. J. Chem., Sect. A.* **2002**, 41A, 712(c) Coluccia, M.; Natile, G. *Anti-Cancer Agents Med. Chem.* **2007**, 111.
- (23) Hambley, T. W. *Coord. Chem. Rev.* **1997**, 166, 181.
- (24) Reedijk, J. *Eur. J. Inorg. Chem.* **2009**, 1303.
- (25) (a) Komeda, S.; Kalayda, G. V.; Lutz, M.; Spek, A. L.; Yamanaka, Y.; Sato, T.; Chikuma, M.; Reedijk, J. *J. Med. Chem.* **2003**, 46, 1210(b) Sorenson, C. M.; Eastman, a. *Cancer Res.* **1988**, 48, 4484.
- (26) Avendano, C.; Menendez, J. C. *Medicinal Chemistry of Anticancer Drugs*; 1<sup>st</sup> ed., Elsevier: New York, 2008, 169-173.
- (27) (a) Ash, D. C. *J. Clin. Hemat. Oncol.* **1980**, 10, 55(b) Chu, G. *J. Biol. Chem.* **1994**, 269, 787(c) Wong, E.; Giandomenico, C. M. *Chem. Rev.* **1999**, 99, 2451(d) Jaimeson, E. R.; Lippard, S. J. *Chem. Rev.* **1999**, 99, 2467(e) Lakomska, I. *Inorg.*

- Chim. Acta.* **2009**, 362, 669(f) Arnesano, F.; Natile, G. *Pure Appl. Chem.* **2008**, 80, 2715.
- (28) (a) Di Blasi, P.; Bernareggi, A.; Beggiolin, L.; Piazzoni, L.; Menta, E. *Anticancer Res* **1998**, 18, 3113(b) Huq, F.; Daghriri, H.; Yu, J. Q.; Tayyem, H.; Beale, P.; Zhang, M. *Eur J Med Chem* **2004**, 39, 947(c) Loehrer, P. J.; Einhorn, L. H. *Ann. Intern. Med* **1984**, 100, 704.
- (29) (a) Goldstein, R. S.; Noordewier, B.; Bond, J. T.; Hook, J. B.; Mayor, G. H. *Toxicol. Appl. Pharmacol.* **1981**, 60, 163(b) Komeda, S.; Lutz, M.; Spek, A. L.; Chikuma, M.; Reedijk, J. *Inorg. Chem.* **2000**, 39, 4230(c) Von Hoff, D. D.; Schilsky, R.; Reichert, C. M.; Reddick, R. L.; Rozencweig, M.; Young, R. C.; Muggia, F. M. *Cancer Treat Rep.* **1979**, 63, 1527(d) Lemma, K.; Shi, T.; Elding, L. I. *Inorg. Chem.* **1999**, 39, 1728(e) Petrovic, D.; Stojimirovic, B.; Petrovic, B.; Bugarcic, Z. M.; Bugarcic, Z. D. *Bioorg. Med. Chem.* **2007**, 15, 4203(f) Cohen, S. M.; Lippard, S. J. *Prog. Nucleic Acid res. Mol. Biol.* **2001**, 67, 93(g) Alberts, D. S.; Noel, J. K. *Anticancer Drugs.* **1995**, 6, 369(h) Goren, M. P.; Wright, R. K.; Horowitz, M. E. *Cancer Chemother. Pharmacol.* **1986**, 18, 69(i) Thurston, D. V. *Chemistry and Pharmacology of Anticancer Drugs*; CRC Press Taylor and Fransis Group: London, 2006, 61(j) Bera, S. K.; Sengupta, P. S.; De, G. S. *Inorg. React. Mech.* **2003**, 5, 65.
- (30) (a) Hay, R. W.; Miller, S. *Polyhedron.* **1998**, 55, 528(b) Perego, P.; Caserini, C.; Gatti, L.; Carenini, N.; Romanelli, S.; Supino, R.; Colangelo, D.; Viano, I.; Leone, R.; Spinelli, S.; Pezzoni, G.; Manzotti, C.; Farrell, N.; Zunino, F. *Mol. Pharmacol.* **1999**, 55, 528(c) Burchenal, J. H.; Kalaher, K.; Dew, K.; Lokys, L.; Gale, G. *Biochimie.* **1978**, 60, 961(d) Eastman, A.; Bresnick, E. *Biochem. Pharmacol.* **1981**, 30, 2721(e) Komeda, S.; Yamane, H.; Chikuma, M.; Reedijk, J. *Eur. J. Inorg. Chem.* **2004**, 4828(f) Kraker, A. J.; Hoeschele, J. D.; Elliott, W. L.; Showalter, H. D.; Sercel, A. D.; Farrell, N. P. *J. Med. Chem.* **1992**, 35, 4526(g) Galanski, M.; Jakupec, M. A.; Keppler, B. K. *Curr. Med. Chem.* **2005**, 12, 2075.
- (31) (a) Kas'yanenko, N. A.; Aia, E. E. E.; Bogdanov, A. A.; Kosmotynskaya, Y. V.; Yakovlev, K. I. *Mol. Biol.* **2002**, 36, 745(b) Tulub, A. A.; Stefanov, V. E. *Int. J. Biol. Macromol.* **2001**, 28, 191.
- (32) Zhen, W.; Link, J. C.; O'Connor, M. P.; Reed, A.; Parker, R.; Howell, S. B.; Bohr, V. *Mol. Cell. Biol.* **1992**, 12, 3689.
- (33) (a) Reedijk, J. *Proc. Natl. Acad. Sci. USA.* **2003**, 100, 3611(b) Johnson, N. P.; Butour, J.-L.; G., V. e. a. *Prog. Clin. Biochem. Med.* **1989**, 10, 1(c) Sengupta, P. S.; Sinha, R.; De, G. S. *Indian J. Chem., Sect. A.* **2001**, 40A, 509(d) Su, H.; Williams, P.; Thompson, M. *Anal. Chem.* **1995**, 67, 1010.

- (34) (a) Puckett, C. A.; Ernst, R. J.; Barton, J. K. *Dalton Trans.* **2010**, 39, 1159(b) Reedijk, J. *Platinum Metals Rev.* **2008**, 52, 2.
- (35) Reedijk, J. *Chem. Commun.* **1996**, 801.
- (36) Kozelka, J.; Legendre, F.; Reeder, F.; Chottard, J.-C. *Coor. Chem. Rev.* **1999**, 190-192, 61.
- (37) Miller, S. E.; A., H. D. *Inorg. Chim. Acta.* **1991**, 187, 125.
- (38) Teuben, J.-M.; i Zubiri, M. R.; Reedijk, J. *J. Chem. Soc., Dalton Trans.* **2000**, 369.
- (39) Bugarčić, Ž. D.; Djordjević, B. V. *Monatshefte für Chemie.* **1998**, 1267.
- (40) (a) Crider, S. E.; Holbrook, R. J.; Franz, K. J. *Metallomics.* **2010**, 2, 74(b) Peleg-Shulman, T.; Najajreh, Y.; Gibson, D. *J. Inorg. Biochem.* **2002**, 91, 306.
- (41) Pasini, A.; Fiore, C. *Inorg. Chim. Acta.* **1999**, 285, 249.
- (42) Vinje, J.; Sletten, E. *Anti-Cancer Agents Med. Chem.* **2007**, 7, 35.
- (43) Wang, X.; Guo, Z. *Anti-Cancer Agents Med. Chem.* **2007**, 7, 19.
- (44) Kelland, L. R. *Nat. Rev. Cancer.* **2007**, 7, 573.
- (45) Swinnen, L. J.; Barnes, D. M.; Fisher, S. G.; Albani, K. S.; Fisher, R. I.; Erickson, L. C. *Cancer Res.* **1989**, 49, 1383.
- (46) Esak, T.; Nakano, S.; Tatsumoto, T.; Kurokawa, M.; Mitsugi, K.; Nakamura, M. N.; Niko, Y. *Cancer Res.* **1992**, 52, 6501.
- (47) Berners-Price, S. J.; Frenkiel, T. A.; Frey, U.; Ranford, J. D.; Sadler, P. J. *J. Chem. Soc., Chem. Commun.* **1992**, 789.
- (48) Hambley, T. W. *J. Chem. Soc., Dalton Trans.* **2001**, 2711.
- (49) Johnson, N. P.; Hoeschele, J. D.; Rahn, R. O. *Chem.-Biol. Interact.* **1980**, 30, 151.
- (50) Barton, S. J.; Barnham, K. J.; Habtemariam, A.; Sue, R. E.; Sadler, P. J. *Inorg. Chim. Acta.* **1998**, 273, 8.
- (51) Ohndrof, U. M.; Rould, M. A.; He, Q. Y.; Pabo, C. O.; Lippard, S. J. *Nature.* **1999**, 399, 708.
- (52) Fuertes, M. A.; Alonso, C.; Perez, J. M. *Chem. Rev.* **2003**, 103, 645.
- (53) (a) Zenker, A.; Galanski, M.; Bereuter, T. L.; Keppler, B. K.; Lindner, W. *J. Chromatogr., B.* **2000**, 745, 211(b) Meroueh, M.; Kjellstrom, J.; Margareta Martensso, K. S.; Elmroth, A. K. C.; Chow, C. S. *Inorg. Chim. Acta.* **2000**, 297, 145(c) Reedijk, J. *Chem. Rev.* **1999**, 99, 2499(d) Baik, M.-H.; Friesner, R. A.; Lippard, S. J. *Inorg. Chem.* **2003**, 42, 8615(e) Bierbach, U.; Farrel, N. *Inorg. Chem.* **1997**, 36, 3657(f) Mellish, K. J.; Qu, Y.; Scarsdale, N.; Farrell, N. P. *Nucleic Acids Res.* **1997**, 25, 1265(g) Zenker, A.; Galanski, M.; Bereuter, T. L.; Keppler, B. K.; Lindner, W. *J. Chromatogr., A* **1999**, 852, 337.

- (54) Bednarski, P. J.; Mackay, F. S.; Sadler, P. J. *Anti-Cancer Agents Med. Chem.* **2007**, *7*, 75.
- (55) <http://www.atdbio.com/content/16/Nucleic-acid-drug-interactions>; Vol. Nucleic acid-drug interactions, Accessed on 14/06/2013.
- (56) (a) Rice, J. A.; Crothers, D. M.; Pinto, A. L.; Lippart, S. J. *Proc. Natl. Acad. Sci. U.S.A.* **1988**, *85*, 4158(b) Bellon, S. F.; Lippard, S. J. *Biophys. Chem.* **1990**, *35*, 179.
- (57) Moyzis, R. K.; Buckingham, J. M.; Cram, L. S.; Dani, M.; Deaven, L. L.; Jones, M. D.; Meyne, J.; Ratliff, R. L.; Wu, J.-R. *Proc. Natl. Acad. Sci. U.S.A.* **1988**, *85*, 6622.
- (58) Counter, C. M. *Mutat. Res.* **1996**, *366*, 45.
- (59) (a) Harley, C. B.; Futcher, A. B.; Greider, C. W. *Nature* **1990**, *345*, 458(b) Ma, D.-L.; Che, C.-M.; Yan, S.-C. *J. Am. Chem. Soc.* **2009**, *131*, 1835.
- (60) Han-Chin, J.; Chang, M. D. *J. Clin. Oncol.* **1999**, *17*, 409.
- (61) Alberto, M. E.; Lucas, M. F. A.; Pavelka, M.; Russo, N. *J. Phys Chem. B.* **2009**, *113*, 14473.
- (62) Su, W.-C.; Chang, S.-L.; Chen, T.-Y.; Chen, J.-S.; Tsao, C.-J. *Jpn J Clin Oncol.* **2000**, *12*, 562.
- (63) Reedijk, J. *J. Chem. Commun.* **1996**, 801.
- (64) Bower, M.; Newlands, E. S.; Holden, L.; Rustin, G. J. S.; Begent, R. H. J. *Ann. Oncol.* **1997**, *8*, 447.
- (65) Hamelers, I. H.; de Kroon, A. I. P. M. *J. Liposome. Res.* **2007**, *17*, 183.
- (66) Ruchdeschel, J. C. *Semin. Oncol.* **1994**, *21*, 114.
- (67) Bolelikas, T.; Vougiouka, M. V. *Oncol. Reports.* **2003**, *10*, 1663.
- (68) Levi, F.; Metzger, G.; Massari, C.; Milano, G. *Clin. Pharmacokinet.* **2000**, *38*, 1.
- (69) Wiseman, L. R.; Adkins, J. C.; Plosker, G. L.; Goa, K. L. *Drugs Aging* **1999**, *14*, 459.
- (70) Lokich, J. *Cancer Invest.* **2001**, *19*, 756.
- (71) Huq, F.; Daghriri, H.; Yu, J. Q.; Tayyem, H.; Beale, P.; Zhang, M. *Eur. J. Med. Chem.* **2004**, *39*, 947.
- (72) Reedijk, J. *Proc. Natl. Acad. Sci. U. S. A.* **2003**, *100*, 3611.
- (73) Farrell, M. *Comments Inorg. Chem.* **1995**, *16*(6), 373.
- (74) (a) Farrell, N. *Met. Ions Biol. Syst.* **2004**, *42*, 251(b) Johnson, S. W.; Ferry, K. V.; Hamilton, T. C. *Drug Resist. Updates.* **1998**, *1*, 243(c) Farrell, N.; De Almeida, S. G.; Skov, K. A. *J. Am. Chem. Soc.* **1988**, *110*, 5018.
- (75) Farrell, N.; Qu, Y.; Feng, L.; Van Houten, B. *Biochemistry.* **1990**, *29*, 9522.
- (76) Brabec, V. *Prog. Nucleic Acid. Res. Mol. Biol.* **2002**, *71*, 1.

- (77) (a) Wheate, N. J.; Collins, J. G. *Curr. Med. Chem. Anticancer Agents*. **2005**, *5*, 267(b) Brabec, V.; Kaspárková, J.; Vrána, O.; Nováková, O.; Cox, J. W.; Qu, Y.; Farrell, N. *Biochem*. **1999**, *38*, 6781.
- (78) Banerjee, T.; Dubey, P.; Mukhopadhyay, R. *Biochimie*. **2010**, *92*, 846.
- (79) Maisonia, A.; Serafin, P.; Traikia, M.; Debiton, E.; Thery, V.; Aitken, D. J.; Lemoine, P.; Viossat, B.; Gautier, A. *Eur. J. Inorg. Chem*. **2008**, 298.
- (80) Zvonok, N.; Williams, J.; Johnston, M.; Pandarinathan, L.; Janero, D. R.; Li, J.; Krishnan, S. C.; Makriyannis, A. *J. Proteome Res*. **2008**, *7*, 2158.
- (81) Roy, S. PhD Thesis, PhD Thesis, University of Leiden, *Synergy of intercalation and coordination binding to design novel DNA-targeting antineoplastic metallodrugs*, 2008, 230- 248.
- (82) Malina, J.; Kasparkova, J.; Farrell, N. P.; Brabec, V. *Nuc. Acids Res*. **2010**, *39*, 720.
- (83) Zhao, G.; Lin, H.; Zhu, S.; Sun, H.; Chen, Y. *Anti- Cancer Drug Des*. **1998**, *13*, 769.
- (84) (a) Wheate, N. J.; Cullinane, C.; Webster, L. K.; Collins, J. G. *Anti-Cancer Drug Des*. **2001**, *16*, 91(b) Broomhead, J. A.; Rendina, L. M.; Sterns, M. *Inorg. Chem*. **1991**, *31*, 1880(c) Broomhead, J. A.; Rendina, L. M.; Webster, L. K. *J. Inorg. Biochem*. **1993**, *49*, 221.
- (85) Zhao, Y.; He, W.; Shi, P. Y.; Zhu, L.; Qia, L.; Lin, L.; Guo, Z. *J. Chem. Soc. Dalton Trans*. **2006**, 2617.
- (86) (a) Komeda, S.; Ohishi, H.; Yamane, H.; Harikawa, M.; Sakaguchi, K.; Chikuma, M. *J. Chem. Soc. Dalton Trans*. **1999**, 2959(b) Komeda, S.; Lutz, M.; Spek, A. L.; Yamanaka, Y.; Sato, T.; Chikuma, M.; Reedijk, J. *J. Am. Chem. Soc*. **2002**, *124*, 4738.
- (87) Nguyen, L.; Kolzeka, J.; Bois, C. *Inorg. Chim. Acta*. **1991**, *190*, 217.
- (88) Wheate, N. J.; Evison, B. J.; Herlt, A. J.; Phillips, D. R.; Collins, J. G. *Daltom Trans*. **2003**, 3486.
- (89) Zhao, G. H.; Lin, H. K.; Zhu, S. R.; Sun, H. W.; Chen, Y. T. *J. Coord. Chem*. **1998**, *46*, 79.
- (90) Links, M.; Lewis, C. *Drugs*. **1999**, *57*, 293.
- (91) Komeda, S.; Bombard, S.; Perrier, S.; Reedijk, J.; Kozelka, J. *J. Inorg. Biochem*. **2003**, *96*, 357.
- (92) Olivova, R.; Kasparkova, J.; Vrana, O.; Vojtiskova, M.; Suchankova, T.; Novakova, O.; He, W.; Guo, Z.; Brabec, V. *Mol. Pharm*. **2011**, *8*, 2368.
- (93) Zhu, J.; Zhao, Y.; Zhu, Y.; Wu, Z.; Lin, M. C.; He, W.; Wang, Y.; Chen, G.; Dong, L.; Zhang, J.; Lu, Y.; Guo, Z. *Chem. Eur. J*. **2009**, *15*, 5245.

- (94) Wheate, N. J.; Day, A. I.; Blanch, R. J.; Arnold, A. P.; Cullinane, C.; Collins, J. G. *Chem. Commun.* **2004**, 1424.
- (95) Hofmann, A.; van Eldik, R. *J. Chem. Soc., Dalton Trans.* **2003**, 2979.
- (96) (a) Jennette, K. W.; Lippard, S. J.; Vassiliades, G. A.; Bauer, W. R. *Proc. Natl. Acad. Sci. U. S. A.* **1974**, *71*, 3839(b) Lowe, G.; Droz, A. S.; Vilaivan, T.; Weaver, G. W.; Tweedale, L.; Pratt, J. M.; Rock, P.; Yardley, V.; Croft, S. L. *J. Med. Chem.* **1999**, *42*, 999(c) Moore, J. J.; Nash, J. J.; Fanwick, P. E.; McMillin, D. R. *Inorg. Chem.* **2002**, *41*, 6387(d) Wheate, N. J.; Talen, R. I.; Krause-Heuer, A. M.; Cook, R. L.; Wang, S.; Higgins, V. J.; Aldrich-Wright, J. R. *Dalton Trans.* **2007**, 5055.
- (97) Hu, Y.-Z.; Wilson, M. H.; Zong, R.; Bonnefous, C.; McMillin, D. R.; Thummel, R. P. *Dalton Trans.* **2005**, 354.
- (98) Neville, D. M.; Daves, D. R. *J. Mol. Biol.* **1966**, *17*, 805.
- (99) (a) Wong, Y.; Lippard, S. J. *J. Am. Chem. Soc.* **1977**, 824(b) Bond, P. J.; Langridge, R.; Jennette, K. W.; Lippard, S. J. *Proc. Natl. Acad. Sci. USA.* **1975**, *72*, 4825.
- (100) Cusumano, M.; Di Pietro, M. L.; Giannetto, A. *Inorg. Chem.* **1999**, *38*, 1754.
- (101) Peyratout, C. S.; Aldridge, T. K.; Crites, D. K.; McMillin, D. R. *Inorg. Chem.* **1995**, *34*, 4484.
- (102) Messori, L.; Marcon, G.; Innocenti, A.; Gallori, E.; Franchi, M.; Orioli, P. *Bioinorg. Chem. Appl.* **2005**, *3*, 239.
- (103) Howe-Grant, M.; Wu, K. C.; Bauer, W. R.; Lippard, S. J. *Biochemistry.* **1976**, *15*, 4339.
- (104) Lowe, G.; McCloskey, J. A.; Ni, J.; Vilaivan, T. *Bioorg. Med. Chem.* **1996**, *4*, 1007.
- (105) Bugarcic, Z. D.; Soldatovic, T.; Jelic, R.; Alguero, B.; Grandas, A. *Dalton Trans.* **2004**, 3869.
- (106) Brothers, H. M.; Kostic, N. M. *Inorg. Chem.* **1988**, *27*, 1761.
- (107) Jaganyi, D.; De Boer, K. L.; Gertenbach, J.; Perils, J. *Int. J. Chem. Kinet.* **2008**, *40*, 808.
- (108) Jaganyi, D.; Reddy, D.; Gertenbach, J. A.; Hofmann, A.; van Eldik, R. *Dalton Trans.* **2004**, 299.
- (109) Hofmann, A.; Dahlenburg, L.; van Eldik, R. *Inorg. Chem.* **2003**, *42*, 6528.
- (110) Romeo, R.; Plutino, M. R.; Scolaro, L. M.; Stoccoro, S.; Minghetti, G. *Inorg. Chem.* **2000**, *39*, 4749.
- (111) (a) Novakova, O.; Kasparkova, J.; Vrana, O.; Van Bliet, P. M.; Reedijk, J.; Brabec, V. *Biochemistry* **1995**, *34*, 12369(b) van der Steen, S.; de Hoog, P.; van der Schilden, K.; Gamez, P.; Pitie, M.; Kiss, R.; Reedijk, J. *Chem. Commun.* **2010**, *46*, 3568(c) Wheate, N. J.; Brodie, C. R.; Collins, J. G.; Kemp, S.; Aldrich-Wright, J. R.

- Mini-Rev. Med. Chem* **2007**, 7, 627(d) van der Schilden, K.; Garcia, F.; Kooijman, H.; Spec, A. L.; Haanoot, J. G.; Reedijk, J. *Angew. Chem. Int. Ed.* **2004**, 43, 5668(e) Zhang, P.; Chen, J.; Liang, Y. *Acta Biochim Biophys Sin.* **2010**, 42, 440(f) Zhang, G.; Wu, C. Y.; Ye, H.; yan, H.; Wang, X. *J. Nanobiotechnol.* **2011**, 9:6(g) Corral, E.; Hotze, A. C. G.; den Dulk, H.; Laczkowska, A.; Rodger, A.; Hannon, M. J.; Reedijk, J. *J. Biol. Inorg. Chem.* **2009**, 14, 439(h) Morris, R. E.; Aird, R. E.; del Socorro Murdoch, P.; Chen, H.; Cummings, J.; Hughes, N. D.; Parsons, S.; Parkin, A.; Boyd, G.; Jodrell, D. I.; Sadler, P. J. *Journal of Medicinal Chemistry* **2001**, 44, 3616.
- (112) Indumathy, R.; Radhika, S.; Kanthimathi, M.; Weyhermuller, T.; Unni Nair, B. *J. Inorg. Biochem.* **2007**, 101, 434.
- (113) Brabec, V.; Novakova, O. *Drug Resist. Updates.* **2006**, 9, 111.
- (114) Cerquetella, A., PhD, (Arene), Universita DiCamerino, *Ruthenium(II) Coordination Chemistry with Chelating and Tripodal Oxygen- and Nitrogen Donor Ligands: Synthesis, Characterization, Reactivity and Application.*, 2008, 1-18.
- (115) Tsenng, H.-W.; Zong, R.; Muckerman, J. T.; Thummel, R. *Inorg. Chem.* **2008**, 47, 11763.
- (116) Halpern, J. *Pure Appl. Chem.* **1987**, 59, 173.
- (117) Pitchkov, V. N. *Plat. Met. Rev.* **1996**, 40, 181.
- (118) Zheng, S., MSc, Nelson Mandela Metropolitan University, *The Reactions of Ruthenium(II) Polypyridyl Complexes.*, 2009, 1-9.
- (119) Cotton, F. A.; Wilkinson, G. *Advanced Inorganic Chemistry*; 5th Edition ed.; 5th Edition, John Wiley & Sons: New York, 1988, 919.
- (120) van der Schilden, K., PhD Thesis, University of Leiden, *The Development of Polynuclear Ruthenium and Platinum Polypyridyl Complexes.*, 2006, 13 - 35, 65 - 85, 133 - 149.
- (121) Sigel, H. *Metal ions in biological systems, metal complexes as anticancer agents*; M. Dekker, 1980, P 9, 11, 64, 241-242.
- (122) Tiba, F., MSc, University of KwaZulu-Natal, *Synthesis and Kinetic Studies of Pd(II), Pt(II) and Ru(II) Polypyridine Monoaqua Complexes.*, 2003, pp: 34 - 45.
- (123) Yukuta, T.; Mori, I.; Kurihara, M.; Muzutani, J.; Kubo, K.; Furusho, S.; Matsumura, K.; Tamai, N.; Nishihara, H. *Inorg. Chem.* **2001**, 40, 4986.
- (124) (a) Murphy, W. R.; Takeuchi, K. J.; Baerley, M. H.; Meyer, T. J. *Inorg. Chem.* **1986**, 25, 1041(b) Arana, C. R.; Abruña, H. D. *Inorg. Chem* **1993**, 32, 194.
- (125) Huang, L.; Seward, K. J.; Sullivan, B. P.; Jones, W. E.; Mecholsky, J. J.; Dressick, W. J. *Inorg. Chim. Acta.* **2000**, 310, 227.



- (126) Kelman, A. D.; Clarke, M. J.; Edmonds, S. D.; Peresie, H. J. *J. Clin. Hemat. Oncol.* **1977**, *7*, 274.
- (127) Mmestroni, G.; ALESSIO, E.; Calligaris, M. e. a. *Prog. Clin. Biochem. Med.* **1989**, *10*, 71.
- (128) Alessio, E.; Mestroni, G.; Nardin, G.; Attia, W. M.; Calligaris, M.; Sava, G.; Zorzet, S. *Inorg. Chem.* **1988**, *27*, 4099.
- (129) Coluccia, M.; Sava, G.; Loseto, F.; Nassi, A.; Boccarelli, A.; Giordano, D.; Alessio, E.; Mestroni, G. *Eur. J. Cancer.* **1993**, *29A*, 1873.
- (130) Bergamo, A.; Gava, B.; Alessio, E.; Mestroni, G.; Serli, B.; Cocchietto, M.; Zorzet, S.; Sava, G. *Int. J. Oncol.* **2002**, *21*, 1331.
- (131) Hartinger, C. G.; Zorbas-Seifried, S.; Jakupec, M. A.; Kynast, B.; Zorbas, H.; Keppler, B. K. *J. Inorg. Biochem.* **2006**, *100*, 891.
- (132) (a) Sava, G.; Bergamo, A.; Zorzet, S.; Gava, B.; Casarsa, C.; Cocchietto, M.; Furlani, A.; Scarcia, V.; Serli, B.; IENGO, e.; aLESSIO, e.; Mestroni, G. *Eur. J. Cancer.* **2002**, *38*, 427(b) Bergamo, A.; Gagliardi, R.; Scarcia, V., et. al *J. Pharmacol. Exp. Ther.* **1999**, *289*, 559(c) Sava, G.; Capozzi, I.; Clerici, K.; gagliardi, G.; Alessi, E.; Mestroni, G. *Clin. Exp. Metastasis.* **1998**, *!6*, 371(d) Sava, G.; Gagliardi, R.; Bergamo, A.; Alessio, E.; Mestroni, G. *Anticancer Res.* **1999**, *19*, 969.
- (133) Pizarro, A. M.; Sadler, P. J. *Biochimie.* **2009**, *91*, 1198.
- (134) Van Vliet, P. M.; Toekimin, S. M. S.; Haasnoot, J. G.; Reedijk, J.; Novakova, O.; Vrana, O.; Brabec, V. *Inorg. Chim. Acta.* **1995**, *231*, 57.
- (135) Zobi, F.; Hohl, M.; Zimmermann, W.; Alberto, R. *Inorg. Chem.* **2004**, *43*, 2771.
- (136) Grover, N.; Welch, T. W.; Fairley, T. A.; Cory, M.; Thorp, H. H. *Inorg. Chem.* **1994**, *33*, 3544.
- (137) Ji, L. N.; Zou, X. H.; Liu, J. G. *Coord. Chem. Rev.* **2001**, *216*, 513.
- (138) Liu, Y. J.; Chao, H.; Tan, L. F.; Yuan, Y. X.; We, W.; Ji, L. N. *J. Inorg. Biochem.* **2005**, *99*, 530.
- (139) Bergamo, A.; Stocco, G.; Gava, B.; Cocchietto, M.; Alessio, E.; Serli, B.; Iengo, E.; Sava, G. *J. Pharmacol. Exp. Ther.* **2003**, *305*, 725.
- (140) Velders, A. H.; Kooijman, H.; Spek, A. L.; Haasnoot, J. G.; de Vos, D.; Reedijk, J. *Inorg. Chem* **2000**, *39*, 2966.
- (141) Grover, N.; Thorp, H. H. *J. Am .Chem. Soc.* **1991**, *113*, 7030.
- (142) (a) Morris, R. E.; Aird, R. E.; Murdoch, P. D.; Chen, H. M.; Cummings, J.; Hughes, N. D.; Parsons, S.; Parkin, A.; Boyd, G.; Jodrell, D. I.; Sadler, P. J. *J. Med. Chem.* **2001**, *44*, 3616(b) Chen, T.; Liu, Y.; Zheng, W.-J.; Liu, J.; Wong, Y.-S. *Inorg. Chem.* **2010**,

- 49, 6366(c) Schmitt, F.; Govindaswamy, P.; Süss-Fink, G.; Ang, W. H.; Dyson, P. J.; Juillerat-Jeanneret, L.; Therrien, B. *J. Med. Chem.* **2008**, *51*, 1811.
- (143) Meng, X.; Leyva, M. L.; Jenny, M. e. a. *Cancer Res.* **2009**, *69*, 5458.
- (144) Bloemink, M. J.; Reedijk, J. *Met Ions. Biol. Syst.* **1996**, *32*, 641.
- (145) Yamada, H.; Koike, T.; Hurst, J. K. *J. Am. Chem. Soc.* **2001**, *123*, 12775.
- (146) (a) Stanbury, D. M.; Haas, O.; taube, H. *Inorg. Chem.* **1980**, *19*, 518(b) Stanbury, D. M.; Mulac, W. A.; Sullivan, J. C.; Taube, H. *Inorg. Chem.* **1980**, *19*, 3735.
- (147) Clarke, M. J.; Zhu, F. C.; Frasca, D. R. *Chem. Rev.* **1999**, *99*, 2511.
- (148) Kratz, F.; Messori, L. *J. Inorg. Biochem.* **1993**, *49*, 79.
- (149) Sava, G.; Bergamo, A. *Int. J. Oncol.* **2000**, *17*, 353.
- (150) Liu, H.-K.; Sadler, P. J. *Acc. Chem. Res.* **2010**, *44*, 349.
- (151) Zheng, C.-G.; Ma, C.-L.; Yu, X.-W.; Qian, Q.-L.; Song, Y.; Kong, J.; Xu, Y. *Chem. Biodivers.*, *8*, 1486.
- (152) Hotze, A. C. G.; Broekhuisen, M. E. T.; Velders, A. H.; Kooijman, H.; Spek, A. L.; Haasnoot, J. G.; Reedijk, J. *J. Chem. Soc. Dalton Trans.* **2002**, 2809.
- (153) Proudfoot, E. M.; Mackay, J. P.; Vagg, R. S.; Vickery, K. A.; Williams, P. A.; Karuso, P. *Chem. Commun.* **1997**, 1623.
- (154) Foley, F. M.; keene, F. R.; Collins, J. G. *J. Chem. Soc., Dalton Trans.* **2001**, 2968.
- (155) Hsi, R. A.; Rosenthal, D. I.; Glaststein, E. *Drugs.* **1999**, *57*, 725.
- (156) Pogozelski, W. K.; Tullius, T. D. *Chem. Rev.* **1998**, *98*, 1089.
- (157) Singh, T. N., PhD Thesis, The Ohio State University, *Ru(II) Complexes as Photoactivated Cisplatin Analogs*, 2006, 1 - 9, 14 - 33.
- (158) Fernandez, R.; Melchart, M.; Habtemariam, A.; Parsons, S.; Sadler, P. L. *Chem. Eur. J.* **2004**, *10*, 5173.
- (159) (a) Clarke, M. J.; Buchbinder, M.; Kelman, A. D. *Inorg. Chim. Acta.* **1978**, *27*, L87(b) Rodriguez-Bailey, V. M.; La Chance-Galang, K. J.; Doan, P. E.; Clarke, M. J. *Inorg. Chem.* **1997**, *36*, 1873
- (160) Khalaila, I.; Bergamo, A.; Bussy, F.; Sava, G.; Dyson *Int. J. Oncol.* **2006**, *29*, 261.
- (161) Brabec, V.; Nováková, O. *Drug Resist. Updates.* **2006**, *9*, 111.
- (162) Groessl, M.; Reisner, E.; Hartinger, C. G.; Eichinger, R.; Semenova, O.; Timerbaev, A. R.; Jakupec, M. A.; Arion, V. B.; Keppler, B. K. *J. Med. Chem.* **2007**, *50*, 2185.
- (163) Schluga, P.; Hartinger, C. G.; Egger, A.; Reisner, E.; Galanski, M.; Jakupec, M. A.; Keppler, B. K. *Dalton Trans.* **2006**, *14*, 1796.
- (164) Ang, W. H.; Dyson, P. J. *Eur. J. Inorg. Chem.* **2006**, 4003.
- (165) Chen, H. M.; Parkinson, J. A.; Parsons, S.; Coxall, R. A.; Gould, R. O.; Sadler, P. J. *J. Am. Chem. Soc.* **2002**, *124*, 3064.

- (166) Davies, N. R.; Mullins, T. L. *Aust. J. Chem.* **1967**, *20*, 657.
- (167) (a) Matsubara, T.; Creutz, C. *Inorg. Chem.* **1979**, *18*, 1956(b) Isied, S. S.; taube, H. *Inorg. Chem* **1976**, *15*, 3070.
- (168) Shepherd, R. E.; taube, H. *Inorg. Chem.* **1973**, *12*, 1392.
- (169) (a) Bajaj, H. C.; Van Eldik, R. *Inorg. Chem.* **1988**, *27*, 4052(b) Bajaj, H. C.; Van Eldik, R. *Inorg. Chem.* **1988**, *28*, 1980.
- (170) Dozsa, L.; Sutton, J. E.; taube, H. *Inorg. Chem.* **1982**, *21*, 3997.
- (171) Creutz, C.; Chou, M. H.; Hou, H.; Muckerman, J. T. *Inorg.Chem.* **2010**, *49*, 9809.
- (172) Ho, C.; Che, C. M.; Lau, T., *C J.Chem. Soc. Dalton Trans.* **1990**, 967.
- (173) Tiba, F.; Jaganyi, D.; Mambanda, A. *J. Coord. Chem.* **2010**, *63*, 2542.
- (174) Barton, J. K. *Science* **1986**, *233*, 727.
- (175) O'Reilly, F. M.; Kelly, J. M.; Kirsch- De Mesmaeker, A. *Chem. Commun.* **1996**, 1013.
- (176) Aldrich-Wright, J. R.; Brodie, C. R.; Glazer, E. C.; Luedtke, N. W.; Elson-Schwab, L.; Tor, Y. *Chem. Commun.* **2004**, 1018.
- (177) Lincoln, P.; Nordén, B. *Chem. Commun.* **1996**, 2145.
- (178) Jiang, C.-W. *Eur. J. Inorg. Chem.* **2004**, 2277.
- (179) van Gijte, O.; Kirsch-De Mesmaeker, A. *J. Chem. Soc. Dalton Trans.* **1999**, 951.
- (180) Van Houten, B.; Illenye, S.; Qu, Y.; Farrell, N. *Biochemistry.* **1993**, *32*, 11794.
- (181) (a) Bignozzi, C. A.; Scandola, F. *Inorg. Chem.* **1984**, *23*, 1540(b) Chow, C.-F.; Chiu, B. K. W.; Lam, M. H. W.; Wong, W.-Y. *J. Am. Chem. Soc.* **2003**, *125*, 7802(c) Swavey, S.; Fang, Z. L.; Brewer, K. J. *Inorg. Chem.* **2002**, *41*, 2598(d) Miao, R.; Mongelli, M. T.; Zigler, D. F.; Winkel, B. S. J.; Brewer, K. J. *Inorg. Chem.* **2006**, *45*, 10413(e) Higgins, S. L. H.; White, T. A.; Winkel, B. S. J.; Brewer, K. J. *Inorg. Chem.* **2011**, *50*, 463.
- (182) Qu, Y.; Farrell, N. *Inorg. Chem.* **1995**, *34*, 3573.
- (183) Milkevitch, M.; DShirley, B. W.; Brewer, K. J. *Inorg. Chim. Acta.* **1997**, *264*, 249.
- (184) Prussin, A. J.; Zhao, S.; Jain, A.; Winkel, B. S. J.; Brewer, K. J. *J. Inorg. Biochem.* **2009**, *103*, 427.
- (185) (a) Vogler, L. M.; Brewer, K. J. *Inorg. Chem.* **1996**, *35*, 818(b) Zhao, S.; Arachchige, S. M.; Slebodnick, C.; Brewer, K. J. *Inorg. Chem.* **2008**, *47*, 6144.
- (186) Clarke, M. J. *Prog. Clin. Biochem. Med.* **1989**, *10*, 25.
- (187) Suen, H. F.; Wilson, S. W.; Pomerantz, M.; Walsh, J. L. *Inorg. Chem.* **1988**, *28*, 786.

**Tables of Contents- 2**

List of Figures.....	ii
List of Tables.....	iii
List of Schemes .....	iii
Chapter Two .....	1
<b>Substitution Reaction Kinetics .....</b>	<b>1</b>
2.1 General Considerations .....	1
2.2 Mechanistic Classification of Inorganic Substitution Reactions.....	2
2.2.1 Limiting Associative Mechanism.....	3
2.2.2 Dissociative Mechanism.....	4
2.2.3 Interchange Mechanism.....	5
2.3 Substitution Reactions of Square Planar Platinum(II) Complexes.....	5
2.3.1 Kinetics and Mechanism of Substitution Reactions .....	7
2.4 Determining the Rates of Ligand Substitution Reactions .....	7
2.4.1 Reversible Second-Order Reactions .....	7
2.4.2 Activation Parameters.....	11
2.4.2.1 Measurement of enthalpy of activation ( $\Delta H^\ddagger$ ) and entropy of activation ( $\Delta S^\ddagger$ ) .....	11
2.4.2.2 Volume of Activation ( $\Delta V^\ddagger$ ) .....	13
2.4.3 Instrumental Techniques Used in Chemical Kinetics .....	14
2.4.3.1 UV/visible Spectrophotometry .....	15
2.4.4 Flow methods.....	19
2.4.4.1 Continuous flow method .....	20
2.4.4.2 Stopped-Flow Technique.....	20
2.5 Factors Influencing the Reactivity of Square Planar Platinum(II) Complexes ....	22
2.5.1 Effect of the Entering Group .....	22
2.5.2 The Effect of Leaving Group .....	26
2.5.3 Effect of Steric Hindrance.....	27
2.5.4 Effect of Solvent.....	29
2.5.5 Non-Participating Ligand .....	30
2.5.5.1 The <i>trans</i> Effect .....	30
i $\sigma$ - <i>trans</i> effect.....	33
ii $\pi$ - <i>trans</i> effect .....	36
2.5.5.2 <i>Cis</i> - Effect.....	36
2.6 References.....	38

## List of Figures

Figure 2.1	Reaction profiles for (a) associative $A$ , (b) associative interchange, $I_a$ , (c) dissociative interchange $I_d$ and (d) dissociative $D$ .....	3
Figure 2.2	Schematic representation of the energy profile and possible steric changes during an associative substitution of leaving group, X by the entering group, Y of a square planar complex: energies at 2, 4, 6, and 8 represent the transition states and the reaction intermediates would have energies shown at 3, 5 and 7.....	6
Figure 2.3	Schematic representation for substitution in $d^8$ four coordinate square planar complexes showing the alternative D and A or $I_a$ solvolysis.....	7
Figure 2.4	Dependence of the <i>pseudo</i> first-order rate constant ( $k_{obs}$ ) on the concentration of the nucleophiles for the chloride substitution from Pttpytgeg in methanol solution ( $I = 0.02$ M $LiCF_3SO_3$ , adjusted with LiCl) at 298 K.....	10
Figure 2.5	Schematic diagram of a UV/visible spectrophotometry setup.....	16
Figure 2.6	Photograph of a double-beam-in-space Varian Cary 100 Bio UV/visible spectrophotometer used by the University of KwaZulu Natal, Pietermaritzburg campus kinetics research group.....	17
Figure 2.7	Spectrum obtained from Cary UV/visible spectrophotometer for the substitution of $Cl^-$ from $[ClPt(tppz)Ru(tppz)PtCl](PF_6)_4$ ( $2.0 \times 10^{-5}$ M) by thiourea (0.0004 M) in methanol solution ( $I = 0.02$ M (adjusted with $LiCF_3SO_3$ and LiCl) at 383 nm and 298 K. ....	19
Figure 2.8	Diagrammatic representation of a continuous flow kinetic system. The letter $d$ represents the distance from the mixture to the point of observation. ....	20
Figure 2.9	Diagrammatic representation of stopped-flow apparatus.....	21
Figure 2.10	Photograph of the Applied Photophysics SX 20 stopped-flow system coupled to an online data acquisition system setup used by the University of KwaZulu Natal, Pietermaritzburg campus kinetics research group.....	22
Figure 2.11	Correlation of the rates of reaction of Pt(II) complexes with the standard <i>trans</i> - $Pt(py)_2Cl_2$ for different nucleophiles: •, <i>trans</i> - $Pt(PEt_3)_2Cl_2$ in methanol at 30 °C; ■, $Pt(en)Cl_2$ in water at 35 °C, produced from references. ....	26
Figure 2.12	The steric effect of the aryl square planar complex showing the steric bulk for the <i>cis</i> isomer blocking the attacking site. ....	29

Figure 2.13	$\pi$ -back donation of the electrons from the filled $d$ orbital to the vacant orbitals of the trans ligand in $\text{PtA}_2\text{LXY}$ . ....	32
Figure 2.14	Distribution of Charge induced dipoles in the $\text{L-Pt-X}$ coordinate of <i>trans</i> - $\text{PtA}_2\text{LX}$ . ....	33
Figure 2.15	Molecular orbital representation showing the relative orbital energies in $\text{PtCl}_4^{2-}$ .....	34
Figure 2.16	Representation of $\text{L-Pt-X}$ bonding using $\sigma_x$ MO (a) The $\sigma$ -bond strength of L and X are almost equal. (b) Strong $\sigma$ -donor ligand L, the $\sigma$ -bond strength of L is much greater than that of X. ....	35
Figure 2.17	The $\sigma$ - <i>trans</i> effect due to the stabilization of the trigonal bipyramidal intermediate. (a) Only one $p$ orbital is available for $\sigma$ -bond formation of L and X. (b) Two $p$ orbitals are available for the $\sigma$ -bonding of L, X and Y. ....	35

### List of Tables

Table 2.1	Some nucleophilic constants given for $\text{Pt}(\text{py})_2\text{Cl}_2$ with different nucleophiles of donor atoms.....	25
Table 2.2	Effects of leaving group on the rates of reaction of $\text{Pt}(\text{dien})$ complexes in water at 25 °C.....	27
Table 2.3	Rate constants and activation parameters for the substitution of $\text{Cl}^-$ by $\text{I}^-$ in $[\text{Pd}(\text{R}_n\text{dien})\text{Cl}]^+$ ( $n = 0, 3-5$ ) in aqueous solution at 25 °C.....	28
Table 2.4	Effect of solvent on the chloride exchange reaction ( <i>Equation 2.39</i> ) at 25 °C. ....	30

### List of Schemes

Scheme 2.1	Associative mode of substitution at the metal centre.....	3
------------	---	---

# Chapter Two

## Substitution Reaction Kinetics

### 2.1 General Considerations

A substitution reaction occurs when a ligand in a coordination sphere of a reactive centre is replaced by another molecule or an ion,<sup>1</sup> causing a temporary change in coordination number due to breaking of bonds and formation of new bonds with the incoming species.<sup>2</sup> Two important aspects need to be considered when describing substitution reactions. The first is based on the changes in the electron distribution that takes place during bond breaking and new bond making while the second aspect addresses the timing of the bond breaking and making processes.<sup>1</sup>

In the decisive work reported by Ingold and Hughes<sup>3</sup> the modes of bond breaking in a substitution reaction at a carbon centre were classified either as homolytic or heterolytic, depending on the type of bond breaking.<sup>1</sup> Homolytic bond breaking involves dividing the bonding electron pair evenly between the products such that each species gets an electron. Heterolytic reactions can be further subdivided into electrophilic or nucleophilic reactions. When the electron pair departs with the leaving group, it is classified as nucleophilic heterolysis. In electrophilic heterolysis, the electron pair remains in the reactive centre when the leaving group departs.<sup>1</sup> These reactions can be represented as:<sup>1-2</sup>



Although the method is adequate for describing substitutions on carbon centres, it can not meet most of the classification criteria for inorganic reaction mechanisms.<sup>2</sup> Inorganic reactions can be divided into electrophilic substitution ( $S_E$ ) or nucleophilic substitutions ( $S_N$ ), and the latter could be represented by  $S_N1$  or  $S_N2$  depending on the molecularity of the rate determining step of the mechanism.<sup>1,4</sup> Often most substitution reaction pathways are based on  $S_N1$  or  $S_N2$  mechanisms.<sup>4</sup>

## 2.2 Mechanistic Classification of Inorganic Substitution Reactions

A reaction mechanism illustrates the progress of different steps by which a chemical transformation occurs which culminates in the observed overall reaction.<sup>5</sup> Langford and Gray<sup>6</sup> used an operational way to classify inorganic reactions based on the concepts of stoichiometric mechanism and intimate mechanisms.<sup>2</sup> The stoichiometric mechanism can be determined from the kinetic behaviour and classified in one of the three forms.<sup>2,7</sup>

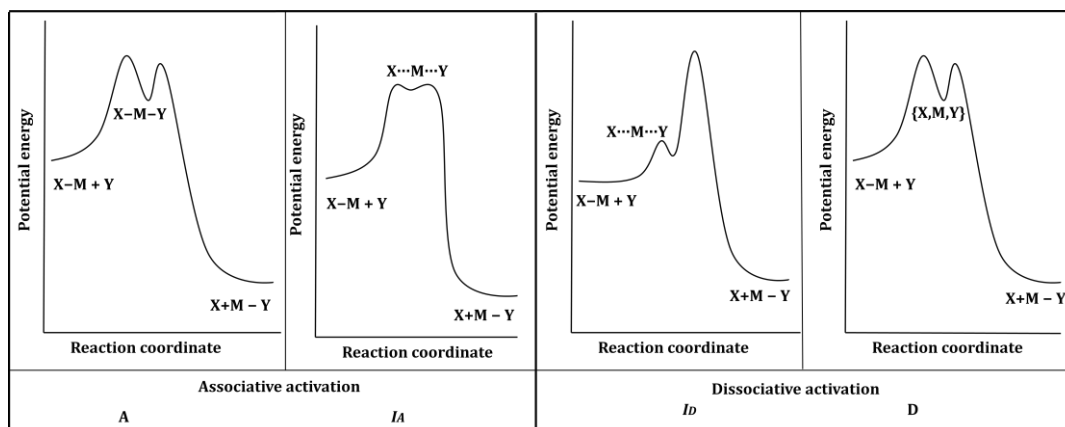
- a. **Limiting associative (A)**- a mechanism having an intermediate with higher coordination number. The 'A' term replaces the older  $S_N2$  term.
- b. **Limiting dissociative (D)**- a mechanism having an intermediate with lower coordination number. The 'D' term replaces the older  $S_N1$  term.
- c. **Interchange (I)**- a mechanism in which the bond breaking and bond forming take place in a pre-formed aggregate. No observable intermediate forms for this pathway.

The stoichiometric interchange mechanism is further classified based on intimacy:<sup>1-2</sup>

- a. **Associatively activated ( $I_A$ )** – an intimate mechanism which has a transition state which involve the bonding between the incoming group and the reactive centre.
- b. **Dissociatively activated ( $I_D$ )** – an intimate mechanism where no direct interaction between the reactive centre and the entering group in the transition state, *i.e.* the reaction centre is more sensitive to changes in the leaving group,

For the intimate mechanism, the incoming group, **Y**, and the leaving group, **X**, are interchanged in the inner coordination sphere of the metal centre. Therefore, the rate is independent of the incoming nucleophile and the relative reaction coordinates from associative to dissociative can be represented as in *Figure 2.1*.<sup>8</sup>



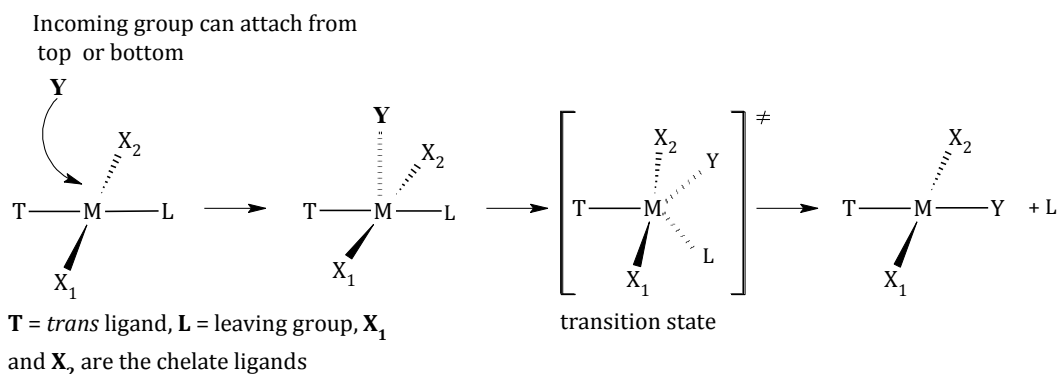


**Figure 2.1** Reaction profiles for (a) associative *A*, (b) associative interchange *I<sub>a</sub>*, (c) dissociative interchange *I<sub>d</sub>* and (d) dissociative *D*.<sup>8</sup>

### 2.2.1 Limiting Associative Mechanism

In this mechanism, the intermediate is formed *via* two transition states in which bond formation is more dominant than bond breaking (*Scheme 2.1*). Here, the rate determining step is one which involves formation of a bond between the metal centre and the incoming nucleophile. When the entering group, **Y**, and the leaving group, **X**, are chemically identical, the bond making and the bond breaking transition states have the same energy. In a non-coordinating medium and in the presence of an excess of **Y**, the substitution is strongly dependent on the nature of the incoming nucleophile. **Y** participates in the early stages of the transition state and at the end stereochemistry of the complex is retained.<sup>9</sup>

In an associative mechanism, all the species involved such as the incoming group, the leaving group and the chelate ligand can influence the stability and the activation energy of the reaction. Thus, all the groups will influence the rate of substitution reaction of the complex. For this reason many ligand substitution reactions are performed by varying the character of the ligands.<sup>10</sup>



**Scheme 2.1** Associative mode of substitution at the metal centre.<sup>11</sup>

It has been reported<sup>12</sup> that Pt(II) complexes containing strong *cis* Pt–C bonds result in the mechanistic changeover in Pt(II) complexes of the form *cis*-[Pt(L)<sub>2</sub>R<sub>2</sub>] (where L<sub>2</sub> = Me, Ph and R<sub>2</sub> = thioethers or DMSO). The *trans* effect due to the strong  $\sigma$ -donor increases the electron density at the Pt(II) centre and weakens the Pt–S bond length in case of DMSO. The fourteen-electron transition state intermediate is stabilized by the strong  $\sigma$ -donor carbene ligands. However, when one of the thioethers were replaced by a strong  $\pi$ -acceptor ligand such as CO or CN<sup>-</sup>, an associative mechanism was favoured for the Pt(II) complexes. The stronger  $\pi$ -accepting ligands remove the electron density from the metal centre thereby increasing the electrophilicity of the Pt(II) centre. This enhances the acceptance of the electron density from the incoming nucleophile and removing the added electron density from the metal centre in a five-coordinate transition state. Thus, the type of the reaction mechanism depends on the nature of the chelate ligand at the Pt(II) centre.

### 2.2.2 Dissociative Mechanism

Depending on the electronic and the steric effects, a dissociative pathway may be favoured by weakening of the metal-leaving group bond. In dissociative (D) mechanism, the bond between the leaving group and the metal breaks completely before incoming group attaches to the metal centre resulting in an intermediate with lower coordination number. This allows the intermediate to discriminate the potential ligands in the surrounding medium before it reacts with the entering group.<sup>9a</sup> The rate of reaction with the entering group depends on the nature of the leaving group and is independent of the concentration and the nature of the incoming group. The leaving group moves from the coordination shell, which favours the solvent attack as the solvent is present in large excess. Therefore, the formation of the product will occur while the leaving group is still in close proximity.

One of the important aspects of dissociative mechanism in square planar Pt(II) complexes is the non-stereo specific products formed. During dissociation mechanism, the complex forms a T-shaped three coordinate intermediate, which undergoes intermolecular rearrangements of '*cis*-like' configuration to a '*trans*-like' configuration. The mechanism is rare for square planar Pt(II) complexes because increase of electron density at the Pt(II) centre hinders the approach of the nucleophiles and stabilization of the coordinatively unsaturated 14-electron intermediate.<sup>12d</sup>

### 2.2.3 Interchange Mechanism

In between the limiting associative and limiting dissociative mechanisms, there exists a set of mechanisms which involves a single activated complex in which bond formation between the metal centre and the incoming nucleophile and bond breaking between the metal and the leaving group are concurrent. These mechanisms are considered as interchange mechanisms. They are:

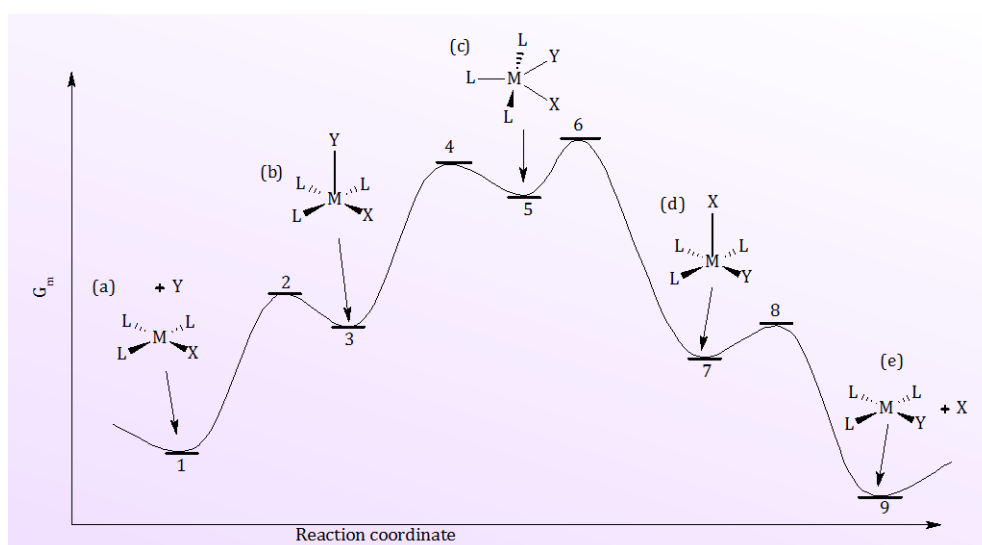
- i. *Associatively Activated Interchange Mechanism*: In this mechanism, the rate of reaction depends on the nature of the incoming species since the rate limiting step involves bond formation between the entering group and the reactive centre in the transition state. The bond breaking is less important even though the two steps co-exist leading to a single activated complex.<sup>13</sup>
- ii. *Dissociatively Activated Interchange Mechanism*: In a dissociatively activated mechanism, the leaving group starts to break away from the inner coordination sphere to the outer coordination sphere at the same time while the entering group moves from the outer coordination sphere to the inner coordination sphere. In this mechanism, if there is a reagent whose concentration is much less than that of the solvent which is already in the inner coordination sphere when the dissociation takes place, then the probability of the solvent attaching to the reactive metal centre is higher. Thus, the discrimination between the entering group and the solvent molecules is minimized.

## 2.3 Substitution Reactions of Square Planar Platinum(II) Complexes

A full understanding of four coordinate substitution reactions dates back to 1920s.<sup>13</sup> Square planar complexes often contain  $d^8$ , low-spin, 2+ oxidation state metal centres.<sup>9</sup> Common examples of square planar complexes include coordinated complexes commonly formed by Ni(II), Pd(II), Au(III), Rh(I) and Pt(II).<sup>9b</sup> Of these, substitution reactions of platinum are the most well studied and understood in inorganic reaction mechanisms due to its redox stability and moderately slow reactivity.<sup>14</sup> This allows the synthesis of specifically designed platinum complexes and investigation of their kinetic behaviour.<sup>2,9b,13,14b</sup> To date, appreciable amount of research has been reported on the kinetic and the mechanistic behaviour of substitution reactions of Pt(II) complexes.<sup>6,7b,13,14b</sup> Since the mechanism of substitution behaviour of Pt(II) is similar to other square planar  $d^8$ -metal complexes, the information collected on Pt(II) complexes can therefore be useful to the other  $d^8$ -metal complexes. For example, substitution

reactions of Pd(II) complexes are very similar to Pt(II)'s. However, Pd(II) complexes are often five order of magnitude faster than the Pt(II) analogues.<sup>15</sup>

During substitution, the coordinatively unsaturated square planar  $d^8$  Pt(II) metal complexes often undergo an associative mechanism which proceeds *via* a five coordinate, trigonal bipyramidal transition state having eighteen electrons in the valence shell.<sup>16</sup> Pt(II)  $d^8$  complexes have vacant  $6p_z$  orbitals which can easily accommodate the extra electrons from the incoming nucleophile.<sup>2,9b,14b</sup> Moreover, square planar complexes being four coordinate, are not sterically hindered. Thus, the incoming ligand can approach the metal centre both from above and below the plane, retaining the stereochemistry of the complex as shown in *Figure 2.2(e)*.<sup>7b</sup>



**Figure 2.2** Schematic representation of the energy profile and possible steric changes during an associative substitution of leaving group, X by the entering group, Y of a square planar complex: energies at 2, 4, 6, and 8 represent the transition states and the reaction intermediates would have energies shown at 3, 5 and 7.<sup>7b,17</sup>

Therefore, the incoming ligand binds to the metal centre before the leaving group leaves, resulting in a trigonal bipyramidal complex<sup>7b,9b,13</sup> (*Figure 2.2, c*). Although an associative mechanism is more common for square planar complexes, recently, some dissociative mechanisms for square planar complexes have been also reported.<sup>12a,12d,18</sup>

### 2.3.1 Kinetics and Mechanism of Substitution Reactions

The nature of the reactants and the solvent play an important role during the substitution reactions of Pt(II) complexes. The substitution kinetics of square planar complexes may take place in any one of the three pathways shown in Figure 2.3.<sup>2</sup> This involves an associative pathway either by direct attack of the nucleophile or the solvent and a dissociative pathway which involves a three coordinate intermediate.<sup>2</sup>

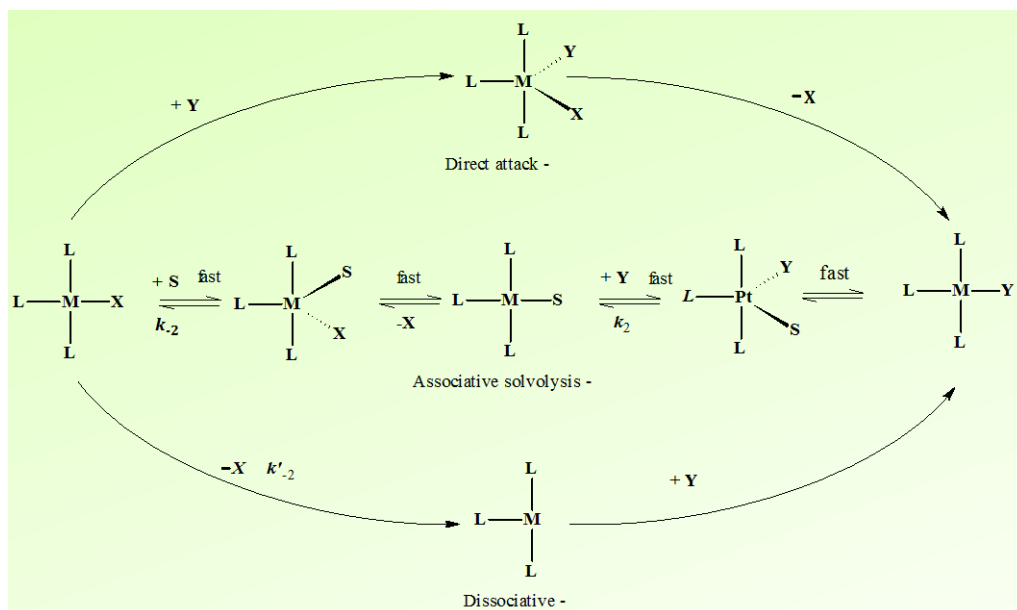
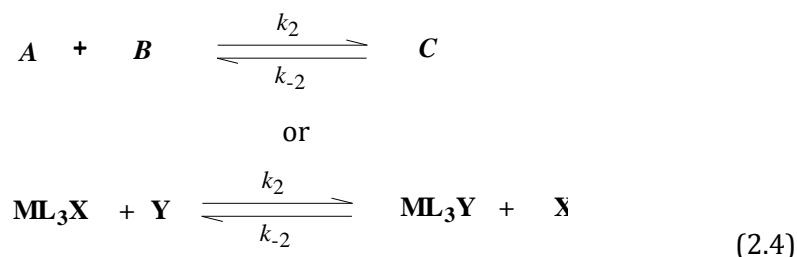


Figure 2.3 Schematic representation for substitution in  $d^8$  four coordinate square planar complexes showing the alternative D and A or  $I_a$  solvolysis.<sup>2</sup>

## 2.4 Determining the Rates of Ligand Substitution Reactions

### 2.4.1 Reversible Second-Order Reactions

Second-order reactions may not always go to completion but rather may attain equilibrium as represented below



where, A = metal complex ( $\text{ML}_3\text{X}$ ), X is the leaving group

B = incoming nucleophile, Y

$k_2$  = second-order rate constant

$k_{-2}$  = observed first-order rate constant for the reverse reaction

The reaction involves a mixed-order behaviour where the forward reaction is second-order and the reverse reaction is first-order. Therefore, to resolve the complexity, *pseudo* first-order conditions is applied for the forward reaction where  $[B]_0 \gg [A]_0$ . Thus, the equation can then be simplified to reversible first-order reaction.

The rate of formation of  $C$  can be expressed as:

$$-\frac{d[A]}{dt} = -\frac{d[B]}{dt} = \frac{d[C]}{dt} = k_2[A]_t[B]_t - k_{-2}[C]_t \quad (2.5)$$

Taking the stoichiometric ratio of the reaction as 1:1:, the mass balances at any time,  $t$  can be written as

$$[A]_t = [A]_0 - [C]_t \text{ and } [B]_t = [B]_0 - [C]_t \quad (2.6)$$

At equilibrium the mass balance becomes:

$$[A]_{eqm} = [A]_0 - [C]_{eqm} \text{ and } [B]_{eqm} = [B]_0 - [C]_{eqm} \quad (2.7)$$

Also at equilibrium the two opposing reactions take place at the same rate. That is,

$$-\frac{d[A]}{dt} = k_2[A]_{eqm}[B]_{eqm} - k_{-2}[C]_{eqm} = 0 \quad (2.8)$$

hence,

$$k_2[A]_{eqm}[B]_{eqm} = k_{-2}[C]_{eqm} \quad (2.9)$$

Using *Equation 2.7* and *Equation 2.9*, the following equation can be obtained

$$k_2[A]_{eqm}[B]_{eqm} = k_{-2}([A]_0 - [A]_{eqm}) \quad (2.10)$$

Thus, rearranging *Equation 2.10* leads to

$$k_{-2}[A]_0 = k_2[A]_{eqm}[B]_{eqm} + k_{-2}[A]_{eqm} \quad (2.11)$$

Substituting *Equation 2.6* for  $[C]_t$  and substituting into *Equation 2.5* gives

$$\begin{aligned} -\frac{d[A]}{dt} &= k_2[A]_t[B]_t - k_{-2}([A]_0 - [A]_t) \\ &= k_2[A]_t[B]_t - k_{-2}[A]_0 = k_{-2}[A]_t \end{aligned} \quad (2.12)$$

Combining *Equations 2.11* and *Equation 2.12* gives:

$$-\frac{d[A]}{dt} = k_2[A]_t[B]_t - k_2[A]_{eqm}[B]_{eqm} - k_{-2}[A]_{eqm} + k_{-2}[A]_t \quad (2.13)$$

Substitution of  $[B]_t$  and  $[B]_{eqm}$  according to *Equations 2.6* and *2.7* and approximating that  $k_2[A]_t[A]_0 \approx k_2[A]_{eqm}[A]_0$  and  $k_2[A]_t^2 \approx k_2[A]_{eqm}^2$  leads to

$$\begin{aligned} -\frac{d[A]}{dt} &= k_2[A]_t[B]_0 - k_2[A]_{eqm}[B]_0 - k_{-2}[A]_{eqm} + k_{-2}[A]_t \\ &= (k_2[B]_0 + k_{-2})([A]_t - [A]_{eqm}) \end{aligned} \quad (2.14)$$

Rewriting *Equation 2.14* followed by integration leads to

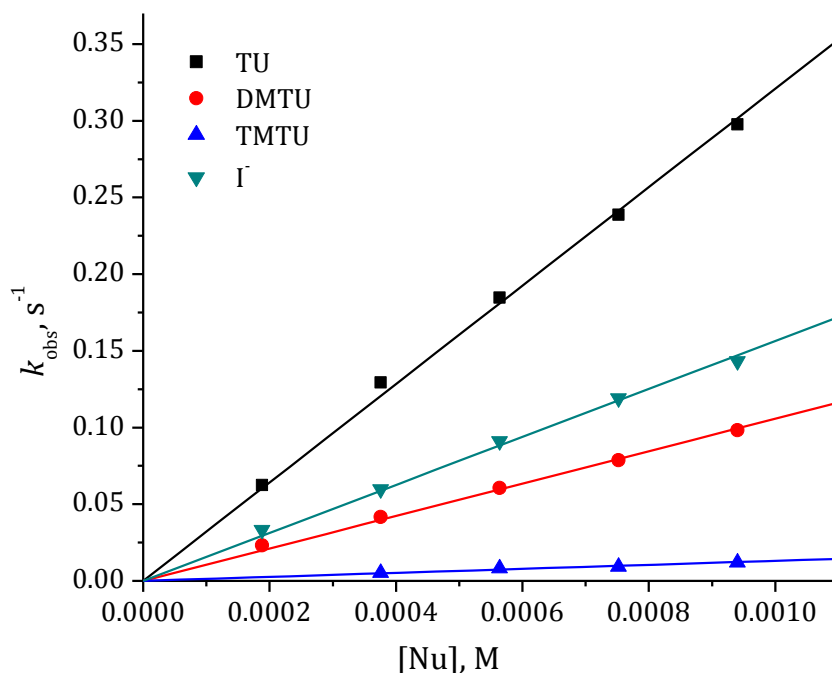
$$\begin{aligned} \int_{[A]_0}^{[A]_t} \frac{d[A]}{([A]_t - [A]_{eqm})} &= -(k_2[B]_0 + k_{-2}) \int_0^t dt \\ \ln \left( \frac{[A]_t - [A]_{eqm}}{[A]_0 - [A]_{eqm}} \right) &= -(k_2[B]_0 + k_{-2})t \\ &= -k_{obs}t \end{aligned} \quad (2.15)$$

$$\text{where } k_{obs} = k_2[B]_0 + k_{-2}$$

$k_{obs}$  = observed first-order or observed pseudo first-order rate constant

$[B]_0$  = is the initial concentration of the nucleophile.

Thus, plotting  $k_{obs}$  against  $[B]_0$  gives a straight line with a slope of  $k_2$  and an intercept of  $k_{-2}$ . The ratio of  $k_2/k_{-2}$  gives the equilibrium constant,  $K$ , which is a measure of the thermodynamic equilibrium position of the reaction.<sup>19</sup> *Figure 2.4* shows an example of such plots obtained for the substitution reaction of **Pttpytteg** with different nucleophiles (where tpy is 2,2':6',2''-terpyridine and tteg is tetraethylene glycoxy ether).



**Figure 2.4** Dependence of the *pseudo* first-order rate constant ( $k_{obs}$ ) on the concentration of the nucleophiles for the chloride substitution from Ptptpyteg in methanol solution ( $I = 0.02$  M  $LiCF_3SO_3$ , adjusted with  $LiCl$ ) at 298 K.

From Figure 2.4, it can be seen that  $k_2$  is sensitive to the nature of the entering nucleophile as this is a nucleophile dependent path.<sup>14a</sup> A plot which passes through zero implies that the forward reaction is irreversible and goes to completion. Noteworthy is that a positive intercept may also be attributed to the reverse reaction or a parallel solvolysis.<sup>20</sup> Some kinetic studies are carried out in coordinating solvents<sup>2,15</sup> such as water and methanol which are present in large excess. In cases where the contribution from the reverse reaction is negligible, then  $k_2$  term can be ascribed as a measure of the solvolysis pathway.<sup>9b,13,14b</sup> This solvent associated pathway has been reported<sup>21</sup> for the substitution kinetics of several square planar complexes.

As mentioned earlier, associative substitution reactions of square planar Pt(II) complexes are just order with respect to both the metal complex and the nucleophile. However, in order to simplify the kinetics of substitution of Pt(II) complexes, *pseudo* first-order conditions are adopted by keeping the concentration of the nucleophile at least 10 fold greater than that of the metal complex in order to force the reaction to go to completion. This simplifies the concentration dependence of rate to first order.

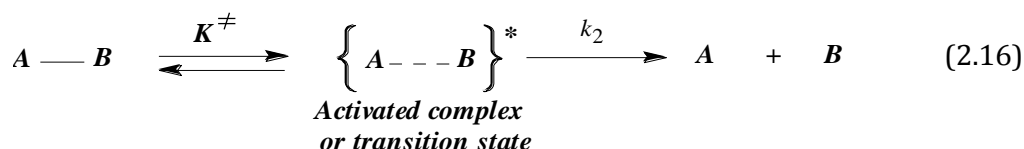


### 2.4.2 Activation Parameters

The temperature dependence of a rate constant is often studied to determine the reaction's activation parameters.<sup>4,7c,9b</sup> In inorganic reactions, this is important in assigning the mechanism that the reaction undergoes. The enthalpy of activation ( $\Delta H^\ddagger$ ) and entropy of activation ( $\Delta S^\ddagger$ ) are determined as stipulated in the Transition State Theory.<sup>4,9b</sup> Practically, to measure  $\Delta H^\ddagger$  and  $\Delta S^\ddagger$ , the observed second-order rate constant is measured at various temperatures. The third activation parameter, volume of activation,  $\Delta V^\ddagger$  is measured by varying the pressure of the reaction medium. The activation parameters along with the second-order rate constants obtained can therefore be used to postulate the reaction mechanism of the system.

#### 2.4.2.1 Measurement of enthalpy of activation ( $\Delta H^\ddagger$ ) and entropy of activation ( $\Delta S^\ddagger$ )

According to the Transition State Theory many reactions occur *via* a formation of a pre-equilibrium between the reactants and the activated transition state complex which is in equilibrium with the reactants and can be described as follows<sup>7b,c,22</sup>



The reaction rate can thus be written as

$$\begin{aligned} -\frac{d[A]}{dt} &= \frac{k_b T}{h} [A \cdots B]^* \\ &= \frac{k_b T}{h} K^\ddagger [A][B] \end{aligned} \quad (2.17)$$

where  $k_b$  = Boltzmann constant ( $1.38 \times 10^{-23} \text{ J K}^{-1}$ ) and  $h$  = Planck's constant ( $6.62 \times 10^{-34} \text{ J s}^{-1}$ ).

The experimental second-order rate constant,  $k_2$  can be written as

$$k_2 = \frac{k_b T}{h} K^\ddagger \quad (2.18)$$

The Gibbs free energy of activation,  $\Delta G^\ddagger$ , is expressed as

$$\Delta G^\ddagger = -RT \ln K^\ddagger = \Delta H^\ddagger - T\Delta S^\ddagger$$

(2.19)

Substituting Equation 2.19 into Equation 2.18 gives

$$k_2 = \frac{k_b T}{h} e^{\left(\frac{-\Delta G^\ddagger}{RT}\right)} = \frac{k_b T}{h} e^{\left(\frac{-\Delta H^\ddagger}{RT}\right)} e^{\left(\frac{\Delta S^\ddagger}{R}\right)}$$

(2.20)

Rearranging and taking logarithm results in

$$\ln\left(\frac{k_2}{T}\right) = \frac{-\Delta H^\ddagger}{RT} + \left[ \ln\left(\frac{k_b}{h} + \frac{\Delta S^\ddagger}{R}\right) \right]$$

(2.21)

Subsequent linearization affords

$$\ln\left(\frac{k_2}{T}\right) = \frac{-\Delta H^\ddagger}{R} \cdot \frac{1}{T} + \left[ 23.8 + \frac{\Delta S^\ddagger}{R} \right]$$

(2.22)

Equation 2.22 is in the form  $y = mx + c$ . A plot of  $\ln(k_2/T)$  against  $1/T$  is linear with a slope from which the enthalpy of activation,  $\Delta H^\ddagger$  can be calculated. The entropy of activation,  $\Delta S^\ddagger$  can be determined from the y-intercept. This plot is generally known as Eyring plot.<sup>7b,9b,23</sup> The magnitude of the two activation parameters can be used to assign the reaction mechanism. In an associatively activated mechanism, the value of  $\Delta H^\ddagger$  tend to be relatively small while  $\Delta S^\ddagger$  are normally negative compared to a dissociatively activated mechanism where the  $\Delta H^\ddagger$  is large and  $\Delta S^\ddagger$  is positive.<sup>2</sup> If the mechanism of the reaction is assigned solely based on the activation parameters, it is necessary to draw such a conclusion from kinetic data taken from several nucleophiles. A drawback is that  $\Delta S^\ddagger$  is obtained from the intercept by extrapolating the graph to infinite temperatures. The error associated with its determination is usually three times higher than that of  $\Delta H^\ddagger$ .<sup>24</sup> Thus, a more reliable parameter in assigning a reaction mechanism is the volume of activation, ( $\Delta V^\ddagger$ ) which can be determined by the measurements of the bimolecular rate constants,  $k_2$  when the pressure of the medium is varied.<sup>25</sup> However, to make a meaningful assignment on the mode of activation, the sign and the magnitude of the two activation parameters, *i.e.*  $\Delta H^\ddagger$  and  $\Delta S^\ddagger$ , are crucial.

### 2.4.2.2 Volume of Activation ( $\Delta V^\ddagger$ )

The volume of activation is an important parameter for elucidating the underlying reaction mechanisms. The volume of activation represents the change in partial volume on moving from reactants to the transition state of the reaction, in such a way that the volume profile of the reaction can be analysed in terms of the changes in volume of the reactant.<sup>26</sup> If the reaction mechanism is associative, this change in volume is greater than one. The activation volume is determined from a series of observed rate constants,  $k_{\text{obs}}$ , obtained at different applied pressures.<sup>2,24</sup> It is a useful supplement to the activation parameters ( $\Delta S^\ddagger$  and  $\Delta H^\ddagger$ ).

The thermodynamic equation:

$$dG = -SdT + VdP \quad (2.23)$$

the partial derivatives can be written as:

$$\left( \frac{d\Delta G^\circ}{dP} \right)_T = \Delta V^\circ \quad (2.24)$$

where  $V^\circ$  is the difference in partial molar volume between products and reactants.

Since

$\Delta G = -RT \ln K$ , Equation 2.24 can be written as:

$$\left( \frac{d \ln k_2}{dP} \right)_T \frac{d(\ln k)}{dP} = \left( \frac{-d \frac{\Delta G^\circ}{(RT)}}{dP} \right)_T - \frac{\Delta V^\circ}{RT} \quad (2.25)$$

Since the equilibrium constant,  $K = k_2/k_{-2}$ , the expression can be written as:

$$\frac{d(\ln k_2)}{dP} = \frac{\Delta V^\ddagger}{RT} \quad (2.26)$$

where  $\Delta V^\ddagger$  is the volume of activation for the forward reaction and it the difference in the molar volumes of the activated complex and the reactant under the experimental conditions. Integrating both sides within an applied pressure range of  $P = 0$  to  $P = P$ ,  $k_2 = (k_2)_0$  to  $k_2$  gives

$$\ln k_2 = \ln(k_2)_0 - \frac{\Delta V^\ddagger}{RT} P \text{ and is in the form } y = c - mx \quad (2.27)$$

where  $(k_2)_0$  is the rate constant at zero pressure (coefficient compressibility of the solvent).

A plot of  $\ln k_2$  verses  $P$  gives a straight line with a slope of  $-\frac{\Delta V^\ddagger}{RT}$ . The value of  $\Delta V^\ddagger$  is a combination of both an intrinsic contribution ( $\Delta V_{\text{int}}^\ddagger$ ) due to changes in internuclear distances within the reactants in forming the transition state and an electrostrictive contribution ( $\Delta V_{\text{elec}}^\ddagger$ ).<sup>27</sup> Ligand substitution reactions involving charged species,  $\Delta V_{\text{elec}}^\ddagger$  may be dominated by changes in charge occurring during the reaction. For the solvent exchange interpretations the  $\Delta V_{\text{elec}}^\ddagger$  term is absent and  $\Delta V^\ddagger$  is due to the activation step for bond making.<sup>27</sup> A positive value of  $\Delta V^\ddagger$  indicates a dissociative mechanism while a negative value means the mechanism is associative. The errors associated with volume of activation are relatively small compared to  $\Delta S^\ddagger$  since the activation volumes are determined from the slope of the graph. Thus, to have an appreciable effect on the rate of reaction, a high pressure (100 - 200 MPa) is required. Recently, Jaganyi *et al.*<sup>28</sup> and van Eldik *et al.*<sup>29</sup> reported  $\Delta V^\ddagger$  for mechanistic investigations of ligand substitution reactions.

### 2.4.3 Instrumental Techniques Used in Chemical Kinetics

Kinetic investigations are normally performed by monitoring the dependence of a physical variable such as pressure, pH, conductivity, absorbance and density<sup>30</sup> which is proportional to the concentration of the products or the reactants as a function of time. The data is then analyzed by fitting to an appropriate model to determine the rate constant.<sup>9b</sup> A number of different techniques such as nuclear magnetic resonance (NMR), UV/visible spectrophotometry and pulsed methods are used to study the rate of reactions.<sup>23</sup> However, the choice of technique used to follow the kinetics depends on the nature and rapidity of the reaction.<sup>31</sup> Regardless of the technique employed, the physical property measured must be proportional to concentration as a function of time after mixing. The reactants must be mixed in the shortest time possible within the time scale of the reaction. The physical conditions such as temperature and pressure must be controlled accurately.

A chemical reaction is generally considered as fast if 50% of the reaction completes in 10 seconds or less.<sup>31</sup> Kinetic studies of very fast reactions such as reactions involving proton transfer, enzymes and non-covalent complex formation,<sup>23</sup> that lie outside the time frame of the normal laboratory operations are studied using specialised techniques and instruments. Normally, for fast reactions, the time varies from 1 minute to  $10^{-14}$  seconds.<sup>24</sup> One approach of analysing fast reactions is to bring their rates into the conventional time range by changing the conditions such as temperature, concentration or the solvent which is reliable only if the half-life is greater than 1 hour.<sup>32</sup> The two main methods often used to study fast reactions include flow methods and pulse methods.<sup>23</sup>

Sufficiently slow reactions are often studied using conventional methods such as UV/visible spectrophotometry which involve first mixing of the reagents and then determining the decrease in the concentration of the reactant(s) or the increase in the concentration of the product(s) with respect to time. Thus, the time taken to mix the reagents and take the necessary measurements should be short enough so that it does not interfere with the actual rate of the reaction. Despite the number of methods available,<sup>23</sup> only the techniques of UV/visible absorption spectrophotometry and the stopped-flow method would be highlighted in this thesis.

#### **2.4.3.1 UV/visible Spectrophotometry**

A substitution reaction which is slow (a reaction which generally takes longer than 16 minutes) are monitored using UV/visible spectrophotometer. UV/visible spectrophotometry is a sensitive technique<sup>14b</sup> which can detect the sample concentrations ranging from  $10^{-4}$  to  $10^{-6}$  mol dm<sup>-3</sup>.<sup>32</sup> The instrument comprises of two light sources, one in the visible (tungsten lamp, 800 to 400 nm) and the other in ultra-violet (deuterium lam, 400 - 200 nm), monochromator, reference and sample compartment, temperature control unit, detector, the data processor and the output-readout system.<sup>31</sup> The commonly used detector is a photomultiplier tube. In a UV/visible spectrophotometer, radiation from the light sources is passed through a monochromator. The light gets dispersed by the grating prisms and the monochromator allows a particular wavelength to pass through. The light of the single wavelength with intensity,  $I_0$ , passes through the sample cell called a cuvette of length,  $l$  where the sample absorbs some light. Modern spectrophotometers are based on a double-beam design where it manages the light alternatively to pass through the sample cell and the reference cell using a chopper which is a motor that rotates a

mirror into and out of the light path.<sup>31,33</sup> The basic set-up of the UV/visible spectrophotometer is illustrated in *Figure 2.5* while the photograph is as shown in *Figure 2.6*.<sup>34</sup>

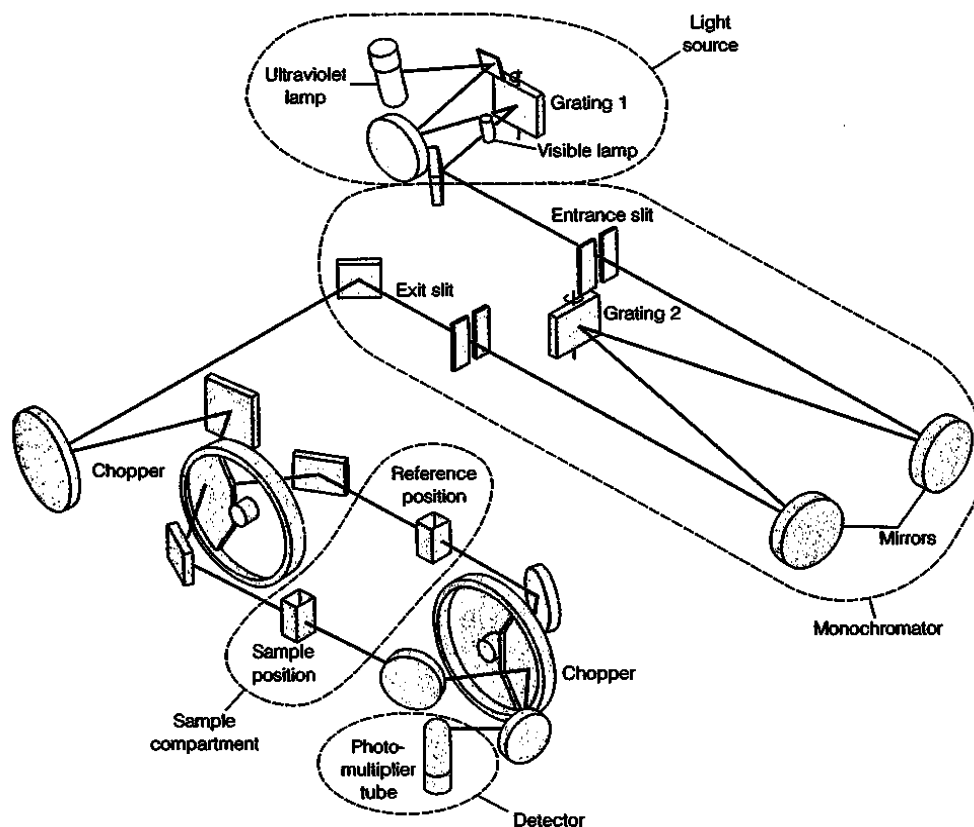
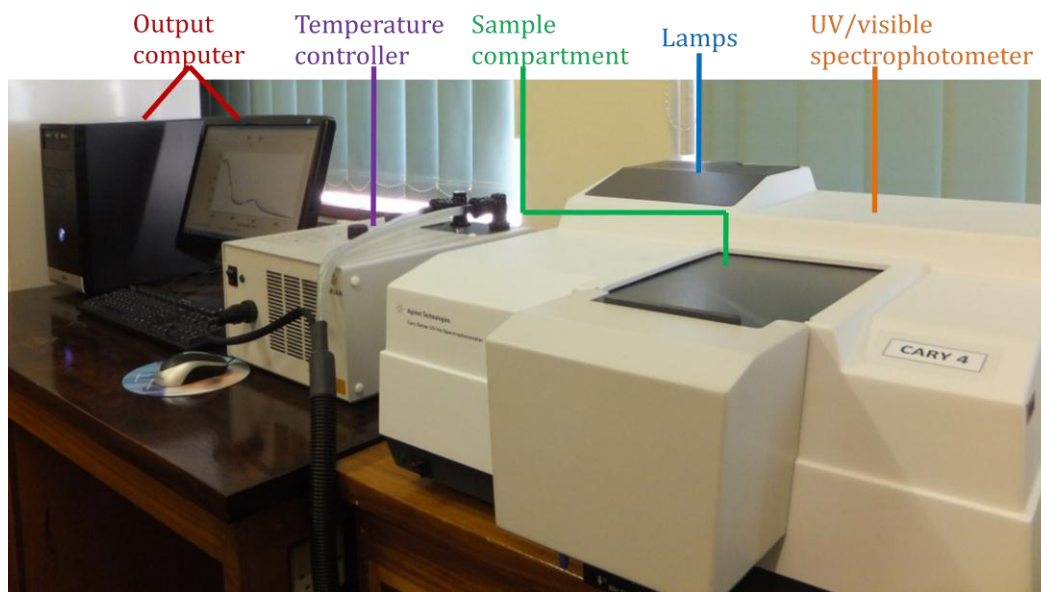


Figure 2.5 Schematic diagram of a UV/visible spectrophotometry setup.<sup>34</sup>



**Figure 2.6** Photograph of a double-beam-in-space Varian Cary 100 Bio UV/visible spectrophotometer used by the University of KwaZulu Natal, Pietermaritzburg campus kinetics research group.

The spectrophotometer measures the transmitted light ( $T$ ) from the sample which can be represented as

$$T = \frac{I_0}{I} \quad (2.28)$$

where  $I_0$  is the intensity of the incident light and  $I$  is the intensity of the transmitted light.

The transmittance is converted into absorbance by use of Equation 2.29 and is displayed on the screen.

$$A = -\log T \quad (2.29)$$

In Beer's law (Equation 2.30), concentration of the sample is directly proportional to the absorbance and thus, can be determined from its absorbance.<sup>31</sup>

$$A = \epsilon cl \quad (2.30)$$

where  $A$  is the absorbance,  $\epsilon$  is the molar absorptivity in  $\text{mol}^{-1} \text{ dm}^3 \text{ cm}^{-1}$ ,  $c$  is the concentration in  $\text{mol dm}^{-3}$  and  $l$  is the path length in cm (1 cm).

For a simple first-order reaction,



The absorption at any time  $t$ , ( $A_t$ ) is

$$A_t = \varepsilon_X [X] + \varepsilon_Y [Y] \quad (2.32)$$

where  $\varepsilon_X, \varepsilon_Y$  = molar absorptivity of  $X$  and  $Y$  respectively

Upon completion of the reaction, the absorption is given by

$$A_\infty = \varepsilon_X [X]_0 + \varepsilon_Y [Y]_0 \quad (2.33)$$

where  $A_\infty$  = absorbance at infinity

$[X]_0$  and  $[Y]_0$  = initial concentration of  $X$  and  $Y$  respectively

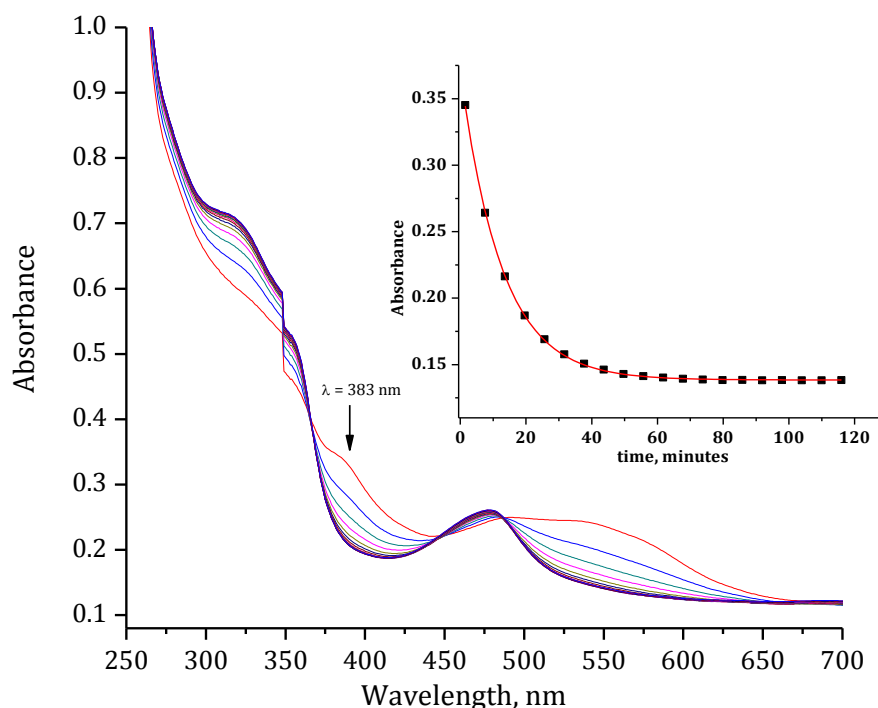
For the kinetic analysis, absorbance can be obtained from the following equation

$$\ln \frac{[X]_0}{[X]_t} = \ln \left( \frac{A_0 - A_\infty}{A_t - A_\infty} \right) = k_1 t \quad (2.34)$$

The observed rate constant for the reaction can be obtained by a least squares fit of the observed absorbance versus time trace at a specific wavelength. The second-order rate constant for the reaction is obtained by monitoring the reaction at different concentrations. The reactions can also be performed at different temperatures to determine the activation parameters.

*Figure 2.7* shows the reaction profile obtained for the substitution of  $[\text{ClPt}(\text{tppz})\text{Ru}(\text{tppz})\text{PtCl}](\text{PF}_6)_4$  (where  $\text{tppz}$  = tetra-2-pyridyl-1,4-pyrazine) with thiourea. The kinetics for the reaction was studied at 383 nm and the kinetic trace obtained for the reaction at 298 K is shown as an inset in *Figure 2.7*. The rate constant for the reaction was obtained by fitting first-order exponential decay function using Origin 7.5®.<sup>35</sup>





**Figure 2.7** Spectrum obtained from Cary UV/visible spectrophotometer for the substitution of  $\text{Cl}^-$  from  $[\text{ClPt}(\text{tppz})\text{Ru}(\text{tppz})\text{PtCl}](\text{PF}_6)_4$  ( $2.0 \times 10^{-5} \text{ M}$ ) by thiourea ( $0.0004 \text{ M}$ ) in methanol solution ( $I = 0.02 \text{ M}$  (adjusted with  $\text{LiCF}_3\text{SO}_3$  and  $\text{LiCl}$ ) at  $383 \text{ nm}$  and  $298 \text{ K}$ .

Apart from its use in the direct monitoring of conventionally slow kinetics of ligand substitution reactions, UV/visible spectroscopy is also used to perform UV/visible spectroscopic titrations to determine the  $\text{pK}_a$  values of the coordinated protic ligands such as aqua ligands. In such titrations, the aqua complex is titrated against a suitable strong base and the resulting change in the absorbance is spectroscopically monitored. By analysing the data obtained at a specific wavelength, the  $\text{pK}_a$  values for the complex are obtained. Such thermodynamic  $\text{pK}_a$  values of the coordinated aqua ligands are important for probing the electrophilicity of the metal complexes as reported by Jaganyi *et al.*<sup>36</sup> and van Eldik *et al.*<sup>29,36a,b,37</sup> An example of a spectroscopic titration spectrum is given in **Chapter 4**, *Figure 4.2*.

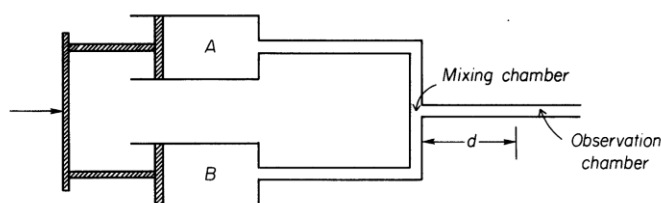
#### 2.4.4 Flow methods

Chemical reactions which are too fast to study using absorption spectrophotometry are analysed using flow methods pioneered by Hartridge and Roughton.<sup>9b</sup> The mixing time of flow methods varies approximately from  $1 \text{ ms}$  to  $10 \text{ seconds}$ . Fast reactions with half-lives of about  $10^{-2} \text{ seconds}$  are normally followed by flow methods.<sup>31</sup> In flow

methods two reactant solutions are rapidly mixed under pressure in a reaction mixing chamber. Concentrations of the reactants or products are then measured at various time intervals at different positions of the tube. The most common types of flow methods are continuous flow method and stopped-flow method.

#### 2.4.4.1 Continuous flow method

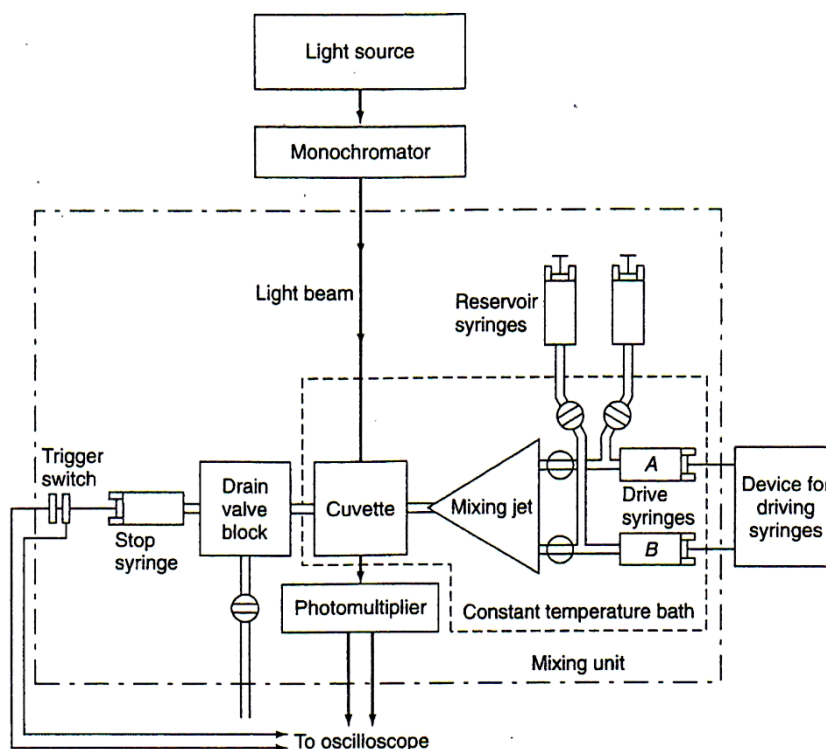
This technique is used to study rapid reactions (which take less than one second) in solution.<sup>30</sup> This method works on the idea where the two reacting solution (A and B, *Figure 2.8*) are forced into the mixing chamber by the pistons and the resulting solution then flows through the observation tube, where it gets spectroscopically detected at a specific distance ( $d$ ) from the mixer where a steady state is attained. This method requires a larger amount of solutions. The use of stopped-flow reaction technique is an alternative to overcome this problem.<sup>30</sup>



**Figure 2.8** Diagrammatic representation of a continuous flow kinetic system. The letter  $d$  represents the distance from the mixture to the point of observation.<sup>38</sup>

#### 2.4.4.2 Stopped-Flow Technique

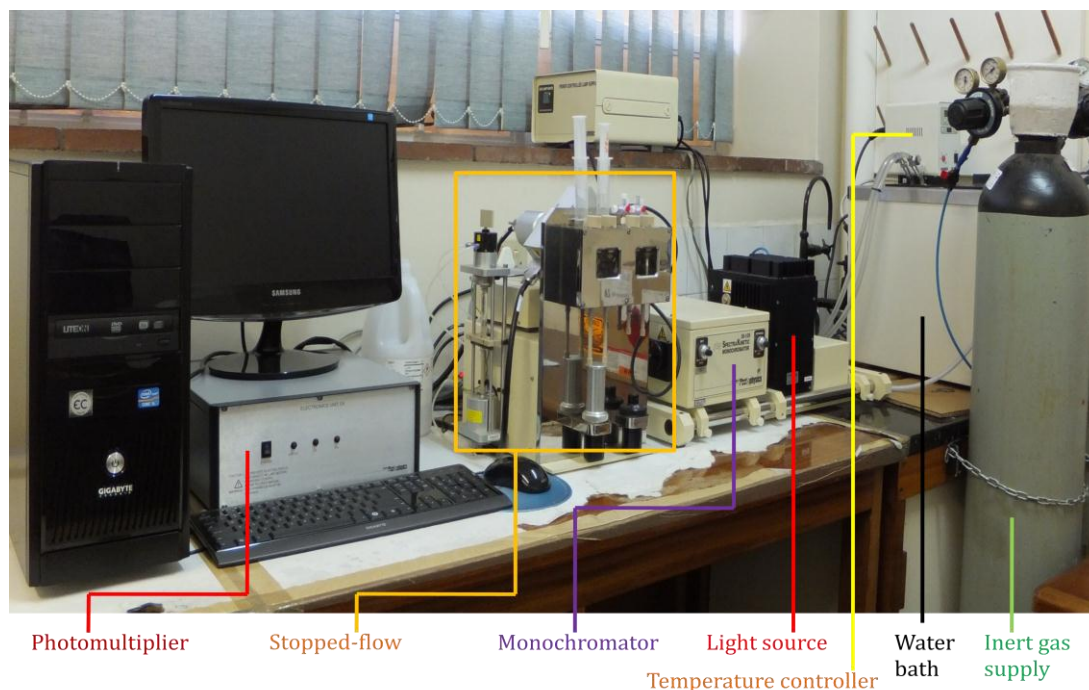
The stopped-flow technique is the most popular for studying reactions which are very fast and having a half-life range of about  $10^0$  to  $10^3$  seconds.<sup>31</sup> A schematic diagram of the stopped-flow technique is shown in *Figure 2.9* and a photograph of SX 20 stopped-flow spectrophotometer is shown in *Figure 2.10*.



**Figure 2.9** Diagrammatic representation of stopped-flow apparatus.<sup>23</sup>

The apparatus is designed to study a reaction between two substances in solution where one of the reactant is placed in drive syringe **A** and the other in syringe **B** and equilibrated at the desired temperature. The reactants are then charged into the mixing chamber by a compressed gas-driven piston (800 kPa) where they get mixed rapidly in about 0.001 seconds.<sup>31</sup> The reaction solution then goes into the stop syringe, causing the plunger to strike the stop block which ceases the flow of solution thereby leaving the solution of the reaction mixture in the observation cell.<sup>14b,23,31</sup> UV/visible spectrophotometry is the most commonly used detector for the reaction analyzer. The amount of light transmitted through the observation chamber in a given wavelength is measured as the reaction goes to completion. The transmitted light is converted into electric current by the photomultiplier. The computer computes and interprets the data as a kinetic trace of absorbance verses time.<sup>14b,23,31</sup>

Some advantages of stopped-flow technique includes its capacity to measure very fast reactions constants and the analysis require only a very small amount of sample ( $\approx 0.2$  mL).<sup>14b</sup>



**Figure 2.10** Photograph of the Applied Photophysics SX 20 stopped-flow system coupled to an online data acquisition system setup used by the University of KwaZulu Natal, Pietermaritzburg campus kinetics research group.

## 2.5 Factors Influencing the Reactivity of Square Planar Platinum(II) Complexes

The magnitude of rate constants of square planar Pt(II) complexes depend on a number of factors. Some of these factors will be discussed here in detail.

### 2.5.1 Effect of the Entering Group

It is well understood that in an associative substitution reaction mechanism, the second order rate constant,  $k_2$  is dependent on the nucleophilicity of the entering group. Nucleophilicity is a measure of how readily a nucleophile can attack an electron deficient centre such as Pt(II). Thus, the stronger the nucleophile, the faster the rate at which the substitution occurs.<sup>9b</sup>

The nucleophilicity of the ligand is often influenced by several factors:<sup>7b</sup>

- (a) Polarisability: Polarisability is an important aspect for the rates than for equilibria<sup>14a</sup> which is often explained by using Pearson's "Hard Soft Acid Base" †(HSAB) theory.<sup>7b,39</sup> Increasing polarisability of the metal centre increases the effectiveness of the incoming nucleophile.
- (b) Basicity: The basicity of a nucleophile depends on its  $pK_a$  which often correlates with the nucleophilicity of the entering nucleophile towards the metal centre. The relationship between the  $\log k_2$  and the basicity of the entering nucleophiles for the substitution reaction of Pt(II) terpyridine type complexes with azole nucleophiles has been reported recently.<sup>21a</sup>
- (c) Oxidability: Ligands which are easily oxidised are considered as good nucleophiles (strong reducing agents) and their strength can be identified based on their electrode reduction potential.
- (d) Metal Centre: The nature of the reaction centre affects the rate of substitution of square planar complexes. Thus, the nature of metal centre limits the applicability of nucleophilicity scales in inorganic chemistry since reactions show dependence on the nature of the metal centre. Heavier elements are better polarised in the transition state following the order: Ni(II) > Pd(II) > Pt(II).
- (e) Solvation Energy: Ligands which are easily solvated are weak nucleophiles because energy is required to remove the solvent shell before it gets coordinated with the metal centre.

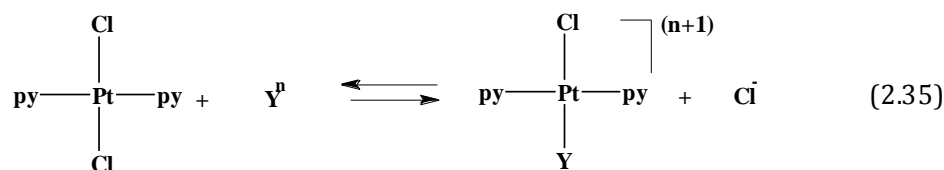
---

<sup>†</sup> Hard acids (metal ions) are small and highly charged (eg:  $Li^+$  and  $Mg^{2+}$ ) and their valence electron shell is not easily distorted while soft acids (metal ions) are large and possess low charge having an easily distortable or removable valence electron shell. Polarisability refers to the "softness" of the nucleophile, i.e. "Hard" nucleophiles prefers "hard" metal centres and "soft" nucleophiles prefers "soft" substrates or metal centres. Pt(II) being a soft metal centre is more effective towards large and soft donors.

Studies reported on Pt(II) complexes show that the nucleophilic reactivity order for commonly used nucleophiles follow the order:<sup>14a,14c,40</sup>



It is also important to note that the nucleophilicity of the reagents is independent of their base strength. Based on earlier studies,<sup>14c,40</sup> the most detailed study on nucleophilicity was reported by Bellucco<sup>41</sup> for *trans*-Pt(py)<sub>2</sub>Cl<sub>2</sub> in methanol at 30 °C (Equation 2.38).<sup>2</sup>



By using *trans*-Pt(py)<sub>2</sub>Cl<sub>2</sub> as the standard, the nucleophilic reactivity constants,  $n_{\text{Pt}}$  was defined as:<sup>9b</sup>

$$n_{\text{Pt}}^{\circ} = \log \frac{k_Y^{\circ}}{k_s^{\circ}} \quad (2.36)$$

where  $k_Y$  = the measured second order rate constant for the entering nucleophile

$k_s^{\circ}$  = the second order rate constant for the attack of solvent in an associative mechanism and is equal to  $k_s / [\text{Methanol}]$

$k_s$  = the observed rate constant for solvent attack (methanol) on the complex.

Plots of  $\log k_Y$  for different Pt(II) complexes with various number of nucleophiles yielded linear free energy relationship (LFER).<sup>42</sup> Such a linear free energy relationship is given by:<sup>9b,14a</sup>

$$\begin{aligned} \log k_Y &= s n_{\text{Pt}} + \log k_s \\ \text{or} \\ \log k_2 &= s n_{\text{Pt}} + \log k_2 \end{aligned} \quad (2.37)$$

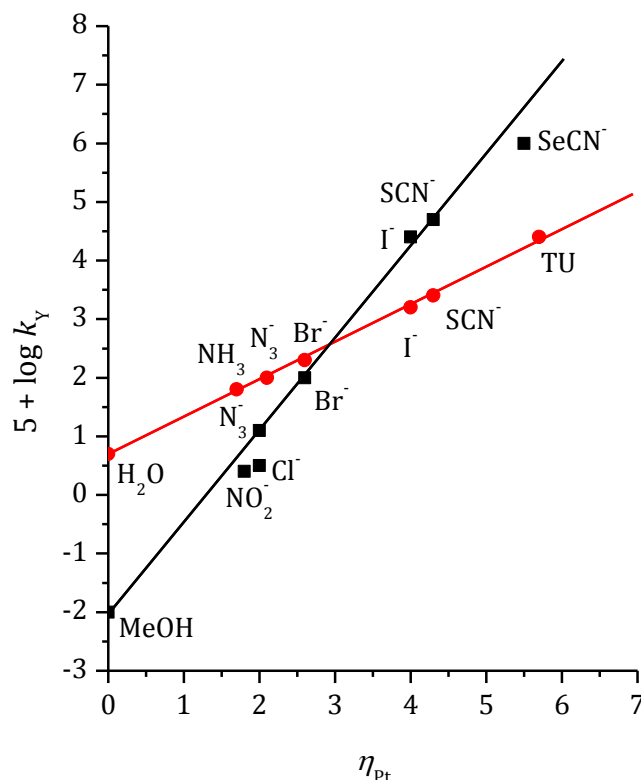
where the slope,  $s$  depends on the complex and is called the *nucleophilic discrimination factor*, a measure of the sensitivity of the metal centre to the nucleophilicity of the incoming ligand.<sup>14a</sup> A larger value of  $s$  means that the reaction is very sensitive to the

changes in nucleophilicity of the substituting ligands. Ligands that are capable of forming dative  $\pi$ -bonding with Pt(II) centre in the transition state have larger values of  $s$  (smaller  $k_s$ )<sup>14a</sup> which enhances the addition of the electrons from the nucleophile. Generally, Pt(II) complexes with softer ligands have larger  $s$  values. The intercept  $\log k_s$  is the intrinsic reactivity. A smaller value of intrinsic reactivity is accompanied with very fast reactions and hence, a greater nucleophilic discrimination factor. Thus, the nucleophilic reactivity constant is a measure of the reactivity of a nucleophile towards a Pt(II) metal centre.

After a number of investigations, it was also reported that the nucleophilicity of the incoming ligand also depends on other properties<sup>14a</sup> such as biphilicity of the ligand and the charge effect<sup>14c,43</sup> while steric hindrance plays a minor role.<sup>44</sup> Some of the experimental results obtained are presented in *Table 2.1*. For many nucleophiles, a plot of  $k_Y$  against  $n_{Pt}$  is a straight line as represented in *Figure 2.11*.

**Table 2.1**      **Some nucleophilic constants given for Pt(py)<sub>2</sub>Cl<sub>2</sub> with different nucleophiles of donor atoms.**<sup>14a,41,45</sup>

Nucleophile	$n_{Pt}^o$	Nucleophile	$n_{Pt}^o$	Nucleophile	$n_{Pt}^o$
<b>O-Donor</b>		<b>N-Donor</b>		Halogens	
CH <sub>3</sub> O <sup>-</sup>	<2.4	C <sub>6</sub> H <sub>5</sub> NH <sub>2</sub>	3.02	<sup>36</sup> Cl <sup>-</sup>	3.04
<b>S-Donor</b>		NH <sub>3</sub>	3.06	Br <sup>-</sup>	4.18
(C <sub>6</sub> H <sub>5</sub> ) <sub>2</sub> S	4.38	C <sub>5</sub> H <sub>5</sub> N	3.13	I <sup>-</sup>	5.42
S=C(NH <sub>2</sub> ) <sub>2</sub>	7.17	H <sub>2</sub> N-NH <sub>2</sub>	3.85	<b>Se-Donor</b>	
(CH <sub>3</sub> ) <sub>2</sub> S	4.73	<b>P-Donor</b>		(C <sub>6</sub> H <sub>5</sub> CH <sub>2</sub> ) <sub>2</sub> Se	5.39
SCN <sup>-</sup>	6.65	(C <sub>6</sub> H <sub>5</sub> )P	8.79	(CH <sub>3</sub> ) <sub>2</sub> Se	5.56
<b>C-Donor</b>		(C <sub>2</sub> H <sub>5</sub> ) <sub>3</sub> P	8.85	<b>As-Donor</b>	
CN <sup>-</sup>	7.14			(C <sub>2</sub> H <sub>5</sub> ) <sub>3</sub> As	7.54



**Figure 2.11** Correlation of the rates of reaction of Pt(II) complexes with the standard *trans*-Pt(py)<sub>2</sub>Cl<sub>2</sub> for different nucleophiles: •, *trans*-Pt(PEt<sub>3</sub>)<sub>2</sub>Cl<sub>2</sub> in methanol at 30 °C; ■, Pt(en)Cl<sub>2</sub> in water at 35 °C, produced from references.<sup>14a,41,46</sup>

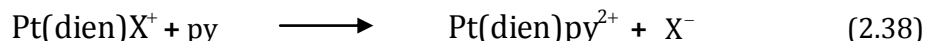
In a study van Eldik *et al.*<sup>47</sup> reported the nucleophilic discrimination ability of Pt(II) complexes of [Pt(N-N-C)Cl] (N-N-CH = 6-phenyl-2,2'-bipyridine), [Pt(N-C-N)Cl] (N-CH-N = 1,3-di(2-pyridyl)benzene), and [Pt(N-N-N)Cl]Cl (N-N-N = 2,2':6',2''-terpyridine) where the rate constants for the substitution of Cl<sup>-</sup> by MeOH, Br<sup>-</sup> and I<sup>-</sup> were measured as well as the corresponding log *k*<sub>2</sub> verse *n*<sub>Pt</sub>. In that study, it was found that due to the biphilic nature of thiourea, its nucleophilic discriminating factor was misleading from plot. The resulting values for *s* were reported to be 0.61 ± 0.04 (NCN), 0.9 ± 0.1 (NNC), 1.39 ± 0.02 (NNN) respectively.

### 2.5.2 The Effect of Leaving Group

Since square planar Pt(II) complexes mainly follow associative mode of substitution reactions, the effect of the leaving group is less important on the rate of substitution compared to the incoming group. However, some substitution reactions have shown a dependence on the nature of the leaving group.



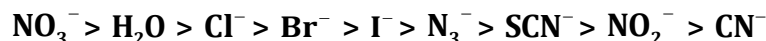
For this purpose,  $\text{Pt}(\text{dien})\text{X}^+$  systems (*Equation 2.38*) has been studied extensively. Data obtained is represented in *Table 2.2*.



**Table 2.2** Effects of leaving group on the rates of reaction of  $\text{Pt}(\text{dien})$  complexes in water at 25 °C.<sup>48</sup>

Ligand, X	$10^6 k_{\text{obs}}, \text{s}^{-1}$
$\text{NO}_3^-$	very fast
$\text{H}_2\text{O}$	1900
$\text{Cl}^-$	35
$\text{Br}^-$	23
$\text{I}^-$	10
$\text{N}_3^-$	0.83
$\text{SCN}^-$	0.3
$\text{NO}_2^-$	0.05
$\text{CN}^-$	0.017

The decrease in the rate of substitution of X from the substitution by pyridine ligand follows the order:



In general, it is easier to substitute ligands which are less nucleophilic than those which are more nucleophilic. For example, the rate of substitution in the  $\text{Pt}(\text{dien})$  is reduced by a factor of 2000 when the cyano is replaced by a chloride as a leaving group while replacement of  $\text{Cl}^-$  by  $\text{CN}^-$  is  $10^4$  times greater than that of  $\text{Cl}^-$ .<sup>41,48a</sup> Thus, for a square planar complex, it is clear that even though the reactivity of a complex strongly depends on the nature of the incoming group, is also dependent on the leaving group.<sup>2,14b</sup> Pitteri *et al.*<sup>49</sup> had reported the effect of displacement of halides from several square planar  $\text{Pt}(\text{II})$  complexes with different nucleophiles depend on the nature of the leaving groups.

### 2.5.3 Effect of Steric Hindrance

Associative mode of mechanisms involves an increase in the steric hindrance in the transition state. Therefore, for a sterically hindered complex, the rate is expected to be slower due to the transition state destabilization. The influence to the rate of reaction

could be either due to the steric bulk in the spectator ligand or in the incoming nucleophile.

It is rationalized that increasing the steric bulk of the spectator ligands usually decrease the rate of substitution. Studies have reported that steric hindrance due to methyl and ethyl substituents on the tridentate ( $R_n$ dien) ligands slows down the substitution rate of  $[Pt(R_n\text{dien})Cl]^+$  complexes on increasing the size of the substituent, R, by five orders of magnitude compared to the unhindered molecule (Table 2.3). The corresponding Pt(II) complexes, even though not yet been studied extensively, based on the available data a similar trend is expected to be followed for Pt(II) complexes.

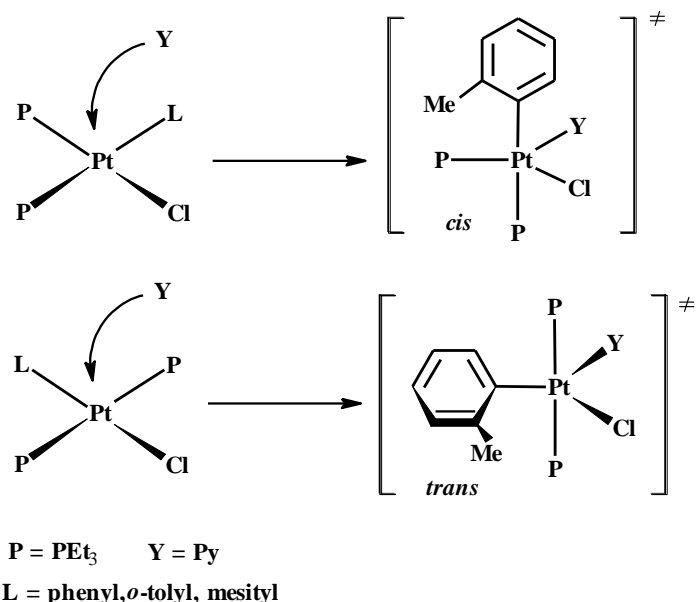
**Table 2.3** Rate constants and activation parameters for the substitution of  $Cl^-$  by  $I^-$  in  $[Pd(R_n\text{dien})Cl]^+$  ( $n = 0, 3-5$ ) in aqueous solution at 25 °C.<sup>50</sup>

$R_n\text{dien}$	$k_1 \text{ s}^{-1}$	$\Delta H^\ddagger \text{ kJ mol}^{-1}$	$\Delta S^\ddagger \text{ J K}^{-1} \text{ mol}^{-1}$	$\Delta V^\ddagger \text{ cm}^3 \text{ mol}^{-1}$
dien	44	43	-69	-10.0
1,4,7-Et <sub>3</sub> dien	10	41	-86	-10.8
1,1,7,7-Et <sub>4</sub> dien	$2.2 \times 10^{-3}$	66	-74	-14.9
1,1,4,7,7-Me <sub>5</sub> dien	0.28	50	-88	-10.9
1,1,4,7,7-Et <sub>5</sub> dien	$7.2 \times 10^{-4}$	59	-106	-12.8

The steric effect of the spectator ligand might influence differently for *cis* and the *trans* positions. This steric effect, using *cis* and *trans* isomers was reported by using *cis/trans*- $[Pt(P\text{Et}_3)_2LX]$  (L= phenyl, *o*-tolyl, mesityl, X = MeOH,  $Cl^-$  and  $Br^-$ ).<sup>7c,9b,51</sup> The substitution of chloro ligand in *trans* - $[Pt(P\text{Et}_3)_2LX]$  complex by thiourea showed that by having one or two *ortho*-methyl groups on the phenyl rings decelerated the reactivity by a factor of only 130 : 10 : 1 respectively for R = phenyl, *o*-tolyl and mesityl.<sup>51b</sup> The decrease in reactivity was reported to be even greater for the *cis* complex, *cis* - $[Pt(P\text{Et}_3)_2LBr]$  ( 32000 : 110 : 1), with the same modification on the phenyl ring.<sup>51c</sup>

The larger decrease in the rates observed for *cis* complex can be explained in terms of transition state complex of the *cis* isomer where the leaving group and the entering group are in equatorial positions (Figure 2.12). In the case of the *cis* isomer, in the transition state, the group L occupies the axial position thus, L interacts with the leaving group at 90° which causes more steric repulsion between the *ortho*-methylene substituents and the entering and the leaving group. For the *trans* isomer, L occupies an equatorial position in the transition state, which lies at 120° to the incoming group

which is further apart.<sup>7c</sup> Also in the trigonal bipyramidal intermediate the *cis* isomer offers more shielding than the *trans* isomer. Recently Jaganyi *et al.*<sup>36f</sup> reported mechanistic elucidation of substitution reactions of Pt(II) dinuclear complexes bridged by pyrazine units where the rate of substitution was found to be controlled by the steric hindrance at the Pt(II) centres due to the linker groups.



**Figure 2.12** The steric effect of the aryl square planar complex showing the steric bulk for the *cis* isomer blocking the attacking site.<sup>7c</sup>

### 2.5.4 Effect of Solvent

Since the solvent is the reaction medium in which the reaction takes place, it can rapidly substitute the labile group rendering the rate to be independent of the entering nucleophile and has been reported<sup>21</sup> for substitution reactions of Pt(II) complexes proceeding *via* the solvent pathway. This contribution of the solvent to the overall rate of reaction depends on the coordination ability of the solvent.<sup>2,14a</sup> The effect was experimentally investigated for the chloride exchange reaction for *trans*-Pt(py)<sub>2</sub>Cl<sub>2</sub> (Table 2.4, Equation 2.39).<sup>9b</sup>



**Table 2.4** Effect of solvent on the chloride exchange reaction (Equation 2.39) at 25 °C.<sup>52</sup>

Coordinating	$k_2 / (10^{-5} \text{ s}^{-1})$	Weakly coordinating	$k_2 / \text{M}^{-1} \text{ s}^{-1}$
DMSO	380	CCl <sub>4</sub>	10 <sup>4</sup>
H <sub>2</sub> O	3.5	C <sub>6</sub> H <sub>6</sub>	10 <sup>2</sup>
EtOH	1.4	<i>i</i> -BuOH	10 <sup>-1</sup>
PrOH	0.4	Me <sub>2</sub> C(O)	10 <sup>-2</sup>
		DMF	10 <sup>-3</sup>

Results obtained show that for the strongly coordinating solvents, the reaction preceded *via* a solvolytic pathway which is independent of the concentration of the chloride while the opposite is true for the weakly or non-coordinating solvents. For coordinating solvents such as DMSO, the rates of the reaction showed a direct dependence on the nucleophilicity of the solvent, ( $k_s \gg k_{Cl}[\text{Cl}^-]$ ). This is also because the soft Pt(II) metal centre prefers to bond with larger S in DMSO. For poorly coordinating (or non-coordinating) solvents such as CCl<sub>4</sub>, larger rates of reaction have been reported where the chloride acts as a nucleophile ( $k_{Cl}[\text{Cl}^-] > k_s$ ).<sup>14a</sup> Romeo *et al.*<sup>53</sup> have reported similar effects. Linear free energy relationships between several parameters that are commonly used to describe the Lewis acidity of the solvent and reactivity were found to depend strongly on the salvation of the incoming nucleophile.

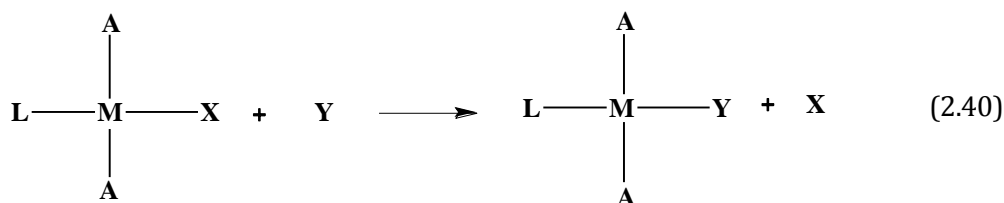
### 2.5.5 Non-Participating Ligand

Substitution reactions of square planar Pt(II) complexes are influenced to a great extent by the nature of the spectator ligand. A number of research studies has been reported on the effect of reactivity on changing the properties such as the  $\pi$ - and  $\sigma$ -bond strengths and the steric factors of the spectator ligands which are *trans* and *cis* to the leaving group.<sup>36b,54</sup> It is known that the influence on the reactivity due to the *trans* ligand is much stronger than the two *cis* ligands.<sup>14d</sup>

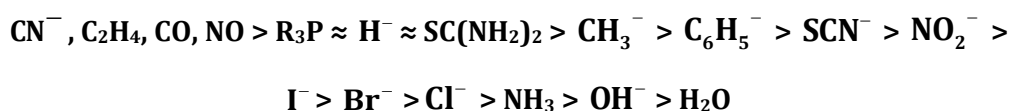
#### 2.5.5.1 The *trans* Effect

The *trans* effect is the influence exerted by a non-labile ligand in a square planar complex on the rate of replacement of a labile ligand *trans* to it.<sup>4</sup> This concept of *trans* influence was first observed by Werner in the early 20<sup>th</sup> century.<sup>9b,55</sup> By 1926 Chernyaev used the concept of *trans* effect to synthesize isomeric square planar Pt(II) complexes.<sup>14a</sup> The *trans* ligand (L) labilize the ligand *trans* to it (X). In this case the

spectator ligands ( $A_2$ ) facilitate the replacement by the incoming nucleophile  $Y$ .<sup>14b</sup> (Equation 2.40).



In an associative mechanism, a greater *trans* effect increases the rate of substitution for square planar complexes. Using a standard complex, studies have established the general order of labilization by *trans*-directing ligands to be:<sup>2,9b,14a,b</sup>



A ligand high up in the *trans* effect series would have a greater *trans* effect. Kinetically, the *trans* effect can be large, hence, with a good *trans* labilizing ligand the effect may increase up to  $10^6$  or more.<sup>14a</sup> Since *trans* effect is a kinetic phenomenon, in order to understand it better, its effect at the ground state and the transition state should be considered. For example, a stabilization of the transition state and destabilization of the ground state leads to a reaction coordinates marked by smaller energy barrier leading to a higher reactivity.

At this point it is important for one to differentiate the two closely related but characteristically distinct concepts, *trans* effect and *trans* influence. The *trans* effect provides information about the *trans* ligand on ground state as well as the transition state, while *trans* influence is a ground state phenomenon which involves the ground state effects such as ground state bond length.<sup>7c,9b,46</sup> To understand the *trans* effect better, it is important to know both  $\sigma$ - and  $\pi$ -bonding effects. These effects involve the ground state orbitals shared by the metal  $M$ , the leaving group  $X$  and the *trans* ligand  $L$ <sup>7c</sup> (Equation 2.40).

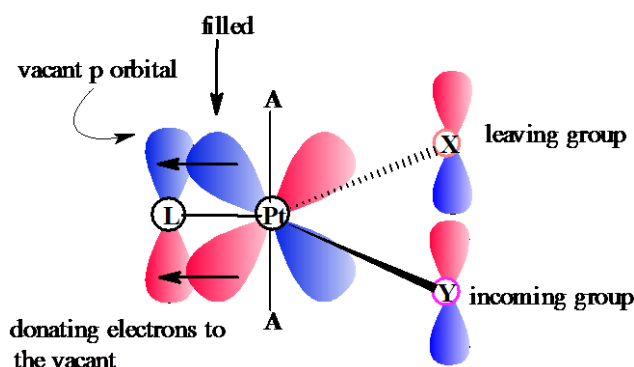
In a square planar Pt(II) complex, a good  $\pi$ -accepting *trans* ligand can stabilise the five coordinate transition state intermediate by accepting the electron density from metal centre.<sup>14a</sup> The  $\pi$ -orbital in the metal centre is a filled  $d_{xy}$ ,  $d_{zy}$  or  $d_{yz}$  orbital and the electrons are transferred from these orbital to the empty  $p$  orbitals on the *trans* ligand,  $L$ .<sup>14a</sup> This makes the metal centre highly electrophilic. Thus, the increase in the electron

density due to the five coordinate transition state on the metal centre is reduced. Hence, the activation energy is reduced and thus, the rate of substitution increases.

In the transition state, the leaving group and the *trans* ligand do not directly share the same *p* orbital. Thus, such a ligand has a greater  $\sigma$ -donacity in the ground state and is the dominant contributor for the ground state *trans* influence. Of the studies conducted to explain *trans* effect,<sup>56</sup> the  $\pi$ -bonding theory and the polarisation theory are the two very common theories.<sup>4</sup> *Trans* effect due to an appended alkyldiammine pendent groups have been recently reported by Jaganyi *et al.*<sup>28,36c</sup> for the substitution kinetics of mono and dinuclear Pt(II) complexes with thiourea nucleophiles.

The  $\pi$ -back bonding effect in a metal complexes was first introduced by Pauling<sup>57</sup> to account for the short Ni—C bond distances in Ni(CO)<sub>4</sub>. The  $\pi$ -bonding theory states that ligands with  $\pi$ -bonds, such as C<sub>2</sub>H<sub>4</sub>, PR<sub>3</sub> and CO have stronger  $\pi$ -acceptor abilities thus, stabilise the transition state and therefore appear higher in the *trans*-effect series.<sup>14a,46</sup> A pair of electrons is donated from the ligand to platinum centre to form the  $\sigma$ -bond while the  $\pi$ -bond is formed by the overlap of electrons from the filled *d* orbital (either *d<sub>xz</sub>* or *d<sub>yz</sub>*) of platinum with the vacant orbital of the ligand.<sup>14a,46</sup>

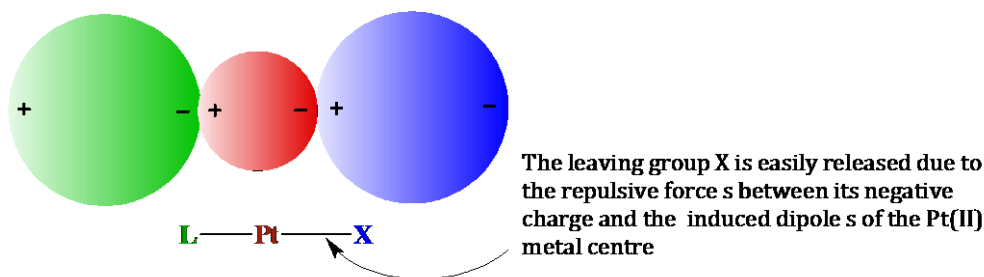
In general, removal of electron density from the platinum centre to the empty orbitals of the ligand weakens the **M—X** bond in the ground state.<sup>14a</sup> Chatt *et al.*<sup>58</sup> and Orgel<sup>59</sup> independently proposed a  $\pi$ -bonding stabilization of the trigonal bipyramidal intermediate complex for the reaction of *trans*-PtA<sub>2</sub>LX with **Y** to form *trans*-PtA<sub>2</sub>LY where **Y** is the entering group, **X** is the leaving group and **L** is the *trans* ligand (Figure 2.13).



**Figure 2.13**  $\pi$ -back donation of the electrons from the filled *d* orbital to the vacant orbitals of the *trans* ligand in PtA<sub>2</sub>LXY.<sup>14a,46</sup>

Chatt *et al.*, stated that strong *trans* directing ligands enhance the substitution reactions by removing the electron density from the metal centre to the  $\pi$ -backbonding ligand.<sup>58</sup> One of the hybrid orbitals, either  $d_{xz}$  or  $p_z$  overlaps with the empty orbital on the *trans* ligand.<sup>46</sup> Thus, the other two orbitals readily accept the electron density from the incoming ligand thereby favouring a rapid reaction.<sup>2,14a</sup> Orgel<sup>59</sup> also supported this theory indicating that the presence of the  $\pi$ -acceptor ligand in the five coordinate transition state lowers the energy of the intermediate because the electron density on the Pt(II) is reduced along the **Pt–X** and **Pt–Y** directions, thereby retaining the original configuration.<sup>14a</sup>

Polarization theory, reported by Meerwein,<sup>60</sup> is based on weakening of the **Pt–X** bond due to the strong *trans* effect caused by the *trans* ligand in  $\text{PtA}_2\text{LX}$ .<sup>14a</sup> The charge on the Pt(II) induces a dipole in **L**, which in turn induces a dipole in the platinum metal which repels the negative charge in **X**<sup>14a</sup> resulting in a weakening of the **Pt–X** bond. A diagrammatic representation of charge induced dipoles in **L–Pt–X** is shown in Figure 2.14. However, there are some contradictions to this theory. Thus, the effect of covalent bonding in such systems needs to be considered. Ligands of high polarisability are expected to form the strongest bonds with Pt(II).



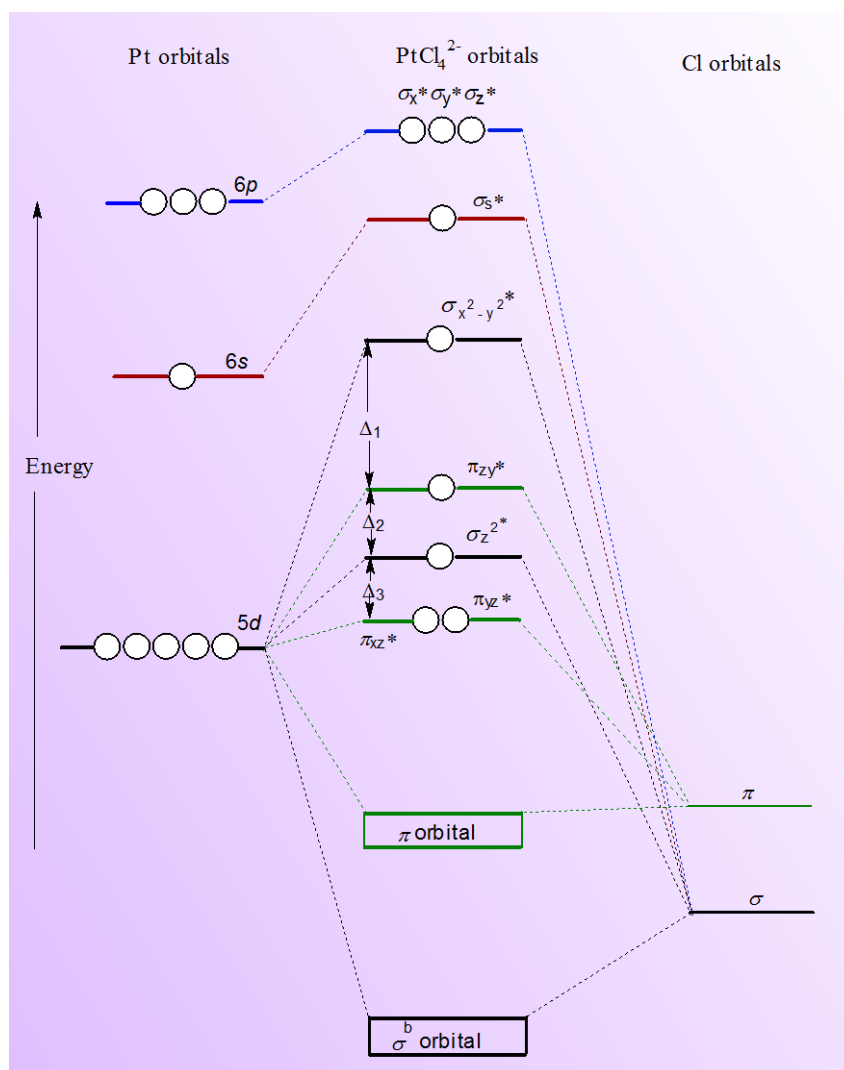
**Figure 2.14** Distribution of Charge induced dipoles in the **L–Pt–X** coordinate of *trans*- $\text{PtA}_2\text{LX}$ .<sup>14a</sup>

The  $\sigma$ - and  $\pi$ -*trans* effect is best described in the molecular orbital theory (MO theory).<sup>14a</sup>

### i $\sigma$ -*trans* effect

A simplified MO diagram for  $\text{PtCl}_4^{2-}$  is given in Figure 2.15. The most stable  $\sigma$ -orbitals tailed by the  $\pi$ -bonding orbitals are located mostly on the chloride groups followed by the anti-bonding orbitals of the  $\sigma$  and  $\pi$ -orbitals.<sup>46</sup> These orbitals are derived from the

5d orbitals of Pt(II) and have four probable MO of which the  $\pi_{xy}^*$  is the most stable and the  $\sigma_{x^2-y^2}^*$  is relatively the least stable MO.<sup>14a,46</sup> The higher energy  $p_z$  valence orbitals are not involved in the  $\sigma$ -bond formation and the higher energy anti-bonding  $\sigma$  orbitals;  $\sigma_s^*$ ,  $\sigma_x^*$  and  $\sigma_y^*$  are relatively the least stable from all.<sup>14a</sup>

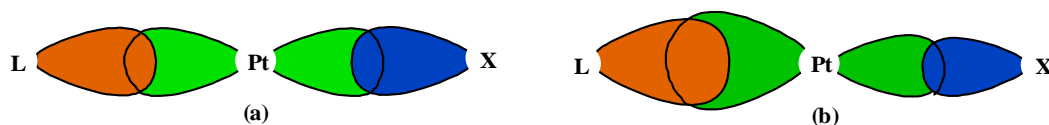


**Figure 2.15** Molecular orbital representation showing the relative orbital energies in  $\text{PtCl}_4^{2-}$ .<sup>14a,46</sup>

In a square planar complexes,  $d_{x^2-y^2}$ ,  $s$ ,  $p_x$ ,  $p_y$  and  $5d_{z^2}$  metal valence orbitals are used for the  $\sigma$ -bond formation.<sup>46</sup> However, only the two  $p$  orbitals have the right geometry for the *trans* directing properties. Therefore, in *trans*-PtA<sub>2</sub>LX, the leaving group, **X** and the *trans* ligand, **L** must share the same  $dsp^2$  orbital in the ground state.<sup>14a</sup> It is known that *trans* effect causes destabilization of the  $\sigma$ -*trans* ligand by elongation of the **Pt–L** bond *via*  $\sigma$ -donation. This in turn weakens the **Pt–X** bond due to the smaller share of

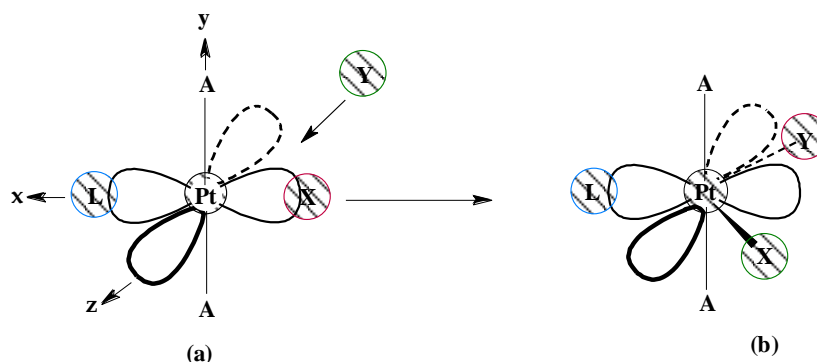


the electrons available for the bonding,<sup>14a</sup> thus, increases the rate of substitution of **X** (Figure 2.16). If the *trans* ligand is a stronger  $\sigma$ -donor, then the **Pt–L** shortens as a result of less electron density available for this bond and the **Pt–X** bond lengthens as reported by Jaganyi *et al.*<sup>36c</sup>



**Figure 2.16** Representation of **L–Pt–X** bonding using  $\sigma$  MO (a) The  $\sigma$ -bond strength of **L** and **X** are almost equal. (b) Strong  $\sigma$ -donor ligand **L**, the  $\sigma$ -bond strength of **L** is much greater than that of **X**.<sup>9b,14a</sup>

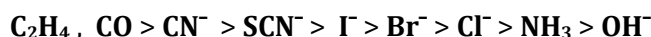
Langford and Gray<sup>6</sup> used the  $\sigma$ -donation to explain the increase in the stabilization of the trigonal bipyramidal intermediate. In a ground state square planar complex, the same  $p_x$  orbital is used to form the **L–Pt–X** bonds.<sup>14a</sup> Addition of the incoming ligand, **Y** from above the *xy* plane shifts **X** out of plane resulting in two suitable  $p$  orbitals ( $p_x$  and  $p_z$ ) increasing the number of orbitals available for formation of bonds (Figure 2.17).<sup>14a</sup> As a result, good  $\sigma$ -bonding ligands such as  $\text{H}^-$  and  $\text{CH}_3$  which can donate to the extra  $p$  orbital can stabilize the  $\sigma$  structure in the trigonal bipyramidal intermediate through *trans* effect.<sup>14a</sup> Jaganyi *et al.*<sup>36c</sup> recently reported the *trans* effect due to the  $\sigma$ -donation of the alkyl pendent chains on the substitution kinetics of Pt(II) complexes by thiourea nucleophiles. It was reported that the alkyl chain on the *trans* N-donor atom of the chelate head group increases the rate of substitution of the aqua leaving groups due to the weaker *trans* influence of the alkyl amine donor group.



**Figure 2.17** The  $\sigma$ -*trans* effect due to the stabilization of the trigonal bipyramidal intermediate. (a) Only one  $p$  orbital is available for  $\sigma$ -bond formation of **L** and **X**. (b) Two  $p$  orbitals are available for the  $\sigma$ -bonding of **L**, **X** and **Y**.<sup>14a</sup>

## ii $\pi$ -*trans* effect

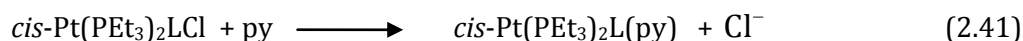
Good *trans* directing groups such as CO and  $C_2H_4$  stabilize the complex by strong  $\pi$ -back donation from the filled Pt(II)  $5d_{xz}$  or  $5d_{yz}$  to the empty  $\pi^*$  ( $p_x$  or  $p_y$ ) orbital of the ligand.<sup>14a</sup> In the trigonal plane, the four orbitals are shared in  $\pi$ -bonding with the three ligands, **L**, **X** and **Y**. This stabilises the trigonal bipyramidal transition state if *trans* ligand, **L**, can form bonds with the  $\pi^*$  orbitals which results in the transfer of electron density from the platinum centre to the  $\pi$ -acceptor ligands thereby lowering the energy of the system.<sup>14a</sup> Thus, a good *trans* ligand lowers the activation energy of the reaction.<sup>9b,14a</sup> This theory rates the *trans* ligands according to the following orders:<sup>14a,17</sup>



Recent studies reported<sup>36a,b</sup> that *trans*  $\pi$ -accepting ligands can cause an increase in the substitution reaction of Pt(II) complexes by increasing the electrophilicity of the Pt(II) centre.

### 2.5.5.2 *Cis*- Effect

For square planar Pt(II) complexes, even though, the *cis* effect has not been studied in detail, it is generally assumed that the *cis* effect is smaller than the *trans* effect. The reactivity of Pt(II) complexes are less sensitive towards the properties of *cis* ligands compared to *trans*. However, the *cis* effect becomes important if the *cis* ligands are bulky as *cis* position can impose greater steric influence.<sup>2</sup> It is known that good *trans* directing ligands have poor *cis* effects.<sup>61</sup> For example, experimental results obtained for *cis*-Pt(PEt<sub>3</sub>)<sub>2</sub>LCl (where L = Cl<sup>-</sup>, C<sub>6</sub>H<sub>6</sub> and CH<sub>3</sub><sup>-</sup>) with pyridine (Equation 2.47) have shown the same trend for the corresponding *trans*-Pt(PEt<sub>3</sub>)<sub>2</sub>LCl with pyridine with the change of the *trans* ligand, **L** in the order of CH<sub>3</sub> ( $6.0 \times 10^2 \text{ s}^{-1}$ ) > C<sub>6</sub>H<sub>5</sub> ( $3.8 \times 10^2 \text{ s}^{-1}$ ) > Cl<sup>-</sup> ( $1.7 \times 10^2 \text{ s}^{-1}$ ).<sup>51a</sup>



van Eldik *et al.*<sup>47</sup> reported that the *cis* effect on the substitution kinetics of Pt(II) complexes viz; [Pt(1,3-di(2-pyridyl)benzene)Cl] (**NCN**), [Pt(6-phenyl-2,2'-bipy)Cl] (**NNC**) and [Pt(terpy)Cl] (**NNN**) using thiourea nucleophiles was much slower than the Pt(II) (**NNN**) complex. Pt(II) (**NNC**) where the Pt—C bond is on the *cis* position. The reactivity was much faster when the Pt—C bond was on the *trans* position due to stronger *trans* effect. The deceleration of the rate of substitution of Pt(II) (**NNC**) complex as compared to (**NNN**) was attributed to the reduced nucleophilic

discrimination of the (**NNC**) complex since the *cis*  $\sigma$ -donor lowers the electrophilicity of the Pt(II) metal centre due to their electron donating effect.<sup>47</sup>

Additionally, Jaganyi *et al.*<sup>62</sup> also reported the Pt—C *cis*  $\sigma$ -donor effect on the substitution reaction of Pt(II) terpyridine type complexes by thiourea nucleophiles. The authors reported a decrease in the reactivity due to the accumulation of electron density at the Pt(II) metal centre of a Pt(II) (**NNC**) thereby decreasing its electrophilicity. This further prevents the approach of the nucleophiles due to a destabilization of the transition state. Furthermore, in different studies Jaganyi *et al.*<sup>21a,63</sup> reported the  $\sigma$ -donor ability of an isoquinoline ligand which is *cis* to the leaving group effectively decreases the electrophilicity of the Pt(II) metal centre thereby decreasing the substitution reactivity.

So far the factors that control the reactivity are studied mostly for mononuclear complexes with square planar Pt(II) geometry. However, not much studies have been reported for multinuclear and heterometallic square planar complexes with bridging linkers. Nevertheless, it is known from literature<sup>28,36d</sup> that the bridging linker confers special structural properties such as flexibility and rigidity which then influences the substitution reactivity of the complex. Thus, an understanding of how the subtle changes in the structural feature of the complex affects the substitution reactivity at the Pt(II) centre is important. In the following chapters, the influence of some of these factors on the rate of substitution kinetics of square planar Pt(II) complexes will be reported based on the experimental findings.

## 2.6 References

- (1) Arnaut, L.; Formosinho, S.; Burrows, H. *Chemical Kinetics From Molecular Structure to Chemical Reactivity*; Elsevier: New York, 2007, 273-294.
- (2) Tobe, M. L.; Burgess, J. *Inorganic Reaction Mechanisms*; Addison Wesley: London, 1999, 30-39, 73-94, 103-106, 128-193.
- (3) Ingold, C. K. *Structure and Mechanism in Organic Chemistry*; 2nd ed.; Cornell University Press, Ithaca: New York, 1969, 241.
- (4) Benson, D. *Mechanisms of inorganic reactions in solution*; McGraw-Hill: London, 1968, 19-31, 60-64.
- (5) Cooke, D. O. *Inorganic Reaction Mechanisms*; The Chemical Society: London, 1979, 1.
- (6) Langford, C. H.; Gray, H. B. *Ligand Substitution Processes*; Benjamin: New York, 1965.
- (7) (a) Miessler, G. L.; Tarr, D. A. *Inorganic Chemistry*; 3rd ed.; Pearson Education International: Singapore, 2004, 415-426 (b) Asperger, S. *Chemical Kinetics and Inorganic Reaction Mechanisms*; 2nd ed.; Kluwer Academic/ Plenum Publisher: New York, 2003, 38-39, 105-106, 140-153 (c) Jordan, R. B. *Reaction mechanisms of Inorganic and Organometallic Systems*; Oxford University Press Inc: New York, 1991, 23-30, 47-54, 58-60.
- (8) Shriver, D. F.; Atkins, P. W.; Langford, C. H. *Inorganic Chemistry*; Oxford University Press: Oxford, 1994, 618-636.
- (9) (a) Murmann, R. K.; Fraser, R. T. M.; Bauman, J. *Mechanisms of Inorganic Reactions*; American Chemical Society: Washington, D. C, 1965, 20-23, 81-97 (b) Atwood, J. D. *Inorganic and Organic Reaction Mechanisms*; 2nd ed.; Wiley- VCH Inc., NY, 1997, 32-34, 43-61, 71-110, 749-771.
- (10) Cattalini, L. *Progr. Inorg. Chem.* **1970**, *13*, 263.
- (11) Cooper, J.; Ziegler, T. *Inorg. Chem.* **2002**, *41*, 6614.
- (12) (a) Lanza, S.; Minniti, D.; Moore, P.; Sachinidis, J.; Romeo, R.; Tobe, M. L. *Inorg. Chem.* **1984**, *23*, 4428 (b) Lanza, S.; Minniti, D.; Romeo, R.; Sachinidis, J.; Moore, P.; Tobe, M. L. *J. Chem. Soc. Chem. Comm.* **1984**, 542 (c) Romeo, R.; Grassi, A.; Scolaro, L. M. *Inorg. Chem.* **1992**, *31*, 4383 (d) Plutino, M. R.; Scolaro, L. M.; Romeo, R.; Grassi, A. *Inorg. Chem.* **2000**, *39*, 2712.
- (13) Henderson, R. A. *The Mechanisms of Reactions at Transition Metal Sites*; Oxford University Press: Oxford, 1993, 1-22.
- (14) (a) Basolo, F.; Pearson, R. G. *Mechanisms of Inorganic Reactions*; 2nd ed.; Wiley: New York, 1967, 193-195, 351-356, 369-400 (b) Wilkins, R. G. *Kinetics and*

- Mechanisms of Reactions of Transition Metal Complexes*; 2nd ed.; VCH: Weinheim, 1991, 136-140, 199-201, 232-237(c) Banerjee, D.; Basolo, F.; Pearson, R. G. *J. Am. Chem. Soc.* **1957**, 79, 4055(d) Catalini, L. *Progr. Inorg. Chem.* **1970**, 13, 263(e) Cross, R. J. *Chem. Soc. Rev.* **1985**, 14, 197(f) Cross, R. J. *Adv. Inorg. Chem.* **1989**, 34, 219.
- (15) Peloso, A. *Coord. Chem. Rev.* **1973**, 10, 123.
- (16) Helm, L.; Merbach, A. E. *Chem. Rev.* **2005**, 105, 1923.
- (17) Richens, D. T. *Chem. Rev.* **2005**, 105, 1961.
- (18) (a) Romeo, R. *Comment. Inorg. Chem.* **1990**, 11, 21(b) Romeo, R.; Scolaro, L. M.; Plutino, M. R.; De Biani, F. F.; Bottari, G.; Romeo, A. *Inorg. Chim. Acta.* **2003**, 350, 143.
- (19) Atkins, P.; de Paula, J. *Atkins' Physical Chemistry*; 8<sup>th</sup> ed.; Oxford University Press, 2006, 479-829.
- (20) (a) Haake, P.; Chan, S. C.; Jones, V. *Inorg. Chem.* **1970**, 9, 1925(b) Beattie, J. K. *Inorg. Chim. Acta* **1983**, 76, L69.
- (21) (a) Shaira, A.; Reddy, D.; Jaganyi, D. *Dalton Trans.* **2013**, 42, 8426(b) Reddy, D.; Akerman, K.; Akerman, M.; Jaganyi, D. *Transition Met. Chem.* **2011**, 36, 593.
- (22) (a) Eyring, H. *J. Chem. Phys.* **1935**, 3, 107(b) Evans, M. G.; Polanyi, M. *Trans. Faraday Soc.* **1935**, 31, 875.
- (23) Laidler, K. J.; Meiser, J. H.; Sanctuary, B. C. *Physical Chemistry*; 4<sup>th</sup> ed.; Houghton Mifflin Company: New York, 2003, 374-379, 390-393.
- (24) Espenson, J. H. *Chemical Kinetic and Reaction Mechanisms*; McGraw-Hill: New York, 1995, 1-80, 155-159, 161-162, 253-256.
- (25) Kotowski, M.; Palmer, D. A.; Kelm, H. *Inorg. Chem.* **1979**, 18, 2555.
- (26) van Eldik, R. *Pure & Appl. Chem.* **1993**, 65, 12.
- (27) Marbach, A. E. *Pure & Appl. Chem.* **1987**, 59, 161.
- (28) Jaganyi, D.; Mambanda, A.; Hochreuther, S.; van Eldik, R. *Dalton Trans.* **2010**, 39, 3595.
- (29) Hochreuther, S.; Puchta, R.; van Eldik, R. *Inorg. Chem.* **2011**, 50, 8984.
- (30) Wilkinson, F. *Chemical Kinetics and Reaction Mechanisms*; Van Nostrand Reinhold Company: New York, 1980, 1-11, 66-99.
- (31) Skoog, D. A.; West, A. M.; Holler, F. J.; Crouch, S. R. *Fundamentals of Analytical Chemistry*; 8<sup>th</sup> ed.; Thomson Brooks/Cole: Canada, 2002, 374-379, 720, 769-775, 878-894.
- (32) Reddy, D., PhD Thesis, Tuning the Reactivity of Platinum(II) Complexes, 2009, 88, 90.

- (33) Bauer, H. H.; Christian, G. D.; O'Reilly, J. E. *Instrumental Analysis*; Allyn and Bacon, Inc. Boston, 1978, 167- 188.
- (34) Harris, D. C. *Quantitative Chemical Analysis*; 4<sup>th</sup> ed.; W. H. Freeman and Company: New York, 1995, 480.
- (35) Origin 7.5<sup>TM</sup> SRO, ; Vol. v7.5714 (B5714), Origin Lab Cooperation, Northampton, One, Northampton, MA, 01060, USA, 2003.
- (36) (a) Jaganyi, D.; Hofmann, A.; van Eldik, R. *Angew. Chem. Int. Ed. Engl.* **2001**, *40*, 1680(b) Hofmann, A.; Jaganyi, D.; Munro, O. Q.; Liehr, G.; van Eldik, R. *Inorg. Chem.* **2003**, *42*, 1688(c) Mambanda, A.; Jaganyi, D. *Dalton Trans.* **2011**, *40*, 79 (d) Mambanda, A.; Jaganyi, D. *Dalton Trans.* **2012**, *41*, 908(e) Reddy, D.; Jaganyi, D. *Int. J. Chem. kinet.* **2011**, *43*, 161(f) Ongoma, P. O.; Jaganyi, D. *Dalton Trans.* **2013**, *42*, 2724.
- (37) Ertürk, H.; Maigut, J.; Puchta, R.; van Eldik, R. *J. Chem. Soc. Dalton Trans.* **2008**, 2759.
- (38) Connors, K. A. *Chemical Kinetics: The Study of Reaction Rates in Solution*; Wiley-VCH: New York, 1990, 1-22, 176-180.
- (39) (a) Pearson, R. G. *J. Am. Chem. Soc.* **1963**, *85*, 3533(b) Pearson, R. G. *J. Chem. Educ.* **1968**, *45*, 643.
- (40) Gray, H. B. *J. Am. Chem. Soc.* **1962**, *84*, 1548.
- (41) Belluco, U.; Cattalini, L.; Basolo, F.; Pearson, R. G.; Turco, A. *J. Am. Chem. Soc.* **1965**, *87*, 241.
- (42) Bronsted, J. N. *J. Am. Chem. Soc.* **1929**, *51*, 428.
- (43) Romeo, R.; Plutino, M. R.; Scolaro, S. *Inorg. Chim. Acta.* **1997**, 225.
- (44) Kruger, H.; van Eldik, R. *J. Chem. Soc., Chem. Commun.* **1990**, 330.
- (45) Pearson, R. G.; Sobel, H.; Songstad, J. *J. Am. Chem. Soc.* **1968**, *90*, 319.
- (46) Belluco, U. *Organometallic Coordination Chemistry of Platinum*; Academic Pressd: London, 1974, 40-53, 138-160, 220-221.
- (47) Hofmann, A.; Dahlenburg, L.; van Eldik, R. *Inorg. Chem.* **2003**, *42*, 6528.
- (48) (a) Basolo, F.; Gray, H. B.; Pearson, R. G. *J. Am. Chem. Soc.* **1960**, *82*, 4200(b) Gray, H. B.; Olcott, R. J. *Inorg. Chem.* **1962**, *1*, 481.
- (49) Pitteri, B.; Marangoni, G.; Cattalini, L.; Bobbo, T. J. *J. Chem. Soc. Dalton Trans.* **1995**, 3853.
- (50) Kotowski, M.; van Eldik, R. *Inorg. Chem.* **1986**, *25*, 3896.
- (51) (a) Basolo, F.; Chatt, J.; Gray, H. B.; Pearson, R. G.; Shaw, B. L. *J. Chem. Soc.* **1961**, 2207(b) Romeo, R.; Tobe, M. L.; Trozzi, M. *Inorg. Chim. Acta.* **1974**, *11*, 231(c) Romeo, R.; Minniti, D.; Trozzi, M. *Inorg. Chem.* **1976**, *15*, 1134.

- (52) Pearson, R. G.; Gray, H. B.; Basolo, F. *J. Am. Chem. Soc.* **1960**, *82*, 787.
- (53) Romeo, R.; Arena, G.; Scolaro, L. M.; Plutino, M. R. *Inorg. Chim. Acta.* **1995**, *240*, 81.
- (54) Weber, C. F.; van Eldik, R. *Eur. J. Inorg. Chem.* **2005**, 4755.
- (55) (a) Pearson, R. G. *J. Amer. Chem. Soc.* **1963**, *85*, 3533 (b) Page, J. D. *J. Chem. Edu.* **1987**, *64*, 561.
- (56) (a) Chernayev, I. I. *Ann. Inn. Platine USSR.* **1928**, *6*, 55 (b) Chernayev, I. I. *Ann. Inst. Platine USSR.* **1926**, *4*, 243 (c) Syrkin, Y. K. *Bull. Acad. Sci. USSR Classe Sci. Chim.* **1948**, 69.
- (57) Pauling, L. *The Nature of the Chemical Bond*; 3rd ed.; Ornell University Press: Ithaca, New York, 1960, 332.
- (58) Chatt, J.; Duncanson, L. A.; Venanzi, L. M. *J. Chem. Soc.* **1955**, 4456.
- (59) Orgel, L. E. *J. Inorg. Nucl. Chem* **1956**, *2*, 137.
- (60) Meerwein, H. R. *Sitzber. Ges. Beforder ges. Naturw. Marburg.*, *64*, 119.
- (61) (a) Grinberg, A. A. *J. Inorg. Chem. (USSR)* **1959**, *4*, 683 (b) Bersuker, I. B. *J. Struct. Chem.* **1963**, *4*, 419.
- (62) Jaganyi, D.; Reddy, D.; Gertenbach, J. A.; Hofmann, A.; van Eldik, R. *Dalton Trans.* **2004**, 299.
- (63) Ongoma, P. O.; Jaganyi, D. *Dalton Trans.* **2012**, *41*, 10724.

**Table Contents- 3**

List of Figures.....	ii
List of Tables.....	iii
List of Schemes .....	iii
Chapter Three .....	1
<b>Mixed-metal Ruthenium(II)-Platinum(II) and Cobalt(II)-Platinum(II) Complexes of Tetra-2-pyridyl-1,4-pyrazine Bridging Ligand. A Kinetic, Mechanistic and Computational Investigation.....</b>	<b>1</b>
3.0    Abstract .....	1
3.1    Introduction.....	2
3.2    Experimental.....	5
3.2.1    Chemicals .....	5
3.2.2    Characterizations and Instrumentations.....	5
3.2.3    Synthesis of Ruthenium Precursors and Intermediate Complexes .....	5
3.2.4    Synthesis of Platinum(II) Complexes .....	6
3.2.5    Preparation of Nucleophile Solutions for Kinetic Measurements .....	8
3.2.6    Kinetic Measurements .....	9
3.2.7    Computational Modelling.....	9
3.3    Results and Discussion.....	12
3.3.1    Synthesis and Characterization .....	12
3.3.2    Computation Calculations .....	12
3.3.3    Kinetic Analyses .....	13
3.4    Conclusion.....	31
3.5    References.....	33
3.6    Supporting Information.....	40



## List of Figures

Figure 3.1	Optimized molecular structure of CoPt, showing the torsion angles of the pyridyl groups.....	13
Figure 3.2	$^1\text{H}$ NMR spectra of PtRuPt (6.48 mM) with TU in acetonitrile at 298 K showing the dechelation of the coordinated platinum complex to form the $(\text{Ru}(\text{tppz})_2)$ unit. The spectra also indicates the formation of other intermediate products, in which some of their chemical shifts merges making it difficult to assign them exactly. The numbering system used to monitor the reaction progress is shown on the structure of PtRuPt (inset). ....	15
Figure 3.3	$^{195}\text{Pt}$ NMR spectra for the reaction of RuPt (6.28 mM) with TU, showing the changes in the chemical shift of the Pt before adding the TU nucleophile and the degradation after addition of TU for the new complex $[\text{Pt}(\text{TU})_4]^{2+}$ .....	16
Figure 3.4	(a) Typical two well-resolved kinetic traces at 382 nm for the two-steps reaction between RuPt ( $2.0 \times 10^{-5}$ M) by TU ( $6.00 \times 10^{-4}$ M) followed on stopped-flow spectrophotometer at 298 K. (b) A typical plot showing the changes in absorbance between 250 – 750 nm wavelength range for the degradation of the chelate ligand in RuPt ( $2.00 \times 10^{-5}$ M) by TU ( $6.00 \times 10^{-4}$ M) at 298 K. Inset is the kinetic trace followed at 382 nm. $I = 0.02$ M (adjusted with $\text{LiCF}_3\text{SO}_3$ and $\text{LiCl}$ ). ....	18
Figure 3.5	Dependence of the <i>pseudo</i> first-order rate constants ( $k_{\text{obs}}$ ) on the concentrations of the nucleophiles (a) for the simultaneous displacement of chloride ligands in $k_{\text{obs.}(1^{\text{st}})}$ , $\text{s}^{-1}$ , (b) for the dechelation of the ligands in $k_{\text{obs.}(2^{\text{nd}})}$ , $\text{s}^{-1}$ , from PtRuPt in methanol solution at 298 K and $I = 0.02$ M (adjusted with $\text{LiCF}_3\text{SO}_3$ and $\text{LiCl}$ ). ....	20
Figure 3.6	Eyring plots obtained for (a) RuPt with the nucleophiles for the substitution of chloride ligand, (b) Plots of $\ln(k_2/T)$ against $1/T$ for the reactions of RuPt with the nucleophiles for the dechelation of the linker at various temperatures in the range 15 - 35 °C.....	22
Figure 3.7	(a) UV/visible spectra of Ptppy, RuPt, PtRuPt, PtRuRuPt and CoPt in methanol (0.01 mM). (b) Energy of highest absorption wavelength peak of band against the number of tppz units in the complexes. CoPt deviates from the straight line. ....	26

**List of Tables**

Table 3.1	Selected bond lengths (Å), bond angles (°), natural bond orbital (NBO) charges, HOMO and LUMO energies and other computational data obtained for the complexes Pttpy, RuPt, PtRuPt, PtRuRuPt and CoPt obtained from the computational studies. Data for Pttpy is included for reference. ....	10
Table 3.2	Density functional theoretical (DFT) calculated minimum energy structures, HOMO and LUMO frontier molecular orbitals for the complexes investigated. The planarity of the molecules is viewed along the propagation axis showing the different planes. ....	11
Table 3.3	Summary of the rate constants and activation parameters for the displacement of the chloride ligand(s) by the nucleophiles studied and the kinetic data for the dechelation of the tppz units by thiourea nucleophiles. Data for Pttpy except with MTU is obtained from references and is included for comparisons. ....	23

**List of Schemes**

Scheme 3.1	Structural formulae of investigated complexes. The numbering schemes used for DFT calculations and the other references are shown on the structure of PtRuRuPt.....	4
Scheme 3.2	Proposed reaction mechanism for the reactions between the complexes, RuPt, PtRuPt, PtRuRuPt and CoPt with thiourea nucleophiles. The full reaction mechanism holds for RuPt, PtRuPt, PtRuRuPt and CoPt with thiourea nucleophiles only. For the ionic nucleophiles studied, I <sup>-</sup> and SCN <sup>-</sup> , the reaction mechanism holds only for the first step. The charges on the complexes are omitted for clarity. ....	17

# Chapter Three

## Mixed-metal Ruthenium(II)-Platinum(II) and Cobalt(II)-Platinum(II) Complexes of Tetra-2-pyridyl-1,4-pyrazine Bridging Ligand. A Kinetic, Mechanistic and Computational Investigation

### 3.0 Abstract

The substitution kinetics of monometallic  $[\text{Pt}(\text{tpy})\text{Cl}]\text{Cl}$  (**Pttpy**) and mixed-metal Ru(II)-Pt(II) and Co(II)-Pt(II) complexes of the form  $[(\text{tpy})\text{Ru}(\text{tppz})\text{PtCl}](\text{PF}_6)_3$  (**RuPt**),  $[\text{ClPt}(\text{tppz})\text{Ru}(\text{tppz})\text{PtCl}](\text{PF}_6)_4$  (**PtRuPt**),  $[\text{ClPtRu}_2(\text{tppz})_3\text{PtCl}](\text{PF}_6)_6$  (**PtRuRuPt**) and  $[(\text{tpy})\text{Co}(\text{tppz})\text{PtCl}](\text{PF}_6)_3$  (**CoPt**) (where tpy = 2,2':6',2''-terpyridine and tppz = tetra-2-pyridyl-1,4-pyrazine) with thiourea nucleophiles and ionic nucleophiles *viz*; thiourea (TU), 1-methylthiourea (MTU), 1,3-dimethyl-2-thiourea (DMTU), 1,1,3,3-tetramethyl-2-thiourea (TMTU) and an ionic nucleophile, iodide ( $\text{I}^-$ ) and thiocynide ( $\text{SCN}^-$ ) were investigated under *pseudo* first-order conditions as a function of concentration and temperature by using UV/visible spectrophotometer and stopped-flow reaction analyzer. The reactions proceeded in two steps. The *pseudo* first-order rate constants,  $k_{\text{obs}(1^{\text{st}}, 2^{\text{nd}})}$  for the substitution of the chloride ligand(s) from the Pt(II) complexes and subsequent displacement of the octahedrally coordinated Co(II)/Ru(II) linker. Incorporation of Ru(tppz) increases the reactivity due to the increased overall charge of the molecule and  $\pi$ -back donation by the tppz ligand which increases the electrophilicity of the Pt(II) metal centre. The increase in the number of tppz ligands further stabilises the LUMO ( $\pi^*$ ). Presence of two Ru(II) metal centres increase the intermetallic electronic communication within the molecule. Changing the metal centre from Ru(II) to Co(II), decreases the reactivity due to the weaker  $\pi$ -back donation. In all cases, the reactivity decrease with increase in the steric hindrance of the nucleophiles. The dechelation process is enhanced by the ligand field strength imposed by the addition of thiourea nucleophiles at the Pt(II) metal centre. The observed relatively low enthalpy of activation,  $\Delta H^\ddagger$  and the negative entropy of activation,  $\Delta S^\ddagger$  support an associative mode of activation for the steps. The observed kinetic results were supported by density functional theory (DFT) studies.

### 3.1 Introduction

The success of cisplatin as an anticancer drug prompted interest in platinum based drugs.<sup>1</sup> However, due to the drawbacks of cisplatin such as nephrotoxicity and neurotoxicity,<sup>2</sup> limited water solubility<sup>3</sup> and resistance in certain tumour cells,<sup>2e,4</sup> chemists were provoked to synthesize a variety of analogues, of which, only few have shown potential for clinical application.<sup>5</sup> Thus, research has given a particular interest on development of effective anticancer agents with fine-tuned performance. In this regard, particular focus is given on the development of combination therapy, consisting of multiple bioactive sites<sup>6</sup> and structurally different complexes of cisplatin derivatives with altered pharmacokinetic and pharmacodynamic properties which can exhibit effective antitumour activity with less side effects and tumour resistance. As such, mixed-metal supramolecular<sup>7</sup> complexes of transition metals such as ruthenium, cobalt and platinum complexes have provided fertile grounds in modern chemistry due to their increased potency as anticancer agents.<sup>6,8</sup> Today, a number of supramolecular systems with various applications are known. These complexes are expected to disclose improved new chemical, physiological and biological activities.<sup>7a,9</sup>

Special attention has been given to such complexes possessing polypyridyl ligands.<sup>8c,10</sup> Polypyridyl ligands form stable complexes with transition metals of different oxidation states.<sup>11</sup> Such polypyridyl complexes consisting of polyazine bridging ligands between the two metal centres have shown enhanced electrostatic interactions with target nucleophiles.<sup>8b,11-12</sup> Focus is given to multinuclear polyazine complexes of ruthenium due to their rich photophysical, redox properties,<sup>6a,13</sup> their metal to ligand charge transitions (MLCT)<sup>8a,14</sup> and biological activities such as cleaving DNA in the presence of oxygen.<sup>15</sup> These MLCT states undergo intermolecular electron transfers with easily tunable ground state and excited state redox properties.<sup>8a</sup>

In multinuclear complexes, the design of bridging ligand is important given that electron transfer between the metal centres depend on the type and nature of the bridging ligand.<sup>8c,16</sup> In this regard, the ligand, tetra-2-pyridyl-1,4-pyrazine (tppz), is one of the known polyazine bridging ligand which is capable of forming monomeric and back-to-back<sup>8b,17</sup> polymeric transition metal complexes.<sup>11,14</sup> Homo and heterodimetalic analogues of tppz with ruthenium,<sup>6a,8a,17-18</sup> osmium,<sup>8a</sup> cobalt,<sup>19</sup> palladium<sup>20</sup> and platinum<sup>6a</sup> have been recently reported.<sup>6a,11,14,21</sup>

Mixed-metal supramolecular bioactive complexes of ruthenium of the form  $[(\text{tpy})\text{RuCl}(\text{BL})\text{PtCl}_2](\text{PF}_6)$  and  $[(\text{bpy})_2\text{Ru}(\text{dpp})\text{PtCl}_2]^{2+}$  (BL = dpp, dpq (dpq = 3 bis-(2-pyridyl)benzoquinoxaline), dpb (dpb = 2,3- bispyridyl)benzoquinoxaline) and (bpy ) 2,2'-bipyridine)) coupled with a *cis*-Pt(II)Cl<sub>2</sub> moiety *via* a bridging ligand have been investigated recently<sup>6a,22</sup> and the latter complex was found to photo-cleave DNA through ruthenium chromophore.<sup>9</sup> Recently, Higgins *et al.*<sup>22b,23</sup> reported DNA interaction with mixed-metal Ru(II)-Pt(II) complexes of the form  $[(\text{Ph}_2\text{phen})_2\text{Ru}(\text{BL})\text{PtCl}_2]^{2+}$  where Ph<sub>2</sub>phen = 4,7-diphenyl-1,10-phenanthroline. These complexes were reported to modify DNA by a new mechanism of photobinding that involves metal to ligand charge transfer (MLCT) excitations using visible light.<sup>22b</sup> Furthermore, the spectroscopic properties of Ru(II) chromophore are imparted onto the Pt(II) bioactive site demonstrating the significance of supramolecular architecture<sup>22b</sup> thus, enhancing the antitumour activity of the complex.

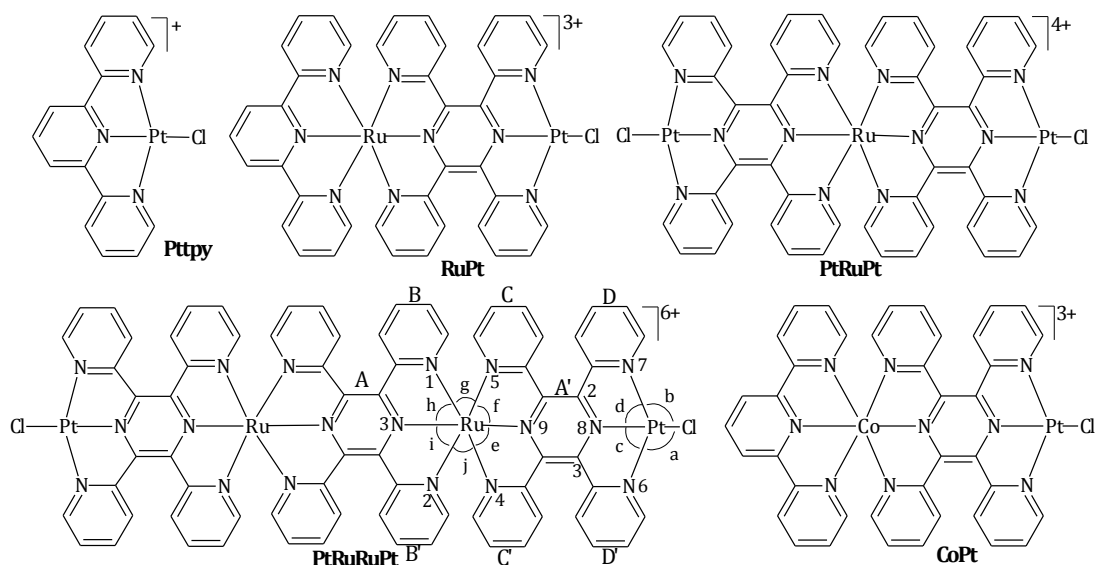
Another aspect of mixed-metal interest is complexes consisting of cobalt, due to its usefulness as bimetallic catalysis,<sup>24</sup> electrochemistry<sup>25</sup> luminescent properties<sup>26</sup> and interaction with biological systems.<sup>27</sup> The biological role of cobalt has shown antitumour, antiproliferative,<sup>27b</sup> antimicrobial,<sup>28</sup> antifungal,<sup>29</sup> antiviral<sup>30</sup> and antioxidant activities.<sup>27a</sup> Apart from direct covalent coordination with DNA, cobalt complexes show noncovalent bindings such as hydrogen bonding and electrostatic groove bindings. Additionally, coupled with planar aromatic ligands, cobalt complexes undergo intercalation with DNA.<sup>27a,31</sup>

DNA intercalation and binding activity of Co(II) phenanthroline, terpyridine and dipyrido complexes have been reported.<sup>27a,31e-g</sup> The Co(II) complexes,  $[\text{Co}(\text{abz})\text{Cl}_2(\text{H}_2\text{O})]\cdot 3\text{H}_2\text{O}$  where abz = albendazole reported by Lopez-Sandoval *et al.*<sup>27b</sup> showed stronger anticancer activity towards human cancer cell lines than cisplatin. However, there is no literature available on ligand substitution reactions of mixed-metal Co(II) complexes<sup>32</sup> with a few reported on cobalt by van Rudi and co-workers.<sup>33</sup>

Recently, Ru(II)-Pt(II) mixed-metal complexes of  $[(\text{tpy})\text{Ru}(\text{tppz})\text{PtCl}](\text{PF}_6)_3$  and  $[\text{ClPt}(\text{tppz})\text{Ru}(\text{tppz})\text{PtCl}](\text{PF}_6)_4$  where a ruthenium light absorber is coupled with a platinum bioactive site through the bridging ligand tppz were synthesized by Zhao *et al.*<sup>6a</sup> The bioactive site, Pt(II) tpy moiety, in these complexes, has been reported to intercalate with the DNA double strands,<sup>8b</sup> thus, labilizing the Pt–Cl bond.<sup>6a</sup> Modification of DNA by these complexes was found to be more intense than by the well-

known anticancer drug, cisplatin.<sup>8b</sup> The mode of interaction of the complexes with DNA was found to be different from cisplatin. Coupling with light absorbing ruthenium improves solubility due to the high overall charge. Furthermore, interaction of these complexes with DNA was found to exhibit strong charge transitions from Ru(II) to anti-bonding orbitals ( $\pi^*$ ) of tppz

Since these complexes are potential anticancer agents, understanding the mechanism of action of these complexes with human cells is important. Thus, this work reports for the first time the kinetic and mechanistic study of mixed-metal Ru(II)-Pt(II) and Co(II)-Pt(II) complexes of the form  $[(\text{tpy})\text{Ru}(\text{tppz})\text{PtCl}](\text{PF}_6)_3$ ,  $[\text{ClPt}(\text{tppz})\text{Ru}(\text{tppz})\text{PtCl}](\text{PF}_6)_4$ ,  $[\text{ClPtRu}_2(\text{tppz})_3\text{PtCl}](\text{PF}_6)_6$  and  $[(\text{tpy})\text{Co}(\text{tppz})\text{PtCl}](\text{PF}_6)_3$  with biorelevant thiourea nucleophiles *viz*; TU, MTU, DMTU, TMTU and ionic nucleophiles,  $\text{I}^-$  and  $\text{SCN}^-$ . For comparisons, data from literature was used for the well-known Pt(II) complex, **Ptttpy**. The two complexes,  $[(\text{tpy})\text{Ru}(\text{tppz})\text{PtCl}](\text{PF}_6)_3$  and  $[\text{ClPt}(\text{tppz})\text{Ru}(\text{tppz})\text{PtCl}](\text{PF}_6)_4$  were the first Ru(II)-Pt(II) rigid tridentate bridged mixed-metal complexes shown to bind with DNA.<sup>6a</sup> The complexes studied are given in *Scheme 3.1*.



**Scheme 3.1** Structural formulae of investigated complexes. The numbering schemes used for DFT calculations and the other references are shown on the structure of PtRuRuPt.

## 3.2 Experimental

### 3.2.1 Chemicals

Potassium tetrachloroplatinate ( $\text{K}_2\text{PtCl}_4$ , 99.99%), ruthenium(III) chloride trihydrate (98%), 1,5-cyclooctadiene (99%) and silver tetrafluoroborate ( $\text{AgBF}_4$ , 98%) were purchased from Aldrich and stored in a dessicator prior to use. Methanol (Merck, South Africa) was distilled over magnesium<sup>34</sup> prior to use in kinetic analysis. Ammonium hexafluorophosphate (98%) was purchased from Fluka. Acetonitrile (BDH,  $\geq 99.5\%$ ), dimethylsulfoxide (99.9%) were purchased from Aldrich and used as supplied. The ligand, tetra-2-pyridyl-1,4-pyrazine (97%) was bought from Aldrich. All other chemicals were purchased from Sigma Aldrich and used as received.

### 3.2.2 Characterizations and Instrumentations

$^1\text{H}$  NMR were recorded on either a Bruker Avance 400 or 500 MHz spectrometer, at 303 K using tetramethylsilane,  $\text{Si}(\text{CH}_3)_4$  as the reference for the chemical shifts.  $^{195}\text{Pt}$  NMR were studied on a 500 MHz spectrometer ( $^{195}\text{Pt}$ , 107.5 MHz) chemical shifts externally referenced to  $\text{K}_2\text{PtCl}_6$ . Both  $^1\text{H}$  and  $^{195}\text{Pt}$  NMR spectroscopy are useful techniques to determine the coordination behaviour of the metal centres since their chemical shifts are influenced by the coordinating atoms, solvent and the temperature.<sup>35</sup> Mass spectra were obtained on a Hewlett Packard HP5988A GC-MS using electron impact (IE) negative ionisation mode. Elemental analyses were performed by a Thermal Scientific Flash 2000. Kinetic analyses were studied either on Varian Cary 100 Bio UV/visible spectrophotometer with an attached Varian Peltier temperature-controller an online kinetic applications or on an Applier Photophysics SX 20 stopped-flow reaction analyser coupled with an online data acquisition. The temperature of the instrument was controlled within  $\pm 0.1$  °C.

### 3.2.3 Synthesis of Ruthenium Precursors and Intermediate Complexes

The  $[\text{Ru}(\text{tpy})\text{Cl}_3]$ ,<sup>36</sup> precursor and the intermediate complexes, viz;  $[(\text{tpy})\text{Ru}(\text{tppz})](\text{PF}_6)_2$ ,<sup>11</sup>  $[\text{Ru}(\text{tppz})_2](\text{PF}_6)_2$ ,<sup>11</sup> and  $[\text{Ru}_2(\text{tppz})_3](\text{PF}_6)_4$ <sup>11</sup> were synthesized according to the literature procedures. Details of experimental procedures are given under Supporting Information.

The purity of the intermediate complexes was confirmed by using  $^1\text{H}$  NMR and mass spectroscopy. The mass spectra obtained for the all complexes show characteristic peaks due to different species. Due to the poor solubility<sup>37</sup> and the paramagnetic nature, the  $\text{Ru}(\text{tpy})\text{Cl}_3$  precursor was used as synthesized.<sup>36</sup>

**[Ru(tpy)Cl<sub>3</sub>]<sup>36</sup>**

Yield: 191 mg, 433 mmol, (76%), brown precipitate.

**[(tpy)Ru(tppz)](PF<sub>6</sub>)<sub>2</sub>**<sup>11</sup> Yield: 70 mg, (60%), brown powder <sup>1</sup>HNMR(400 MHz, CH<sub>3</sub>CN)  $\delta$  (ppm)<sup>†</sup>: 8.77 (2H, ds, *J* = 8.5 Hz), 8.50 (1H, t), 8.54 (2H, s), 7.99 (2H, t, *J* = 8.05, 7.63, 1.2 Hz), 7.25 (2H, t, *J* = 7.5, 6.0, 1.0 Hz), 7.58 (2H, t, *J* = 6.0, 1.0 Hz), 8.37 (2H, t, *J* = 7.5, 1.8 Hz), 8.24 (2H, t, *J* = 8.0, 6.5, 1.7 Hz), 7.75 (2H, d, *J* = 7.8, 6.8, 1.7 Hz), 8.75 (2H, d, *J* = 5.0, 2.0 Hz), 7.55 (2H, t, *J* = 8.0, 6.0, 1.8 Hz), 7.61 (2H, t, *J* = 8.0, 6.0, 1.8 Hz), 7.15 (2H, t, *J* = 7.8, 6.2, 1.5 Hz), 7.41 (2H, d, *J* = 5.4, 1.6 Hz). TOF MS-ES+, *m/z*: 361.5719 (*M*<sup>2+</sup>).

**[Ru(tppz)<sub>2</sub>](PF<sub>6</sub>)<sub>2</sub>**<sup>11</sup> Yield: 98 mg, (39%), brown powder <sup>1</sup>HNMR(400 MHz, CH<sub>3</sub>CN)  $\delta$  (ppm): 8.38 (4H, d, *J* = 8.0 Hz), 8.26 (4H, t, *J* = 8.3, 7.8, 1.4 Hz), 7.78 (4H, dd, *J* = 7.8, 2.1 Hz), 8.77 (4H, d, *J* = 5.0 Hz), 7.64 (4H, d, *J* = 7.4 Hz), 7.66 (4H, d, *J* = 8.0 Hz), 7.22 (4H, dt, 6.9, 6.3, 1.2 Hz), 7.67 (4H, d, 5.1 *J* = Hz). TOF MS-ES+, *m/z*: 439.0962, (*M*<sup>2+</sup> + 1).

**[Ru<sub>2</sub>(tppz)<sub>3</sub>](PF<sub>6</sub>)<sub>4</sub>**<sup>11</sup> Yield: 50 mg, (12%), dark purple powder <sup>1</sup>HNMR(400 MHz, CH<sub>3</sub>CN)  $\delta$  (ppm): 9.06 (4H, d, *J* = 8.7, 1.2 Hz), 8.78 (4H, d, *J* = 4.8 Hz), 8.54 (4H, d, *J* = 8.1 Hz), 8.33 (4H, dt, *J* = 8.1, 7.5, 1.7 Hz), 8.03 (4H, br), 8.01 (4H, br), 7.84 (4H, br), 7.81 (4H, br), 7.77 (4H, dd, *J* = 7.5, 1.3 Hz), 7.73 (4H, br), 7.54 (4H, dt, *J* = 7.1, 7.0, 1.2 Hz), 7.31 (4H, dt, *J* = 7.1, 6.7, 1.6 Hz). TOF MS-ES+, *m/z*: 342.0604, (*M*<sup>4+</sup>).

**3.2.4 Synthesis of Platinum(II) Complexes**

The Pt(II) complexes, [Pt(DMSO)<sub>2</sub>Cl<sub>2</sub>]<sup>38</sup> and [Pt(tpy)Cl]Cl·H<sub>2</sub>O (**Pttpy**)<sup>39</sup> were synthesized as in literature. The heterometallic complexes, [(tpy)Ru(tppz)PtCl](PF<sub>6</sub>)<sub>3</sub> (**RuPt**)<sup>8b</sup> and the analogous complex [(tpy)Ru(tppz)PtCl](PF<sub>6</sub>)<sub>3</sub> (**CoPt**)<sup>8b</sup> [ClPt(tppz)Ru(tppz)PtCl](PF<sub>6</sub>)<sub>4</sub> (**PtRuPt**)<sup>8b</sup> and [PtCl(tppz)Ru(tppz)Ru(tppz)PtCl](PF<sub>6</sub>)<sub>6</sub> (**PtRuRuPt**)<sup>8b</sup> were synthesized following the literature method reported by Zhao *et al.*<sup>8b</sup> Details of experimental procedures and respective spectra are given under Supporting Information.

<sup>†</sup>  $\delta$  ppm, s = singlet, quat = quaternary, m = multiplet, dd = doublet of doublet, dt = doublet of triplets



The identity and the purity of the complexes were confirmed by using  $^1\text{H}$  NMR,  $^{195}\text{Pt}$  NMR, elemental analyses and mass spectroscopy. The  $^1\text{H}$  NMR spectra obtained show the symmetric nature of the heterometallic complexes. The  $^{195}\text{Pt}$  NMR of all the complexes exhibited a characteristic signal between -2500 to -2600 ppm which confirms the coordination of platinum to the Ru(II) moieties. Due to the high charge and complexity of the molecules, the mass spectra obtained show characteristic fragmentation of the molecules.

**[PtCl<sub>2</sub>(DMSO)<sub>2</sub>]<sup>38</sup>**

Yield: 1.25 g, 65%, fine yellow crystals. *Anal. Calc. for* C<sub>4</sub>H<sub>12</sub>Cl<sub>2</sub>O<sub>2</sub>PtS<sub>2</sub>: C 11.38, H 2.86. *Found*: C 11.67, H 3.10.

**[Pt(tpy)Cl]Cl·H<sub>2</sub>O (Pttpy)<sup>39</sup>** Yield: 0.64 g, 1.19 mmol (89%), Orange crystalline powder. *Anal. Calc. for* C<sub>15</sub>H<sub>13</sub>N<sub>3</sub>Cl<sub>2</sub>OPt: C 34.83, H 2.53, N 8.12. *Found*: C 34.92, H 2.98, N 7.75.

**[(tpy)Ru(tppz)PtCl](PF<sub>6</sub>)<sub>3</sub> (RuPt)** The complex was synthesized by modification of the literature method reported by Zhao *et al.*<sup>8b</sup> To a refluxing solution of [Pt(DMSO)<sub>2</sub>Cl<sub>2</sub>] (80 mg, 0.38 mmol) in acetonitrile (10 mL), a solution of [(tpy)Ru(tppz)](PF<sub>6</sub>)<sub>2</sub> (48 mg, 48 mmol) in acetonitrile (10 mL) was added drop wise under nitrogen. The reaction mixture was refluxed for 6 hours. After cooling to room temperature, the mixture was filtered and the filtrate was added to an aqueous solution of ammonium hexafluoro phosphate (50 mL, 3 M). The purple precipitate formed was vacuum filtered, washed with ethanol (5 mL), distilled water (20 mL) and copious amount of diethyl ether. Yield: 50 mg, 36 mmol, (76%), very dark purple powder.  $^1\text{H}$ NMR(500 MHz, CH<sub>3</sub>CN)  $\delta$  (ppm): 9.45 (2H, dd,  $J$  = 5.6, 1.3 Hz), 8.89 (2H, d,  $J$  = 8.2 Hz), 8.87 (2H, d,  $J$  = 8.5, 1.0 Hz), 8.75 (2H, d,  $J$  = 8.7, 1.1 Hz), 8.63 (1H, t,  $J$  = 16.7, 8.3 Hz), 8.56 (2H, d,  $J$  = 7.7 Hz), 8.45 (dt, 2H,  $J$  = 8.0, 7.8, 1.6 Hz), 8.12 (2H, dt,  $J$  = 6.9, 6.7, 1.2 Hz), 8.02 (2H, t,  $J$  = 8.0, 7.9, 1.4 Hz), 7.99 (2H, t,  $J$  = 7.8, 6.3, 1.5 hz), 7.69 (2H, d,  $J$  = 6.3, 1.1 Hz), 7.49 (2H, d,  $J$  = 6.2, 1.0 Hz), 7.45 (2H, d,  $J$  = 7.8, 6.8, 1.5 Hz), 7.18 (2H, t,  $J$  = 7.8, 6.3, 1.5 Hz),  $^{195}\text{Pt}$  NMR (CH<sub>3</sub>CN)  $\delta$ / ppm: -2593. TOF MS-ES+,  $m/z$ : 318.0260, ( $\text{M}^{3+}$ ). *Anal. Calc. for* C<sub>39</sub>H<sub>27</sub>ClF<sub>18</sub>N<sub>9</sub>P<sub>3</sub>PtRu·5H<sub>2</sub>O: C 31.68, N 8.56, H 2.52. *Found*: C 31.96, N 8.10, H 2.03.

**[ClPt(tppz)Ru(tppz)PtCl](PF<sub>6</sub>)<sub>4</sub> (PtRuPt)<sup>8b</sup>** This compound was synthesized by a similar approach as [(tpy)Ru(tppz)PtCl](PF<sub>6</sub>)<sub>3</sub>. Yield: 62 mg, 32 mmol (77%), very dark purple powder. <sup>1</sup>H NMR (500 MHz, CH<sub>3</sub>CN)  $\delta$  (ppm): 9.51 (4H, dd,  $J$  = 5.5 Hz), 8.91 (4H, d,  $J$  = 8.4 Hz), 8.77 (4H, d,  $J$  = 8.5, 1.0 Hz), 8.51 (4H, dt,  $J$  = 8.2, 7.9, 1.3 Hz), 8.19 (4H, dt,  $J$  = 6.6, 7.1, 1.0 Hz), 8.09 (4H, t,  $J$  = 8.1, 8.01.0 Hz), 7.89 (4H, br, ), 7.50 (4H, br), <sup>195</sup>Pt NMR (CH<sub>3</sub>CN)  $\delta$ / ppm: -2568. TOF MS-ES+,  $m/z$ : calculated: 318.0258, experimental: 318.0260  $\pm$  0.6). *Anal. Calc. for* C<sub>48</sub>H<sub>32</sub>Cl<sub>2</sub>F<sub>24</sub>N<sub>12</sub>P<sub>4</sub>Pt<sub>2</sub>Ru·H<sub>2</sub>O: C 29.77, N 8.68, H 1.77. *Found*: C 29.35, N 8.28, H 2.24.

**[ClPt(tppz)Ru(tppz)Ru(tppz)PtCl](PF<sub>6</sub>)<sub>4</sub> (PtRuRuPt)<sup>8b</sup>** The compound was synthesized by using an approach similar to [ClPt(tppz)Ru(tppz)PtCl](PF<sub>6</sub>)<sub>4</sub>. Yield: 0.0201 g, (75%), dark purple powder. <sup>1</sup>H NMR (500 MHz, CH<sub>3</sub>CN),  $\delta$  (ppm): 9.56 (4H, dd,  $J$  = 6.2, 1.1 Hz), 9.07 (4H, d,  $J$  = 8.0 Hz), 9.01 (4H, d,  $J$  = 8.0 Hz), 8.91 (4H, d,  $J$  = 7.9 Hz), 8.55 (4H, dt,  $J$  = 8.2, 8.0, 1.3 Hz), 8.23 (4H, dt,  $J$  = 7.2, 7.0, 1.1 Hz), 8.17 (4H, br), 8.11 (4H, br), 8.08 (4H, br), 7.97 (4H, d,  $J$  = 6.2 Hz), 7.64 (4H, t,  $J$  = 7.7.2, 7.0 Hz), 7.52 (4H, t,  $J$  = 7.8 Hz), <sup>195</sup>Pt NMR (CH<sub>3</sub>CN)  $\delta$ / ppm: -2574. TOF MS-ES+,  $m/z$ : 342.0879, (M<sup>6+</sup> -6H, where one chloride ligand is substituted by a DMSO molecule). *Anal. Calc. for* C<sub>72</sub>H<sub>48</sub>Cl<sub>2</sub>F<sub>36</sub>N<sub>18</sub>P<sub>6</sub>Pt<sub>2</sub>Ru<sub>2</sub>·5H<sub>2</sub>O: C 31.01, N 9.08, H 2.10. *Found*: C 31.45, N 8.74, H 1.82.

**[(tpy)Co(tppz)PtCl](PF<sub>6</sub>)<sub>3</sub> (CoPt)<sup>8b</sup>** This complex was synthesized following the method used for [(tpy)Ru(tppz)PtCl](PF<sub>6</sub>)<sub>3</sub>. Yield: 20 mg, (58%), dark brown powder. TOF MS-ES+,  $m/z$ : 625.1257, (C<sub>34</sub>H<sub>23</sub>CoN<sub>8</sub> species)<sup>+</sup>. *Anal. Calc. for* C<sub>39</sub>H<sub>27</sub>ClF<sub>18</sub>N<sub>9</sub>P<sub>3</sub>PtCo: C 34.80, N 9.37, H 2.02. *Found*: C 34.82, N 8.96, H 2.18.

### 3.2.5 Preparation of Nucleophile Solutions for Kinetic Measurements

The solutions of nucleophiles, *viz.* TU, MTU, DMTU, TMTU, I<sup>-</sup> and SCN<sup>-</sup> were prepared by dissolving the required amount of the nucleophile in methanol solution of fixed ionic strength of 0.02 M (adjusted with LiCF<sub>3</sub>SO<sub>3</sub> and LiCl) to afford a concentration of approximately equal to 50 times greater than that of the metal complex for mono chloro compounds and approximately 100 times greater for dichloro compounds. The other nucleophile solutions were prepared by subsequent dilutions of the same stock solution to afford a series of standards of 10, 20, 30 and 40 (for mono chloro compounds) or 20, 40, 60 and 80 (for dichloro compounds) times that of the platinum complex. The concentration of the nucleophiles were kept *pseudo* first-order conditions to push the substitution reactions to completion.<sup>40</sup>

### 3.2.6 Kinetic Measurements

To establish a wavelength to perform the kinetic measurements, the spectral changes resulting in from mixing the metal complexes with the ligand solutions were predetermined on a UV/visible spectrophotometer over the wavelength range of 200 – 800 nm. The wavelengths are summarised in *Table S3.1* (Supporting Information). The fast substitution reactions were studied on an Applied Photophysics SX 20 stopped-flow system which is coupled with an online data acquisition system. The substitution kinetics of the slower reactions were purposely analysed on UV/visible spectrophotometer. A typical kinetic trace obtained from the stopped-flow spectrophotometry for the reaction of **CoPt** with TU at 298 K is shown in *Figure 3.4* and *Figure S3.1* (Supporting Information). Temperature dependence studies were performed within the range of 15 – 40 °C. All data were mathematically analysed using Origin 7.5®.<sup>41</sup> Representative graphs are given in *Figures 3.5, 3.6, and Figure S3.2* to *Figure S3.9*.

### 3.2.7 Computational Modelling

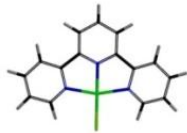
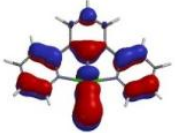
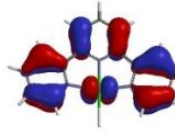

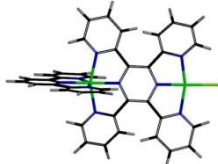
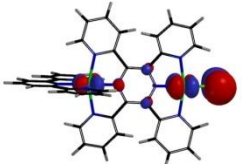
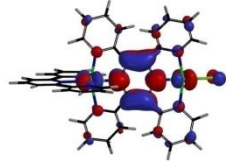
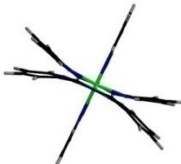
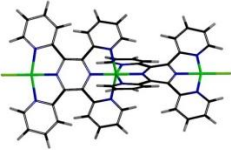
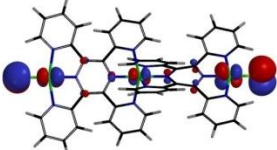
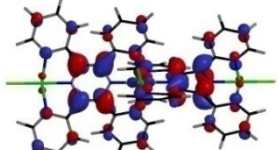
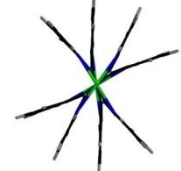
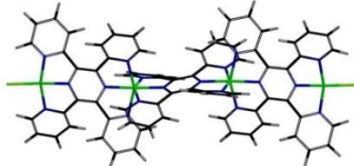
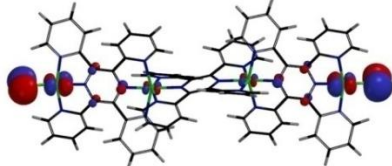
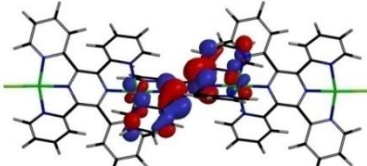
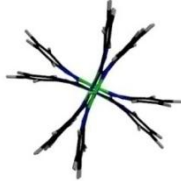
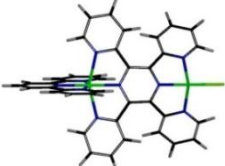
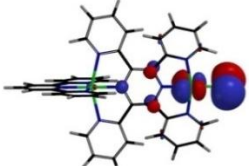
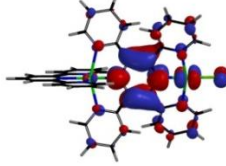
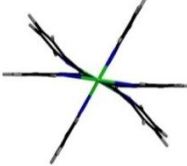
Computational calculations for the complexes **Ptppy**, **RuPt**, **PtRuPt**, **PtRuRuPt**, and **CoPt** were performed in gas phase as cations for the chloro complexes, using the software package Spartan® '04 for Windows®.<sup>42</sup> using the B3LYP<sup>43</sup>, density functional method (DFT)<sup>44</sup> and the LACVP+\*\* (Los Alamos Core Valence Potentials)<sup>45</sup> pseudo potential basis set. The LACVP basis set employs effective core potentials for K-Cu, Pb-Ag, Cs-La and Hf-Au.<sup>46</sup> Data obtained are summarized in *Tables 3.1, 3.2 and Tables S3.2 and S3.3*. The numbering scheme used is as given in *Scheme 3.1*.

**Table 3.1** Selected bond lengths (Å), bond angles (°), natural bond orbital (NBO) charges, HOMO and LUMO energies and other computational data obtained for the complexes Pttpy, RuPt, PtRuPt, PtRuRuPt and CoPt obtained from the computational studies. Data for Pttpy is included for reference.

	Pttpy	RuPt	PtRuPt	PtRuRuPt	CoPt
<b>Bond lengths (Å)</b>					
Pt–N ( <i>trans</i> )	1.966	1.972	1.969	1.967	1.961
Pt–Cl	2.347	2.320	2.313	2.303	2.317
N–N(pyrzine)		2.657	2.646	2.662	2.660
Ru–Pt		6.624	6.651	6.663	
Co–Pt					6.649
Pt–Pt			13.30	24.61	
N–N(pyridine)		2.657	2.646	2.662	2.660
Ru–N(pyrzine <i>cis</i> )		2.020	2.036	2.058	2.028
<b>Torsion Angles(°)</b>					
C–C–C- C of tppz central/terminal		10.39	24.15	11.10	25.00
N7C2C3N6 <sub>(with Pt)</sub>		0.44	11.62	0.03	13.02
<b>NBO charges</b>					
Pt <sub>1/2</sub>	1.227	1.255	1.266	1.283	1.263
N <sub>trans</sub>	-0.565	-0.567	-0.560	-0.565	-0.547
Cl	-0.637	-0.565	-0.541	-0.504	-0.562
Ru/Co		0.997	0.989	1.000	1.319
N1		-0.502	-	-0.496	-0.546
N2		-0.498	-	-0.494	-0.546
N3		-0.492	-	-0.474	-0.533
N4		-0.489	-0.496	-0.500	-0.547
N5		-0.491	-0.495	-0.502	-0.547
N9		-0.471	-0.474	-0.484	-0.554
HOMO/eV	-9.45	-13.22	-14.76	-16.76	-13.42
LUMO/eV	-6.16	-10.75	-12.52	-15.09	-10.81
$\Delta E$ /eV	3.29	2.47	2.24	1.67	2.61
$\eta$ /eV	1.65	1.24	1.12	0.84	1.31
$\mu$ /eV	-7.81	-11.99	-13.64	-15.93	-12.12
$\omega$ /eV	18.46	57.92	83.06	150.96	56.02

$\eta$  = chemical hardness,  $\mu$  = chemical potential and  $\omega$  = global electrophilicity index.<sup>47</sup> NBO = natural bond orbital.

**Table 3.2** Density functional theoretical (DFT) calculated minimum energy structures, HOMO and LUMO frontier molecular orbitals for the complexes investigated. The planarity of the molecules is viewed along the propagation axis showing the different planes.

Structure	HOMO Map	LUMO Map	Planarity
<b>Pttpy</b> 			
<b>RuPt</b> 			
<b>PtRuPt</b> 			
<b>PtRuRuPt</b> 			
<b>CoPt</b> 			

### 3.3 Results and Discussion

#### 3.3.1 Synthesis and Characterization

In this study, one mono nuclear **Ptppy** and four heterometallic Ru(II)/Co(II)-Pt(II) complexes were synthesized. The data obtained is in good agreement with the literature<sup>8b</sup> and the chemical structures. Details of the characterisation are given under experimental section. Exemplary spectra are presented under Supporting Information (*Figures S3.10 to S3.23*).

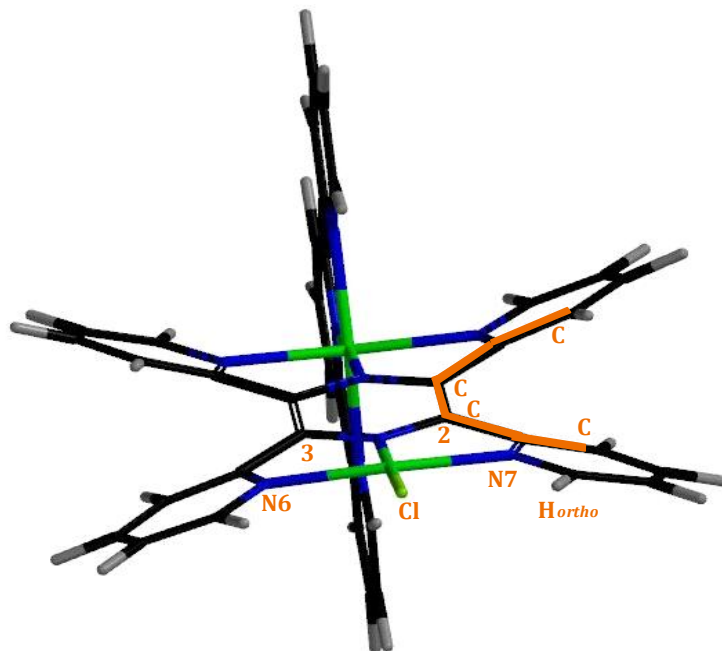
The Ru(III) metal centre gets reduced to Ru(II) during refluxing in ethanol water mixture. The paramagnetic nature of **CoPt** complex hindered the characterization using normal <sup>1</sup>H NMR studies due to broadening of signals.<sup>8c</sup> Thus, the complex was characterized using micro analysis and mass spectroscopy. The novel heterometallic complex, **PtRuRuPt** was synthesized and characterized using <sup>1</sup>H NMR, <sup>195</sup>Pt NMR, mass spectroscopy and micro analysis. In the <sup>1</sup>H NMR (*Figures S3.12 and S3.15*), only twelve signals were seen in the aromatic region, a clear indication that the complexes are symmetric. The <sup>195</sup>Pt NMR for all the complexes appeared around -2500 to -2700 ppm, typical of NNN coordinated Pt(II) centre.<sup>48</sup> For all the complexes, the mass spectra show great fragmentations.

#### 3.3.2 Computation Calculations

In order to understand the structural and electronic properties of the complexes studied, computational calculations were performed at density functional theory (DFT) level. The geometry at the Ru(II) centres is distorted octahedral<sup>6a,49</sup> while the Pt(II) centres exhibit a distorted square planar, typical for Pt(II) centres.<sup>50,46</sup> The capping tpy ligand in **RuPt** and **CoPt** is coordinated to the Ru(II) metal centre meridionally along the equatorial plane. This *mer*-tpy chelating ligand exerts steric repulsion from its extended electron cloud towards the coordinated tppz ligand maintaining some degree of stereogenic rigidity.

The optimized geometrical structures show that in all the heterometallic complexes the Co/Ru—N pyrazine bond orients along the z axis<sup>51</sup> and hence the Co/Ru—N pyrazine bond length is shorter than the Co/Ru—N pyridine which reflects the steric constraints due to the tridentate coordination and the strong back donation facilitated by the bridge-mediated intermetallic electronic interactions.<sup>17</sup> The capping pyridine groups are tilted from the central pyrazine group as can be seen in *Figure 3.1*.<sup>17,51</sup> The intermetallic Ru—Pt distances increase with increase in the number of tppz ligands in

the complex suggesting that the rigid tppz ligand controls the steric influences of the complexes throughout the series.<sup>51</sup> DFT calculations for paramagnetic **CoPt** were performed at doublet spin state.<sup>52</sup>



**Figure 3.1** Optimized molecular structure of CoPt, showing the torsion angles of the pyridyl groups.

The DFT calculated frontier orbitals show the electron density of highest occupied molecular orbital (HOMO) orbitals are predominantly located on the Pt(II) and the chloride ligands while the lowest unoccupied molecular orbital (LUMO) electron density predominantly lies on the bridging tppz ligand, an indication of the contribution from the metal centres due the strong  $\pi$ -accepting ability<sup>53</sup> which develops a high density condition in both the unoccupied and occupied orbitals,<sup>18a</sup> and hence the  $\Delta E_{\text{(gap)}}$  decreases with the number of tppz units.

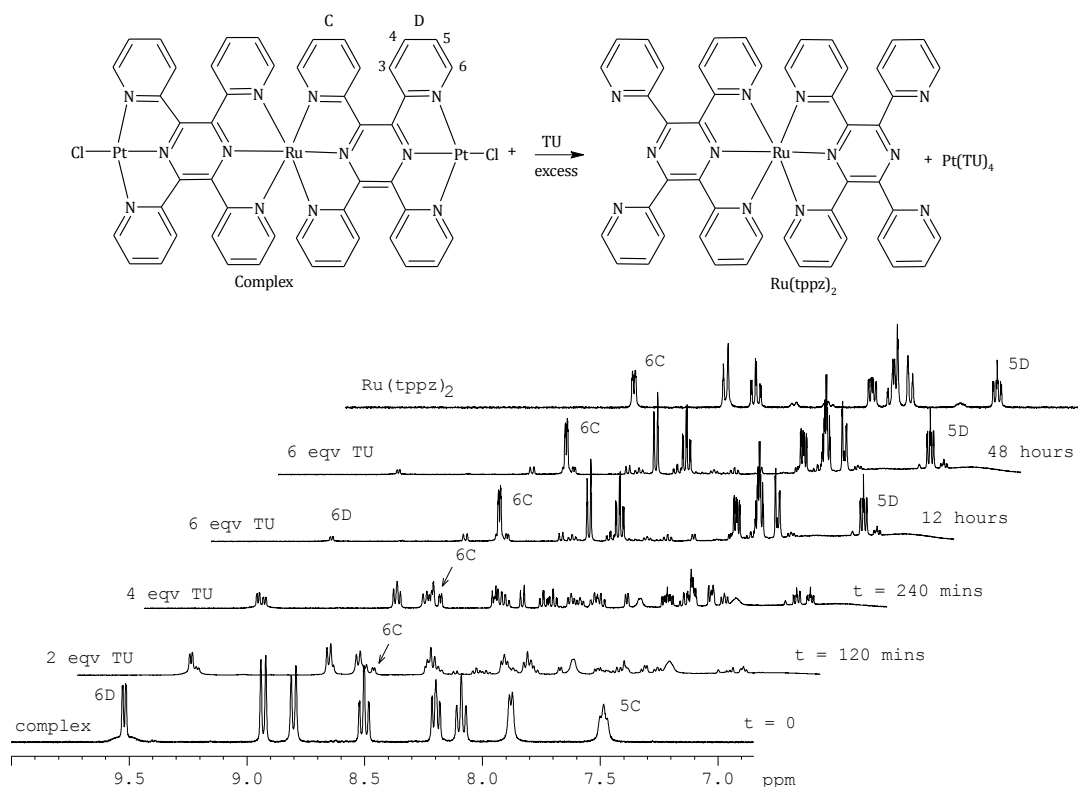
### 3.3.3 Kinetic Analyses

The substitution reactions of the heterometallic complexes with thiourea nucleophiles *viz*; TU, MTU, DMTU, TMTU and ionic nucleophiles,  $\text{I}^-$  and  $\text{SCN}^-$  were carried out in methanol. Representative data are given in *Table 3.3* and *Table S3.4* to *Table S3.20* (Supporting Information). The substitution reactions occurred *via* two separated steps *i.e.* substitution of the coordinated chloride ligand(s) followed by the release of the

coordinated linker as comprehended from NMR study (*Figures 3.2, 3.4, S3.24 and S3.25*).

This conclusion was drawn after monitoring the reaction between **PtRuPt** with TU (6 eqv) and **RuPt** with TU (3 equivalence, eqv) as a nucleophile by  $^1\text{H}$  NMR and  $^{195}\text{Pt}$  NMR spectroscopy in acetonitrile. To rule out solvolysis, a freshly prepared solution of **PtRuPt** in acetonitrile (0.02 mM) was monitored under UV/visible spectrophotometer over 12 hours and change in absorbance was observed (*Figure S3.26*). Arrays of the  $^1\text{H}$  NMR and  $^{195}\text{Pt}$  NMR spectra recorded for **PtRuPt** with 6 eqv of TU and **RuPt** with 3 eqv TU are given in *Figures 3.2 and 3.3* respectively. Representative  $^{195}\text{Pt}$  NMR spectra for **PtRuPt** with TU (6 eqv) is depicted in *Figure S3.25*. As seen in *Figure 3.2* a new set of  $^1\text{H}$  NMR signals, slightly upfield were observed after mixing **PtRuPt** with TU. The intensity of the distinctive signals of the coordinated complex, 6D (9.52 ppm) and 5C (7.49 ppm) decreased during the reaction. The two signals nearly disappeared after 240 minutes of the reaction and new signals at 8.78 ppm (doublet) and 7.23 ppm (triplet) were well formed. The spectrum obtained after twelve hours with 6 equivalence of TU produced a spectrum same as that of the linking Ru(II) complex,  $(\text{Ru}(\text{tppz})_2)$ , indicating complete dechelation of the terminal Pt(II) centre. Furthermore, the  $^1\text{H}$  NMR spectrum obtained after 48 hours is similar to the spectrum obtained after twelve hours, hence re-chelation of the  $(\text{Ru}(\text{tppz})_2)$  ligand with platinum is ruled out. Since the first step of the reaction is fast and takes less than 5 seconds to complete, this substitution step cannot be followed by the NMR technique.<sup>50</sup> Thus, it can be concluded that the subsequent changes with the addition of TU in the spectra are due to the dechelation of the coordinated ligand.

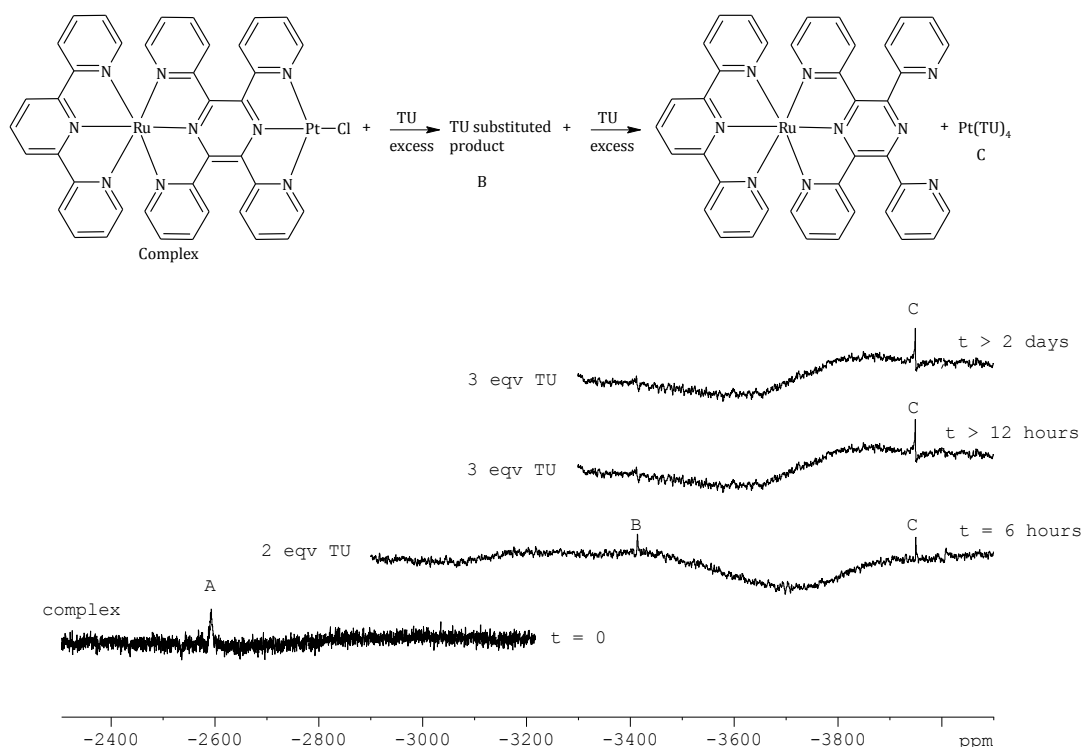




**Figure 3.2**  $^1\text{H}$  NMR spectra of PtRuPt (6.48 mM) with TU in acetonitrile at 298 K showing the dechelation of the coordinated platinum complex to form the  $(\text{Ru}(\text{tppz})_2)$  unit. The spectra also indicates the formation of other intermediate products, in which some of their chemical shifts merges making it difficult to assign them exactly. The numbering system used to monitor the reaction progress is shown on the structure of PtRuPt (inset).

This was further confirmed by the  $^{195}\text{Pt}$  NMR spectra obtained for **RuPt** and **PtRuPt** (Figures 3.3, S3.24 and S3.25) after addition of 3 and 6 equivalence of TU respectively. By looking at Figure 3.3, at  $t = 0$ , the signal due to starting complex, **RuPt**, was observed at -2590 ppm. To elucidate the substitution reaction pathway with the nucleophiles, we first added two equivalence (eqv) of TU. The  $^{195}\text{Pt}$  NMR obtained after this addition shows complete disappearance of  $\text{PtN}_3\text{Cl}$  signal at -2590 ppm. The  $^1\text{H}$  NMR and  $^{195}\text{Pt}$  NMR spectra show the formation of intermediate species. After 6 hours, two species, labelled as B (-3410 ppm) and C (-3950 ppm) are formed which is typical of  $\text{PtN}_2\text{S}_2$  and  $\text{Pt}(\text{TU})_4$ <sup>2+54</sup> respectively.<sup>35a,48b,54</sup> After 12 hours, there exists uncoordinated ligand in solution as indicated by a strong doublet at 8.77 ppm (6C, Figure 3.2). Furthermore, the singlet at -3950 ppm due to the  $\text{Pt}(\text{TU})_4$  as the end product when the linking Ru(II) complex is released by TU, support the observed substitution kinetics. Additionally, when **RuPt** and **PtRuPt** were reacted with a large excess of TU (10 eqv) and (6 eqv) respectively, the  $^{195}\text{Pt}$  NMR spectra obtained for **RuPt** after 4 - 6 hours (Figure S3.24)

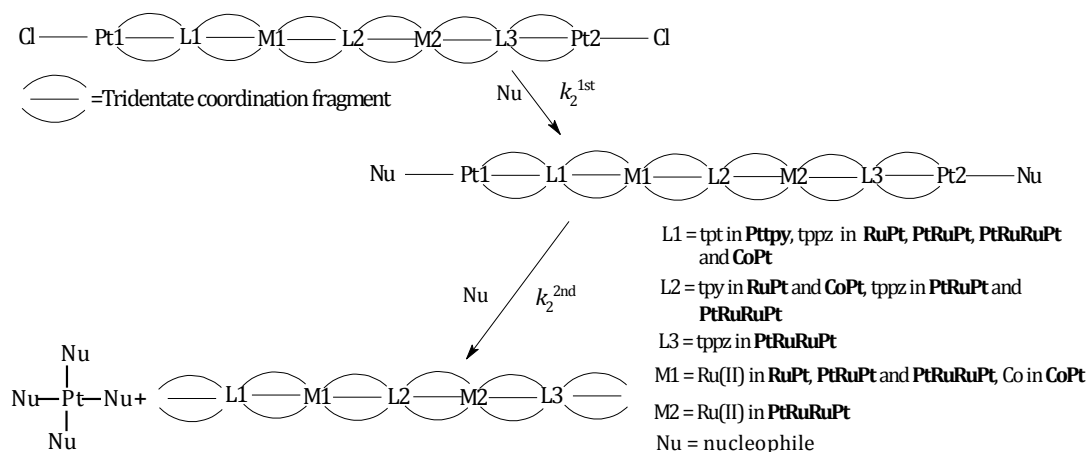
and the  $^{195}\text{Pt}$  NMR spectra obtained for **PtRuPt** after 10 - 30 hours (Figure S3.25) shows no peak corresponding to any intermediate products. In both the cases only one peak corresponding to the final product,  $[\text{Pt}(\text{TU})_4]^{2+}$  at around -4000 ppm was observed. This indicates that under *pseudo* first-order conditions the dechelation step is not stepwise and hence occurs simultaneously releasing the terminal Pt(II) centre, further supporting the observed kinetics.



**Figure 3.3**  $^{195}\text{Pt}$  NMR spectra for the reaction of RuPt (6.28 mM) with TU, showing the changes in the chemical shift of the Pt before adding the TU nucleophile and the degradation after addition of TU for the new complex  $[\text{Pt}(\text{TU})_4]^{2+}$ .

Based on NMR studies one can infer that the coordination of strong thiourea nucleophiles at terminal Pt(II) centre enhances simultaneous dissociation of the linker. Dechelation is in accord with recent reports by Jaganyi *et al.*<sup>35a,50</sup> for substitution reactions of thiourea with Pt(II) dinuclear complexes bridged by rigid pyrazine and flexible diammine linkers and van Eldik and co-workers<sup>48b,50</sup> for ring opening of bis-(2-pyridylmethyl)amine chelate groups by strong labilizing thiourea nucleophiles. It is also noted that in this study dechelation of terpyridine type chelated Pt(II) complexes is observed for the first time. Noteworthy here is that for the weaker ionic nucleophiles,  $\text{I}^-$  and  $\text{SCN}^-$ , only one step taken as the substitution of the chloride ligand was observed.

If all the facts are put together, it clearly shows that the substitution of the chloride ligand(s) occurred simultaneously from the diPt(II) complexes irrespective of the number of metal centres or the number of linking tppz groups. The second step is due to the displacement of the ligand<sup>35a</sup> caused by labilizing thiourea nucleophiles. Further support for this comes from the second substitution step, which occurs at least 2400 times slower compared to the first step in **RuPt**, **PtRuPt** and **PtRuRuPt** while it is 1400 times slower in **CoPt**. Thus, the rate of dechelation depends on the type of metal centres and irrespective of the electronic properties of the linker, ring opening is pervasive for Pt(NNN) coordinated complexes with strong labilizing thiourea nucleophiles.<sup>50</sup> Hence, the overall substitution reaction can be represented by the mechanism given in *Scheme 3.2*.



**Scheme 3.2** Proposed reaction mechanism for the reactions between the complexes, **RuPt**, **PtRuPt**, **PtRuRuPt** and **CoPt** with thiourea nucleophiles. The full reaction mechanism holds for **RuPt**, **PtRuPt**, **PtRuRuPt** and **CoPt** with thiourea nucleophiles only. For the ionic nucleophiles studied,  $I^-$  and  $SCN^-$ , the reaction mechanism holds only for the first step. The charges on the complexes are omitted for clarity.

In all cases, the first step was fast and was studied on stopped-flow method while the subsequent slower step was studied by UV/visible spectrophotometer. An example of the combined time resolved kinetic trace obtained from the stopped-flow spectrophotometer showing the two substitution steps recorded at 298 K and 382 nm using **RuPt** ( $2.00 \times 10^{-5}$  M) with TU ( $6.00 \times 10^{-4}$  M) is given in *Figure 3.4*. Included in this *Figure* is a typical kinetic trace obtained from a UV/visible spectrophotometer for the reaction between **RuPt** ( $2.00 \times 10^{-5}$  M) with TU ( $6.00 \times 10^{-4}$  M) for the second step in methanol solution ( $I = 0.02$  M) at 330 nm at 298 K. Even though, stopped-flow

analyzer could also be used to study the slower second step, the reaction was slow enough to be analyzed using UV/visible spectrophotometer, and hence, the kinetics of this step was followed under UV/visible spectrophotometer.

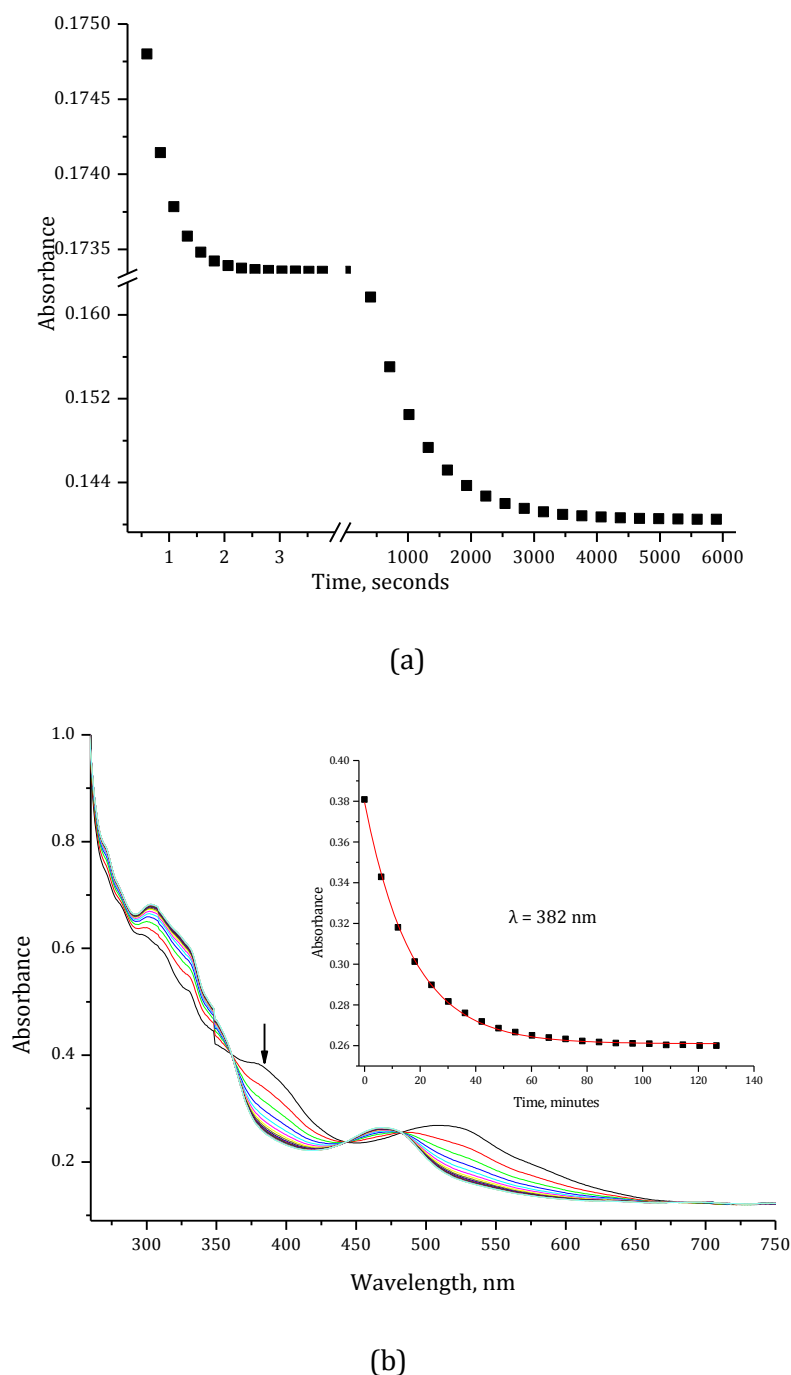


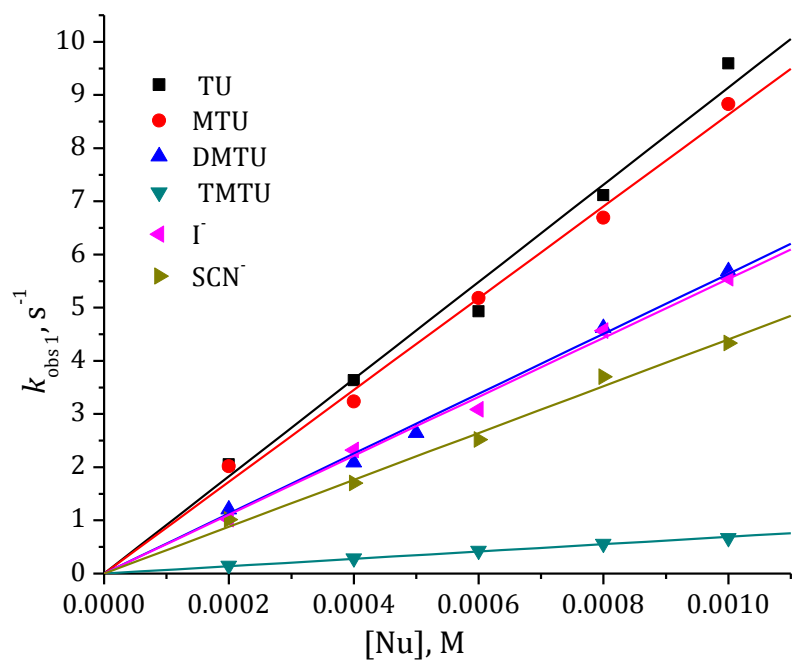
Figure 3.4

(a) Typical two well-resolved kinetic traces at 382 nm for the two-steps reaction between RuPt ( $2.0 \times 10^{-5} \text{ M}$ ) by TU ( $6.00 \times 10^{-4} \text{ M}$ ) followed on stopped-flow spectrophotometer at 298 K. (b) A typical plot showing the changes in absorbance between 250 – 750 nm wavelength range for the degradation of the chelate ligand in RuPt ( $2.00 \times 10^{-5} \text{ M}$ ) by TU ( $6.00 \times 10^{-4} \text{ M}$ ) at 298 K. Inset is the kinetic trace followed at 382 nm.  $I = 0.02 \text{ M}$  (adjusted with  $\text{LiCF}_3\text{SO}_3$  and  $\text{LiCl}$ ).

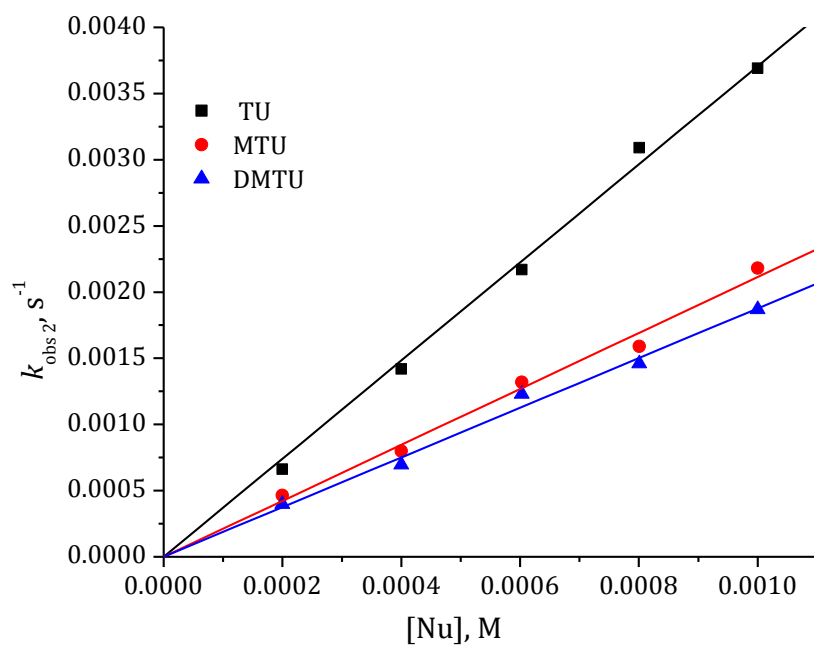
Both substitution steps fitted well to a single exponential model to obtain the observed first-order rate constant,  $k_{\text{obs}(1^{\text{st}}/2^{\text{nd}})}$ . The observed *pseudo* first-order rate constants  $k_{\text{obs}(1^{\text{st}})}$  and  $k_{\text{obs}(2^{\text{nd}})}$  were plotted against the concentration of the nucleophiles. Absence of non-zero intercepts indicated that the reactions were irreversible in nature and that they do not follow the solvotoc pathway and hence, the rate law can be written as shown in *Equation 3.1*.<sup>55</sup> The second-order rate constants,  $k_{2(1^{\text{st}}/2^{\text{nd}})}$  were obtained from the slopes of the plots. Representative plots for **PtRuPt** are shown in *Figure 3.5*. The data obtained is summarized in *Table 3.3*. Included in *Table 3.3* is the literature kinetic data for **Ptppy**<sup>56</sup> for comparison purposes except **Ptppy** with MTU which is new data.

$$k_{\text{obs}(1^{\text{st}}/2^{\text{nd}})} = k_{2(1^{\text{st}}/2^{\text{nd}})}[Nu] \quad (3.1)$$

where  $k_2$  is the second-order rate constant for the forward reaction.



(a)

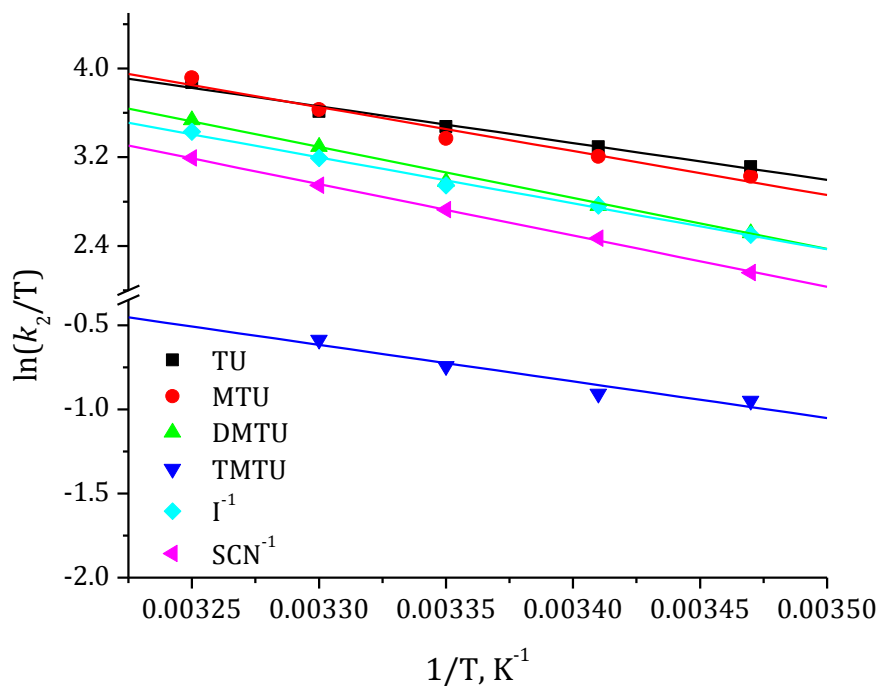


(b)

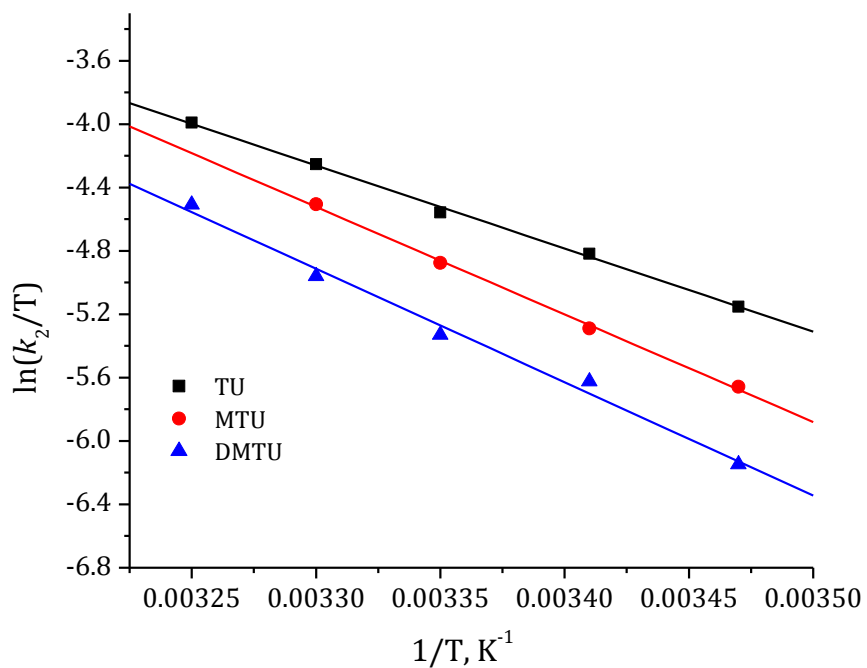
Figure 3.5

Dependence of the *pseudo* first-order rate constants ( $k_{obs}$ ) on the concentrations of the nucleophiles (a) for the simultaneous displacement of chloride ligands in  $k_{obs,(1^{st})}$ , s<sup>-1</sup>, (b) for the dechelation of the ligands in  $k_{obs,(2^{nd})}$ , s<sup>-1</sup>, from PtRuPt in methanol solution at 298 K and  $I = 0.02$  M (adjusted with LiCF<sub>3</sub>SO<sub>3</sub> and LiCl).

The temperature dependence studies were performed between 15 - 40 °C in 5 °C intervals. Activation parameters, entropy of activation ( $\Delta S^\ddagger$ ) and enthalpy of activation ( $\Delta H^\ddagger$ ) for both the substitution of the chloride ligand and the subsequent dechelation step were calculated from the slopes and the intercepts of the Eyring plots.<sup>55</sup> Representative plots are presented in *Figure 3.6* and respective activation parameters are in *Table 3.3*.



(a)



(b)

**Figure 3.6** Eyring plots obtained for (a) RuPt with the nucleophiles for the substitution of chloride ligand, (b) Plots of  $\ln(k_2/T)$  against  $1/T$  for the reactions of RuPt with the nucleophiles for the dechelation of the linker at various temperatures in the range 15 - 35 °C.



**Table 3.3** Summary of the rate constants and activation parameters for the displacement of the chloride ligand(s) by the nucleophiles studied and the kinetic data for the dechelation of the tppz units by thiourea nucleophiles. Data for Ptppy except with MTU is obtained from references<sup>56</sup> and is included for comparisons.

Complex	Nu	Second-order rate constant/ $\text{M}^{-1} \text{s}^{-1}$		Enthalpy of activation / $\text{kJ mol}^{-1}$		Entropy of activation / $\text{J K}^{-1} \text{mol}^{-1}$	
		$k_2 / 1^{\text{st}}$	$k_2 / 2^{\text{nd}}$	$\Delta H_1^\ddagger$	$\Delta H_2^\ddagger$	$\Delta S_1^\ddagger$	$\Delta S_2^\ddagger$
<b>Ptppy</b>	TU	1494 $\pm$ 10		29 $\pm$ 2		-88 $\pm$ 5	
	MTU	1306 $\pm$ 19		38 $\pm$ 0.3		-68 $\pm$ 0.9	
	DMTU	448 $\pm$ 10		36 $\pm$ 1		-73 $\pm$ 4	
	TMTU	82 $\pm$ 4		35 $\pm$ 2		-91 $\pm$ 8	
	I <sup>-</sup>	243 $\pm$ 4		47 $\pm$ 3		-42 $\pm$ 11	
	SCN <sup>-</sup>	17 $\pm$ 0.2		48 $\pm$ 2		-61 $\pm$ 1	
<b>RuPt</b>	TU	8921 $\pm$ 100	3.0 $\pm$ 0.03	27 $\pm$ 2	43 $\pm$ 1	-78 $\pm$ 6	-93 $\pm$ 3
	MTU	8359 $\pm$ 155	2.5 $\pm$ 0.06	32 $\pm$ 3	56 $\pm$ 1	-61 $\pm$ 9	-50 $\pm$ 4
	DMTU	5395 $\pm$ 113	1.4 $\pm$ 0.04	38 $\pm$ 2	58 $\pm$ 3	-46 $\pm$ 6	-47 $\pm$ 9
	TMTU	288 $\pm$ 2		17 $\pm$ 0.6		-146 $\pm$ 2	
	I <sup>-</sup>	5443 $\pm$ 73		34 $\pm$ 1		-60 $\pm$ 3	
	SCN <sup>-</sup>	4334 $\pm$ 78		38 $\pm$ 1		-49 $\pm$ 3	
<b>PtRuPt</b>	TU	9141 $\pm$ 260	3.7 $\pm$ 0.06	46 $\pm$ 0.4	35 $\pm$ 1	-17 $\pm$ 1	-118 $\pm$ 2
	MTU	8630 $\pm$ 157	2.1 $\pm$ 0.06	40 $\pm$ 0.2	41 $\pm$ 1	-34 $\pm$ 0.7	-101 $\pm$ 3
	DMTU	5684 $\pm$ 89	1.9 $\pm$ 0.05	41 $\pm$ 2	46 $\pm$ 2	-37 $\pm$ 7	-85 $\pm$ 7
	TMTU	690 $\pm$ 12		51 $\pm$ 3		-20 $\pm$ 9	
	I <sup>-</sup>	5541 $\pm$ 73		32 $\pm$ 2		-67 $\pm$ 6	
	SCN <sup>-</sup>	4405 $\pm$ 92		45 $\pm$ 0.3		-35 $\pm$ 0.9	
<b>PtRuRuPt</b>	TU	10035 $\pm$ 100	3.2 $\pm$ 0.08	33 $\pm$ 2	36 $\pm$ 2	-57 $\pm$ 6	-115 $\pm$ 8
	MTU	8860 $\pm$ 198	2.8 $\pm$ 0.06	45 $\pm$ 2	32 $\pm$ 2	-18 $\pm$ 7	-128 $\pm$ 7
	DMTU	6659 $\pm$ 139	1.5 $\pm$ 0.02	39 $\pm$ 2	45 $\pm$ 2	-41 $\pm$ 7	-93 $\pm$ 5
	TMTU	4159 $\pm$ 72		52 $\pm$ 3		-7 $\pm$ 11	
	I <sup>-</sup>	6962 $\pm$ 74		22 $\pm$ 0.4		-96 $\pm$ 1	
	SCN <sup>-</sup>	4536 $\pm$ 75		28 $\pm$ 1		-87 $\pm$ 3	
<b>CoPt</b>	TU	2090 $\pm$ 31	1.5 $\pm$ 0.02	37 $\pm$ 1	37 $\pm$ 2	-56 $\pm$ 4	-118 $\pm$ 5
	MTU	2043 $\pm$ 38	1.4 $\pm$ 0.02	45 $\pm$ 2	38 $\pm$ 3	-33 $\pm$ 6	-116 $\pm$ 8
	DMTU	1707 $\pm$ 7	0.5 $\pm$ 0.01	47 $\pm$ 3	53 $\pm$ 2	-27 $\pm$ 9	-74 $\pm$ 7
	TMTU	989 $\pm$ 16		46 $\pm$ 2		-33 $\pm$ 6	
	I <sup>-</sup>	1813 $\pm$ 39		49 $\pm$ 4		-38 $\pm$ 7	
	SCN <sup>-</sup>	994 $\pm$ 16		45 $\pm$ 2		-19 $\pm$ 2	

Data in *Table 3.3* show the results obtained for the displacement of the chloro ligand(s) for the complexes and subsequent dechelation of the coordinated ligand. By using **Ptppy**'s rate constant as a standard value, the ratio of the rate of substitution of chloride ligand(s) by TU is 1 : 6.0 : 6.1 : 6.7 : 1.4 respectively for **Ptppy** : **RuPt** : **PtRuPt** : **PtRuRuPt** : **CoPt**. Thus, the order of reactivity of displacement of chloride ligand(s) by the nucleophiles studied follows the order **PtRuRuPt** > **PtRuPt** > **RuPt** > **CoPt** > **Ptppy**. The difference in reactivity can be attributed to the electronic effects of the linking complex unit(s) and the number and type of metal centres.

The reactivity increases at least six folds from **Ptppy** to **RuPt**, by incorporation of the Ru(tppz) moiety. This could be attributed to the increased  $\pi$ -back donation along with the increased overall charge of the complex<sup>48b,57</sup> and hence the electrophilicity of the Pt(II) centre<sup>56a,58</sup> as supported by the DFT calculated higher NBO charge on the Pt(II) centre of **RuPt** (1.255) to that of **Ptppy** (1.227). The back donation from the tpnz ligand is greater than the tpy ligand which makes the Pt(II) centre in **RuPt** more electrophilic than that of **Ptppy**. The crystal structure reported<sup>59</sup> for Cu(tpnz)(SCN)<sub>2</sub> shows that the dihedral angles between the pyridyl rings are fairly small. Thus, supports the greater  $\pi$ -back donation in **RuPt** due to its extended  $\pi$  conjugation. Since in a chemical reaction, the interactions occur only between the frontier molecular orbitals,<sup>60</sup> the considerable decrease in the LUMO energy of **RuPt** along with the decrease in the frontier orbital gap makes it easier for the transfer of electrons into the anti-bonding  $\pi^*$  LUMO orbital, thereby stabilizing the transition state. This destabilizes the ground state of **RuPt** as supported by the smaller chemical hardness,  $\eta$  ( $= (\epsilon_{\text{LUMO}} - \epsilon_{\text{HOMO}})/2$ )<sup>47a</sup> value of **RuPt**. As expected, this significantly increases the global electrophilicity index,  $\omega$  ( $= \mu^2/2\eta$ )<sup>47b,c</sup> obtained for **RuPt** and hence, the reactivity of **RuPt** is remarkably higher than that of **Ptppy**.

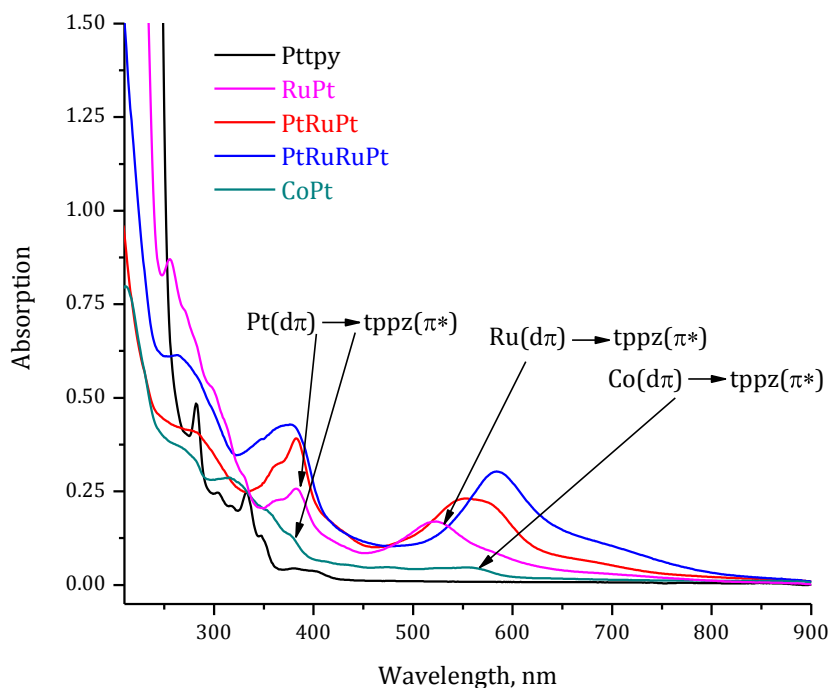
Similarly, when compared the reactivity of **Ptppy** with **CoPt**, the increase is only by 1.4 times. This increase in reactivity of **CoPt** can be attributed to the increase in the overall charge<sup>48b,58</sup> along with the increased electrophilicity of the Pt(II) metal centre<sup>57a,59</sup> due to the  $\pi$ -back donation from the tpnz ligand. As expected, this decreases the anti-bonding  $\pi^*$  LUMO energy level and thus, the chemical hardness of **CoPt**. However, the increased overall charge from **Ptppy** to **CoPt** (from +1 to +3) and the increased global electrophilicity index of **CoPt** (56.02 eV), despite significant, do not reflect on the observed reactivity for **CoPt** to that of **Ptppy** as in the case of **RuPt**. Therefore, the

reactivity of **CoPt** is influenced by the presence of the Co metal centre than that of tppz ligand.

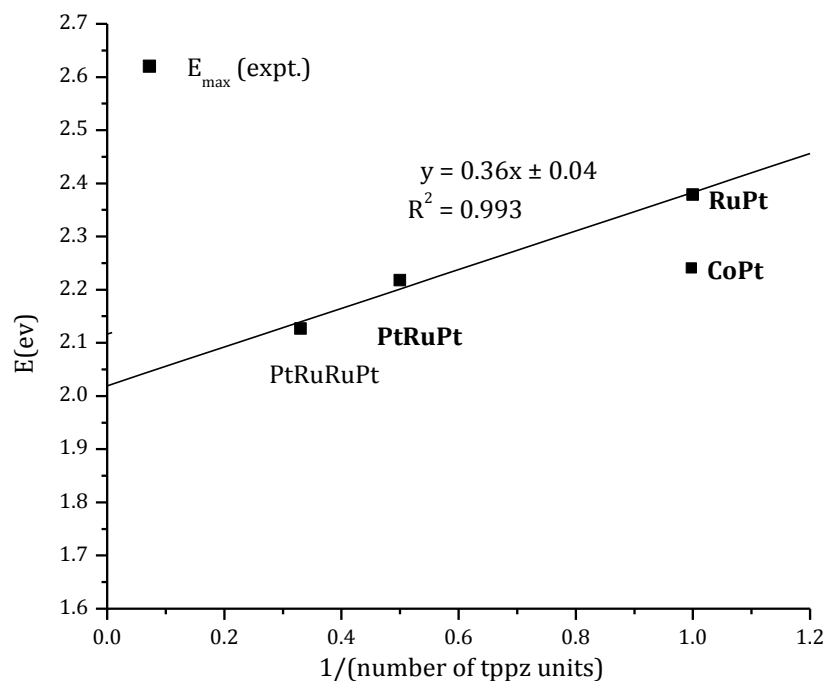
By keeping the overall charge and the ligand system constant, when the metal centre is changed from Ru(II) (**RuPt**) to a Co(II) (**CoPt**), the substitution rates of displacement of chloride ligand decreases by more than 4 times while the dechelation was 2 times slower. A glance at the  $N_{trans}$  atom to Pt(II) centre (N8), one notices that the nitrogen atom in **RuPt** (-0.567) is more negative than that of **CoPt** (-0.547). However, the NBO charges on the N atoms around Ru(II) metal centre are less negative in **RuPt** (Table 3.1) than that of the corresponding N atoms around Co(II) in **CoPt**. Conversely, the NBO charge on the Ru(II) metal centre of **RuPt** (0.997) is less positive compared to the Co(II) centre (1.319). This difference in the DFT calculated NBO charges indicate that Ru(II) enhances  $\pi$ -back donation in **RuPt** by accommodating the electron density at the Ru(II) metal centre, while in **CoPt**, the Co(II) metal centre donates the electron density into the capped tpy ligand and the linking tppz ligand as can be seen from the NBO charges on the N atoms. Thus, replacing the Ru(II) metal centre for a Co(II) changes the electron accepting property of the ligand system. Further support is the electron donor property of  $\text{Co}(\text{bpy})_3^{2+}$  reported by Song *et al.*<sup>61</sup> based on photophysical investigations performed on ruthenium and cobalt heterometallic complexes. This electron donation lowers the  $\pi$ -acceptability of the tppz ligand in **CoPt** as supported by the smaller NBO charge on the N8. Furthermore, the tilt angle, C–C–C (Figure 3.1), in **CoPt** is 25.00 ° while it is 10.39 ° in **RuPt**. This tilt angle between the subunits of the bridging linker is critical for aromatic linkers containing  $\pi$  systems.<sup>62</sup> This may have significant influences on the degree of metal-metal interactions.<sup>62a</sup>

The weaker  $\pi$ -back donation in **CoPt** is also supported by the nearly absent ( $\text{Co}(d\pi) \rightarrow \text{tppz}(\pi^*)$ ) transitions at 500 to 590 nm as reported for  $\text{Co}(\text{II})(\text{tpy})_2$  complex<sup>63</sup> and the observed weaker ( $\text{Pt}(d\pi) \rightarrow \text{tppz}(\pi^*)$ )<sup>64</sup> between 370 to 400 nm (Figure 3.7a) indicating the weak  $\pi$ -back donation and metal-metal electronic transitions.<sup>62a</sup> This is further backed by the DFT calculated smaller HOMO-LUMO energy gap. The slightly higher HOMO-LUMO gap in **CoPt** indicates that the compound is thermodynamically more stable<sup>65</sup> and is supported by the calculated greater chemical hardness value<sup>47b</sup> for **CoPt**, which is an indication of its ground state stability to that of **RuPt**. Additionally, the higher electronegativity of Ru (2.2 eV)<sup>66</sup> compared to Co (1.9 eV)<sup>66</sup> along with the

global electrophilicity index,  $\omega$  of **RuPt**, despite small, indicates the greater propensity of the molecule to accept electrons from the incoming nucleophiles.<sup>47c,d</sup>



(a)



(b)

**Figure 3.7** (a) UV/visible spectra of Ptppy, RuPt, PtRuPt, PtRuRuPt and CoPt in methanol (0.01 mM). (b) Energy of highest absorption wavelength peak of band against the number of tppz units in the complexes. CoPt deviates from the straight line.

The difference in reactivity might also be due to the spacial arrangement of the tppz ligand in both the complexes as can be seen from the DFT calculated minimum energy structures (See *Table 3.2*) which may influence the electronic properties of  $\pi^*$  orbitals of the bridging tppz ligand.<sup>11</sup> Since cobalt is a first row transition metal, the radial extension of its 3d orbital is smaller than 4d orbital in ruthenium. Thus, the  $\pi \rightarrow \pi^*$  transitions are stronger for 4d because of its stronger orbital diffuse compared to a 3d which is reflected on the observed much smaller absorption coefficient for **CoPt** ( $\epsilon_{557} = 4769 \text{ M}^{-1} \text{ cm}^{-1}$ , *Figure S3.25*) compared to its analogous complex, **RuPt**. This might be the controlling factor for the observed slower reactivity of **CoPt** to that of **RuPt**.

Furthermore, to understand the spacial conjugation in the  $\pi$ -conjugated systems, we determined the effective conjugation length (ECL),<sup>51,67</sup> reported by Osuka *et al.*<sup>68</sup> Thus, a plot of absorption maxima, ( $\Delta E_{\text{max}}$ ) (*Equation 3.2*)<sup>69</sup> obtained from the UV/visible spectra (*Figure 3.7a*) against the number of tppz units (*Figure 3.7b*),<sup>51,70</sup> the resultant slope indicates the extent of delocalization,<sup>18a</sup> which is observed to be greater for **RuPt** than that of **CoPt** with the other complexes, further supporting the greater  $\pi$ -conjugation in **RuPt** (also see *Figures S3.27 to S3.29*).<sup>69a,18a,71</sup>

$$\Delta E_{\text{max}} = \frac{hc}{\lambda} \quad (3.2)$$

where  $h$  = is planks constant,  $c$  is the speed of light.

The reactivity of a metal complex is influenced by the number of valence electronic configuration of the metal. In  $d^7$  octahedral symmetry, the Co(II) coordinated system, even though it enormously favours high spin (HS) state,<sup>52,72</sup> might undergo spin-crossover transitions between low spin  $^2E \ t_{2g}^6 e_g^1$  and high spin  $^4T_1 \ t_{2g}^5 e_g^2$  state.<sup>52,73</sup> These transitions between the two states can significantly affect the thermodynamic and the kinetic processes of the complex.<sup>52,61</sup> The electron transfer from a nonbonding  $t_{2g}$  to anti-bonding  $e_g$  orbitals might result in concurrent loss of  $\pi$ -backbonding in **CoPt**,<sup>73a</sup> as a consequence affects the ligand field strength which in turn impacts on the strength of MLCT charge transfer transitions as can be seen in *Figure 3.7a* and from the DFT calculated NBO charges. For high spin state Co(II) complexes, the metal-ligand bond length is longer and hence the longer bond length does not allow a better overlapping of the orbitals.<sup>73a</sup> Moreover, the octahedral  $d^7$  Co(II) undergoes distinct

Jahn-Teller distortions,<sup>63,74</sup> which might result in a large first-order splitting of the  $^2E$  level<sup>73a</sup> that can change the electronic property of the bridging ligand system, hence influence the reactivity of Pt(II) centre. This is accounted for by the slightly bigger HOMO-LUMO gap for **CoPt** (2.61 eV) compared to **RuPt** (2.47 eV).

When a second platinum centre is introduced, the results obtained show a slight increase in lability of the chloride ligands in **PtRuPt** compared to **RuPt** when two tppz ligands are orthogonally bonded to the Ru(II) metal centre. The slightly higher reactivity of **PtRuPt** can be ascribed to the increased cationic charge and the higher  $\pi$ -backbonding from the two tppz ligands in **PtRuPt**<sup>6a</sup> thereby decreasing the LUMO,  $\pi^*$  energy (Table 3.1), resulting in a more electrophilic metal centre in **PtRuPt** as can be seen from the DFT calculated greater NBO charge on the Pt(II) metal centre. Consequently, the positive charge on the Ru(II) centre in **PtRuPt** decreases slightly. This observation is in line with the observed smaller HOMO-LUMO gap obtained for **PtRuPt** and is supported by the less negative tppz based reduction (tppz<sup>0/-</sup> couple) for **RuPt** (-0.16 V) than **PtRuPt** (-0.03 V), reported by Zhao *et al.*<sup>8b</sup> This was explained as a result of the extra stability gained by the  $\pi^*$  orbitals of tppz, by increasing the  $\pi$ -accepting ability and the intermetal electronic transitions *via* electron exchange pathway within the complex,<sup>8b,17,51,75</sup> on increasing the number of tppz ligands. This intermetal communications take place among the contiguous metal centres since the bridging tppz ligands are orthogonal to each other as a result of the octahedral geometry imposed by the Ru(II) metal centre.<sup>51</sup> Coordination of this ligand to the Pt(II) metal centres<sup>76</sup> pulls the electron density from the Pt(II) metal centres whereby making them more electrophilic. This makes the ground state **PtRuPt** complex more unstable as can be seen from the smaller chemical harness value of **PtRuPt** and hence, more reactive.<sup>47d</sup> This explanation is in line with the observed kinetic behaviour. A similar behaviour in reactivity was reported for the two complexes when incubated with DNA on agarose gel, where modification of DNA structures was higher for **PtRuPt** than that of **RuPt**.<sup>6a</sup>

By keeping in mind that increasing the number of tppz ligands in the complex enhances the  $\pi$ -accepting ability, a second Ru(II) and a tppz ligand was then introduced into **PtRuPt**. As expected, this has increased the overall  $\pi$ -backbonding (Figure 3.7b) at the Pt(II) metal centre and the intermetallic communication within the molecule<sup>53a,77</sup> as can be seen from the very low LUMO energy level of **PtRuRuPt**, enhancing the transfer of electrons from the 18 electron five coordinate intermediate, hence the DFT calculated

positive NBO charge on the Pt(II) centre of **PtRuRuPt** increases. This is further supported by the DFT calculated smallest  $\Delta E_{\text{gap}}$  in **PtRuRuPt** as a result of the  $\pi$ -backbonding interactions between the  $t_{2g}$  orbitals of the two Ru(II) centres and the  $p$  orbitals of the nitrogen atoms of pyrazine in the central tppz ligand which increases the stability of the tppz based ( $\pi^*$ ) LUMO electrons<sup>51</sup> and decreases the stability of the Ru( $d\pi$ ) HOMO electrons<sup>11,18a</sup> and is well supported by the very small chemical hardness value<sup>78</sup> of **PtRuRuPt**. The destabilization of the HOMO electrons arises due to the repulsion between the charges among the metal centres<sup>51,79</sup> together with the  $\pi$ - $\pi^*$  ligand transitions move to lower energy levels because the anti-bonding  $\pi^*$  orbitals of the bridging tppz ligand<sup>51</sup> which gets stabilized on adding the second Ru(II) metal centre.<sup>18a</sup> Thus, the lower  $\Delta E_{\text{(gap)}}$  is due to the intermetal communication between Ru1–Ru2 in **PtRuRuPt** through the central tppz ligand<sup>51</sup> which stabilizes the LUMO orbital<sup>18a</sup> as supported by Arana *et al.*<sup>11</sup> for the two electron reduction observed (+1.53 V and +0.99 V) for  $[\text{Ru}_2(\text{tppz})_3]^{4+}$  synthon, despite its symmetrical structure. Thus, this intermetal electronic communication between Ru1–Ru2 metals ions might be the main reason for the slightly higher reactivity of **PtRuRuPt** compared to **RuPt** and **PtRuPt**.

If one considers the two diPt(II) complexes, **PtRuPt** and **PtRuRuPt**, it is noticeable that due to the orthogonal geometry at the Ru(II) metal centres, orbital overlapping between the tppz ligands is absent. Due to this geometry along with the symmetrical nature of the two complexes, the two Pt(II) centres are kinetically indistinguishable and hence, react independently. As a result, the two Pt(II) metal centres cannot be discriminated by the incoming nucleophile which results in a simultaneous displacement of the chloride ligands<sup>80</sup> as reported previously for dinuclear Pt(II) complexes.<sup>81,82</sup> If there was any orbital overlapping between the tppz ligands, one would expect a considerable increase in the reactivity as anticipated from the significant change in the DFT calculated global electrophilicity index,  $\omega$ , on moving from **RuPt** to **PtRuPt** to **PtRuRuPt**. However, the increased global electrophilicity index is as a result of the increased aromatic systems in the complexes. In each complex, the electronic environment around the reactive Pt(II) metal centre varies only slightly and hence their substitution reactivity. The slight differences in reactivity observed is due to the increased intermetal communication on increasing the number of metal centres and the improved  $\pi$ -acceptor effect facilitated by the tppz ligands which stabilises the energy of anti-bonding LUMO orbitals as explained earlier.<sup>51</sup>

The reaction rates for the second step are much slower by a factor of at least 2400 for **RuPt**, **PtRuPt** and **PtRuRuPt** while it is about 1400 times slower for **CoPt**. Binding the nucleophile to the Pt(II) centre increases the steric effect on the Pt(II) centre.<sup>35a</sup> This in turn blocks the approach of the nucleophile from above and below the Pt(II) centre, hence, the observed second step is slower.<sup>35a</sup> Furthermore, the results show that the rate of dissociation of the chelate ligand is less sensitive to the structural and electronic nature of the chelate ligand moiety as previously reported by Jaganyi *et al.*<sup>35a,83</sup> and van Eldik *et al.*<sup>48b</sup> and explained this dechelation arising most likely due to the increased constraints perched on the incoming nucleophiles as the Pt(II) centre in the transition state is already hindered.<sup>48b,83-84</sup> Once strong donor thiourea coordinates the Pt(II) centre, the electronegativity of the metal centre increases thereby enhancing the direct attack of the incoming nucleophile.<sup>85</sup> This weakens the Pt–N<sub>tpz</sub> bonds, thereby enhancing further substitution of thiourea ligands, resulting in the simultaneous release of the linker and formation of [Pt(TU)<sub>4</sub>]<sup>2+</sup> in the case of TU.<sup>35a</sup> Furthermore, the increased steric distortions, along with the higher ligand field strength around the Pt(II) centre enhances the dechelation process as thiourea attacks to an already thiourea substituted Pt(II) centre.<sup>35a</sup> Dechelation of the coordinated ligands from square planar transition metal complexes such as Pt(II),<sup>86</sup> Au(III)<sup>84,87</sup> and Pt(II)<sup>35a,40b,83,88</sup> metal centres by sulphur donor have been reported previously. Pt(II) being a soft metal centre has more tendency to form bonds with sulphur donor than hard nitrogen donor atoms<sup>83</sup> in the tppz ligand.

In all cases, the substitution reactivity of the chloride(s) by the ionic nucleophiles was less than the strong donor TU and MTU. The reactivity of I<sup>−</sup> was comparable to DMTU. The reactivity with the ionic nucleophiles were greater for I<sup>−</sup> than SCN<sup>−</sup> due to the higher polarisability of the I<sup>−</sup> along with its stronger electrostatic attraction towards the softer cationic Pt(II) metal centre.<sup>39</sup>

In terms of steric effects, the complexes investigated are sensitive towards the steric hindrance of the incoming nucleophiles studied where the fastest rate of chloride substitution was observed for TU in all cases. Thus, the reactivity of the nucleophiles followed the order, TU > MTU > DMTU, I<sup>−</sup> > SCN<sup>−</sup> > TMTU. For all the complexes studied, TMTU was the slowest due to the presence of methyl groups which hinder the approach of the nucleophile thereby decreasing its reactivity.<sup>40b,56a,83,88-89</sup>



The results obtained for enthalpy for activation ( $\Delta H^\ddagger$ ) and entropy of activation ( $\Delta S^\ddagger$ ) support an associative mode of activation typical for square planar Pt(II) complexes as a result of bond formation in the transition state.<sup>80,89a,90</sup> Some of the activation entropies for the first step are small and negative. This may be because the substitution steps are accompanied by charge neutralization by the solvent molecules. The release of the electrostatically attracted solvent molecules results in an increase in entropy and counterweigh the negative intrinsic contributions due to the bond formation.<sup>80</sup> Nevertheless, the substitution reactions proceeded *via* an associated mode of activation.

### 3.4 Conclusion

Incorporation of Ru(tppz) in **RuPt** increases the reactivity almost six times compared to the monometallic **Ptpty**. The significant increase in reactivity is ascribed mainly to the increased  $\pi$ -back donation from the tppz ligand which increases the electrophilicity of the metal centre,<sup>56a,58a,58c,91</sup> along with the increased overall charge and the global electrophilicity index of the complex. On adding the second tppz ligand further stabilises the LUMO ( $\pi^*$ ) thereby enhancing  $\pi$ -back donation of the molecule. The intermetal communication between the two Ru(II) metal centres *via* the bridging tppz linker even stabilises the LUMO orbitals. Thus, the overall reactivity is driven by the increased  $\pi$ -backbonding and the overall electrophilicity of the molecules along with the decrease in the HOMO-LUMO gap obtained on adding more metal centres and tppz ligands to the complex. Thus, the reactivity followed the order **PtRuRuPt** > **PtRuPt** > **RuPt** > **CoPt** > **Ptpty**.

Changing the metal centre from Ru(II) to Co(II) decreases the substitution reactivity of **CoPt** by four times that of **RuPt**. UV/visible spectrophotometric analysis along with the DFT calculations show that for **CoPt** electronic transitions from ( $Pt(d\pi) \rightarrow tppz(\pi^*)$ ) are very weak which is an indication of weak  $\pi$ -backbonding from the Pt(II)  $d$  orbitals to the tppz ligand. Based on the facts discussed, we conclude that the Ru(II) is better at accepting the electron density than Co(II) from the Pt(II) centre through the bridging tppz ligand.

<sup>1</sup>H NMR and <sup>195</sup>Pt NMR spectroscopic data confirms the observed dechelation of the coordinated ligand from the Pt(II) centre which was enhanced by the ligand field strength imposed by the addition of thiourea nucleophiles at the Pt(II) metal centre.

The substitution reactions were sensitive towards the steric hindrance of the incoming nucleophiles. The observed enthalpy of activation,  $\Delta H^\ddagger$  and the entropy of activation,  $\Delta S^\ddagger$  support an associative mode of substitution.

### 3.5 References

- (1) Milkevitch, M.; Storrie, H.; Brauns, E.; Brewer, K. J.; Shirley, B. W. *Inorg. Chem.* **1997**, *36*, 4534.
- (2) (a) Yu, Y.; Lou, L.-G.; Liu, W.-P.; Zhu, H.-J.; Ye, Q.-S.; Chen, X.-Z.; Gao, W.-G.; Hou, S.-Q. *Eur. J. Med. Chem.* **2008**, *43*, 1438(b) Komeda, S.; Lutz, M.; Spek, A. L.; Chikuma, M.; Reedijk, J. *Inorg. Chem.* **2000**, *39*, 4230(c) Cohen, S. M.; Lippard, S. J. *Prog. Nucleic Acid res. Mol. Biol.* **2001**, *67*, 93(d) Alberts, D. S.; Noel, J. K. *Anti-Cancer Drugs.* **1995**, *6*, 369(e) Bera, S. K.; Sengupta, P. S.; De, G. S. *Inorg. React. Mech.* **2003**, *5*, 65.
- (3) Gielen, M.; Tiekink, E. R. T. *Metallotherapeutic Drugs and Metal-Based Diagnostic Agents: The Use of Metals in Medicine*; John Wiley and Sons, Ltd: Canada, 2005, 489-502.
- (4) (a) Hay, R. W.; Miller, S. *Polyhedron.* **1998**, *55*, 528(b) Perego, P.; Caserini, C.; Gatti, L.; Carenini, N.; Romanelli, S.; Supino, R.; Colangelo, D.; Viano, I.; Leone, R.; Spinelli, S.; Pezzoni, G.; Manzotti, C.; Farrell, N.; Zunino, F. *Mol. Pharmacol.* **1999**, *55*, 528(c) Burchenal, J. H.; Kalaher, K.; Dew, K.; Lokys, L.; Gale, G. *Biochimie.* **1978**, *60*, 961(d) Eastman, A.; Bresnick, E. *Biochem. Pharmacol.* **1981**, *30*, 2721(e) Komeda, S.; Yamane, H.; Chikuma, M.; Reedijk, J. *Eur. J. Inorg. Chem.* **2004**, 4828(f) Galanski, M.; Jakupiec, M. A.; Keppler, B. K. *Curr. Med. Chem.* **2005**, *12*, 2075.
- (5) Reedijk, J. *Platinum Metals Rev.* **2008**, *52*, 2.
- (6) (a) Prussin, A. J.; Zhao, S.; Jain, A.; Winkel, B. S. J.; Brewer, K. J. *J. Inorg. Biochem.* **2009**, *103*, 427(b) Boerner, L. J. K.; Zaleski, J. M. *Curr. Opin. Chem. Biol.* **2005**, *7*, 481.
- (7) (a) Hofmeier, H.; Schubert, U. S. *Chem. Soc. Rev.* **2004**, *33*, 373(b) Holder, A. A.; Swavey, S.; Brewer, K. J. *Inorg. Chem.* **2003**, *43*, 303.
- (8) (a) Vogler, L. M.; Brewer, K. J. *Inorg. Chem.* **1996**, *35*, 818(b) Zhao, S.; Arachchige, S. M.; Slebodnick, C.; Brewer, K. J. *Inorg. Chem.* **2008**, *47*, 6144(c) Downward, A. M.; Jane, R. T.; Polson, M. I. J.; Moore, E. G.; Hartshorn, R. M. *Dalton Trans.* **2012**, *41*, 14425(d) Constable, E. C.; Harris, K.; Housecroft, C. E.; Neuburger, M.; Zampese, J. A. *Dalton Trans.* **2011**, *40*, 11441.
- (9) Miao, R.; Mongelli, M. T.; Zigler, D. F.; Winkel, B. S. J.; Brewer, K. J. *Inorg. Chem.* **2006**, *45*, 10413.
- (10) Swavey, S.; Fang, Z. L.; Brewer, K. J. *Inorg. Chem.* **2002**, *41*, 2598.
- (11) Arana, C. R.; Abruña, H. D. *Inorg. Chem.* **1993**, *32*, 194.

- (12) Juris, A.; Balzani, V.; Barigelletti, F.; Campagna, S.; Belser, P.; Von Zelewsky, V. *Coor. Chem. Rev.* **1988**, *84*, 85.
- (13) Kalyanasundaram, K. *Coord. Chem. Rev.* **1982**, *46*, 159.
- (14) Chen, X.; Femia, F. J.; Babich, J. W.; Zubieta, J. *Inorg. Chim. Acta.* **2001**, *315*, 66.
- (15) Clark, M. J. *Coord. Chem. Rev.* **2003**, *236*, 209.
- (16) (a) Isied, S. S.; Taube, H. *J. Am. Chem. Soc.* **1973**, *95*, 8198(b) Fischer, H.; Tom, G. M.; Taube, H. *J. Am. Chem. Soc.* **1976**, *98*, 5512(c) Rieder, K.; Taube, H. *J. Am. Chem. Soc.* **1977**, *99*, 7891(d) Zawacky, S. K. S.; Taube, H. *J. Am. Chem. Soc.* **1981**, *103*, 3379.
- (17) Kundu, T.; Sarkar, B.; Mondal, T. K.; Fiedler, J.; Mobin, S. M.; Kaim, W.; Lahiri, G. K. *Inorg. Chem.* **2010**, *49*, 6565.
- (18) (a) Flores-Torres, S.; Hutchison, G. R.; Soltzberg, L. J.; Abruña, H. D. *J. Am. Chem. Soc.* **2006**, *128*, 1513(b) Wadman, S. H.; Havenith, R. W. A.; Hartl, F.; Lutz, M.; Spek, A. L.; van Klink, G. P. M.; van Koten, G. *Inorg. Chem.* **2009**, *48*, 5685.
- (19) Campos- Fernandez, C. S.; Smucker, B. W.; Clerac, R.; Dunbar, K. R. *Isr. J. Chem.* **2001**, *41*, 207.
- (20) (a) Yamada, Y.; Miyashita, Y.; Fujisawa, K.; Okamoto, K.-i. *Bull. Chem. Soc. Jpn.* **2000**, *73*, 1843(b) Corcoran, A. M.; Haines, R. I. *Inorg React Mech.* **2011**, *6*.
- (21) Thummel, R. P.; Chirayil, S. *Inorg. Chim. Acta.* **1988**, *154*, 77.
- (22) (a) Williams, R. L.; Toft, H. N.; Winkel, B. S. J.; Brewer, K. J. *Inorg. Chem.* **2003**, *42*, 4394(b) Higgins, S. L. H.; Tucker, A. J.; Winkel, B. S. J.; Brewer, K. J. *Chem. Commun.* **2012**, *48*, 67.
- (23) Higgins, S. L. H.; White, T. A.; Winkel, B. S. J.; Brewer, K. J. *Inorg. Chem.* **2010**, *50*, 463.
- (24) Ho, E. N.-M.; Lin, Z.; Wong, W.-T. *Eur. J. Inorg. Chem.* **2001**, *2001*, 1321.
- (25) Ramprasad, D.; Gilicinski, A. G.; Markley, T. J.; Pez, G. P. *Inorg. Chem.* **1994**, *33*, 2841.
- (26) Feskov, S. V.; Kichigina, A. O.; Ivanov, A. I. *J. Phys. Chem. A.* **2011**, *115*, 1462.
- (27) (a) Shahabadi, N.; Mahdavi, M. *ISRN Inorg. Chem.* **2013**, *2013*, 7(b) López-Sandoval, H.; Londoño-Lemos, M. E.; Garza-Velasco, R.; Poblano-Meléndez, I.; Granada-Macías, P.; Gracia-Mora, I.; Barba-Behrens, N. *J. Inorg. Biochem.* **2008**, *102*, 1267.
- (28) Miodragović, D. U.; Bogdanović, G. A.; Miodragović, Z. M.; Radulović, M. Đ.; Novaković, S. B.; Kaluđerović, G. N.; Kozłowski, H. *J. Inorg. Biochem.* **2006**, *100*, 1568.

- (29) Lv, J.; Liu, T.; Cai, S.; Wang, X.; Liu, L.; Wang, Y. *J. Inorg. Biochem.* **2006**, *100*, 1888.
- (30) Böttcher, A.; Takeuchi, T.; Hardcastle, K. I.; Meade, T. J.; Gray, H. B.; Cwikel, D.; Kapon, M.; Dori, Z. *Inorg. Chem.* **1997**, *36*, 2498.
- (31) (a) Zhang, Q.-L.; Liu, J.-G.; Chao, H.; Xue, G.-Q.; Ji, L.-N. *J. Inorg. Biochem.* **2001**, *83*, 49(b) Zhang, Q.-L.; Liu, J.-G.; Xu, H.; Li, H.; Liu, J.-Z.; Zhou, H.; Qu, L.-H.; Ji, L.-N. *Polyhedron*. **2001**, *20*, 3049(c) Jiao, K.; Wang, Q. X.; Sun, W.; Jian, F. F. *J. Inorg. Biochem.* **2005**, *99*, 1369(d) Souza, E. T.; Castro, L. C.; Castro, F. A. V.; Visentin, L. D.; Pinheiro, C. B.; Pereira, M. D.; Machado, S. D.; Scarpellini, M. *J. Inorg. Biochem.* **2009**, *103*, 1355(e) Sastri, C. V.; Eswaramoorthy, D.; Giribabu, L.; Maiya, B. G. *J. Inorg. Biochem.* **2003**, *94*, 138(f) Indumathy, R.; Kanthimathi, M.; Weyhermuller, T.; Nair, B. U. *Polyhedron*. **2008**, *27*, 3443(g) Indumathy, R.; Radhika, S.; Kanthimathi, M.; Weyhermuller, T.; Nair, B. U. *J. Inorg. Biochem.* **2007**, *101*, 434.
- (32) Shinohara, N.; Lilie, J. *Inorg. Chem.* **1990**, *29*, 3812.
- (33) Alzoubi, B. M.; Hamza, M. S. A.; Ducker- Benfer, C.; van Eldik, R. *Eur. J. Inorg. Chem.* **2003**, 2972.
- (34) Perrin, D. D.; Armarego, W. L. F.; Perrin, D. R. *Purification of Laboratory Chemicals*; 2<sup>nd</sup> ed.; Pergamon: Oxford, 1980.
- (35) (a) Ongoma, P. O.; Jaganyi, D. *Dalton Trans.* **2013**, *42*, 2724(b) Connors, K. A. *Chemical Kinetics: The Study of Reaction Rates in Solution*; Wiley-VCH: New York, 1990, 334- 337.
- (36) Takeuchi, K. J.; Thompson, M. S.; Pipes, D. W.; Meyer, T. J. *Inorg. Chem.* **1984**, *23*, 1845.
- (37) Constable, E. C. *Adv. Inorg. Chem. Radiochem.* **1986**, *30*, 69.
- (38) Price, J. H.; Williamson, A. N.; Schramm, R. F.; Wayland, B. B. *Inorg. Chem.* **1971**, *11*, 1280.
- (39) Annibale, G.; Brandolisio, M.; Pitteri, B. *Polyhedron*. **1995**, *14*, 451.
- (40) (a) Hofmann, A.; van Eldik, R. *J. Chem. Soc., Dalton Trans.* **2003**, 2979(b) Mambanda, A.; Jaganyi, D. *Dalton Trans.* **2011**, *40*, 79
- (41) Origin 7.5™ SRO, ; Vol. v7.5714 (B5714), Origin Lab Cooperation, Northampton, One, Northampton, MA, 01060, USA, 2003.
- (42) (a) Sparttan '04, w., Ink., 18401 Von Karman Avenue, Suite 370, Irvine, CA, 92612, USA; Q-Chem, Ink., The design center, Suite 690, 5001 BAum Blvd., Pittsburgh, PA, 15213, USA., 2004(b) Kong, J.; White, C. A.; Krylov, A. I.; Sherrill, C. D.; Adamson, R. D.; Furlani, T. R.; Lee, M. S.; Lee, A. M.; Gwaltney, S. R.; Adams, T. R.; Ochsenfeld, C.; Gilbert, A. T. B.; Kedziora, G. S.; Rassolov, V. A.;

- Maurice, D. R.; Nair, N.; Shao, Y.; Besley, N. A.; Maslen, P. E.; Dombroski, J. P.; Daschel, H.; Zhang, W.; Korambath, P. P.; Baker, J.; Byrd, E. F. C.; Van Voorhuis, T.; Oumi, M.; Hirata, S.; Hsu, C.-P.; Ishikawa, N.; Florian, J.; Warshel, A.; Johnson, B. G.; Gill, P. M. W.; Head-Gordon, M. a.; Pople, J. A. *J. Computational Chem.* **2000**, *21*, 1532.
- (43) Becke, A. G. *J. Chem. Phys.* **1993**, *98*, 5648.
- (44) (a) Friesner, R. A. *Chem. Phys. Lett.* **1985**, *116*, 39(b) Friesner, R. A. *Ann. Rev. Phys. Chem.* **1991**, *42*, 341.
- (45) Hay, P. J.; Wadt, W. R. *J. Chem. Phys.* **1985**, *82*, 299.
- (46) (a) Rassolov, V. A.; Pople, J. A.; Ratner, M. A. a.; Windus, T. L. *J. Chem. Phys.* **1998**, *109*, 1223(b) Francl, M. M.; Pietro, W. J.; Hehre, W. J.; Binkley, J. S.; Gordon, M. S.; DeFrees, D. J. a.; Pople, J. A. *J. Chem. Phys.* **1982**, *77*, 3654.
- (47) (a) Parr, P. G.; Pearson, R. G. *J. Am. Chem. Soc.* **1983**, *105*, 7512(b) Mebi, C. A. *J. Chem. Sci.* **2011**, *123*, 727(c) Parr, R. G.; Szentpaly, L.; Liu, S. *J. Am. Chem. Soc.* **1999**, *121*, 1922(d) Chattaraj, P. K.; Giri, S.; Duley, S. *Chem. Rev.* **2011**, *111*, PR43(e) Cedillo, A.; Contreras, R. *J. Mex. Chem. Soc.* **2012**, *56*, 257(f) Elango, M.; Parthasarathi, R.; Narayanan, G. K.; Sabeelullah, A. M.; Sarkar, U.; Venkatasubramanian, N. S.; Subramanian, V.; Chattaraj, P. K. *J. Chem. Sci.* **2005**, *117*, 61.
- (48) (a) Zhao, G.; Hu, X. *Trans. Met. Chem.* **2004**, *29*, 607 (and references there in)(b) Ertürk, H.; Maigut, J.; Puchta, R.; van Eldik, R. *J. Chem. Soc. Dalton Trans.* **2008**, 2759(c) Field, J. S.; Haines, R. J.; McMillin, D. R.; Summerton, G. C. *J. Chem. Soc., Dalton Trans* **2002**, 1369.
- (49) Tiba, F.; Jaganyi, D.; Mambanda, A. *J. Coord. Chem.* **2010**, *63*, 2542.
- (50) Jaganyi, D.; Mambanda, A.; Hochreuther, S.; van Eldik, R. *Dalton Trans.* **2010**, 39, 3595.
- (51) Fantacci, S.; De Angelis, F.; Wang, J.; Bernhard, S.; Selloni, A. *J. Am. Chem. Soc.* **2004**, *126*, 9715.
- (52) Pietrzyk, P.; Srebro, M.; Radoń, M.; Sojka, Z.; Michalak, A. *J. Chem. Phys. A.* **2011**, *115*, 2316.
- (53) (a) Jaganyi, D.; Hofmann, A.; van Eldik, R. *Angew. Chem., Int. Ed.* **2001**, *40*, 1680(b) Bugarčić, Z. D.; Liehr, G.; van Eldik, R. *Dalton Trans.* **2002**, 951.
- (54) Puchta, R.; Meier, R.; van Elikema Hommes, N. J. R.; van Eldik, R. *Eur. J. Inorg. Chem.* **2006**, 4063.
- (55) Atwood, J. D. *Inorganic and Organometallic Reaction Mechanisms*, Wiley-VCH Inc., NY; 2nd ed., 1997.

- (56) (a) Jaganyi, D.; Reddy, D.; Gertenbach, J. A.; Hofmann, A.; van Eldik, R. *Dalton Trans.* **2004**, 299(b) Ongoma, P. O.; Jaganyi, D. *Dalton Trans.*, **2012**, 41, 10724.
- (57) Davies, M. S.; Thomas, D. S.; Hegmans, A.; Berners-Price, S. J.; Farrell, N. *Inorg. Chem.* **2002**, 41, 1101.
- (58) (a) Reddy, D.; Jaganyi, D. *Int. J. Chem. Kinet.* **2011**, 43, 161(b) Pantoja, E.; Gallipoli, A.; van Zutphen, S.; Komeda, S.; Reddy, D.; Jaganyi, D.; Lutz, M.; Tooke, D. M.; Spek, A. L.; Navarro-Ranninger, C.; Reedijk, J. *J. Inorg. Biochem.* **2006**, 100, 1955(c) Reddy, D.; Jaganyi, D. *Dalton Trans.* **2008**, 6724.
- (59) Machura, B.; Świtlicka, A.; Palion, J.; Kruszynski, R. *Struct. Chem.* **2013**, 24, 89.
- (60) Fang, J.; Li, J. *J. Mol. Struct.* **2002**, 593, 179.
- (61) Song, X.; Lei, Y.; S., V. W.; Perkovic, M. W.; Jackman, D. C.; Endicott, J. F.; Rillema, D. P. *J. Phys Chem.* **1993**, 97, 3225.
- (62) (a) Indelli, M. T.; Scandola, F.; Collin, J. P.; Sauvage, J. P.; Sour, A. *Inorg. Chem.* **1996**, 35, 303(b) Welter, S.; Salluce, N.; Benetti, A.; Rot, N.; Belser, P.; Sonar, P.; Grimsdale, A. C.; Müllen, K.; Lutz, M.; Spek, A. L.; De Cola, L. *Inorg. Chem.* **2005**, 44, 4706.
- (63) Indumathy, R.; Weyhermüller, T.; Rajapandian, V.; Subramanian, V.; Nair, B. U. *Polyhedron*. **2012**, 43, 159.
- (64) Aldridge, T. K.; Stacy, E. M.; McMillin, D. R. *Inorg. Chem.* **1994**, 33, 722.
- (65) Parr, P. G.; Zhou, Z. *Acc. Chem. Res.* **1993**, 26, 256.
- (66) Lee, J. D. *Concise Inorganic Chemistry*; Blackwell Science: India, 1996, 160.
- (67) Zerbi, G.; Galbiati, E.; Gallazzi, M. C.; Castiglioni, C.; Del Zoppo, M.; Schenk, R.; Müllen, K. *J. Chem. Phys.* **1996**, 106, 2509.
- (68) Tsuda, A.; Osuka, A. *Science*. **2001**, 293, 79.
- (69) (a) Kuhn, H. *J. Chem. Phys.* **1949**, 17, 1198(b) Kuhn, H. *Fortschr. Chem. Org. Naturst.* **1958**, 16, 169.
- (70) (a) Martin, R. E.; Diederich, F. *Angew. Chem. Int. Ed.* **1999**, 38, 1350(b) Meier, H.; Stalmach, U.; Kolshorn, H. *Acta. Polym.* **1997**, 48, 379.
- (71) (a) Hutchison, G. R.; Zhao, Y. J.; Delley, B.; Freeman, A. J.; Ratner, M. A.; Marks, T. *J. Phys. Rev. B.* **2003**, 68, 035204(b) Taubmann, G. *J. Chem. Educ.* **1992**, 69, 96.
- (72) Radoń, M.; Srebro, M.; Broclawik, E. *J. Chem. Theory. Comput.* **2009**, 5, 1237.
- (73) (a) Krivokapic, I.; Zerara, M.; Daku, M. L.; Vargas, A.; Enachescu, C.; Ambrus, C.; Tregenna-Piggott, P.; Amstutz, N.; Krausz, E.; Hauser, A. *Cood. Chem. Rev.* **2007**, 251, 364(b) Childs, B. J.; Craig, D. C.; Scudder, M. L.; Goodwin, H. A. *Inorg. Chim. Acta.* **1998**, 274, 32(c) Constable, E. C.; Kulke, T.; Neuburger, M.; Zehnder, M. *New. J. Chem.* **1997**, 21, 1091(d) Enachescu, C.; Krivokapic, I.; Zerara, M.; Real, J.

- A.; Amstutz, N.; Hauser, A. *Inorg. Chim. Acta.* **2007**, *360*, 3945(e) Goodwin, H. A. In *Spin Crossover in Transition Metal Compounds II*; Springer Berlin Heidelberg, Vol. 234, 2004, 23-47.
- (74) Maslen, E. N.; Raston, C. L.; White, A. H. *J. Chem. Soc. Dalton Trans.* **1974**, *0*, 1803.
- (75) Yuasa, J.; Fukuzumi, S. *J. Am. Chem. Soc.* **2007**, *130*, 566.
- (76) Fang, Z., MSc Thesis, Virginia Polytechnic Institute and State University, *The Synthesis and Characterization of A New Kind of Tagged Ru-Pt Bimetallic DNA Binding Agent*, 2000, 26- 80.
- (77) Summa, N.; Schiessl, W.; Puchta, R.; Hommes, N. E.; van Eldik, R. *Inorg. Chem.* **2006**, *45*, 2948.
- (78) Geerlings, P.; De Proft, F. *Int. J. Mol. Sci.* **2002**, *3*, 276.
- (79) (a) Sutton, J. E.; Taube, H. *Inorg. Chem.* **1981**, *20*, 3126(b) Sutton, J. E.; Sutton, P. M.; Taube, H. *Inorg. Chem.* **1979**, *18*, 1017.
- (80) Ertürk, H.; Hofmann, A.; Puchta, R.; van Eldik, R. *Dalton Trans.* **2007**, 2295.
- (81) (a) Ruhayel, R. A.; Langner, J. S.; Oke, M.-J.; Berners-Price, S. J.; Zgani, I.; Farrell, N. P. *J. Amer. Chem. Soc.* **2012**, *134*, 7135(b) Davies, M. S.; Cox, J. W.; Berners-Price, S. J.; Barklage, W.; Qu, Y.; Farrell, N. *Inorg. Chem.* **2006**, *39*, 1710.
- (82) (a) Hochreuther, S.; Puchta, R.; van Eldik, R. *Inorg. Chem.* **2011**, *50*, 8984(b) Summa, N.; Maigut, J.; Puchta, R.; van Eldik, R. *Inorg. Chem.* **2007**, *46*, 2094.
- (83) Mambanda, A.; Jaganyi, D. *Dalton Trans.* **2012**, *41*, 908.
- (84) Annibale, G.; Cattalini, L.; Natile, G. *J. Chem. Soc. Dalton Trans.* **1975**, *0*, 188.
- (85) Cotton, F. A.; Willkinson, G. *Advanced Inorganic Chemistry*; 5th Edition ed.; John Wiley & Sons: New York, 1966, 710- 754.
- (86) Tauben, J.; Rodriguez, M.; Zubiri, I.; Reedijk, J. *J. Chem. Soc. Dalton Trans.* **2000**, 369.
- (87) Annibale, G.; Cattalini, L.; El-Awady, A. A.; Natile, G. *J. Chem. Soc. Dalton Trans.* **1974**, *0*, 802.
- (88) Jaganyi, D.; Mambanda, A.; Hochreuther, S.; van Eldik, R. *Dalton Trans.* **2010**, *39*, 3595.
- (89) (a) Jaganyi, D.; De Boer, K. L.; Gertenbach, J.; Perils, J. *Int. J. Chem. Kinet.* **2008**, *40*, 808(b) Reddy, D.; Jaganyi, D. *Transition Met. Chem.* **2006**, *31*, 792.
- (90) Atwood, J. D. *Inorganic and Organic Reaction Mechanisms*; 2nd ed.; Wiley- VCH Inc.: New York, 1997, 32-34, 43-61.
- (91) (a) Pantoja, E.; Gallipoli, A.; van Zutphen, S.; Komeda, S.; Reddy, D.; Jaganyi, D.; Lutz, M.; Tooke, D. M.; Spek, A. L.; Navarro-Ranninger, C.; Reedijk, J. *J. Inorg.*



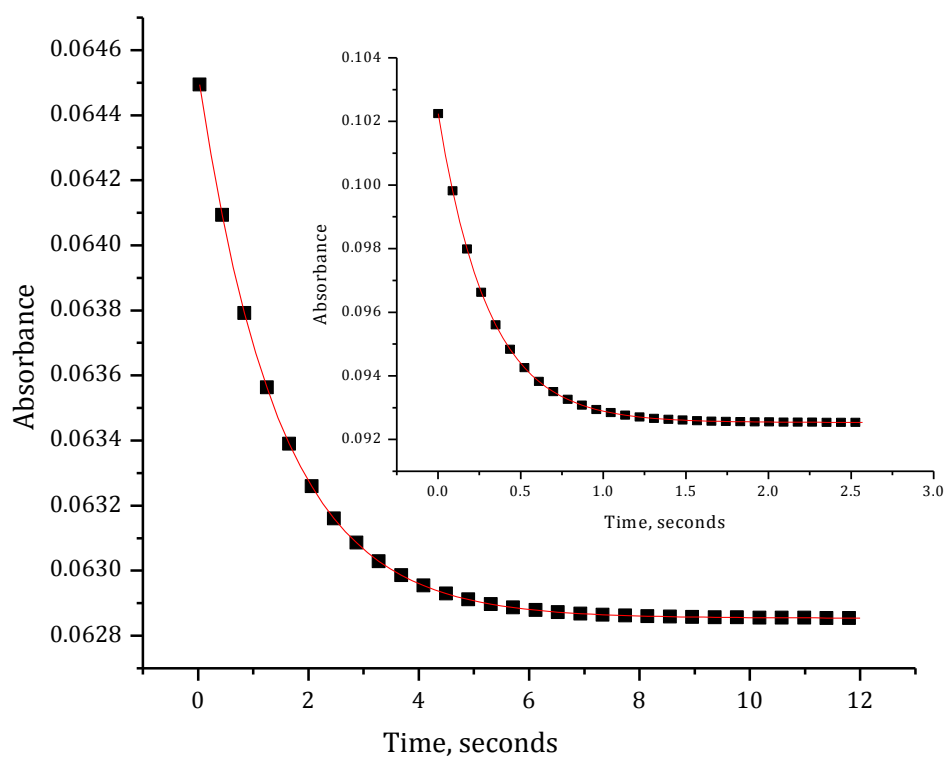
*Biochem.* **2006**, *100*, 1955(b) Hofmann, A.; Dahlenburg, L.; van Eldik, R. *Inorg. Chem.* **2003**, *42*, 6528.

### 3.6 Supporting Information

A summary of the wavelengths used for kinetic studies; representative DFT calculated structures of the complexes; representative mass spectra, NMR spectra, exemplary spectra for microanalysis, exemplary tables of kinetic data and the respective plots and graphs on concentration and temperature dependence studies for the complexes studied are given as supporting information.

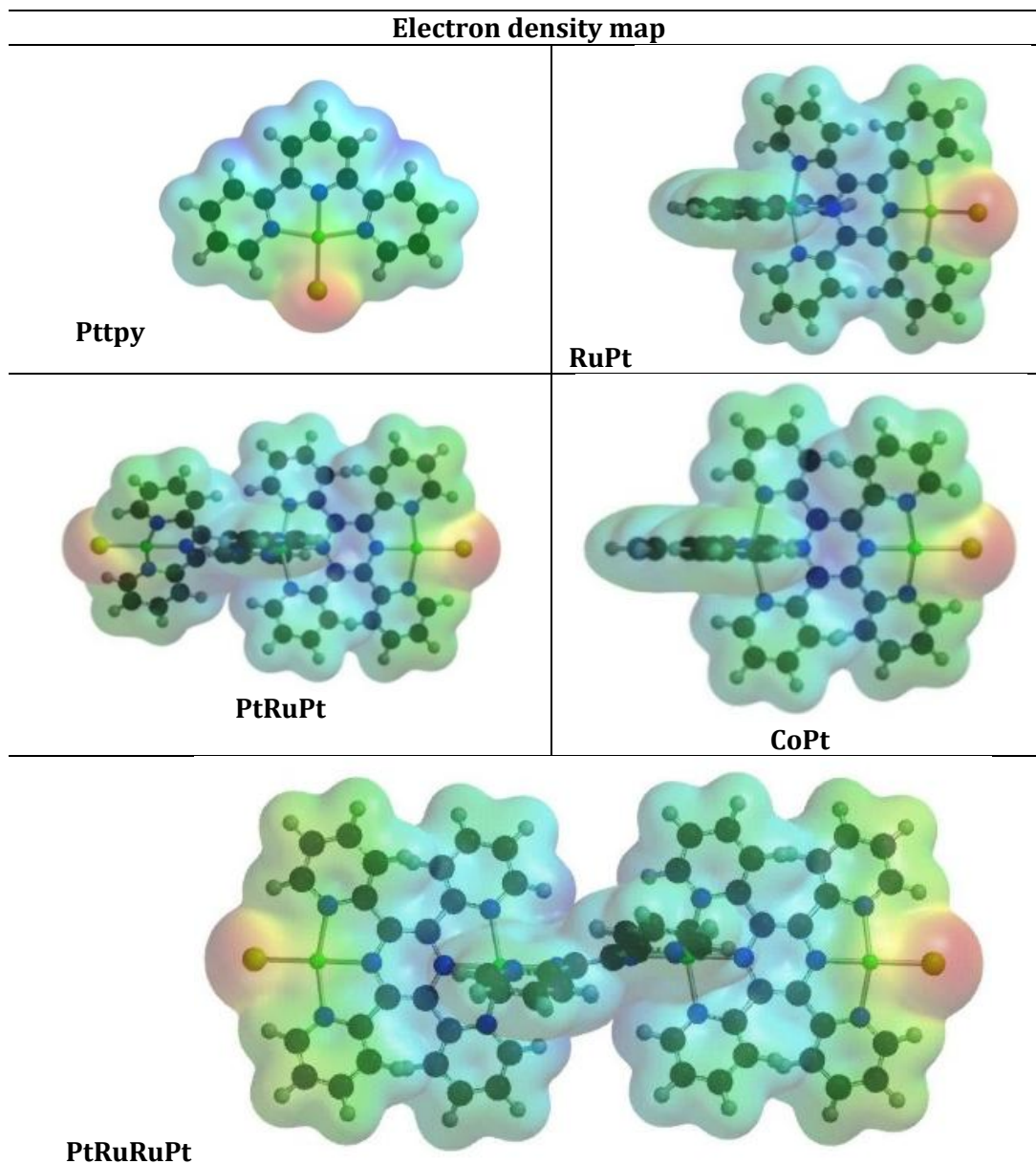
**Table S 3.1** Summary of selected wavelengths (nm) used for the kinetic investigations for the heterometallic Ru(II)-Pt(II) and Co(II)-Pt(II) complexes of pyrazine, 2,3,5,6-tetra-2-pyridyl with thiourea and the ionic nucleophiles.

Complex	Nu	Wavelength ( $\lambda$ ), nm	
		step 1 (Stopped-flow)	Step 2 (UV/visible)
<b>Ptpty</b>	mtu	333	-
<b>RuPt</b>	TU	382	382
	MTU	382	382
	DMTU	380	382
	TMTU	382	-
	I <sup>-</sup>	382	-
	SCN <sup>-</sup>	382	-
<b>PtRuPt</b>	TU	383	383
	MTU	383	382
	DMTU	382	383
	TMTU	383	-
	I <sup>-</sup>	383	-
	SCN <sup>-</sup>	383	-
<b>PtRuRuPt</b>	TU	390	390
	MTU	385	385
	DMTU	384	384
	TMTU	385	-
	I <sup>-</sup>	303	-
	SCN <sup>-</sup>	382	-
<b>CoPt</b>	TU	292	270
	MTU	377	280
	DMTU	377	370
	TMTU	405	-
	I <sup>-</sup>	370	-
	SCN <sup>-</sup>	410	-



**Figure S 3.1** Kinetic trace obtained at 292 nm for CoPt ( $4.0 \times 10^{-5}$  M) with TU ( $6.0 \times 10^{-4}$  M) on stopped flow at 298 K,  $I = 0.02$  M  $\text{LiCF}_3\text{SO}_3$ , adjusted with LiCl. Inset is the kinetic trace obtained at 382 nm for RuPt ( $2.0 \times 10^{-5}$  M) with TU ( $3.0 \times 10^{-5}$  M) at 298 K,  $I = 0.02$  M  $\text{LiCF}_3\text{SO}_3$ , adjusted with LiCl.

Table S 3.2      Geometry-optimised structures of the platinum complexes investigated and distribution of the electron density on the platinum complexes and the planarity of the molecules investigated. The blue area indicates the most electropositive areas and the red region indicates the most electronegative areas.



**Table S 3.3** Selected bond lengths (Å), bond angles (°), NBO charges, HOMO and LUMO energies and other computational data obtained for the complexes Pttpy, RuPt, PtRuPt, PtRuRuPt and CoPt obtained from the computational studies and the X-ray crystal structures. The values in brackets are obtained from the X-ray crystallographic structure.

	Pttpy	RuPt	PtRuPt	PtRuRuPt	CoPt
<b>Bond lengths (Å)</b>					
Pt–N ( <i>trans</i> )	1.966	1.972 (1.947)	1.969 (1.929)	1.967	1.961
Pt–Cl	2.347	2.320 (2.297)	2.313 (2.394)	2.303	2.317
N–N(pyridine)		2.657 (2.638)	2.646 (2.644)	2.662	2.660
Ru–Pt		6.624 (6.534)	6.651 (6.654)	6.663	6.649
Ru–Cl		8.932 (8.830)	8.964 (8.824)	8.939	8.967
Ru–N(pyrzine <i>cis</i> )		2.020 (2.012)	2.036 (2.070)	2.058	2.028
Pt–Pt			13.302 (17.622)	24.613	
Ru–Ru				6.759	
Cl---Py-H <sub>ortho</sub>		2.70 (2.812)	2.700 (2.806)	2.703	2.713
Ru–N( <i>cis</i> Py terminal)		2.123	2.130	2.140	2.252
Ru–N( <i>cis</i> Py central)	-	-	-	2.128	-
Ru–N( <i>tpy trans</i> )		2.036			1.902
Ru–N( <i>tpy cis</i> )		2.141			2.031
Pt – N( <i>Py cis</i> )					
<b>Bond Angles(°)</b>					
N <sub>cis</sub> –Pt1–N <sub>cis</sub>	161.58	161.31 (162.68)	162.25 (162.95)	161.48	162.14
Cl1–Pt1–N <sub>trans</sub>	179.93	176.52 (179.59)	180.00 (179.05)	175.29	180
c/d	80.79	81.26 (81.52)	81.13 (81.37)	81.42	81.07
a/b	99.25	98.89 (98.09)	98.87 (98.33)	98.79	98.93
N5–Ru/Co–N4		156.75 (157.32)	156.80 (158.03)	154.88/155.84	154.35
N1–Co–N2		155.88			162.00
e/f		78.92 (80.32)	78.40 (79.39)	77.95	77.18
g/j		89.55 (89.98)	94.13 (96.46)	91.91	93.29
h/i		78.01	78.40	78.40	81.00
<b>NBO charges</b>					
N6	-0.599	-0.601	-0.599	-0.601	-0.601
N7	-0.599	-0.601	-0.599	-0.601	-0.601

.....Continuation of Table S 3.3

<b>Torsion Angles(°)</b>				
C-C-C- C of tppz	10.39	24.15	11.10	25.00
central/terminal	(21.23)	(31.85)		
NCCN-inside-	6.36	20.37	5.91	21.00
(terminal)	(18.67)	(17.50)		
Cl from Pt plan	13.30	7.65	14.73	7.74
	(8.29)	(11.57)		
N7-Pt-Ru-N5	8.41	24.13	8.46	21.67
	(20.76)	(28.14)		
N7-Pt-Ru-N <sub>(1 of RuPt</sub>	85.28			69.67
and CoPt)				
NCCN <sub>(central Pyrazine)</sub>			6.67	
N-C-C-N <sub>(with Pt)</sub>	0.44	11.62	0.03	13.02
<i>Dipole</i>	0.01 16.47	0.13	0.00	18.33

Pz = pyrazine, py = pyridyl

**Table S 3.4**      **Average observed rate constants,  $k_{\text{obs}}$  ( $\text{s}^{-1}$ ),  $\text{s}^{-1}$  at 298.15 K for Ptppy with MTU at various concentrations and temperature dependence of  $k_2$   $\text{M}^{-1}\text{s}^{-1}$ , for the replacement of chloride ligand in Ptppy by MTU at 30-fold excess over [Ptppy],.  $I = 0.02$  M (adjusted with  $\text{LiCF}_3\text{SO}_3$  and  $\text{LiCl}$ ).**

<b>Conc., mM</b>	<b><math>k_{\text{obs}}</math>, <math>\text{s}^{-1}</math></b>	<b><math>1/T</math>, <math>\text{K}^{-1}</math></b>	<b><math>\ln(k_2/T)</math></b>
0.100	0.10967	0.00347	0.2399
0.200	0.24957	0.00341	0.51451
0.300	0.38307	0.00335	0.76144
0.400	0.52425	0.0033	1.0077
0.5000	0.6664	0.00325	1.23732

**Table S 3.5** Average observed rate constants,  $k_{\text{obs}}$  ( $1^{\text{st}}$ ),  $\text{s}^{-1}$  at 298.15 K for the replacement of chloride ligand in RuPt ( $3.0 \times 10^{-5} \text{ M}$ ) with the nucleophiles at various concentrations.  $I = 0.02 \text{ M}$  (adjusted with  $\text{LiCF}_3\text{SO}_3$  and  $\text{LiCl}$ ).

TU		MTU		DMTU		TMTU		$\text{I}^-$		$\text{SCN}^-$	
Conc., M	$k_{\text{obs}}, \text{s}^{-1}$	Conc., M	$k_{\text{obs}}, \text{s}^{-1}$	Conc., M	$k_{\text{obs}}, \text{s}^{-1}$	Conc., M	$k_{\text{obs}}, \text{s}^{-1}$	Conc., M	$k_{\text{obs}}, \text{s}^{-1}$	Conc., M	$k_{\text{obs}}, \text{s}^{-1}$
0.00015	1.6266	0.0003	2.74185	0.00015	0.98054	0.00020	0.057864	0.00015	0.9077	0.00015	0.7221
0.00029	2.96973	0.00037	3.2127	0.0003	1.6780	0.00025	0.07023	0.0003	1.6629	0.0003	1.3888
0.00045	4.02429	0.00045	3.89585	0.00045	2.5553	0.00029	0.085163	0.00045	2.5523	0.00045	2.0500
0.0006	5.20728	0.0006	4.8251	0.0006	3.1224	0.00040	0.116908	0.0006	3.2482	0.0006	2.5441
0.00075	6.62738	0.00075	6.18877	0.00075	4.0031	0.00050	0.144108	0.00075	4.0017	0.00075	3.1855

**Table S 3.6** Average observed rate constants,  $k_{\text{obs}}$  ( $2^{\text{nd}}$ ),  $\text{s}^{-1}$  at 298.15 K for the dechelation of the pyridyl units in RuPt ( $3 \times 10^{-5} \text{ M}$ ) with the nucleophiles at various concentrations.  $I = 0.02 \text{ M}$  (adjusted with  $\text{LiCF}_3\text{SO}_3$  and  $\text{LiCl}$ ).

TU		MTU		DMTU	
Conc., M	$k_{\text{obs}}, \text{s}^{-1}$	Conc., M	$k_{\text{obs}}, \text{s}^{-1}$	Conc., M	$k_{\text{obs}}, \text{s}^{-1}$
0.00015	$2.76 \times 10^{-4}$	0.00015	$2.87 \times 10^{-4}$	0.00015	$1.61 \times 10^{-4}$
0.0003	$6.17 \times 10^{-4}$	0.0003	$4.36 \times 10^{-4}$	0.0003	$2.99 \times 10^{-4}$
0.00045	$9.37 \times 10^{-4}$	0.00045	$7.28 \times 10^{-4}$	0.00045	$4.34 \times 10^{-4}$
0.0006	0.00119	0.0006	0.001	0.0006	5.52E-04
0.00075	0.00149	0.00075	0.00129	0.00075	6.42E-04

**Table S 3.7** Average observed rate constants,  $k_{\text{obs}}$  ( $1^{\text{st}}$ ),  $\text{s}^{-1}$  at 298.15 K for the replacement of chloride ligand in PtRuPt ( $2.0 \times 10^{-5} \text{ M}$ ) with the nucleophiles at various concentrations.  $I = 0.02 \text{ M}$  (adjusted with  $\text{LiCF}_3\text{SO}_3$  and  $\text{LiCl}$ ).

TU		MTU		DMTU		TMTU		$\text{I}^-$		$\text{SCN}^-$	
Conc., M	$k_{\text{obs}}, \text{s}^{-1}$	Conc., M	$k_{\text{obs}}, \text{s}^{-1}$	Conc., M	$k_{\text{obs}}, \text{s}^{-1}$	Conc., M	$k_{\text{obs}}, \text{s}^{-1}$	Conc., M	$k_{\text{obs}}, \text{s}^{-1}$	Conc., M	$k_{\text{obs}}, \text{s}^{-1}$
0.0002	2.0542	0.0002	2.01688	0.0002	1.2045	0.0002	0.14769	0.0002	1.0192	0.0002	1.0166
0.0004	3.6365	0.0004	3.23528	0.0004	2.08718	0.0004	0.28915	0.0004	2.3226	0.0004	1.7023
				0.0005	2.64321						
0.0006	4.93334	0.0006	5.17973	0.0006	--	0.0006	0.43196	0.0006	3.08438	0.0006	2.5216
0.0008	7.11465	0.0008	6.6906	0.0008	4.6178	0.0008	0.56124	0.0008	4.5658	0.0008	3.7033
0.001	9.59337	0.001	8.8281	0.001	5.68903	0.001	0.6656	0.001	5.55345	0.001	4.3316

**Table S 3.8** Average observed rate constants,  $k_{\text{obs}}$  ( $2^{\text{nd}}$ ),  $\text{s}^{-1}$  at 298.15 K for the dechelation of the pyridyl units in PtRuPt ( $2.0 \times 10^{-5} \text{ M}$ ) with the nucleophiles at various concentrations.  $I = 0.02 \text{ M}$  (adjusted with  $\text{LiCF}_3\text{SO}_3$  and  $\text{LiCl}$ ).

TU		MTU		DMTU	
Conc., M	$k_{\text{obs}}, \text{s}^{-1}$	Conc., M	$k_{\text{obs}}, \text{s}^{-1}$	Conc., M	$k_{\text{obs}}, \text{s}^{-1}$
0.0002	$6.62 \times 10^{-4}$	0.0002	$4.63 \times 10^{-4}$	0.0002	$3.98 \times 10^{-4}$
0.0004	0.00142	0.0004	$7.98 \times 10^{-4}$	0.0004	$6.95 \times 10^{-4}$
0.0006	0.00217	0.0006	0.00132	0.0006	0.00123
0.0008	0.00309	0.0008	0.00159	0.0008	0.00146
0.001	0.00369	0.001	0.00218	0.001	0.00187



**Table S 3.9** Average observed rate constants,  $k_{\text{obs}}$  (1<sup>st</sup>), s<sup>-1</sup> at 298.15 K for the replacement of chloride ligand in PtRuRuPt (1.0 x 10<sup>-5</sup> M) with the nucleophiles at various concentrations.  $I = 0.02$  M (adjusted with LiCF<sub>3</sub>SO<sub>3</sub> and LiCl).

TU		MTU		DMTU		TMTU		I <sup>-</sup>		SCN <sup>-</sup>	
Conc., M	$k_{\text{obs}}$ , s <sup>-1</sup>	Conc., M	$k_{\text{obs}}$ , s <sup>-1</sup>	Conc., M	$k_{\text{obs}}$ , s <sup>-1</sup>	Conc., M	$k_{\text{obs}}$ , s <sup>-1</sup>	Conc., M	$k_{\text{obs}}$ , s <sup>-1</sup>	Conc., M	$k_{\text{obs}}$ , s <sup>-1</sup>
0.0001		0.0001	0.97715	0.0001	0.8144	0.0001	0.4852	0.0001	0.6521	0.0001	0.4925
0.0002	2.0800	0.0002	1.76353	0.0002	1.426	0.0002	0.871	0.0002	1.47213	0.0002	0.9835
0.0003	3.08633	0.0003	2.422	0.0003	1.97418	0.0003	1.2996	0.0003	2.03665	0.0003	1.3011
0.0004	3.94305	0.0004	3.5174	0.0004	2.714	0.0004	1.6482	0.0004	2.81407	0.0004	1.783
0.0005	5.0000	0.0005	4.5784	0.0005	3.2362	0.0005	2.0312	0.0005	3.46587	0.0005	2.2901

**Table S 3.10** Average observed rate constants,  $k_{\text{obs}}$  (2<sup>nd</sup>), s<sup>-1</sup> at 298.15 K for the dechelation of the coordinated ligand in PtRuRuPt with the nucleophiles at various concentrations.  $I = 0.02$  M (adjusted with LiCF<sub>3</sub>SO<sub>3</sub> and LiCl).

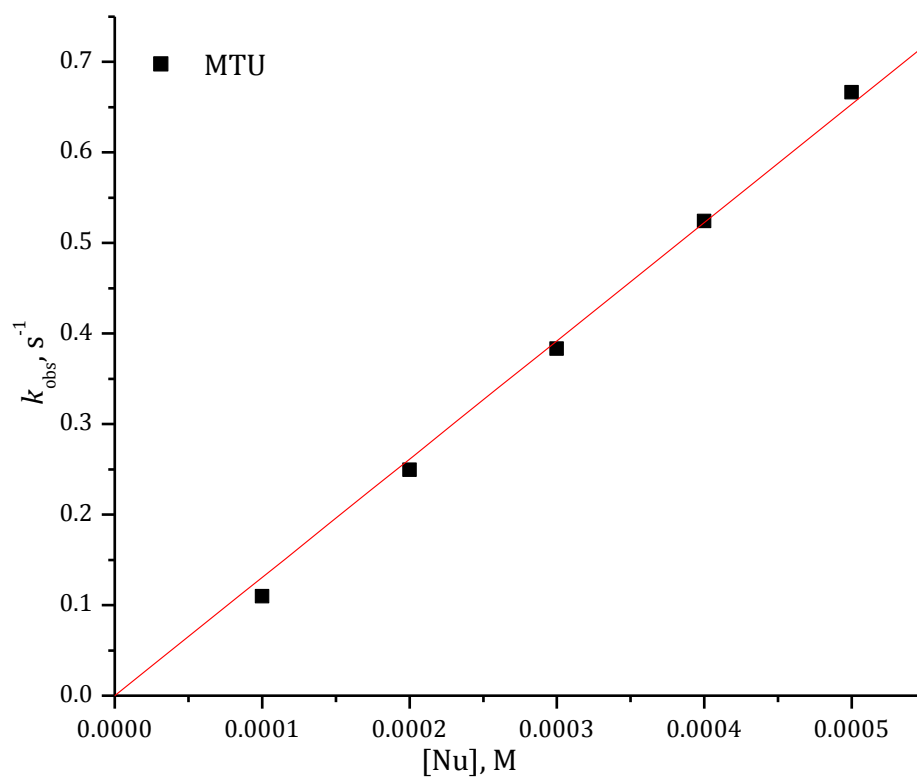
TU		MTU		DMTU	
Conc., M	$k_{\text{obs}}$ , s <sup>-1</sup>	Conc., M	$k_{\text{obs}}$ , s <sup>-1</sup>	Conc., M	$k_{\text{obs}}$ , s <sup>-1</sup>
0.0001	3.92 x 10 <sup>-4</sup>	0.0001	2.82 x 10 <sup>-4</sup>	0.0001	1.51 x 10 <sup>-4</sup>
0.0002	6.40 x 10 <sup>-4</sup>	0.0002	6.06 x 10 <sup>-4</sup>	0.0002	3.06 x 10 <sup>-4</sup>
0.0003	9.35 x 10 <sup>-4</sup>	0.0003	8.67 x 10 <sup>-4</sup>	0.0003	4.30 x 10 <sup>-4</sup>
0.0004	0.00129	0.0004	0.00109	0.0004	6.13 x 10 <sup>-4</sup>
0.0005	0.0016	0.0005		0.0005	7.21 x 10 <sup>-4</sup>

**Table S 3.11** Average observed rate constants,  $k_{\text{obs}}$  (1<sup>st</sup>), s<sup>-1</sup> at 298.15 K for the replacement of chloride ligand in CoPt (4.0 x 10<sup>-5</sup> M) with the nucleophiles at various concentrations.  $I = 0.02$  M (adjusted with LiCF<sub>3</sub>SO<sub>3</sub> and LiCl).

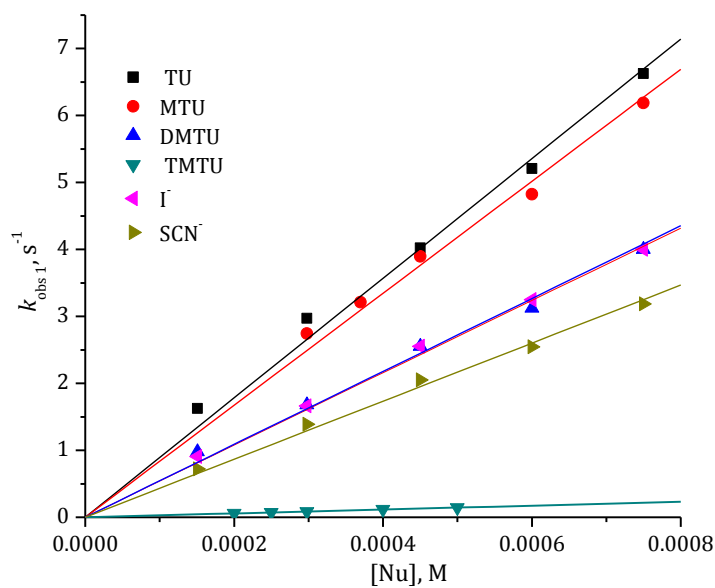
TU		MTU		DMTU		TMTU		I <sup>-</sup>		SCN <sup>-</sup>	
Conc., M	$k_{\text{obs}}$ , s <sup>-1</sup>	Conc., M	$k_{\text{obs}}$ , s <sup>-1</sup>	Conc., M	$k_{\text{obs}}$ , s <sup>-1</sup>	Conc., M	$k_{\text{obs}}$ , s <sup>-1</sup>	Conc., M	$k_{\text{obs}}$ , s <sup>-1</sup>	Conc., M	$k_{\text{obs}}$ , s <sup>-1</sup>
0.0002	0.496	0.0002	0.4631	0.0002	0.3269	0.0002	0.2129	0.0002	0.290433	0.0002	0.2447
0.0004	0.842667	0.0004	0.83014	0.0004	0.6915	0.0004	0.4171	0.0004	0.68285	0.0004	0.3696
0.0006	1.28935	0.0006	1.21424	0.0006	1.0338	0.0006	0.6195	0.0006	1.025714	0.0006	0.6215
0.0008	1.66195	0.0008	1.553	0.0008	1.3575	0.0008	0.796	0.0008	1.47965	0.0008	0.7579
0.001	2.05865	0.001	2.0986	0.001	1.7079	0.001	0.9592	0.001	1.8585	0.001	1.010

**Table S 3.12** Average observed rate constants,  $k_{\text{obs}}$  (2<sup>nd</sup>), s<sup>-1</sup> at 298.15 K for the dechelation of the pyridyl units in CoPt (4.0 x 10<sup>-5</sup> M) with the nucleophiles at various concentrations.  $I = 0.02$  M (adjusted with LiCF<sub>3</sub>SO<sub>3</sub> and LiCl).

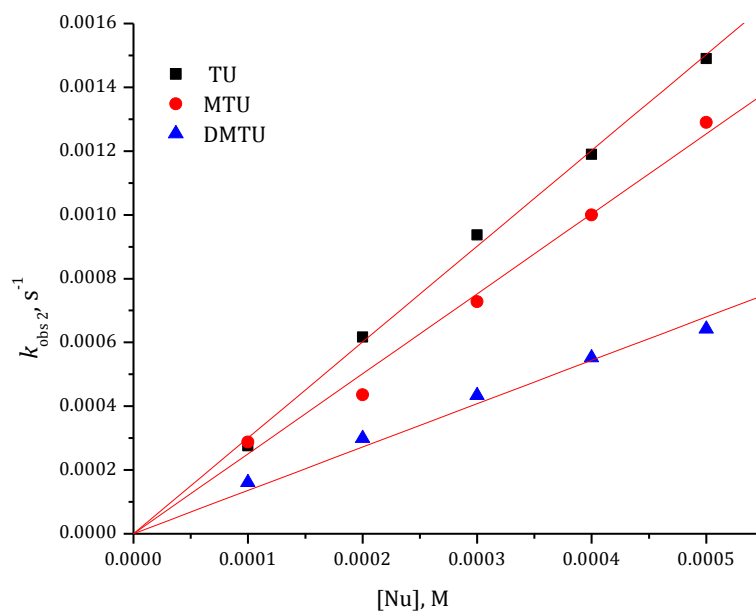
TU		MTU		DMTU	
Conc., M	$k_{\text{obs}}$ , s <sup>-1</sup>	Conc., M	$k_{\text{obs}}$ , s <sup>-1</sup>	Conc., M	$k_{\text{obs}}$ , s <sup>-1</sup>
0.0002	0.000297	0.0002	0.000239	0.0002	9.71 x 10 <sup>-5</sup>
0.0004	0.000571	0.0004	0.000556	0.0004	0.000191
0.0006	0.000924	0.0006	0.000864	0.0006	0.000261
0.0008	0.001197	0.0008	0.001107	0.0008	0.000355
0.001	0.001531	0.001	0.00146	0.001	0.000448



**Figure S 3.2** Dependence of the *pseudo* first-order rate constants ( $k_{\text{obs}}$ ) on the concentrations of MTU for the displacement of chloride ligand in from Ptpty in methanol solution at 298 K and  $I = 0.02$  M (adjusted with  $\text{LiCF}_3\text{SO}_3$  and  $\text{LiCl}$ ).

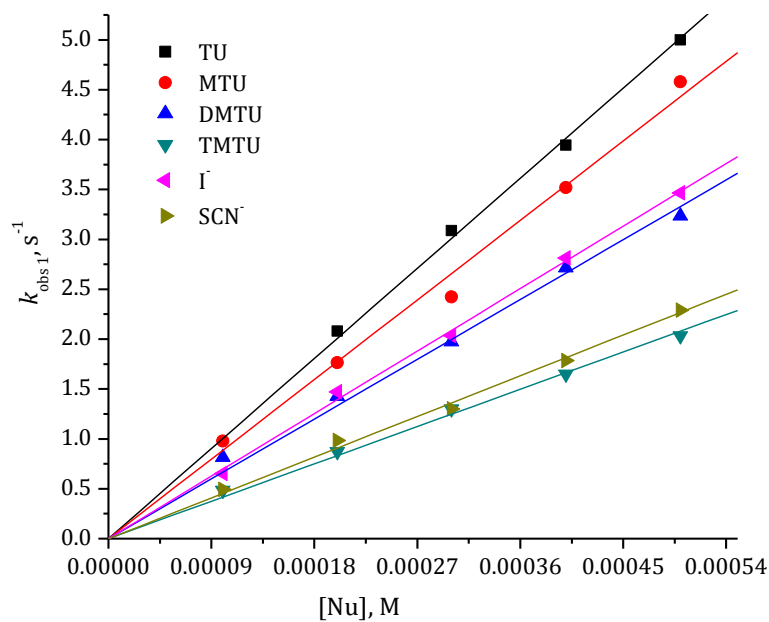


(a)

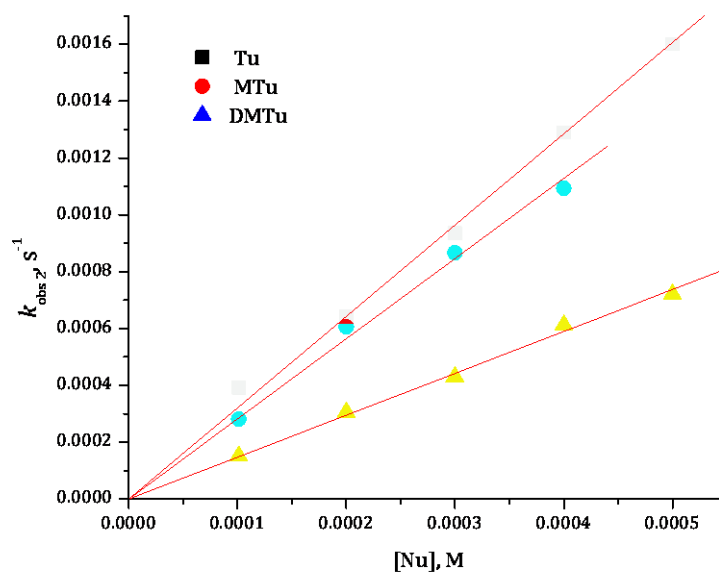


(b)

**Figure S 3.3** Dependence of the *pseudo* first-order rate constants ( $k_{obs}$ ) on the concentrations of the nucleophiles (a) for the displacement of chloride ligands in  $k_{obs\ 1^{st}}, s^{-1}$  (b) for the dechelation of the ligands in  $k_{obs\ 2^{nd}}, s^{-1}$ , from RuPt in methanol solution at 298 K and  $I = 0.02$  M (adjusted with  $LiCF_3SO_3$  and  $LiCl$ ).

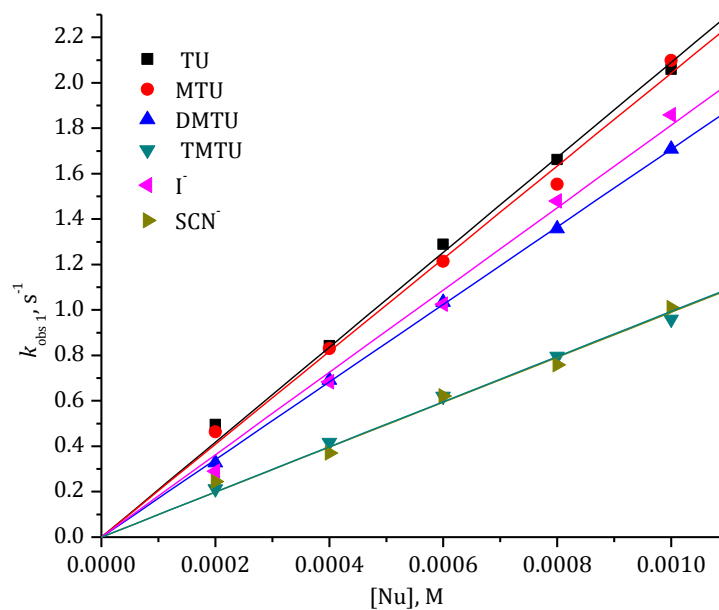


(a)

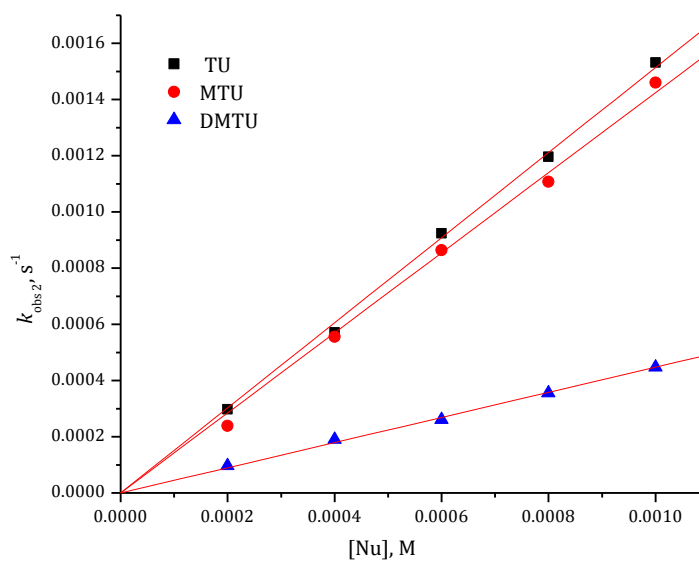


(b)

**Figure S 3.4** Dependence of the *pseudo* first-order rate constants ( $k_{obs}$ ) on the concentrations of the nucleophiles (a) for the simultaneous displacement of the chloride ligands,  $k_{obs}^{1st}$ , s<sup>-1</sup> (b) for the dechelation of the ligands,  $k_{obs}^{2nd}$ , s<sup>-1</sup>, from PtRuRuPt in methanol solution at 298 K and  $I = 0.02$  M (adjusted with LiCF<sub>3</sub>SO<sub>3</sub> and LiCl).



(a)



(b)

**Figure S 3.5** Dependence of the *pseudo* first-order rate constants ( $k_{obs}$ ) on the concentrations of the nucleophiles (a) for the displacement of the chloride ligand,  $k_{obs}^{1st}$ ,  $s^{-1}$  (b) for the dechelation of the ligand,  $k_{obs}^{2nd}$ ,  $s^{-1}$  from CoPt in methanol solution at 298 K and  $I = 0.02$  M (adjusted with  $LiCF_3SO_3$  and  $LiCl$ ).

**Table S 3.13** Temperature dependence of  $k_2 \text{ M}^{-1}\text{s}^{-1}$ , for the displacement of the aqua ligand in RuPt by nucleophiles at 30-fold excess over [RuPt],  $I = 0.02 \text{ M}$  (adjusted with  $\text{LiCF}_3\text{SO}_3$  and  $\text{LiCl}$ ).

TU		MTU		DMTU		TMTU		$\text{I}^-$		$\text{SCN}^-$	
$1/T, \text{K}^{-1}$	$\ln(k_2/T)$	$1/T, \text{K}^{-1}$	$\ln(k_2/T)$	$1/T, \text{K}^{-1}$	$\ln(k_2/T)$	$1/T, \text{K}^{-1}$	$\ln(k_2/T)$	$1/T, \text{K}^{-1}$	$\ln(k_2/T)$	$1/T, \text{K}^{-1}$	$\ln(k_2/T)$
0.00347	3.11454	0.00347	3.02634	0.00347	2.51549	0.00347	-0.94815	0.00347	2.50021	0.00347	2.15772
0.00341	3.29369	0.00341	3.2077	0.00341	2.7604	0.003411	-0.90704	0.00341	2.76462	0.00341	2.46757
0.00335	3.47705	0.00335	3.36858	0.00335	2.9768	0.003354	-0.74221	0.00335	2.94567	0.00335	2.72646
0.0033	3.61121	0.0033	3.6287	0.0033	3.29297	0.003299	-0.5863	0.0033	3.19257	0.0033	2.94714
0.00325	3.87124	0.00325	3.91634	0.00325	3.53436	0.003245		0.00325	3.43044	0.00325	3.19083

**Table S 3.14** Temperature dependence of  $k_2 \text{ M}^{-1}\text{s}^{-1}$ , for the dechelation of the pyridyl units in RuPt by thiourea nucleophiles at 30-fold excess over [RuPt],  $I = 0.02 \text{ M}$  (adjusted with  $\text{LiCF}_3\text{SO}_3$  and  $\text{LiCl}$ ).

TU		MTU		DMTU	
$1/T, \text{K}^{-1}$	$\ln(k_2/T)$	$1/T, \text{K}^{-1}$	$\ln(k_2/T)$	$1/T, \text{K}^{-1}$	$\ln(k_2/T)$
0.00347	-5.15171	0.00347	-5.65839	0.00347	-6.1472
0.00341	-4.81778	0.00341	-5.29034	0.00341	-5.62497
0.00335	-4.55839	0.00335	-4.87543	0.00335	-5.32898
0.0033	-4.25257	0.0033	-4.5053	0.0033	-4.95961
0.00325	-3.99009	0.00325	-3.55479	0.00325	-4.50809

**Table S 3.15** Temperature dependence of  $k_2$   $\text{M}^{-1}\text{s}^{-1}$ , for the displacement of the aqua ligand in PtRuPt by nucleophiles at 60-fold excess over [PtRuPt],  $I = 0.02$  M (adjusted with  $\text{LiCF}_3\text{SO}_3$  and  $\text{LiCl}$ ).

TU		MTU		DMTU		TMTU		$\text{I}^-$		$\text{SCN}^-$	
$1/T, \text{K}^{-1}$	$\ln(k_2/T)$	$1/T, \text{K}^{-1}$	$\ln(k_2/T)$	$1/T, \text{K}^{-1}$	$\ln(k_2/T)$	$1/T, \text{K}^{-1}$	$\ln(k_2/T)$	$1/T, \text{K}^{-1}$	$\ln(k_2/T)$	$1/T, \text{K}^{-1}$	$\ln(k_2/T)$
0.00347	2.63302	0.00347	2.85908	0.00347	2.16223	0.00347	0.23565	0.00347	2.33553	0.00347	2.14869
0.003411	2.87183	0.003411	3.165	0.003411	2.49082	0.003411	0.63654	0.003411	2.5531	0.003411	2.34985
0.003354	3.317	0.003354	3.36574	0.003354	2.80685	0.003354	0.88157	0.003354	2.84733	0.003354	2.64588
0.003299	3.48409	0.003299	3.68863	0.003299	2.97359	0.003299	1.35142	0.003299	2.99342	0.003299	2.98392
0.003245	3.88284	0.003245	3.96378	0.003245	3.31565	0.003245	1.5959	0.003245	3.19942	0.003245	3.24761

**Table S 3.16** Temperature dependence of  $k_2$   $\text{M}^{-1}\text{s}^{-1}$ , for the dechelation of the pyridyl units in PtRuPt by thiourea nucleophiles at 60-fold excess over [PtRuPt],  $I = 0.02$  M (adjusted with  $\text{LiCF}_3\text{SO}_3$  and  $\text{LiCl}$ ).

TU		MTU		DMTU	
$1/T, \text{K}^{-1}$	$\ln(k_2/T)$	$1/T, \text{K}^{-1}$	$\ln(k_2/T)$	$1/T, \text{K}^{-1}$	$\ln(k_2/T)$
0.00347		0.00347	-5.43628	0.00347	-5.67936
0.00341	-4.63896	0.00341	-5.14642	0.00341	-5.25566
0.00335	-4.41349	0.00335	-4.88489	0.00335	-5.0225
0.0033	-4.17073	0.0033	-4.60967	0.0033	-4.69338
0.00325	-3.95086	0.00325	-4.31259	0.00325	-4.4332



**Table S 3.17** Temperature dependence of  $k_2 \text{ M}^{-1}\text{s}^{-1}$ , for the displacement of the aqua ligand in PtRuRuPt by nucleophiles at 60-fold excess over [PtRuRuPt],  $I = 0.02 \text{ M}$  (adjusted with  $\text{LiCF}_3\text{SO}_3$  and  $\text{LiCl}$ ).

TU		MTU		DMTU		TMTU		$\text{I}^-$		$\text{SCN}^-$	
$1/T, \text{K}^{-1}$	$\ln(k_2/T)$	$1/T, \text{K}^{-1}$	$\ln(k_2/T)$	$1/T, \text{K}^{-1}$	$\ln(k_2/T)$	$1/T, \text{K}^{-1}$	$\ln(k_2/T)$	$1/T, \text{K}^{-1}$	$\ln(k_2/T)$	$1/T, \text{K}^{-1}$	$\ln(k_2/T)$
0.00347	2.95076	0.00347	2.74097	0.00347	2.4655	0.00347	1.43943	0.00347	2.97357	0.00347	1.61336
0.003411	3.17488	0.003411	3.10021	0.003411	2.8066	0.003411	1.87015	0.003411	3.14176	0.003411	1.80233
0.003354	3.42384	0.003354	3.29873	0.003354	3.09428	0.003354	2.09131	0.003354	3.27928	0.003354	1.98302
0.003299	3.57999	0.003299	3.67861	0.003299	3.34262	0.003299	2.44511	0.003299	3.44608	0.003299	2.16699
0.003245	3.86461	0.003245	3.98884	0.003245	3.52507	0.003245	2.89783	0.003245	3.57409	0.003245	2.38369

**Table S 3.18** Temperature dependence of  $k_2 \text{ M}^{-1}\text{s}^{-1}$ , for the dechelation of the pyridyl units in PtRuRuPt by thiourea nucleophiles at 60-fold excess over [PtRuRuPt],  $I = 0.02 \text{ M}$  (adjusted with  $\text{LiCF}_3\text{SO}_3$  and  $\text{LiCl}$ ).

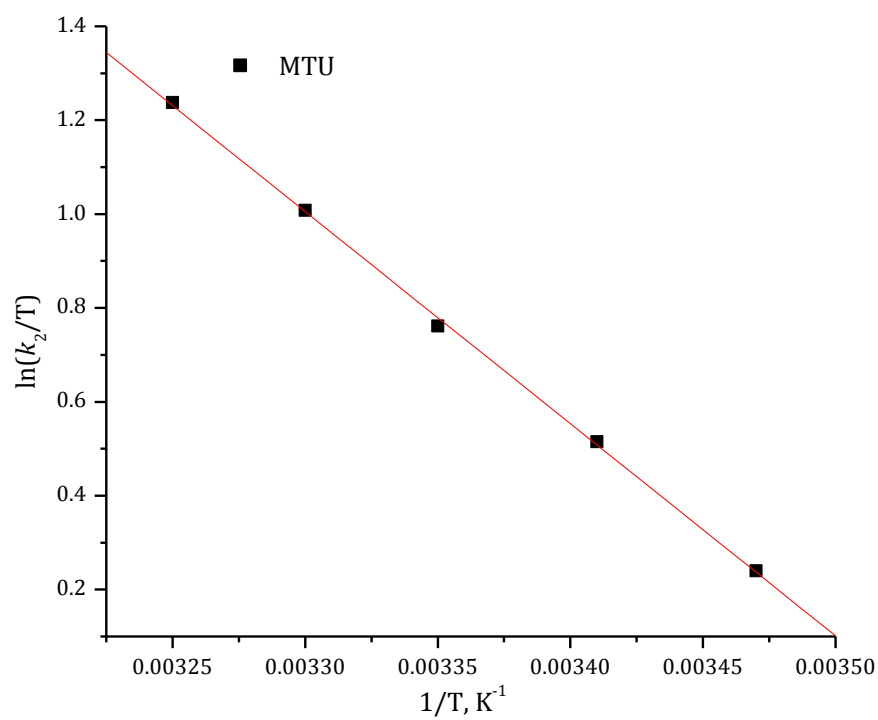
TU		MTU		DMTU	
$1/T, \text{K}^{-1}$	$\ln(k_2/T)$	$1/T, \text{K}^{-1}$	$\ln(k_2/T)$	$1/T, \text{K}^{-1}$	$\ln(k_2/T)$
0.00347	-5.1066	0.00347	-5.1674	0.00347	-6.02278
0.00341	-4.73573	0.00341	-4.90997	0.00341	-5.67055
0.00335	-4.56057	0.00335	-4.62736	0.00335	-5.33713
0.0033	-4.31535	0.0033	-4.50979	0.0033	-5.05952
0.00325	-4.09525	0.00325	-4.27272	0.00325	-4.82319

**Table S 3.19** Temperature dependence of  $k_2 \text{ M}^{-1}\text{s}^{-1}$ , for the displacement of the aqua ligand in CoPt by nucleophiles at 30-fold excess over [CoPt],  $I = 0.02 \text{ M}$  (adjusted with  $\text{LiCF}_3\text{SO}_3$  and  $\text{LiCl}$ ).

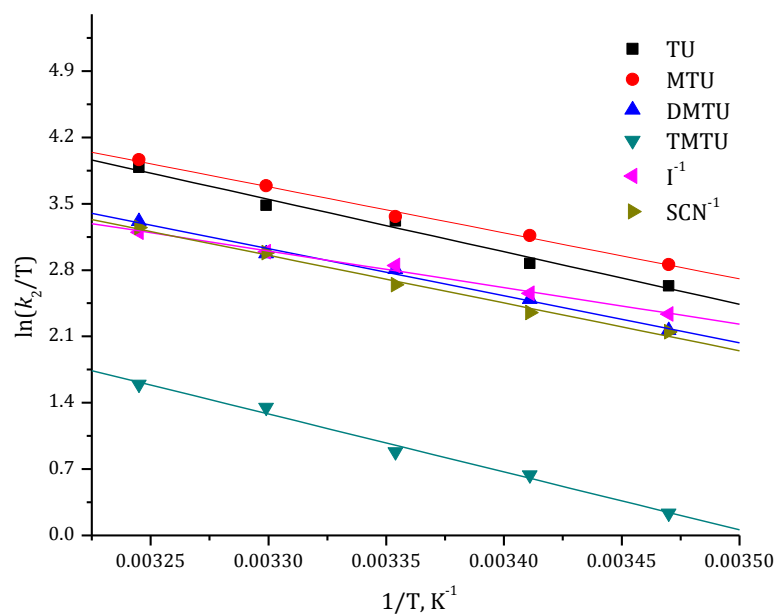
TU		MTU		DMTU		TMTU		$\text{I}^-$		$\text{SCN}^-$	
$1/T, \text{K}^{-1}$	$\ln(k_2/T)$	$1/T, \text{K}^{-1}$	$\ln(k_2/T)$	$1/T, \text{K}^{-1}$	$\ln(k_2/T)$	$1/T, \text{K}^{-1}$	$\ln(k_2/T)$	$1/T, \text{K}^{-1}$	$\ln(k_2/T)$	$1/T, \text{K}^{-1}$	$\ln(k_2/T)$
0.00347	1.4983994	0.00347	1.20850	0.00347	0.9611372	0.00347	0.5454441	0.00347	0.51538	0.00347	1.17197
0.00341	1.7305361	0.00341	1.58010	0.00341	1.3452242	0.00341	0.904107	0.00341	0.88256	0.00341	1.49729
0.00335	1.9751224	0.00335	1.915102	0.00335	1.7542578	0.00335	1.2421416	0.00335	1.24528	0.00335	1.74637
0.00329	2.2394616	0.00329	2.166765	0.00329	2.0009207	0.00329	1.5665842	0.00329	1.47286	0.00329	2.14308
0.00325	2.5117602	0.00325	2.417184	0.00325	2.2072244	0.00325	1.7787942	0.00325	1.72404	0.00325	2.51055

**Table S 3.20** Temperature dependence of  $k_2 \text{ M}^{-1}\text{s}^{-1}$ , for the dechelation of the pyridyl units in CoPt by thiourea nucleophiles at 30-fold excess over [CoPt],  $I = 0.02 \text{ M}$  (adjusted with  $\text{LiCF}_3\text{SO}_3$  and  $\text{LiCl}$ ).

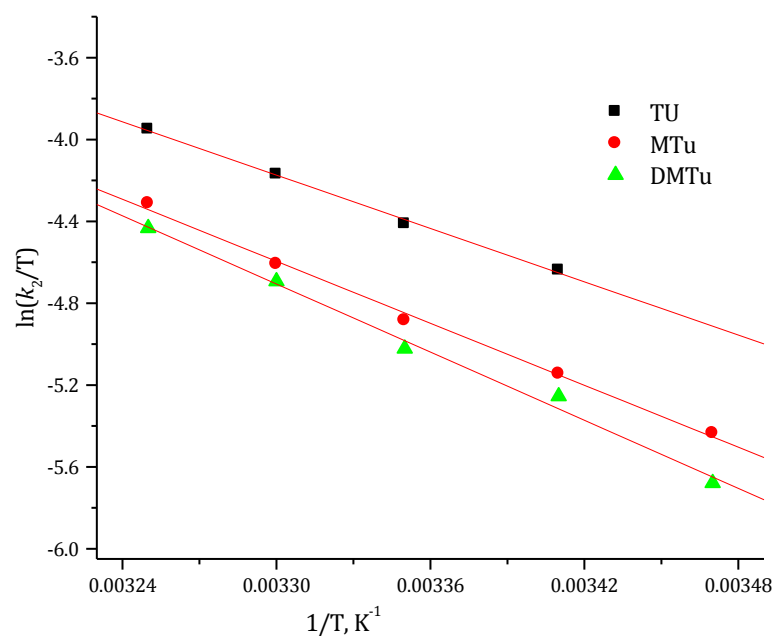
TU		MTU		DMTU	
$1/T, \text{K}^{-1}$	$\ln(k_2/T)$	$1/T, \text{K}^{-1}$	$\ln(k_2/T)$	$1/T, \text{K}^{-1}$	$\ln(k_2/T)$
0.003470415	-5.71353	0.00347	-5.87206	0.00347	-7.08116
0.003411223	-5.47388	0.003411	-5.49783	0.003411	-6.76303
0.003354016	-5.26543	0.003354	-5.33283	0.003354	-6.35325
0.003298697	-4.94821	0.003299	-5.09471	0.003299	-6.07875
0.003245173	-4.7254	0.003245	-4.80536	0.003245	-5.63694



**Figure S 3.6** Eyring plot obtained for the substitution of chloride ligand in  $\text{Pt}(\text{tpy})$ , with MTU nucleophile at various temperatures in the range 15 - 40 °C

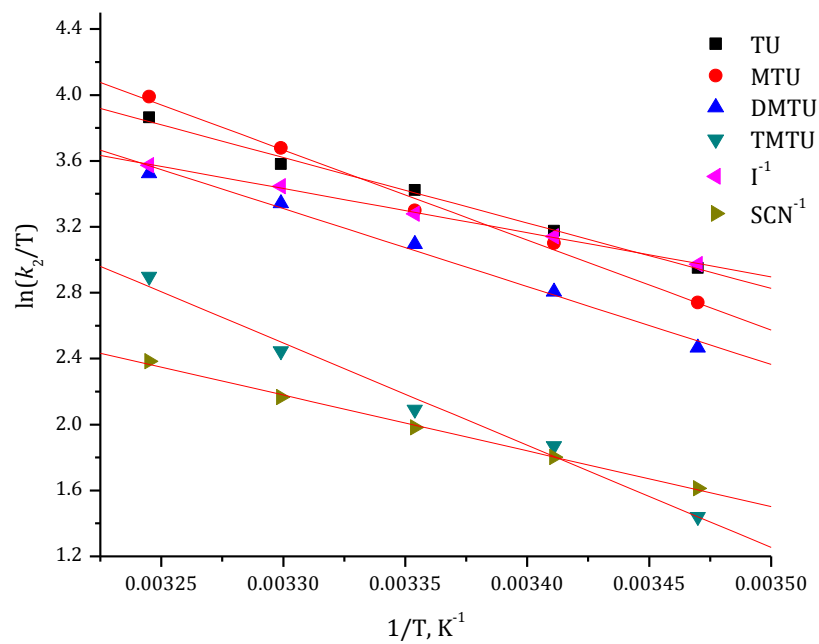


(a)

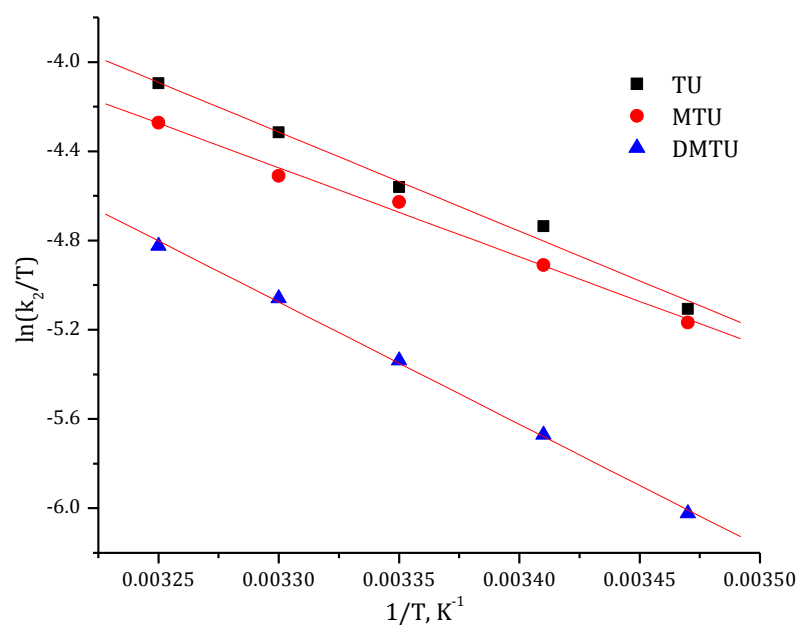


(b)

**Figure S 3.7** Eyring plots obtained, as  $\ln(k_2/T)$  against  $1/T$  (a) for the reactions of PtRuPt with the nucleophiles for the substitution of chloride ligands (b) for the dechelation of the linker at various at various temperatures in the range 15 - 40 °C

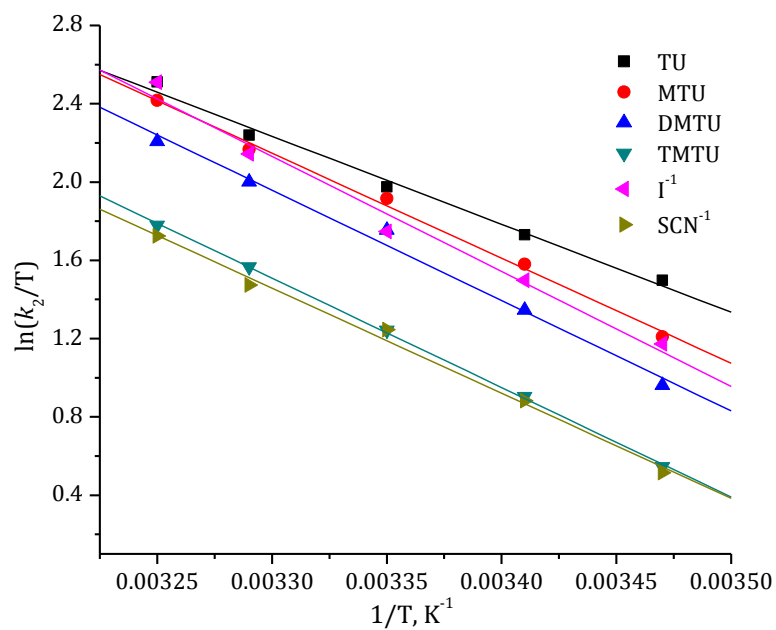


(a)

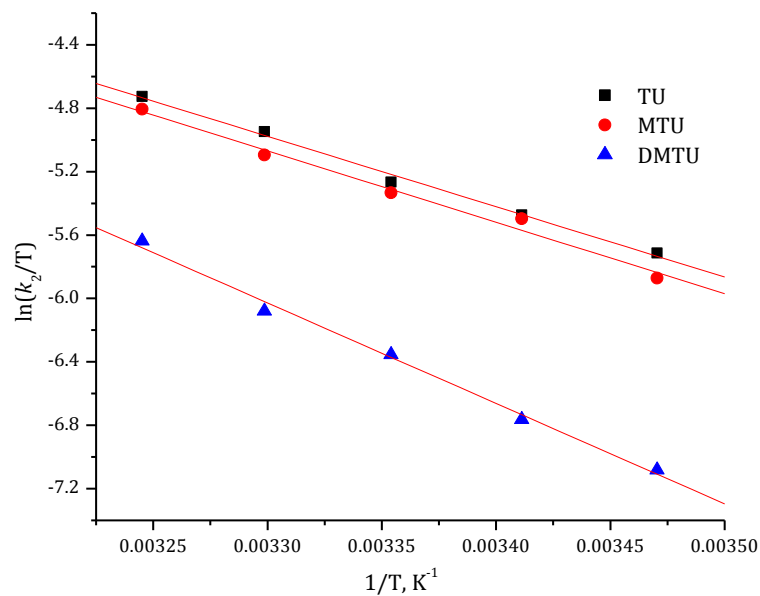


(b)

**Figure S 3.8** Eyring plots obtained, as  $\ln(k_2/T)$  against  $1/T$  (a) for the reactions of PtRuRuPt with the nucleophiles for the substitution of chloride ligands (b) for the dechelation of the linker at various temperatures in the range 15 - 40 °C



(a)



(b)

**Figure S 3.9** Eyring plots obtained, as  $\ln(k_z/T)$  against  $1/T$  (a) for the reactions of CoPt with the nucleophiles for the substitution of chloride ligands (b) for the dechelation of the linker at various temperatures in the range 15 - 40 °C

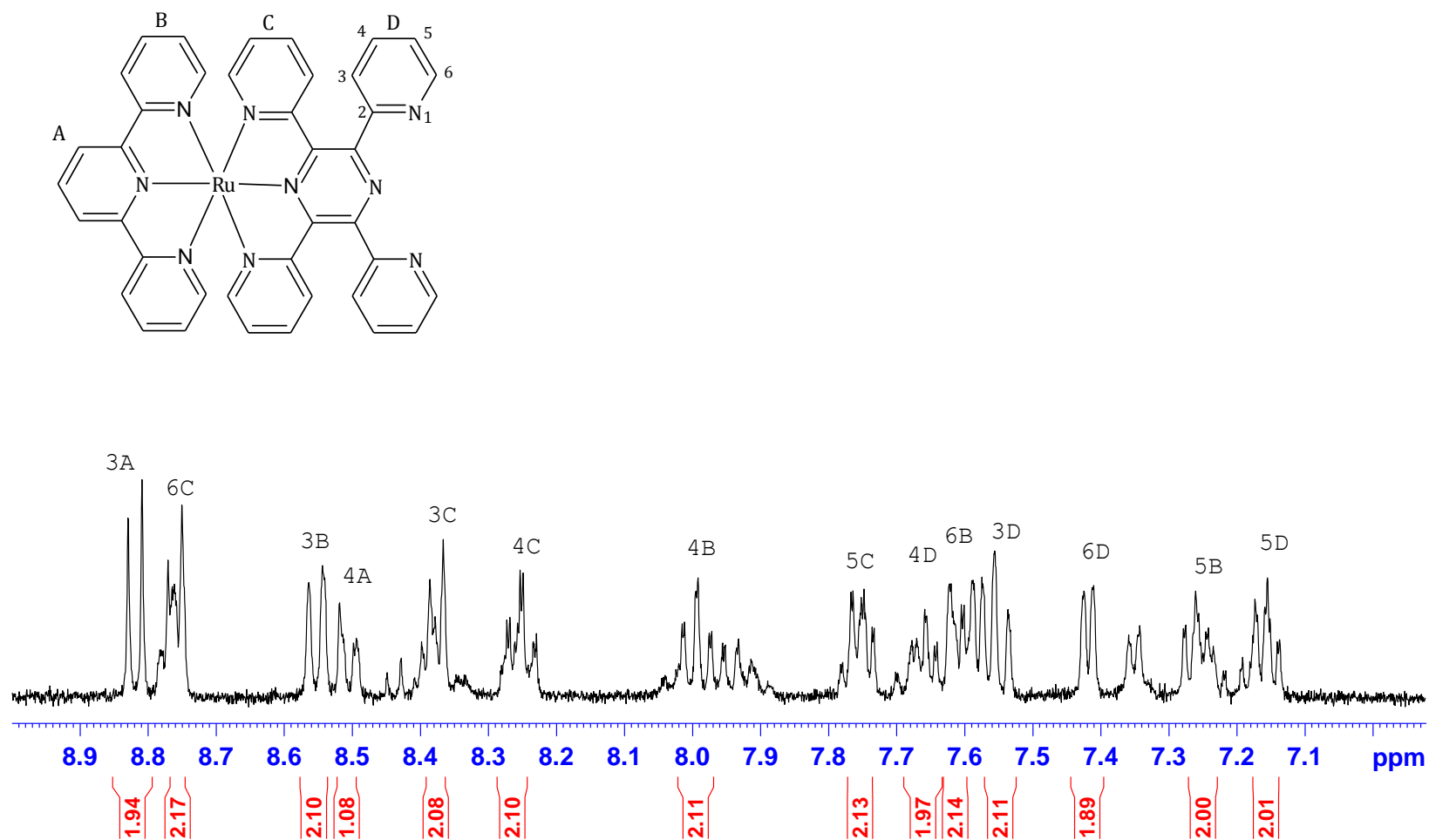


Figure S 3.10  $^1\text{H}$ NMR spectrum of  $(\text{tpy})\text{Ru}(\text{tppz})(\text{PF}_6)_2$ . Spectrum zoomed in to show the signals due to the protons in the aromatic rings.

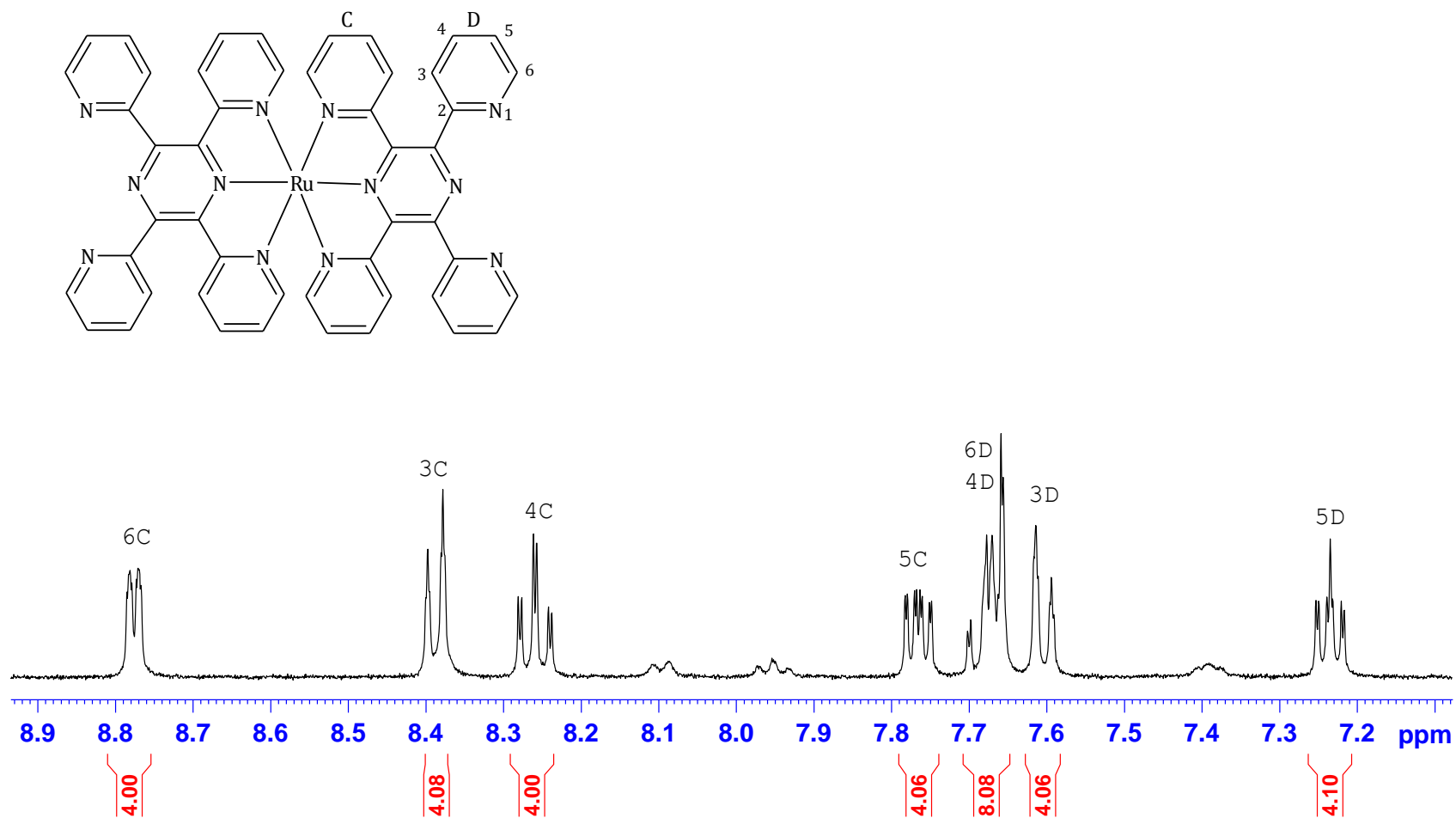


Figure S 3.11  $^1\text{H}$ NMR spectrum of  $\text{Ru}(\text{tppz})_2(\text{PF}_6)_2$ . Spectrum zoomed in to show the signals due to the protons in the aromatic rings.



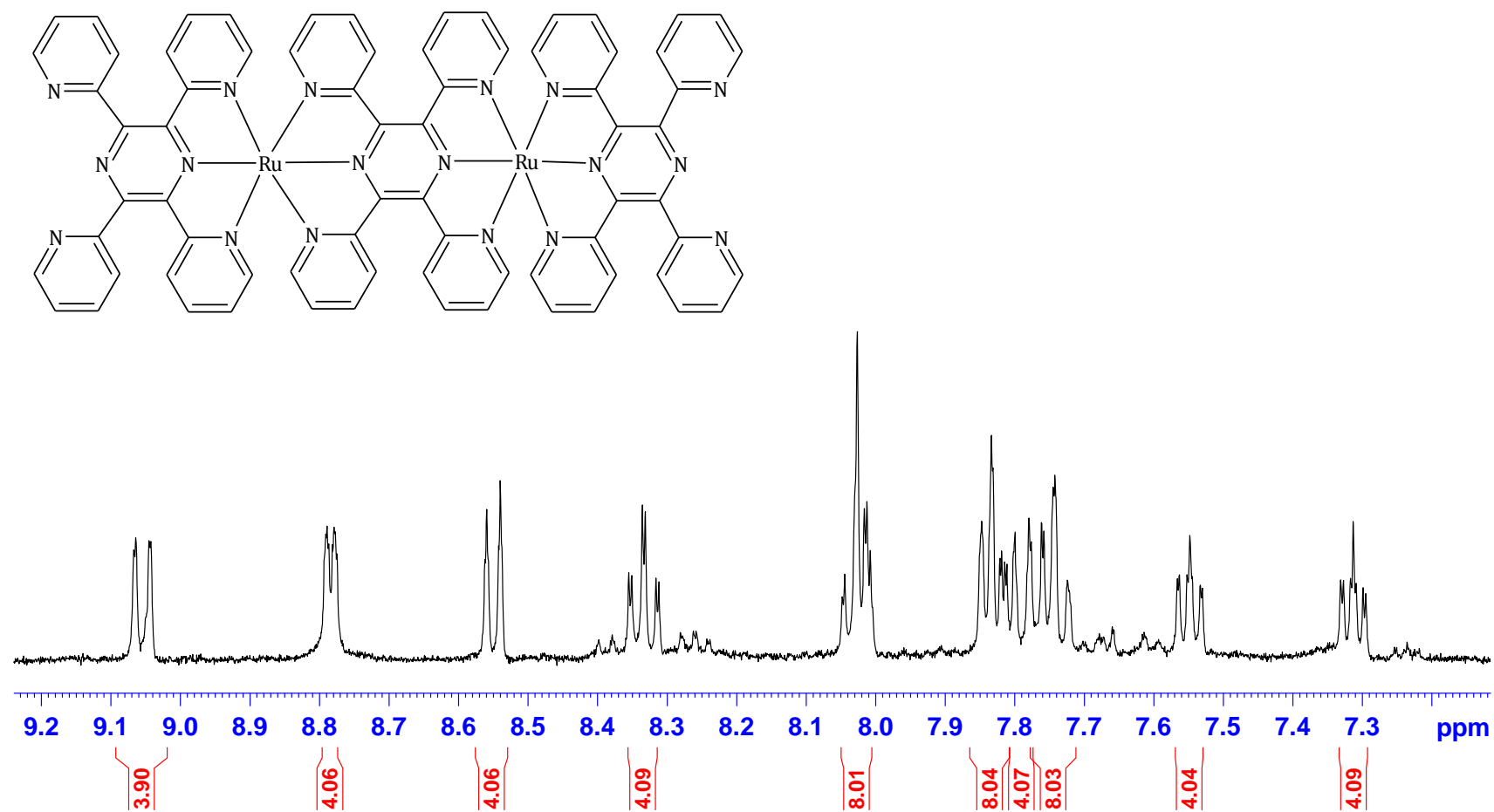


Figure S3.12  $^1\text{H}$ NMR spectrum of  $\text{Ru}_2(\text{tppz})_3(\text{PF}_6)_4$ . Spectrum zoomed in to show the signals due to the protons in the aromatic rings.

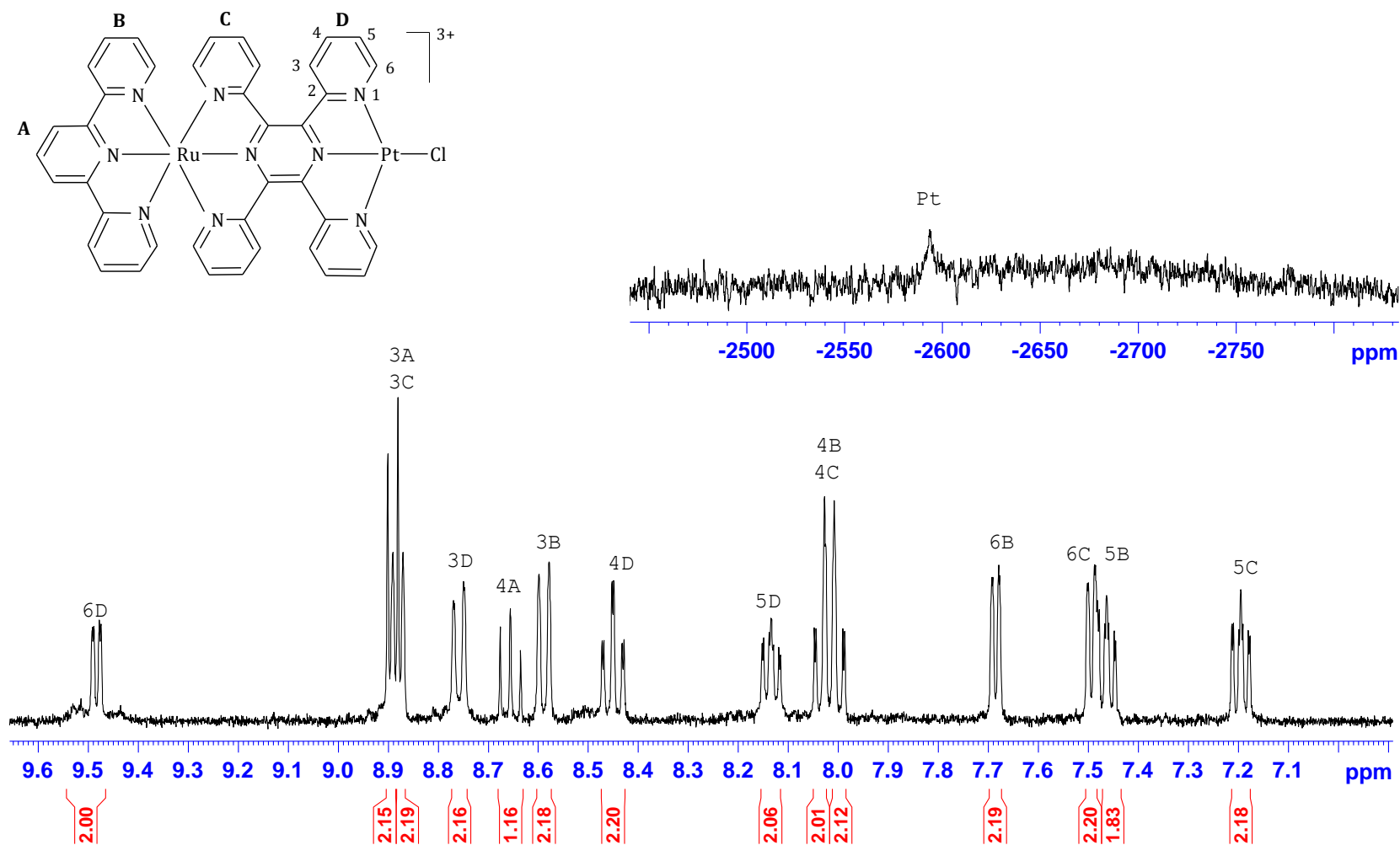


Figure S 3.13  $^1\text{H}$ NMR spectrum of  $[(\text{tpy})\text{Ru}(\text{tppz})\text{PtCl}](\text{PF}_6)_3$ . Spectrum zoomed in to show the signals due to the protons in the aromatic rings. Inset is the  $^{195}\text{Pt}$  NMR for the complex.

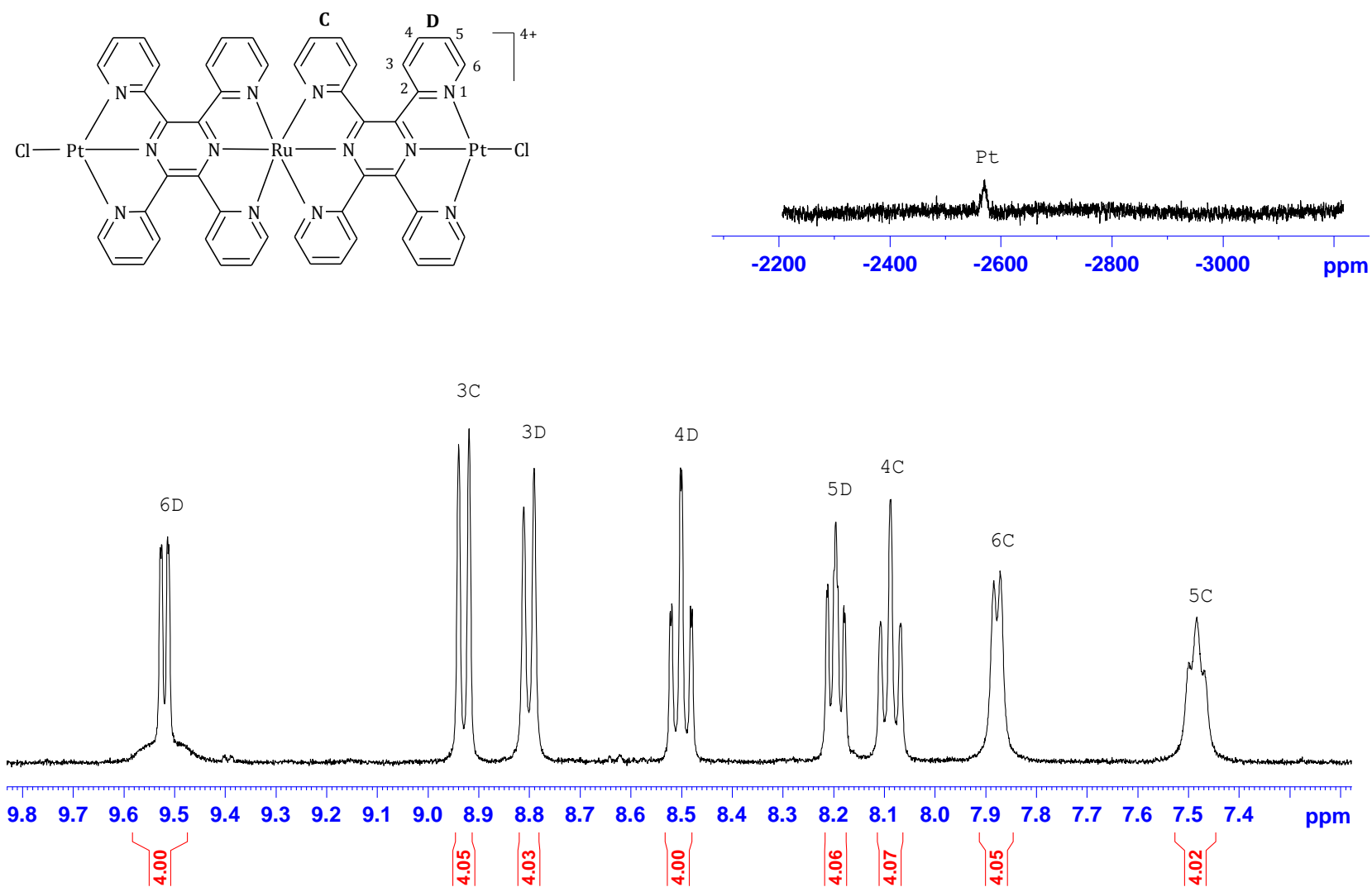


Figure S 3.14  $^1\text{H}$ NMR spectrum of  $[\text{ClPt}(\text{tppz})\text{Ru}(\text{tppz})\text{PtCl}](\text{PF}_6)_4$ . Spectrum zoomed in to show the signals due to the protons in the aromatic rings. Inset is the  $^{195}\text{Pt}$  NMR for the complex.

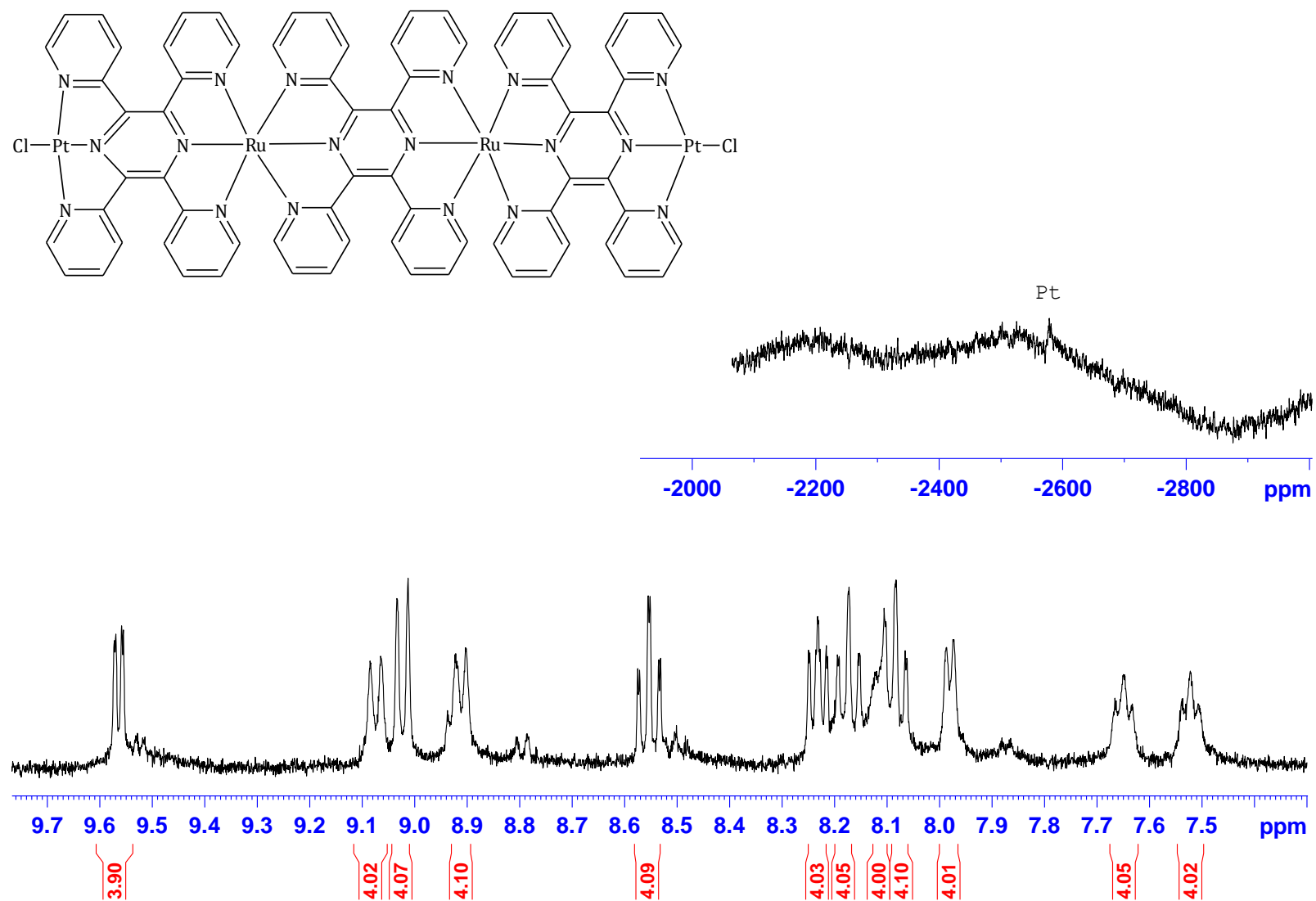
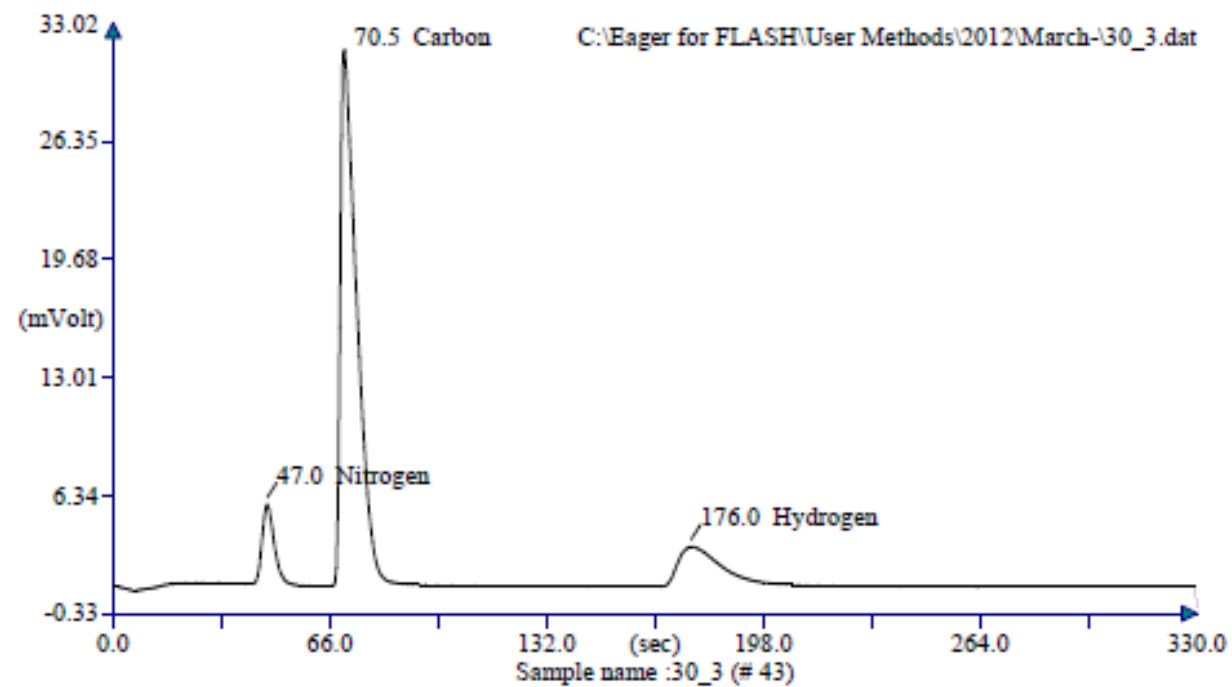


Figure S 3.15  $^1\text{H}$ NMR spectrum of  $[[\text{ClPtRu}_2(\text{tppz})_3\text{PtCl}](\text{PF}_6)_6$ . Spectrum zoomed in to show the signals due to the protons on the aromatic rings. Inset is the  $^{195}\text{Pt}$  NMR for the complex.



Retention Time (min)	Element Name	Element %
0.783	Nitrogen	8.955
1.175	Carbon	34.824
2.933	Hydrogen	2.183
		45.962

Figure S 3.16 Exemplary elemental analysis spectrum for CoPt.

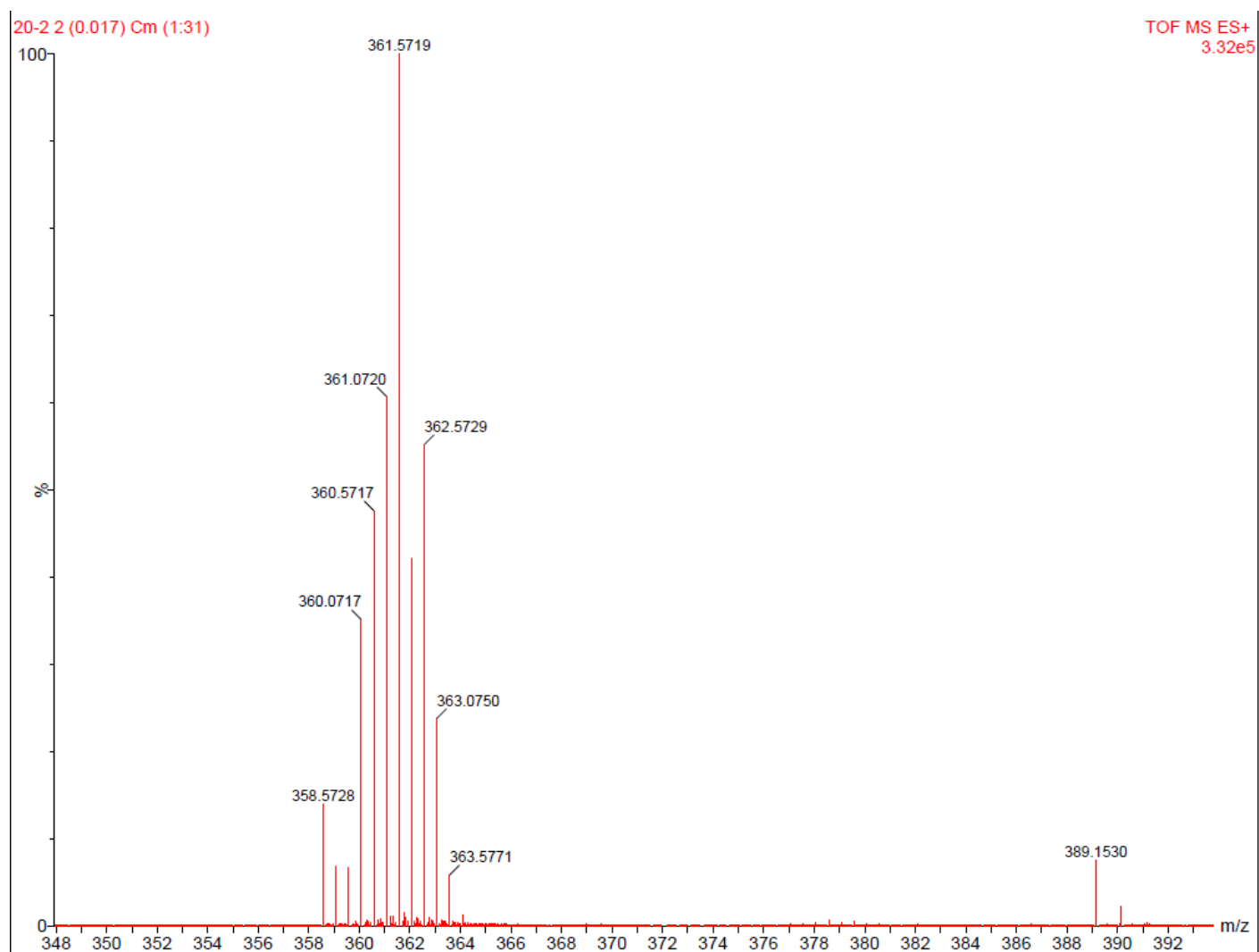


Figure S 3.17 Low resolution ESI mass spectrum of (tpy)Ru(tppz)(PF<sub>6</sub>)<sub>2</sub>.

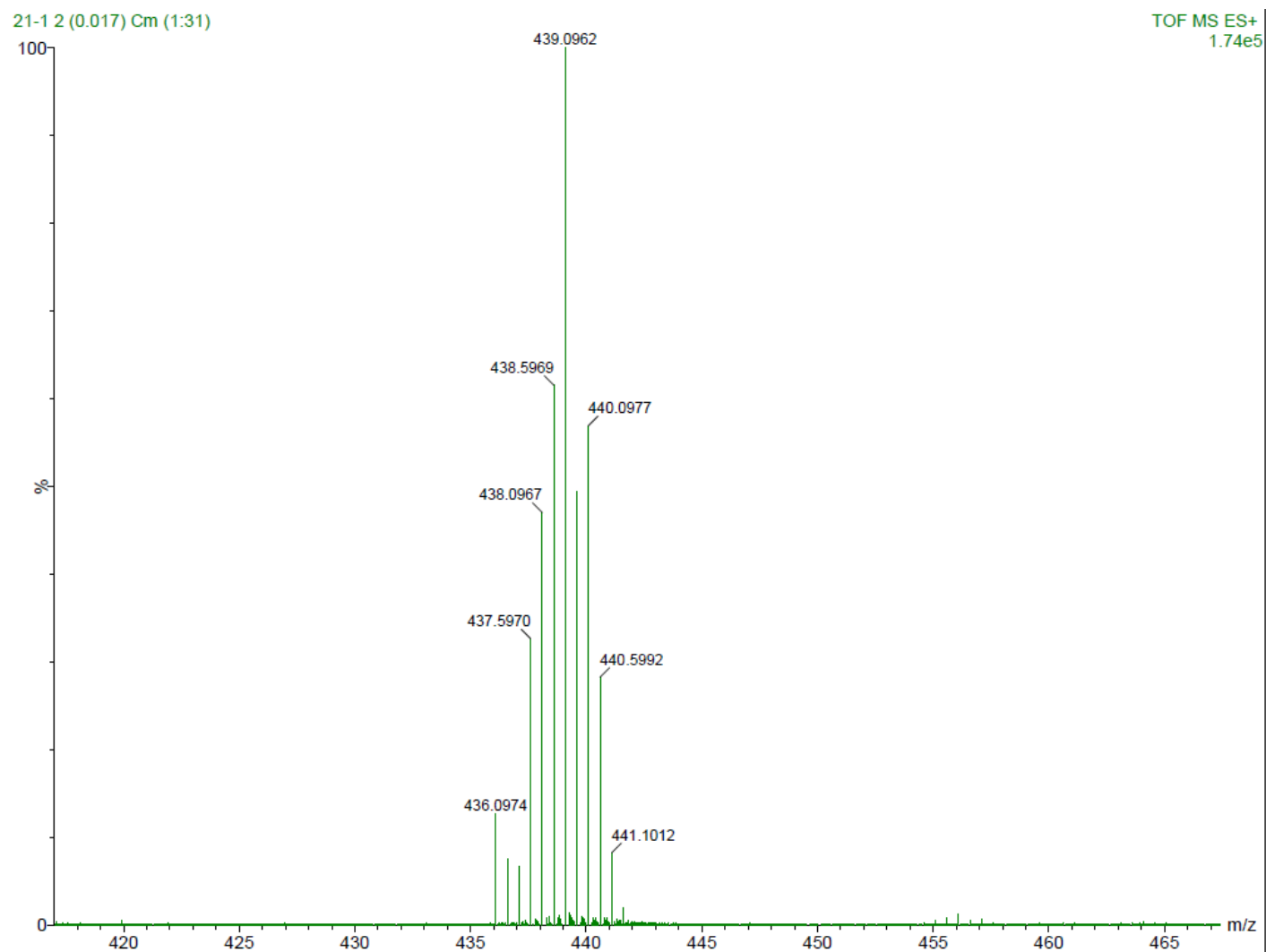


Figure S 3.18 Low resolution ESI mass spectrum of  $\text{Ru}(\text{tppz})_2(\text{PF}_6)_2$ .

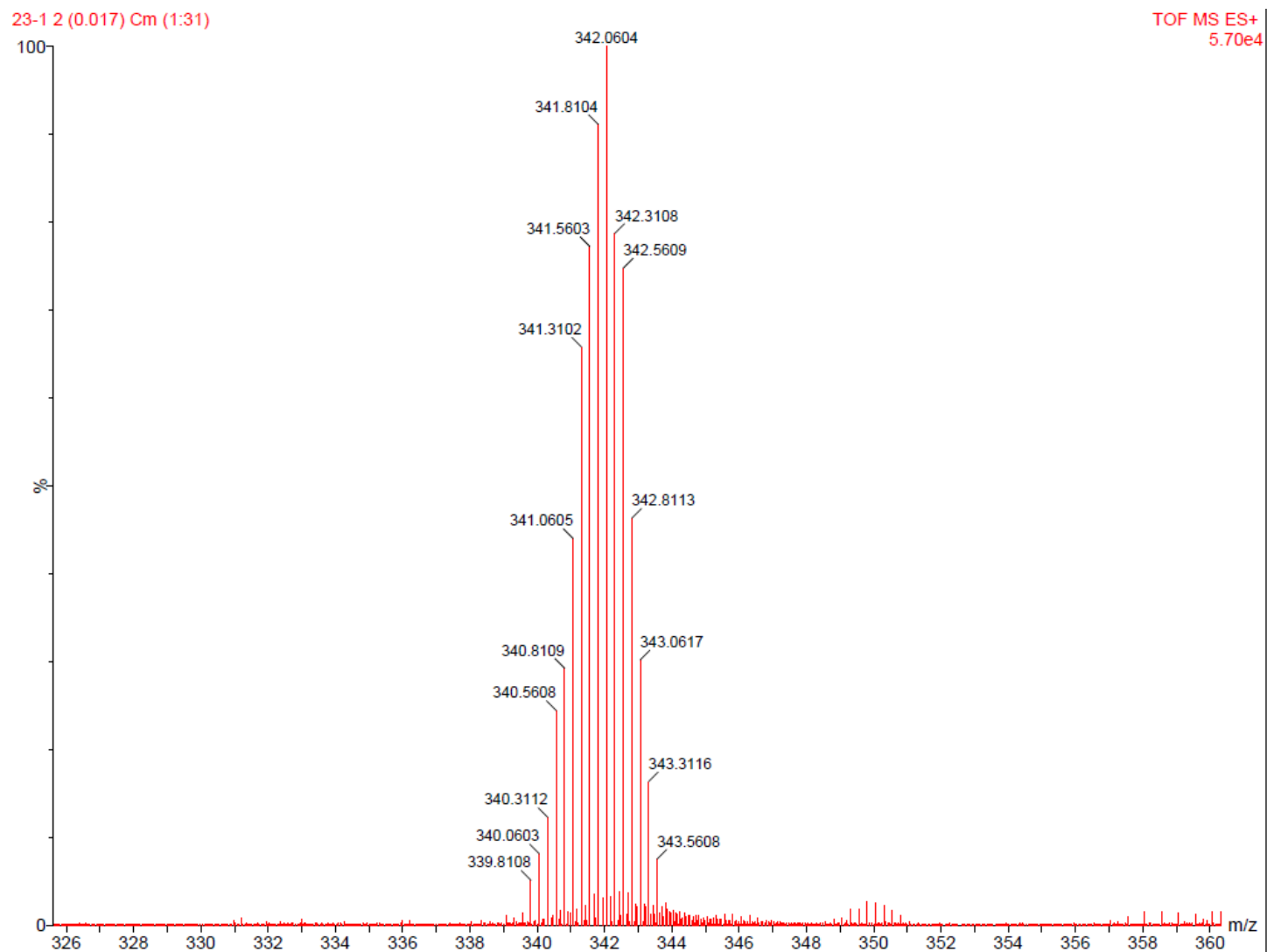


Figure S 3.19 Low resolution ESI mass spectrum of  $\text{Ru}_2(\text{tppz})_3(\text{PF}_6)_4$ .



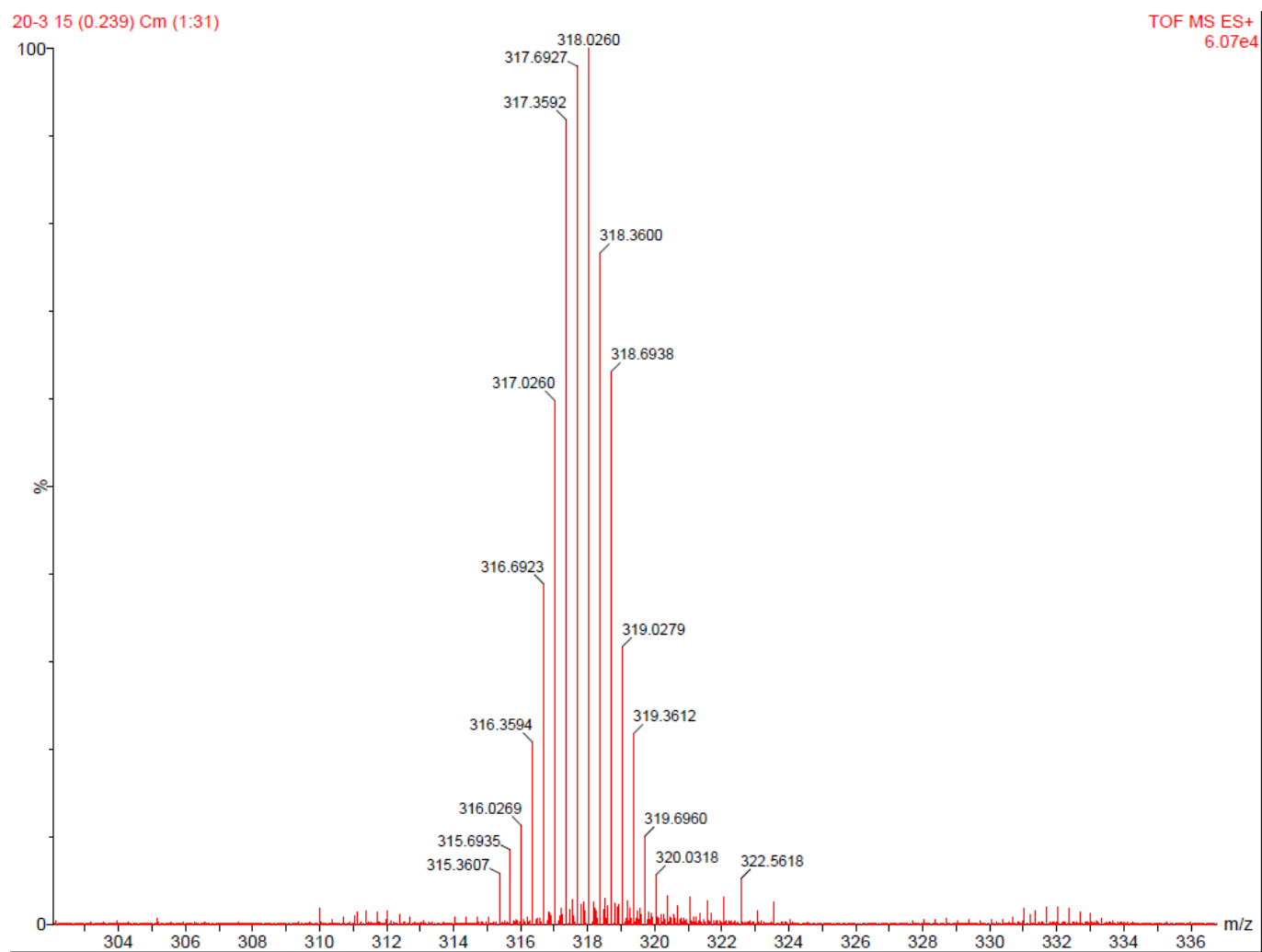


Figure S 3.20 Low resolution ESI mass spectrum of RuPt.

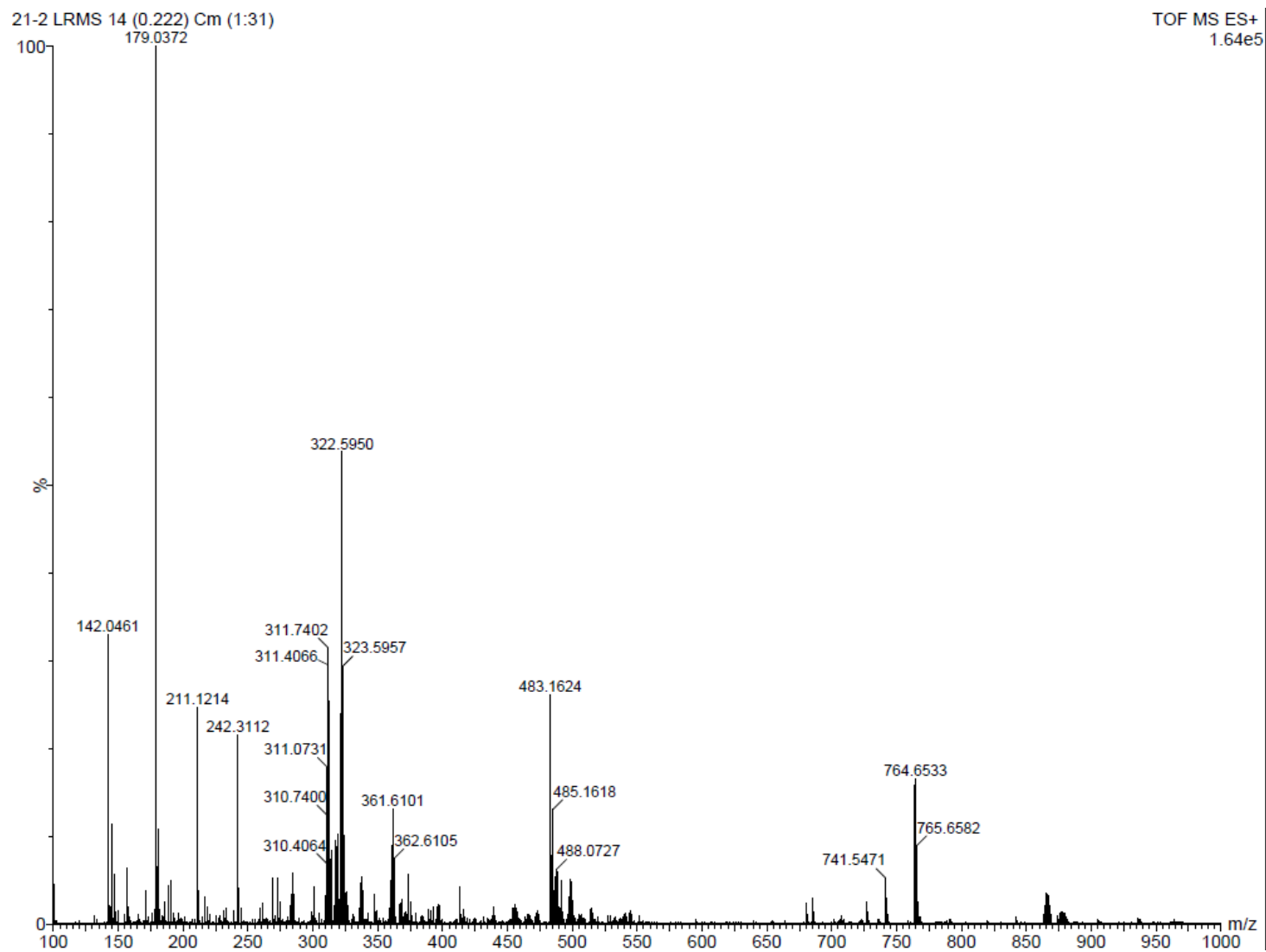


Figure S 3.21 Low resolution ESI mass spectrum of PtRuPt.

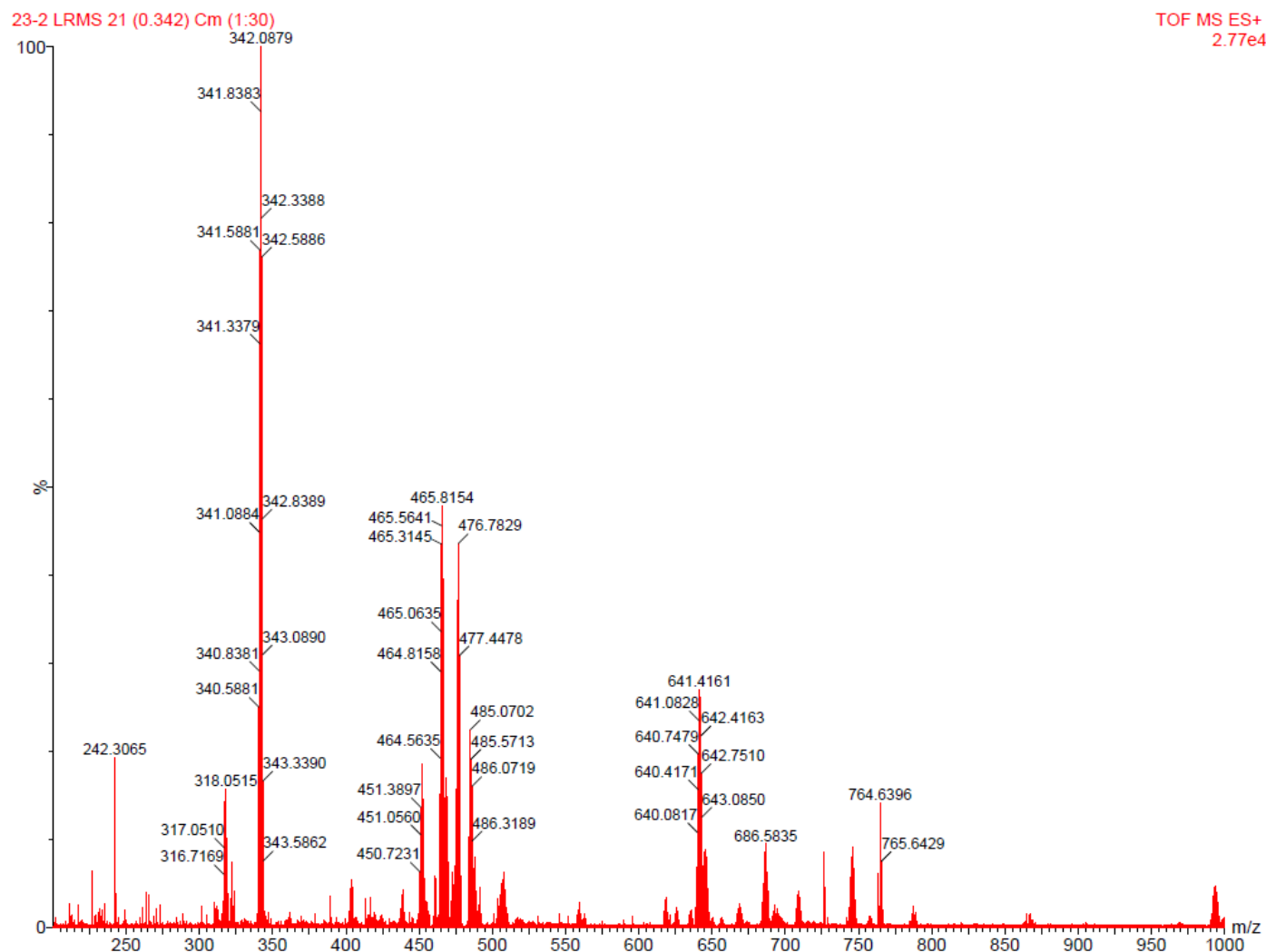


Figure S 3.22 Low resolution ESI mass spectrum of PtRuRuPt

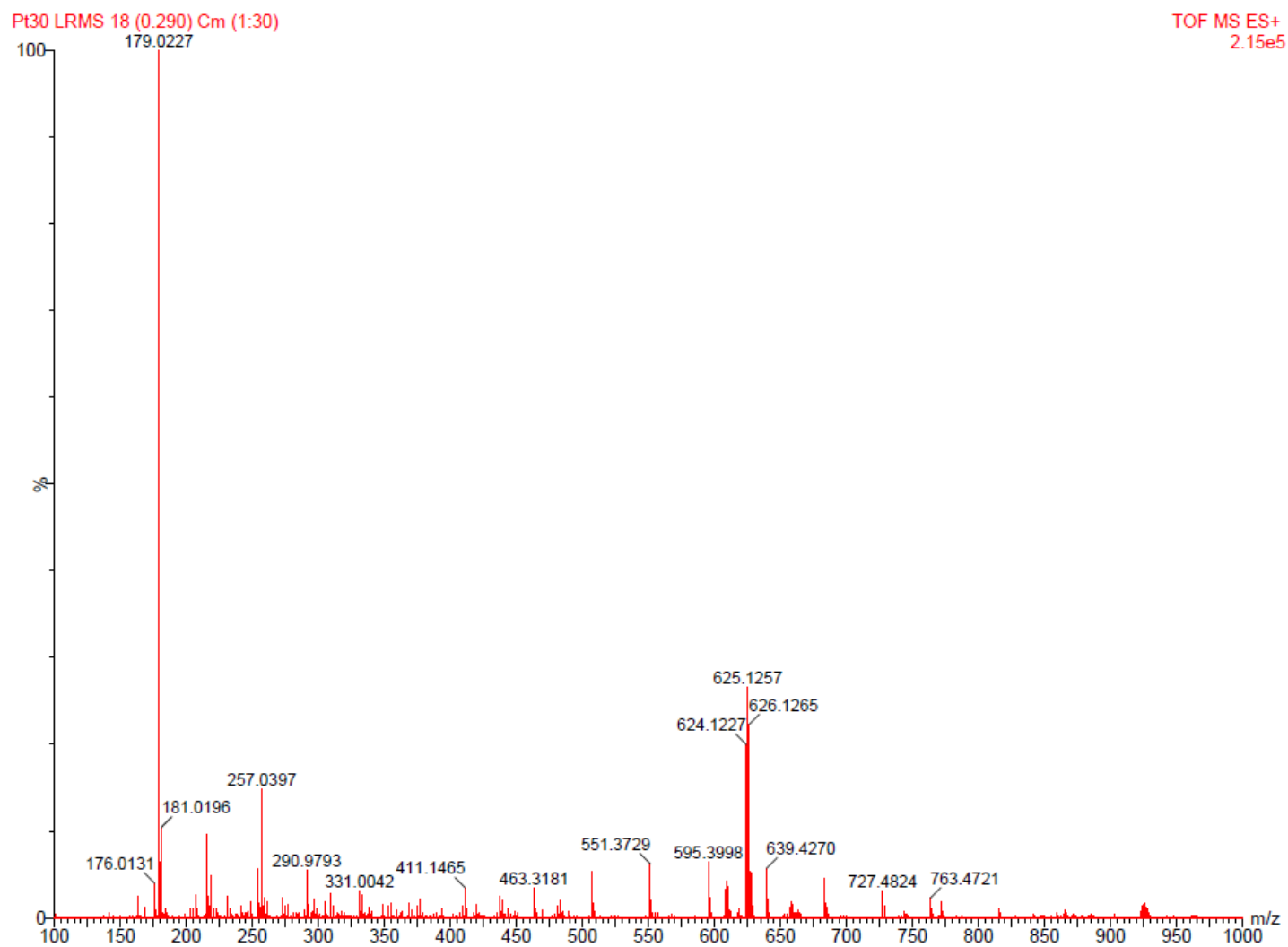
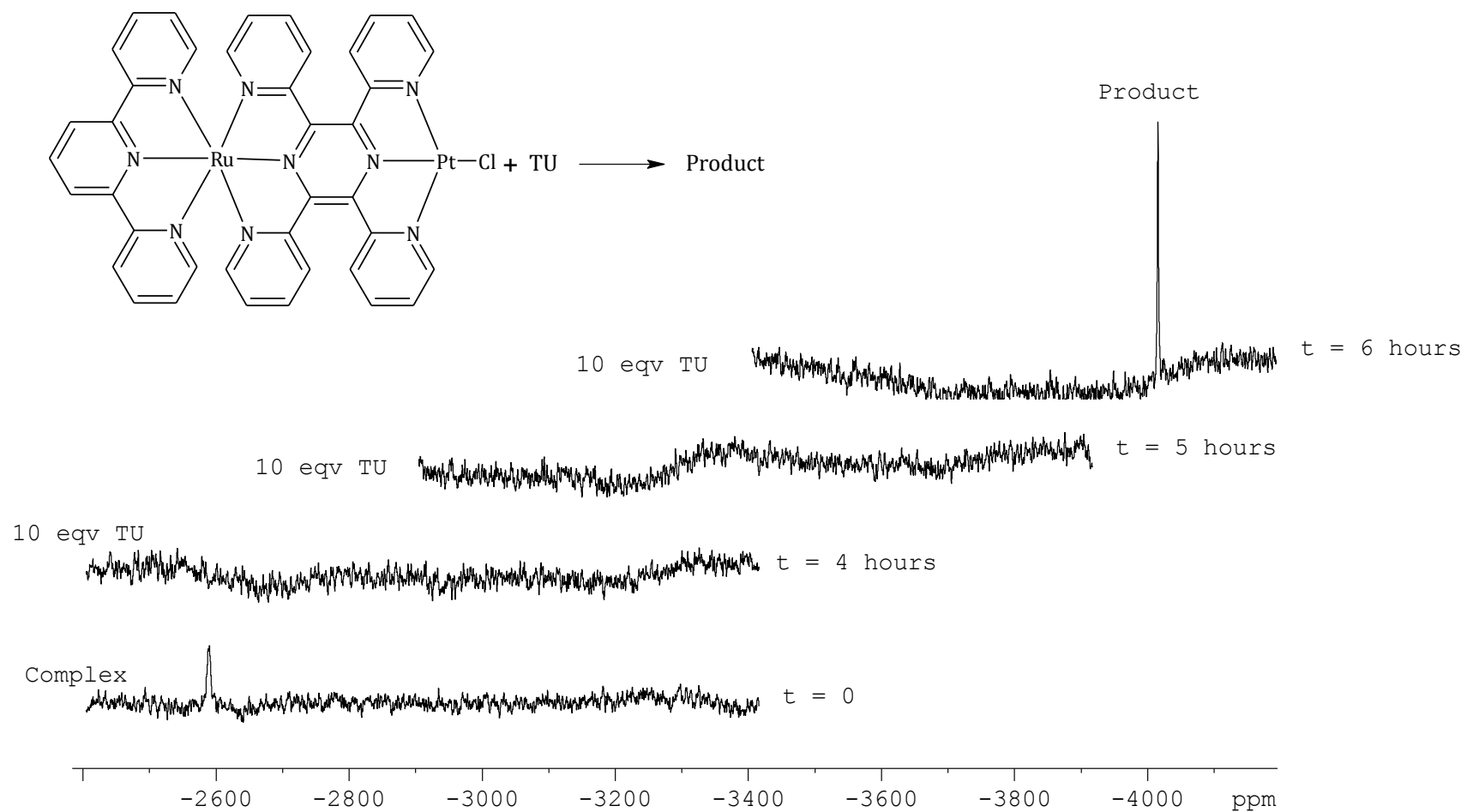
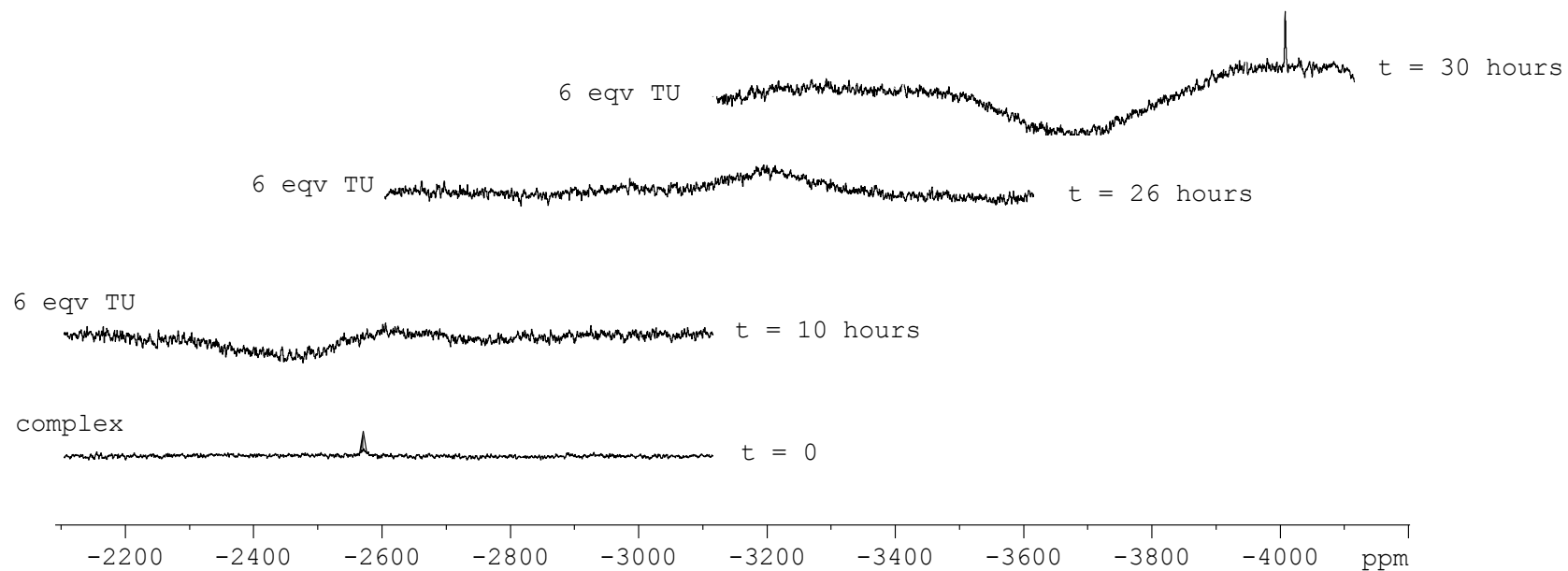
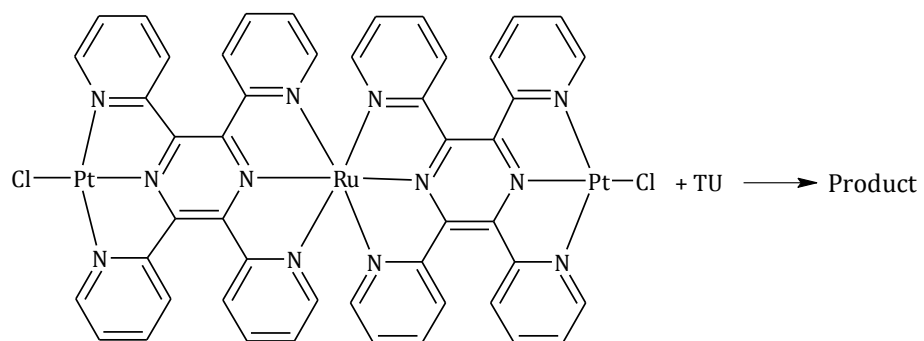


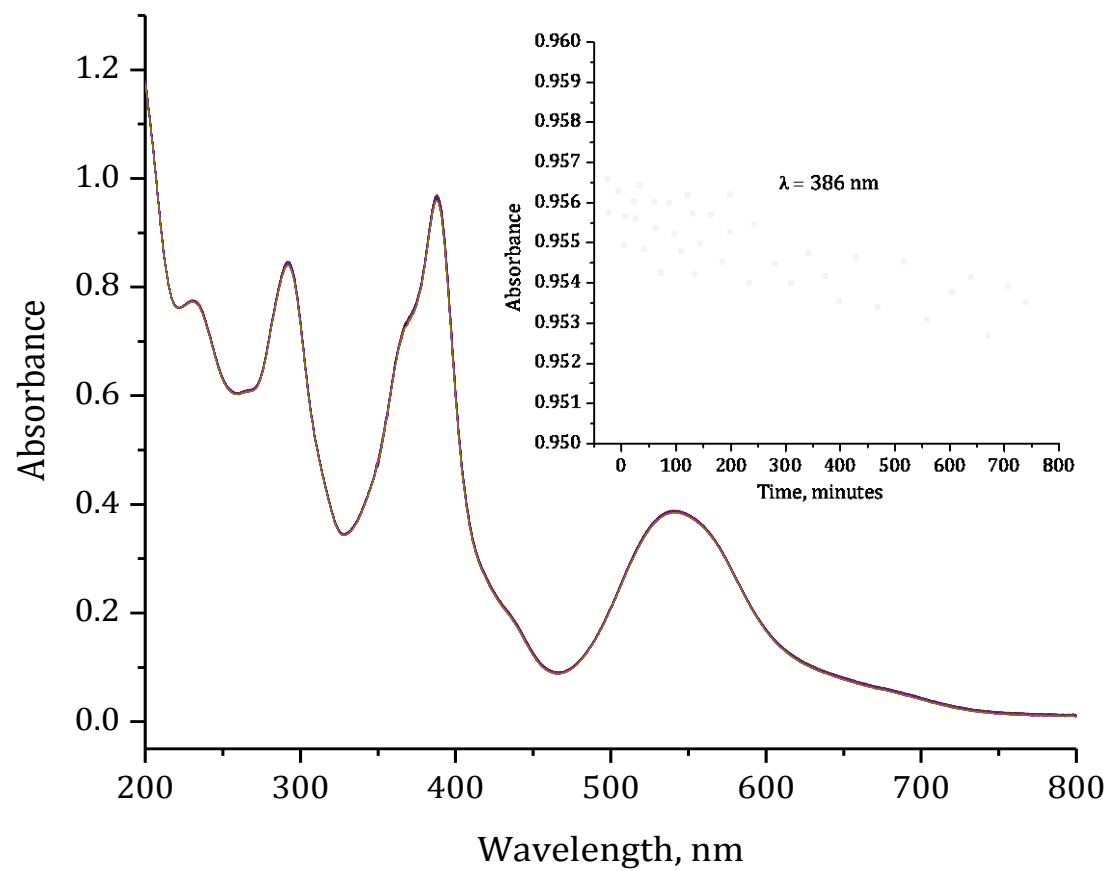
Figure S 3.23 Low resolution ESI mass spectrum of CoPt



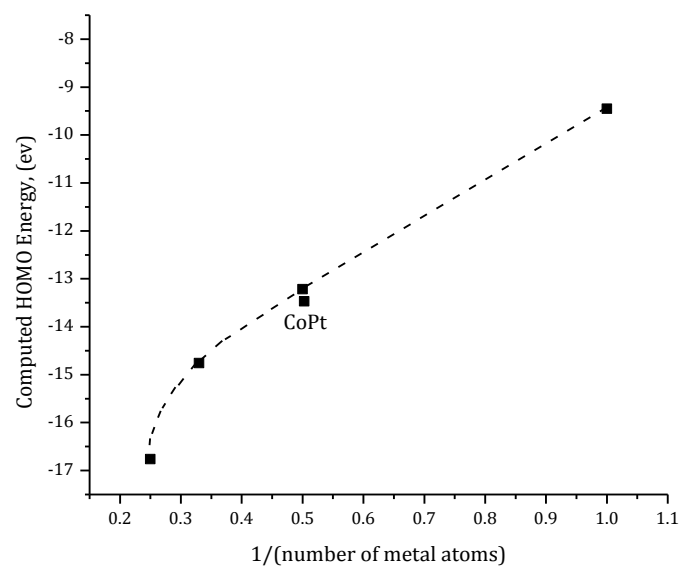
**Figure S 3.24** <sup>195</sup>Pt NMR spectra for the reaction of RuPt (6.28 mM) with TU, showing the changes in the chemical shift of the Pt before adding the TU nucleophile and the degradation after addition of TU for the new complex [Pt(TU)<sub>4</sub>]<sup>2+</sup>.



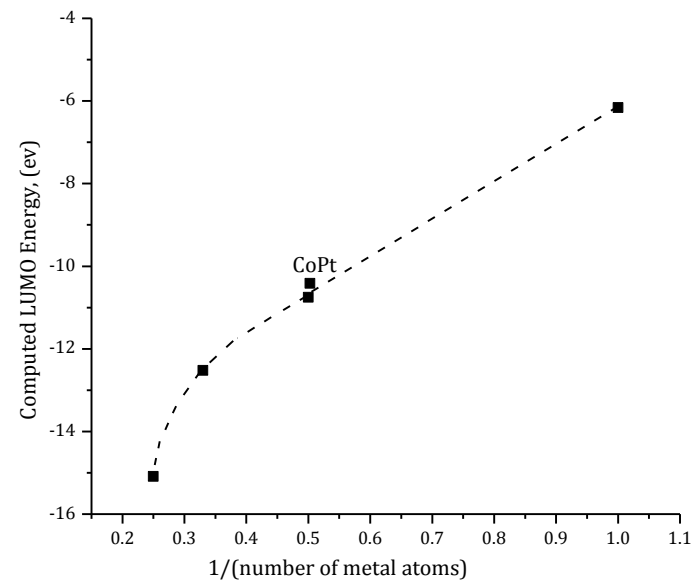
**Figure S 3.25** Kinetic  $^{195}\text{Pt}$  NMR spectra in  $\text{CD}_3\text{CN}$  for the reaction of PtRuPt (0.02 mM) with TU at 298 K. The bottom spectrum is obtained for the pure complex and the top spectrum is obtained by addition of six equivalence of TU after 12 hours. Inset is the trace obtained at 386 nm.



**Figure S 3.26** A typical UV/visible plot showing the changes in absorbance between 250 to 800 nm wavelength range for PtRuPt in acetonitrile (0.02 mM) at 298 K over a period of 12 hours.



(a)



(b)

**Figure S 3.27** (a) Computed HOMO energy against inverse number of metal centres. (b) Computed LUMO energy against inverse number of metal centres.



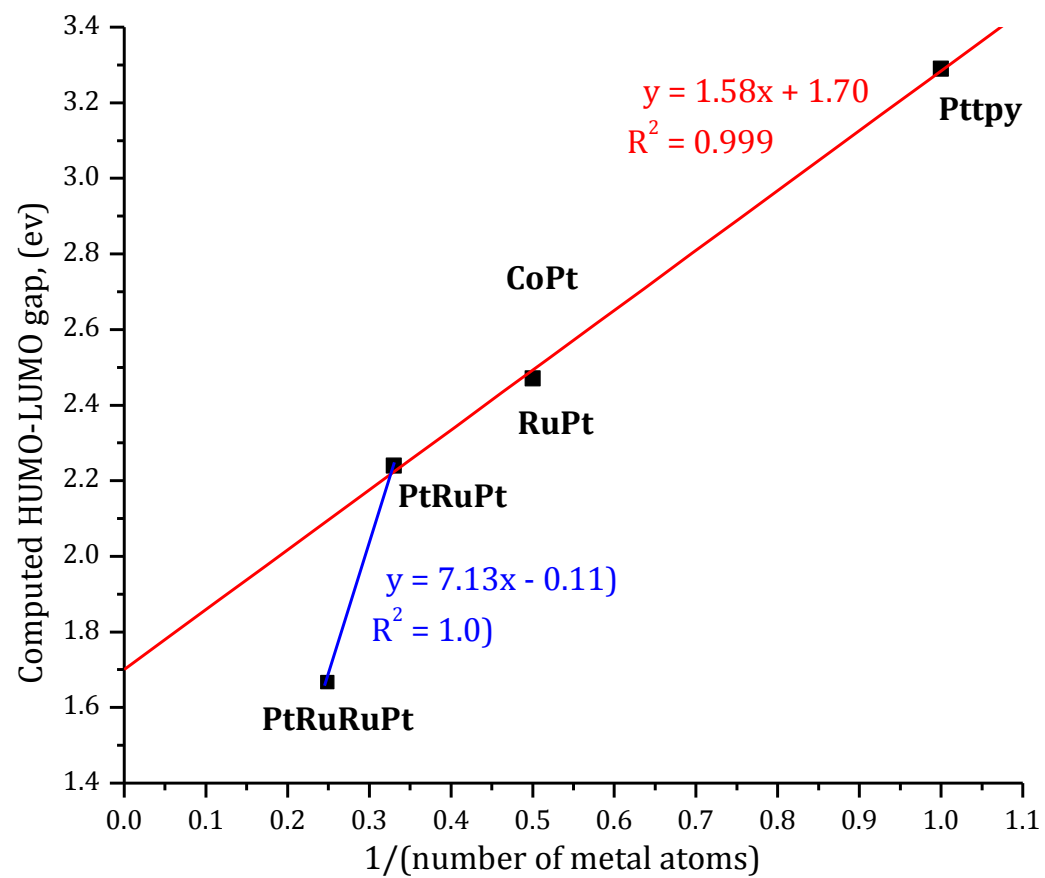


Figure S 3.28 Graph of DFT calculated HOMO-LUMO energy gap against inverse number of metal centres. CoPt deviates from the trend.

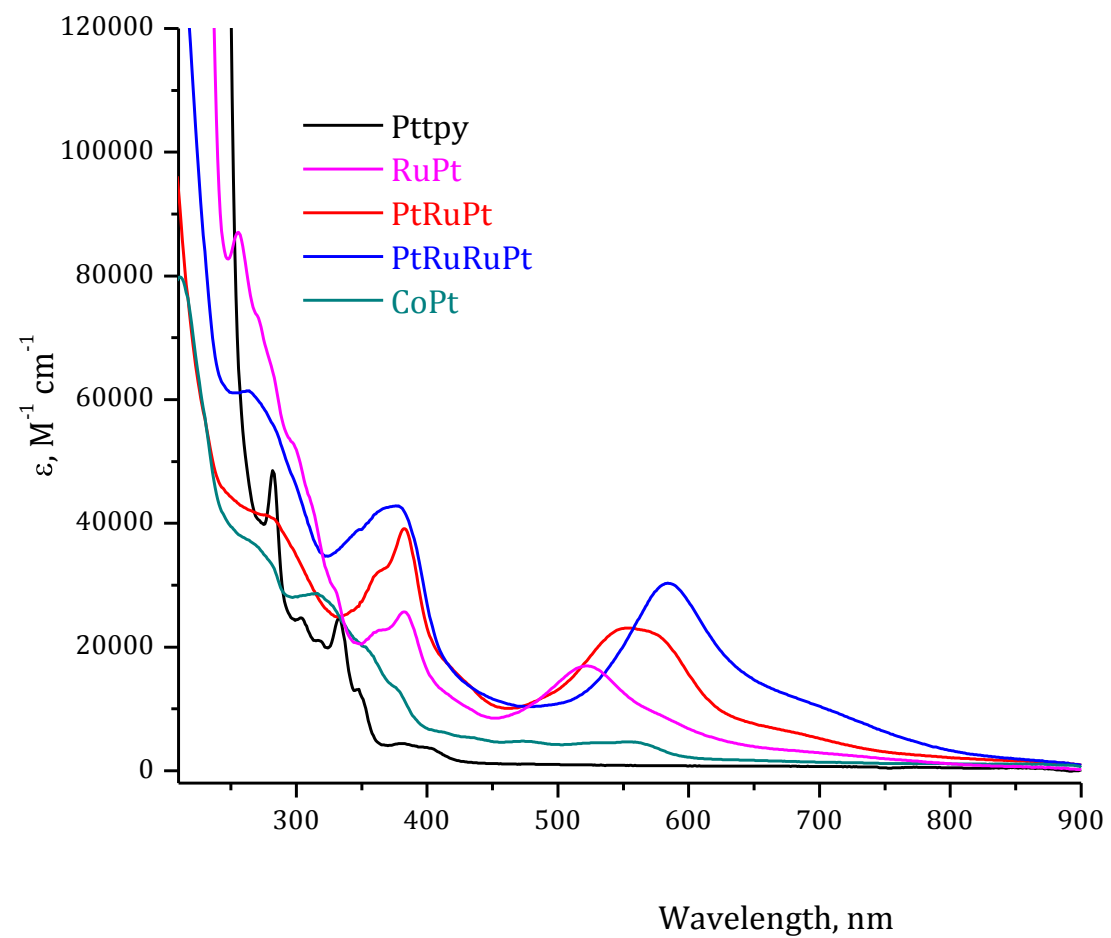


Figure S 3.29 Electronic absorption for the complexes investigated using 0.01 mM concentration for all the complexes measured in methanol at 298 K.

## Experimental

### [Ru(tpy)Cl<sub>3</sub>]

Equal amounts of RuCl<sub>3</sub>·3H<sub>2</sub>O (~150 mg) and tpy were refluxed in absolute EtOH (125 mL) for 3 hours. The resulting reaction mixture was cooled to room temperature and the precipitate was filtered, washed with cold absolute EtOH (10 mL) followed by copious amount of diethyl ether and dried under *vacuo*.

### [(tpy)Ru(tppz)](PF<sub>6</sub>)<sub>2</sub>,

To a stirred solution of Ru(tpy)Cl<sub>3</sub> (50.7 mg, 0.115 mmol) in an ethanol/ water mixture (1: 1) was added the ligand tppz (45 mg, 0.115 mmol). The reaction mixture was flushed with nitrogen for 15 minutes and then refluxed for 12 hours. The resulting reaction mixture was cooled and filtered in order to remove any unreacted tppz. The filtrate was added to an aqueous solution of ammonium hexafluoro phosphate. The resulting black precipitate was filtered and this product was chromatographed on neutral aluminium oxide using acetonitrile and toluene (1: 1) as an eluent. The first main orange band was isolated and solvent removed under *vacuo* and dried under vacuum to yield the desired product.

### [Ru(tppz)<sub>2</sub>](PF<sub>6</sub>)<sub>2</sub>,

The ruthenium complexes; [Ru(tppz)<sub>2</sub>](PF<sub>6</sub>)<sub>2</sub>] and [Ru<sub>2</sub>(tppz)<sub>3</sub>(PF<sub>6</sub>)<sub>4</sub>] were synthesized as from literature. To a stirred solution of Ru(III)Cl<sub>3</sub>·3H<sub>2</sub>O (58.5 mg, 0.22 mmol) in ethanol/ water (1: 1), was added the ligand, tppz (300 mg, 0.77 mmol). The solution was flushed with nitrogen for 15 minutes and then heated to reflux for 48 hours. The purple reaction mixture was allowed to cool and filtered to remove any unreacted tppz. The filtrate was treated with aqueous ammonium hexafluoro phosphate and the black precipitate formed was filtered and chromatographed on neutral alumina using acetonitrile/toluene (1 : 1) as an eluant. The first orange band was collected and solvent removed and dried under *vacuo* to yield the monomeric product, Ru(tppz)(PF<sub>6</sub>)<sub>2</sub>. The homodimetalic complex, [Ru<sub>2</sub>(tppz)<sub>3</sub>(PF<sub>6</sub>)<sub>4</sub>] was obtained as a byproduct which was eluted as a purple band after the orange fraction. This product was obtained after removing the solvent and drying it under *vacuo*.

### PtCl<sub>2</sub>(DMSO)<sub>2</sub>]

Dimethyl sulphoxide (0.64 mL, 0.009 mol) was added to a solution of (10 mL) K<sub>2</sub>PtCl<sub>4</sub> (1.87 g, 0.0045 mol) at room temperature . The solution was left to stand until the yellow crystals were formed. The crystals were filtered, washed with water and diethyl ether and dried under *vacuo*.

**[Pt(tpy)Cl]Cl·H<sub>2</sub>O (Pt<sub>1</sub>tpy)**

To a stirred solution of [Pt(COD)Cl<sub>2</sub>] (500 mg, 1.34 mmol) in water (30 mL), 2,2':6',2''-terpyridine (313 mg, 1.34 mmol) was added. The mixture was stirred and warmed to between 45-50 °C for 15 minutes. The clear orange-red solution obtained was cooled to room temperature and filtered to remove any unreacted [Pt(COD)Cl<sub>2</sub>]. Removal of solvent under reduced pressure gave an orange-red solid, [Pt(terpy)Cl]Cl·2H<sub>2</sub>O, (**Pt<sub>1</sub>tpy**). The product was collected, washed thoroughly with diethyl ether and air dried. Recrystallization of the dried solid in a hot methanol/water mixture (50: 50) gave orange needle like crystals of the titled compound. The crystals were filtered using 0.45 µm nylon filter membrane on millipore filtration unit, washed with diethyl ether and air dried.

**[ClPt(tppz)Ru(tppz)PtCl](PF<sub>6</sub>)<sub>4</sub> (Pt<sub>1</sub>RuPt)**

This compound was synthesized by a similar approach as [(tpy)Ru(tppz)PtCl](PF<sub>6</sub>)<sub>3</sub>. [ClPt(tppz)Ru(tppz)PtCl](PF<sub>6</sub>)<sub>4</sub> was synthesized by dropwise addition of Ru(tppz)<sub>2</sub> (50 mg, 43 µmol) in acetonitrile (10 mL) to a refluxing solution of [Pt(DMSO)<sub>2</sub>Cl<sub>2</sub>] (38 mg, 90 µmol) in acetonitrile (15 mL). The reaction mixture was refluxed for 6 hours under nitrogen and then cooled to room temperature and filtered. The filtrate was added to an aqueous solution of ammonium hexafluoro phosphate. The dark purple precipitate formed was filtered, washed with ethanol (5 mL), distilled water (20 mL) and copious amount of diethyl ether and dried under *vacuo*.

**Tables of Contents- 4**

List of Figures.....	ii
List of Tables .....	iii
List of Schemes .....	iii
Chapter Four.....	1
<b>The Effect of Ruthenium(II) Terpyridine Fragment on the Reactivity of Platinum(II) centre. A Kinetic and Computational Approach.....</b>	<b>1</b>
4.0    Abstract.....	1
4.1    Introduction .....	2
4.2    Experimental.....	4
4.2.1    Materials.....	4
4.2.2    Synthesis of Ligand and Ruthenium Moieties .....	5
4.2.3    Synthesis of Platinum(II) Complexes .....	6
4.2.4    Preparation of Aqua Complexes .....	7
4.2.5    Instrumentation and Measurements .....	8
4.2.6    Determination of $pK_a$ of Aqua Complexes.....	8
4.2.7    Kinetic Measurements .....	9
4.2.8    Computational Modelling .....	10
4.3    Results and Discussion .....	10
4.3.1    Synthesis and Characterization .....	10
4.3.2    Acid-base Equilibria of the Aqua Ptlatinum(II) Complexes .....	11
4.3.3    Computational Calculations.....	13
4.3.4    Kinetics Analyses.....	17
4.4    Conclusion.....	26
4.5    References.....	27
4.6    Supporting Information.....	33

**List of Figures**

Figure 4.1	Structural formulae of the mono, di and tri- nuclear complexes investigated.....	4
Figure 4.2	UV/visible spectrum recorded for the titration of 0.019 mM Pt1 with NaOH, in the pH range 2 - 9 at 298 K. Inset is the plot of absorbance against pH at 275 nm. ....	12
Figure 4.3	Optimized structure of Pt1 (obtained using Gaussian09 software package) showing the steric interactions of the protons on the 4'-pyridyl ring owing to the NH <sub>2</sub> <i>trans</i> protons. Due to the longer distance between the NH <sub>2</sub> <i>cis</i> protons and the aqua ligand, no hydrogen binding is possible. ....	15
Figure 4.4	Kinetic trace obtained at 291 nm for the reaction between Pt2 (2.86 x 10 <sup>-5</sup> M) and DMTU (8.58 x 10 <sup>-4</sup> M) on stopped-flow at 298 K, I = 0.02 M LiCF <sub>3</sub> SO <sub>3</sub> , adjusted with LiCl. ....	17
Figure 4.5	<sup>195</sup> Pt NMR arrays showing the Pt3-Cl with 2 to 6 equivalents of TU, as a function of time. t = 0 spectrum of pure Pt3 ( $\delta$ = -2506 ppm) and the subsequent spectra at t = 3, 6 and 15 hours. ....	18
Figure 4.6	Concentration dependence of the <i>pseudo</i> first-order rate constant, $k_{\text{obs}}$ for the substitution of aqua ligand in Pt2 with the thiourea nucleophiles at pH = 2, T = 298 K, I = 0.02 M HCF <sub>3</sub> SO <sub>3</sub> , adjusted with LiCF <sub>3</sub> SO <sub>3</sub> . ....	19
Figure 4.7	Eyring plots for the reaction of Pt2 with the nucleophiles for the substitution reactions over the temperature range 15 - 40 °C at pH = 2, T = 298 K, I = 0.02 M HCF <sub>3</sub> SO <sub>3</sub> , adjusted with LiCF <sub>3</sub> SO <sub>3</sub> . ....	21
Figure 4.8	Schematic representation of the aerial steric effect due to the <i>ortho</i> -H atoms on the <i>cis</i> pyridyl moiety. Optimized structure obtained for Pt1 from computational calculations using Gaussian09 software package. ....	23
Figure 4.9	UV/visible spectra of Pt1-Cl, Pt2-Cl and Pt3-Cl in methanol (0.008 mM). ....	25

**List of Tables**

Table 4.1	The $pK_a$ values of the deprotonation of the coordinated aqua ligand in mono-, di- and tri-nuclear complexes studied.....	11
Table 4.2	Summary of DFT calculated data for the complexes using Gaussian09 software package based on B3LYP and LanL2DZ basis set. ....	14
Table 4.3	DFT calculated minimum energy structures and frontier molecular orbitals (HOMO and LUMO) of the complexes investigated. Calculations were done using Gaussian09 software package based on B3LYP and LanL2DZ basis set. ....	16
Table 4.4	Summary of the second-order rate constants, $k_2$ and activation parameters, with the corresponding standard deviations for the substitution of the aqua ligand(s) by a series of thiourea nucleophiles at pH = 2, $I = 0.02$ M $\text{HCF}_3\text{SO}_3$ , adjusted with $\text{LiCF}_3\text{SO}_3$ .....	20

**List of Schemes**

Scheme 4.1	Schematic representation of preparation of aqua complexes.....	7
Scheme 4.2	The $pK_a$ titration reactions of the aqua complexes with $\text{OH}^-$ .....	9
Scheme 4.3	Proposed reaction mechanism for the substitution of aqua ligand(s) by thiourea nucleophiles studied.....	20

# Chapter Four

## The Effect of Ruthenium(II) Terpyridine Fragment on the Reactivity of Platinum(II) centre. A Kinetic and Computational Approach

### 4.0 Abstract

The rate of substitution of a series of heterometallic Ru(II)-Pt(II) complexes; *cis*-[Pt(en)(py)H<sub>2</sub>O](CF<sub>3</sub>SO<sub>3</sub>)<sub>2</sub>, **Pt1**, *cis*-[(tpy)Ru(qpy)Pt(en)H<sub>2</sub>O](CF<sub>3</sub>SO<sub>3</sub>)<sub>4</sub>, **Pt2** and *cis*-[H<sub>2</sub>O(en)Pt(qpy)Ru(qpy)Pt(en)H<sub>2</sub>O](CF<sub>3</sub>SO<sub>3</sub>)<sub>6</sub>, **Pt3** (en = 1,2-ethylenediamine, py = pyridine, tpy = 2,2':6',2''-terpyridine and qpy 4'-pyridyl-2,2':6',2''-terpyridine), with thiourea nucleophiles, *viz.* thiourea (TU), 1,3-dimethylthiourea (DMTU) and 1,1,3,3-tetramethylthiourea (TMTU) were studied under *pseudo* first-order conditions as a function of concentration and temperature by using UV/visible spectrophotometer and stopped-flow analyzer. The reactions proceeded *via* a single step, following first-order kinetics. The observed *pseudo* first-order rate constants,  $k_{\text{obs}}$  followed the rate law:  $k_{\text{obs}} = k_2[\text{Nu}]$ . The observed reactivity trend, **Pt3**  $\approx$  **Pt2** > **Pt1** is in line with the observed  $\text{p}K_{\text{a1}}$  trend for the complexes investigated. The substitution reactivities of the heterometallic complexes are enhanced as a result of the increased overall charge and the electrophilicity of the complexes. Replacing the *cis* pyridyl group by a (tpy)Ru(qpy) moiety lowers the energy of anti-bonding LUMO ( $\pi^*$ ) orbitals and increases the metal-metal interactions and electronic transition within the complex whereby enhancing the reactivity of Pt(II) centre. Incorporation of Ru(qpy)<sub>2</sub> in **Pt3** did not double the reactivity to that of **Pt2** due to the orthogonal geometry of the coordinated qpy ligands at the Ru(II) metal centre. The rate of the reactivity of the nucleophiles is depended on the steric hindrance, where the reactivity followed the order: TU > DMTU > TMTU. The observed relatively low enthalpy of activation,  $\Delta H^\ddagger$  and the negative entropy of activation,  $\Delta S^\ddagger$  support an associative mode of activation for the displacement of the aqua ligand(s). Experimental data were supported by density functional theory (DFT) calculations.



## 4.1 Introduction

Development of new effective anticancer drugs has focused on designing new drugs with lesser side effects and drawbacks.<sup>1</sup> In the past, a number of different mono- and multinuclear complexes with potential anticancer activity have been developed.<sup>1c,2</sup> The architecture of the most well-known multinuclear Pt(II) complexes has platinum centres structurally joined by linkers with terminal platinum centres containing labile ligand(s) such as chloro or aqua.<sup>1b,3</sup> These structural linkers are thought to play an important role in influencing the mode of interaction when binding with DNA base pairs. Reaction of such complexes with DNA oligomers have shown different adducts to that formed by cisplatin and its analogues.<sup>1a</sup> For example, multinuclear anticancer Pt(II) complexes linked by 4,4'-dipyrazolylmethane<sup>4</sup> and pyrazole ligands which have one labile group were expected to exhibit different modes of actions with DNA than that of cisplatin.<sup>5</sup>

Recent kinetic studies reported by van Eldik *et al.*<sup>6</sup> and Jaganyi *et al.*<sup>7</sup> for dinuclear Pt(II) complexes with flexible alkyldiamine linkers show that the reactivity depends on the distance between the two Pt(II) centres, their electrostatic interactions and the charge density around the metal centre.<sup>6,7b</sup> Of note, are multinuclear Pt(II) complexes bridged by flexible alkyldiamines,<sup>8</sup> first synthesized by Farrell *et al.*<sup>9</sup> Two good examples are  $[\mu\text{-trans- Pt}(\text{NH}_3)_2\{\text{trans-PtCl}(\text{NH}_3)_2\text{NH}_2(\text{CH}_2)_6\text{NH}_2\}_2](\text{NO}_3)_4$ , (**BBR3464**)<sup>9</sup> and its analogue (**BBR3610**).<sup>9</sup> Both comprise of two or three Pt(II) centres linked *via* flexible alkyldiamine bridges. These compounds have shown strong clinical potential but are limited by *in vitro* degradation to release the linker in the presence of strong S-containing biomolecules.<sup>9</sup> However, it is difficult to generalize on how the factors control the kinetic and thermodynamic behaviour due to structural complexity of multinuclear complexes such as the flexibility<sup>1b,6c,d,7,10</sup> (e.g., aliphatic diamine linkers) or the rigidity<sup>5,11</sup> (e.g., azoles, azines and polypyridines) of the linkers.

Out of the different metal complexes synthesized and tested for biological activity,<sup>12</sup> Ru is of great interest.<sup>13</sup> From the many Ru(II) complexes tested for biological activity, the compound  $[\text{ImH}][\text{trans-RuCl}_4(\text{DMSO-S})\text{Im}]$  (Im = imidazole), NAMI-A and its derivatives are the most studied.<sup>14</sup> Interaction of other Ru complexes such as  $\{[(\text{NH}_3)_4\text{Ru}]_2(\text{dpb})\}^{4+}$  (dpb= 2,3-bis(2-pyridyl)benzoquinoxaline) with DNA has also been reported.<sup>15</sup>

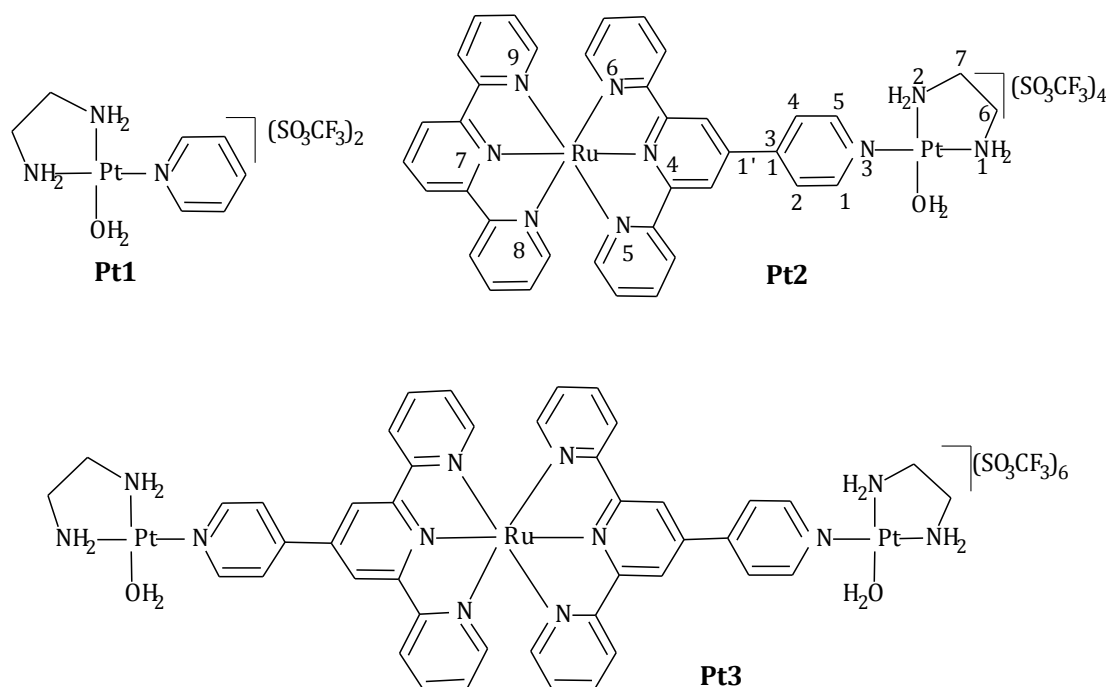
Furthermore, synthesis of heterometallic Ru(II)-Pt(II) complexes<sup>16</sup> of the form,  $[(bpy)_2M(dpb)PtCl_2]Cl_2$  ( $M = Ru(II), Os(II)$ ;  $bpy = 2,2'$ -bipyridine;  $dpb = 2,3$ -bis(2-pyridyl)benzoquinoxaline containing short heterocyclic rigid linkers have been reported.<sup>16</sup> The presence of non-binding metal centres in the complexes increase the overall cationic charge thereby enhancing their water solubility.<sup>16-17</sup> The complexes were also reported to photoreact with DNA through the light absorbing ruthenium metal centre,<sup>18,19,20</sup> which transfers the energy into the platinum metal centres thereby enhancing its reactivity.<sup>16</sup> This property can be a useful switch for kinetic and thermodynamic control of the platinum complexes in their substitution reactions. However, ligand substitution behaviour of heterometallic Pt(II)-Ru(II) complexes have not been studied kinetically to a great extent.

Therefore, it is the aim of this work to investigate the substitution reactions of heterometallic Ru(II)-Pt(II) complexes, where the two metal centres are linked by a 4'-pyridyl-2,2':6',2''-terpyridine (qpy), a ligand which is rigid. Apart from being a tridentate ligand, qpy can also bind with a second metal centre *via* the nitrogen atom of the appended pyridine ring on the terpyridine moiety.<sup>21</sup> This ligand has a very versatile coordination chemistry; forming mononuclear compounds with pendant groups,<sup>21a,22</sup> metal coordinated polygons<sup>23</sup> and polymers.<sup>24</sup> It is postulated to interact with DNA favourably due to its extended aromaticity apart from the substitution at the terminal Pt(II) metal centre.<sup>11c</sup>

We therefore synthesized three complexes *viz*; *cis*-[Pt(en)(py)H<sub>2</sub>O](NO<sub>3</sub>) (**Pt1**), *cis*-[(tpy)Ru(qpy)Pt(en)H<sub>2</sub>O](NO<sub>3</sub>)<sub>3</sub> (**Pt2**) and *cis*-[H<sub>2</sub>O(en)Pt(qpy)Ru(qpy)Pt(en)H<sub>2</sub>O](NO<sub>3</sub>)<sub>4</sub> (**Pt3**). The mononuclear platinum complex, **Pt1** is included for comparison reasons so that the effect on reactivity of the complexes due to the *cis* ligand to the Pt(II) centre or the linker (qpy) could be quantified. The *cis* geometry is purposely chosen as it endows enhanced stability to metabolic deactivation. It is known that the *cis* complexes react slower compared to their *trans* counterparts.<sup>25</sup> Studies have also shown that complexes such as  $[{cis}\text{-PtCl}(\text{NH}_3)_2\text{-}\mu\text{-y}]^{n+}$  (where  $y = \text{NH}_2(\text{CH}_2)_6\text{NH}_2$ )<sup>26</sup> do not undergo degradation of the linker with strong sulfur donor nucleophiles as compared to their *trans* analogues.<sup>1d</sup> However, the factors which facilitate these reactions are not fully understood. Furthermore, the invariant ethylenediamine chelate coordinated to the Pt(II) centre is deliberately designed into all the complexes since our interest was to investigate the effect of the octahedral Ru(tpy)<sub>2</sub> moiety making up the linker on the reactivity of the terminal Pt(II) ions. Thus,

it is anticipated that structurally improved architecture of the complexes will have better advantages over the well-known trinuclear anticancer compound, **BBR3464**<sup>27</sup> and other well-known alkyldiamine<sup>6c,28</sup> complexes since their DNA cross links will be differently recognised by cellular proteins and are potential to cause cell death *via* different pathways.

The reactivities of the complexes were studied in aqueous medium at pH 2 using thiourea nucleophiles. Thiourea nucleophiles are used because of the multiple role of sulfur containing bio molecules inside the cells. This is also facilitated by their solubility, high nucleophilicity and neutral character.<sup>28</sup> The structures of the complexes used in this study are shown in *Figure 4.1*.



**Figure 4.1** Structural formulae of the mono, di and tri- nuclear complexes investigated.

## 4.2 Experimental

### 4.2.1 Materials

pH buffer standards of pH 4.0, 7.0 and 10.0 were bought from Merck. 4'-chloro-2,2':6',2''-terpyridine (99%), ruthenium(III)chloride trihydrate (99%) and 1,5-cyclooctadiene were purchased from Aldrich. All other chemicals were procured from Sigma Aldrich and used as received. For preparation of all aqueous solutions, ultra-pure water was used. The ruthenium precursors; [Ru(tpy)Cl<sub>3</sub>],<sup>29</sup> [Ru(qpy)Cl<sub>3</sub>]<sup>11c</sup> and 0.1 M Ru(III) solution<sup>11c</sup> were synthesized as described in literature.

### 4.2.2 Synthesis of Ligand and Ruthenium Moieties

The ligand, 4'-pyridyl-2,2':6',2''-terpyridine (qpy) was synthesized as in literature.<sup>30</sup> A perspective X-ray crystal structure is given under Supporting Information. Summary of the experimental procedure and the characterization data are given under supporting information. Acidic Ru(III) solution was prepared following the literature procedure.<sup>11c</sup> The Ru complexes, [Ru(tpy)Cl<sub>3</sub>],<sup>29</sup> [Ru(qpy)Cl<sub>3</sub>],<sup>11c</sup> Ru(qpy)(tpy)Cl<sub>2</sub><sup>11c</sup> and [Ru(qpy)<sub>2</sub>]Cl<sub>2</sub><sup>11c</sup> are synthesized following the literatures. Experimental procedures are summarized under Supporting Information.

The purity of the complexes was confirmed by <sup>1</sup>H NMR and mass spectroscopy. The X-ray crystal structure obtained for the ligand qpy further confirms the correct identification of the qpy ligand.

**4'-pyridyl-2,2':6',2''-terpyridine (qpy)** Yield: 0.509 g, (70%), Colourless needles. <sup>1</sup>H NMR (400 MHz, CDCl<sub>3</sub>) δ/ ppm: 8.79 (2H, m, 2''' 6'''), 8.77 (2H, s, 3' 5'), 8.74 (2H, br dm, 6 6''), 8.67 (2H, dd, 3 3''), 7.90 (2H, td, 4 4''), 7.80 (2H, dd, 3''' 5'''), 7.39 (2H, ddd, 5, 5''). TOF MS-ES<sup>+</sup>, m/z: 333.1114, (M+Na)<sup>+</sup>.

**Ru(qpy)(tpy)Cl<sub>2</sub>** Yield: 35 mg, 0.0489 mmol (61%), Dark red powder. <sup>1</sup>H NMR (400 MHz, DMSO-*d*<sub>6</sub>) δ/ ppm: 9.58 (2H, s, I3' 5'), 9.12 (2H, d, I33''), 9.10 (2H, s, II3' 5'), 8.99 (2H, d, I2''' 6'''), 8.85 (2H, d, II3 3'), 8.56 (2H, t, II4'), 8.45 (2H, d, I3''', 5'''), 8.09 (2H, t, I4 4''), 8.03 (2H, t, II4 4''), 7.52 (2H, d, II6 6''), 7.46 (2H, d, I6 6''), 7.30 (2H, t, I5 5''), 7.25 (2H, t, II5 5''). TOF MS-ES<sup>+</sup>, m/z: 366.5616, (M<sup>2+</sup>). *Anal. Calc. for* C<sub>35</sub>H<sub>25</sub>Cl<sub>2</sub>N<sub>7</sub>Ru: C 58.75, N 13.70, H 3.52. *Found:* C 58.32, N 13.21, H 3.12.

**[Ru(qpy)<sub>2</sub>]Cl<sub>2</sub>** Yield: 50 mg, (46 %), Dark maroon powder. <sup>1</sup>H NMR (400 MHz, DMSO-*d*<sub>6</sub>) δ/ ppm: 9.61 (2H, s, 3' 5'), 9.12 (2H, d, 2''' 6'''), 9.00 (2H, d, 3 3''), 8.45 (2H, d, 3''' 5'''), 8.09 (2H, t, 4 4''), 7.57 (2H, d, 6 6''), 7.29 (2H, t, 5 5''). TOF MS-ES<sup>+</sup>, m/z: 361.1088, (M<sup>2+</sup>). *Anal. Calc. for* C<sub>40</sub>H<sub>28</sub>Cl<sub>2</sub>N<sub>8</sub>Ru: C 60.61, N 14.14, H 3.56. *Found:* C 60.99, N 14.57, H 3.72.

### 4.2.3 Synthesis of Platinum(II) Complexes

The platinum precursor, Pt(en)Cl<sub>2</sub> was synthesized following a literature procedure.<sup>31</sup> Details of the experimental procedure and characterization data are summarized under Supporting Information. The platinum complexes, **Pt1-Cl**, **Pt2-Cl** and **Pt3-Cl** are synthesized following a similar approach reported.<sup>11c</sup>

**(Pt1-Cl)** The compound was synthesized by a slight modification of the literature method.<sup>11c</sup> To a stirred solution of [Pt(en)Cl<sub>2</sub>] (42 mg; 0.126 mmol) in 10 mL of DMF at 310 K, silver nitrate (AgNO<sub>3</sub>) (21 mg, 0.126 mmol) in dimethylformamide (DMF) (5 mL) was added drop wise. The reaction mixture was stirred for 24 hours at 313 K. After filtration of silver chloride (AgCl) precipitate using a 0.45 µm nylon membrane filter (Millipore), pyridine (0.010 mL, 0.126 mmol) was added to the filtrate and the mixture was stirred for another 18 hours. The reaction mixture was filtered and coevaporated using EtOH/MeOH (v: v = 50:50) (20 mL) to remove DMF. The precipitate was dissolved in MeOH. The product was precipitated by slow diffusion of diethyl ether.

The purity and the identity of the complexes were confirmed by <sup>1</sup>H NMR, <sup>195</sup>Pt NMR, mass spectroscopy and elemental analyses. The <sup>195</sup>Pt NMR of all the complexes exhibited a characteristic signal at about -2500 ppm, typical to platinum coordinated to NNN chelate and a chloride. Due to the high charge and complexity of the complexes, the mass spectra obtained show characteristic fragmentations.

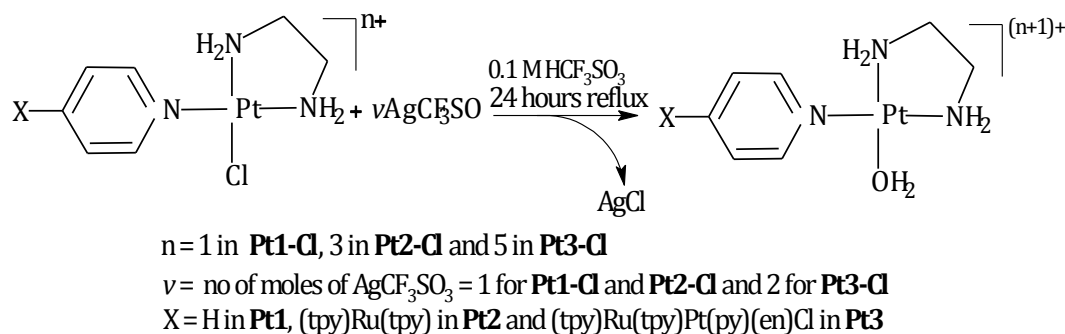
Yield: 0.032 g, (60%), off-white crystalline powder. <sup>1</sup>H NMR (400 MHz, DMF) δ/ ppm: 8.62 (2H, dd, *J* = 6.9, 1.4), 7.89 (1H, tt, *J* = 7.8, 1.5), 7.40 (2H, br), 6.04 (2H, br), 5.65 (2H, br), 3.01 (2H, t), 2.92 (2H, br), <sup>195</sup>Pt NMR (500 MHz, DMF) δ/ ppm: -2501. TOF MS-ES<sup>+</sup>, *m/z*: 369.0449, (M<sup>+</sup>). *Anal. Calc. For* C<sub>7</sub>H<sub>13</sub>ClN<sub>4</sub>O<sub>3</sub>Pt: C 19.47, N 12.98, H 2.96. *Found*: C 19.21, N 12.51, H 2.98.

**(Pt2-Cl)** Yield: 28 mg (15 %), Dark red powder. <sup>1</sup>H NMR (400 MHz, D<sub>2</sub>O) δ/ ppm: 9.11 (2H, s, I3 5'), 9.00 (2H, d, I2''' 6'''), 8.78 (2H, d, II3' 5'), 8.61 (2H, d, I3 3''), 8.50 (2H, d, II3 3''), 8.42 (2H, t, II4'), 8.25 (2H, d, I3''' 5'''), 7.93 (2H, t, I4 4''), 7.89 (2H, t, II4 4''), 7.45 (2H, d, II6 6''), 7.35 (2H, d, I6 6'), 7.17 (2H, t, I5 5''), 7.11 (2H, t, II5 5''), 2.73 (2H, br, b), 2.66 (2H, br, c), <sup>195</sup>Pt NMR (500 MHz, D<sub>2</sub>O) δ/ ppm: -2530. TOF MS-ES<sup>+</sup>, *m/z*: 322.5963, (for water substituted M<sup>4+</sup>). *Anal. Calc. For* C<sub>37</sub>H<sub>33</sub>ClN<sub>12</sub>O<sub>9</sub>PtRu·4H<sub>2</sub>O: C 37.24, N 14.08, H 3.46. *Found*: C 36.81, N 13.76, H 3.01.

**(Pt3-Cl)** Yield: 0.035 g, (22 %), dark red powder.  $^1\text{H}$  NMR (400 MHz,  $\text{D}_2\text{O}$ )  $\delta$ / ppm: 9.13 (2H, s, I3' 5'), 9.01 (2H, d, I2''' 6'''), 8.62 (2H, d, I3 3''), 8.25 (2H, d, I3''' 5'''), 7.93 (2H, t, I4 4''), 7.45 (2H, d, II6 6''), 7.17 (2H, t, I5 5''), 2.80 (2H, br, b), 2.73 (2H, br, c)  $^{195}\text{Pt}$  NMR (500 MHz,  $\text{D}_2\text{O}$ )  $\delta$ / ppm: -2532. TOF MS-ES<sup>+</sup>,  $m/z$ : 2901.0024, (for water substituted  $\text{M}^{6+} \cdot \text{H}_2\text{O}$ ). *Anal. Calc. For*  $\text{C}_{44}\text{H}_{44}\text{Cl}_2\text{N}_{16}\text{O}_{12}\text{Pt}_2\text{Ru} \cdot 5\text{H}_2\text{O}$ : C 32.90, N 13.95, H 3.64. *Found*: C 32.69, N 13.98, H 3.31.

#### 4.2.4 Preparation of Aqua Complexes

The desired solutions for kinetic studies of aqua complexes (**Pt1**, **Pt2** and **Pt3**) were prepared according to the literature procedure which is summarized in *Scheme 4.1*.<sup>32</sup> To a stirred solution of the Pt(II) compound (**Pt1-Cl**, **Pt2-Cl** and **Pt3-Cl**) (0.4 mmol) in 0.01 M triflic acid ( $\text{CF}_3\text{SO}_3\text{H}$ ) (40 mL) was added silver triflate ( $\text{AgSO}_3\text{CF}_3$ ) (equal amounts for mono chloro complexes, (**Pt1-Cl** and **Pt2-Cl**) and 2 equivalences for the dichloro complex, (**Pt3-Cl**)). The mixture was stirred for 24 hours at 50 °C in dark. The precipitated silver chloride was removed by filtration using a 0.45  $\mu\text{m}$  nylon membrane filter (Millipore). The filtrate was made up to 100 mL using 0.01 M  $\text{CF}_3\text{SO}_3\text{H}$  which had an ionic strength of 0.02 M adjusted with  $\text{LiSO}_3\text{CF}_3$ . For all kinetic studies, the pH of the solution was kept at pH 2, ionic strength of 0.02 M adjusted with lithium triflate ( $\text{LiSO}_3\text{CF}_3$ ). A pH of 2 was chosen to prevent the formation of the hydroxo species which are substitutionally inert.<sup>28,33</sup> The solutions for  $pK_a$  determination were prepared by diluting the metal complexes with ultra-pure water and keeping the pH of the desired solution at pH 1 using concentrated  $\text{CF}_3\text{SO}_3\text{H}$ . The initial absorbance of the peaks of the complexes were kept between 0.2 - 1.5. The schematic representation of the aquation process is given in *Scheme 4.1*.



**Scheme 4.1** Schematic representation of preparation of aqua complexes.

#### 4.2.5 Instrumentation and Measurements

$^1\text{H}$  NMR were recorded on either a Bruker Avance DPX 400 or 500 MHz spectrometer, at 303 K using  $\text{Si}(\text{CH}_3)_4$  as the reference for the chemical shifts.  $^{195}\text{Pt}$  NMR were done on a 500 MHz spectrometer ( $^{195}\text{Pt}$ , 107.5 MHz) and chemical shifts externally referenced to  $\text{K}_2[\text{PtCl}_6]$ . Low resolution electron spray ionization (ESI<sup>+</sup>) mass spectra were recorded on a TOF Micromass spectrometer. Elemental analyses were performed by a Thermal Scientific Flash 2000. X-ray crystal structure for the ligand qpy was solved using an Oxford Diffraction Xcalibur 2 CCD 4-circle diffractometer linked to an Oxford Cryostat System. The data collection was done at 100 K.

UV/visible spectra for wavelength determination and kinetic measurements of slow reactions were studied on Varian Cary 100 Bio UV/visible spectrophotometer with an attached Varian Peltier temperature-controller with an online kinetic applications having temperature controlled to within  $\pm 0.05$  °C. Kinetic measurements of fast reactions were studied on an Applied Photophysics SX 20 stopped-flow reaction analyser coupled with an online data acquisition system with controlled temperature having an accuracy of  $\pm 0.1$  °C. The pH measurements were recorded on a Jenway 4330 conductivity/pH meter equipped with a Jenway glass microelectrode calibrated with standard buffer solutions of pH 4.0, 7.0 and 10.0.

#### 4.2.6 Determination of $\text{p}K_{\text{a}}$ of Aqua Complexes

The acidity of the coordinated water ligands were studied prior to kinetic studies. The  $\text{p}K_{\text{a}}$  titrations were carried out as described in literature<sup>28,34</sup> by using NaOH as the base (Scheme 4.2). The pH titrations were carried out starting from pH 2 (0.01 M  $\text{CF}_3\text{SO}_3\text{H}$  solution), and increased by addition of small amounts of NaOH solution until pH 9 (Figures 4.2, S4.1, S4.2). To avoid errors due to dilution effect, a large volume (200 mL) complex solution was used. Crushed NaOH pellets were added until a pH of 3 was reached. NaOH solutions of different concentrations were used to obtain evenly distributed spectra. The solution was stirred after each addition of NaOH before the pH measurement was taken. Small vials were used for sampling out the solution (2 mL) for pH measurements. After each pH measurement the sample aliquot used was discarded to avoid *in situ* precipitation of the chloride. Aliquots from spectral acquisitions were returned back to the titration solution. To ensure the presence of the aqua species in solution, the titrations were carried out using both NaOH and triflic acid with which the





### 4.2.8 Computational Modelling

Computational modelling for the complexes were performed at Density Functional Theoretical (DFT) level based on B3LYP/LanL2DZ<sup>35</sup> (Los Alamos National Laboratory 2 double  $\xi$ ) level theory, with inner core electrons of platinum atom replaced by relative Effective Core Potential (ECP). Due to low electronic spin of Pt(II), the DFT calculations of the complexes were done at singlet state. The complexes were computed in water taking into account the solvolysis effect by means of the Conductor Polarizable Continuum Model (C-PCM).<sup>36</sup> The Gaussian09 suite of programs was used for all computational calculations.<sup>37</sup> A summary of respective bond lengths, the bond angles and DFT-calculated natural bond orbital (NBO) charges, highest occupied molecular orbital (HOMO) and lowest unoccupied molecular orbital (LUMO) energies obtained from the modelled structures of the platinum complexes are given in *Table 4.2* (also see *Tables S4.2 to S4.5*) The numbering scheme used is as shown in *Figure 4.1*.

DFT calculations in gas phase as cations of total charge +2, +4 and +6 respectively for **Pt1**, **Pt2** and **Pt3**, were also repeated by using the software package, Spartan® '08 for Windows<sup>®38</sup> using the B3LYP<sup>35a</sup> density functional method (DFT)<sup>39</sup> and the LACVP+\*\* (Los Alamos Core Valence Potentials)<sup>35c</sup> pseudo potential basis set. The LACVP basis set employs effective core potentials for K-Cu, Pb-Ag, Cs-La and Hf-Au.<sup>40</sup> However, somewhat similar results were obtained and are summarized in *Table S4.5* for further references.

## 4.3 Results and Discussion

### 4.3.1 Synthesis and Characterization

The three chloro derivatives of Pt(II) complexes were synthesized following literature methods<sup>11c,29,30</sup> and characterised using <sup>1</sup>H NMR, <sup>195</sup>Pt NMR, MS and elemental analysis (*Figures S4.9 to S4.22*). The details of the characterisation and spectroscopic data are included in the experimental section and also under Supporting Information. The <sup>1</sup>H NMR spectrum of **(Pt1-Cl)** (*Figure S4.11*), shows that one of the CH<sub>2</sub> protons overlap with the solvent residual peak. Synthesis of Ru(II) moieties, [Ru(tpy)Cl<sub>3</sub>]<sup>29</sup>, [Ru(qpy)Cl<sub>3</sub>],<sup>11c</sup> [Ru(qpy)(tpy)]Cl<sub>2</sub> and [Ru(qpy)<sub>2</sub>]Cl<sub>2</sub> have been reported previously.<sup>21a,41,11c</sup> However, due to the poor solubility<sup>42</sup> and the paramagnetic nature (due to the unpaired electron in one of the *t*<sub>2g</sub> orbital of low-spin Ru(III)<sup>11c</sup>) of [Ru(tpy)Cl<sub>3</sub>]<sup>29</sup> and [Ru(qpy)Cl<sub>3</sub>],<sup>11c</sup> the two precursors were used as synthesized.<sup>21a</sup> In the <sup>1</sup>H NMR spectra of the two heterometallic Ru(II)-Pt(II) complexes, the resonance peaks are well resolved and most importantly the *ortho* protons of the coordinated

pyridyl ring shows a down field shift in the spectrum of **Pt2-Cl** relative to the free ligand (*Figures S4.12 and S4.13*). Due to the low symmetry ( $C_2$ ) of **Pt3-Cl**, chemical shifts corresponding only half of the molecule are detected.<sup>11c</sup> However, signals due to ammine groups are not detectable in  $D_2O$  because of the rapid exchange with the deuterated solvent.<sup>11c</sup> The  $^{195}\text{Pt}$  NMR signals were observed between -2300 ppm to -2600 ppm, typical for square planar NNN coordinated Pt(II) complexes.<sup>6c</sup> The characterization data agreed with the literature and the proposed chemical structures of the complexes.<sup>11c,21a,41</sup>

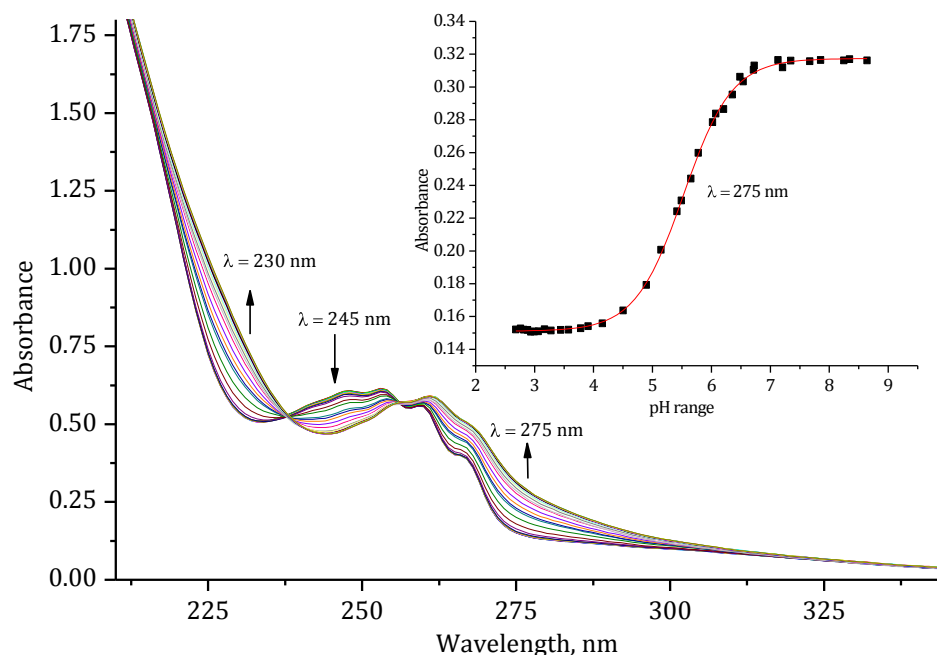
### 4.3.2 Acid-base Equilibria of the Aqua Ptlatinum(II) Complexes

The  $pK_a$  values were determined from the titration spectra at a specific wavelength. Typical UV/visible  $pK_a$  titration spectra obtained for **Pt1** with NaOH is shown in *Figure 4.2*. Distinct isosbestic points at the following wavelengths, 230 nm and 238 nm were observed as the solution became more basic. For **Pt2** and **Pt3**, more absorbance peaks were observed as the ligand systems around the metal centres are more conjugated (*Supporting Information Figures S4.1 and S4.2* for the corresponding spectra for **Pt2** and **Pt3**, respectively).

**Table 4.1** The  $pK_a$  values of the deprotonation of the coordinated aqua ligand in mono-, di- and tri-nuclear complexes studied.

Compound	Pt1	Pt2	Pt3
$^{\dagger}pK_{a1}$	$5.53 \pm 0.01$	$3.61 \pm 0.05$	$3.01 \pm 0.01$
$pK_{a2}$	N/A	N/A	$7.08 \pm 0.03$

$^{\dagger}pK_a$  obtained by fitting the titration data to the Boltzmann equation,  $y = A_2 + (A_1 - A_2) / (1 + \exp((x - x_0)/dx))$  using Origin 7.5<sup>®</sup>



**Figure 4.2** UV/visible spectrum recorded for the titration of 0.019 mM **Pt1** with NaOH, in the pH range 2 - 9 at 298 K. Inset is the plot of absorbance against pH at 275 nm.

The  $pK_{a1}$  values for the deprotonation of the coordinated aqua ligand(s) follow the order, **Pt3** ( $3.01 \pm 0.01$ ) < **Pt2** ( $3.61 \pm 0.05$ ) < **Pt1** ( $5.53 \pm 0.01$ ) even though the chelate effect is kept constant. The observed decrease in the  $pK_a$  in **Pt2** and **Pt3** compared to **Pt1** is probably due to the replacement of the pyridyl by the octahedrally coordinated (qpy)Ru(tpy) or Ru(qpy)<sub>2</sub> moiety as the chelate effect is kept constant.

The  $pK_a$  values indicate the degree of the electrophilicity of the metal complexes,<sup>43</sup> following the order; **Pt3** > **Pt2** > **Pt1**. Thus, introducing the Ru(II) moiety as a *cis* linking unit to the Pt(II) centre increases the overall charge and the electrophilicity of the heterometallic complex thereby increasing the overall acidity of the coordinated aqua ligand(s).<sup>7b</sup> As already known,<sup>6b,7b,34b</sup> this charge addition is prominent if the distance between the two platinum centres is shorter.

The diaqua complex, **Pt3**, showed a stepwise deprotonation, with the lowest  $pK_a$  value. This smallest  $pK_{a1}$  might be attributed to the higher overall positive charge (+6) which is a clear indication of an increased acidity on attaching a second Pt(en)py unit to **Pt2**, a factor which enhances substitution reactivity. It is also noted that the second deprotonation of the coordinated aqua ligand in **Pt3** occurs at a higher  $pK_{a2}$  ( $7.08 \pm$

0.03) than that of the first  $pK_{a1}$  ( $3.01 \pm 0.01$ ) and is attributed to decrease in the overall charge on the platinum complex by deprotonation of the first aqua ligand as reported previously.<sup>6a,b,6d,7b</sup>

Since the position of the  $^{195}\text{Pt}$  NMR resonance influences the donor strength of the ligands coordinated to the Pt(II) centre, the observed  $pK_a$  trend is further supported by the changes in the  $^{195}\text{Pt}$  NMR chemical shifts obtained for **Pt1** (-2501), **Pt2** (-2530) and **Pt3** (-2534 ppm). As the ethylenediamine chelate ligand is kept constant for all the three complexes, the changes in the  $pK_a$  is an indication of the strength of the  $\sigma$ -inductive effect of the *cis* pyridyl moiety attached to the Pt(II) centre which controls the basicity of the aqua complexes. The smaller difference between the  $pK_{a1}$  values of **Pt2** and **Pt3** (0.6) units indicate the similarity of the *cis* pyridyl moieties in **Pt2** and **Pt3** and hence the difference between them is a result of the increase in the overall charge.<sup>44</sup>

### 4.3.3 Computational Calculations

In order to understand the relation between the electronic structures and the substitution reactions of the aqua complexes, the molecules were optimized at the DFT level using B3LYP functional with LANL2DZ basis set as this setting has been reported to be reliable for Ru(II) complexes.<sup>45</sup> An extract of the data obtained from gaussian09 software package are summarized in *Tables 4.2* and *4.3* (also *Tables S4.2* to *S4.5*)

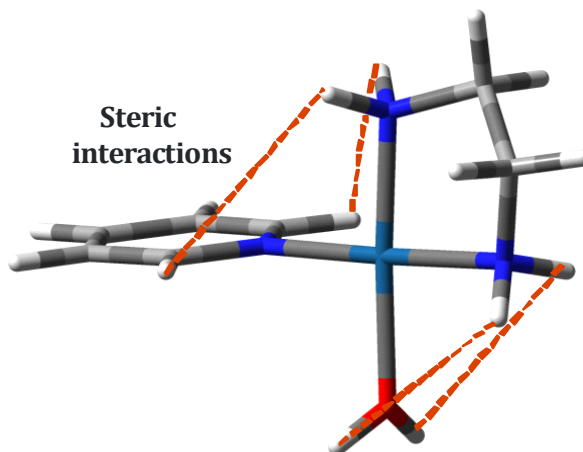
**Table 4.2** Summary of DFT calculated data for the complexes using Gaussian09 software package based on B3LYP and LanL2DZ basis set.

Parameter	Pt1	Pt2	Pt3
<b>Bond lengths, Å</b>			
Pt-OH <sub>2</sub>	2.110	2.111	2.107
Pt-N <sub>trans</sub>	2.052	2.052	2.050
Pt-N <sub>cis</sub> (HN2)	2.082	2.085	2.085
Pt-N <sub>cis</sub> (py)	2.051	2.057	2.058
Ru-Pt		11.15	11.15
Pt-Pt			22.31
H <sub>(py) ortho</sub> -Pt	2.993	3.037	3.051
<b>Bond angles, °</b>			
Twist of 4'-py from plane of terpyridine ligand		35.53	30.31
deviation of py (relative to Pt(II) coord. plane)	87.93	92.84	92.95
<b>NBO charges</b>			
Pt	0.736	0.740	0.742
Ru		0.315	0.320
N <sub>trans</sub>	-0.813	-0.837	-0.812
N <sub>cis</sub> (py)	-0.516	-0.510	-0.510
N <sub>cis</sub> (NH <sub>2</sub> )	-0.837	-0.812	-0.812
O (H <sub>2</sub> O)	-0.913	-0.915	-0.914
<b>Orbital Energy / eV</b>			
HOMO	-7.00	-6.30	-6.40
LUMO	-2.11	-3.16	-3.25
$\Delta E_{\text{HOMO-LUMO}}$	4.89	3.14	3.15
$\eta$ / eV	2.44	1.57	1.58
$\mu$ / eV	-4.56	-4.73	-4.83
$\omega$ / eV	4.25	7.13	7.38
Point group	C <sub>1</sub>	C <sub>1</sub>	C <sub>2</sub>

$\eta$  = chemical hardness,  $\mu$  = chemical potential and  $\omega$  = global electrophilicity index.<sup>46</sup>

DFT calculations reveal that the Pt(II) centres exhibit slightly distorted square planar arrangement, typical for Pt(NNN) coordinated centres (*Table S4.4*).<sup>47</sup> The bite angle of octahedrally coordinated qpy to the Ru(II) centre is smaller than a typical square planar Pt(II)<sup>42a</sup> centre as expected for octahedral geometry.<sup>48</sup> As exhibits from the perspective view of the complexes in *Table 4.3*, the 4'-pyridyl group of qpy is not coplanar with the terpyridine ligand backbone which is bonded to Ru(II). This is necessary to reduce the steric strain due to the hydrogens on the 4'-pyridyl group and the hydrogens attached on the central pyridine ring of the terpyridine ligand.<sup>47a,49</sup> Due

to the steric effects caused by the *trans* NH<sub>2</sub> protons of the ethylenediamine chelate, the monodentate pyridyl group lies in a plane which is nearly orthogonal to the plane containing the Pt, N, N atoms<sup>7b</sup> (Figure 4.3). Thus, the  $\pi$ -backbonding between the Pt(II) metal centre and the *cis* pyridyl moiety is minimised<sup>11b,50</sup> since the  $\pi$ -acceptor ligand is out of plane with the coordination geometry of the Pt(II) metal centre.<sup>47c,51</sup>

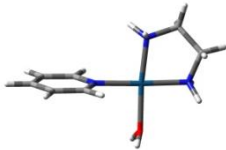
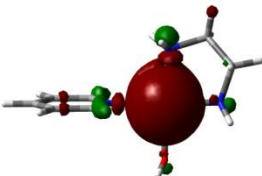
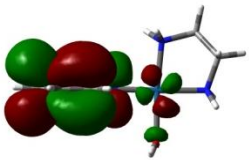
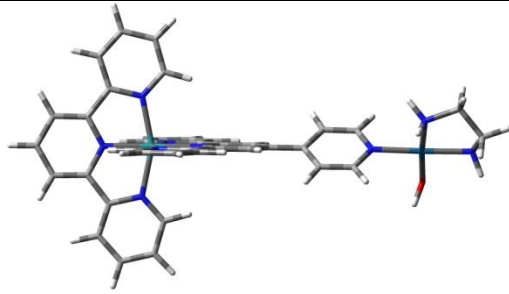
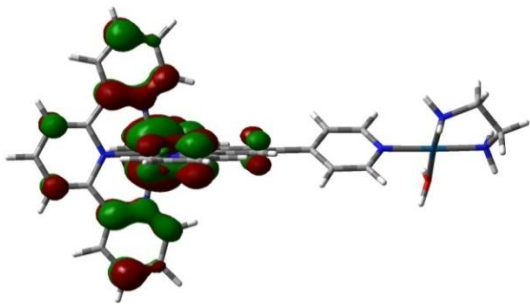
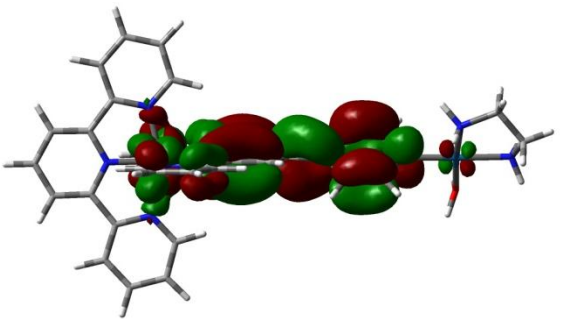
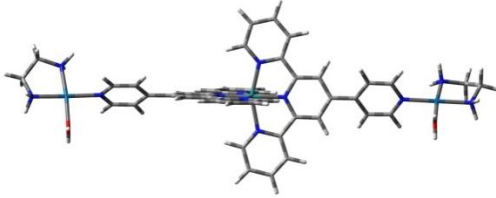
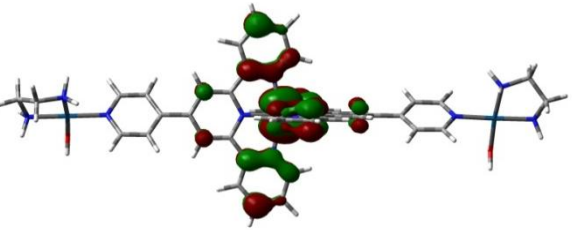
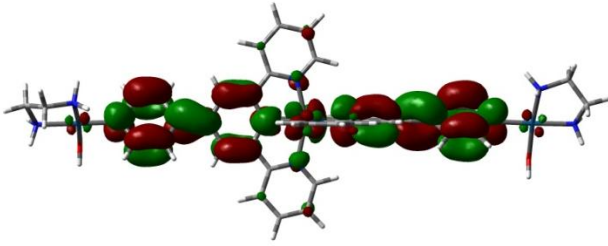


**Figure 4.3** Optimized structure of Pt1 (obtained using Gaussian09 software package) showing the steric interactions of the protons on the 4'-pyridyl ring owing to the NH<sub>2</sub> *trans* protons. Due to the longer distance between the NH<sub>2</sub> *cis* protons and the aqua ligand, no hydrogen binding is possible.

DFT calculated HOMO electron density of **Pt1** is predominantly on the Pt(II) metal centre while in heterometallic complexes, the HOMO electron density mainly lies on the Ru(II) metal centre and sparsely on the coordinated pyridyl rings with no electron density at the Pt(II) metal centre. The LUMO electron density comprises the contributions from the metal centre to the ligands. Thus, the LUMO electrons are concentrated on the pyridyl ring in **Pt1** while in **Pt2** and **Pt3**, they are located on the qpy ligand. This is supported by the decrease in the HOMO-LUMO energy gap by incorporation of Ru(II) moiety as indicated in Table 4.2.

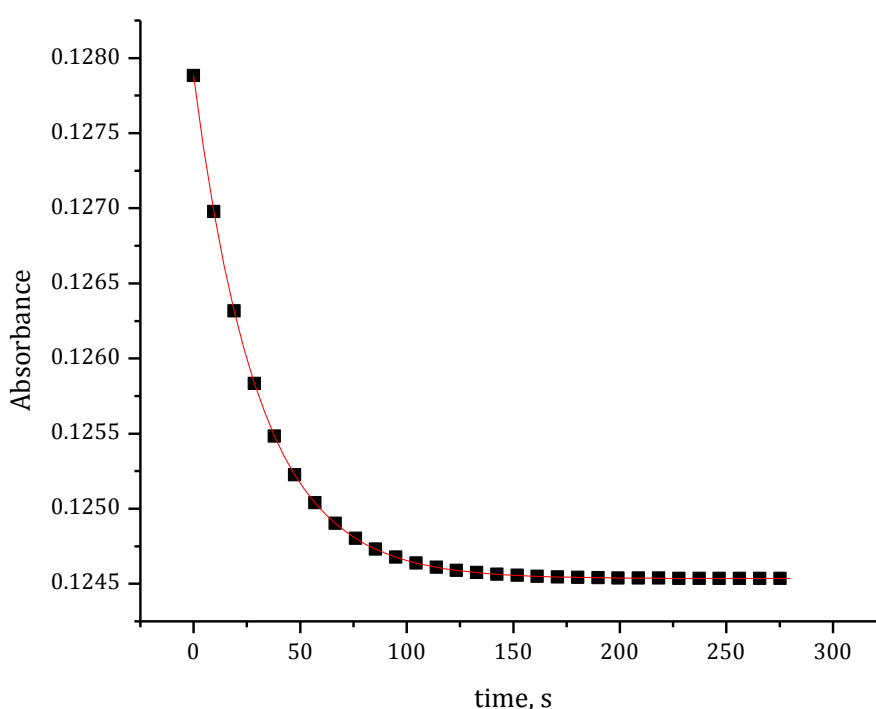
A change in the *cis*-coordinated pyridyl group to a back coordinated Ru(qpy) increases the electrophilicity of the Pt(II) centres. However, when increased the number of qpy to 2, linked by an octahedral Ru(II) does not double the electrophilicity and the reactivity. The reactivity of **Pt2** and **Pt3** are almost equal. This is because the two qpy ligands lie orthogonal to each other at the Ru(II) metal centre. Thus, prevents the continuous flow of electron density across the two qpy ligands because of orthogonal cut of extended  $\pi$ -conjugation at the octahedral Ru(II) centre.

**Table 4.3** DFT calculated minimum energy structures and frontier molecular orbitals (HOMO and LUMO) of the complexes investigated. Calculations were done using Gaussian09 software package based on B3LYP and LanL2DZ basis set.

Geometry optimised structure	HOMO map	LUMO map
		
<b>Pt1</b>		
		
<b>Pt2</b>		
		
<b>Pt3</b>		

#### 4.3.4 Kinetics Analyses

The ligand substitution reactions of the coordinated aqua ligand(s) by thiourea nucleophiles were studied as a function of concentration of the nucleophiles at 25 °C. The substitution reactions of **Pt1** with the nucleophiles were studied on the UV/visible spectrophotometer while those of **Pt2** and **Pt3** were studied on stopped-flow reaction analyzer. Only one reaction step, taken to be the substitution of the coordinated aqua ligand(s) was observed for all the studied complexes. A representative of time resolved kinetic step of the complex **Pt2** with DMTU is shown in Figure 4.4. Representative spectra for the **Pt1** and **Pt3** are shown in Figures S4.3 and S4.4.

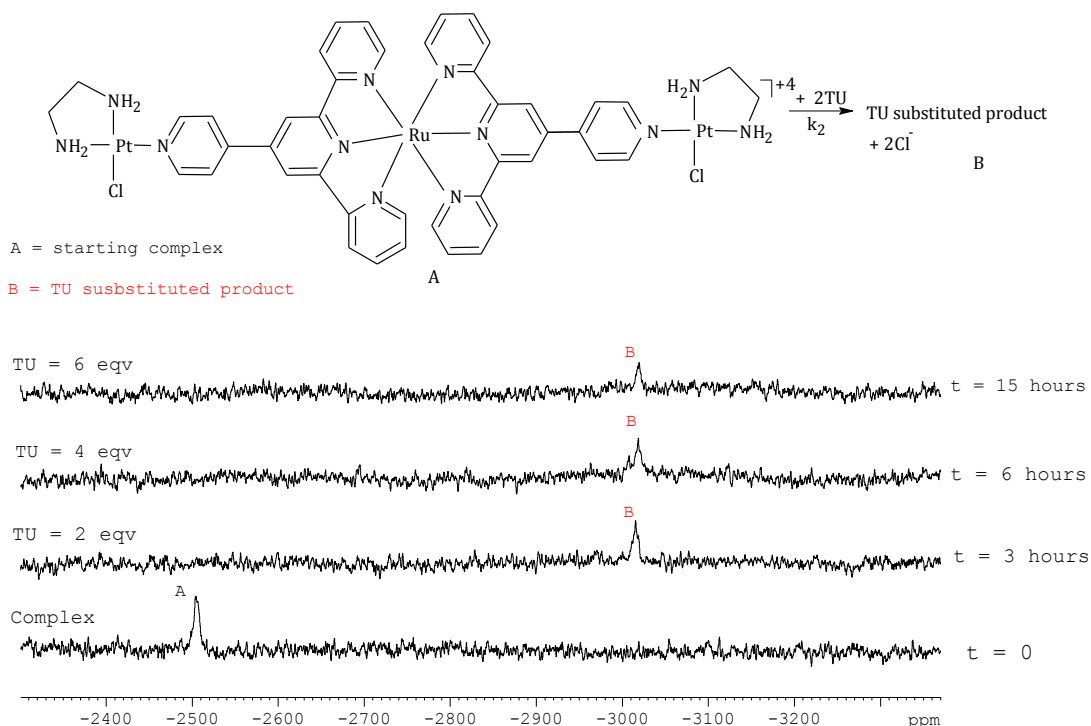


**Figure 4.4** Kinetic trace obtained at 291 nm for the reaction between **Pt2** ( $2.86 \times 10^{-5}$  M) and DMTU ( $8.58 \times 10^{-4}$  M) on stopped-flow at 298 K,  $I = 0.02$  M  $\text{LiCF}_3\text{SO}_3$ , adjusted with LiCl.

The heterometallic complex, **Pt3** is symmetrical and the terminal Pt(II) centres are spaced sufficiently far apart ( $22.31 \text{ \AA}$ ), thus, their behaviour is expected to be independent from each other.<sup>52</sup> Hence, the two square planar Pt(II) centres cannot be differentiated by the strong labile thiourea nucleophiles<sup>7b,52a</sup> as reported by Jaganyi *et al.*<sup>7b</sup> and van Rudi *et al.*<sup>6b,c</sup> for dinuclear Pt(II) complexes. Thus, reactivity at each Pt(II) centre is independent of the other metal centre. This assertion is further supported by the calculated NBO charges on the platinum atoms for **Pt3**. As a result, the aqua ligands



of **Pt3** are simultaneously substituted. To confirm this, the substitution reaction of **Pt3** as a chloride compound,  $[\text{Cl}(\text{en})\text{Pt}(\text{qpy})\text{Ru}(\text{qpy})\text{Pt}(\text{en})\text{Cl}](\text{NO}_3)_4$  with excess TU (2 to 6 equivalence, eqv), was studied by  $^{195}\text{Pt}$  NMR spectroscopy at 25 °C.  $^{195}\text{Pt}$  NMR spectroscopy is a useful method to study the coordination behaviour of Pt(II) complexes since the  $^{195}\text{Pt}$  resonance is influenced characteristically by the nature of the atoms coordinated to the platinum centre.<sup>52b</sup> An array of the  $^{195}\text{Pt}$  NMR spectra for the substitution reaction is shown in Figure 4.5.

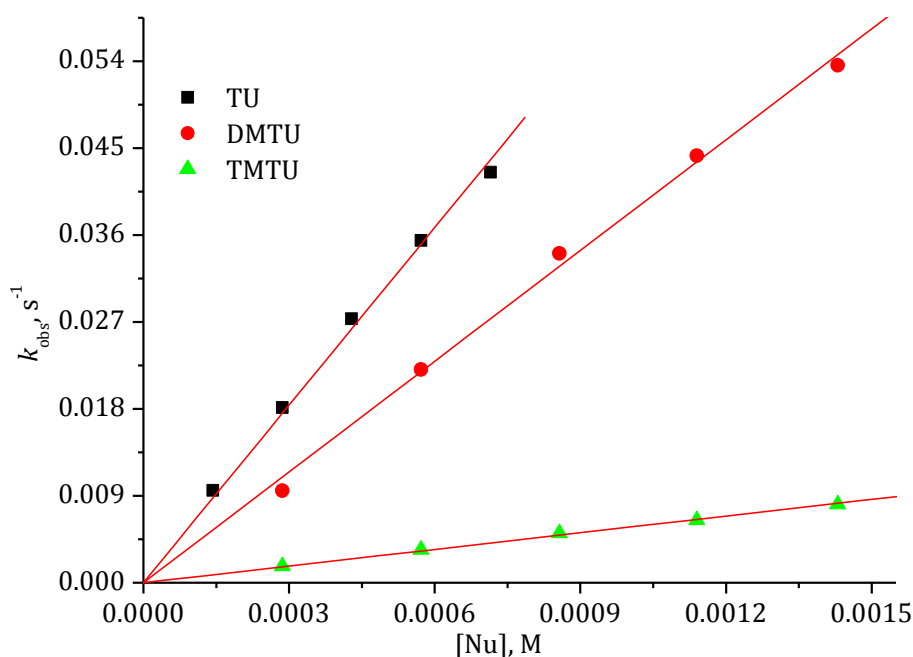


**Figure 4.5**  $^{195}\text{Pt}$  NMR arrays showing the **Pt3-Cl** with 2 to 6 equivalents of TU, as a function of time.  $t = 0$  spectrum of pure **Pt3** ( $\delta = -2506$  ppm) and the subsequent spectra at  $t = 3, 6$  and 15 hours.

Prior to the addition of the nucleophile, a signal ( $\delta = -2506$  ppm) due to the starting complex **Pt3** was observed. A new upfield resonance peak, at  $\delta = -3015$  ppm appeared after 3 hours upon mixing the complex with 2 equivalents of TU. The  $^{195}\text{Pt}$  NMR reveals the formation of the TU substituted complex,  $[\text{TU}(\text{en})\text{Pt}(\text{qpy})\text{Ru}(\text{qpy})\text{Pt}(\text{en})\text{TU}]^{6+}$ , which exhibits a chemical shift at  $\delta = -3015$  ppm, typical of  $\text{PtN}_3\text{S}$  coordinated environment.<sup>53</sup> Based on the results obtained for **Pt3-Cl** by NMR spectroscopy, it is clear that the aqua ligands in **Pt3** are substituted simultaneously. Furthermore,  $^{195}\text{Pt}$  NMR spectrum shows that there was no dechelation of the chelate ligand, induced by the substituted thiourea nucleophile. A similar observation for complexes that possess

*cis* geometry at the Pt(II) centre have been reported with strong sulfur donor nucleophiles.<sup>26</sup>

In all cases the substitution reactions fitted perfectly to a single exponential equation. The observed *pseudo* first-order rate constant,  $k_{\text{obs}}$  varied linearly with the concentration of the nucleophiles and their plots passed through the origin. Representative plots of  $k_{\text{obs}}$  against nucleophiles of the concentration are shown in Figure 4.6 (also Supporting Information, Figures S4.5 and S4.6).

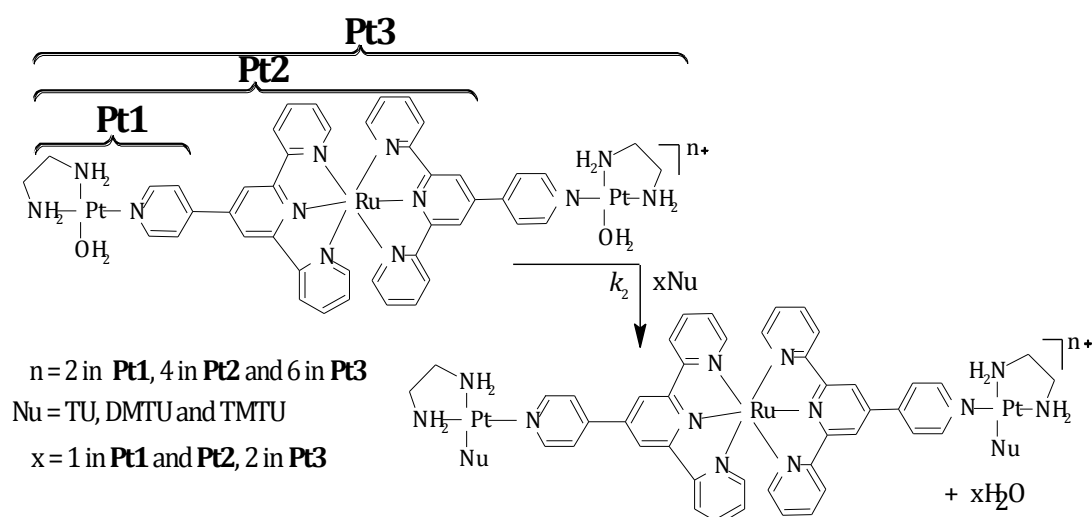


**Figure 4.6** Concentration dependence of the *pseudo* first-order rate constant,  $k_{\text{obs}}$  for the substitution of aqua ligand in Pt2 with the thiourea nucleophiles at pH = 2, T = 298 K, I = 0.02 M HCF<sub>3</sub>SO<sub>3</sub>, adjusted with LiCF<sub>3</sub>SO<sub>3</sub>.

The slopes of the concentration dependence graphs gave the second-order rate constants,  $k_2$ , at 25 °C for the direct attack of the nucleophiles and are summarized in Table 4.4. The absence of non-zero intercepts for all the complexes suggest that the reactions are irreversible in nature as proposed in Scheme 4.3.

**Table 4.4** Summary of the second-order rate constants,  $k_2$  and activation parameters, with the corresponding standard deviations for the substitution of the aqua ligand(s) by a series of thiourea nucleophiles at pH = 2,  $I = 0.02$  M  $\text{HCF}_3\text{SO}_3$ , adjusted with  $\text{LiCF}_3\text{SO}_3$ .

Complex	Nu	$k_2/\text{M}^{-1}\text{s}^{-1}$	$\Delta S^\ddagger/\text{J K}^{-1}\text{mol}^{-1}$	$\Delta H^\ddagger/\text{kJ mol}^{-1}$
<b>Pt1</b>	TU	$22 \pm 0.5$	$-109 \pm 6$	$33 \pm 2$
	DMTU	$12 \pm 0.2$	$-116 \pm 5$	$33 \pm 2$
	TMTU	$6 \pm 0.1$	$-88 \pm 3$	$42 \pm 1$
<b>Pt2</b>	TU	$61 \pm 0.9$	$-24 \pm 9$	$57 \pm 3$
	DMTU	$38 \pm 0.5$	$-30 \pm 10$	$57 \pm 3$
	TMTU	$6 \pm 0.1$	$-68 \pm 2$	$48 \pm 1$
<b>Pt3</b>	TU	$66 \pm 0.7$	$-23 \pm 5$	$56 \pm 2$
	DMTU	$41 \pm 0.7$	$-81 \pm 4$	$39 \pm 1$
	TMTU	$8 \pm 0.2$	$-53 \pm 11$	$54 \pm 4$

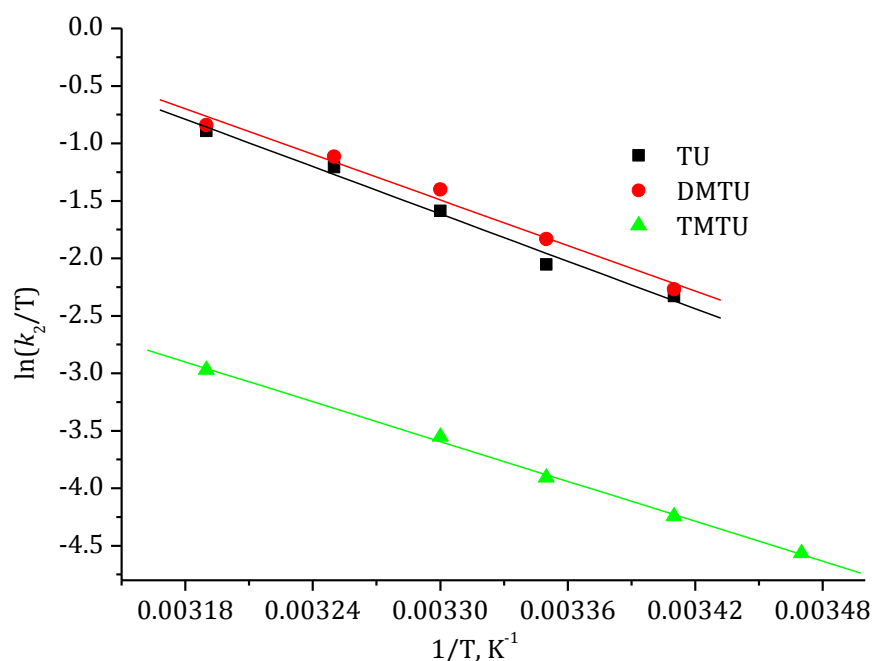


**Scheme 4.3** Proposed reaction mechanism for the substitution of aqua ligand(s) by thiourea nucleophiles studied.

Thus, the corresponding associative rate law can be written as *Equation 4.4*:

$$k_{\text{obs}} = k_2[\text{Nu}] \quad (4.4)$$

The temperature dependence of the second-order rate constants were studied over a temperature range of  $15\text{ }^\circ\text{C}$  -  $40\text{ }^\circ\text{C}$  in  $5\text{ }^\circ\text{C}$  intervals. The resulting thermodynamic activation parameters, entropy of activation ( $\Delta S^\ddagger$ ) and enthalpy of activation ( $\Delta H^\ddagger$ ) were obtained by Eyring equation and the data obtained are summarized in *Table 4.4* and representative Eyring plots are shown in *Figure 4.7* (also Supporting Information *Figures S4.7, S4.8* and *Tables S4.6* to *S4.11*).



**Figure 4.7** Eyring plots for the reaction of **Pt2** with the nucleophiles for the substitution reactions over the temperature range 15 - 40 °C at pH = 2, T = 298 K, I = 0.02 M HCF<sub>3</sub>SO<sub>3</sub>, adjusted with LiCF<sub>3</sub>SO<sub>3</sub>.

Data in *Table 4.4* clearly indicate that when a Ru(qpy) moiety replaces the pyridyl ligand of Pt(en)(py) through the 4'-pyridine ring of Ru(qpy), the resultant *cis* heterometallic complex is more reactive towards the incoming nucleophiles studied. When the rate constants of the aqua complexes are compared, using **Pt1**'s rate constant as the common denominator, the ratio of the rate constants for the substitution of aqua ligands by TU is 1 : 2.78 : 2.98, respectively for **Pt1**, **Pt2** and **Pt3**. A similar trend is observed for the substitution of aqua ligand by DMTU and TMTU. Thus, the rate of substitution of aqua ligand(s) by the S-donor thiourea nucleophiles increased in the order: **Pt3** ≈ **Pt2** > **Pt1**.

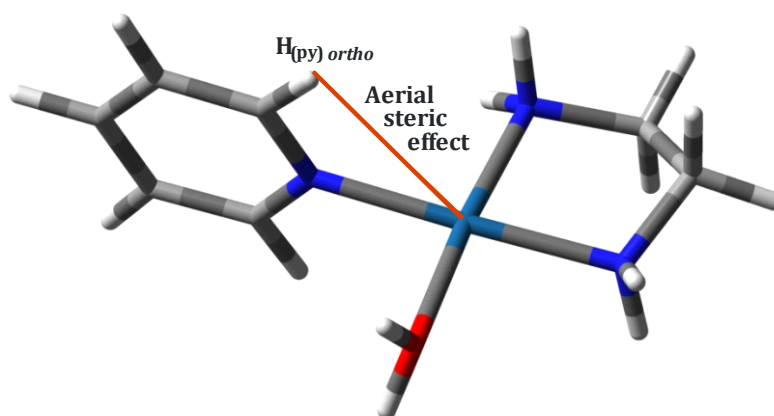
The reactivity increased by almost three fold from **Pt1** to **Pt2** by incorporation of the (tpy)Ru(qpy) moiety. DFT calculations show that attachment of the (qpy)Ru(tpy) moiety slightly increases the Pt–N<sub>cis(py)</sub> bond from **Pt1** (2.051 Å) to **Pt2** (2.057 Å), this small change may be attributed to the pulling of bonding electrons towards the qpy linker. The net effect of this is a slight increase in the positive NBO charge on the Pt(II) metal centre of **Pt2**. Thus, it seems that tridentate coordination of qpy to Ru(II) enhances the electronic transitions from the Pt(II) metal centre towards the pyridyl

group.<sup>54</sup> Electrochemical and TD-DFT computational studies reported by Gagliardo *et al.*<sup>55</sup> for heterometallic Ru(II)-Pd(II) complexes linked by a similar terpyridine linker, 4'-{4-BrC<sub>6</sub>H<sub>2</sub>(CH<sub>2</sub>NMe<sub>2</sub>)<sub>2</sub>-3,5}-2,2':6',2''-terpyridine (**TPBr**) showed the existence of electronic intermetal communication between Ru(II) and Pd(II) metal centers, due to the presence of the aromatic linker.<sup>55</sup> Such intermetal electronic communications between the adjoining metal centers have also been reported for polymetallic Ru(II) complexes with tetra-2-pyridyl-1,4-pyrazine (tppz) aromatic linkers.<sup>56</sup> However, unlike the work reported in **Chapter 3**, electronic interactions between the metal centres decrease when the pyridyl group was attached to the 4'-position of the terpyridine moiety as such electronic interactions become less effective with longer separations between the metal centres.<sup>57</sup> Also, in **Pt2**, the orthogonal geometry of the *cis* pyridyl moiety to the plane of Pt(II) centres further reduces possible electronic transitions between the two metal centres.

Coordination of Ru(II) moiety to **Pt1** decreases the energy of LUMO ( $\pi^*$ ) orbitals resulting in a smaller HOMO-LUMO gap as in **Pt2** (3.14 eV) to that of **Pt1** (4.89 eV). This makes it easier to transfer the electrons from the HOMO to the empty LUMO ( $\pi^*$ ) orbitals. Such decrease in HOMO-LUMO gaps have been reported<sup>12d</sup> for heterometallic Ru(II)-Pt(II) complexes and was attributed to the stabilization of the anti-bonding orbital of the aromatic bridging ligand on coordinating the Ru(II) moiety to the Pt(II) metal centre. The decrease in LUMO energy stabilizes the five coordinate transition state complex by enhancing the transfer of electrons from the 18 electron transition state complex to the qpy ligand, which in turn enhances the approach of the incoming nucleophile.<sup>11b,42b,52</sup> Furthermore, reactivity increases with the increase in deviation of the pyridyl group from the square planar Pt(II) plane from 87.93° to 92.84° respectively for **Pt1** to **Pt2**, however small, might enhancing the ease of the nucleophile to approach the metal centre.<sup>11b</sup>

Additionally, in each case, the *cis* pyridyl group is nearly perpendicular to the Pt(II) centre, in such a way that the *ortho*-hydrogen atoms ( $H_{ortho}$ ) on the pyridyl group imposes some degree of steric hindrance to the aerial approach of the nucleophiles.<sup>44</sup> An equal amount of steric hindrance would be felt on both above and below the square planar Pt(II) metal centre. This aerial steric hindrance, despite small, decreases on moving from **Pt1** (2.993 Å) to **Pt2** (3.037 Å) to **Pt3** (3.051 Å) (*Figure 4.8, Table 4.2*). As expected, the decrease in steric hindrance results in an increase in the substitution

reactivity from **Pt1** to **Pt2** to **Pt3**. This steric influence certainly plays a role in controlling the reactivity of the complexes.



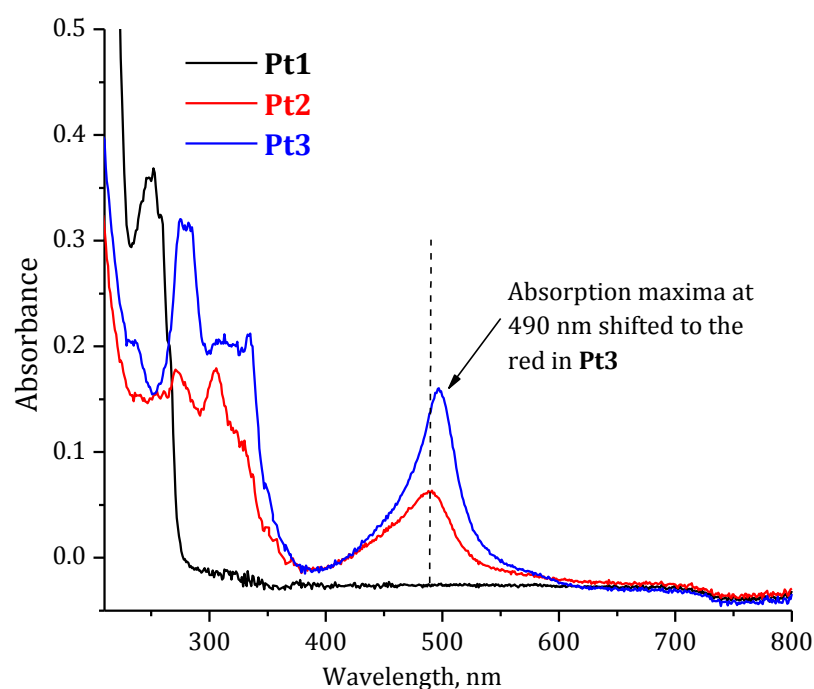
**Figure 4.8** Schematic representation of the aerial steric effect due to the *ortho*-H atoms on the *cis* pyridyl moiety. Optimized structure obtained for **Pt1** from computational calculations using Gaussian09 software package.

Another factor which may lead to the higher reactivity of **Pt2** compared to **Pt1** is the increase in the overall charge of the complex which enhances the electrophilicity and hence, the reactivity of the complex. The DFT calculated HOMO electron density of **Pt1** lies on the Pt(II) metal centre while in **Pt2** it is centred on the Ru(II) metal centre and the capped tpyridine ligand leaving the Pt(II) metal centre electron free. This indicates that Ru(II) moiety accommodates the electron density. DFT calculated higher global electrophilicity index<sup>46c</sup> along with the smaller  $pK_{a1}$  obtained for **Pt2** further support its higher electrophilicity compared to that of **Pt1**.<sup>6a,b,11b,47c</sup> If all the facts are combined together, it can be concluded that the (tpy)Ru(qpy) lowers the energy of anti-bonding LUMO, hence enhances the removal of electron density from the Pt(II) centre making it more electrophilic whereby increasing the substitution reactivity.

A comparison of the reactivity of **Pt3** is not significantly different from that of **Pt2** despite the increase in the overall charge of the complex.<sup>6c,9</sup> The octahedral geometry of the linking Ru(qpy)<sub>2</sub> does not permit extended  $\pi$ -conjugation between the coordinated qpy ligands, which would further increase the reactivity. As such, the effect of the octahedrally coordinated qpy ligands on the reactivity is independent of each other since the  $\pi$ -extended molecular orbital in each qpy are mutually orthogonal at the Ru(II) metal centre. The Ru(II) ion acts as an orthogonal shatter to the flow of delocalization of  $\pi$ -electron density across the entire semi-rigid linker.

Keeping in mind that coordination of the Ru(II) moiety to the Pt(II) metal centre stabilizes the  $\pi^*$  orbitals of the aromatic bridging linker, one notices that when the second Pt(II) moiety is added to **Pt2**, the resulting LUMO orbitals of **Pt3** decreases slightly compared to the difference observed between **Pt1** and **Pt2**. The slightly higher reactivity of **Pt3** to that of **Pt2** is attributed to the increased overall charge along with the DFT calculated slightly decreased LUMO ( $\pi^*$ ) energy and the higher global electrophilicity index, ( $\omega$ ) of **Pt3**.<sup>46a,b,58</sup> Thus, **Pt3** has a slightly greater potential to accept electrons from the incoming nucleophiles, despite its lower HOMO energy,<sup>46a,59</sup> hence, the observed reactivity.<sup>46c,d</sup> The similar reactivity is further supported by the similar  $pK_{a1}$  values obtained for both **Pt2** and **Pt3**.

The slightly higher reactivity of **Pt3** can also be due to the enhanced metal-metal couplings in **Pt3**. Since qpy is a semi-rigid linker, there is some degree of conformational freedom in terms of rotation around the C–C single bond (C1–C1', *Figure 4.1* and also see *Figure S4.23, Table S4.12*) between the parent terpyridine backbone and the 4'-pyridyl moiety. Such tilt angles between the subunits of aromatic linkers play a crucial role on the degree of metal-metal interactions and electronic transitions in supramolecular complexes.<sup>60</sup> Since the DFT calculated tilt angle between the 4'-pyridyl group and the plane of terpyridine backbone, in **Pt3** (30.31 °) is slightly smaller than that of **Pt2** (35.53 °), the metal-metal interactions and electronic transitions in **Pt3** is expected to be slightly higher. This somewhat influences the reactivity. Furthermore, the slight increase in the planarity of the qpy linker in **Pt3** is also responsible for the observed red shifted metal to ligand charge transfer (MLCT) absorption maximum in **Pt3** as depicted in *Figure 4.9*. This has been reported<sup>60-61</sup> and was attributed to the enhanced metal-metal coupling and electronic interactions along with the enhanced  $\pi$ -backbonding within the complex.<sup>60</sup>



**Figure 4.9** UV/visible spectra of Pt1-Cl, Pt2-Cl and Pt3-Cl in methanol (0.008 mM).

The complexes investigated are sensitive towards the steric hindrance of the incoming nucleophiles. In all cases, the rate was fastest for TU, following the order TU > DMTU > TMTU and is in line with the steric effect of DMTU and TMTU.<sup>7b,47a</sup> TMTU was the slowest due to the bulkiness of the nucleophile.

The observed relatively low enthalpy of activation ( $\Delta H^\ddagger$ ) and negative entropy of activation ( $\Delta S^\ddagger$ ) support for associative mode of activated process, typical for square planar platinum complexes.<sup>6b,62</sup> The characteristic negative  $\Delta S^\ddagger$  values is a result of bond formation in the transition state.<sup>6b,62e</sup> However, the smaller entropy of activation obtained for both **Pt2** and **Pt3** compared to that **Pt1** might be due to the re-organisation of the solvent<sup>52a</sup> causing an increase in the entropy which cancels out the negative intrinsic contribution resulting from the bond formation.<sup>6b</sup>



#### 4.4 Conclusion

In conclusion, the results of the  $^{195}\text{Pt}$  NMR experiment shows that *cis* geometry confers stability<sup>26</sup> which precludes labilization of the Ru(qpy) linker unlike what has been reported for substitution reactions involving complexes of *trans* geometry with sulfur donors.<sup>63,44</sup> Also unlike bridged *cis* Pt(II) complexes reported,<sup>28,50</sup> the *cis* Ru(II) moiety enhances the substitution reactivity. Apart from the increased overall charge and the electrophilicity, the octahedrally coordinated Ru(II) moiety lowers the energy of anti-bonding LUMO ( $\pi^*$ ) orbitals whereby enhancing the metal-metal interactions and electronic transitions within the molecule. This seems to have changed the electronic structure of the system sufficiently enough to promote the reactions as observed from the reactivity trend **Pt3**  $\approx$  **Pt2** > **Pt1**. The reactivity of **Pt2** and **Pt3** are almost equal since the qpy ligands lie near orthogonal planes at the Ru(II) metal centre, which prevents the efficient flow of extended  $\pi$ -electron density through the three metal centres as supported by the  $\text{p}K_{\text{a1}}$ . However, DFT calculations and the spectroscopic data show a slight increase in metal-metal coupling on increasing the number of metal centres and the qpy ligand in **Pt3** compared to **Pt2**. The observed enthalpy of activation,  $\Delta H^\ddagger$  and the entropy of activation,  $\Delta S^\ddagger$  support an associative mode of substitution.

## 4.5 References

- (1) (a) Wheate, N. J.; Collins, J. G. *Coord. Chem. Rev.* **2003**, *241*, 133(b) Farrell, M.; De Almeida, S. G.; Skov, K. A. *J. Am. Chem. Soc.* **1988**, *110*, 5018(c) Reedijk, J. *Proc. Natl. Acad. Sci. U. S. A.* **2003**, *100*, 3611(d) Summa, N.; Maigut, J.; Puchta, R.; van Eldik, R. *Inorg. Chem.* **2007**, *46*, 2094.
- (2) Huq, F.; Daghriri, H.; Yu, J. Q.; Tayyem, H.; Beale, P.; Zhang, M. *Eur. J. Med. Chem.* **2004**, *39*, 947.
- (3) (a) Farrell, N.; Qu, Y. *Inorg. Chem.* **1989**, *28*, 3416(b) Ruhayel, R. A.; Berners-Price, S. J.; Farrell, N. P. *Dalton Trans.* **2013**, *42*, 3181.
- (4) (a) Broomhead, J. A.; Rendina, L. M.; Sterns, M. *Inorg. Chem.* **1991**, *31*, 1880(b) Broomhead, J. A.; Rendina, L. M.; Webster, L. K. *J. Inorg. Biochem.* **1993**, *49*, 221.
- (5) (a) Komeda, S.; Lutz, M.; Spek, A. L.; Chikuma, M.; Reedijk, J. *Inorg. Chem.* **2000**, *39*, 4230(b) Komeda, S.; Lutz, M.; Spek, A. L.; Yamanaka, Y.; Sato, T.; Chikuma, M.; Reedijk, J. *J. Am. Chem. Soc.* **2002**, *124*, 4738.
- (6) (a) Hofmann, A.; van Eldik, R. *J. Chem. Soc., Dalton Trans.* **2003**, 2979(b) Ertürk, H.; Hofmann, A.; Puchta, R.; van Eldik, R. *Dalton Trans.* **2007**, 2295(c) Ertürk, H.; Maigut, J.; Puchta, R.; van Eldik, R. *J. Chem. Soc. Dalton Trans.* **2008**, 2759(d) Ertürk, H.; Puchta, R.; van Eldik, R. *Eur. J. Inorg. Chem.* **2009**, 2009, 1331.
- (7) (a) Jaganyi, D.; Munisamy, V. M.; Reddy, D. *Int. J. Chem. Kinet.* **2006**, *38*, 202(b) Jaganyi, D.; Mambanda, A.; Hochreuther, S.; van Eldik, R. *Dalton Trans.* **2010**, *39*, 3595.
- (8) (a) Farrell, N.; Spinelli, S. *Dinuclear and trinuclear platinum anticancer Agents*; In: N. Farrell (Ed.), *Uses of Inorganic Chemistry in Medicine*, Royal Society of Chemistry, , 1999, p.124(b) Zhao, G.; Lin, H.; Zhu, S.; Sun, H.; Chan, Y. *Anti-Cancer Drug Des.* **1998**, *13*, 769.
- (9) Davies, M. S.; Thomas, D. S.; Hegmans, A.; Berners-Price, S. J.; Farrell, N. *Inorg. Chem.* **2002**, *41*, 1101.
- (10) (a) Farrell, N.; Qu, Y.; Hacker, M. P. *J. Med. Chem.* **1990**, *33*, 2179(b) Rauter, H.; Di Domenico, R.; Menta, E.; Oliva, A.; Qu, Y.; Farrell, N. *Inorg. Chem.* **1997**, *36*, 3919.
- (11) (a) Komeda, S.; Kalayda, G. V.; Lutz, M.; Spek, A. L.; Yamanaka, Y.; Sato, T.; Chikuma, M.; Reedijk, J. *J. Med. Chem.* **2003**, *46*, 1210(b) Reddy, D.; Jaganyi, D. *Int. J. Chem. Kinet.* **2011**, *43*, 161(c) van der Schilden, K., University of Leiden, PhD Thesis, *The Development of Polynuclear Ruthenium and Platinum Polypyridyl Complexes in Search of New Anticancer Agents*, 2006, 13- 35, 133-148(d) Wheate, N. J.; Cullinane, C.; Webster, L. K.; Collins, J. G. *Anti-Cancer Drug*

- Des. **2001**, 16, 91(e) Kalayda, G. V.; Jansen, B. A. J.; Wielard, P.; Tanke, H. J.; Reedijk, J. *J. Biol. Inorg. Chem.* **2005**, 10, 305.
- (12) (a) Holder, A. A.; Swavey, S.; Brewer, K. J. *Inorg. Chem.* **2004**, 43, 303(b) Miao, R.; Mongelli, M. T.; Zigler, D. F.; Winkel, B. S. J.; Brewer, K. J. *Inorg. Chem.* **2006**, 45, 10413(c) Higgins, S. L. H.; Tucker, A. J.; Winkel, B. S. J.; Brewer, K. J. *Chem. Commun.* **2012**, 48, 67(d) Higgins, S. L. H.; White, T. A.; Winkel, B. S. J.; Brewer, K. J. *Inorg. Chem.* **2011**, 50, 463.
- (13) (a) Clarke, M. J. *Coord. Chem. Rev.* **2003**, 236, 209(b) Dougan, S. J.; Sadler, P. J. *Chimia* **2007**, 61, 704(c) Ang, W. H.; Dyson, P. J. *Eur. J. Inorg. Chem.* **2006**, 4003(d) Bratsos, I.; Birarda, G.; Jedner, S.; Zangrando, E.; Alessio, E. *Dalton Trans.* **2007**, 40(e) Mijatović, A.; Šmit, B.; Rilak, A.; Petrović, B.; Čanović, D.; Bugarčić, Ž. D. *Inorg. Chim. Acta.* **2013**, 394, 552(f) Fricker, S. B. *Dalton Trans.* **2007**, 4903.
- (14) Alessio, E.; Mestroni, G.; Bergamo, A.; Sava, G. *Metal Ions in Biological Systems.* **2004**, 42, 323.
- (15) Carlson, D. L.; Huchital, D. H.; Mantilla, E. J.; Sheardy, R. D.; Murphy, W. R. *J. Am. Chem. Soc.* **1993**, 115, 6424.
- (16) Milkevitch, M.; Storrie, H.; Brauns, E.; Brewer, K. J.; Shirley, B. W. *Inorg. Chem.* **1997**, 36, 4534.
- (17) Kelly, J. M.; Tossi, A. B.; McConnell, D. J.; Ohuigin, C. *Nucleic Acids Res.* **1985**, 13, 6017.
- (18) (a) Wenger, O. S. *Coord. Chem. Rev.* **2009**, 253, 1439(b) Hanss, D.; Walther, M. E.; Wenger, O. S. *Coord. Chem. Rev.* **2010**, 254, 2584.
- (19) (a) Eryazici, I.; Moorefield, C. N.; Newkome, G. R. *Chem. Rev.* **2008**, 108, 1834(b) Medlycott, E. A.; Hanan, G. S. *Chem. Soc. Rev.* **2005**, 34, 133.
- (20) Constable, E. C. *Chem. Soc. Rev.* **2007**, 36, 246.
- (21) (a) Constable, E. C.; Cargill Thompson, A. M. W. *J. Chem. Soc. Dalton Trans.* **1994**, 1409(b) Metcalf, C.; Spey, S.; Adams, H.; Thomas, J. A. *J. Chem. Soc. Dalton Trans.*, **2002**, 4732.
- (22) (a) Constable, E. C.; Cargill Thomson, A. M. W. *J. Chem. Soc. Dalton Trans.* **1992**, 2947(b) Figgemeier, E.; Merz, L.; Hermann, B. A.; Zimmermann, Y. C.; Housecroft, C. E.; Guntherrodt, H.-J.; Constable, E. C. *J. Phys. Chem. B.* **2003**, 107, 1157(c) Granifo, J.; Garland, M. T.; Baggio, R. *Inorg. Chem. Commun.* **2004**, 7, 77(d) Constable, E. C.; Housecroft, C. E.; Kulke, T.; Lazzarini, C.; Schofield, E. R.; Zimmerman, Y. *J. Chem. Soc. Dalton Trans.* **2001**, 2864.

- (23) (a) Sun, S.-S.; Lees, A. J. *Inorg. Chem.* **2001**, *40*, 3154(b) Sun, S.-S.; Silva, A. S.; Brinn, I. M.; Lees, A. J. *Inorg. Chem.* **2000**, *39*, 1344.
- (24) (a) Hayami, S.; Hashiguchi, K.; Jugasz, G.; Ohba, M.; Okawa, H.; Maeda, Y.; Kato, K.; Osaka, K.; Takata, M. *Inorg. Chem.* **2004**, *43*, 4124(b) Constable, E. C.; Dunphy, E. L.; Housecroft, C. E.; Kylberg, W.; Neuburger, M.; Schaffner, S.; Schofield, E. R.; Smith, C. B. *Chem. Eur. J.* **2006**, *12*, 4600.
- (25) Oehlsen, M.; Hegmans, A.; Qu, Y.; Farrell, N. *J. Biol. Inorg. Chem.* **2005**, *10*, 433.
- (26) Williams, J. W.; Qu, Y.; Bulluss, G. H.; Alvarado, E.; Farrell, N. P. *Inorg. Chem.* **2007**, *46*, 5820.
- (27) Brabec, V.; Kašpárková, J.; Vrána, O.; Nováková, O.; Cox, J. W.; Qu, Y.; Farrell, N. *Biochemistry*. **1999**, *38*, 6781.
- (28) Hochreuther, S.; Puchta, R.; van Eldik, R. *Inorg. Chem.* **2011**, *50*, 8984.
- (29) Takeuchi, K. J.; Thompson, M. S.; Pipes, D. W.; Meyer, T. J. *Inorg. Chem.* **1984**, *23*, 1845.
- (30) Smith, C. B.; Raston, C. L.; Sobolev, A. N. *Green Chem.* **2005**, *7*, 650.
- (31) Brunner, H.; Schellerer, K.-M. *Inorg. Chim. Acta.* **2003**, *350*, 39.
- (32) Bugarčić, Z. D.; Petrović, B. V.; Jelić, R. *Transition Met. Chem.* **2001**, *26*, 668.
- (33) (a) Mahal, G.; van Eldik, R. *Inorg. Chem.* **1985**, *24*, 4165(b) Mahal, G.; van Eldik, R. *Inorg. Chem.* **1987**, *127*, 203.
- (34) (a) Jaganyi, D.; Tiba, F.; Munro, O. Q.; Petrovic, B.; Bugarčić, Z. D. *Dalton Trans.* **2006**, 2943(b) Mambanda, A.; Jaganyi, D. *Dalton Trans.* **2011**, *40*, 79
- (35) (a) Becke, A. G. *J. Chem. Phys.* **1993**, *98*, 5648(b) Lee, C. T.; Yang, W. T.; Parr, R. G. *Phys. Rev. B* **1988**, *37*, 785(c) Hay, P. J.; Wadt, W. R. *J. Chem. Phys.* **1985**, *82*, 299.
- (36) (a) Barone, V.; Cossi, M. *J. Phys Chem. A.* **1998**, *102*, 1995(b) Cossi, M.; Rega, N.; Scalmani, G.; Barone, V. *J. Comput. Chem.* **2003**, *24*, 669.
- (37) Frisch, M. J.; Trucks, G. W.; Schlegel, H. B.; Scuseria, G. E.; Robb, M. A.; Cheeseman, J. R.; Scalmani, G.; Barone, V.; Mennucci, B.; Petersson, G. A.; Nakatsuji, H.; Caricato, M.; Hratchian, X. L.; H. P. ; Izmaylov, A. F.; Bloino, J.; Zheng, G.; Sonnenberg, J. L.; Hada, M.; Ehara, M.; Toyota, K.; Fukuda, R.; Hasegawa, J.; Ishida, M.; Nakajima, T.; Honda, Y.; Kitao, O.; Nakai, H.; Vreven, T.; Montgomery, J. A.; Peralta, J., J. E. ; Ogliaro, F.; Bearpark, M.; Heyd, J. J.; Brothers, E.; Kudin, K. N.; Staroverov, V. N.; Kobayashi, R.; Normand, J.; Raghavachari, K.; Rendell, A.; Burant, J. C.; Iyengar, S. S.; Tomasi, J.; Cossi, M.; Rega, N.; M. Millam, J.; Klene, M.; Knox, J. E.; Cross, J. B.; Bakken, V.; Adamo, C.; Jaramillo, J.; Gomperts, R.; Stratmann, R. E.; Yazyev, O.; Austin, A. J.; Cammi, R.; Pomelli, C.; Ochterski, J. W.; Martin, R. L.; Morokuma, K.; Zakrzewski, V. G.; Voth, G. A.

- Salvador, P.; Dannenberg, J. J.; Dapprich, S.; Daniels, A. D.; Farkas, O.; Foresman, J. B.; Ortiz, J. V.; Cioslowski, J.; Fox, D. J.; Gaussian, I., Wallingford CT, 2009., Ed.; Gaussian, Inc., Wallingford CT., 2009.
- (38) (a) Spartan '04, W., Inc. (2008) 18401 Von Karman Avenue, Suite 370, Irvine, CA, 92612, USA; Q-Chem, Inc., The Design Center, Suite 690, 5001 Baum Blvd., Pittsburgh, PA15213, USA. [http://www.wavefun.com/\(b\)](http://www.wavefun.com/(b)) Kong, J.; White, C. A.; Krylov, A. I.; Sherrill, C. D.; Adamson, R. D.; Furlani, T. R.; Lee, M. S.; Lee, A. M.; Gwaltney, S. R.; Adams, T. R.; Ochsenfeld, C.; Gilbert, A. T. B.; Kedziora, G. S.; Rassolov, V. A.; Maurice, D. R.; Nair, N.; Shao, Y.; Besley, N. A.; Maslen, P. E.; Dombroski, J. P.; Daschel, H.; Zhang, W.; Korambath, P. P.; Baker, J.; Byrd, E. F. C.; Van Voorhuis, T.; Oumi, M.; Hirata, S.; Hsu, C.-P.; Ishikawa, N.; Florian, J.; Warshel, A.; Johnson, B. G.; Gill, P. M. W.; Head-Gordon, M. a.; Pople, J. A. *J. Computational Chem.* **2000**, *21*, 1532.
- (39) (a) Friesner, R. A. *Chem. Phys. Lett.* **1985**, *116*, 39(b) Friesner, R. A. *Annu Rev Phys Chem* **1991**, *42*, 341.
- (40) (a) Rassolov, V. A.; Pople, J. A.; Ratner, M. A. a.; Windus, T. L. *J. Chem. Phys.* **1998**, *109*, 1223(b) Francl, M. M.; Pietro, W. J.; Hehre, W. J.; Binkley, J. S.; Gordon, M. S.; DeFrees, D. J. a.; Pople, J. A. *J. Chem. Phys.* **1982**, *77*, 3654.
- (41) Metcalfe, C.; Spey, S.; Adams, H.; Thomas, J. A. *J. Chem. Soc. Dalton Trans.* **2002**, 4732.
- (42) Constable, E. C. *Inorg. Chem. Radiochem.* **1986**, *30*, 69.
- (43) Dadci, L.; Elias, H.; Frey, U.; Hornig, A.; Koelle, U.; Merbach, A. E.; Paulus, H.; Schneider, J. S. *Inorg. Chem.* **1995**, *34*, 306.
- (44) Ongoma, P. O., PhD Thesis, University of KwaZulu-Natal, *Tuning Reactivity of Platinum(II) Complexes. A Kinetic and Mechanistic Investigation into Substitution Behaviour of Mono- and Dinuclear Platinum(II) Complexes*, 2012, CH4, 1- 30, CH6, 1-29, CH7, 1-28, .
- (45) (a) Li, J.; Xu, L.-C.; Chen, J.-C.; Zheng, K.-C.; Ji, L.-N. *J. Phys Chem. A.* **2006**, *110*, 8174(b) Salassa, L.; Garino, C.; Salassa, G.; Gobetto, R.; Nervi, C. *J. Chem. Soc.* **2008**, *130*, 9590.
- (46) (a) Parr, R. G.; Szentpaly, L.; Liu, S. *J. Am. Chem. Soc.* **1999**, *121*, 1922(b) Elango, M.; Parthasarathi, R.; Narayanan, G. K.; Sabeelullah, A. M.; Sarkar, U.; Venkatasubramanian, N. S.; Subramanian, V.; Chattaraj, P. K. *J. Chem. Sci.* **2005**, *117*, 61(c) Mebi, C. A. *J. Chem. Sci.* **2011**, *123*, 727(d) Chattaraj, P. K.; Giri, S.; Duley, S. *Chem. Rev.* **2011**, *111*, PR43.

- (47) (a) Jaganyi, D.; De Boer, K. L.; Gertenbach, J.; Perils, J. *Int. J. Chem. Kinet.* **2008**, *40*, 808(b) Jaganyi, D.; Reddy, D.; Gertenbach, J. A.; Hofmann, A.; van Eldik, R. *Dalton Trans.* **2004**, 299(c) Hofmann, A.; Jaganyi, D.; Munro, O. Q.; Liehr, G.; van Eldik, R. *Inorg. Chem.* **2003**, *42*, 1688(d) Willermann, M.; Mulcahy, C.; Sigel, R. K. O.; Cerda, M. M.; Freisinger, E.; Sanz Migul, P. J.; Roitzsch, M.; Liperet, B. *Inorg. Chem.* **2006**, *45*, 2093(e) Field, J. S.; Haines, R. J.; McMillin, D. R.; Summerton, G. C. *J. Chem. Soc., Dalton Trans.* **2002**, 1369(f) Buchner, R.; Cunningham, C. T.; S. Field, J.; H. Aines, R. J.; McMillin, D. R.; Summerton, G. C. *J. Chem. Soc., Dalton Trans.* **1999**, 711(g) Müller, J.; Freisinger, E.; Lax, P.; Megger, D. A.; Polonius, F., - A. *Inorg. Chim. Acta.* **2007**, *360*, 255(h) Sengul, A. *Turk. J. Chem.* **2004**, *28*, 667(i) Ledwaba, P.; Munro, O. Q.; Stewart, K. *Acta Cryst.* **2009**, *E65*, 0376.
- (48) Tiba, F.; Jaganyi, D.; Mambanda, A. *J. Coord. Chem.* **2010**, *63*, 2542.
- (49) Summerton, G. C., PhD Thesis, University of Natal, Pietermaritzburg, RSA, *Solid State Structures and Photophysical Properties of Polypyridyl Complexes of platinum(II)*, 1997, 23-25, 32-33, 70-75, 153-154, 182-190.
- (50) Ongoma, P. O.; Jaganyi, D. *Dalton Trans.* **2013**, *42*, 2724.
- (51) Jaganyi, D.; Hofmann, A.; van Eldik, R. *Angew Chem. Int. Ed. Engl.* **2001**, *40*, 1680.
- (52) (a) Ruhayel, R. A.; Langner, J. S.; Oke, M.-J.; Berners-Price, S. J.; Zgani, I.; Farrell, N. P. *J. Amer. Chem. Soc.* **2012**, *134*, 7135(b) Ertürk, H.; Maigut, J.; Puchta, R.; van Eldik, R. *Dalton Transactions* **2008**, 2759.
- (53) (a) Ertürk, H.; Maigut, J.; Puchta, R.; van Eldik, R. *dalton Trans.* **2008**, 2759(b) Appleton, F. D.; Hall, J. R.; Ralph, S. F. *Inorg. Chem.* **1985**, *24*, 4685.
- (54) Schindler, S.; Szalda, D. J.; Creutz, C. *inorg. Chem.* **1992**, *31*, 2255.
- (55) Gagliardo, M.; Rodríguez, G.; Dam, H. H.; Lutz, M.; Spek, A. L.; Havenith, R. W. A.; Coppo, P.; De Cola, L.; Hartl, F.; van Klink, G. P. M.; van Koten, G. *Inorg. Chem.* **2006**, *45*, 2143.
- (56) Fantacci, S.; De Angelis, F.; Wang, J.; Bernhard, S.; Selloni, A. *J. Am. Chem. Soc.* **2004**, *126*, 9715.
- (57) (a) Sauvage, J. P.; Collin, J. P.; Chambron, J. C.; Guillerez, S.; Coudret, C.; Balzani, V.; Barigelletti, F.; De Cola, L.; Flamigni, L. *Chem. Rev.* **1994**, *94*, 993(b) Levy, S. T.; Rubin, M. B.; Speiser, S. *J. Am. Chem. Soc.* **1992**, *114*, 10747(c) Levy, S. T.; Speiser, S. *J. Chem. Phys.* **1992**, *96*, 3585(d) Scholes, G. D.; Ghiggino, K. P.; Oliver, A. M.; Paddon-Row, M. N. *J. Phys. Chem.* **1993**, *97*, 11871(e) Grosshenny, V.; Harriman, A.; Hissler, M.; Ziessel, R. *J. Am. Chem. Soc. Faraday Trans.* **1996**, *92*, 2223.
- (58) Vektariene, A.; Vektaris, G.; Svoboda, J. *ARKIVOC.* **2009**, *7*, 311.

- (59) Parr, P. G.; Pearson, R. G. *J. Am. Chem. Soc.* **1983**, *105*, 7512.
- (60) Indelli, M. T.; Scandola, F.; Collin, J. P.; Sauvage, J. P.; Sour, A. *Inorg. Chem.* **1996**, *35*, 303.
- (61) Welter, S.; Salluce, N.; Benetti, A.; Rot, N.; Belser, P.; Sonar, P.; Grimsdale, A. C.; Müllen, K.; Lutz, M.; Spek, A. L.; De Cola, L. *Inorg. Chem.* **2005**, *44*, 4706.
- (62) (a) Tobe, M. L.; Burgess, J. *Inorganic Reaction Mechanisms*; Addison Wesley: London, 1999, 30- 33, 73-112 (b) Atwood, J. D. *Inorganic and Organic Reaction Mechanisms*; 2nd ed.; Wiley-VCH Inc.: New York, 1997, 32-34, 43-61 (c) Wilkins, R. G. *Kinetics and Mechanisms of Reactions of Transition Metal Complexes*; 2nd ed.; VCH: Weinheim, 1991, 199- 201, 232- 238 (d) Basolo, F.; Pearson, R. G. *Mechanisms of Inorganic Reactions*; 2nd ed.; Wiley: New York, 1967, pp. 80-115 (e) Summa, N.; Schiessl, W.; Puchta, R.; Hommes, N. E.; van Eldik, R. *Inorg. Chem.* **2006**, *45*, 2948.
- (63) (a) Wong, E.; Giandomenico, C. M. *Chem. Rev.* **1999**, *99*, 2451 (b) Montero, E. I.; Zhang, J.; Moniodis, J. J.; Berners-Price, S. J.; Farrell, N. P. *Chem. Eur. J.* **2010**, *16*, 1975.

## 4.6 Supporting Information

A summary of wavelengths at which the kinetic studies were performed, spectra obtained for titrations of **Pt2**, **Pt3** with NaOH, spectral absorbance change for **Pt1** with TU and plots of the dependence of  $k_{\text{obs}}$  against concentration of the nucleophiles and plots from temperature dependence studies along with tables of kinetic data, graphs of exemplary mass spectra for qpy ligand and **Pt1**, exemplary spectrum for microanalysis of **Pt1** and the representative spectra for  $^1\text{H}$  NMR and  $^{195}\text{Pt}$  NMR work reported in this study are given as electronic supporting information (ESI).

**Table S 4.1** Summary of the wavelengths (nm) used to study the substitution reactions of the complexes with thiourea nucleophiles.

Complex	Nu	Wavelength ( $\lambda$ ), nm
<b>Pt1</b>	TU	273
	DMTU	274
	TMTU	274
<b>Pt2</b>	TU	291
	DMTU	291
	TMTU	296
<b>Pt3</b>	TU	284
	DMTU	284
	TMTU	350



**Table S 4.2**      **Geometry-optimised structures of the platinum complexes investigated and distribution of the electron density on the platinum complexes investigated. The blue area indicates the most electropositive areas and the red region indicates the most electronegative areas.**

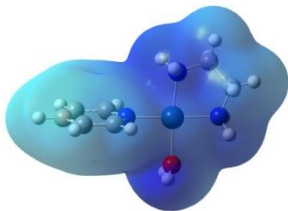
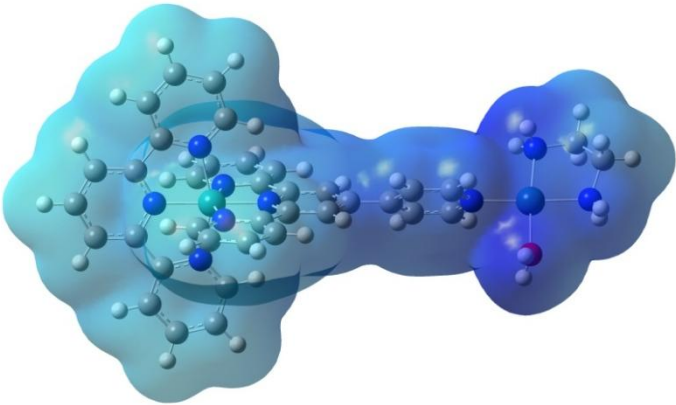
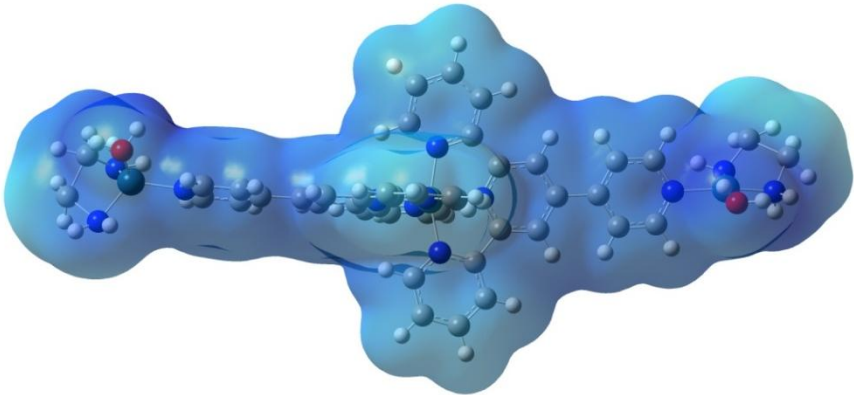
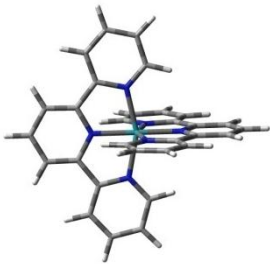
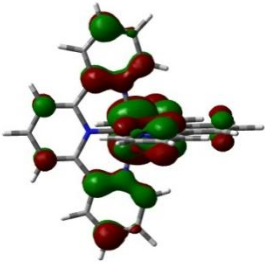
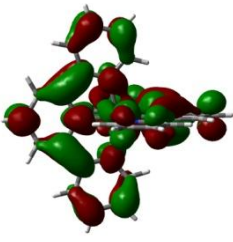
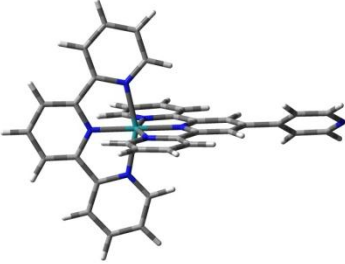
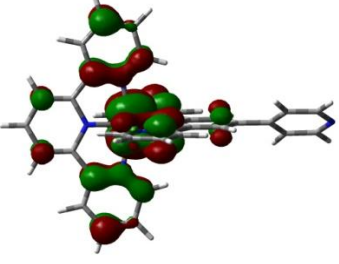
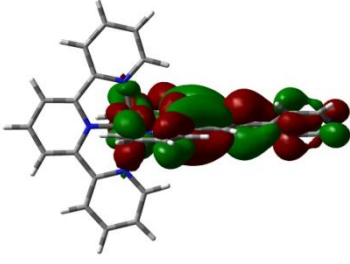
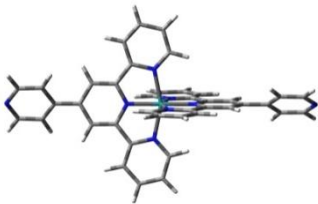
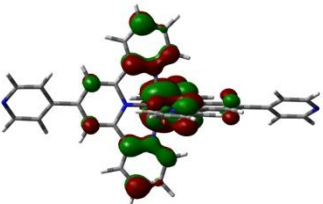
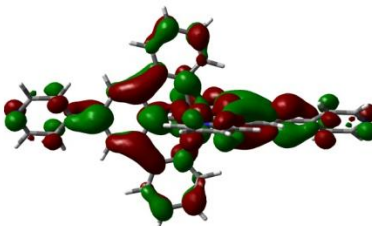
Compound	Structure
d	
Pt1	
Pt2	
Pt3	

Table S 4.3      Calculated minimum energy structures, frontier molecular orbitals (HOMO and LUMO) for the Ru terpyridine moieties; Ru(tpy)<sub>2</sub> and Ru(qpy)<sub>2</sub>.

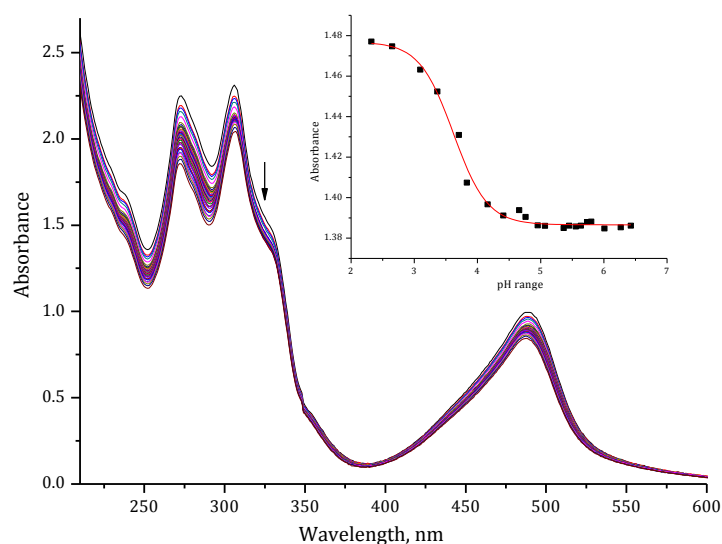
Complex	HOMO	LUMO
 <b>Ru(tpy)<sub>2</sub></b>		
 <b>Ru(tpy)(qpty)</b>		
 <b>Ru(qpy)<sub>2</sub></b>		

**Table S 4.4** Summary of DFT calculated data for the complexes investigated. Included are the data obtained for the DFT calculated Ru(II) analogues; Ru(tpy)<sub>2</sub>, Ru(tpy)(qpy) and Ru(qpy)<sub>2</sub> for comparisons.

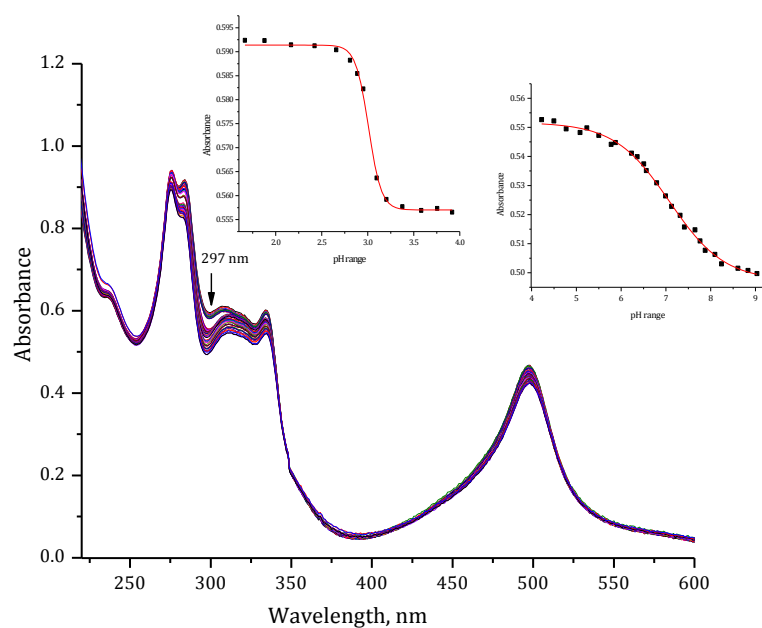
Parameter	Pt1	Pt2	Pt3	Ru(tpy) <sub>2</sub>	Ru(tpy)(qpy)	Ru(qpy) <sub>2</sub>
<b>Bond lengths, Å</b>						
Ru – Pt		11.15	11.247			
C3–C1'(dipyridine)		1.485	1.488		1.488	1.488
Ru–N <sub>trans</sub> (qpy)		2.002	2.016		2.004	2.005
Ru– N <sub>trans</sub> (tpy)		2.013	-	2.009	2.011	
<b>Bond angles, °</b>						
N <sub>cis</sub> –Pt–N <sub>cis</sub>	177.99	177.95	178.16			
OH <sub>2</sub> – Pt - N <sub>trans</sub>	174.51	175.36	174.99			
N <sub>trans</sub> –Pt–N <sub>cis</sub> (py)	94.07	94.25	94.46			
N <sub>trans</sub> –Pt–N <sub>cis</sub> (NH <sub>2</sub> )	83.93	83.76	83.83			
N <sub>cis</sub> (py) –Pt–OH <sub>2</sub>	91.17	90.35	90.57			
N <sub>cis</sub> (NH <sub>2</sub> ) –Pt–OH <sub>2</sub>	90.83	91.62	91.18			
N <sub>cis</sub> –Ru–N <sub>cis</sub> (tpy)		157.64		157.80	157.77	
N <sub>cis</sub> –Ru–N <sub>cis</sub> (qpy)		157.82	157.65		157.72	157.60
N <sub>trans</sub> –Ru–N <sub>trans</sub>		179.97	179.90	179.99	179.97	179.99
Deviation of (en) (relative to coord. plane)	12.23	14.13	14.29			
Angle of inclination of water from Pt plane	1.64	4.59	5.23			
<b>NBO charges</b>						
O (H <sub>2</sub> O)	-0.913	-0.915	-0.914			
Ru				0.302	0.312	0.316
N <sub>cis</sub> (py)					-0.528	-0.528
N4		-0.404	-0.510	-0.410	-0.408	-0.409
N5		-0.420	-0.405	-0.421	-0.420	-0.421
N6		-0.420	-0.420	-0.421	-0.420	-0.421
N7		-0.412	-0.510	-0.410	-0.421	
N8		-0.421	-0.420	-0.421	-0.411	
N9		-0.421	-0.420	-0.421	-0.421	
C1	-0.087	0.105	0.104		0.061	0.061
C2	-0.226	-0.212	-0.211		-0.234	-0.234
C3	-0.148	0.005	0.004		-0.030	-0.030
C4	-0.226	-0.212	-0.211		-0.234	-0.234
C5	-0.088	0.103	0.106		0.061	0.061
C1'	-	-0.008	0.005		0.002	0.002
C6	-0.207	-0.207	-0.207		-	-
C7	-0.210	-0.209	-0.210		-	-
<b>Energy gap, eV</b>						
HOMO				-6.18	-6.23	-6.26
LUMO				-2.78	-2.99	-2.96
ΔE <sub>HOMO</sub> - LUMO				3.40	3.24	3.30
Symmetry				D <sub>2d</sub>	C <sub>2</sub>	C <sub>2</sub>

**Table S 4.5** Summary of DFT calculated data from Spartan08 Computational calculations for the complexes investigated. Data included for references.

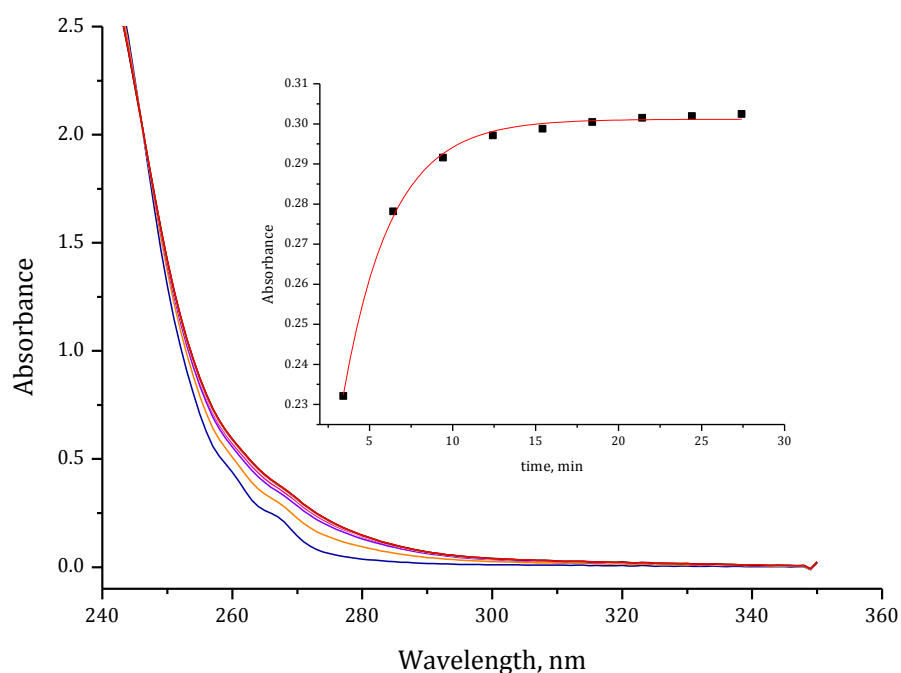
Parameter	Pt1	Pt2	Pt3
<b>Bond lengths, Å</b>			
Pt-OH <sub>2</sub>	2.136	2.136	2.136
Pt-N <sub>trans</sub>	2.052	2.056	2.057
Pt - N <sub>cis</sub> (HN2)	2.105	2.093	2.088
Pt - N <sub>cis</sub> (py)	2.066	2.091	2.108
Ru - Pt		11.19	11.24
Pt-Pt			22.49
<b>Bond angles, °</b>			
Twist of 4'-py from plane of tpy ligand deviation of py (relative to Pt(II) coord. plane)	89.83	36.10 94.98	39.44 96.61
<b>NBO charges</b>			
Pt	1.182	1.185	1.186
Ru		0.999	0.996
N <sub>trans</sub>	-0.943	-0.943	-0.944
N <sub>cis</sub> (py)	-0.653	-0.652	-0.642
N <sub>cis</sub> (NH <sub>2</sub> )	-0.974	-0.967	-0.963
<b>Energy gap, eV</b>			
HOMO	-14.52	-14.14	-16.78
LUMO	-9.37	-11.87	-13.77
$\Delta E_{\text{HOMO-LUMO}}$	5.15	2.27	3.01
$\eta$ /eV	2.58	1.14	1.51
$\mu$ / eV	-11.95	-13.01	-15.28
$\omega$ / eV	27.65	74.19	77.26



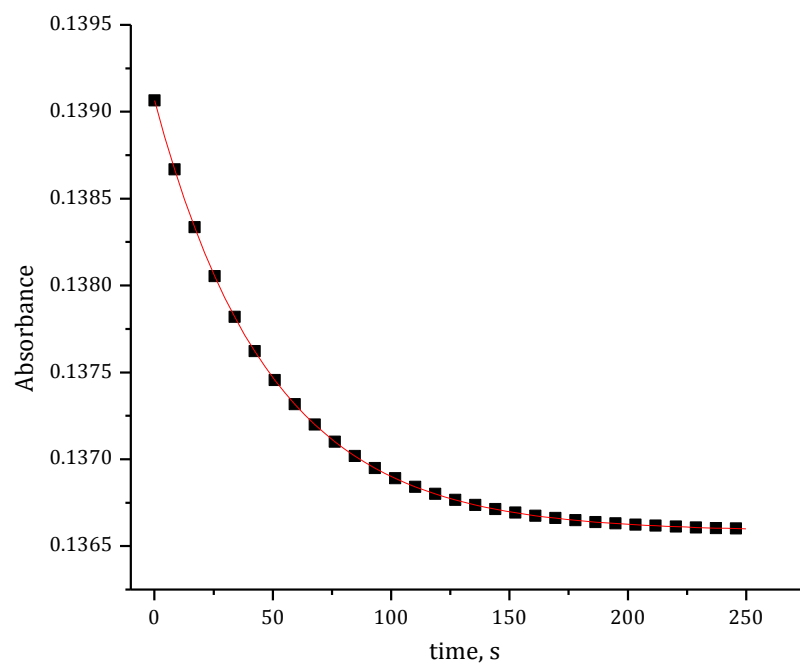
**Figure S 4.1** UV/visible spectrum for the titration of Pt2 ( $5.0 \times 10^{-5}$  M) with NaOH, pH range from 2 - 9 at 298 K. Inset is the titration graph of absorbance verses pH at 327 nm from pH 2 - 6.



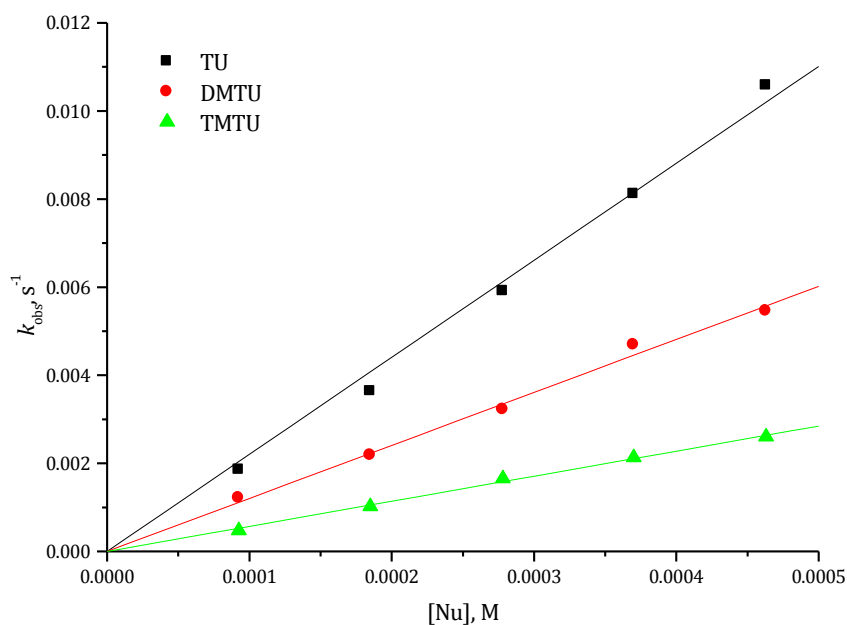
**Figure S 4.2** UV/visible spectrum for the titration of Pt3 ( $2.5 \times 10^{-5}$  M) with NaOH from pH 2 - 9 at 298 K. Inset are the titration graphs of absorbance versus pH at 297 nm.



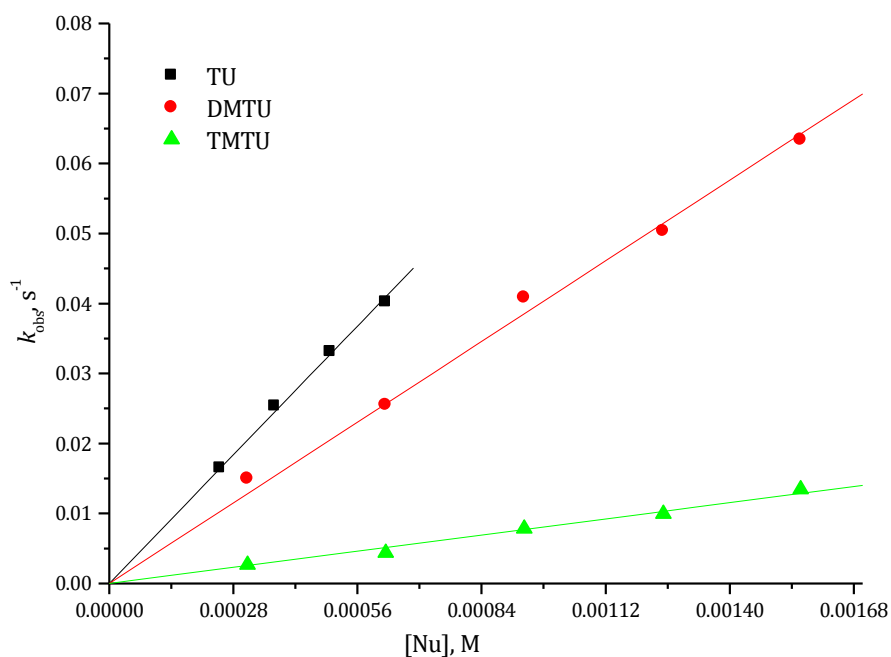
**Figure S 4.3** Spectrum obtained from Cary UV/Visible spectrophotometer for the substitution of H<sub>2</sub>O from Pt1 ( $1.850 \times 10^{-5}$  mol dm<sup>-3</sup>) with Tu ( $2.780 \times 10^{-4}$  mol dm<sup>-3</sup>) in methanol solution at pH = 2, T = 298 K, I = 0.02 M HCF<sub>3</sub>SO<sub>3</sub>, adjusted with LiCF<sub>3</sub>SO<sub>3</sub>. Inset is the time resolved kinetic trace obtained at 273 nm.



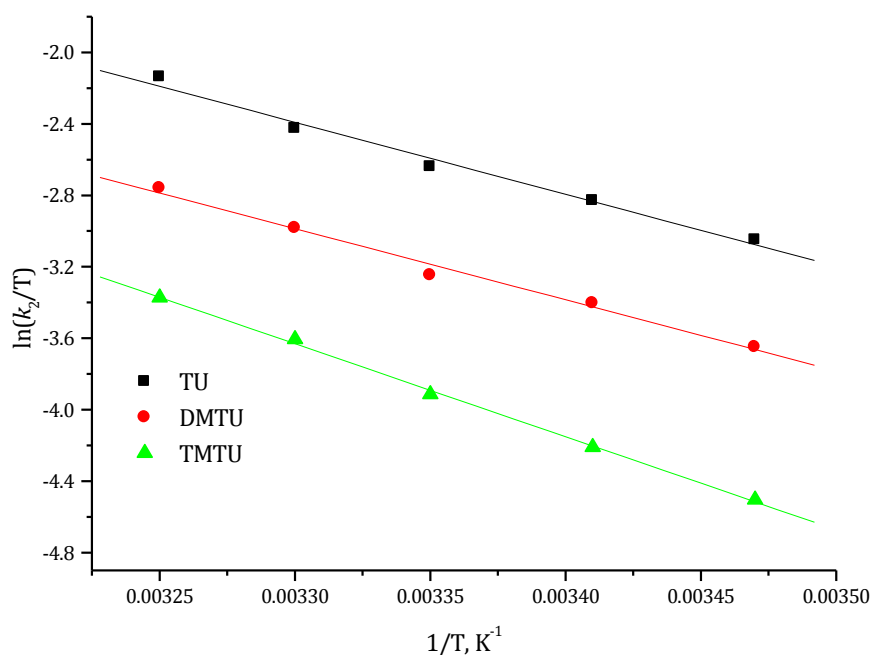
**Figure S 4.4** Kinetic trace at 284 nm for the reaction of Pt3 ( $1.248 \times 10^{-5} \text{ mol dm}^{-3}$ ) with TU ( $3.744 \times 10^{-4} \text{ mol dm}^{-3}$ ) at 298 K, pH = 2.0,  $I = 0.02 \text{ M HCF}_3\text{SO}_3$ , adjusted with  $\text{LiCF}_3\text{SO}_3$ .



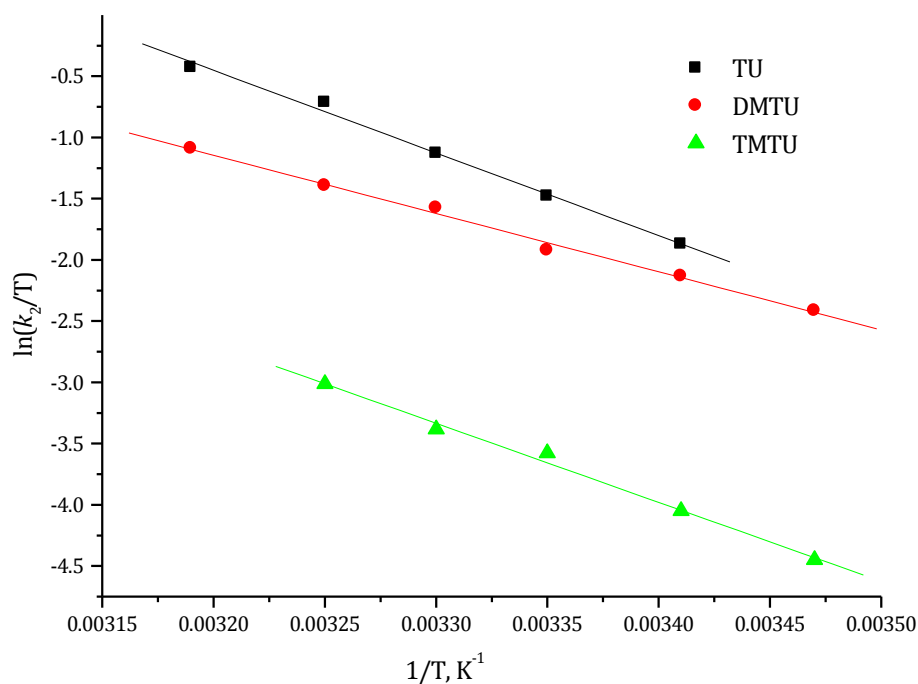
**Figure S 4.5** Concentration dependence of the pseudo first-order  $k_{\text{obs}}$  for the substitution of aqua ligand in Pt1 with the thiourea nucleophiles at pH = 2,  $T = 298 \text{ K}$ ,  $I = 0.02 \text{ M HCF}_3\text{SO}_3$ , adjusted with  $\text{LiCF}_3\text{SO}_3$ .



**Figure S 4.6** Concentration dependence of the pseudo first-order  $k_{obs}$  for the substitution of aqua ligand in Pt3 with the thiourea nucleophiles at pH = 2, T = 298 K, I = 0.02 M  $HCF_3SO_3$ , adjusted with  $LiCF_3SO_3$ .



**Figure S 4.7** Eyring plots obtained for Pt1 with the nucleophiles for the substitution reactions over the temperature range 15-40 °C at pH = 2, T = 298 K, I = 0.02 M  $HCF_3SO_3$ , adjusted with  $LiCF_3SO_3$ .



**Figure S 4.8** Eyring plots obtained for Pt3 with the nucleophiles for the substitution reactions over the temperature range 15-40 °C at pH = 2, T = 298 K, I = 0.02 M HCF<sub>3</sub>SO<sub>3</sub>, adjusted with LiCF<sub>3</sub>SO<sub>3</sub>.

**Table S 4.6** Average observed rate constants,  $k_{\text{obs}}$  s<sup>-1</sup>, for the displacement of the aqua ligand in Pt1 with thiourea nucleophiles, at pH = 2, T = 298 K, I = 0.02 M HCF<sub>3</sub>SO<sub>3</sub>, adjusted with LiCF<sub>3</sub>SO<sub>3</sub>.

TU		DMTU		TMTU	
Conc, mM	$k_{\text{obs.}}, \text{s}^{-1}$	Conc, mM	$k_{\text{obs.}}, \text{s}^{-1}$	Conc, mM	$k_{\text{obs.}}, \text{s}^{-1}$
0.093	0.00185	0.093	0.00121	0.093	0.000473
0.185	0.00363	0.185	0.00218	0.185	0.00102
0.278	0.00591	0.278	0.00322	0.278	0.00165
0.370	0.00811	0.370	0.00469	0.370	0.00213
0.463	0.01058	0.463	0.00546	0.463	0.0026



**Table S 4.7** Temperature dependence of  $k_2$  M<sup>-1</sup>s<sup>-1</sup>, for the displacement of the aqua ligand in Pt1 by thiourea nucleophiles at 30-fold excess over [Pt1], pH = 2,  $I = 0.02$  M HCF<sub>3</sub>SO<sub>3</sub>, adjusted with LiCF<sub>3</sub>SO<sub>3</sub>.

TU		DMTU		TMTU	
1/T, K <sup>-1</sup>	ln( $k_2$ /T)	1/T, K <sup>-1</sup>	ln( $k_2$ /T)	1/T, K <sup>-1</sup>	ln( $k_2$ /T)
0.00347	-3.04956	0.00347	-3.65076	0.00347	-4.5056
0.00341	-2.8304	0.00341	-3.40433	0.00341	-4.21024
0.00335	-2.64079	0.00335	-3.24791	0.00335	-3.91537
0.0033	-2.4258	0.0033	-2.98288	0.0033	-3.60702
0.00325	-2.13686	0.00325	-2.76149	0.00325	-3.37426

**Table S 4.8** Average observed rate constants,  $k_{\text{obs}}$  s<sup>-1</sup>, for the displacement of the aqua ligand in Pt2 with thiourea nucleophiles, at pH = 2, T = 298 K,  $I = 0.02$  M HCF<sub>3</sub>SO<sub>3</sub>, adjusted with LiCF<sub>3</sub>SO<sub>3</sub>.

TU		DMTU		TMTU	
Conc, mM	$k_{\text{obs.}}$ s <sup>-1</sup>	Conc, mM	$k_{\text{obs.}}$ s <sup>-1</sup>	Conc, mM	$k_{\text{obs.}}$ s <sup>-1</sup>
0.143	0.00956	0.286	0.00954	0.286	0.00172
0.286	0.01813	0.572	0.02208	0.572	0.00343
0.429	0.02732	0.857	0.0341	0.857	0.00513
0.572	0.03543	1.14	0.04421	1.14	0.00647
0.715	0.04252	1.43	0.05356	1.43	0.0081

**Table S 4.9** Temperature dependence of  $k_2$  M<sup>-1</sup>s<sup>-1</sup>, for the displacement of the aqua ligand in Pt2 by thiourea nucleophiles at 60-fold excess over [Pt1], pH = 2,  $I = 0.02$  M HCF<sub>3</sub>SO<sub>3</sub>, adjusted with LiCF<sub>3</sub>SO<sub>3</sub>.

TU		DMTU		TMTU	
1/T, K <sup>-1</sup>	ln( $k_2$ /T)	1/T, K <sup>-1</sup>	ln( $k_2$ /T)	1/T, K <sup>-1</sup>	ln( $k_2$ /T)
0.00341	-2.32889	0.00341	-2.26821	0.00347	-4.56526
0.00335	-2.0545	0.00335	-1.8327	0.00341	-4.24356
0.0033	-1.58638	0.0033	-1.40179	0.00335	-3.90906
0.00325	-1.20635	0.00325	-1.11602	0.0033	-3.55237
0.00319	-0.89219	0.00319	-0.84015	0.00319	-2.96939

**Table S 4.10** Average observed rate constants,  $k_{\text{obs}}$  s<sup>-1</sup>, for the displacement of the aqua ligand in Pt3 with thiourea nucleophiles, at pH = 2, T = 298 K,  $I = 0.02$  M HCF<sub>3</sub>SO<sub>3</sub>, adjusted with LiCF<sub>3</sub>SO<sub>3</sub>.

TU		DMTU		TMTU	
Conc, mM	$k_{\text{obs}}$ , s <sup>-1</sup>	Conc, mM	$k_{\text{obs}}$ , s <sup>-1</sup>	Conc, mM	$k_{\text{obs}}$ , s <sup>-1</sup>
0.25	0.01647	0.312	0.01496	0.312	0.00266
		0.624	0.02546	0.624	0.00435
0.374	0.02535	0.936	0.04083	0.936	0.0078
0.499	0.0331	1.25	0.05032	1.25	0.00991
0.624	0.0402	1.56	0.06337	1.56	0.01342

**Table S 4.11** Temperature dependence of  $k_2$  M<sup>-1</sup>s<sup>-1</sup>, for the displacement of the aqua ligand in Pt3 by thiourea nucleophiles at 60-fold excess over [Pt1], pH = 2,  $I = 0.02$  M HCF<sub>3</sub>SO<sub>3</sub>, adjusted with LiCF<sub>3</sub>SO<sub>3</sub>.

TU		DMTU		TMTU	
1/T, K <sup>-1</sup>	ln( $k_2$ /T)	1/T, K <sup>-1</sup>	1/T, K <sup>-1</sup>	ln( $k_2$ /T)	1/T, K <sup>-1</sup>
		0.00347	-2.41624	0.00347	-4.45185
0.00341	-1.87293	0.00341	-2.13461	0.00341	-4.05136
0.00335	-1.48116	0.00335	-1.92194	0.00335	-3.57791
0.0033	-1.13116	0.0033	-1.57576	0.0033	-3.3836
0.00325	-0.71432	0.00325	-1.39421	0.00325	-3.01378
0.00319	-0.42996	0.00319	-1.09062		

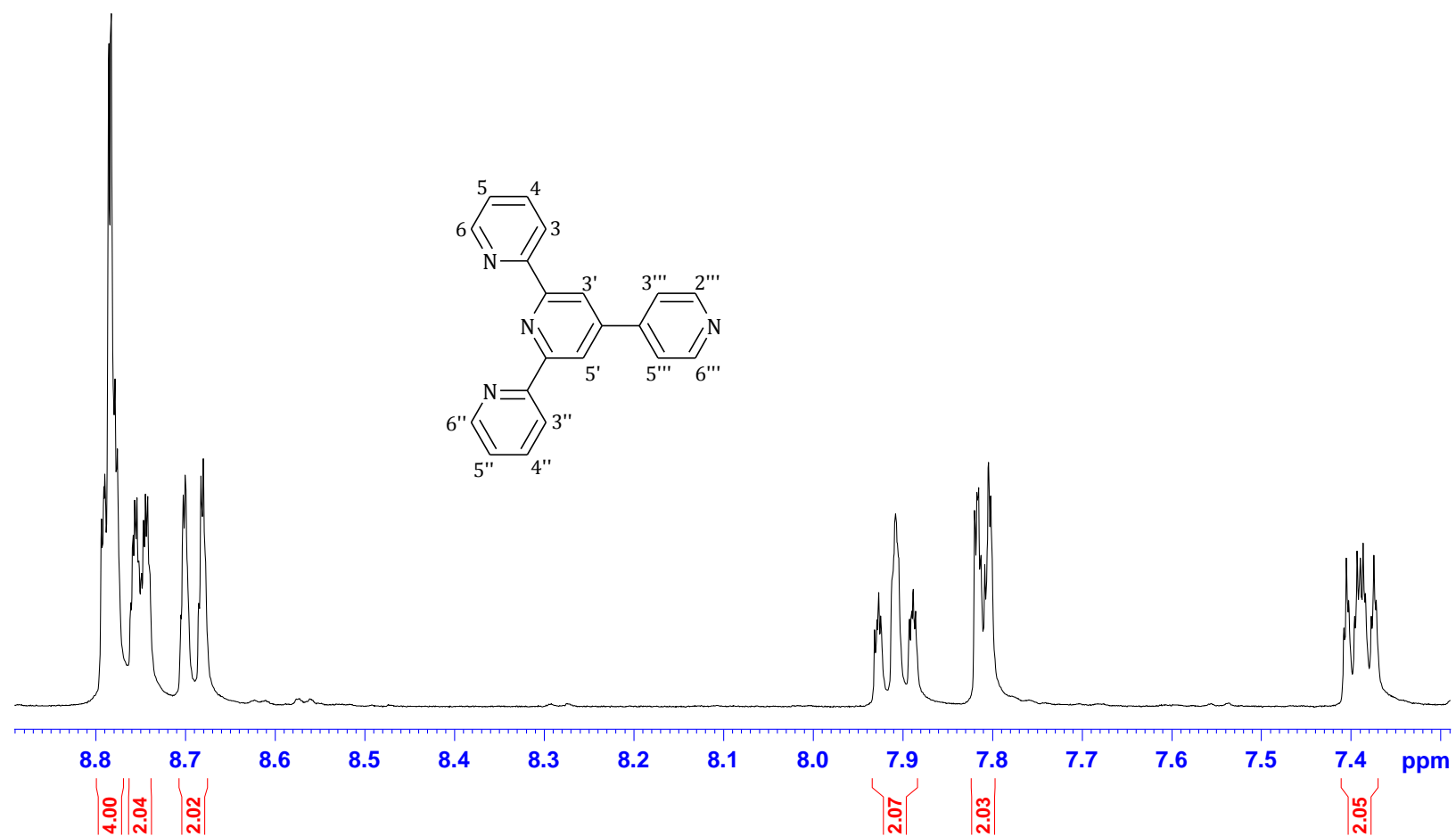


Figure S 4.9 <sup>1</sup>H NMR spectrum of 4'-(4'''-pyridyl)2,2':6',2''-terpyridine in CDCl<sub>3</sub>. Spectrum zoomed in to show the signals due to the protons on the aromatic rings.

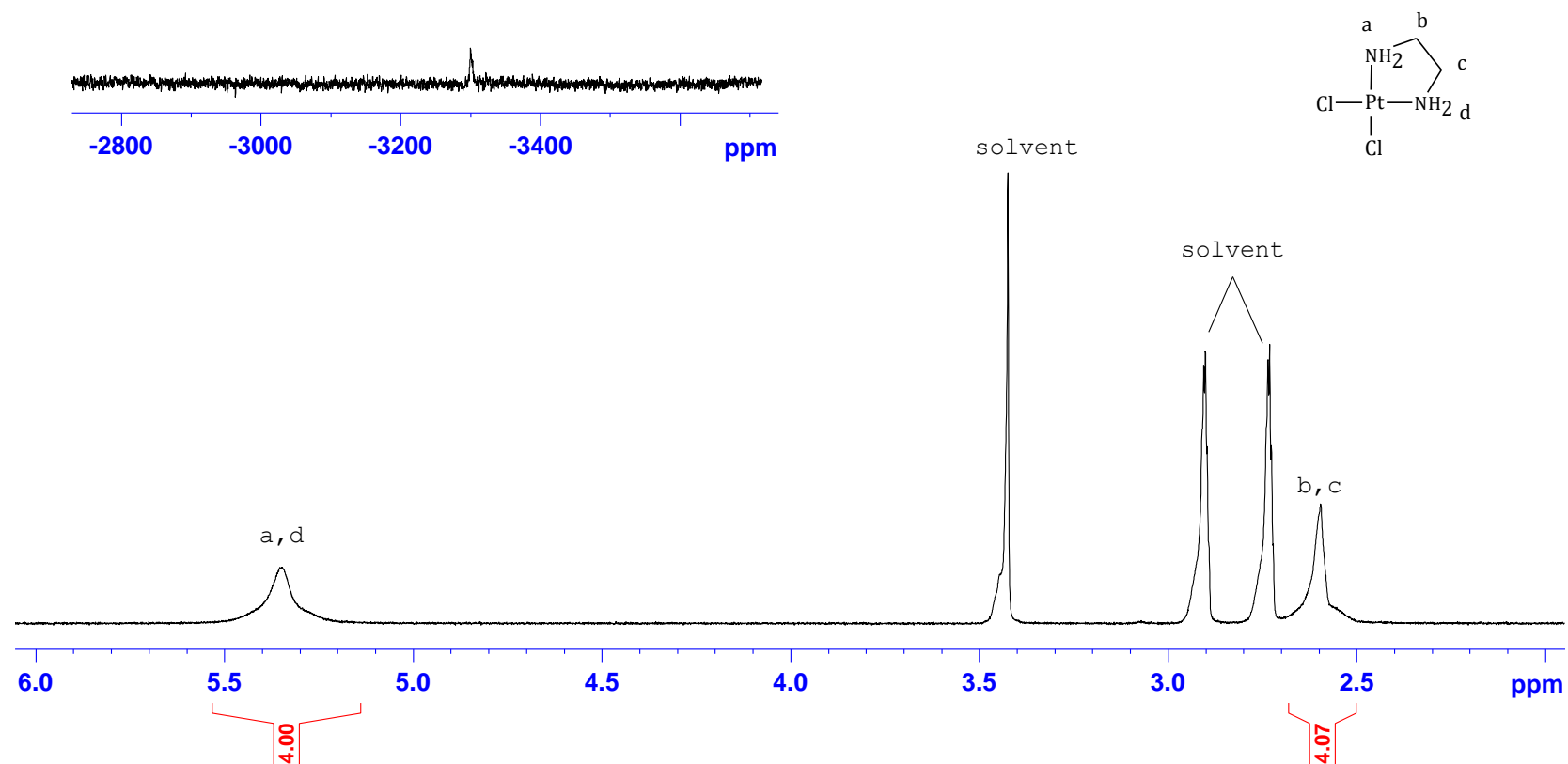


Figure S 4.10  $^1\text{H}$  NMR and  $^{195}\text{Pt}$  NMR spectra of  $\text{Pt}(\text{en})\text{Cl}_2$  in  $\text{DMF-}d_7$ .

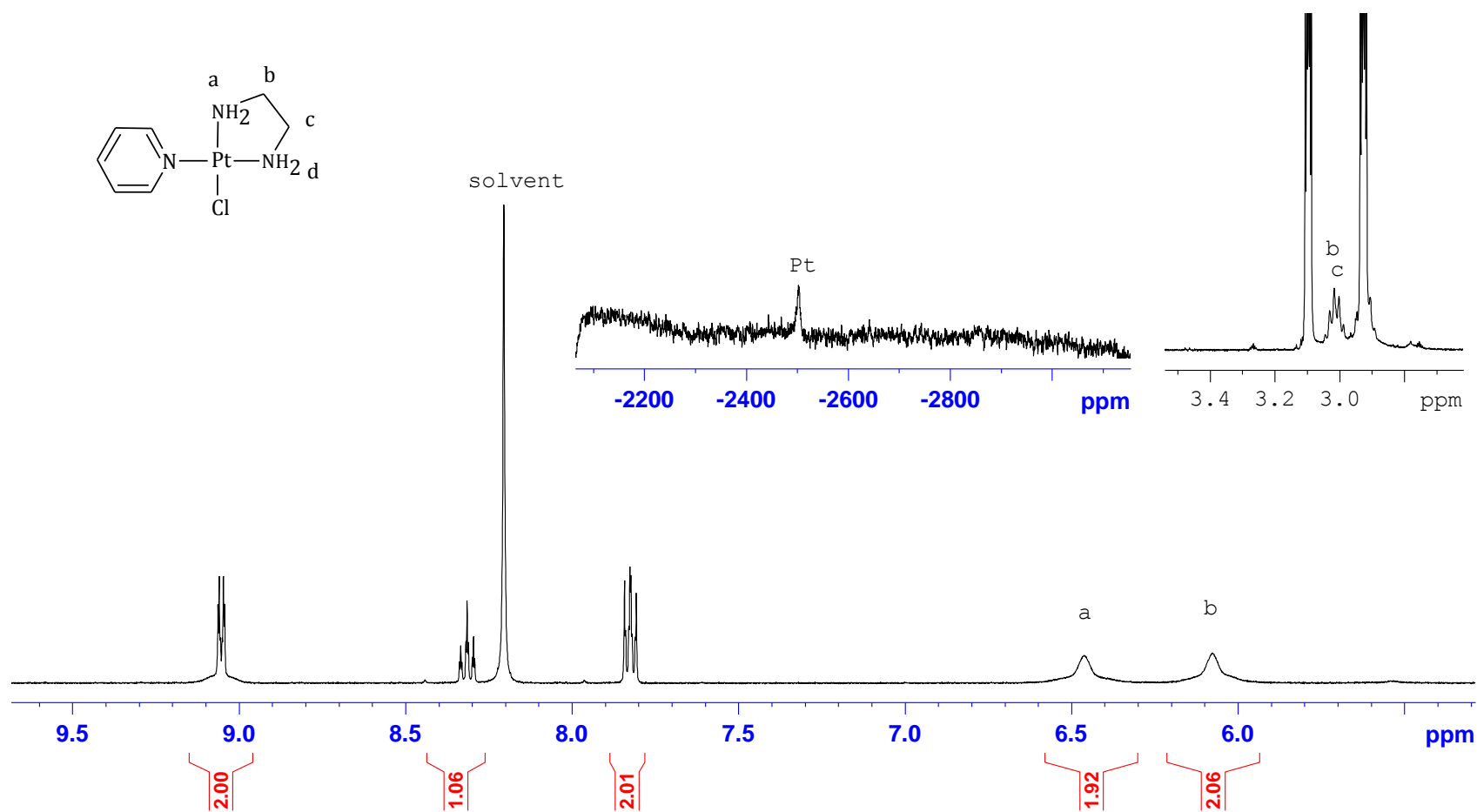


Figure S 4.11  $^1\text{H}$  NMR and  $^{195}\text{Pt}$  NMR spectrum of Pt1-Cl in  $\text{DMF-d}_7$ .

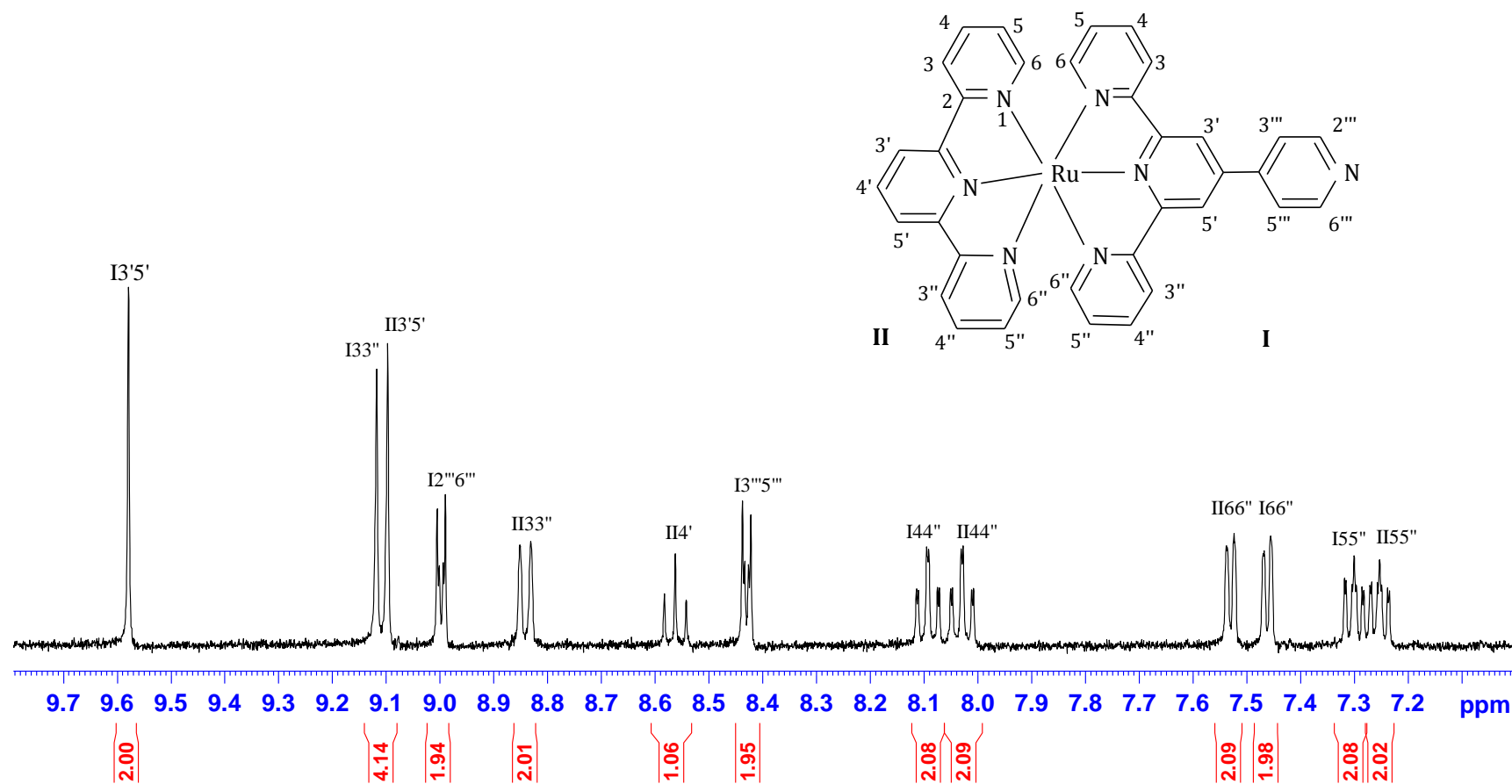


Figure S 4.12  $^1\text{H}$  NMR spectrum of  $\text{Ru}(\text{qpy})(\text{tpy})\text{Cl}_2$ . Spectrum zoomed in to show the signals due to the protons on the aromatic rings.

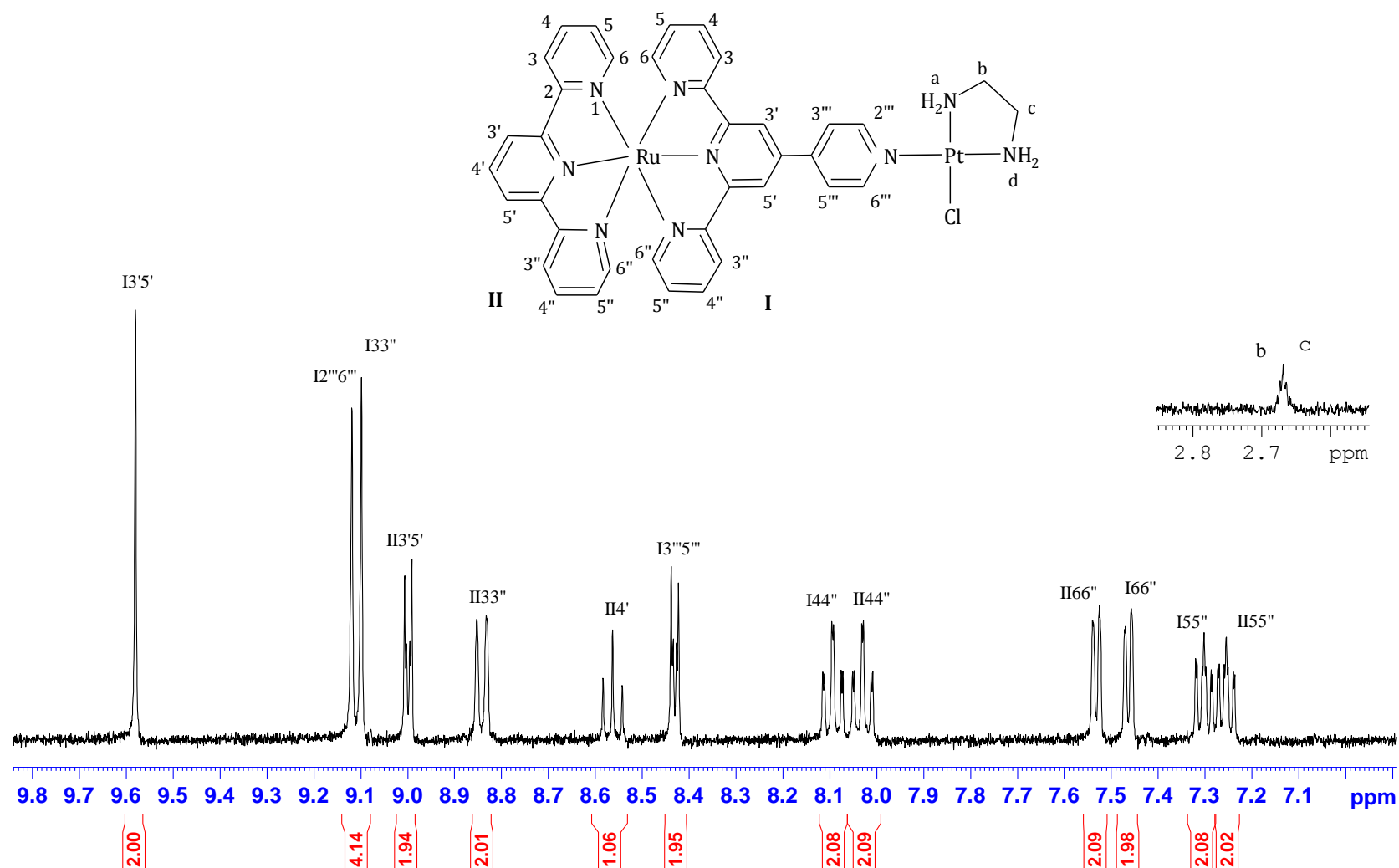


Figure S 4.13 <sup>1</sup>H NMR spectrum of Pt<sub>2</sub>-Cl. Inset is the signal due to the alkyl protons.

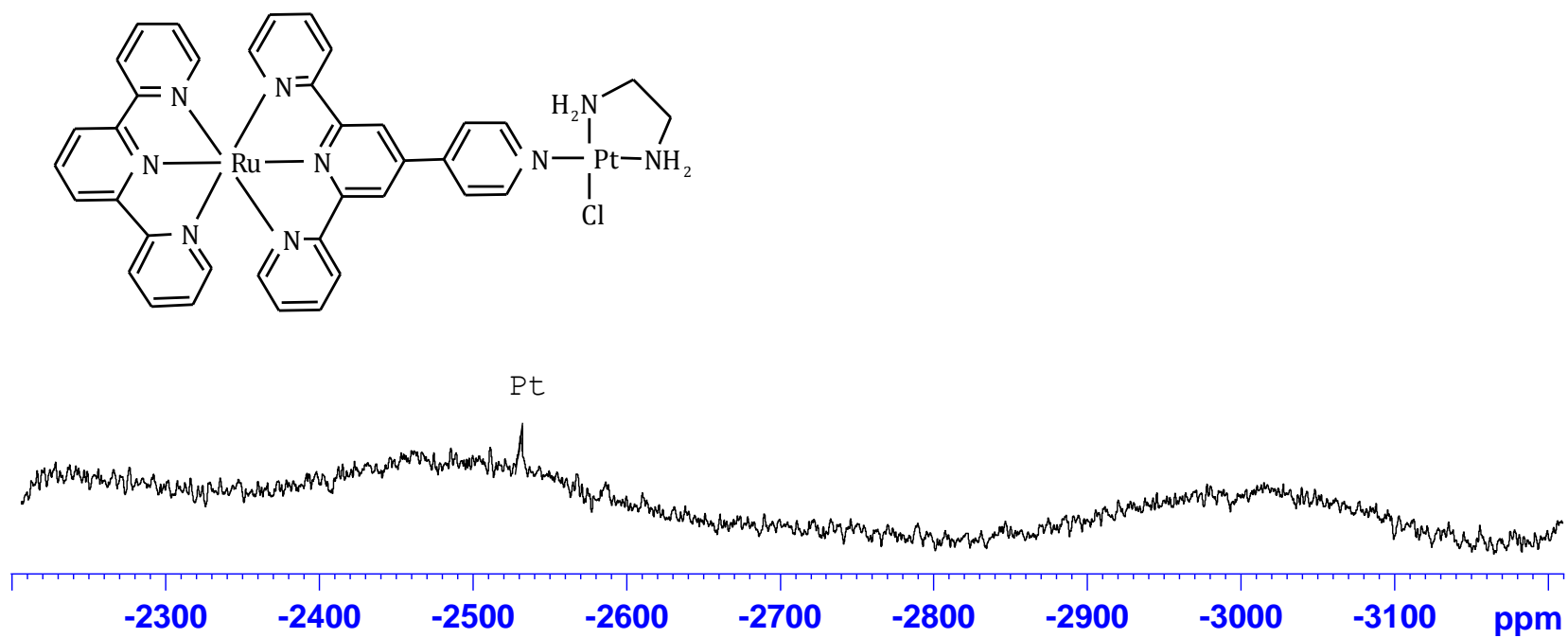


Figure S 4.14  $^{195}\text{Pt}$  NMR spectrum of Pt3-Cl.



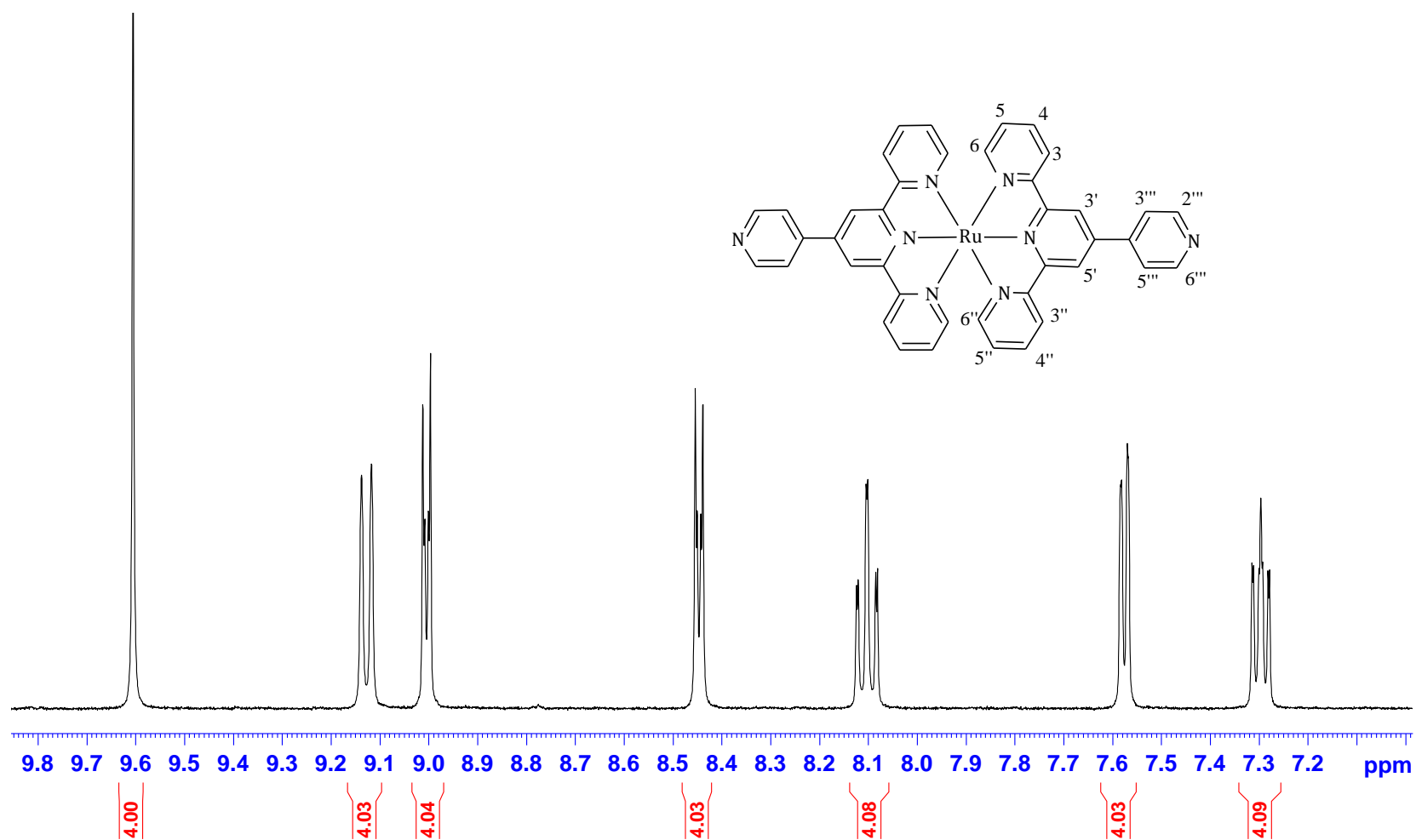


Figure S 4.15  $^1\text{H}$ NMR spectrum of  $[\text{Ru}(\text{qpy})_2]\text{Cl}_2$ . Spectrum zoomed in to show the signals due to the protons on the aromatic rings.

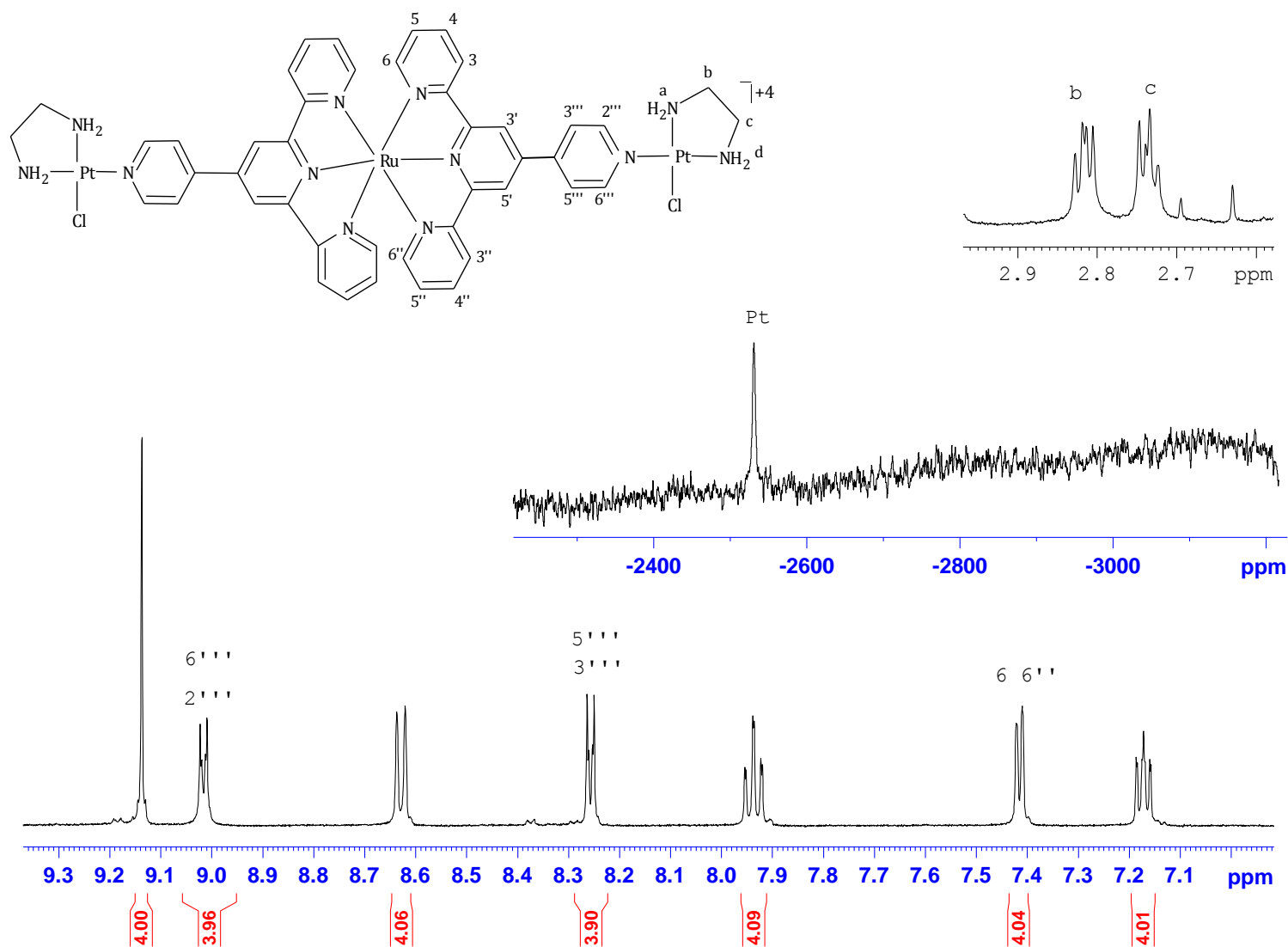


Figure S 4.16  $^1\text{H}$  NMR and  $^{195}\text{Pt}$  NMR spectra of Pt3-Cl. Insets are the signals due to the alkyl protons and due to Pt.

## Elemental Composition Report

Page 1

## Single Mass Analysis

Tolerance = 5.0 PPM / DBE: min = -1.5, max = 50.0

Element prediction: Off

Number of isotope peaks used for i-FIT = 3

Monoisotopic Mass, Even Electron Ions

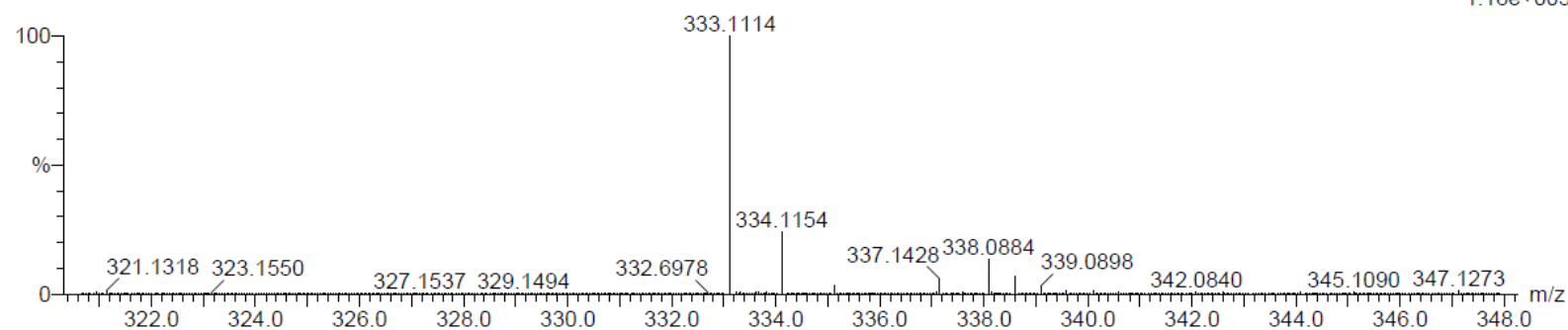
6 formula(e) evaluated with 1 results within limits (all results (up to 1000) for each mass)

Elements Used:

C: 15-20 H: 10-15 N: 0-5 Na: 0-1

Aishath

qtpy 11 (0.170) Cm (1:30)

TOF MS ES+  
1.18e+005

Minimum: -1.5  
Maximum: 5.0 5.0 50.0

Mass	Calc. Mass	mDa	PPM	DBE	i-FIT	i-FIT (Norm)	Formula
333.1114	333.1116	-0.2	-0.6	15.5	540.3	0.0	C20 H14 N4 Na

Figure S 4.17 High resolution ESI mass spectrum of 4'-(4'''-pyridyl)2,2':6',2''-terpyridine (qpy).

## Elemental Composition Report

Page 1

## Single Mass Analysis

Tolerance = 5.0 PPM / DBE: min = -1.5, max = 50.0

Element prediction: Off

Number of isotope peaks used for i-FIT = 3

Monoisotopic Mass, Even Electron Ions

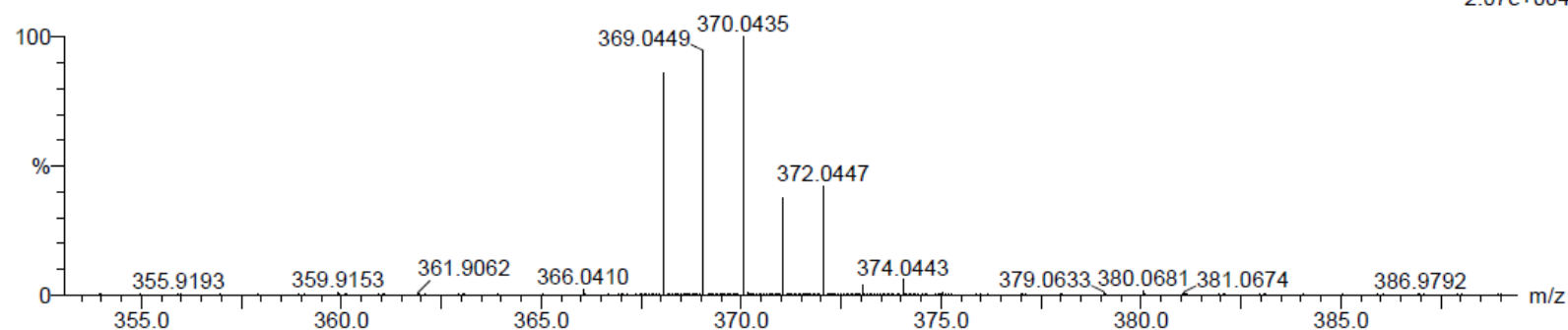
19 formula(e) evaluated with 1 results within limits (all results (up to 1000) for each mass)

Elements Used:

C: 5-10 H: 10-15 N: 0-5 Cl: 0-1 Pt: 0-1

Aishath

Ptenpy 2 (0.017) Cm (1:29)

TOF MS ES+  
2.07e+004

Minimum: -1.5  
Maximum: 5.0 5.0 50.0

Mass	Calc. Mass	mDa	PPM	DBE	i-FIT	i-FIT (Norm)	Formula
369.0449	369.0446	0.3	0.8	3.5	450.2	0.0	C7 H13 N3 Cl Pt

Figure S 4.18 High resolution ESI mass spectrum of Pt1-Cl.

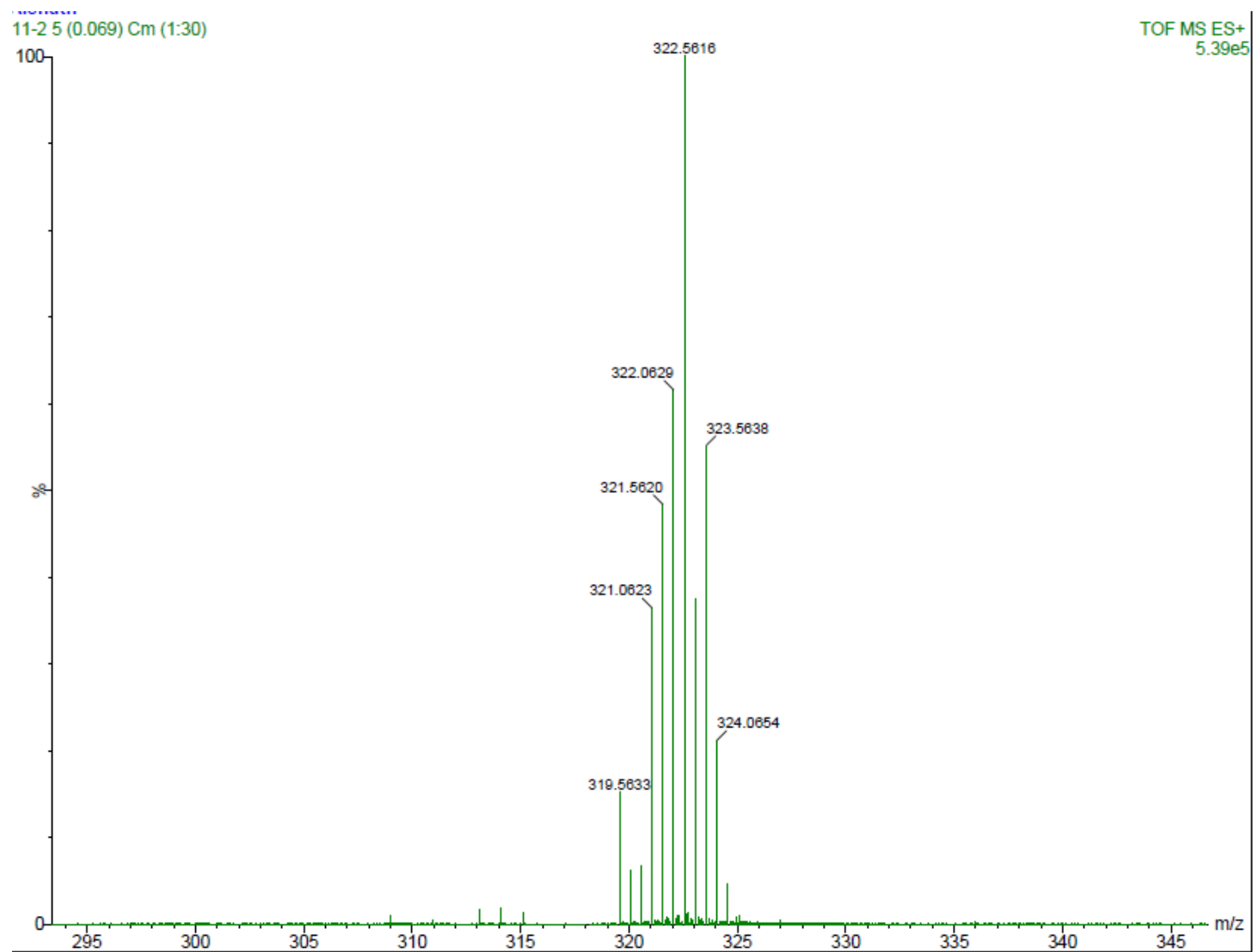


Figure S 4.19 Low resolution ESI mass spectrum of  $[\text{Ru}(\text{qpy})(\text{tpy})\text{Cl}_2]$ .

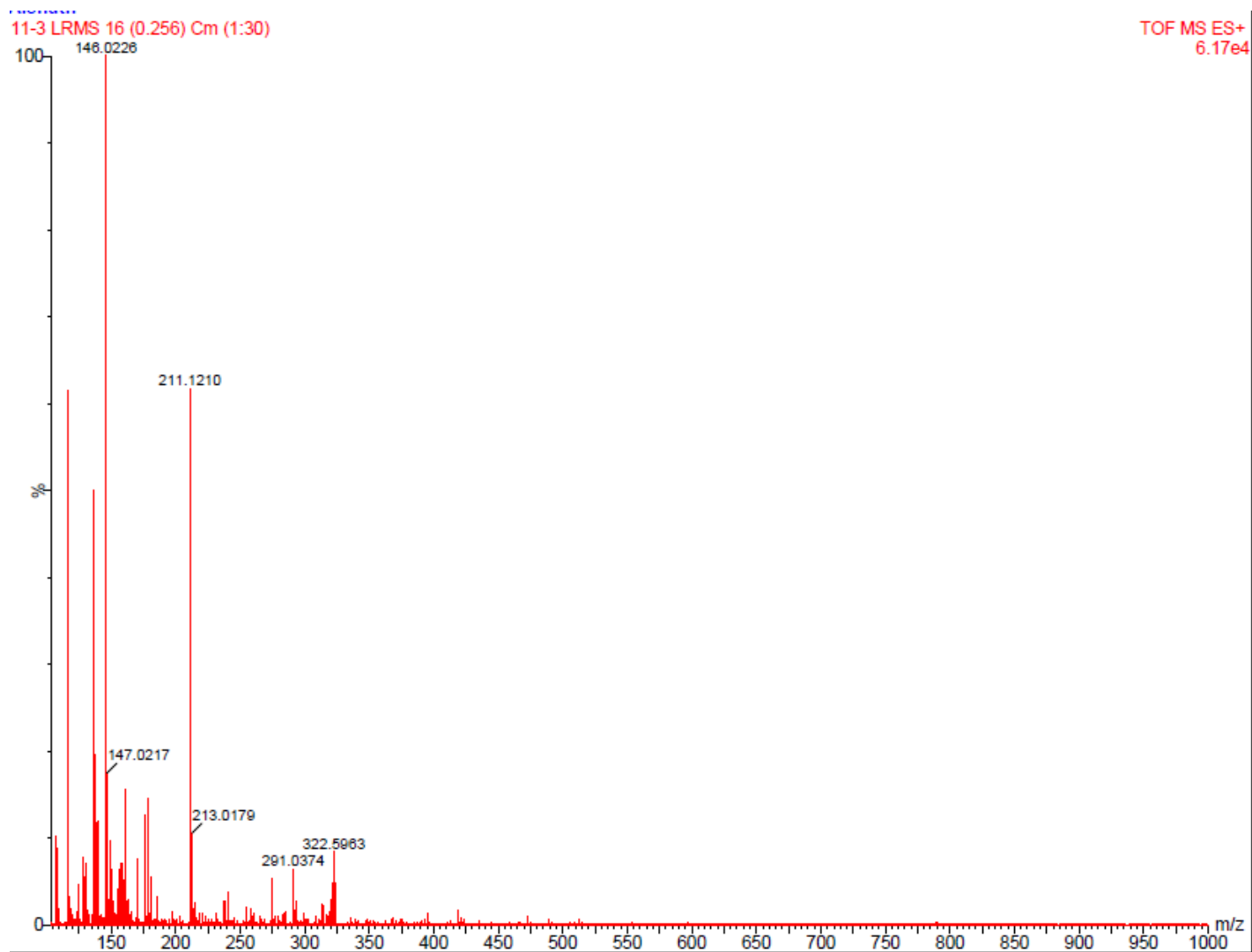


Figure S 4.20 Low resolution ESI mass spectrum of Pt<sub>2</sub>-Cl.

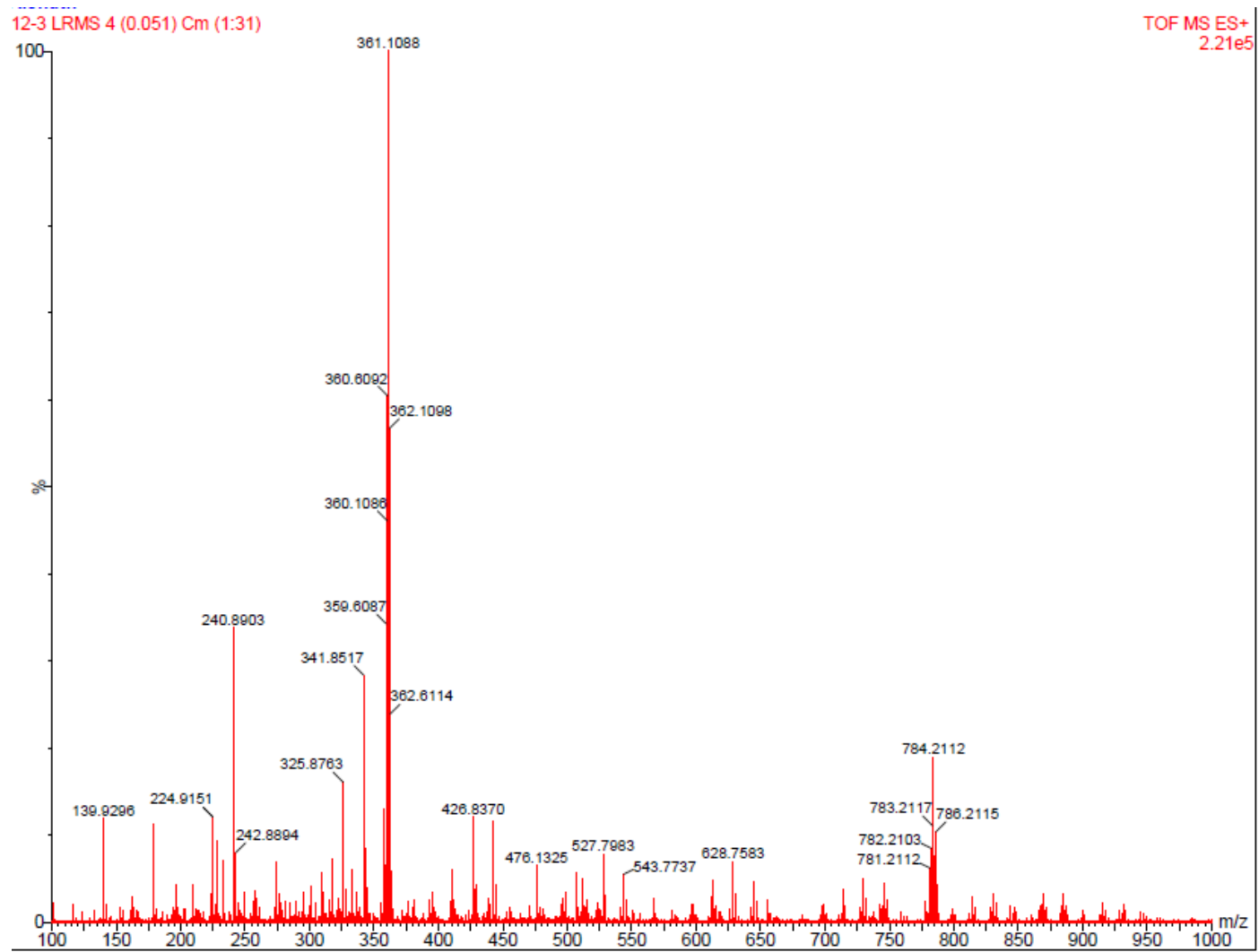


Figure S 4.21 Low resolution ESI mass spectrum of  $[\text{Ru}(\text{qpy})_2\text{Cl}_2]$ .

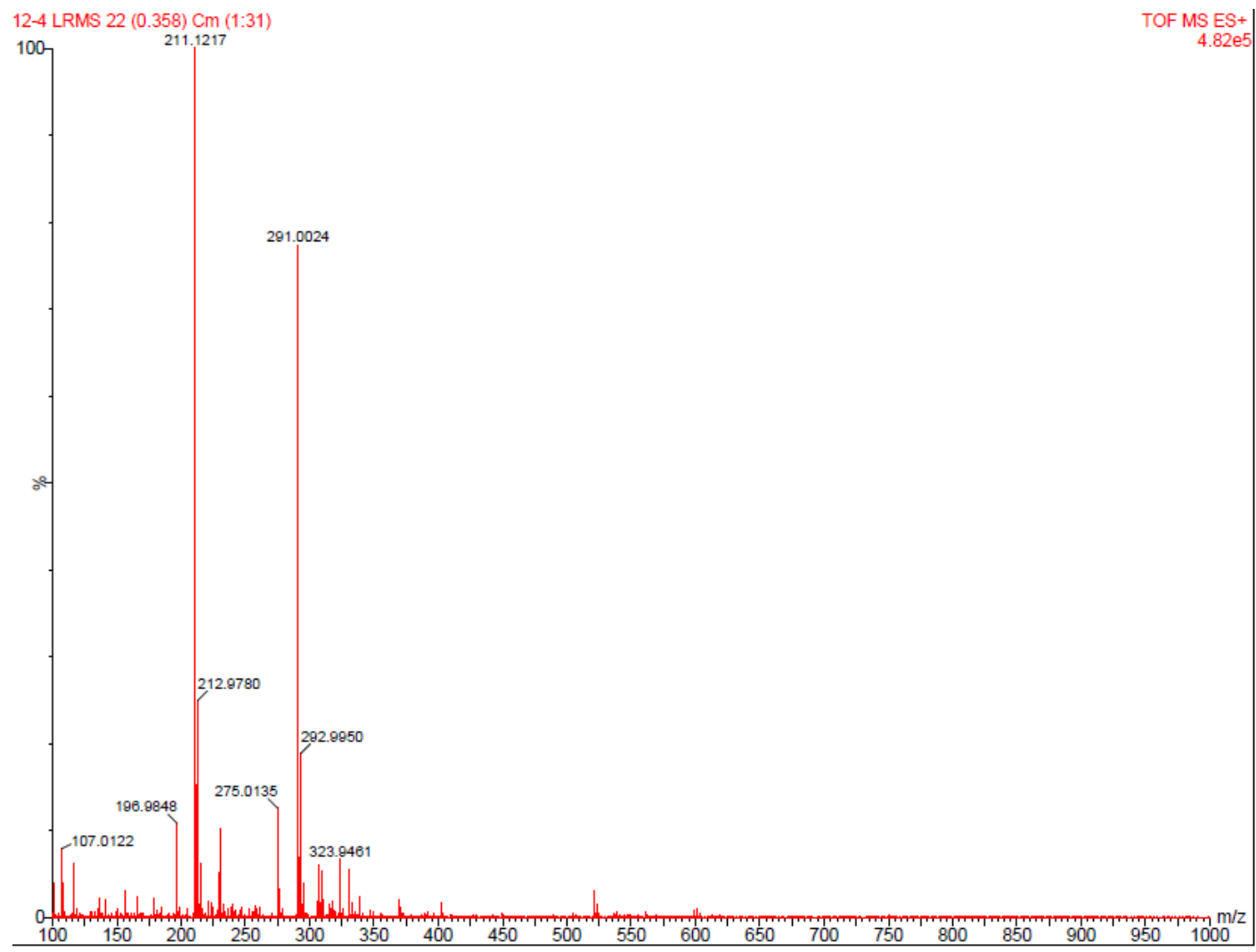


Figure S 4.22 Low resolution ESI mass spectrum of Pt<sub>3</sub>-Cl.



## Experimental

### 4'-pyridyl-2,2':6',2''-terpyridine (qpy)

2-acetylpyridine (5 g, 4.13 mol), was added to a suspension of NaOH in polyethylene glycol (PEG 300) (35 mL) and the reaction mixture was stirred for 10 minutes at 0 °C. 4-pyridine carboxaldehyde (2.21 g, 2.06 mol) was added to the suspension and left at 0 °C for 2 hours. The reaction mixture was stirred manually in every 15 minutes due to the high viscosity of the reaction mixture. After this time, excess  $\text{NH}_4\text{OAc}$  (10 g) was added and the suspension was heated at 100 °C for 2 hours. Brown precipitate was formed from the initially formed red solution. Water (75 mL) was added to the precipitate. The precipitate was filtered, washed with more water (50 mL) followed by cold ethanol (10 mL). The ligand was recrystallized from ethanol. Yield: 3.5 g, (55 %). Crystal good for X-ray determinations were obtained by recrystallizing the ligand in ethanol and slow evaporation of the solvent.

### Preparation of about 0.1 M Ruthenium(III) Solution

$\text{RuCl}_3 \cdot 3\text{H}_2\text{O}$  (~1.5 g, 5.7 mmol) was refluxed in a mixture (70 mL) of a 1 M HCl and EtOH (v:v = 1:1) for 3 hours. The mixture was cooled and filtered. The filtrate was reduced *in vacuo* to 10 mL. An aqueous solution of 1 M HCl was used to dilute the solution to the required acidified ~ 0.1 M Ru(III) solution.

### [Ru(tpy)Cl<sub>3</sub>]

Equal amounts of  $\text{RuCl}_3 \cdot 3\text{H}_2\text{O}$  (~150 mg, 0.574 mmol) and terpyridine were refluxed in absolute EtOH (125 mL) for 3 hours. The resulting reaction mixture was cooled to room temperature and the precipitate was filtered, washed with cold absolute EtOH (5 mL) followed by copious amount of diethylether and dried under *vacuo*. Yield: 191 mg, 433  $\mu\text{mol}$ , (76 %), brown precipitate.

### [Ru(qpy)Cl<sub>3</sub>]

The Ru moiety was synthesized following the literature. The ligand qpy (100 mg; 0.323 mmol) was refluxed in MeOH (25 mL) until it dissolved. To this solution, a 0.1 M Ru(III) solution (3.25 mL; 0.33 mmol) was added drop-wisely. The reaction mixture was refluxed for 1.5 hours. The precipitated crude product was filtered hot. The filtrate was cooled to 253 K, which resulted in the precipitation of a relatively pure product. The product was filtered and dried. Yield: 84 mg, 0.162 mmol (49%).

**Ru(qpy)(tpy)Cl<sub>2</sub>**

This Ru moiety was synthesized by a slight modification of the literature method.<sup>11c</sup> To a filtered solution of AgBF<sub>4</sub> (240 mg; 1.232 mmol) in acetone (15 mL), [Ru(tpy)Cl<sub>3</sub>] (40 mg; 0.080 mmol) was added. The reaction mixture was refluxed for 18 hours in the dark after which the precipitated AgCl was removed by filtration. The filtrate was concentrated to 1 mL in *vacuo*. Into the resulting green oil the ligand qpy (43 mg, 0.148 mmol) was added and the mixture was refluxed for 2 hours in DMF (20 mL) which reduced Ru(III) to Ru(II). The reaction mixture was filtered and concentrated in *vacuo* to (1.0 mL) which gave a red oil. A saturated solution of LiCl (2 mL) in EtOH was added to the red oil. A precipitate was formed on adding the oil to acetone (200 mL). The precipitate obtained was purified by column chromatography on neutral alumina using CH<sub>3</sub>CN: EtOH (50: 50) as the eluent. The first red band was collected and was lyophilised with diethylether. Recrystallization of the precipitate with a mixture of MeOH and diethylether yielded a relatively pure product.

**[Ru(qpy)<sub>2</sub>]Cl<sub>2</sub>**

The Ru moiety was synthesized by a slight modification of the literature method.<sup>11c</sup> To a filtered solution of AgBF<sub>4</sub> (350 mg; 1.798 mmol) in acetone (20 mL), [Ru(qpy)Cl<sub>3</sub>] (68.9 mg; 0.133 mmol) was added. The reaction mixture was refluxed for 18 hours in the dark after which the precipitated AgCl was removed by filtration. The filtrate was concentrated to 1 mL in *vacuo*. To the resulting green oil, the ligand qpy (46 mg, 0.147 mmol) was added and the mixture was refluxed for 2 hours in DMF (25 mL) which reduced Ru(III) to Ru(II). The reaction mixture was cooled to room temperature and filtered. The red filtrate was reduced to 1 mL to afford a red oil. A saturated solution of LiCl (6 mL) in EtOH was then added to the red oil. A precipitate was formed on adding acetone (400 mL). The precipitate was purified by column chromatography on neutral alumina using acetone: MeOH: EtOH (3: 6: 1) as the eluent. The first red band was collected and lyophilized with diethylether gave a relatively pure product.

**Pt(en)Cl<sub>2</sub>**

The platinum complex was synthesized following a literature procedure.<sup>31</sup> Into an aqueous solution of K<sub>2</sub>PtCl<sub>4</sub> (125 mg, 0.300 mmol), an aqueous solution of ethane-1,2-diamine (0.018, 0.300 mmol) was added drop wise. The pH of the solution was brought to 6. The reaction mixture was stirred at 313 K. During the reaction, the pH of the solution was maintained between 5- 6 using 0.1 M NaOH. The reaction was stopped

when the pH of the solution no longer changed. The yellow precipitate which formed was filtered, washed with water and ethanol and dried.

Yield: 0.068 g, (70%), yellow powder.  $^1\text{H}$ NMR (400 MHz, DMF)  $\delta$ / ppm: 5.54 (4H, br, NH), 2.79 (4H, br),  $^{195}\text{Pt}$  (-3298).

### **Pt2-Cl**

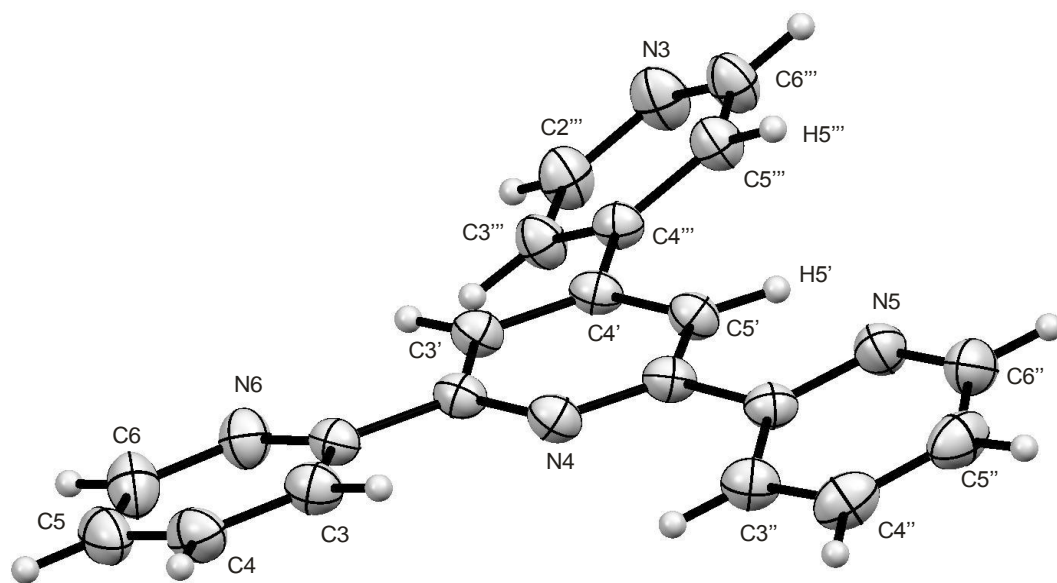
This compound was synthesized by a slight modification of the literature method.<sup>11c</sup> To a stirred solution of  $[\text{Pt}(\text{en})(\text{py})\text{Cl}]\text{Cl}$  (56 mg, 0.168 mmol) in 5 mL of DMF at 310 K,  $\text{AgNO}_3$  (28 mg, 0.168 mmol) in DMF (10 mL) was added drop wise over three hours. Subsequently the reaction mixture was stirred for 24 hours at 313 K. After removing the formed AgCl precipitate using a 0.45  $\mu\text{m}$  nylon membrane filter (Millipore),  $[\text{Ru}(\text{tpy})(\text{qpy})]\text{Cl}_2$  (120 mg, 0.168 mmol) was added to the filtrate and the mixture was stirred for another 18 hours. The reaction mixture was cooled to room temperature and filtered. The filtrate was concentrated in *vacuo* and co-evaporated three times with EtOH/MeOH (50: 50) (20 mL) to remove DMF. The precipitate formed was redissolved in MeOH. The desired product was precipitated with slow addition of diethylether.

### **Pt3-Cl**

The compound was synthesized by a slight modification of the literature method.<sup>11c</sup> To a stirred solution of  $[\text{Pt}(\text{en})(\text{py})\text{Cl}]\text{Cl}$  (84 mg, 0.252 mmol) in 20 mL of DMF at 310 K,  $\text{AgNO}_3$  (43 mg, 0.252 mmol) in DMF (15 mL) was added drop wise over three hours. Subsequently the reaction mixture was stirred for 24 hours at 313 K. After removing the formed AgCl precipitate using a 0.45  $\mu\text{m}$  nylon membrane filter (Millipore),  $[\text{Ru}(\text{qpy})_2\text{Cl}_2]$  (100 mg, 0.126 mmol) was added to the filtrate and the mixture was stirred for another 18 hours. The reaction mixture was cooled to room temperature and filtered. The filtrate was concentrated in *vacuo* and co-evaporated three times with EtOH/MeOH (50: 50) (25 mL) to remove DMF. The precipitate formed was redissolved in MeOH. The desired product was precipitated with slow addition of diethylether.

### X-ray Crystallography

Needle-like crystals good for X-ray crystallography were obtained by recrystallizing the ligand in ethanol. The X-ray crystal structure obtained for qpy ligand which shows that the qpy ligand is not planar. The terminal pyridine ring systems adopt a *trans-trans* conformation about the interannular bonds C2—C2' and C6'—C2'' (Figure S4.23, Table S4.12) as reported previously for terpyridine and 4'-functionalized terpyridine ligand systems. Of particular interest is the C5'''—C4'''—C4'—C5' torsion angle since this has been shown to be important in determining the crystal structures of platinum complexes of the 4'-pyridyl (terpyridine) ligand systems. The value is 25.95°, showing a large twist of the 4'-pyridyl group about the C4'''—C4' interannular bond *i.e.* the 4'-pyridyl group twists out of the plane of the central pyridine ring by a large amount in order to minimise steric repulsion between the methyl group and the hydrogen atom attached to C5'.



**Figure S 4.23** Perspective view showing the molecular geometry and atom numbering scheme for the qpy ligand. Non-H atoms are drawn as 50% thermal ellipsoids and the H atoms as spheres of arbitrary radius.

**Table S 4.12** Crystal structure, data collection and refinement details

<b>Parameter</b>	
Empirical formula	C10 H7 N2
Formula weight	155.18
Temperature	100(2) K
Wavelength	0.71073 Å
Crystal system	Orthorhombic
Space group	pbcn
Unit cell dimensions	$a = 11.082(5) \text{ Å}$ $\alpha = 90.000(5)^\circ$ $b = 11.408(5) \text{ Å}$ $\beta = 90.000(5)^\circ$ $c = 12.140(5) \text{ Å}$ $\gamma = 90.000(5)^\circ$
Volume	$1534.8(12) \text{ Å}^3$
Z	8
Density (calculated)	$1.343 \text{ Mg/m}^3$
Absorption coefficient	$0.083 \text{ mm}^{-1}$
F(000)	648
Crystal size	$0.10 \times 0.100 \times 0.35 \text{ mm}^3$
Theta range for data collection	$2.56 \text{ to } 31.08^\circ$
Index ranges	$-15 \leq h \leq 16, -16 \leq k \leq 16, -12 \leq l \leq 17$
Reflections collected	9744
Independent reflections	2440 [ $R(\text{int}) = 0.0319$ ]
Completeness to $\theta = 25.00^\circ$	99.3 %
Refinement method	Full-matrix least-squares on $F^2$
Data / restraints / parameters	2440 / 0 / 111
Goodness-of-fit on $F^2$	1.041
Final R indices [ $I > 2\sigma(I)$ ]	$R1 = 0.0519, wR2 = 0.1421$
R indices (all data)	$R1 = 0.0713, wR2 = 0.1563$
Largest diff. peak and hole	0.308 and $-0.224 \text{ e.Å}^{-3}$

**Table of Contents- 5**

List of Figures.....	ii
List of Tables.....	ii
List of Schemes .....	ii
Chapter Five.....	1
<b>Understanding the Role of Flexible 4'-Functionalised Polyethylene glycoxy Chains on the Behaviour of Platinum(II) (4'-(ethylene glycoxy)-2,2':6',2''-terpyridine- A kinetic and a Mechanistic Study .....</b>	<b>1</b>
5.0    Abstract .....	1
5.1    Introduction.....	1
5.2    Experimental.....	4
5.2.1    Materials.....	4
5.2.2    Synthesis of Ligands .....	4
5.2.3    Synthesis of Platinum(II) Complexes .....	5
5.2.4    Physical Measurements.....	7
5.2.5    Computational Modelling.....	7
5.2.6    Kinetic Analyses .....	7
5.3    Results and Discussion.....	10
5.3.1    Synthesis and Characterization .....	10
5.3.2    DFT Calculations .....	11
5.3.3    Kinetics.....	14
5.4    Conclusions.....	19
5.5    References .....	20
5.6    Supporting Information.....	24

**List of Figures**

Figure 5.1	Structures of polyethylene glycoxy appended Pt(II) complexes studied. Shown on the diagram is the numbering scheme used. Ptppy is included for reference. ....	3
Figure 5.2	Kinetic trace for the reaction of Ptppydeg ( $4.0 \times 10^{-5}$ M) with TU ( $6.0 \times 10^{-4}$ M) in methanol solution ( $I = 0.02$ M) at 330 nm at 298 K. ....	8
Figure 5.3	Dependence of the <i>pseudo</i> first-order rate constants ( $k_{\text{obs}}$ ) on the concentrations of the nucleophiles for the chloride substitution from Ptppydeg ( $4.0 \times 10^{-5}$ M) in methanol solution ( $I = 0.02$ M) at 298 K. ....	9
Figure 5.4	Eyring plots obtained for Ptppydeg with the nucleophiles for the forward reactions over the temperature range 15 - 35 °C. ....	10
Figure 5.5	DFT calculated minimum energy structures, frontier molecular orbitals (HOMO and LUMO) and the planarity of the complexes investigated. Included is the data obtained for the DFT calculated Ptppy complex for comparisons. ....	13
Figure 5.6	Aerial view showing the angles of inclination, $\alpha$ , of the pendant units in the DFT calculated structures of Ptppyeg and Ptppytdeg. ....	18

**List of Tables**

Table 5.1	Summary of DFT calculated data for the complexes investigated. Included is the data obtained for the DFT calculated Ptppy complex for comparisons. ....	12
Table 5.2	Summary of second-order rate constants, $k_2$ and activation parameters, with the corresponding standard deviations for the substitution of the chloro ligand by a series of thiourea nucleophiles and iodide at $I = 0.02$ M $\text{LiCF}_3\text{SO}_3$ , adjusted with LiCl. Given in brackets for TU is the data for Ptppy taken from literature and included for comparison. ....	16

**List of Schemes**

Scheme 5.1	Proposed mechanism for the substitution of chloride ligand from the Pt(II) complexes. ....	14
------------	--	----

# Chapter Five

## Understanding the Role of Flexible 4'-Functionalised Polyethylene glycoxy Chains on the Behaviour of Platinum(II) (4'-(ethylene glycoxy)-2,2':6',2''-terpyridine- A kinetic and a Mechanistic Study

### 5.0 Abstract

The ligand substitution kinetics of 4'-functionalized mono nuclear Pt(II) (4'-(ethylene glycoxy)-2,2':6',2''-terpyridine complexes of the form;  $[\text{Pt}(\text{nY-tpy})\text{Cl}]\text{Cl}$  (where Y = ethylene glycoxy, n = number of ethylene glycoxy units = 1, 2, 3 and 4, tpy = 2,2':6',2''-terpyridine) with thiourea (TU), 1,3-dimethyl-2-thiourea (DMTU), 1,1,3,3-tetramethyl-2-thiourea (TMTU) and iodide ( $\text{I}^-$ ) were investigated under *pseudo* first-order conditions as a function of concentration and temperature by conventional stopped-flow technique. The observed first-order rate constants followed the simple rate law  $k_{\text{obs}} = k_2[\text{Nu}]$ . The data obtained shows that the ethylene glycoxy pendant, *trans* to the leaving group, acts as a  $\sigma$ -donor into the terpyridine ligand and is effective only up to n = 1, beyond which the substitution reactivity of the complexes are controlled by the steric influence of the appended ethylene glycoxy pendant units, which decreases with the increase in the number of ethylene glycoxy units. The activation parameters obtained support an associative mode of mechanism, where bond formation in the transition state is favoured. The observed reactivity trends were supported by density functional theory (DFT) calculations.

### 5.1 Introduction

The tridentate N-donor ligand, 2,2':6',2''-terpyridine, also known as tpy, first reported by Burstall<sup>1</sup> and Morgan,<sup>1-2</sup> is one of the most attractive ligands for metal coordination. The ligand has very rich chemistry since it can easily form transition metal complexes with potential applications in various fields such as biochemistry, photochemistry,<sup>3</sup> nanoscience and supramolecular chemistry.<sup>4</sup> In the biomedical applications, terpyridine and its derivatives are used as potential sensors for tumour cells<sup>5</sup> due to their ability to interact with double strand DNA and proteins.<sup>3c,6</sup> Some complexes of terpyridine were found to be cytotoxic against human ovarian cancer.<sup>6b,7</sup> However, interactions of some of these complexes with certain biomolecules such as sulfur



donors were found to exhibit toxic side effects.<sup>8</sup> Therefore, the search for obtaining better cytotoxic agents with improved side effects is of great focus. So there is need for investigating the mechanism of interactions of these compounds with biomolecules and DNA.

Recent synthetic techniques have opened new possibilities for the synthesis of functionalized terpyridine complexes. More importantly, functionalization in the 4' position by using substituted terpyridine ligands such as 4'-chloro-terpyridine or 4'-hydroxyterpyridine derivatives are of great interest today.<sup>9</sup> However, applications of functionalized terpyridine complexes have not been fully studied.

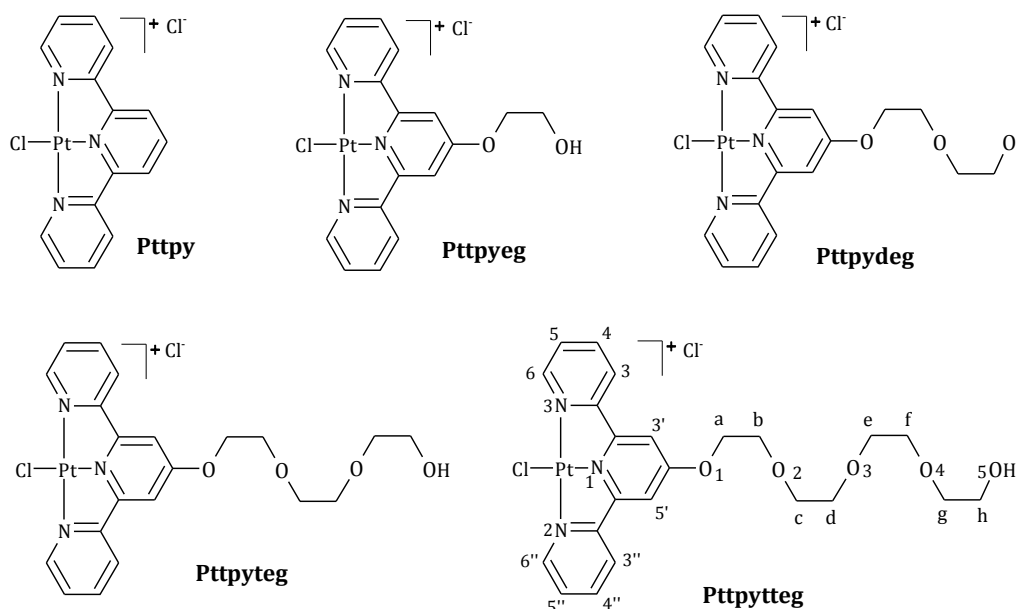
In this regard, square planar terpyridine derivatives are useful models for studying the substitution behaviour of Pt(II) complexes.<sup>9b,10</sup> Only the ligand in the fourth coordinate position of terpyridine is replaced in a simple substitution reaction.<sup>11</sup> During substitution, the  $\pi$ -acceptor orbitals of pyridine units in terpyridine ligand accept the electrons from metal centre including those from the incoming ligand and stabilizes the transition state intermediate.<sup>12</sup> This  $\pi$ -acceptor effect is responsible for the high reactivity of the unfunctionalized Pt(II) terpyridine type complexes. Literature data focusing on understanding the substitution kinetics of unfunctionalized terpyridine complexes and its derivatives is available.<sup>9b,10,13</sup>

Mono nuclear Pt(II) terpyridine complexes have been useful in understanding the effect of a non-carrier ligand on the rate of substitution at the metal centres.<sup>14</sup> It has been illustrated from previous studies, that the structure and the electronic properties of the chelate ligand backbone control the rate of the ligand substitution of square planar metal complexes.<sup>10,15</sup> Furthermore, it has also been established that the degree of lability of the leaving group is influenced by the  $\sigma$  and  $\pi$ - structural features of the ancillary group of the terpyridine ligand system.<sup>10,15</sup>

The effect of the ancillary group on the  $\pi$ -acceptor property of the terpyridine complexes of the form:  $[\text{Pt}(\text{R-tpy})\text{X}]^+$  (where R = H; Ph; Ph(o-CH<sub>3</sub>); Ph(o-Cl); where Ph = phenyl group, X = Cl, OH) has been investigated previously.<sup>10,13g,15h</sup> Data obtained from these studies reveals that electron withdrawing groups on the terpyridine ancillary ligand increases the rate of ligand substitution while electron donating groups have the opposite effect. The influence of the ligand substitution is also controlled by the extent of the  $\pi$ -backbonding from the metal centre to the terpyridine ligand backbone.<sup>10,15</sup>

Basolo *et al.*<sup>16</sup> and Tobe *et al.*<sup>17</sup> reported that substitution kinetics of bis(2-pyridylmethyl)amine complexes possessing appending ancillary groups on the *trans* position of the non-labile ligand system showed that the *trans* effect was more dominant over  $\pi$ -acceptor effect. When electron donating head groups were attached to the *trans* N atom, an increase in the rate of ligand substitution was observed.<sup>18</sup> This increase in the reactivity was thought to be due to the increased ground state stabilization caused by the *trans* effect of the appended group. Structural variations due to such appending groups were thought to enhance the anti-tumour activity of the complex in biological systems.<sup>19</sup>

To extend this understanding we functionalized the terpyridine at 4'-position by polyethylene glycoxy groups. We have investigated the ligand substitution behaviour of 4'-functionalized mono nuclei Pt(II) terpyridine complexes of the form;  $[\text{Pt}(\text{nY-tpy})\text{Cl}]\text{Cl}$  (where Y = ethylene glycoxy, n = number of ethylene glyco units = 1, 2, 3 and 4, tpy = 2,2':6',2''-terpyridine) with TU, DMTU, TMTU and I. The length of the polyethylene glycoxy tail is systematically increased by incorporating base 2 – 4 units. It is our expectation that the results of this study will reveal the role of flexible poly glycoxy pendant groups on the substitution reactions of Pt(II) terpyridine. The structures of the investigated complexes are shown in *Figure 5.1*.



**Figure 5.1** Structures of polyethylene glycoxy appended Pt(II) complexes studied. Shown on the diagram is the numbering scheme used. Pttpy is included for reference.

## 5.2 Experimental

### 5.2.1 Materials

Methanol (Merck) was distilled over magnesium<sup>20</sup> prior to use for kinetic analysis. Dimethylsulfoxide (99.9%) from Aldrich was used without any further purification. Ethylene glycol (99.8%), diethylene glycol (99%) and triethylene glycol (99%) were bought from Sigma Aldrich. The ligand, 4'-chloro,2,2':6',2''-terpyridine (97%), tetraethylene glycol (99%), and the platinum salt, potassium tetrachloroplatinate (II) (99.9%) were bought from Aldrich. All other chemicals were purchased from Sigma Aldrich and were used without further purification.

### 5.2.2 Synthesis of Ligands

The syntheses of ligands were carried out by literature procedures.<sup>21</sup> To a suspension of KOH in dry DMSO at 50 °C was added the ethylene glycol and its respective polymer (n = 2, 3, 4) in excess. After stirring for 30 minutes, 4'-chloro-2,2':6',2''-terpyridine was added and the reaction mixture stirred for 20 hours at this temperature. Upon cooling to room temperature, the reacting mixture was treated with deionised water and filtered. The crude product was extracted from the filtrate in dichloromethane (3 x 30 mL) dried over anhydrous magnesium sulfate and the solvent removed. 4'-[2-(2-Hydroxyethoxy)ethoxy]-2,2':6',2''-terpyridine (**tpyeg**) and 4'-[2-(2-Hydroxyethoxy)ethoxy]-2,2':6',2''-terpyridine (**tpydeg**) gave a white paste and a white powder respectively. Crude products were purified in THF to give white solids. Ligands, 4'-{2-[2-(2-Hydroxyethoxy)ethoxy]ethoxy-2,2':6',2''-terpyridine (**tpyteg**) and 4'-{2-[2-(2-Hydroxyethoxy)ethoxy]ethoxy}ethoxy}-2,2':6',2''-terpyridine (**tpytteg**) yielded pale yellow oils, pure enough for platination.

The purity of the ligands was confirmed by <sup>1</sup>H NMR and mass spectroscopy. The <sup>1</sup>H NMR spectra obtained show similarity in the aromatic region for the ligands.

**(tpyeg):** Yield: 250 mg, (70%), off white paste. <sup>1</sup>H NMR (400 MHz, CDCl<sub>3</sub>)<sup>†</sup> δ / ppm: 8.63 (d, 2H, 6 6''), 8.55 (2H, d, 3 3''), 7.99 (2H, s, 3' 5'), 7.79 (dt, 2H, 4 4''), 7.29 (dt, 2H, 5 5''), 4.23 (t, 2H, CH<sub>2</sub>), 3.97 (t, 2H, CH<sub>2</sub>). <sup>13</sup>C NMR (77 MHz, CDCl<sub>3</sub>), δ / ppm: 61.1, 69.6, 107.6, 121.5, 123.8, 136.9, 148.9, 155.6, 157.2, 167.1. TOF MS-ES<sup>+</sup>, m/z: 316.1062, (M+Na)<sup>+</sup>.

---

<sup>†</sup> s = singlet, d = doublet, t = triplet, dt = doublet of a triplet. The same representation is used for the other complexes.

**(tpydeg):** Yield: 190 mg, (80%), white powder.  $^1\text{H}$  NMR (400 MHz,  $\text{CDCl}_3$ )  $\delta$ / ppm: 8.69 (d, 2H, 6''), 8.62 (d, 2H, 3''), 8.13 (s, 2H, 3' 5'), 7.87 (t, 2H, 4''), 7.35 (t, 2H, 5''), 4.46 (t, 2H,  $\text{CH}_2$ ), 3.94 (t, 2H,  $\text{CH}_2$ ), 3.77 (t, 2H,  $\text{CH}_2$ ), 3.69 (t, 2H,  $\text{CH}_2$ ).  $^{13}\text{C}$  NMR (77 MHz,  $\text{CDCl}_3$ )  $\delta$  / ppm: 61.7, 68.1, 69.9, 72.8, 108.3, 121.6, 124.0, 137.1, 148.9, 155.7, 156.7, 167.3. *Anal. Calc. for  $\text{C}_{19}\text{H}_{19}\text{N}_3\text{O}_3$ :* C, 67.64; H, 5.68; N, 12.46; *Found:* C, 68.00; H, 5.81; N, 11.97. TOF MS-ES $^+$ ,  $m/z$ : 360.1324,  $(\text{M}+\text{Na})^+$ .

**(tpyteg):** Yield: 175 mg, colourless oil (70%).  $^1\text{H}$  NMR (400 MHz,  $\text{CDCl}_3$ )  $\delta$ / ppm: 8.66 (d, 2H, 6''), 8.59 (d, 2H, 3''), 8.03 (s, 2H, 3' 5'), 7.83 (t, 2H, 4''), 7.31 (t, 2H, 5''), 4.40 (t, 2H,  $\text{CH}_2$ ), 3.92 (t, 2H,  $\text{CH}_2$ ), 3.73 (m, 4H,  $\text{CH}_2$ ), 3.69 (t, 2H,  $\text{CH}_2$ ), 3.60 (t, 2H,  $\text{CH}_2$ ).  $^{13}\text{C}$  NMR (77 MHz,  $\text{CDCl}_3$ )  $\delta$  / ppm: 61.7, 67.9, 69.8, 70.4, 71.0, 72.9, 107.8, 121.4, 123.9, 136.9, 148.9, 155.9, 157.0, 167.1. TOF MS-ES $^+$ ,  $m/z$ : 404.1580,  $(\text{M}+\text{Na})^+$ .

**(tpyttg):** Yield: 183 mg, (74%), pale brown oil.  $^1\text{H}$  NMR (400 MHz,  $\text{CDCl}_3$ )  $\delta$ / ppm: 8.38 (d, 2H, 6''), 8.30 (d, 2H, 3''), 7.72 (s, 2H, 3' 5'), 7.58 (t, 2H, 4''), 7.07 (t, 2H, 5''), 4.11 (t, 2H,  $\text{CH}_2$ ), 3.63 (t, 2H,  $\text{CH}_2$ ), 3.44 (t, 2H,  $\text{CH}_2$ ), 3.37 (m, 6H,  $\text{CH}_2$ ), 3.27 (m, 4H,  $\text{CH}_2$ ).  $^{13}\text{C}$  NMR (77 MHz,  $\text{CDCl}_3$ )  $\delta$ / ppm: 39.5, 40.6, 42.4, 60.9, 60.9, 67.5, 69.1, 69.8, 70.0, 70.2, 70.3, 70.5, 72.5, 72.5, 107.2, 121.1, 123.8, 136.8, 148.8, 155.4, 156.7, 166.7. TOF MS-ES $^+$ ,  $m/z$ : 448.1848,  $(\text{M}+\text{Na})^+$ .

### 5.2.3 Synthesis of Platinum(II) Complexes

The synthesis of the complexes was carried out using the following procedure: To a stirred solution of  $[\text{Pt}(\text{cod})\text{Cl}_2]^{15\text{h}}$  in dry methanol at room temperature, a suspension of the ligand in dry methanol was added at 55 °C. The reaction mixture was stirred for 24 hours at the same temperature, after which the solution was cooled and filtered. When the bright yellow filtrate was concentrated under *vacuo*, the desired compound precipitated as pale yellow solid. The compound was filtered, washed with chloroform (20 mL), cold methanol (1 x 5 mL), diethylether (2 x 15 mL) and dried and stored in a desiccator.

The identity and the purity of the final complexes were confirmed by using  $^1\text{H}$  NMR,  $^{13}\text{C}$  NMR,  $^{195}\text{Pt}$  NMR, elemental analyses, IR and mass spectroscopy. The  $^1\text{H}$  NMR spectra obtained show similarity in the aromatic region. Presence of a peak at about -2700 ppm on the  $^{195}\text{Pt}$  NMR spectra confirms the  $\text{Pt}(\text{NNN})$  coordination.

**(Ptppyeg):** Yield: 35 mg, (55%), pale yellow powder.  $^1\text{H}$  NMR (400 MHz,  $\text{CD}_3\text{OH}$ )  $\delta$ / ppm: 10.23 (2H, d, 6  $6''$ ), 9.79 (2H, d, 3  $3''$ ), 9.78 (t, 2H, 4  $4''$ ), 9.39 (2H, s, 3' 5'), 9.20 (t, 2H, 5  $5''$ ), 5.88 (t, 2H, CH<sub>2</sub>), 5.44 (t, 2H, CH<sub>2</sub>).  $^{195}\text{Pt}$  NMR ( $\text{CD}_3\text{OH}$ )  $\delta$ / ppm: -2715. IR (4000-650  $\text{cm}^{-1}$ )  $\nu$ : 3237 (O-H), 3062 (C-H stretch), 1607 (C=H, pyridine), 1476 - 1423 (C-H stretch), 1222.43 (C-O), 788 (C-H stretch). *Anal. Calc. for*  $\text{C}_{17}\text{H}_{15}\text{Cl}_2\text{N}_3\text{O}_2$ : C, 36.51; H, 2.70; N, 7.51; *Found*: C, 36.38; H, 3.20; N, 7.92. TOF MS-ES+,  $m/z$ : 524.0482, (M+1)<sup>+</sup>.

**(Ptppydeg):** Yield: 46 mg, (64%), crystalline yellow powder.  $^1\text{H}$  NMR (400 MHz,  $\text{CD}_3\text{OH}$ )  $\delta$ / ppm: 9.76 (d, 2H, 6  $6''$ ), 9.67 (d, 4H, 3  $3''$ ), 9.65 (t, 2H, 4  $4''$ ), 9.17 (s, 2H, 3' 5'), 9.07 (t, 2H, 5  $5''$ ), 5.87 (t, 2H, CH<sub>2</sub>), 5.38 (t, 2H, CH<sub>2</sub>), 5.21 (t, 2H, CH<sub>2</sub>), 5.11 (t, 2H, CH<sub>2</sub>).  $^{13}\text{C}$  NMR (77 MHz,  $\text{CD}_3\text{OH}$ ),  $\delta$  / ppm: 62.26, 69.93, 72.01, 74.07, 112.07, 126.95, 130.28, 142.73, 152.27, 156.70, 159.58, 170.89.  $^{195}\text{Pt}$  NMR ( $\text{CD}_3\text{OH}$ )  $\delta$ / ppm: -2705. IR (4000-650  $\text{cm}^{-1}$ )  $\nu$ : 3338 (O-H), 3071 (C-H stretch), 1607 (C=H, pyridine), 1476 - 1430 (C-H stretch), 1219 (C-O), 773 (C-H stretch). *Anal. Calc. for*  $\text{C}_{19}\text{H}_{21}\text{Cl}_2\text{N}_3\text{O}_4$ : C, 37.73; H, 3.41; N, 6.76; *Found*: C, 37.35; H, 3.75; N, 6.34. TOF MS-ES+,  $m/z$ : 568.0847, (M+1)<sup>+</sup>.

**(Ptppyteg):** Yield: 38 mg, dark orange powder (60%).  $^1\text{H}$  NMR (400 MHz,  $\text{CD}_3\text{OH}$ )  $\delta$ / ppm: 9.98 (dd, 2H, 6  $6''$ ), 9.73 (s, 2H, 3' 5'), 9.71 (d, 2H, 3  $3''$ ), 9.29 (t, 2H, 4  $4''$ ), 9.13 (t, 2H, 5  $5''$ ), 5.90 (t, 2H, CH<sub>2</sub>), 5.40 (t, 2H, CH<sub>2</sub>), 5.22 (m, 2H, CH<sub>2</sub>), 5.14 (t, 2H, CH<sub>2</sub>), 5.11 (t, 2H, CH<sub>2</sub>), 5.04 (t, 2H, CH<sub>2</sub>).  $^{195}\text{Pt}$  NMR ( $\text{CD}_3\text{OH}$ )  $\delta$ / ppm: -2708. IR (4000-650  $\text{cm}^{-1}$ )  $\nu$ : 3332 (O-H), 3071 (C-H stretch), 1607 (C=H, pyridine), 1448 - 1429 (C-H stretch), 1220 (C-O), 774 (C-H stretch). *Anal. Calc. for*  $\text{C}_{21}\text{H}_{23}\text{Cl}_2\text{N}_3\text{O}_4$ : C, 38.96; H, 3.58; N, 6.49; *Found*: C, 38.48; H, 3.41; N, 6.32. TOF MS-ES+,  $m/z$ : 612.1027, (M+1)<sup>+</sup>.

**(Ptppytteg):** Yield: 30 mg, (65%), mustard yellow powder.  $^1\text{H}$  NMR (400 MHz,  $\text{CD}_3\text{OH}$ )  $\delta$ / ppm: 8.75 (d, 2H, 6  $6''$ ), 8.60 (d, 2H, 3  $3''$ ), 8.49 (t, 2H, 4  $4''$ ), 8.25 (s, 2H, 3' 5'), 7.90 (t, 2H, 5  $5''$ ), 4.51 (t, 2H, CH<sub>2</sub>), 3.90 (t, 2H, CH<sub>2</sub>), 3.67 (t, 2H, CH<sub>2</sub>), 3.60 (t, 2H, CH<sub>2</sub>), 3.53 (m, 4H, CH<sub>2</sub>), 3.47 (t, 2H, CH<sub>2</sub>), 3.40 (t, 2H, CH<sub>2</sub>).  $^{13}\text{C}$  NMR (77 MHz,  $\text{CD}_3\text{OH}$ ),  $\delta$ / ppm: 39.4, 40.7, 41.0, 60.7, 70.2, 70.4, 70.5, 72.8, 111.2, 125.3, 126.3, 129.9, 143.2, 155.9, 158.9, 169.5.  $^{195}\text{Pt}$  NMR ( $\text{CD}_3\text{OH}$ )  $\delta$ / ppm: -2710. IR (4000-650  $\text{cm}^{-1}$ )  $\nu$ : 3246 (O-H), 3064 (C-H stretch), 1607 (C=H, pyridine), 1476 - 1423 (C-H stretch), 1220 (C-O), 773 (C-H stretch). *Anal. Calc. for*  $\text{C}_{23}\text{H}_{27}\text{Cl}_2\text{N}_3\text{O}_5$ : C, 40.47; H, 3.54; N, 5.92; *Found*: C, 40.27; H, 3.17; N, 5.60. TOF MS-ES+,  $m/z$ : 657.1368, (M+1)<sup>+</sup>.

### 5.2.4 Physical Measurements

$^1\text{H}$  NMR and  $^{13}\text{C}$  NMR were recorded on either a Bruker Avance DPX 400 or 500 MHz spectrometer, at 303 K using  $\text{Si}(\text{CH}_3)_4$  as the reference for the chemical shifts.  $^{195}\text{Pt}$  NMR were done on a 500 MHz spectrometer ( $^{195}\text{Pt}$ , 107.5 MHz) chemical shifts externally referenced to  $\text{K}_2[\text{PtCl}_6]$ . Low resolution electron spray ionization (ESI<sup>+</sup>) mass spectra were recorded on a TOF Micromass spectrometer. Infrared (IR) spectra were recorded by using Perkin Elmer Spectrum 100 FT-IR spectrometer. Elemental analyses were performed by a Thermal Scientific Flash 2000. Kinetic analyses were studied on an Applied Photophysics SX 20 stopped-flow reaction analyser coupled with an online data acquisition system with controlled temperature within  $\pm 0.1$  °C. The wavelengths for the kinetic analysis were predetermined on Varian Cary 100 Bio UV/visible spectrophotometer with an attached Varian Peltier temperature-controller and an online kinetic application. X-ray crystal structure for the ligand qpy was solved using an Oxford Diffraction Xcalibur 2 CCD 4-circle diffractometer linked to an Oxford Cryostat System. The data collection was done at 100 K.

### 5.2.5 Computational Modelling

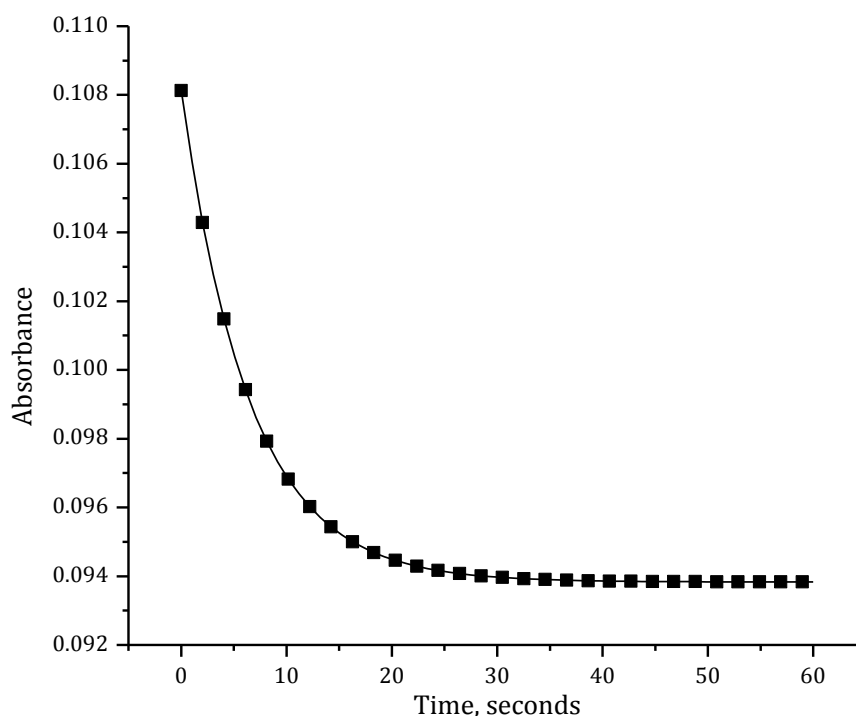
Computational modelling for the complexes was performed at Density Functional Theoretical (DFT) level based on B3LYP/LanL2DZ<sup>22</sup> (Los Alamos National Laboratory 2 double  $\xi$ ) level theory, with inner core electrons of Pt atom replaced by relative Effective Core Potential (ECP). Due to low electronic spin of Pt(II), the DFT calculations of the complexes were done at singlet state. The complexes were computed in methanol solution taking into account the solvolysis effect by means of the Conductor Polarizable Continuum Model (C-PCM).<sup>23</sup> The Gaussian09 suite of programs was used for all computational calculations.<sup>24</sup>

### 5.2.6 Kinetic Analyses

All kinetic measurements were performed under *pseudo* first-order conditions using at least 10-fold excess of the nucleophile in 0.02 M ionic solution, made by dissolving the required amount of  $\text{LiCF}_3\text{SO}_3$  (0.018 M) and  $\text{LiCl}$  (0.002 M) in dry methanol.  $\text{LiCl}$  was added to suppress the solvolysis reactions. Since  $\text{CF}_3\text{SO}_3^-$  does not coordinate with the Pt(II) metal centre<sup>25</sup>, all substitution kinetics were studied in this media.

Pt(II) complex solutions were prepared by dissolving the required amount of the complex in the ionic solution. Nucleophile solutions were prepared at 50 times the concentration of the Pt(II) complex. Subsequent dilutions of the nucleophile stock

solution afforded solutions of 10, 20, 30 and 40 times the concentration of metal complex. The wavelengths chosen for the kinetic investigations were pre-determined using UV/visible absorption spectra (See *Table S5.1*). A typical kinetic trace for the reaction of **Ptppydeg** with TU at 330 nm and 298 K is shown in *Figure 5.2* and *Figure S5.1*.



**Figure 5.2** Kinetic trace for the reaction of Ptppydeg ( $4.0 \times 10^{-5}$  M) with TU ( $6.0 \times 10^{-4}$  M) in methanol solution ( $I = 0.02$  M) at 330 nm at 298 K.

Substitution reactions were fast, and were studied on an Applied Photophysics SX 20 stopped-flow system coupled with an online data acquisition system. All measurements were carried out in a thermostatted environment to within  $\pm 0.1$  °C. All data were graphically analysed using the software package, Origin 7.5<sup>®26</sup> to determine the observed rate constants,  $k_{\text{obs}}$ . All kinetic data obtained were fitted to first-order exponential decay function to generate the observed *pseudo* first-order rate constants, ( $k_{\text{obs}}$ ), using *Equation 5.1*<sup>27</sup> at all concentrations and temperatures.

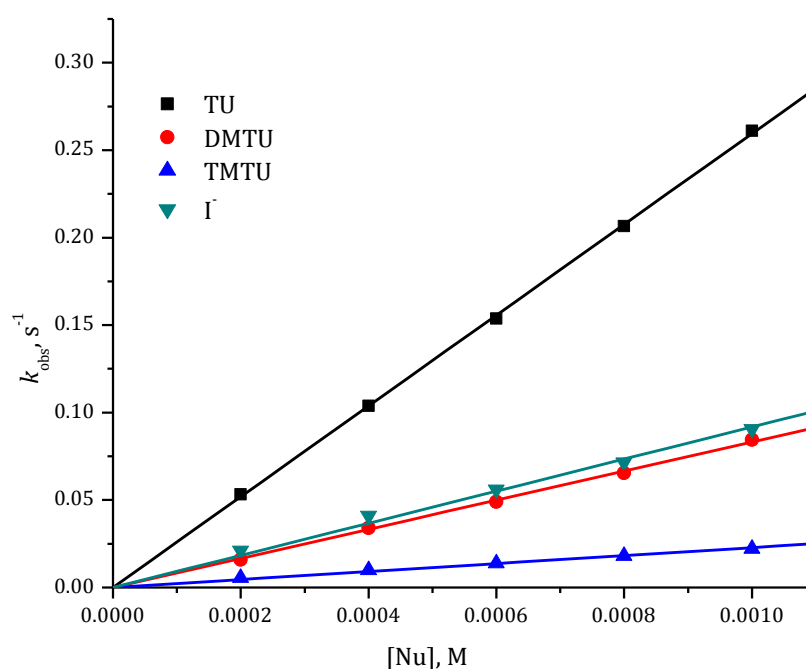
$$A_t = A_0 + (A_\infty - A_0) \exp(-k_{\text{obs}} t) \quad (5.1)$$

where  $A_0$ ,  $A_t$  and  $A_\infty$  represent the absorbance of the reaction mixture initially, at time,  $t$  and at the end of the reaction respectively.

The observed rate constants,  $k_{\text{obs}}$ , for the nucleophiles at different concentrations were determined in the same manner. The values used were averages of seven to ten independent runs. Linear graphs with zero intercepts were obtained for the nucleophiles studied. The second-order rate constants,  $k_2$ , for the reactions of the platinum complexes with the nucleophiles were obtained from the slopes and the intercepts of the graphs of  $k_{\text{obs}}$  versus the concentration of the nucleophiles (Equation 5.2).<sup>27</sup> Representative plots for **Ptptydeg**, shown in Figure 5.3 clearly indicate that the substitution reactions were first-order with respect to the incoming nucleophile.

$$k_{\text{obs}} = k_2[\text{Nu}] \quad (5.2)$$

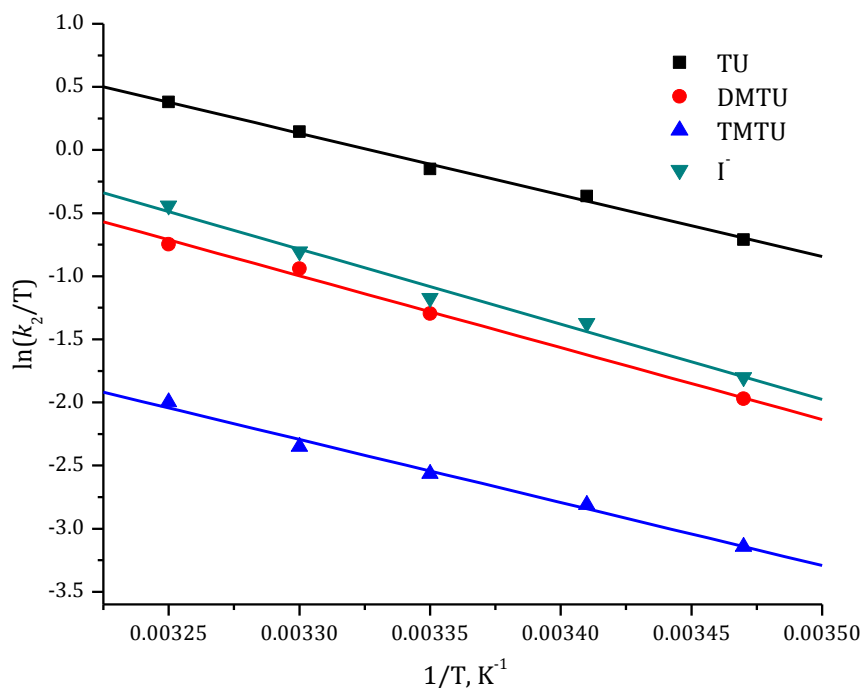
where  $k_2$  is the second-order rate constant.



**Figure 5.3** Dependence of the *pseudo* first-order rate constants ( $k_{\text{obs}}$ ) on the concentrations of the nucleophiles for the chloride substitution from Ptptydeg ( $4.0 \times 10^{-5}$  M) in methanol solution ( $I = 0.02$  M) at 298 K.



The temperature dependence studies were done in a similar manner, using a single nucleophile concentration in the temperature range 15 - 40 °C in 5 °C intervals. The activation parameters, entropy of activation ( $\Delta S^\ddagger$ ) and enthalpy of activation ( $\Delta H^\ddagger$ ) were obtained using the Eyring equation.<sup>27</sup> Figure 5.4 shows the representative plots obtained for **Ptppydeg** with the nucleophiles for the forward reactions with the nucleophiles. Representative graphs are also given in Figures S5.2 to S5.9.



**Figure 5.4** Eyring plots obtained for Ptppydeg with the nucleophiles for the forward reactions over the temperature range 15 - 35 °C.

## 5.3 Results and Discussion

### 5.3.1 Synthesis and Characterization

In this study, four square planar 4'-functionized Pt(II) terpyridine complexes of polyethylene glycoxy pendant groups, which vary by the number of appended ethylene glycoxy units or monomers, were synthesized and characterized. The ligands have been synthesized by different methods.<sup>21a,b,28</sup> Details of the synthesis and the spectroscopic data were given under experimental. The spectroscopic data obtained were in good agreement with the literature<sup>22b</sup> and the proposed chemical structures of the ligands and the complexes. To avoid the formation of the diterpyridine ligand, ethylene glycol reagent was added in large excess.<sup>21b</sup> Representative <sup>1</sup>H NMR, <sup>13</sup>C NMR, <sup>195</sup>Pt NMR, IR and mass spectra are given in Figure S5.10 to Figure S5.34 (Supporting Information). The peak due to the OH proton is not seen in any of the <sup>1</sup>H NMR spectra due to the

proton exchange with the solvent, methanol.<sup>28</sup> The  $^{195}\text{Pt}$  NMR signals for all the complexes appeared at around -2700 ppm, typical for  $\text{N}^{\wedge}\text{N}^{\wedge}\text{N}$  coordinated square planar Pt(II) centre.<sup>18,29</sup> Furthermore, the IR spectra of the complexes show distinct broad bands at around 3200 to 3300  $\text{cm}^{-1}$  due to the O–H stretches along with the C–H peaks at around 3000  $\text{cm}^{-1}$ .<sup>30</sup> Additionally, the crystal structure obtained for **Ptttpydeg** (Figure S5.35) confirms the synthesis of the anticipated complex. However, the compound could not be resolved to a satisfactory quality due to desolvation.

### 5.3.2 DFT Calculations

In order to obtain further insight on how the ethylene glycoxy pendant groups influence the substitution kinetics of the Pt(II) complexes, the electronic properties of the complexes were investigated at DFT level. The DFT calculated geometry optimized structures (also Table S5.2) along with the DFT calculated data are given in Figure 5.5 and Table 5.1 respectively. Table S5.3 (Supporting Information) shows that the geometry at the Pt(II) centre is slightly distorted square planar which is common to **Ptttpy** type of complexes.<sup>10,13g</sup>

When compared the DFT calculated natural bond orbital (NBO) charges on the platinum and  $\text{N}_{\text{trans}}$  atoms of **Ptttpy** and **Ptttpyeg**, the value for platinum decreases from **Ptttpy** to **Ptttpyeg**. The same is true for the charge on  $\text{N}_{\text{trans}}$ , i.e., it becomes more negative. This difference can be linked to the attachment of ethylene glycoxy pendant to the 4'-position of the parent **Ptttpy** molecule. However, when the NBO charges of the corresponding atoms of the ethylene glycoxy appended molecules (i.e. **Ptttpyeg** to **Ptttpytteg**) are compared, the values are observed to be constant. The results show that the inductive effect to the 4'-position of the complex is limited to the first glycoxy unit only. The subsequent units have little or no effect. This implies that the electronic effect beyond the first unit have little or no influence on the reactivity of the complexes.

Since reactivity parameters are explained by various associated electronic structure principles, the DFT calculated computational data was further analysed to understand the global chemical reactivity descriptors<sup>31</sup> such as chemical hardness ( $\eta$ , which relates to the thermodynamic stability of the molecule),<sup>32</sup> electronic chemical potential ( $\mu$ , which defines the electronegativity of the molecule) and electrophilicity index ( $\omega$ , which measures the propensity of a species to accept electrons).<sup>33</sup> DFT calculated  $\mu$  and  $\omega$  further support the observed changes in the NBO charges as already discussed. The electrophilicity index shows that the ability of the complex to accept electron decreases

from **Ptppy** to **Ptppyeg** after which it remains constant. This is an indication of reduction of  $\pi$ -backbonding ability of the terpyridine moiety from **Ptppy** to **Ptppyeg** due to the introduction of the attachment of ethylene glycoxy pendant.

**Table 5.1** Summary of DFT calculated data for the complexes investigated. Included is the data obtained for the DFT calculated Ptppy complex for comparisons.

Complex	Ptppy	Ptppyeg	Ptppydeg	Ptppyteg	Ptppytteg
<b>Bond Length (Å)</b>					
Pt1–Cl	2.446	2.445	2.446	2.446	2.446
Pt–N1(trans)	1.961	1.961	1.961	1.961	1.961
4'C–O1		1.368	1.368	1.368	1.386
N <sub>trans</sub> –O1		4.111	4.110	4.110	4.121
<b>Bond angles (°)</b>					
Elevation angle of ethylene glycoxy pendant ( $\alpha$ )		37.55	36.44	19.38	17.32
<b>NBO charges</b>					
Pt1	0.604	0.592	0.591	0.591	0.590
N1(trans)	-0.453	-0.471	-0.470	-0.471	-0.470
Cl	-0.502	-0.505	-0.505	-0.505	-0.504
$E_{\text{HOMO/eV}}$	-7.04	-6.87	-6.88	-6.87	-6.86
$E_{\text{LUMO/eV}}$	-3.35	-3.21	-3.22	-3.23	-3.24
$\Delta E$	3.69	3.66	3.66	3.64	3.62
Dipole moment	13.30	11.21	10.72	6.83	4.20
$\eta$ /eV	1.85	1.83	1.83	1.82	1.81
$\mu$ / eV	-5.20	-5.04	-5.05	-5.05	5.05
$\omega$ / eV	7.31	6.94	6.97	7.00	7.05

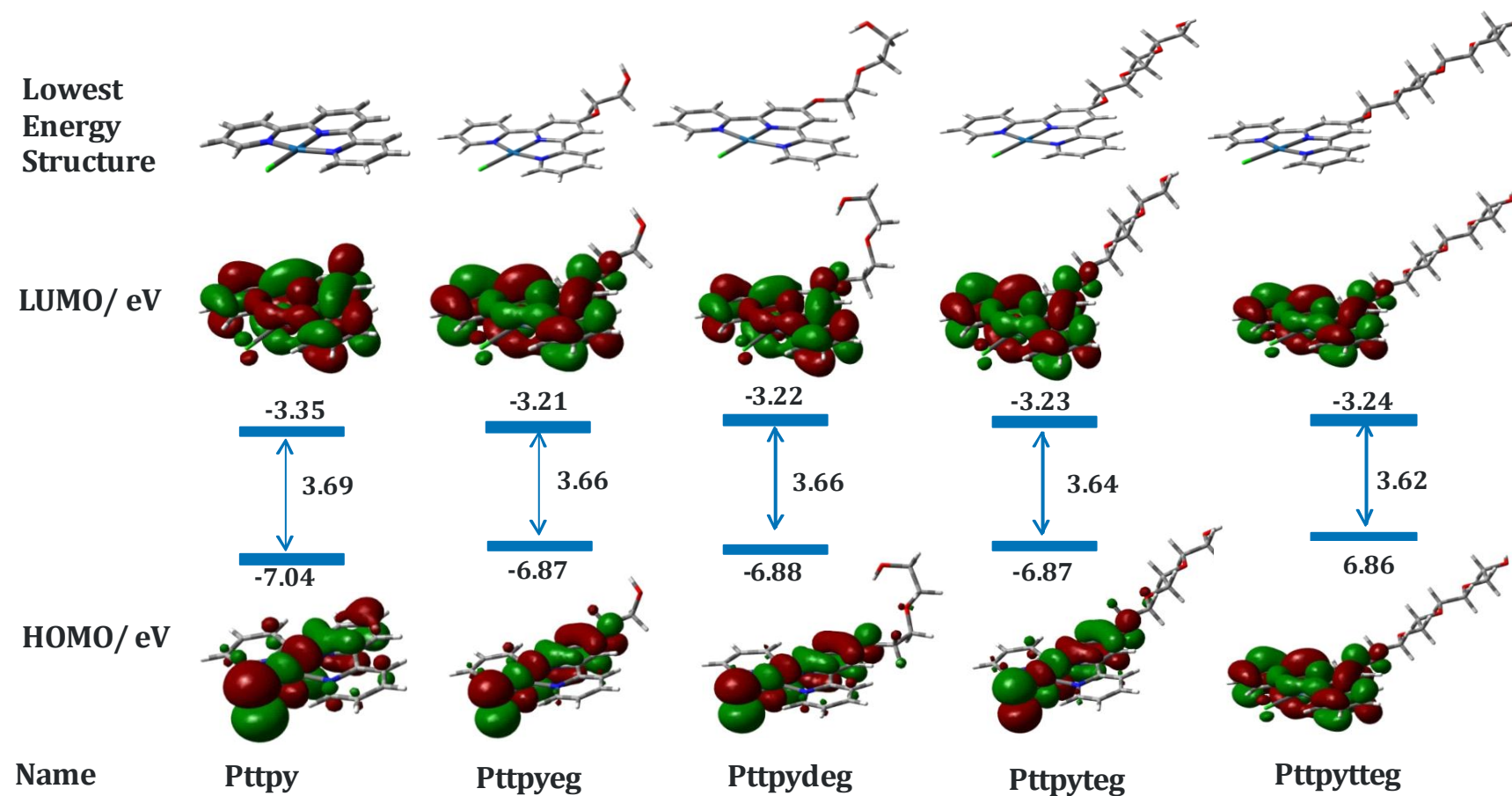
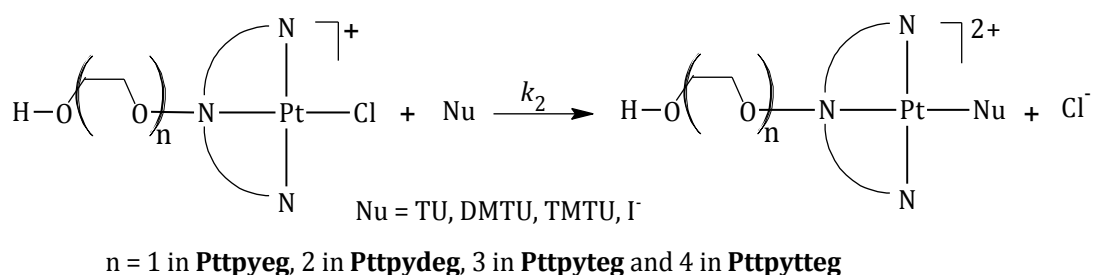


Figure 5.5 DFT calculated minimum energy structures, frontier molecular orbitals (HOMO and LUMO) and the planarity of the complexes investigated. Included is the data obtained for the DFT calculated Ptppy complex for comparisons.

### 5.3.3 Kinetics

Substitution kinetics of coordinated chloride from the Pt(II) complexes (Figure 5.1) by four different nucleophiles, *i.e.* TU, DMTU, TMTU and an ionic nucleophile, I<sup>-</sup> were studied under *pseudo* first-order conditions using the conventional stopped-flow technique. Only one step, taken to be the substitution of the chloride ligand was observed with no solvation pathway. Thus, the proposed substitution mechanism for the complexes studied can be represented as shown in Scheme 5.1. The kinetic data obtained are summarized in Table 5.2. Additional data are given in Tables S5.4 to S5.12)



**Scheme 5.1** Proposed mechanism for the substitution of chloride ligand from the Pt(II) complexes.

To understand the role of the polyethylene glycoxy pendant units on the rate of chloride substitutions, the reactivities of **Ptppy** and **Ptppyeg** were compared. The difference between them is the appended ethylene glycoxy pendant group in **Ptppyeg**. When a single ethylene glycoxy pendant group is attached to the 4'-position of the terpyridine chelate ligand, the reactivity of the resultant metal complexes is reduced by almost five times that of **Ptppy** showing that the polyethylene glycoxy pendant is acting as a  $\sigma$ -donor including the *trans* phenyl ring as supported by the DFT calculations. Furthermore, through  $\pi$ -resonance effect, the lone pair of electrons on the O1 atom of the glycoxy pendant is donated towards the Pt(II) centre. As can be seen from Table 5.1, the inductive  $\sigma$ -electron donation along with the  $\pi$ -electron contribution from the ethylene glycoxy pendant increases the negative charge on the N<sub>trans</sub> atom of **Ptppyeg** compared to **Ptppy**. Consequently, the positive charge on the Pt(II) centre decreases marginally from 0.604 (**Ptppy**) to 0.592 (**Ptppyeg**), indicating that the electron density flow is towards the metal centre, and can be attributed to the well-known *trans* effect.<sup>34</sup> As reported previously, electron donating groups on the ancillary position of terpyridine reduces the positive charge at the metal centre, thereby lowering the electrophilicity of the metal centre.<sup>13g,h,15h,35</sup> This observation in this study is supported

by the DFT calculated global electrophilicity index,  $\omega$ , which clearly indicates that the ability of the parent **Ptppy** to accept the electron density from the incoming nucleophile gets considerably decreased when the ethylene glycoxy pendant unit is attached to 4'-position of the terpyridine backbone.<sup>31,36</sup> In addition, from the perspective that a high dipole moment favours higher  $\pi$ -back donation character,<sup>37</sup> the observed smaller dipole moment of **Ptppyeg** further supports its lower reactivity relative to **Ptppy**. Additional support is obtained by the energy levels of the molecular orbitals, HOMO and LUMO. The fact that the LUMO energy of the **Ptppyeg** is slightly raised (-3.21 eV) related to **Ptppy** (-3.35 eV), makes it difficult to  $\pi$ -back donate. Thus, reduces the transfer of electron density from the 18- electron five coordinate Pt(II)  $d_{xz}$  orbital into the tridentate terpyridine ligand, thereby making the transition state less stable. This can be reflected on from the observed slightly higher activation enthalpy,  $\Delta H^\ddagger$  of **Ptppyeg**, which indicates the slightly higher energy barrier associated with the formation of transition state complex. The net effect is the observed decrease in the electron acceptability of the terpyridine moiety in comparison to that of **Ptppy**, resulting in a decreased rate of substitution of chloride in **Ptppyeg**.

**Table 5.2** Summary of second-order rate constants,  $k_2$  and activation parameters, with the corresponding standard deviations for the substitution of the chloro ligand by a series of thiourea nucleophiles and iodide at  $I = 0.02$  M  $\text{LiCF}_3\text{SO}_3$ , adjusted with  $\text{LiCl}$ . Given in brackets for TU is the data for **Ptppy** taken from literature<sup>13g</sup> and included for comparison.

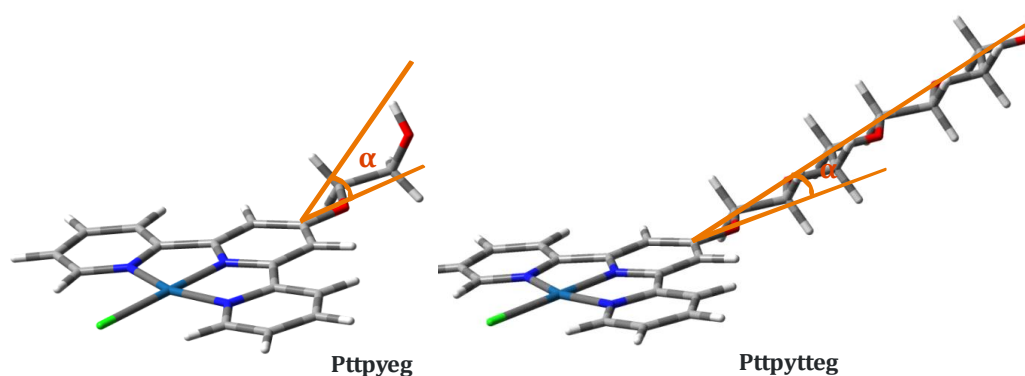
Complex	Nu	$k_2/\text{M}^{-1} \text{s}^{-1}$	$\Delta S^\ddagger / \text{J K}^{-1} \text{mol}^{-1}$	$\Delta H^\ddagger / \text{kJ mol}^{-1}$
<b>Ptppy</b>	TU	(1494 $\pm$ 10)	(-88 $\pm$ 5)	(29 $\pm$ 2)
		1421 $\pm$ 25	-76 $\pm$ 4	35 $\pm$ 1
	DMTU	448 $\pm$ 10	-73 $\pm$ 4	36 $\pm$ 1
	TMTU	82 $\pm$ 4	-91 $\pm$ 8	35 $\pm$ 2
	I <sup>-</sup>	243 $\pm$ 4	-42 $\pm$ 11	47 $\pm$ 4
<b>Ptppyeg</b>	TU	257 $\pm$ 5	-56 $\pm$ 6	43 $\pm$ 2
	DMTU	81 $\pm$ 1	-98 $\pm$ 6	33 $\pm$ 2
	TMTU	22 $\pm$ 1	-57 $\pm$ 7	40 $\pm$ 2
	I <sup>-</sup>	95 $\pm$ 2	-32 $\pm$ 9	53 $\pm$ 3
<b>Ptppydeg</b>	TU	265 $\pm$ 1	-66 $\pm$ 5	40 $\pm$ 2
	DMTU	83 $\pm$ 1	-54 $\pm$ 9	46 $\pm$ 3
	TMTU	23 $\pm$ 1	-83 $\pm$ 7	41 $\pm$ 2
	I <sup>-</sup>	91 $\pm$ 2	-44 $\pm$ 9	48 $\pm$ 3
<b>Ptppyteg</b>	TU	277 $\pm$ 1	-60 $\pm$ 3	41 $\pm$ 1
	DMTU	93 $\pm$ 1	-57 $\pm$ 3	45 $\pm$ 1
	TMTU	19 $\pm$ 0.3	-65 $\pm$ 6	46 $\pm$ 2
	I <sup>-</sup>	91 $\pm$ 1	-48 $\pm$ 6	48 $\pm$ 2
<b>Ptppytteg</b>	TU	321 $\pm$ 4	-67 $\pm$ 5	39 $\pm$ 2
	DMTU	102 $\pm$ 1	-46 $\pm$ 2	48 $\pm$ 2
	TMTU	13 $\pm$ 1	-88 $\pm$ 6	40 $\pm$ 2
	I <sup>-</sup>	156 $\pm$ 2	-44 $\pm$ 5	48 $\pm$ 2

This retardation effect observed between **Ptppy** and **Ptppyeg** has also been noted previously by Schmülling *et al.*<sup>38</sup> where an electron donating methoxy ( $\text{OCH}_3$ ) group was attached to the ancillary ligand of a  $\text{Pt(II)}$  complex of the form  $[\text{Pt}\{\text{C}_6\text{H}_3\text{X}(\text{CH}_2\text{NMe}_2)\}(\text{NC}_5\text{H}_4\text{SO}_3)(\text{H}_2\text{O})]$  where  $\text{X} = \text{OMe}$ . The decrease in the reactivity was accounted for in terms of the  $\sigma$ -inductive donation from the methoxy group to the metal centre making it less electrophilic. A similar effect due to electron donating groups attached at the 4'-position of the terpyridine ligand has also been reported previously by Jaganyi *et al.*<sup>13g,15h</sup>

Furthermore, the decrease in the rate of substitution of **Pttpyeg** is also attributed to the steric contribution imposed on one side of the Pt(II) coordination sphere by the inclined appended ethylene glycoxy unit (*Figure 5.6*) thereby hindering the approach of the axially incoming nucleophile. This steric influence exists in **Pttpyeg** since the angle of inclination,  $\alpha$ , is absent in **Pttpy**. Therefore, it can be concluded that the difference in the rate of substitution between **Pttpy** and **Pttpyeg** is due to both steric and electronic effects.

The analysis of the reactivity of the other complexes having ethylene glycoxy pendant shows a slight increase in the rate of substitution with the increase in the number of ethylene glycoxy units. One would have expected the reactivity to decrease due to increase in the  $\sigma$ -inductive effect, however that is not the case and is supported by the DFT calculations. The observed NBO charges on the Pt(II) centre and N<sub>trans</sub> atom of **Pttpyeg** to **Pttpytteg** are all constant indicating that no change is being experienced by the Pt(II) centres as the pendant unit is increased. The  $\sigma$ -donation and the  $\pi$ -resonance contribution (due to O1) is effective only up to the first glycol unit. The global electrophilicity index shows a very small increase with an increase in the pendant unit which might be linked to the increase in electrons within each pendant unit. Therefore, the remaining factor that accounts for the observed reactivity from **Pttpyeg** to **Pttpytteg** is steric hindrance due to the inclination of the ethylene glycoxy pendant group to the plane containing Pt(II). This angle  $\alpha$ , which has also been reported in literature by Jaganyi *et al.*,<sup>39</sup> when investigating the reactivity of Pt(II) complexes having appended poly alkyl groups, decreases from **Pttpyeg** (37.55 °) to **Pttpytteg** (17.32 °) as depicted in *Figure 5.6*. This means that one side of these complexes experiences steric hindrance which decreases as the angle of inclination decreases with increase in the number of pendant unit. This results in reactivity increasing slightly from **Pttpyeg** to **Pttpytteg**.





**Figure 5.6** Aerial view showing the angles of inclination,  $\alpha$ , of the pendant units in the DFT calculated structures of Pttpyeg and Pttpytteg

There is also a possibility that very weak intramolecular hydrogen bonding between the lone pair of electrons on the oxygen atoms and the neighbouring H atoms or the OH,<sup>40</sup> might be contributing to the stabilization of the five coordinate transition state, which increases with the increase in the number of oxygen atoms in the pendant (*Scheme S5.1, Supporting Information*).

If all the facts are put together, it explains the observed substitution reactivity trend: **Pttpy** >> **Pttpytteg** > **Pttpyteg** > **Pttpydeg** > **Pttpyeg**. If the reactivity of **Pttpy** with TU is taken as a reference, the ratio of reactivity follows: 1.00 : 0.17: 0.18: 0.19: 0.22 respectively for **Pttpy**, **Pttpyeg**, **Pttpydeg**, **Pttpyteg** and **Pttpytteg**. The slight changes in reactivity for the ethylene glycoxy pendant complexes are sterically controlled with minor or no electronic effects.

The data in *Table 5.2* clearly shows a dependence of the chloride substitution on the steric hindrance of the incoming nucleophiles. In all cases, TU has the highest rate constant and the rate constant decreases as the incoming nucleophile gets more bulky; *i.e.*, rate constants for DMTU and TMTU are significantly lower compared to TU. The results show that the complexes are sensitive to the steric hindrance of the incoming nucleophiles which is typical of an associative substitution reaction. In case of the ionic nucleophile,  $\Gamma^-$ , the rate of substitution of the chloride ligand was slower than TU. This difference in reactivity has been explained to be a result of the electrostatic attraction between the anionic iodide and the cationic metal centre facilitated by the high polarisability of the  $\Gamma^-$  ion.<sup>39</sup>

The activation parameters obtained for the substitution of the chloride ligands support an associative mode of mechanism.<sup>41</sup> The large and negative entropy of activation ( $\Delta S^\ddagger$ ) suggests a more ordered transition state. The small enthalpies of activation ( $\Delta H^\ddagger$ ) support the ease of bond formation in the transition state.<sup>10,13g</sup> This is typical for substitution of  $d^8$  square planar Pt(II) complexes.<sup>10,15h,18,39,40b,42</sup>

## 5.4 Conclusions

This study demonstrates that the polyethylene glyoxy pendant attached *trans* to the leaving group of **Pttpy**, acts as a  $\sigma$ -donor towards the Pt(II) centre, thereby decreasing the reactivity compared to the parent **Pttpy** molecule. The  $\sigma$ -donation due to the pendant unit and the  $\pi$ -electronic contribution due to O1 is effective only up to one unit of the ethylene glycoxy pendant, beyond which there is no significant electronic effect on the Pt(II) metal centre. Thus, the retardation of the reactivity from **Pttpy** to **Pttpyeg** is mostly due to both steric and electronic effects caused by the appended ethylene glycoxy pendant. However, the slight increase in substitution reactivity from **Pttpyeg** to **Pttpytteg** is mainly sterically controlled as the angle of inclination of the appended ethylene glycoxy pendant decreases from the Pt(II) plane. The complexes are sensitive to the incoming nucleophiles as demonstrated by the decrease in rate constant depending on the size. The activation parameters, enthalpy of activation and entropy of activation well support an associative mode of mechanism, where bond formation in the transition state is favoured.

## 5.5 References

- (1) Burstall, F. H. *J. Chem. Soc.* **1938**, 1662.
- (2) Morgan, G. T.; Burstall, F. H. *J. Chem. Soc.* **1932**, 20.
- (3) (a) Tzeng, B.-C.; Fu, W.-F.; Che, C.-M.; Chao, H.-Y.; Cheung, K.-K.; Peng, S.-M. *Journal of the Chemical Society, Dalton Transactions* **1999**, 1017(b) Buchner, R.; Cunningham, C. T.; Field, J. S.; Haines, R. J.; McMillin, D. R.; Summerton, G. C. *J. Chem. Soc., Dalton Trans* **1999**, 711(c) McMillin, D. R.; Moore, J. J. *Coord. Chem. Rev.* **2002**, 229, 113(d) Field, J. S.; Haines, R. J.; McMillin, D. R.; Summerton, G. C. *J. Chem. Soc., Dalton Trans.* **2002**, 1369.
- (4) (a) Constable, E. C. *Adv. Inorg. Chem. Radiochem.* **1986**, 30, 69(b) Sauvage, J. P.; Collin, J. P.; Chambron, J. C.; Guillerez, S.; Couret, C.; Balzani, V.; Barigelletti, F.; De Cola, L.; Flamigni, L. *Chem. Rev.* **1994**, 94, 993(c) Andres, P. R.; Lunkwitz, R.; Pabst, G. R.; Bohn, K.; Wouters, D.; Schmatloch, S.; Schuber, U. S. *Eur. J. Org. Chem.* **2003**, 3769.
- (5) Zhang, Y.; Murphy, C. B.; Jones, W. E. *Macromolecules.* **2002**, 35, 630.
- (6) (a) Bonse, S.; Richards, J. M.; Ross, S. A.; Lowe, G.; Krauth-Siegel, R. L. *J. Med. Chem.* **2000**, 43, 4812(b) Lowe, G.; Droz, A. S.; Vilaivan, T.; Weaver, G. W.; Park, J. J.; Pratt, J. M.; Tweeddale, L.; Kelland, L. R. *J. Med. Chem.* **1999**, 42, 3167(c) Messori, L.; Abbate, F.; Marcon, G.; Orioli, P.; Fontani, M.; Mini, E.; Mazzei, T.; Carooti, S.; O'Connel, T.; Zanello, P. *J. Med. Chem.* **2000**, 43, 3541(d) Peyratout, C. S.; Aldridge, T. K.; Crites, D. K.; McMillin, D. R. *Inorg. Chem.* **1995**, 34, 4484(e) Cusumano, M.; Di Pietro, M. L.; Giannetto, A. *Inorg. Chem.* **1999**, 38, 1754(f) Howe-Grant, M.; Wu, K. C.; Bauer, W. R.; Lippard, S. J. *Biochemistry* **1976**, 15, 4339.
- (7) Lowe, G.; Droz, A. S.; Vilaivan, T.; Weaver, G. W.; Tweeddale, L.; Pratt, J. M.; Rock, P.; Yardley, V.; Croft, S. L. *J Med Chem* **1999**, 42, 999.
- (8) Bugarčić, Z. D.; Liehr, G.; van Eldik, R. *J. Chem. Soc. Dalton Trans.* **2002**, 2825.
- (9) (a) Jiang, H.; Lee, S. J.; Lin, W. *Org. Lett.* **2002**, 4, 2149(b) Reddy, D.; Akerman, K. J.; Akerman, M. P.; Jaganyi, D. *Transition Met. Chem.* **2011**, 36, 593.
- (10) Jaganyi, D.; De Boer, K. L.; Gertenbach, J.; Perils, J. *Int. J. Chem. Kinet.* **2008**, 40, 808.
- (11) Jaganyi, D.; Tiba, F.; Munro, O. Q.; Petrovic, B.; Bugarcic, Z. D. *Dalton Trans* **2006**, 2943.
- (12) Romeo, R.; Plutino, M. R.; Scolaro, L. M.; Stoccoro, S.; Minghetti, G. *Inorg Chem* **2000**, 39, 4749.

- (13) (a) Jaganyi, D.; Tiba, F.; Munro, O. Q.; Petrovic, B.; Bugarčić, Z. D. *Dalton Trans.* **2006**, 2943(b) Pitteri, B.; Marangoni, G.; Cattalini, L.; Bobbo, T. J. *J. Chem. Soc. Dalton Trans.*, **1995**, 3853(c) Basolo, F.; Gray, H. B.; Pearson, R. G. *J. Am. Chem. Soc.* **1960**, *82*, 4200(d) Hofmann, A.; Jaganyi, D.; Munro, O. Q.; Liehr, G.; van Eldik, R. *Inorg. Chem.* **2003**, *42*, 1688(e) Jaganyi, D.; Hofmann, A.; van Eldik, R. *Angew. Chem. Int. Ed. Engl.* **2001**, *40*, 1680(f) Jaganyi, D.; Tiba, F. *Trans. Met. Chem.* **2003**, *28*, 803(g) Jaganyi, D.; Reddy, D.; Gertenbach, J. A.; Hofmann, A.; van Eldik, R. *Dalton Trans.* **2004**, 299(h) Hofmann, A.; Dahlenburg, L.; van Eldik, R. *Inorg. Chem.* **2003**, *42*, 6528(i) Bugarčić, Z. D.; Heinemann, F. W.; van Eldik, R. *Dalton Trans.* **2004**, 279(j) Bugarčić, Z. D.; Soldatovic, T.; Jelic, R.; Alguero, B.; Grandas, A. *Dalton Trans.* **2004**, 3869.
- (14) (a) Werner, A. Z.; Cheryaev, I. *Ann. Instr. Platne SSSR.* **1926**, *4*, 261(b) Werner, A. *Z. Anorg. Allg. Chem.* **1893**, *3*, 367.
- (15) (a) Romeo, R.; Plutino, M. R.; Scolaro, L. M.; Stoccoro, S.; Minghetti, G. *Inorg. Chem.* **2000**, *39*, 4749(b) Basolo, F.; Chatt, J.; Gray, H. B.; Pearson, R. G.; Shaw, B. L. *J. Chem. Soc.* **1961**, 2207(c) Gray, H. B. *J. Am. Chem. Soc.* **1962**, *84*, 1548(d) Schmülling, M.; Ryabov, A. D.; van Eldik, R. *J. Chem. Soc. Chem. Comm.* **1992**, 1609(e) Deubel, V. *J. Am. Chem. Soc.* **2002**, *124*, 5834(f) Pitteri, B.; Marangoni, G.; Cattalini, L.; Visentin, F.; Bertolasi, V.; Gilli, P. *Polyhedron.* **2001**, *20*, 869(g) Annibale, G.; Brandolisio, M.; Pitteri, B. *Polyhedron.* **1995**, *14*, 451(h) Reddy, D.; Jaganyi, D. *Dalton Trans.* **2008**, 6724.
- (16) Basolo, F.; Pearson, R. G. *Mechanisms of Inorganic Reactions*; 2nd ed.; Wiley: New York, 1967, pp. 80- 115.
- (17) Tobe, M. L.; Burgess, J. *Inorganic Reaction Mechanisms*; Addison Wesley, Longman: London, 1999, pp. 30- 33, 70- 112.
- (18) Mambanda, A.; Jaganyi, D. *Dalton Trans.* **2011**, *40*, 79.
- (19) Kapp, T.; Dullin, A.; Gust, R. *J. Med. Chem.* **2006**, *49*, 1182.
- (20) Perrin, D. D.; Armarego, W. L. F.; Perrin, D. R. *Purification of Laboratory Chemicals*; 2<sup>nd</sup> ed.; Pergamon: Oxford, 1980.
- (21) (a) Sampath, U.; Putnam, W. C.; Osiek, T. A.; Touami, S.; Xie, J.; Cohen, D.; Cagnolini, A.; Droege, P.; Klug, D.; Barnes, C. L.; Modak, A.; Bashkin, J. K.; Jurisson, S. S. *J. Chem. Soc., Dalton Trans.* **1999**, 2049(b) Andres, P. R., Eindhoven University of Technology, 2004(c) Chow, H. S., PhD Thesis, University of Basel, Metal Complexes of 4'-Substituted-2,2':6',2''-Terpyridines in Supramolecular Chemistry, 33- 66, 2005.

- (22) (a) Becke, A. D. *Chem. Phys.* **1993**, *98*, 5648(b) Lee, C. T.; Yang, W. T.; Parr, R. G. *Phys. Rev. B* **1988**, *37*, 785(c) Hay, P. J.; Wadt, W. R. *Chem. Phys.* **1985**, *82*, 220.
- (23) (a) Barone, V.; Cossi, M. *J. Phys Chem. A* **1998**, *102*, 1995(b) Cossi, M.; Rega, N.; Scalmani, G.; Barone, V. *J. Comput. Chem.* **2003**, *24*, 669.
- (24) Frisch, M. J.; Trucks, G. W.; Schlegel, H. B.; Scuseria, G. E.; Robb, M. A.; Cheeseman, J. R.; Scalmani, G.; Barone, V.; Mennucci, B.; Petersson, G. A.; Nakatsuji, H.; Caricato, M.; Hratchian, X. L.; H. P. ; Izmaylov, A. F.; Bloino, J.; Zheng, G.; Sonnenberg, J. L.; Hada, M.; Ehara, M.; Toyota, K.; Fukuda, R.; Hasegawa, J.; Ishida, M.; Nakajima, T.; Honda, Y.; Kitao, O.; Nakai, H.; Vreven, T.; Montgomery, J. A.; Peralta, J., J. E. ; Ogliaro, F.; Bearpark, M.; Heyd, J. J.; Brothers, E.; Kudin, K. N.; Staroverov, V. N.; Kobayashi, R.; Normand, J.; Raghavachari, K.; Rendell, A.; Burant, J. C.; Iyengar, S. S.; Tomasi, J.; Cossi, M.; Rega, N.; M. Millam, J.; Klene, M.; Knox, J. E.; Cross, J. B.; Bakken, V.; Adamo, C.; Jaramillo, J.; Gomperts, R.; Stratmann, R. E.; Yazyev, O.; Austin, A. J.; Cammi, R.; Pomelli, C.; Ochterski, J. W.; Martin, R. L.; Morokuma, K.; Zakrzewski, V. G.; Voth, G. A.; Salvador, P.; Dannenberg, J. J.; Dapprich, S.; Daniels, A. D.; Farkas, O.; Foresman, J. B.; Ortiz, J. V.; Cioslowski, J.; Fox, D. J.; Gaussian, I., Wallingford CT, 2009., Ed.; Gaussian, Inc., Wallingford CT., 2009.
- (25) Appleton, T. G.; Hall, J. R.; Ralph, S. F.; Thompson, C. S. M. *Inorg. Chem.* **1984**, *23*, 3521.
- (26) Origin 7.5™ SRO, ; Vol. v7.5714 (B5714), Origin Lab Cooperation, Northampton, One, Northampton, MA, 01060, USA, 2003.
- (27) Atwood, J. D. *Inorganic and Organic Reaction Mechanisms*; 2nd ed.; Wiley- VCH Inc.: New York, 1997, 32-34, 43-61.
- (28) Sarkar, S.; Li, S.; Wayland, B. B. *Inorg. Chem.* **2011**, *50*, 3313.
- (29) Ertürk, H.; Maigut, J.; Puchta, R.; van Eldik, R. *J. Chem. Soc. Dalton Trans.* **2008**, 2759.
- (30) (a) Bruice, P. Y. *Organic Chemistry*; 6<sup>th</sup> ed., Pearson Prentice Hall: Clifonia, 2011, 90- 97, 516- 544, A-18(b) Shirver, D. F.; Atkins, P. W.; Langford, C. H. *Inorganic Chemistry*; Oxford University Press: Oxford, 1994, 406.
- (31) Mebi, C. A. *J. Chem. Sci.* **2011**, *123*, 727.
- (32) Chattaraj, P. K.; Sarkar, U. *arXiv:physics/0509089* **2005**, 1.
- (33) (a) Vektariene, A.; Vektaris, G.; Svoboda, J. *ARKIVOC* **2009**, *7*, 311(b) Parr, R. G.; Szentpaly, L.; Liu, S. *J. Am. Chem. Soc.* **1999**, *121*, 1922(c) Elango, M.; Parthasarathi, R.; Narayanan, G. K.; Sabeelullah, A. M.; Sarkar, U;

- Venkatasubramaniyan, N. S.; Subramanian, V.; Chattaraj, P. K. *J. Chem. Sci.* **2005**, *117*, 61.
- (34) Cotton, F. A.; Willkinson, G. *Advanced Inorganic Chemistry*; 5th Edition ed.; 5th Edition, John Wiley & Sons: New York, 1988, 919.
- (35) (a) Pantoja, E.; Gallipoli, A.; van Zutphen, S.; Komeda, S.; Reddy, D.; Jaganyi, D.; Lutz, M.; Tooke, D. M.; Spek, A. L.; Navarro-Ranninger, C.; Reedijk, J. *J. Inorg. Biochem.* **2006**, *100*, 1955(b) Reddy, D.; Jaganyi, D. *Int. J. Chem. kinet.* **2011**, *43*, 161.
- (36) (a) Parr, P. G.; Pearson, R. G. *J. Am. Chem. Soc.* **1983**, *105*, 7512(b) Chattaraj, P. K.; Maiti, B. *J. Am. Chem. Soc.* **2003**, *125*, 2705.
- (37) Rillema, D. P.; Cruz, A. J.; Moore, C.; Siam, K.; Jehan, A.; Base, D.; Nguyen, T.; Huang, W. *Inorg. Chem.* **2012**, *52*, 596.
- (38) Schmülling, M.; Ryabov, A. D.; van Eldik, R. *J. Chem. Soc. Dalton Trans.* **1994**, 1257.
- (39) Jaganyi, D.; Mambanda, A.; Hochreuther, S.; van Eldik, R. *Dalton Trans.* **2010**, *39*, 3595.
- (40) (a) Thalladi, V. R.; Gehrke, A.; Boese, R. *New J. Chem.* **2000**, *24*, 463(b) Ongoma, P. O.; Jaganyi, D. *Dalton Trans.* **2013**, *42*, 2724(c) Klein, A.; Schurr, T.; Knödler, A.; Gudat, D.; Klinkhammer, K. W.; Jain, V.; Zális, S.; Kaim, W. *Organometallics.* **2005**, *24*, 4125.
- (41) Jaganyi, D.; Reddy, D.; Gertenbach, J. A.; Hofmann, A.; van Eldik, R. *Dalton Trans.* **2003**, 299.
- (42) Asperger, S. *Chemical Kinetics and Inorganic Reaction Mechanisms*; 2nd ed.; Kluwer Academic/ Plenum Publisher: New York, 2003, 152-153.

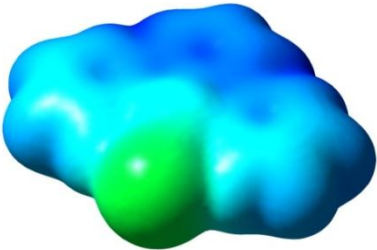
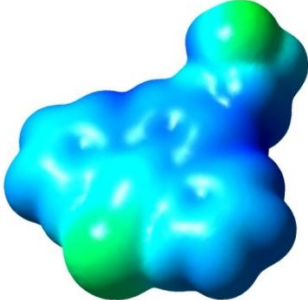
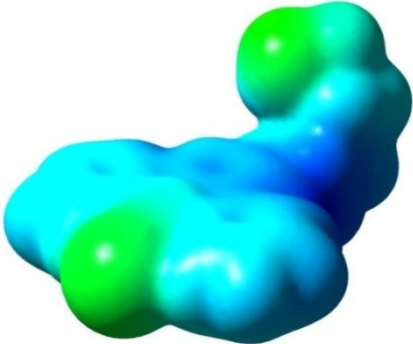
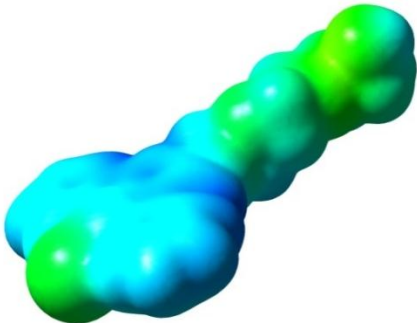
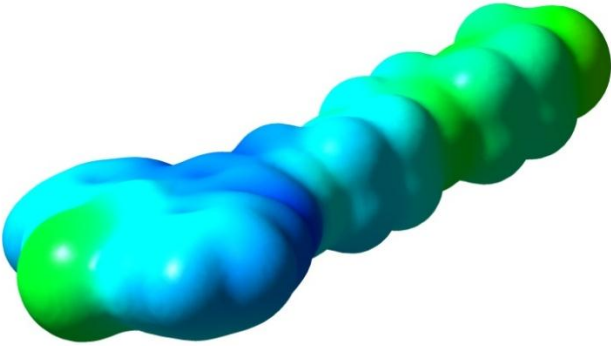
## 5.6 Supporting Information

A summary of wavelengths at which the kinetic studies were performed, plots of the dependence of  $k_{\text{obs}}$  against concentration of the nucleophiles and plots from temperature dependence studies along with tables of kinetic data, graphs of exemplary mass spectra and the representative spectra for  $^1\text{H}$  NMR and  $^{195}\text{Pt}$  NMR work reported in this study are given as electronic supporting information (ESI).

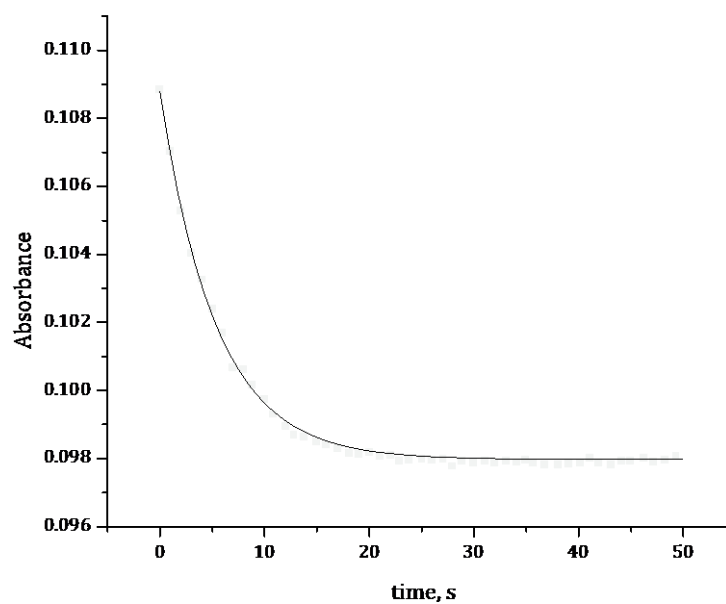
**Table S5.1** Summary of the wavelengths (nm) used to study the substitution reactions of the complexes with thiourea nucleophiles.

Complex	Nu	Wavelength ( $\lambda$ ), nm
<b>Ptppyeg</b>	TU	330
	DMTU	296
	TMTU	297
	I <sup>-</sup>	330
<b>Ptppydeg</b>	TU	330
	DMTU	330
	TMTU	330
	I <sup>-</sup>	297
<b>Ptppyteg</b>	TU	330
	DMTU	329
	TMTU	329
	I <sup>-</sup>	329
<b>Ptppytteg</b>	TU	330
	DMTU	400
	TMTU	295
	I <sup>-</sup>	330

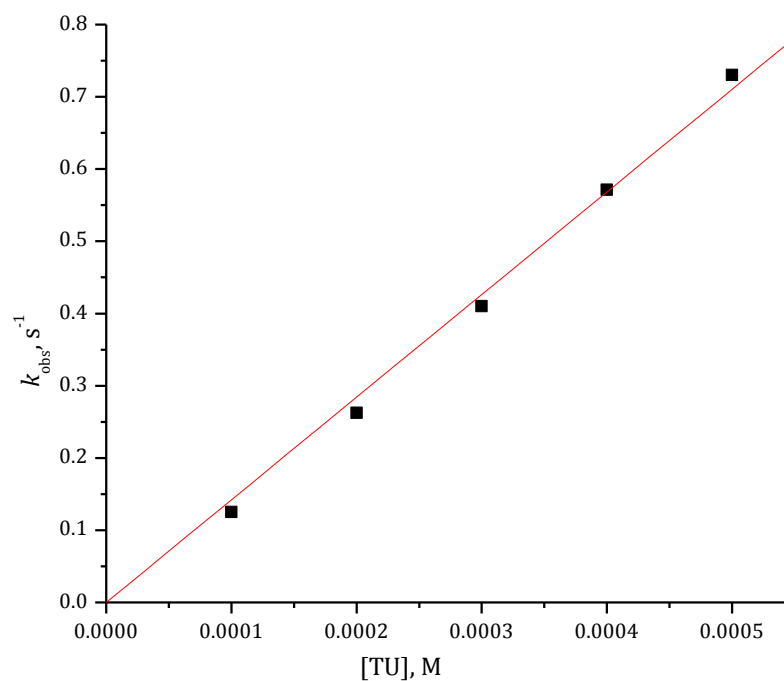
**Table S5.2** Geometry-optimised structures of the platinum complexes investigated and distribution of the electron density on the platinum complexes investigated. The blue area indicates the most electropositive areas and the green region indicates the most electronegative areas.

Compound	Structure
 Ptppy	 Ptppyeg
 Ptppydeg	 Ptppyteg
	 Ptppytteg

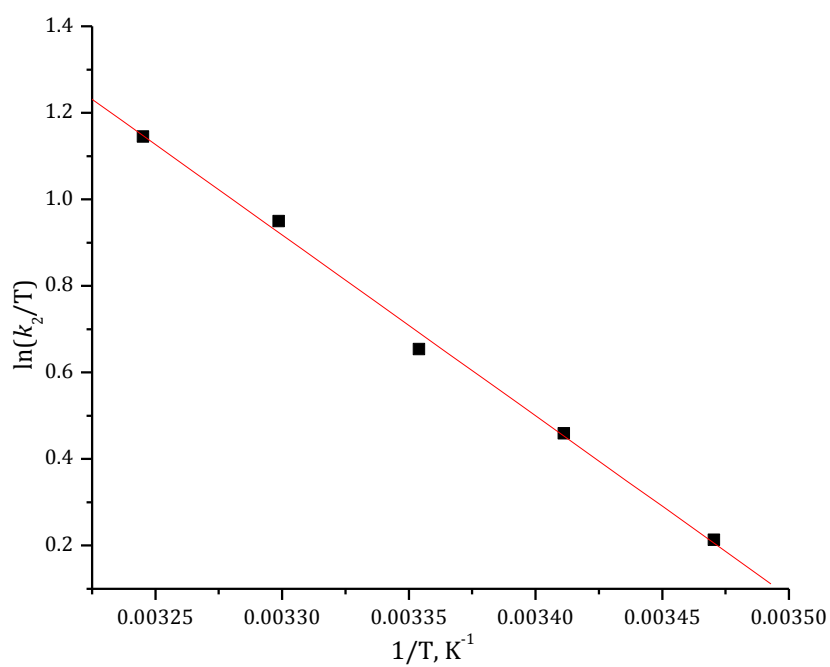




**Figure S5.1** Kinetic trace at 284 nm for the reaction of Ptpyeg ( $1.3 \times 10^{-5} \text{ mol dm}^{-3}$ ) with Tu ( $3.7 \times 10^{-4} \text{ mol dm}^{-3}$ ) at 298 K,  $I = 0.02 \text{ M LiCF}_3\text{SO}_3$ , adjusted with LiCl.



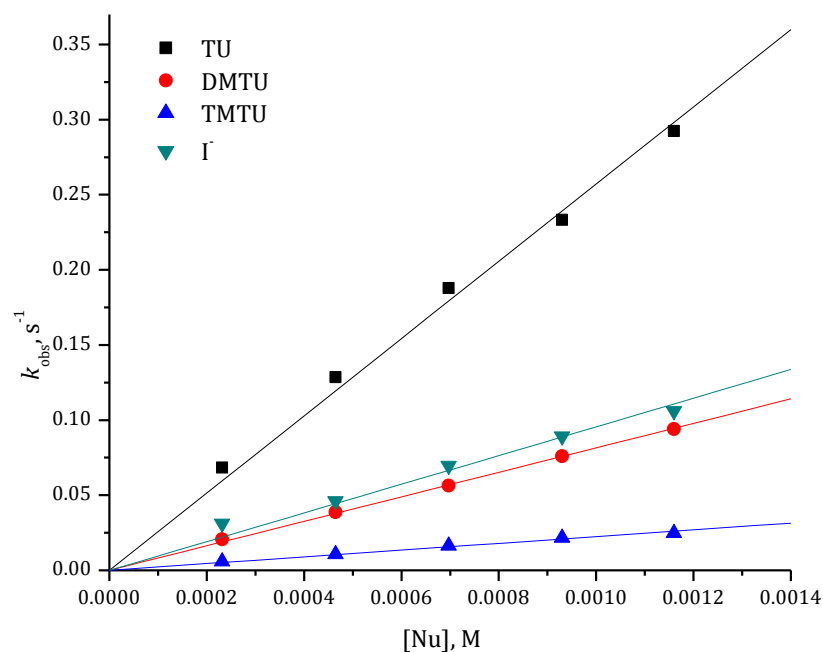
**Figure S5.2** Dependence of the *pseudo* first-order rate constants ( $k_{\text{obs}}$ ) on the concentrations of TU for the chloride substitution from Ptpy ( $4.0 \times 10^{-5} \text{ M}$ ) and



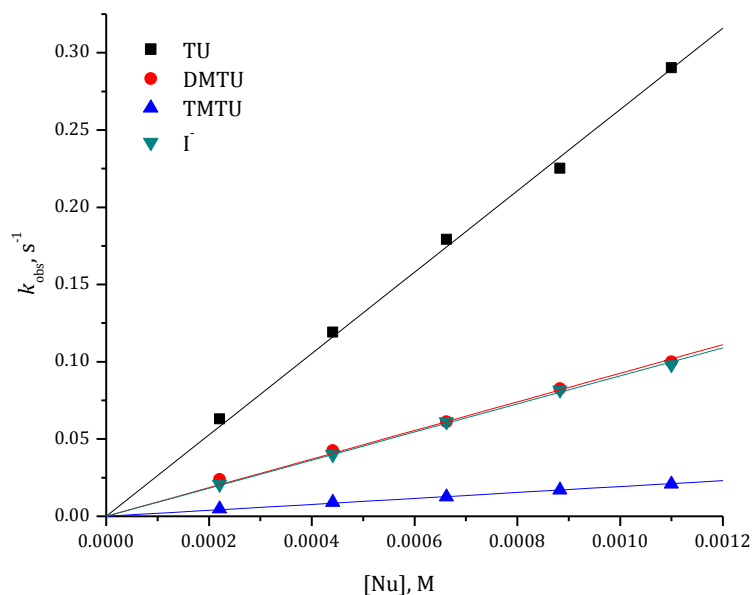
**Figure S5.3** (a) Dependence of the *pseudo* first-order rate constants ( $k_{\text{obs}}$ ) on the concentrations of TU for the chloride substitution from Pttpy ( $4.0 \times 10^{-5} \text{ M}$ ) and (b) Eyring plot obtained for Pttpy with TU for the over the temperature range 15-35 °C in methanol solution ( $I = 0.02 \text{ M LiCF}_3\text{SO}_3$ , adjusted with LiCl.) at 298 K.

**Table S5.3** Summary of DFT calculated data for the complexes investigated. Included is the data obtained for the DFT calculated Pttpy complex for comparisons.

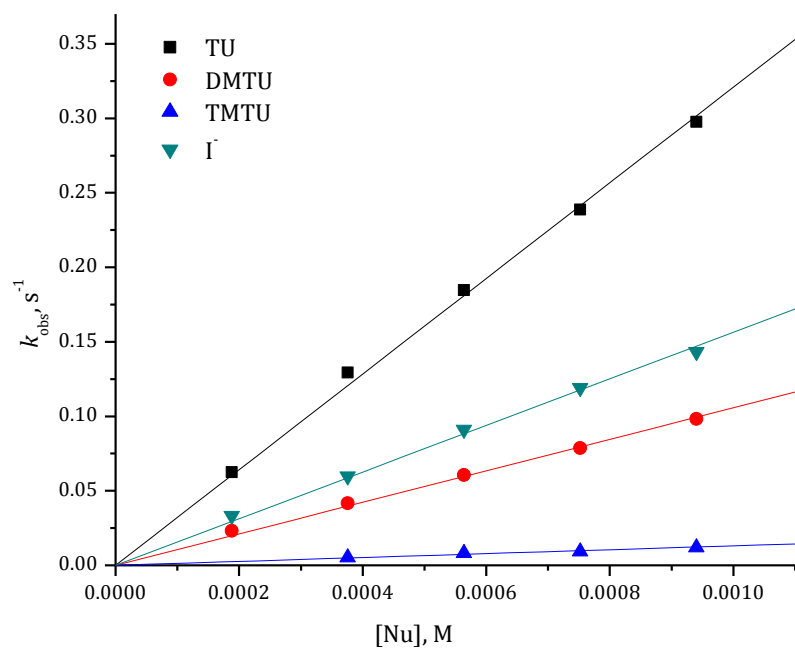
Complex	Pttpy	Ptptyeg	Ptptydeg	Ptptyteg	Ptptytteg
<b>Bond Length (Å)</b>					
Pt1–N2(cis)	2.0486	2.0510	2.0490	2.0508	2.0488
Pt–N3(cis)	2.0486	2.0491	2.0532	2.0513	2.0501
O1–O2		2.9737	2.9705	2.9734	2.9709
O2–O3			2.8311	3.1122	3.0948
O3–O4				2.8679	3.1265
O4–O5					3.6670
O1-O5/O1-O3/O1-O4			4.4784	8.3258	9.0097
Pt1–O1		6.0703	6.0704	6.0701	6.0814
Cl–H/O3/O4/O5		11.4700	10.7616	16.4473	17.0570
Pt–O2/ O3/O4/O5		8.8644	9.0628	14.2687	14.0313
N <sub>trans</sub> –O1		4.11104	4.1102	4.1101	4.1210
<b>Bond angles (°)</b>					
N1–Pt–Cl	179.99	179.543	179.60	179.40	179.57
N2–Pt–Cl	99.05	99.030	98.92	99.31	98.72
N3–Pt–Cl	99.05	99.426	99.52	99.14	99.50
N3–Pt–N2	161.90	161.544	161.56	161.55	161.78
N2–Pt–N1	80.95	80.799	80.73	80.86	80.90
N1–Pt–N3	80.95	80.746	80.83	80.69	80.88
Dihedral -cl	0.007	0.848	0.118	0.698	0.678
<b>NBO charges</b>					
N2	-0.493	-0.493	-0.492	-0.492	-0.493
N3	-0.493	-0.492	-0.494	-0.493	-0.493
O1		-0.559	-0.560	-0.560	-0.608
O2		-0.814	-0.658	-0.650	-0.656
O3			-0.821	-0.665	-0.658
O4				-0.824	-0.657
O5					-0.826
C 4	-0.134	0.408	0.408	0.408	0.387
Point Group	$C_2$	$C_1$	$C_1$	$C_1$	$C_1$
Ground state energy	-876.46	-1105	-1259	-1413	-1567



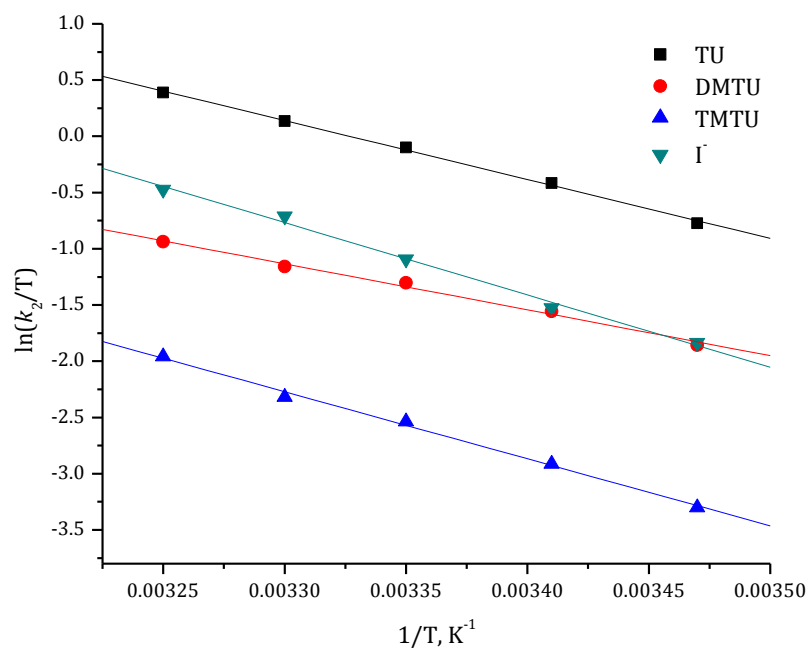
**Figure S5.4** Dependence of the *pseudo* first-order rate constants ( $k_{obs}$ ) on the concentrations of the nucleophiles for the chloride substitution from Ptppyeg ( $4.0 \times 10^{-5}$  M) in methanol solution ( $I = 0.02$  M  $LiCF_3SO_3$ , adjusted with  $LiCl$ ) at 298 K.



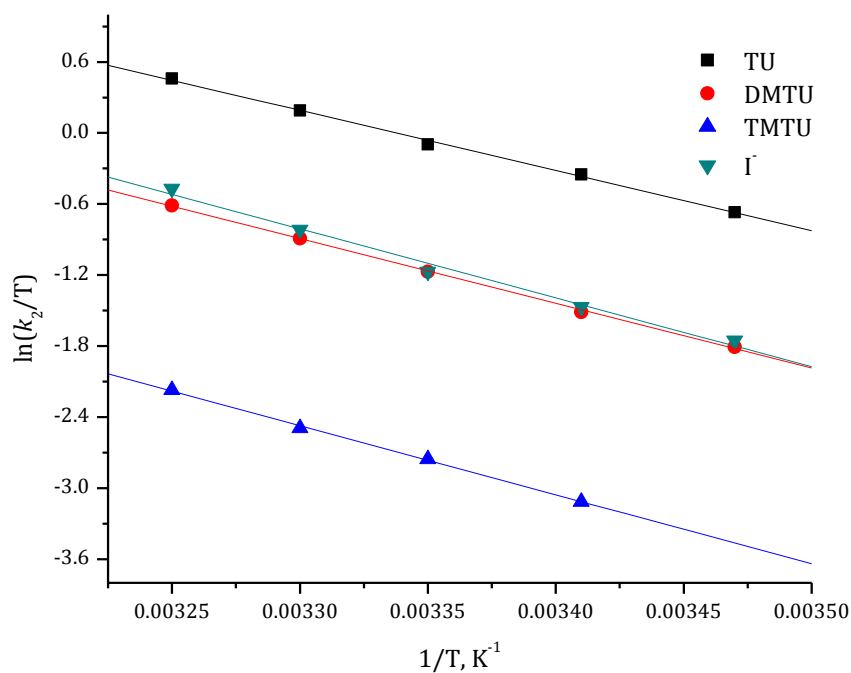
**Figure S5.5** Dependence of the *pseudo* first-order rate constants ( $k_{obs}$ ) on the concentration of the nucleophiles for the chloride substitution from Ptppyeg ( $4.00 \times 10^{-5}$  M) in methanol solution ( $I = 0.02$  M  $LiCF_3SO_3$ , adjusted with  $LiCl$ ) at 298 K.



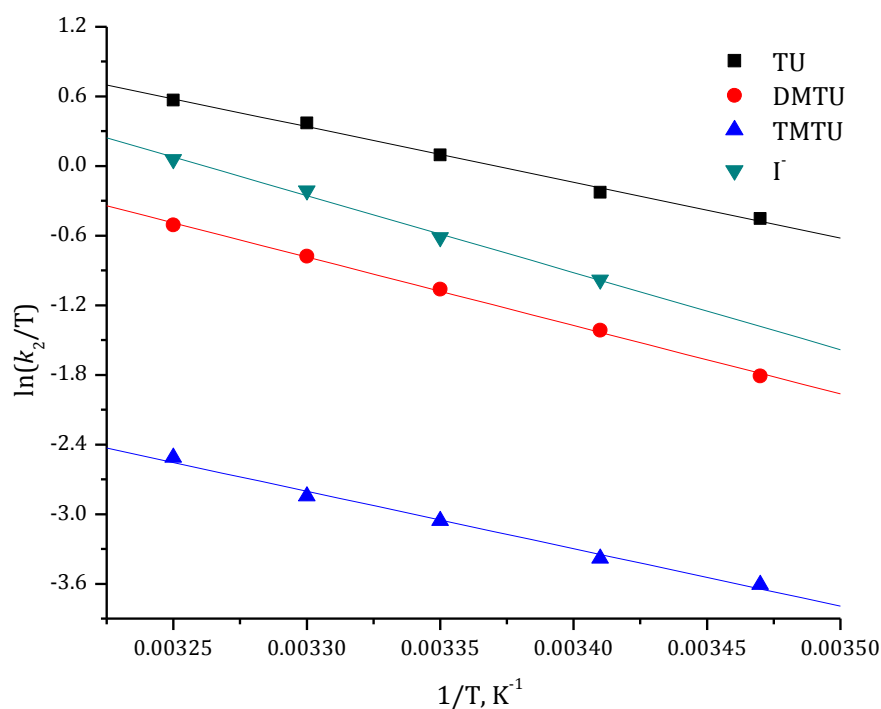
**Figure S5.6** Dependence of the *pseudo* first-order rate constant ( $k_{obs}$ ) on the concentration of the nucleophiles for the chloride substitution from Ptppyteg ( $4.00 \times 10^{-5}$  M) in methanol solution ( $I = 0.02$  M  $LiCF_3SO_3$ , adjusted with  $LiCl$ ) at 298 K.



**Figure S5.7** Eyring plots obtained for Ptppydeg with the nucleophiles for the forward reactions over the temperature range 15 - 35 °C.



**Figure S5.8** Eyring plots obtained for Ptptpyteg with the nucleophiles for the forward reactions over the temperature range 15 - 35 °C.



**Figure S5.9** Eyring plots obtained for Ptptpyteg with the nucleophiles for the forward reactions over the temperature range 15 - 35 °C.

**Table S5.4** Average observed rate constants, for the displacement of the chloride ligand in Ptppy with TU, at T = 298 K and Temperature dependence of  $k_2$  M<sup>-1</sup>s<sup>-1</sup>, for the displacement of the chloride ligand in Ptppy by TU at 30-fold excess over [Ptppy],  $I = 0.02$  M LiCF<sub>3</sub>SO<sub>3</sub>, adjusted with LiCl.

Conc, mM	$k_{\text{obs.}}, \text{s}^{-1}$	1/T, K <sup>-1</sup>	ln( $k_2$ /T)
0.100	0.12503	0.00347	0.21285
0.200	0.26255	0.00341	0.45944
0.300	0.40997	0.00335	0.65416
0.400	0.57142	0.0033	0.94986
0.500	0.73003	0.00325	1.14465

**Table S5.5** Average observed rate constants,  $k_{\text{obs.}} \text{s}^{-1}$ , for the displacement of the chloride ligand in Ptppyeg with the nucleophiles, at T = 298 K,  $I = 0.02$  M LiCF<sub>3</sub>SO<sub>3</sub>, adjusted with LiCl.

TU		DMTU		TMTU		I <sup>-</sup>	
Conc., mM	$k_{\text{obs.}}, \text{s}^{-1}$	Conc., mM	$k_{\text{obs.}}, \text{s}^{-1}$	Conc., mM	$k_{\text{obs.}}, \text{s}^{-1}$	Conc., mM	$k_{\text{obs.}}, \text{s}^{-1}$
0.232	0.06831	0.232	0.02068	0.232	0.00588	0.232	0.03115
0.465	0.12859	0.465	0.03861	0.465	0.01073	0.465	0.04615
0.697	0.18792	0.697	0.0564	0.697	0.01632	0.697	0.06969
0.930	0.2332	0.930	0.07593	0.930	0.02168	0.930	0.08915
1.160	0.29235	1.160	0.09408	1.160	0.02474	1.160	0.1061

**Table S5.6** Temperature dependence of  $k_2$  M<sup>-1</sup>s<sup>-1</sup>, for the displacement of the chloride ligand in Ptppyeg by the nucleophiles at 30-fold excess over [Ptppyeg], at T = 298 K,  $I = 0.02$  M LiCF<sub>3</sub>SO<sub>3</sub>, adjusted with LiCl.

TU		DMTU		TMTU		I <sup>-</sup>	
1/T, K <sup>-1</sup>	ln( $k_2$ /T)	1/T, K <sup>-1</sup>	1/T, K <sup>-1</sup>	ln( $k_2$ /T)	1/T, K <sup>-1</sup>	1/T, K <sup>-1</sup>	ln( $k_2$ /T)
0.00347	-0.77375	0.00347	-1.85666	0.00347	-3.29982	0.00347	-1.83455
0.00341	-0.41648	0.00341	-1.55805	0.00341	-2.91201	0.00341	-1.52821
0.00335	-0.1006	0.00335	-1.30418	0.00335	-2.53604	0.00335	-1.09253
0.0033	0.13394	0.0033	-1.15741	0.0033	-2.31879	0.0033	-0.71143
0.00325	0.38996	0.00325	-0.93678	0.00325	-1.9588	0.00325	-0.47234

**Table S5.7** Average observed rate constants,  $k_{\text{obs}}$   $\text{s}^{-1}$ , for the displacement of the chloride ligand in Ptppydeg with the nucleophiles, at  $T = 298 \text{ K}$ ,  $I = 0.02 \text{ M LiCF}_3\text{SO}_3$ , adjusted with LiCl.

TU		DMTU		TMTU		$\text{I}^-$	
Conc., mM	$k_{\text{obs.}}, \text{s}^{-1}$	Conc., mM	$k_{\text{obs.}}, \text{s}^{-1}$	Conc., mM	$k_{\text{obs.}}, \text{s}^{-1}$	Conc., mM	$k_{\text{obs.}}, \text{s}^{-1}$
0.200	0.0533	0.200	0.01594	0.200	0.00557	0.200	0.02111
0.400	0.10391	0.400	0.03404	0.400	0.00991	0.400	0.04101
0.600	0.15373	0.600	0.04892	0.600	0.01392	0.600	0.05605
0.800	0.20663	0.800	0.06539	0.800	0.01813	0.800	0.07142
1.00	0.26106	1.00	0.0845	1.00	0.02223	1.00	0.09049

**Table S5.8** Temperature dependence of  $k_2$   $\text{M}^{-1}\text{s}^{-1}$ , for the displacement of the chloride ligand in Ptppydeg by the nucleophiles at 30-fold excess over [Ptppyeg], at  $T = 298 \text{ K}$ ,  $I = 0.02 \text{ M LiCF}_3\text{SO}_3$ , adjusted with LiCl.

TU		DMTU		TMTU		$\text{I}^-$	
$1/T, \text{K}^{-1}$	$\ln(k_2/T)$	$1/T, \text{K}^{-1}$	$1/T, \text{K}^{-1}$	$1/T, \text{K}^{-1}$	$\ln(k_2/T)$	$1/T, \text{K}^{-1}$	$1/T, \text{K}^{-1}$
0.00347	-0.71115	0.00347	-1.97003	0.00347	-3.1435	0.00347	-1.80055
0.00341	-0.36447	0.00341	--	0.00341	-2.80919	0.00341	-1.37186
0.00335	-0.15161	0.00335	-1.29658	0.00335	-2.56486	0.00335	-1.17219
0.0033	0.14608	0.0033	-0.94055	0.0033	-2.3508	0.0033	-0.80536
0.00325	0.37893	0.00325	-0.74569	0.00325	-1.99632	0.00325	-0.44109

**Table S5.9** Average observed rate constants,  $k_{\text{obs}}$   $\text{s}^{-1}$ , for the displacement of the chloride ligand in Ptppyteg with the nucleophiles, at  $T = 298 \text{ K}$ ,  $I = 0.02 \text{ M LiCF}_3\text{SO}_3$ , adjusted with LiCl.

TU		DMTU		TMTU		$\text{I}^-$	
Conc., mM	$k_{\text{obs.}}, \text{s}^{-1}$	Conc., mM	$k_{\text{obs.}}, \text{s}^{-1}$	Conc., mM	$k_{\text{obs.}}, \text{s}^{-1}$	Conc., mM	$k_{\text{obs.}}, \text{s}^{-1}$
0.221	0.06301	0.221	0.02378	0.221	0.00483	0.221	0.02073
0.441	0.11921	0.441	0.04244	0.441	0.009	0.441	0.03996
0.662	0.1792	0.662	0.06119	0.662	0.01256	0.662	0.0612
0.883	0.2252	0.883	0.08255	0.883	0.01699	0.883	0.0816
1.100	0.29024	1.100	0.09991	1.100	0.02095	1.100	0.09814



**Table S5.10** Temperature dependence of  $k_2$  M<sup>-1</sup>s<sup>-1</sup>, for the displacement of the chloride ligand in Pttpyteg by the nucleophiles at 30-fold excess over [Pttpyteg], at T = 298 K,  $I$  = 0.02 M LiCF<sub>3</sub>SO<sub>3</sub>, adjusted with LiCl.

TU		DMTU		TMTU		I <sup>-</sup>	
1/T, K <sup>-1</sup>	ln( $k_2$ /T)	1/T, K <sup>-1</sup>	1/T, K <sup>-1</sup>	1/T, K <sup>-1</sup>	ln( $k_2$ /T)	1/T, K <sup>-1</sup>	1/T, K <sup>-1</sup>
0.00347	-0.66929	0.00347	-1.80685	0.00347	-	0.00347	-1.75361
0.00341	-0.34999	0.00341	-1.51259	0.00341	-3.11426	0.00341	-1.46934
0.00335	-0.0966	0.00335	-1.17105	0.00335	-2.75475	0.00335	-1.17101
0.0033	0.1892	0.0033	-0.89035	0.0033	-2.49374	0.0033	-0.81608
0.00325	0.46045	0.00325	-0.6124	0.00325	-2.17086	0.00325	-0.47009

**Table S5.11** Average observed rate constants,  $k_{\text{obs}}$  s<sup>-1</sup>, for the displacement of the chloride ligand in Pttpyteg with the nucleophiles, at T = 298 K,  $I$  = 0.02 M LiCF<sub>3</sub>SO<sub>3</sub>, adjusted with LiCl.

TU		DMTU		TMTU		I <sup>-</sup>	
Conc., mM	$k_{\text{obs.}}$ s <sup>-1</sup>	Conc., mM	$k_{\text{obs.}}$ s <sup>-1</sup>	Conc., mM	$k_{\text{obs.}}$ s <sup>-1</sup>	Conc., mM	$k_{\text{obs.}}$ s <sup>-1</sup>
0.188	0.06242	0.188	0.02311	-	-	0.188	0.03314
0.376	0.12927	0.376	0.04156	0.376	0.00529	0.376	0.05969
0.564	0.18476	0.564	0.06049	0.564	0.00823	0.564	0.09101
0.752	0.2388	0.752	0.07858	0.752	0.00931	0.752	0.11915
0.940	0.29756	0.940	0.09822	0.940	0.01206	0.940	0.14317

**Table S5.12** Temperature dependence of  $k_2$  M<sup>-1</sup>s<sup>-1</sup>, for the displacement of the chlorideligand in Pttpyteg by the nucleophiles at 30-fold excess over [Pttpyteg], at T = 298 K,  $I$  = 0.02 M LiCF<sub>3</sub>SO<sub>3</sub>, adjusted with LiCl.

TU		DMTU		TMTU		I <sup>-</sup>	
1/T, K <sup>-1</sup>	ln( $k_2$ /T)	1/T, K <sup>-1</sup>	1/T, K <sup>-1</sup>	1/T, K <sup>-1</sup>	ln( $k_2$ /T)	1/T, K <sup>-1</sup>	1/T, K <sup>-1</sup>
0.00347	-0.45212	0.00347	-1.80917	0.00347	-3.60789		
0.00341	-0.22695	0.00341	-1.41566	0.00341	-3.38006	0.00341	-0.98071
0.00335	0.09414	0.00335	-1.06236	0.00335	-3.05708	0.00335	-0.61393
0.0033	0.37004	0.0033	-0.77722	0.0033	-2.84358	0.0033	-0.21246
0.00325	0.56892	0.00325	-0.50865	0.00325	-2.51069	0.00325	0.05868

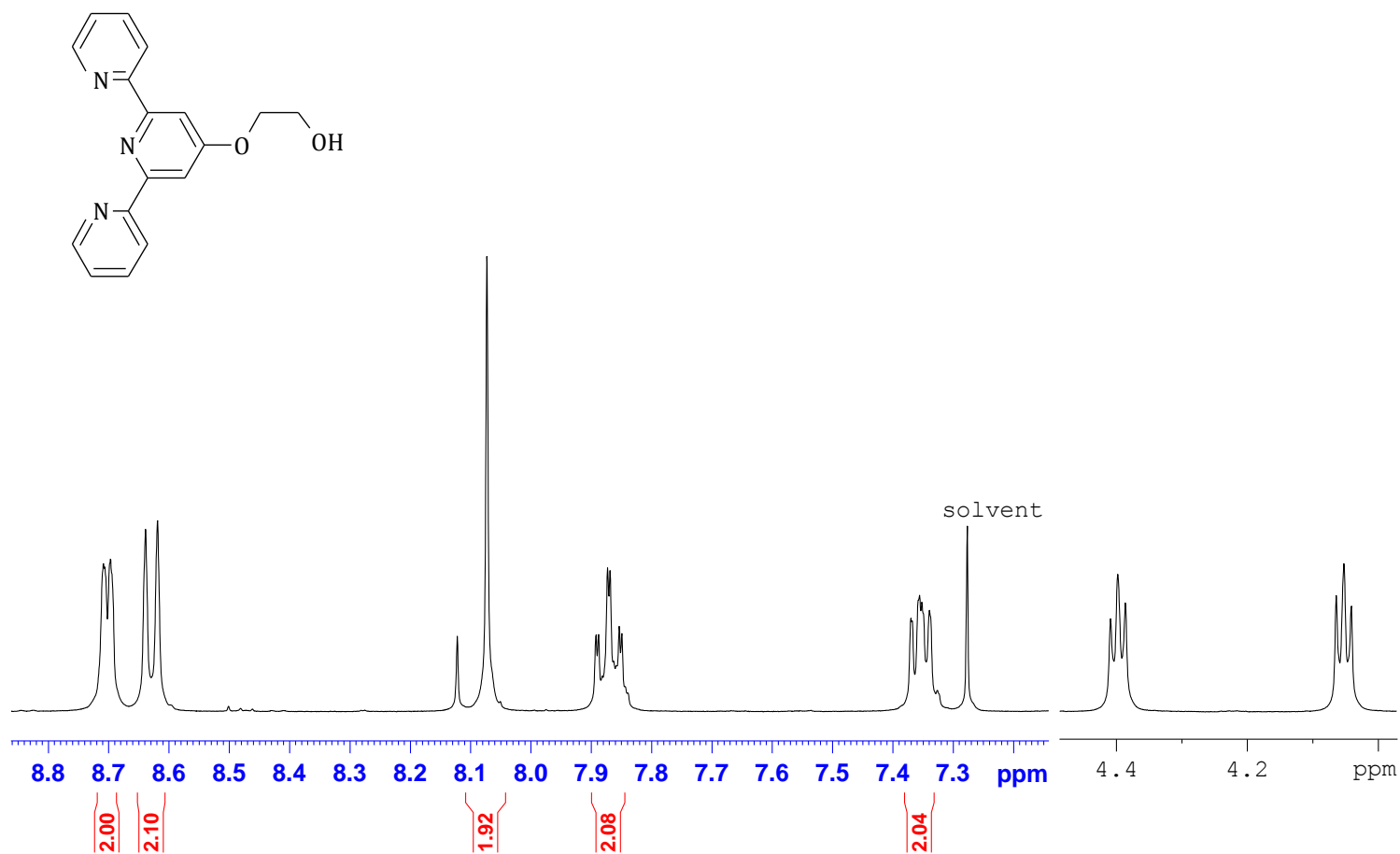


Figure S5.10 <sup>1</sup>H NMR spectrum of 4'-[2-(2-Hydroxyethoxy)ethoxy]-2,2':6',2''-terpyridine in CDCl<sub>3</sub>.

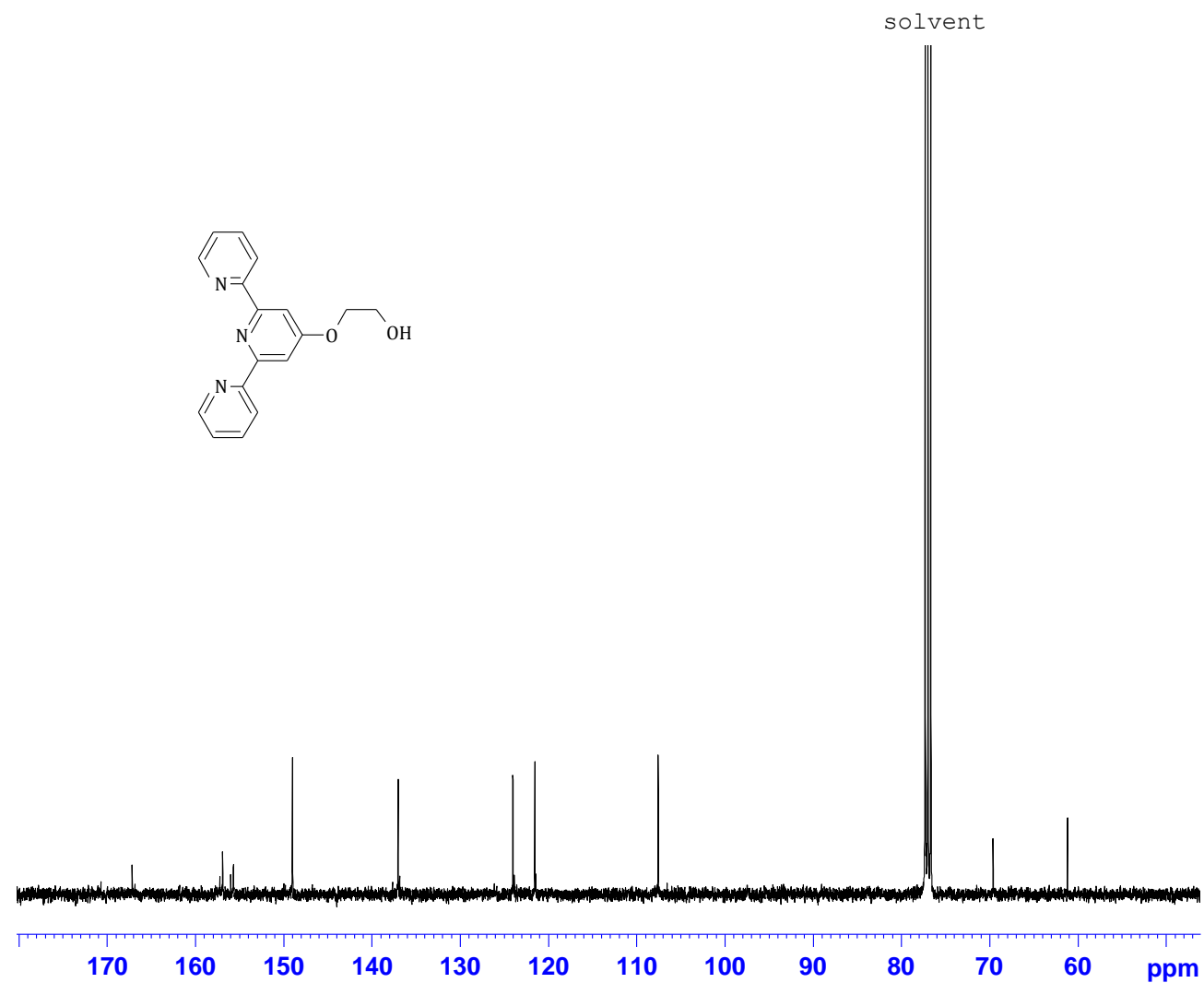


Figure S5.11  $^{13}\text{C}$  Spectrum of 4'-[2-(2-Hydroxyethoxy)ethoxy]-2,2':6',2''-terpyridine in  $\text{CDCl}_3$ .

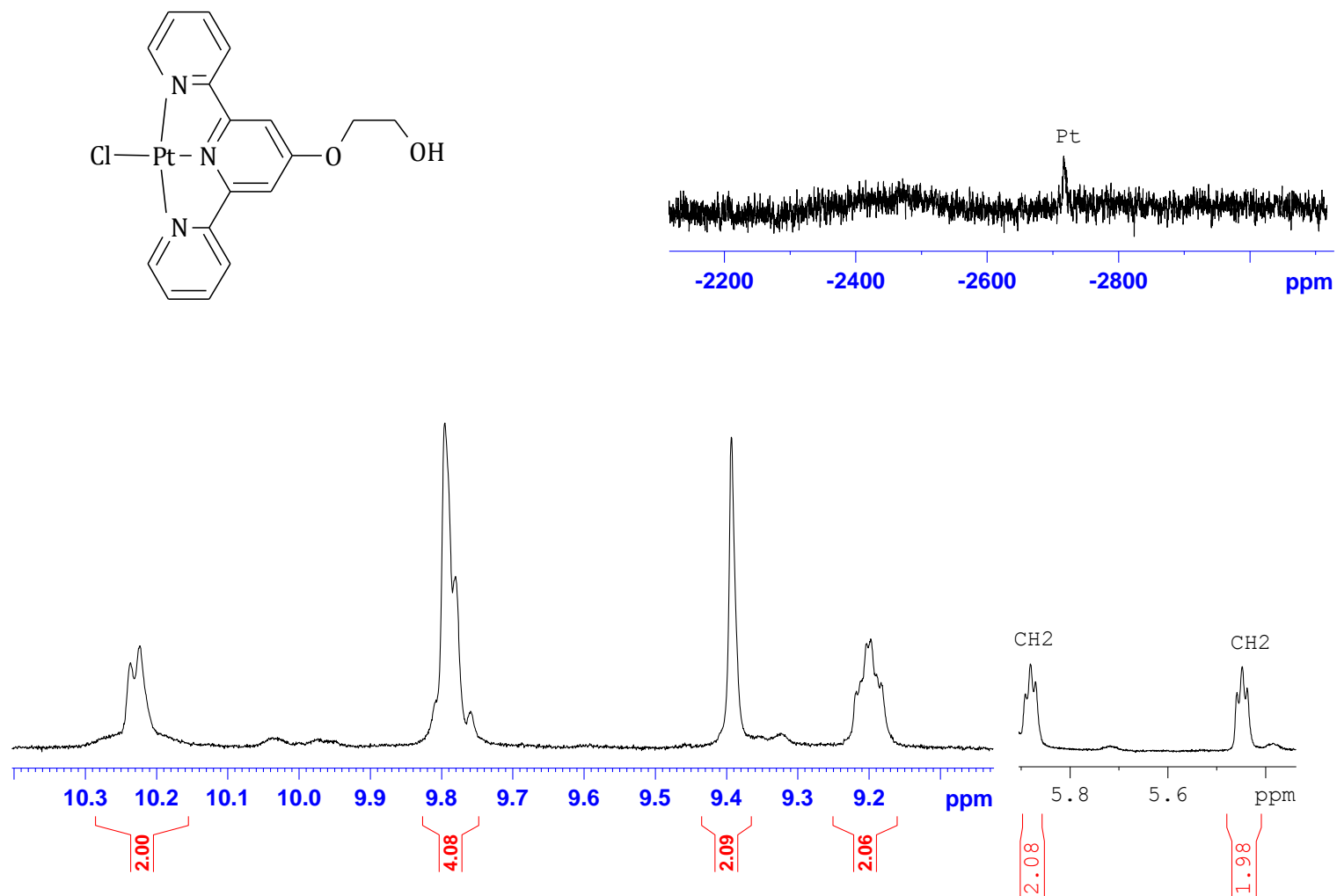


Figure S5.12  $^1\text{H}$  NMR and  $^{195}\text{Pt}$  NMR spectra of Ptptpyeg

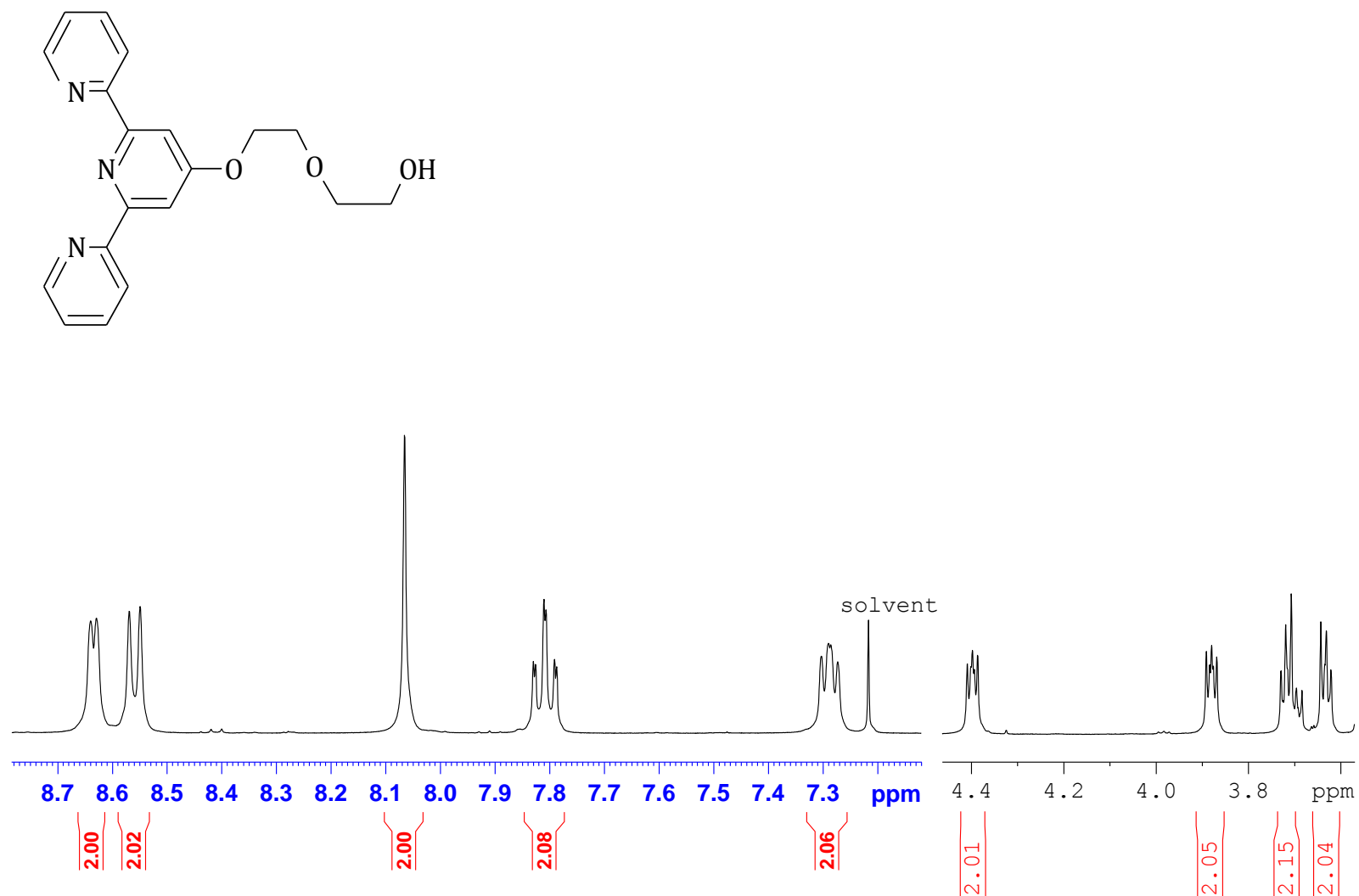


Figure S5.13  $^1\text{H}$  NMR spectrum of 4'-[2-(2-Hydroxyethoxy)ethoxy]-2,2':6',2''-terpyridine in  $\text{CDCl}_3$ .

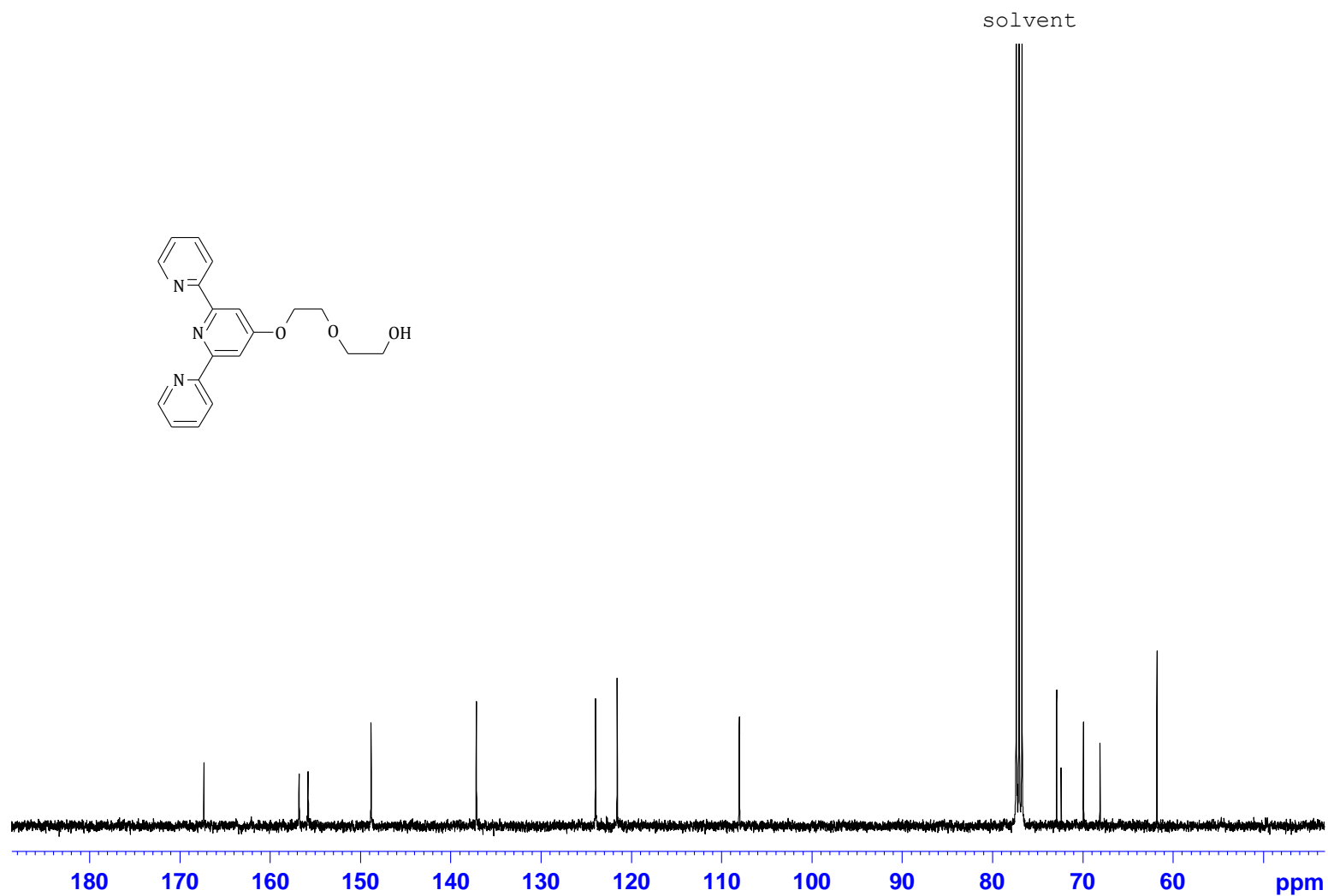


Figure S5.14  $^{13}\text{C}$  NMR spectrum of 4'-[2-(2-Hydroxyethoxy)ethoxy]-2,2':6',2''-terpyridine in  $\text{CDCl}_3$ .

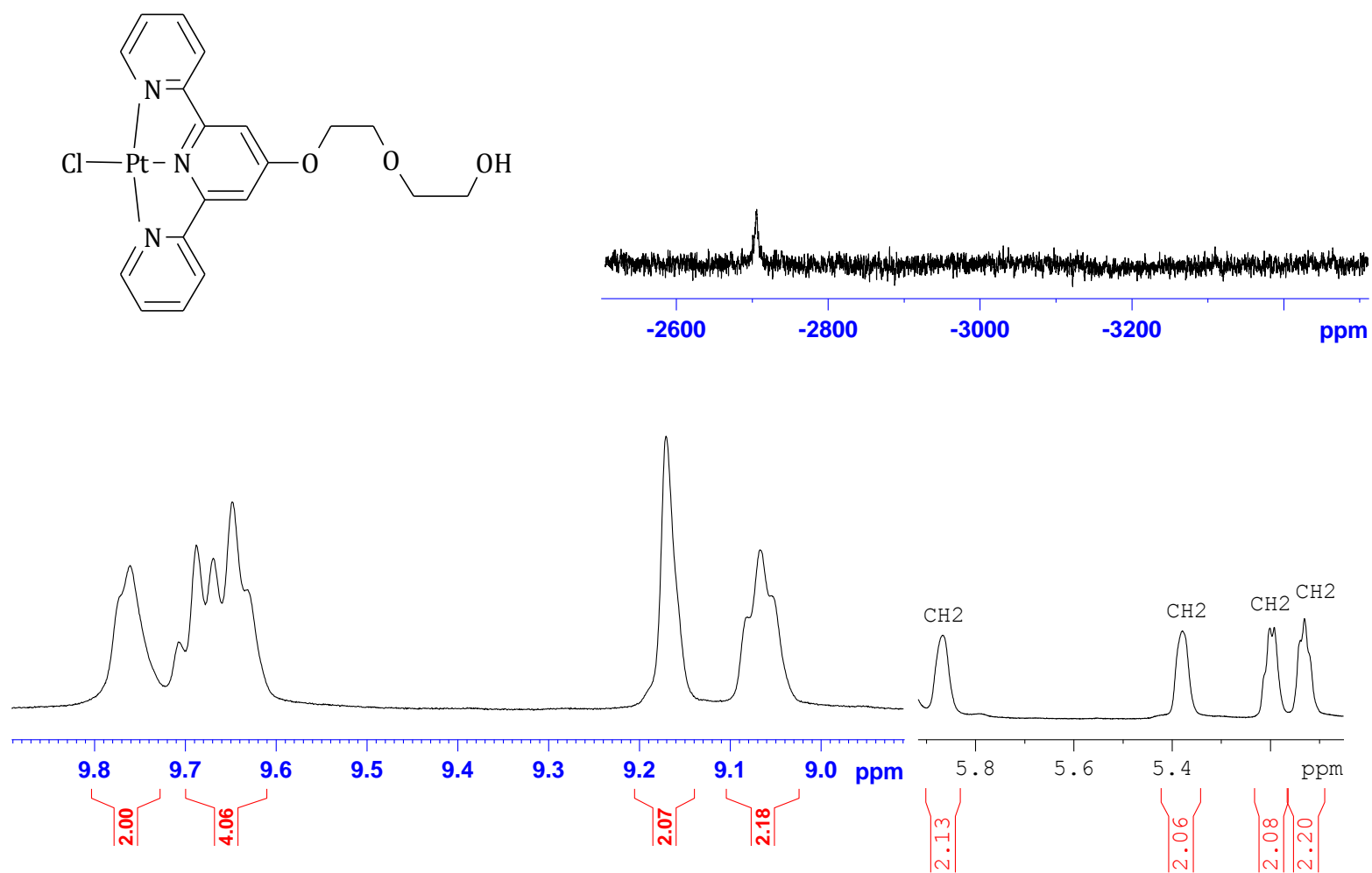


Figure S5.15  $^1\text{H}$  NMR and  $^{195}\text{Pt}$  NMR spectra of ptppydeg.

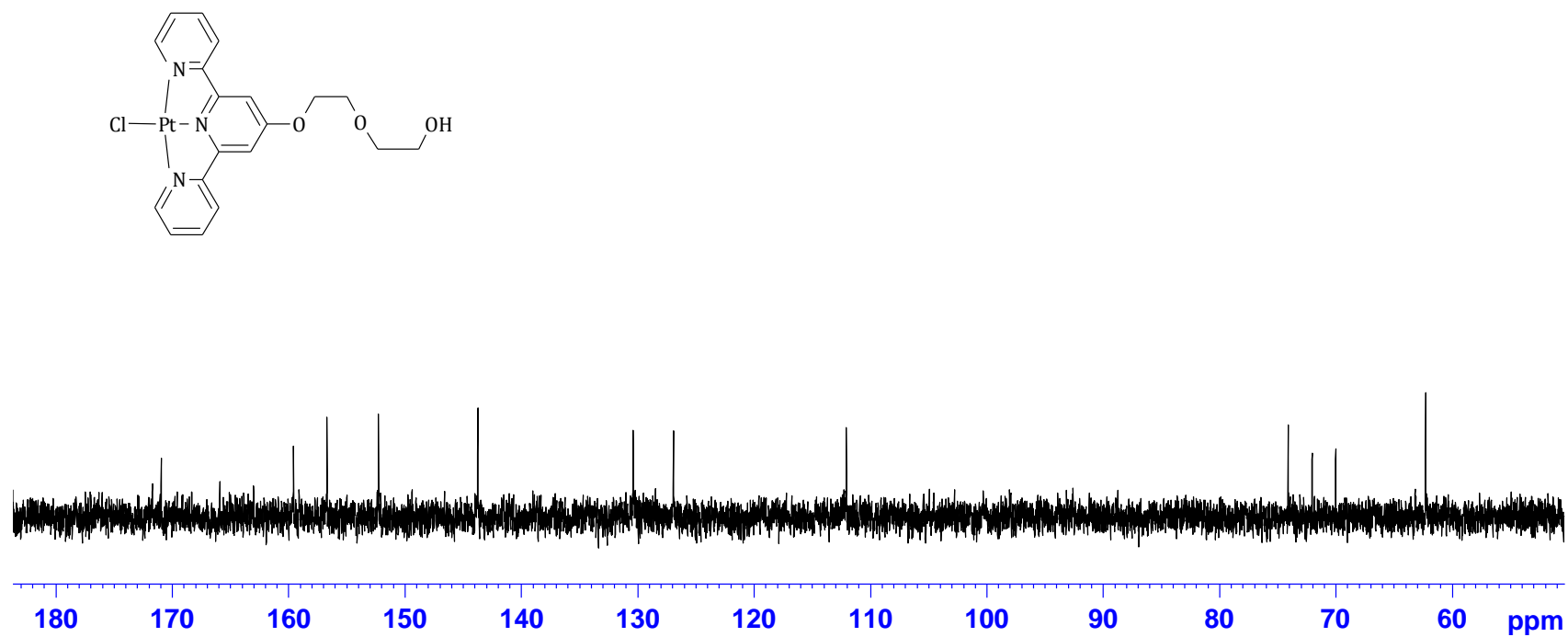


Figure S5.16 <sup>13</sup>C NMR spectrum of Ptttpydeg



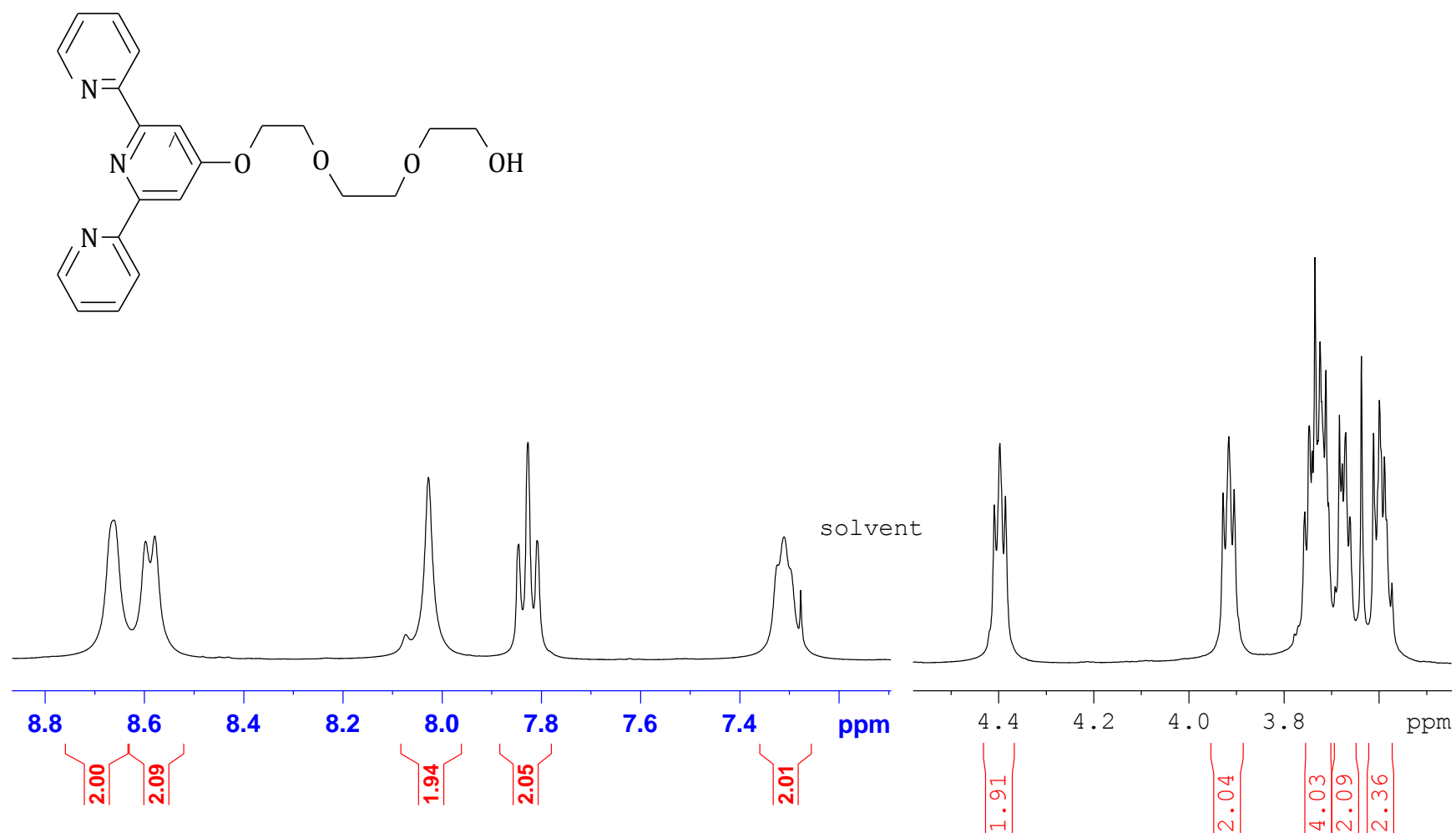


Figure S5.17 <sup>1</sup>H NMR spectrum of 4'-[2-[2-(2-Hydroxyethoxy)ethoxy]ethoxy]-2,2':6',2''-terpyridine in CDCl<sub>3</sub>.

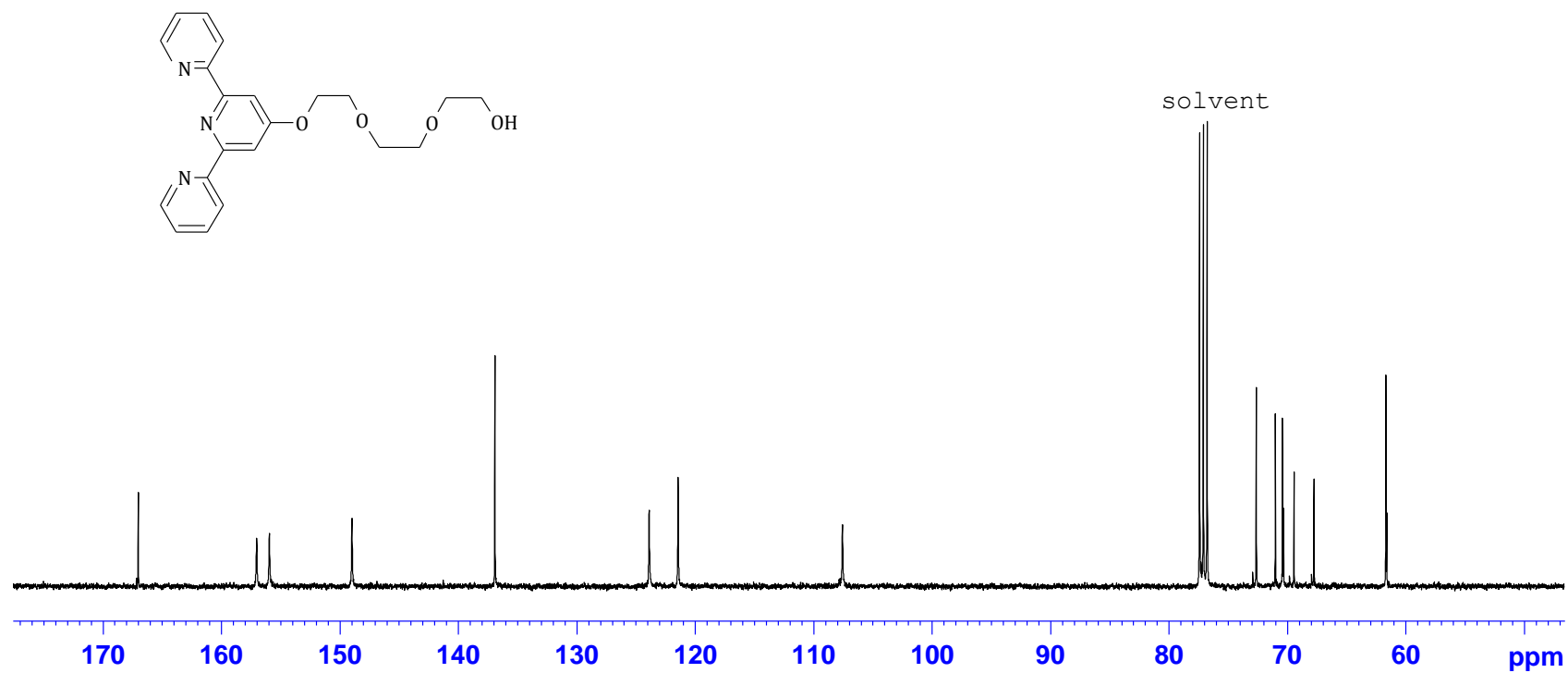


Figure S5.18  $^{13}\text{C}$  NMR spectrum of 4'-{2-[2-(2-Hydroxyethoxy)ethoxy]ethoxy}-2,2':6',2''-terpyridine in  $\text{CDCl}_3$ .

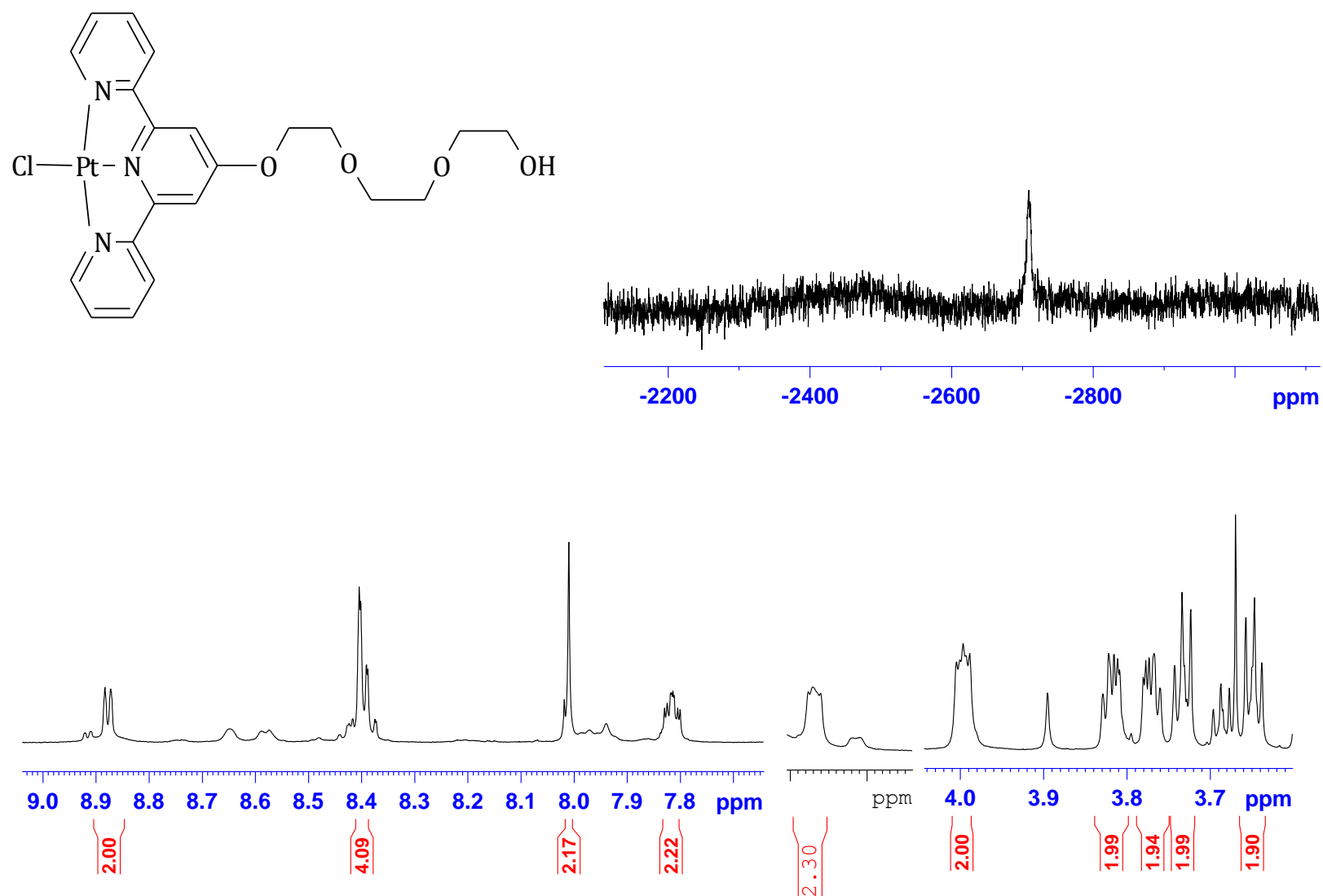
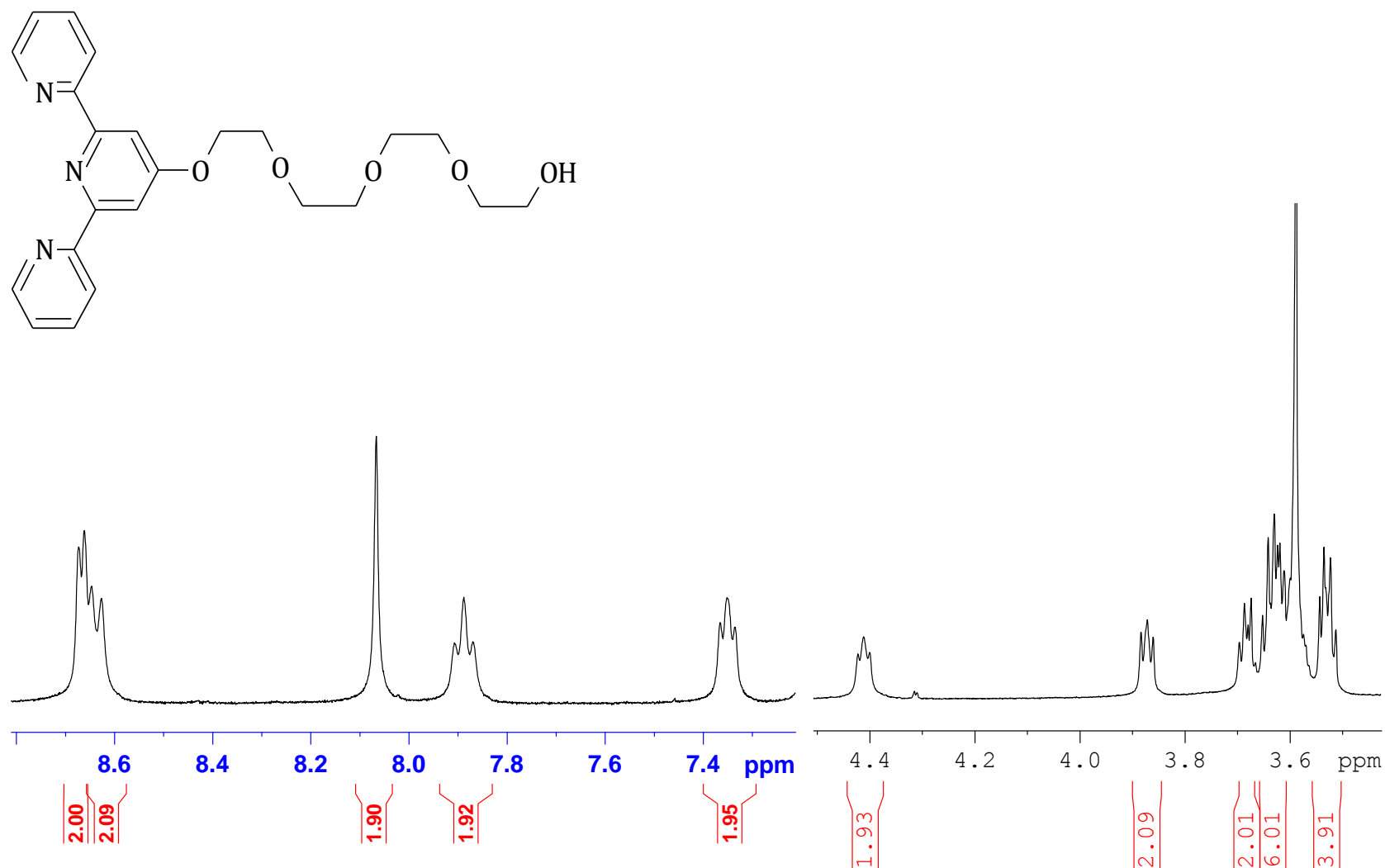
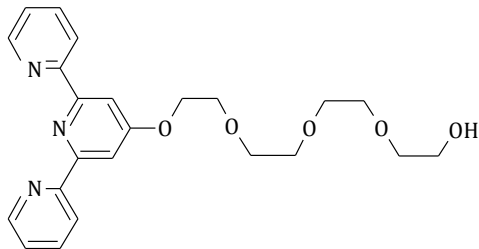
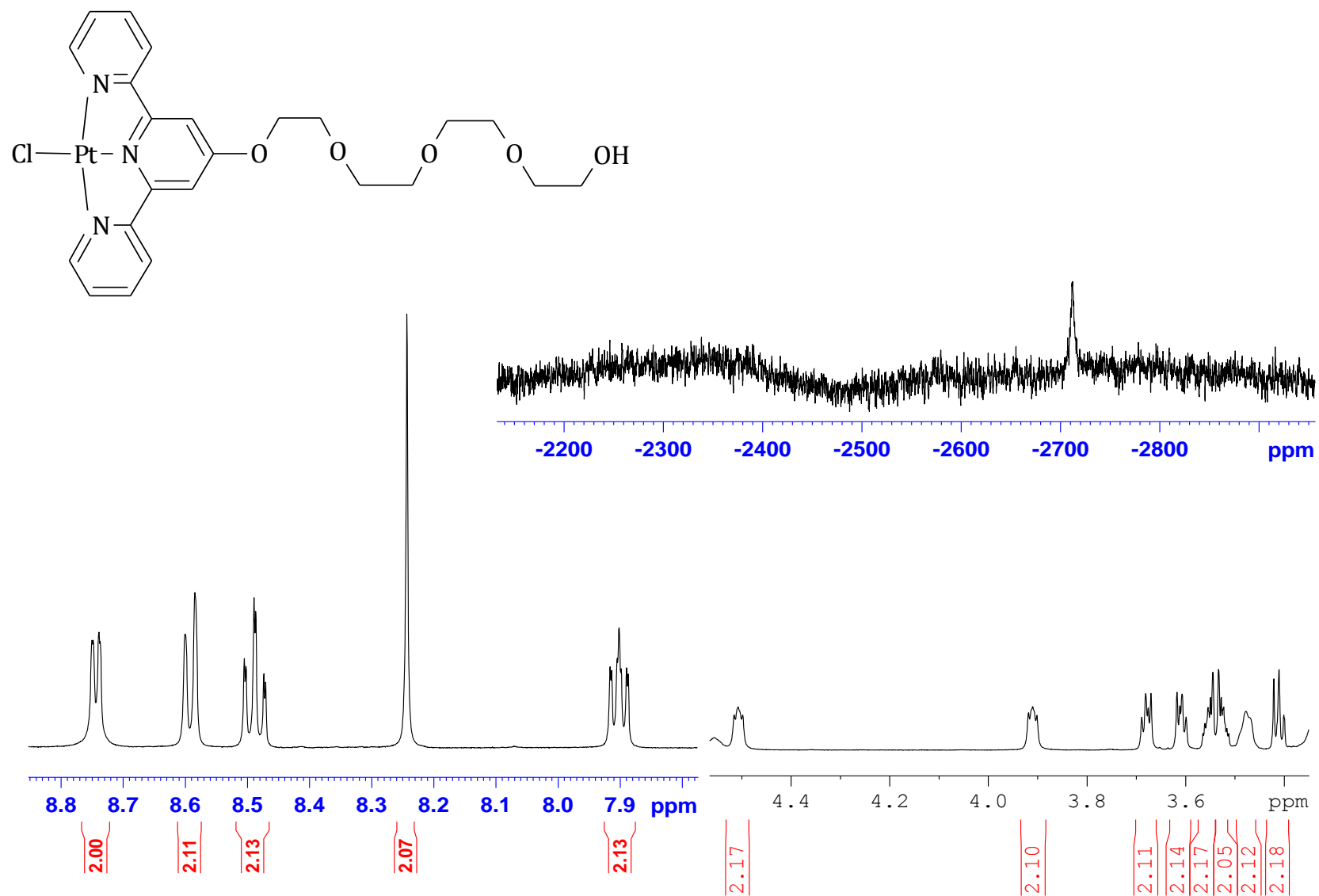


Figure S5.19  $^1\text{H}$  NMR and  $^{195}\text{Pt}$  NMR spectra of Ptptpyteg.





**Figure S5.21**  $^{13}\text{C}$  NMR spectrum of 4'-{2-[2-[2-(2-Hydroxyethoxy)ethoxy]ethoxy]ethoxy}-2,2':6',2'' terpyridine in  $\text{CDCl}_3$ .

Figure S5.22 <sup>1</sup>H NMR and <sup>195</sup>Pt NMR spectrum of Ptptpyteg.

## Elemental Composition Report

Page 1

## Single Mass Analysis

Tolerance = 5.0 PPM / DBE: min = -1.5, max = 50.0

Element prediction: Off

Number of isotope peaks used for i-FIT = 3

Monoisotopic Mass, Even Electron Ions

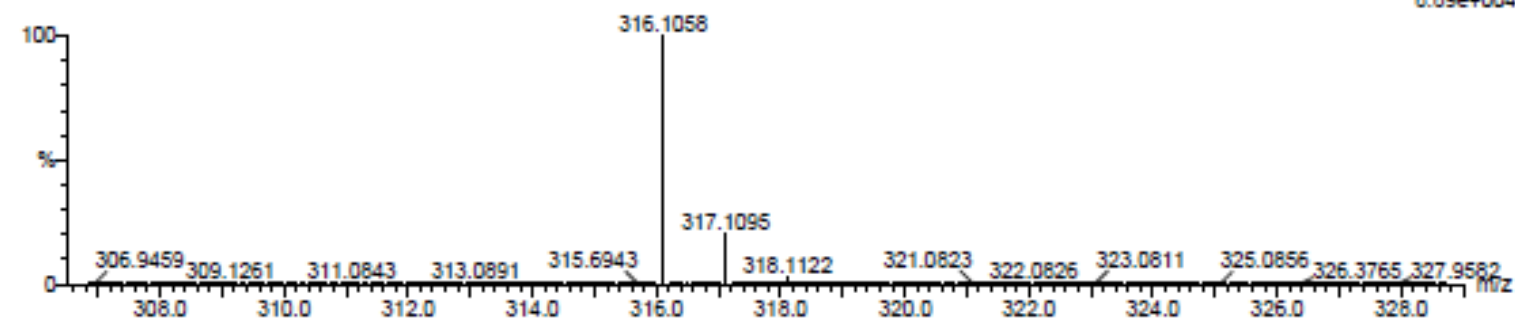
9 formula(e) evaluated with 1 results within limits (all results (up to 1000) for each mass)

Elements Used:

C: 15-20 H: 15-20 N: 0-5 O: 0-3 Na: 1-1

Alshath

tpyeg-ppt 29 (0.478) Cm (1:31)

TOF MS ES+  
8.89e+004

Minimum: -1.5  
Maximum: 5.0 5.0 50.0

Mass	Calc. Mass	mDa	PPM	DBE	i-FIT	i-FIT (Norm)	Formula
316.1058	316.1062	-0.4	-1.3	11.5	519.8	0.0	C17 H15 N3 O2 Na

Figure S5.23 High resolution ESI mass spectrum of tpyeg.

## Elemental Composition Report

Page 1

## Single Mass Analysis

Tolerance = 5.0 PPM / DBE: min = -1.5, max = 50.0

Element prediction: Off

Number of isotope peaks used for i-FIT = 3

Monoisotopic Mass, Even Electron Ions

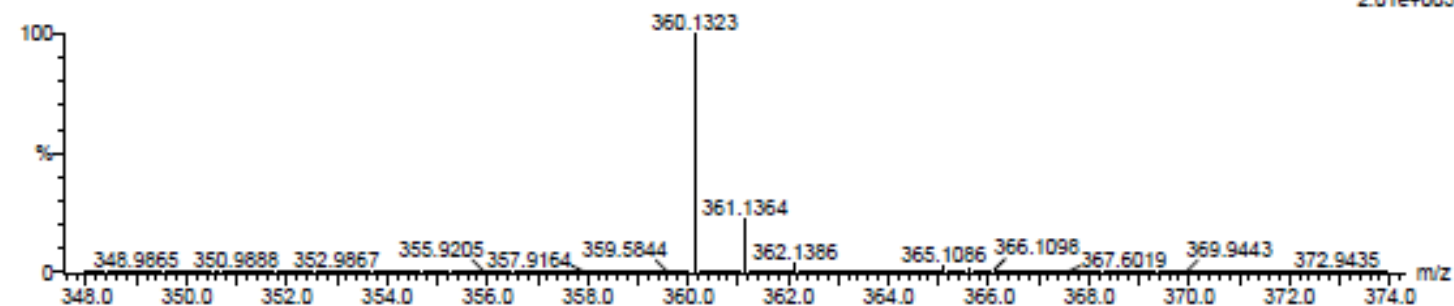
15 formula(e) evaluated with 1 results within limits (all results (up to 1000) for each mass)

Elements Used:

C: 15-20 H: 15-20 N: 0-5 O: 0-5 Na: 1-1

Alshath

tpydeg 16 (0.257) Cm (1:30)

TOF MS ES+  
2.01e+005

Minimum:

Maximum: 5.0 5.0 -1.5

Mass	Calc. Mass	mDa	PPM	DBE	i-FIT	i-FIT (Norm)	Formula
------	------------	-----	-----	-----	-------	--------------	---------

360.1323	360.1324	-0.1	-0.3	11.5	565.0	0.0	C19 H19 N3 O3 Na
----------	----------	------	------	------	-------	-----	------------------

Figure S5.24 High resolution ESI mass spectrum of tpydeg.



## Elemental Composition Report

Page 1

## Single Mass Analysis

Tolerance = 5.0 PPM / DBE: min = -1.5, max = 50.0

Element prediction: Off

Number of isotope peaks used for i-FIT = 3

Monoisotopic Mass, Even Electron Ions

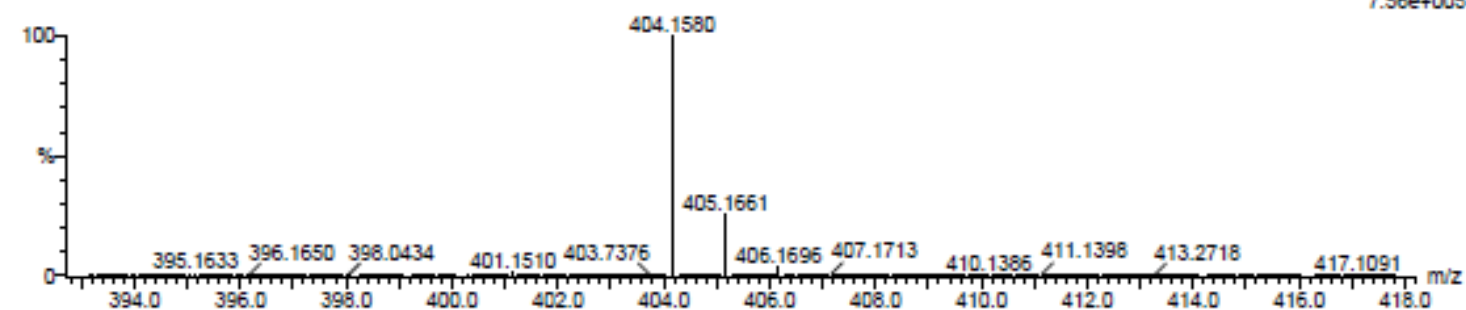
28 formula(e) evaluated with 1 results within limits (all results (up to 1000) for each mass)

Elements Used:

C: 20-25 H: 20-25 N: 0-5 O: 0-5 Na: 0-1

Aishath

tpy teg T1 30 (0.495) Cm (1:31)

TOF MS ES+  
7.56e+005

Minimum: -1.5  
Maximum: 5.0 5.0 50.0

Mass	Calc. Mass	mDa	PPM	DBE	i-FIT	i-FIT (Norm)	Formula
404.1580	404.1586	-0.6	-1.5	11.5	606.7	0.0	C21 H23 N3 O4 Na

Figure S5.25 High resolution ESI mass spectrum of tpyteg.

## Elemental Composition Report

Page 1

## Single Mass Analysis

Tolerance = 5.0 PPM / DBE: min = -1.5, max = 50.0

Element prediction: Off

Number of isotope peaks used for i-FIT = 3

Monoisotopic Mass, Even Electron Ions

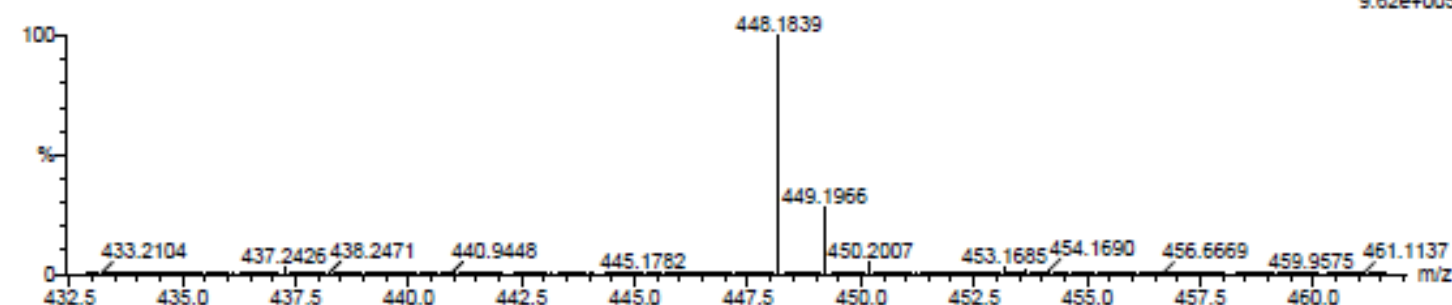
31 formula(e) evaluated with 1 results within limits (all results (up to 1000) for each mass)

Elements Used:

C: 20-25 H: 25-30 N: 0-5 O: 0-5 Na: 0-1

Alshath

tpy t3 T1 2 (0.017) Cm (1:30)

TOF MS ES+  
9.62e+005

Minimum:

Maximum:

-1.5

50.0

Mass	Calc. Mass	mDa	PPM	DBE	i-FIT	i-FIT (Norm)	Formula
------	------------	-----	-----	-----	-------	--------------	---------

448.1839	448.1848	-0.9	-2.0	11.5	588.3	0.0	C23 H27 N3 O5 Na
----------	----------	------	------	------	-------	-----	------------------

Figure S5.26 High resolution ESI mass spectrum of tpytæg.

## Elemental Composition Report

Page 1

## Single Mass Analysis

Tolerance = 5.0 PPM / DBE: min = -1.5, max = 50.0

Element prediction: Off

Number of isotope peaks used for i-FIT = 3

Monoisotopic Mass, Even Electron Ions

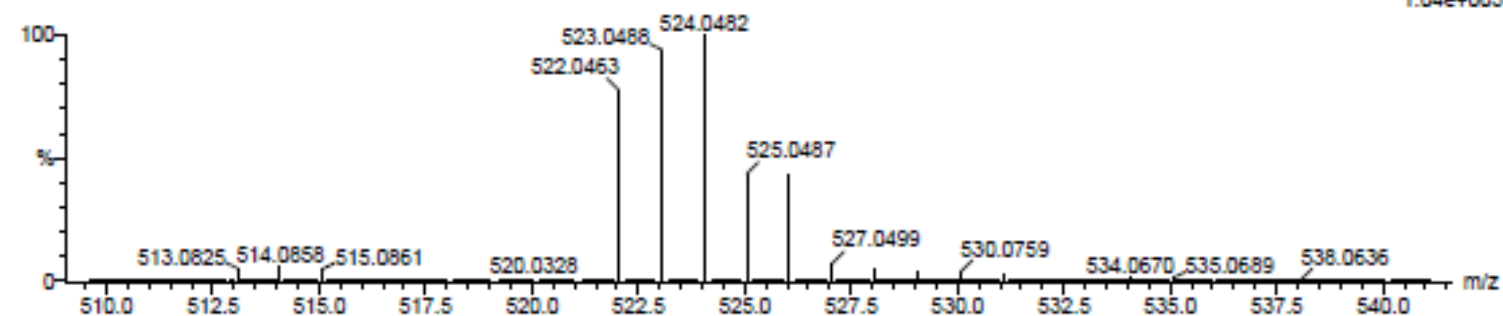
159 formula(e) evaluated with 1 results within limits (all results (up to 1000) for each mass)

Elements Used:

C: 15-20 H: 15-20 N: 0-5 O: 0-5 Cl: 0-2 Pt: 0-1

Aishath

tpy egPt dmso 16 (0.256) Cm (1:30)

TOF MS ES+  
1.04e+005

Minimum:

Maximum:

5.0

5.0

-1.5

50.0

Mass

Calc. Mass

mDa

PPM

DBE

i-FIT

i-FIT (Norm)

Formula

524.0482

524.0471

1.1

2.1

7.5

496.9

0.0

C15 H19 N2 O2 Cl2 Pt

Figure S5.27 High resolution ESI mass spectrum of Ptppyeg.

## Elemental Composition Report

Page 1

## Single Mass Analysis

Tolerance = 4.0 PPM / DBE: min = -1.5, max = 50.0

Element prediction: Off

Number of isotope peaks used for i-FIT = 3

Monoisotopic Mass, Odd and Even Electron Ions

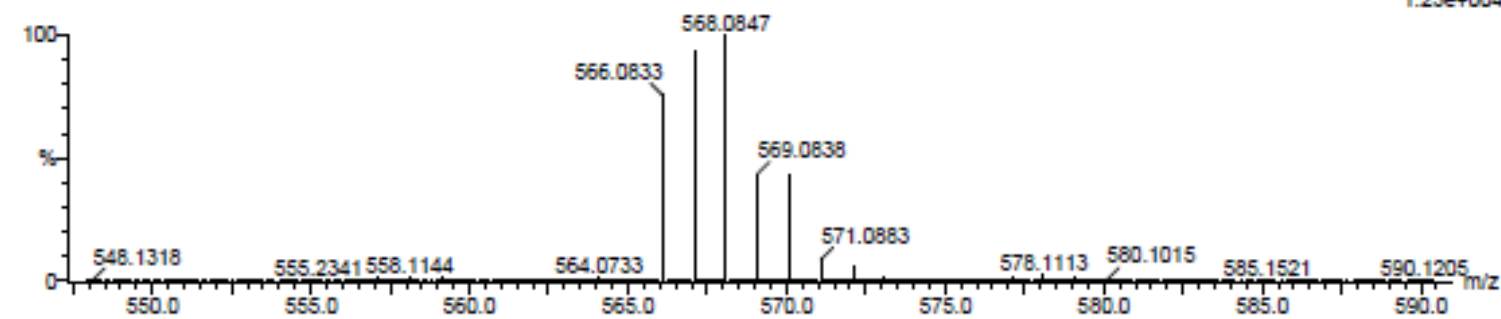
159 formula(e) evaluated with 1 results within limits (all results (up to 1000) for each mass)

Elements Used:

C: 15-20 H: 15-20 N: 0-5 O: 0-5 Cl: 0-2 Pt: 0-1

Alshath

tpydeg pt dmso ppt 25 (0.410) Cm (1:30)

TOF MS ES+  
1.23e+004

Minimum: -1.5  
Maximum: 5.0 4.0 50.0

Mass	Calc. Mass	mDa	PPM	DBE	i-FIT	i-FIT (Norm)	Formula
568.0847	568.0841	0.6	1.1	12.0	384.4	0.0	C19 H20 N3 O3 Cl Pt

Figure S5.28 High resolution ESI mass spectrum of Ptptydeg.

## Elemental Composition Report

Page 1

## Single Mass Analysis

Tolerance = 5.0 PPM / DBE: min = -1.5, max = 50.0

Element prediction: Off

Number of isotope peaks used for i-FIT = 3

Monoisotopic Mass, Even Electron Ions

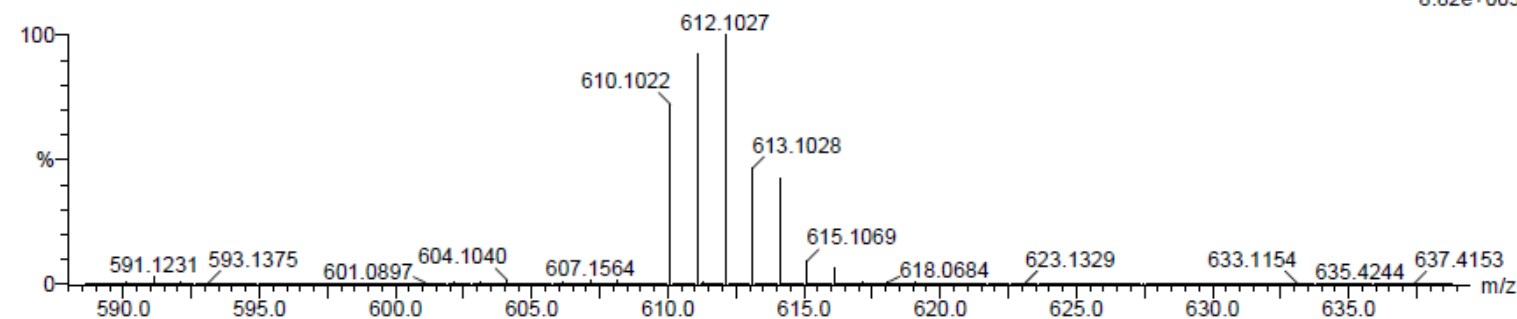
100 formula(e) evaluated with 1 results within limits (all results (up to 1000) for each mass)

Elements Used:

C: 20-25 H: 20-25 N: 0-5 O: 0-5 Cl: 0-1 Pt: 0-1

Aishath

pt tpy teg cod 30 (0.494) Cm (1:31)

TOF MS ES+  
8.82e+003

Minimum: -1.5  
Maximum: 5.0 5.0 50.0

Mass	Calc. Mass	mDa	PPM	DBE	i-FIT	i-FIT (Norm)	Formula
611.1034	611.1025	0.9	1.5	12.5	338.6	0.0	C21 H23 N3 O4 Cl Pt

Figure S5.29 High resolution ESI mass spectrum of Pttpyteg.

## Elemental Composition Report

Page 1

## Single Mass Analysis

Tolerance = 5.0 PPM / DBE: min = -1.5, max = 50.0

Element prediction: Off

Number of isotope peaks used for i-FIT = 3

Monoisotopic Mass, Odd and Even Electron Ions

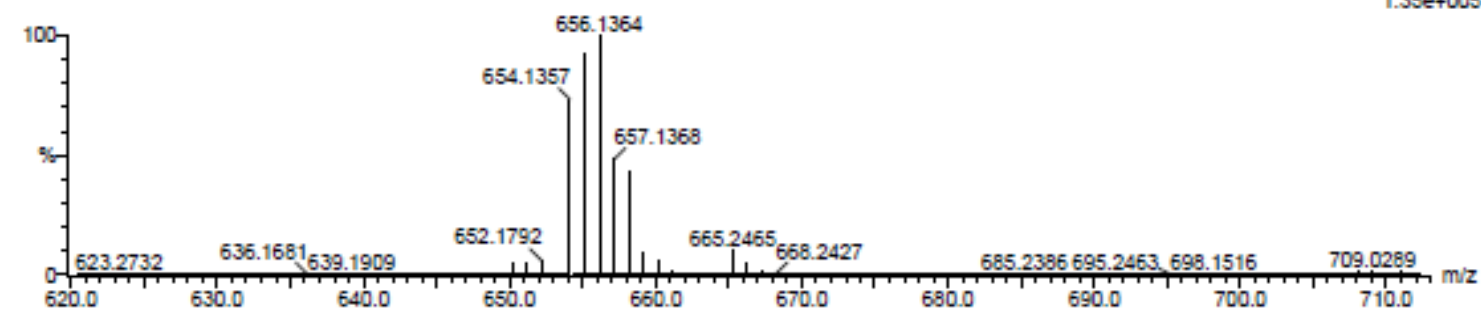
153 formula(e) evaluated with 1 results within limits (all results (up to 1000) for each mass)

Elements Used:

C: 20-25 H: 25-30 N: 0-5 O: 0-5 Cl: 0-2 Pt: 0-1

Alshath

t3 ptoll filtrate dmso 13 (0.205) Cm (1:30)

TOF MS ES+  
1.35e+005

Minimum:

Maximum:

5.0

5.0

-1.5

50.0

Mass

Calc. Mass

mDa

PPM

DBE

i-FIT

i-FIT (Norm)

Formula

656.1364

656.1365

-0.1

-0.2

12.0

460.3

0.0

C23 H28 N3 O5 Cl Pt

Figure S5.30 High resolution ESI mass spectrum of Ptptpytreg.

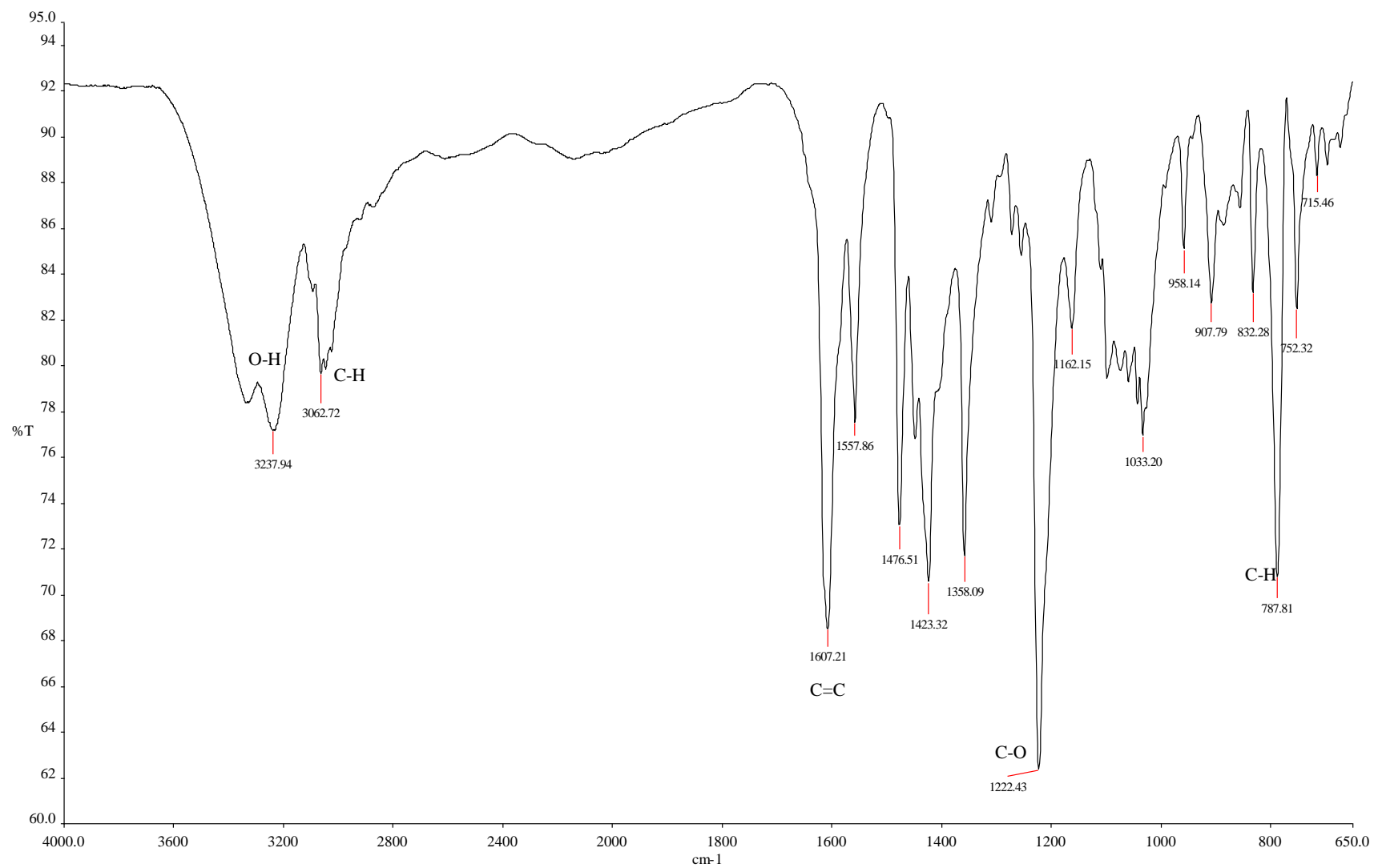


Figure S5.31 IR Spectrum of Pttpyeg.

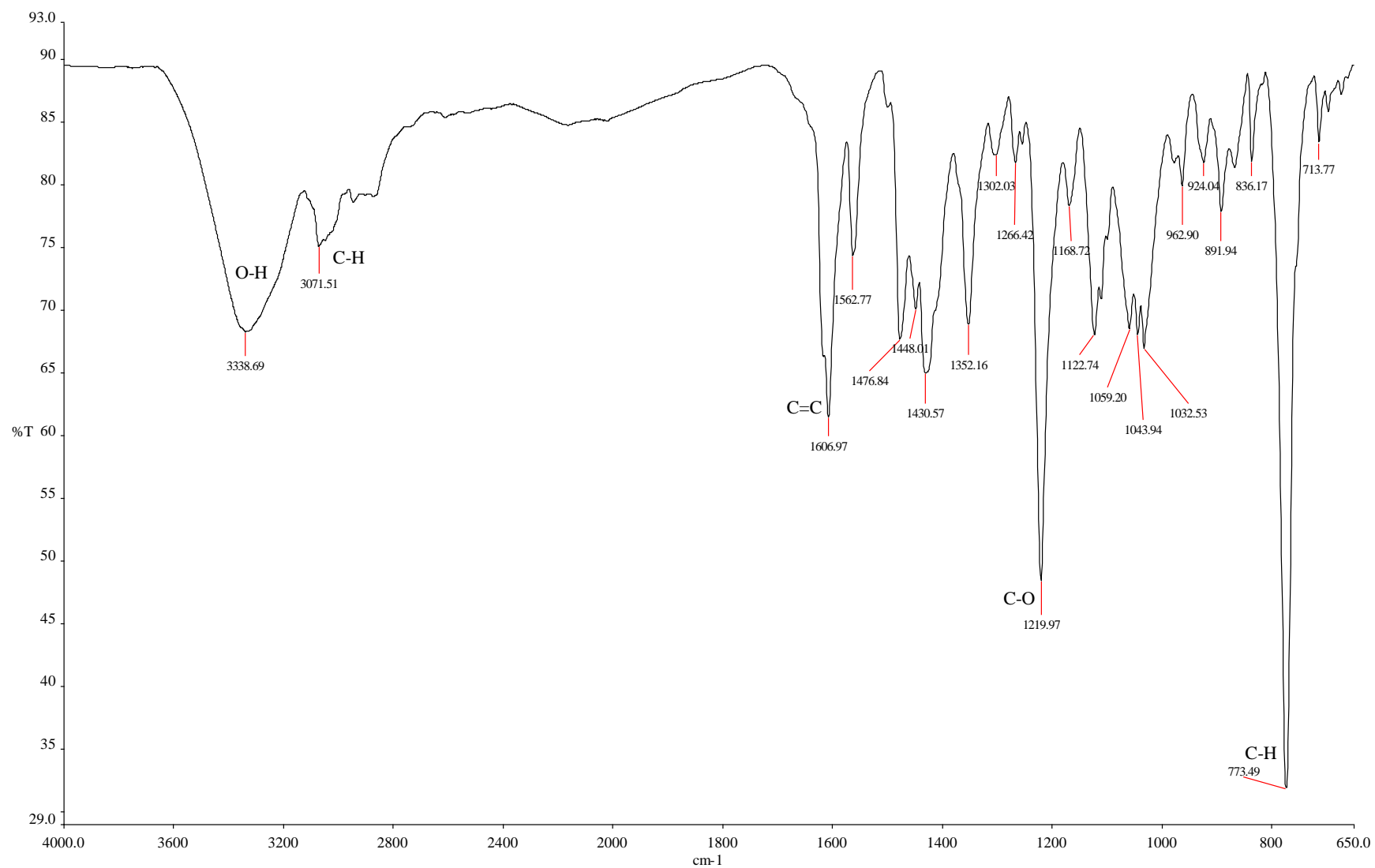


Figure S5.32 IR Spectrum of Pttpydeg.



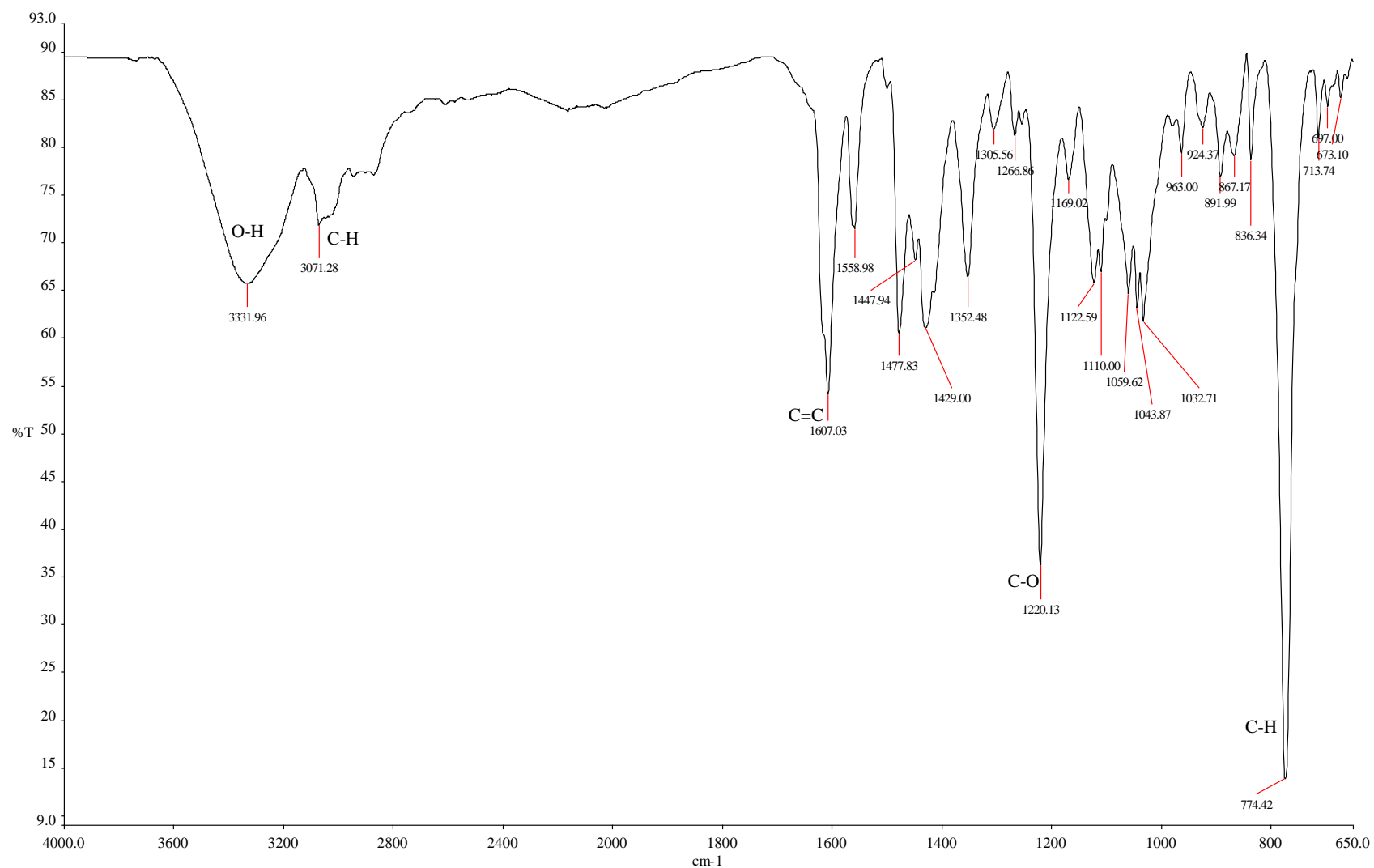


Figure S5.33 IR Spectrum of Pttpyteg.

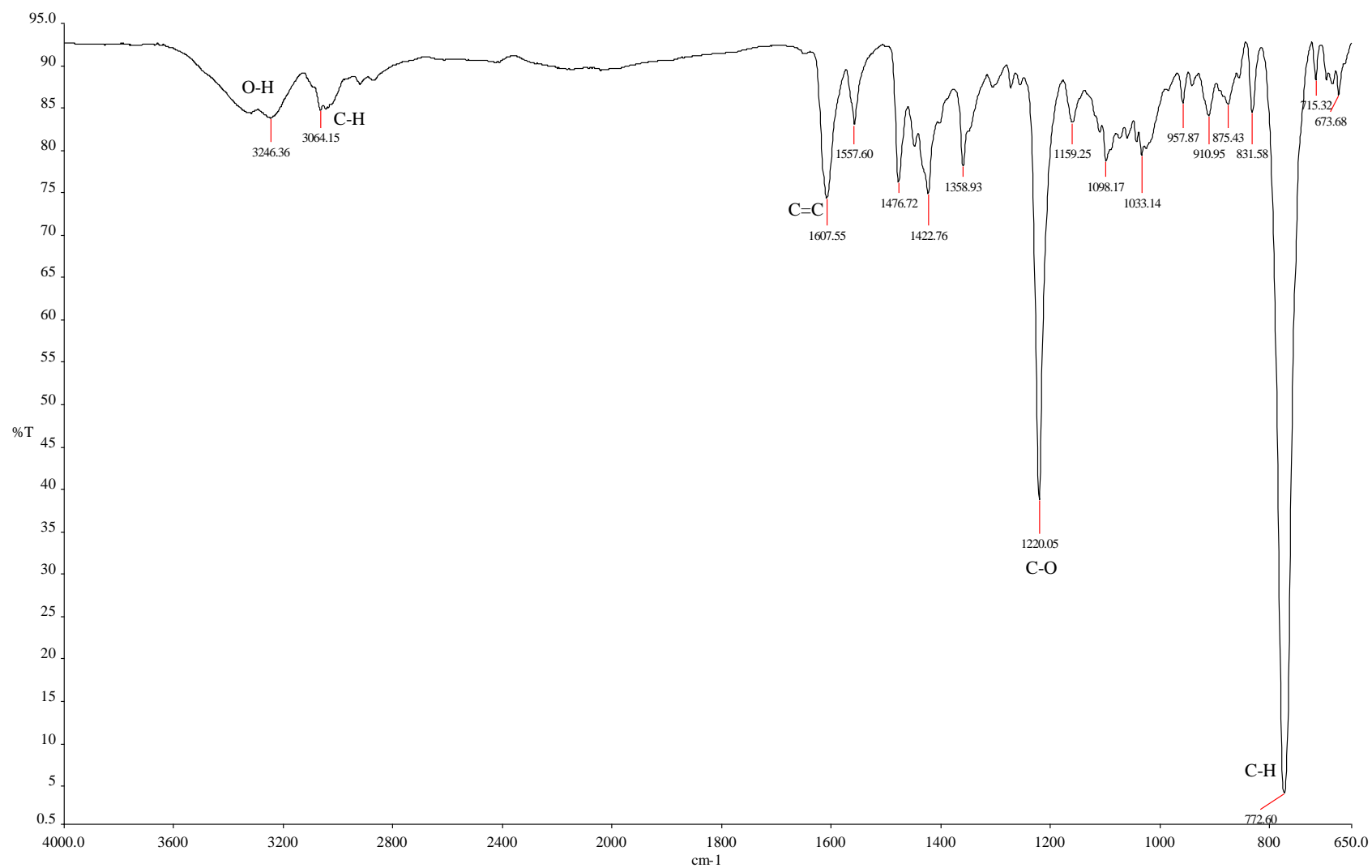
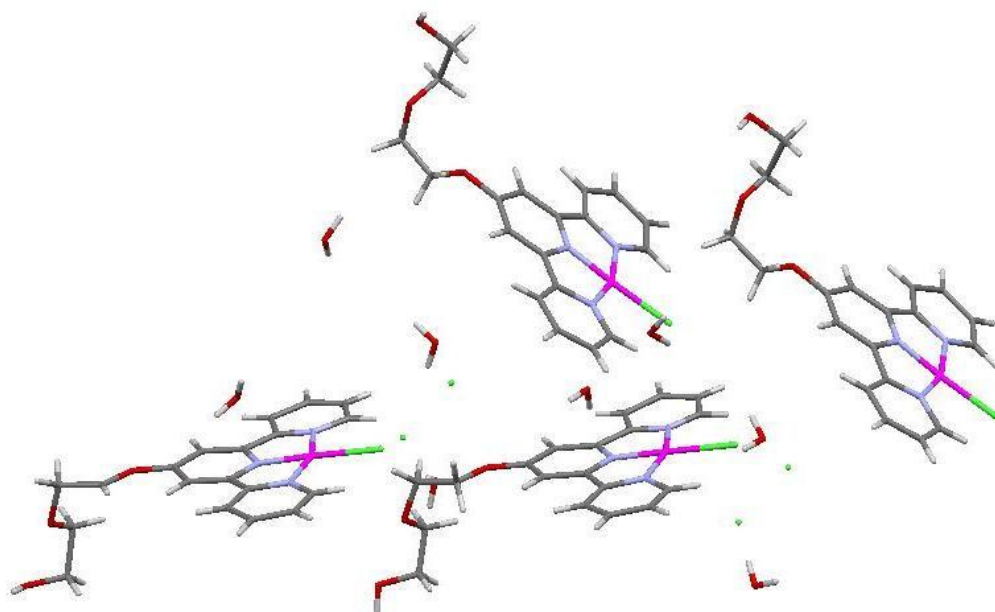
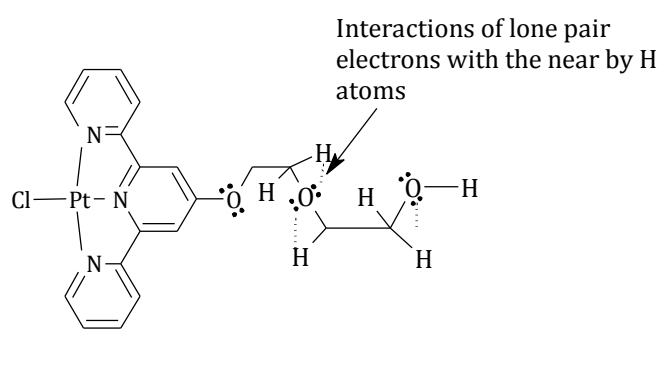


Figure S5.34 IR Spectrum of Pttpytgeg.



**Figure S5.35** Perspective view showing the molecular geometry and atom connectivity for the Pttpydeg complex. Non-H atoms are drawn as 50% thermal ellipsoids and the H atoms as spheres of arbitrary radius.



**Scheme S5.1** Possible electronic interactions and hydrogen bonding within the molecule and between the molecules and solvent.

#### DFT calculations

DFT calculated HOMO and LUMO energies are used to calculate the chemical hardness ( $\eta$ ), electronic chemical potential ( $\mu$ ) and electrophilicity index ( $\omega$ ) by following the Equations (S5.1), (S5.2) and (S5.3) respectively.

$$\eta = (\epsilon_{\text{LUMO}} + \epsilon_{\text{HOMO}})/2 \quad (\text{S5.1})$$

$$\mu = (\epsilon_{\text{HOMO}} + \epsilon_{\text{LUMO}})/2 \quad (\text{S5.2})$$

$$\omega = \mu^2/2\eta \quad (\text{S5.3})$$

**Table of Contents- 6**

List of Figures.....	ii
List of Tables .....	iii
List of Schemes.....	iii
Chapter Six.....	1
<b>A Kinetic and Mechanistic Investigation of Polyethyleneglycol Ether Bridged Dinuclear Platinum(II) 2,2':6',2''-Tpyridine Complexes .....</b>	<b>1</b>
6.0    Abstract.....	1
6.1    Introduction .....	1
6.2    Experimental.....	4
6.2.1    Materials .....	4
6.2.2    Synthesis of Ligands.....	5
6.2.3    Synthesis of Platinum(II) Complexes .....	6
6.2.4    Instrumentation and Physical Measurements .....	8
6.2.5    Computational Modelling.....	8
6.2.6    Kinetic Analyses .....	9
6.3    Results .....	9
6.3.1    Computational Modelling.....	13
6.4    Discussion.....	18
6.5    Conclusions.....	23
6.6    References.....	24
6.7    Supporting Information .....	28

**List of Figures**

Figure 6.1	Structures of polyethyleneglycol ether linked dinuclear Pt(II) complexes studied. Shown on the diagram is the numbering scheme used. Ptppy is included for comparisons.....	4
Figure 6.2	Kinetic trace at 301 nm for the reaction of Ptdtteg ( $3.0 \times 10^{-5} \text{ mol dm}^{-3}$ ) with DMTU ( $8.99 \times 10^{-4} \text{ mol dm}^{-3}$ ) at 298 K, $I = 0.02 \text{ M LiCF}_3\text{SO}_3$ , adjusted with LiCl. ....	10
Figure 6.3	Dependence of the <i>pseudo</i> first-order rate constants ( $k_{\text{obs}}$ ) on the concentrations of the nucleophiles for the chloride substitution from Ptdteg ( $2.65 \times 10^{-5} \text{ M}$ ) in methanol solution ( $I = 0.02 \text{ M}$ ) at 298 K.....	11
Figure 6.4	Eyring plots obtained for Ptdteg with the nucleophiles for the forward reactions over the temperature range 15 - 35 °C.....	13
Figure 6.5	Aerial view showing the angles of inclination, $\alpha$ , in the DFT calculated distorted slip-up stair case like linkers and the angle of twisting ( $\delta$ ) of the tpy moieties from each other. ....	15
Figure 6.6	DFT calculated minimum energy structures, frontier molecular orbitals (HOMO and LUMO) of Ptppy, Ptdt and Ptdteg. Data for Ptppy is included for comparisons. Data for Ptdtdeg, Ptdtteg and Ptdttteg are included in <i>Figure S1</i> (Supporting Information).....	17
Figure 6.7	$^{195}\text{Pt}$ NMR the reaction mixture of Ptdtteg ( $2 \times 10^{-2} \text{ M}$ ) with six equivalents of TU (2.0 M), showing a peak for pure dinuclear Pt(II) complex at $\delta = -2687 \text{ ppm}$ before the reaction ( $t = 0$ ) and the final substituted product (B, $\delta = -3099 \text{ ppm}$ ) corresponding to $[(\text{TU})\text{Pt}(\text{dtteg})\text{Pt}(\text{TU})]^{4+}$ , over a period of 4.5 hours after the reaction begins.....	19
Figure 6.8	$^1\text{H}$ spectra of Ptdttteg (0.02 M) in DMSO- $d_6$ at temperatures, 30 °C to 80 °C.....	22

**List of Tables**

Table 6.1	Summary of the second-order rate constants, $k_2$ and activation parameters, with the corresponding standard deviations for the substitution of the chloro ligands by a series of thiourea nucleophiles at $I = 0.02 \text{ M LiCF}_3\text{SO}_3$ , adjusted with LiCl. Data for Ptpty is taken from literature and included for comparison. ....	12
Table 6.2	Geometry optimised structures of the complexes investigated. ....	16
Table 6.3	Summary of DFT calculated data for the complexes investigated. Included is the data obtained for the DFT calculated Ptpty complex for comparisons.....	18

**List of Schemes**

Scheme 6.1	Proposed substitution mechanism for the dinuclear Pt(II) complex system with thiourea nucleophiles. ....	11
------------	--	----

# Chapter Six

## A Kinetic and Mechanistic Investigation of Polyethyleneglycol Ether Bridged Dinuclear Platinum(II) 2,2':6',2''-Tpyridine Complexes

### 6.0 Abstract

A series of dinuclear Pt(II) complexes bridged with polyethyleneglycol ether of the type  $[\text{ClPt}(\text{tpy})-\text{O}(\text{CH}_2\text{CH}_2\text{O})_n(\text{tpy})\text{PtCl}]\text{Cl}_2$  where  $n = 1$  (**Ptdteg**), 2 (**Ptdtdeg**), 3 (**Ptdtteg**), 4 (**Ptdttteg**) and linker free complex,  $\text{ClPt}(\text{tpy})-(\text{tpy})\text{PtCl}]\text{Cl}_2$ , (**Ptdt**), (where tpy = 2,2':6',2''-terpyridine) were synthesized and characterized to investigate the role of bridging polyethyleneglycol ether linker on the substitution reactivity of the dinuclear Pt(II) complexes. Substitution reactions were studied using thiourea nucleophiles viz. thiourea (TU), 1,3-dimethyl-2-thiourea (DMTU), 1,1,3,3-tetramethyl-2-thiourea (TMTU) under *pseudo* first-order conditions as a function of concentration and temperature by conventional stopped-flow reaction analyser. The reactions gave single exponential fits following the rate law  $k_{\text{obs}} = k_2[\text{Nu}]$ . Introduction of polyethyleneglycol ether linker decreases the electrophilicity of the platinum centre and the whole complex. The results obtained indicate that the rate of substitution reactions is controlled by both electronic and steric hindrance which increases with the length of the linker. Experimental results are supported by the density functional theory (DFT) calculations and structures obtained at LanL2DZ/ B3LYP level. The order of the reactivity of the nucleophiles is  $\text{TU} > \text{DMTU} > \text{TMTU}$ . The magnitude and the size of the enthalpy of activation and entropy of activation support an associative mode of mechanism, where bond formation in the transition state is favoured.

### 6.1 Introduction

Platinum metallodrugs play an important role in the treatment of cancer and modification of nucleic acids.<sup>1</sup> Today, multinuclear platinum complexes comprise a new class of promising anticancer agents with comparable cytotoxicity.<sup>2</sup> Compared to cisplatin, they are more water soluble and offer better DNA interactions due to their high charge.<sup>3</sup> The multinuclear Pt(II) complexes that can interact with DNA were first synthesized by Farrell *et al.*<sup>2f,4</sup> The most successful of these complexes are the monodentate amine complexes,  $[[\{\text{trans-PtCl}(\text{NH}_3)_2\}_2\{\mu\text{-trans-}$

$\text{Pt}(\text{NH}_3)_2(\text{NH}_2(\text{CH}_2)_6\text{NH}_2)_2\}^{4+}$  (**BBR3464**) and  $[\{\text{trans-PtCl}(\text{NH}_3)_2\}_2\{\mu\text{-C}_2\text{H}_4(\text{NH}_2(\text{CH}_2)_6\text{NH}_2)_2\}]^{4+}$  (**BBR3610**).<sup>2i,4b,5</sup> The complexes show enhanced cytotoxicity against lung, pancreatic and melanoma cancers.<sup>2b</sup> The interaction of these complexes with DNA were found to be based on their structural-activity relationships that depend on the length of the linker and the average distance between the Pt(II) centres.<sup>2a,4a,6</sup> Furthermore, for dinuclear Pt(II) complexes it was found that the reactivity of the first metal centre is independent of the other.<sup>7</sup> However, in some cases the interactions between the two Pt(II) centres have been reported.<sup>8</sup> Therefore, there is limited data in literature for one to formulate a clear relationship between the nature of the bridging ligands and the reactivity of the Pt(II) centres.<sup>9</sup>

Apart from the Pt...Pt distances, the nature of the linker or the spacer plays a crucial role in the cytotoxicity and the reactivity of multinuclear complexes.<sup>9-10</sup> For example, the flexibility and the hydrophilicity of the linker influences the reactivity and the cytotoxicity of the complexes in a biological environment.<sup>9</sup> The hydrophilicity of the linker can be increased by introducing polar groups into its linker.<sup>11</sup> The advantage of having a flexible linking unit over a mono nuclear complex is that the linker provides a variable flexibility and reduces the steric hindrance between the two monomer binding units.<sup>11</sup> Furthermore, hydrophilic flexible bridging linkers between two platinum centres can provide additional interactions with the proteins and the biomolecules in the body which in turn might enhance the transport of drug carrying ability in the body.<sup>11</sup> For instance, in the case of **BBR3464**, one of the factors accounted for its higher activity against tumour cells was attributed to its ability to form long range flexible intrastand cross links, straddling over four nucleobases of DNA.<sup>12</sup>

2,2':6',2''-terpyridine, most commonly known as tpy and its derivatives are extensively used in research applications mostly due to their excellent photochemical and DNA intercalating properties.<sup>7a,11</sup> In some cases, coordinated compounds of terpyridine do not show cytotoxic behaviour.<sup>13</sup> However, coupling of two active terpyridine moieties with flexible linkers were found to improve this activity.<sup>10a</sup> Good examples of such flexible linkers include alkyldiamine and ethyleneglycol ligands. The ethyleneglycol ether linker increases the flexibility of the ligand so that it can wrap around the DNA.<sup>10a</sup> Previous studies have shown that a number of multinuclear complexes have been synthesized using this linker and 4'-chloroterpyridine ligand. Biological activities of such complexes have been studied using 9-ethylguanine, (Etg).

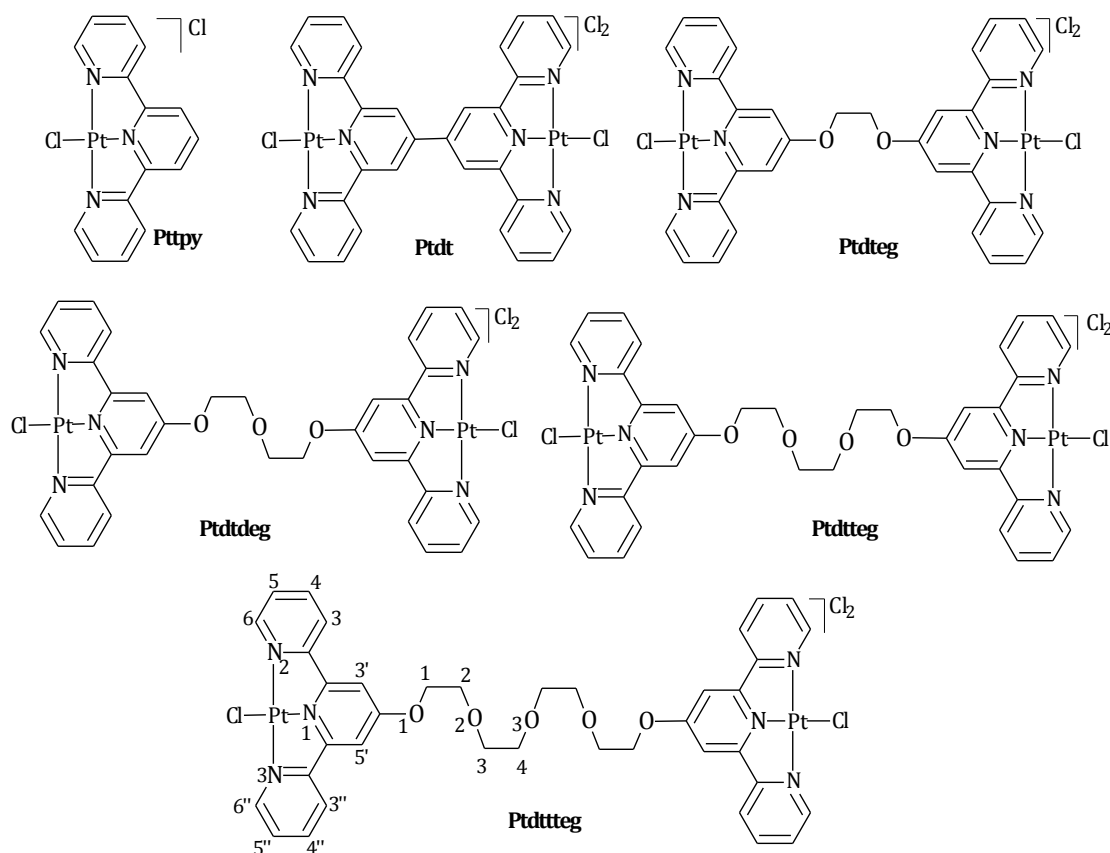


DNA interaction of the dinuclear Pt(II) complex, [ClPt(dtdeg)PtCl] (where dtdeg = bis[4'-(2,2':6',2''-terpyridyl)]-diethyleneglycol ether) studied by using Calf Thymus (CT) DNA as a substrate,<sup>10a</sup> was reported to show very high activity against all the cancer cell lines tested. In some cases the activity was found to be greater than the well known anticancer drug, cisplatin.<sup>10a</sup> Furthermore, the activity of the dinuclear complex was found to be higher than its mononuclear complex, [Pt(tpy)Cl]Cl, indicating that the modification of the primary terpyridine ligand system improves the biological activity of the complex.<sup>10a</sup> However, to understand the behaviour of interaction with DNA, one needs to understand the mechanism of action of substitution behaviour of such complexes with the biological molecules.

The mechanistic understanding of how flexible linkers control the ligand substitution behaviour at the platinum centres has not been studied extensively. Recently, a number of ligand substitution reactions of dinuclear Pt(II) complexes have been reported.<sup>10b,14</sup> Studies have shown that reactivity is controlled by the distance between the platinum centres and the symmetry of the complexes.<sup>14b,c</sup> The increase in reactivity was attributed to an increase in charge density around the platinum centre facilitated by the increase in the electrostatic interactions with simultaneous reduction of the  $\sigma$ -donation to each platinum centre.<sup>14c</sup> Substitution of aqua ligands from an alkyldiamine bridged dinuclear platinum complexes further support the decrease in the reactivity with the increase in the length of the flexible alkyldiamine linker.<sup>14a,b</sup> Furthermore, the results obtained showed a greater reactivity for the odd number of CH<sub>2</sub> groups in the alkyldiamine ligand due to their geometry.<sup>14a,14c</sup>

In **Chapter 5**, with the mononuclear Pt(II) complexes, it was found that the  $\sigma$ -donicity of polyethylene glycoxy linker reduces the  $\pi$ -acceptability of terpyridine. In this study, our aim is to increase our understanding of the role of flexible polyethyleneglycol ether linkers on the reactivity of dinuclear Pt(II) terpyridine complexes when a second terpyridine group is coupled with the polyethylene glycoxy pendant. To accomplish this, we have synthesized and characterized five dinuclear Pt(II) complexes, of which, four complexes are linked by polyethyleneglycol ether units of different monomer units. The linker-free dinuclear complex, **Ptdt** was used to gain an in-depth understanding on the role of the ethyleneglycol ether linker on controlling the reactivity of the dinuclear complexes. The monomeric unit, [Pt(tpy)Cl]<sup>+</sup> and Pt(II) (4'-(ethylene glycoxy)-2,2':6',2''-terpyridine (**Ptptyeg**) from **Chapter 5** is used to compare

the reactivity of the dinuclear complexes. The complexes used in this investigation are shown in *Figure 6.1*.



**Figure 6.1** Structures of polyethyleneglycol ether linked dinuclear Pt(II) complexes studied. Shown on the diagram is the numbering scheme used. Ptpy is included for comparisons.

## 6.2 Experimental

### 6.2.1 Materials

Methanol (Merck) was distilled over magnesium prior to use for kinetic analysis.<sup>15</sup> Dimethylsulfoxide (99.9%) from Aldrich was used without any further purification. Ethylene glycol (99.8%), diethylene glycol (99%) and triethylene glycol (99%) were bought from Sigma Aldrich. The ligand, 4'-chloro,2,2':6',2''-tpyridine (97%), tetraethylene glycol (99%), and the platinum salt, potassium tetrachloroplatinate (II) (99.9%) were bought from Aldrich. All the other chemicals were purchased from Sigma Aldrich and were used without further purification.

### 6.2.2 Synthesis of Ligands

The ligand 6',6''-Bis(2-pyridyl)-2,2':4',4'' :2'',2'''-quaterpyridine (dt) was synthesized following a literature method<sup>16</sup> and ethyleneglycol ether linked ligands were synthesized according to the literature procedure.<sup>17</sup>

#### 6',6''-Bis(2-pyridyl)-2,2':4',4'' :2'',2'''-quaterpyridine (dt)<sup>16</sup>

To a solution of  $[\text{Ni}(\text{PPh}_3)_2\text{Cl}_2]$  (2.94 g, 4.5 mmol) and  $\text{PPh}_3$  (2.36 g, 9 mmol) in DMF (15 mL) was added zinc dust (0.30 g, 4.5 mmol) and the reaction mixture was stirred at room temperature for 30 minutes. The resulting red suspension was treated with 4'-chloro-2,2':6',2''-terpyridine (0.6 g, 4.5 mmol) which immediately changed to dark green. After stirring the reaction mixture at room temperature for 8 hours, the solvent was removed in *vacuo*. The residue obtained was boiled in water (50 mL) for 10 minutes, cooled and filtered. The greenish brown filtrate was treated with ammoniumhexafluorophosphate (1.5 g, 9 mmol). The precipitate formed was filtered and the solid was dissolved in a mixture of acetonitrile and water (1 : 4, 50 mL) and refluxed for one hour with sodium cyanide (1.5 g, 30 mmol). The yellow solid formed was filtered, washed with methanol and dried. Recrystallization of the solid in methanol (20 mL) gave colourless needles.

Yield: 111 mg, (69%), colourless needles. The  $^1\text{H}$  NMR spectra and the mass spectra are in good agreement with the proposed chemical structure.  $^1\text{H}$ NMR (400 MHz,  $\text{CDCl}_3$ )  $\delta$ /ppm<sup>†</sup>: 8.72 (4H, d, 6 6''), 8.61 (4H, d, 3 3''), 8.51 (4H, s, 3' 5'), 7.88 (4H, dt, 4 4''), 7.35 (4H, dt, 5 5''). TOF MS-ES<sup>+</sup>, m/z: 487.1639, (M+Na)<sup>+</sup>.

#### Synthesis of bis[4'-(2,2':6',2''-tpyridyl)]- ethyleneglycol ether Ligands<sup>17</sup>

A mixture of ethyleneglycol (with variable chain lengths viz. ethyleneglycol, diethyleneglycol, triethyleneglycol and tetraethyleneglycol) with 2 equivalents of 4'-chloro-2,2':6',2''-tpyridine and excess KOH were stirred in dry DMSO at 60 °C for 24 hours, under nitrogen. After cooling the reaction mixture to room temperature, water was added, which resulted in a white precipitate. The precipitate was filtered, washed with water and air dried. The crude product was refluxed in Ethanol (98%) for half an hour. The pure product was precipitated upon cooling the mixture in ice for about 30 minutes. The precipitate was filtered, washed with a small amount of ice cold ethanol and air dried.

<sup>†</sup> s = singlet, d = doublet, t = triplet, dt = doublet of a triplet. The same representation is used for the other complexes.

The purity of the ligands was confirmed by using  $^1\text{H}$  NMR and mass spectroscopy. The  $^1\text{H}$  NMR spectra obtained show similarity in the aromatic region for the ethyleneglycol ether linked ligands.

**Bis[4'-(2,2':6',2''-terpyridyl)]- ethyleneglycol ether (dteg):** Yield: 109 mg, (54%), off white powder.  $^1\text{H}$  NMR (400 MHz,  $\text{CDCl}_3$ )  $\delta$ / ppm: 8.72 (4H, d, 6 6''), 8.65 (4H, d, 3 3''), 8.15 (4H, s, 3' 5'), 7.88 (4H, dt, 4 4''), 7.35 (4H, dt, 5 5''), 4.71 (4H, t,  $\text{CH}_2$ ), TOF MS-ES $^+$ , m/z: 547.1857, (M+Na) $^+$ .

**Bis[4'-(2,2':6',2''-terpyridyl)]- diethyleneglycol ether (dtdeg):** Yield: 185 mg, (80%), off white powder.  $^1\text{H}$  NMR (400 MHz,  $\text{CDCl}_3$ )  $\delta$ / ppm: 8.69 (4H, d, 6 6''), 8.61 (4H, d, 3 3''), 8.08 (4H, s, 3' 5'), 7.85 (4H, dt, 4 4''), 7.33 (4H, dt, 5 5''), 4.47 (4H, t,  $\text{CH}_2$ ), 4.07 (4H, t,  $\text{CH}_2$ ), TOF MS-ES $^+$ , m/z: 591.2115, (M+Na) $^+$ .

**Bis[4'-(2,2':6',2''-terpyridyl)]- triethyleneglycol ether (dtteg):** Yield: 103 mg, (65%), off white powder.  $^1\text{H}$  NMR (400 MHz,  $\text{CDCl}_3$ )  $\delta$ / ppm: 8.69 (4H, d, 6 6''), 8.61 (4H, d, 3 3''), 8.05 (4H, s, 3' 5'), 7.84 (4H, dt, 4 4''), 7.32 (4H, dt, 5 5''), 4.42 (4H, t,  $\text{CH}_2$ ), 3.97 (4H, t,  $\text{CH}_2$ ), 3.81 (4H, t,  $\text{CH}_2$ ), TOF MS-ES $^+$ , m/z: 635.2371, (M+Na) $^+$ .

**Bis[4'-(2,2':6',2''-terpyridyl)]- tetraethyleneglycol ether (dtteg):** Yield: 98 mg, (67%), off white powder.  $^1\text{H}$  NMR (400 MHz,  $\text{CDCl}_3$ )  $\delta$ / ppm: 8.69 (4H, d, 6 6''), 8.61 (4H, d, 3 3''), 8.05 (4H, s, 3' 5'), 7.84 (4H, dt, 4 4''), 7.31 (4H, dt, 5 5''), 4.40 (4H, t,  $\text{CH}_2$ ), 3.94 (4H, t,  $\text{CH}_2$ ), 3.78 (4H, t,  $\text{CH}_2$ ), 3.72 (4H, t,  $\text{CH}_2$ ), TOF MS-ES $^+$ , m/z: 679.2626, (M+Na) $^+$ .

### 6.2.3 Synthesis of Platinum(II) Complexes

#### Synthesis of 6',6''-Bis(2-pyridyl)-2,2':4',4'' :2 ',2'''-quaterpyridine Platinum(II), (Ptdt)

The silver salt  $\text{AgSbF}_6$  (68.5 mg, 0.200 mmol) was dissolved in acetonitrile (5 mL) and added to a suspension of platinum salt,  $[\text{Pt}(\text{PhCN})_2\text{Cl}_2]$  (99 mg, 0.200 mmol) in acetonitrile (10 mL). The mixture was refluxed overnight under an inert atmosphere and the resultant precipitate of  $\text{AgCl}$  was filtrated. An equimolar amount of 6',6''-Bis(2-pyridyl)-2,2':4',4'' :2 ',2'''-quaterpyridine (92.9 mg, 0.200 mmol) was added to the filtrate and the mixture was refluxed for an additional 24 hours. Once the reflux was complete, the mixture was filtered hot and the solvent partially removed under *vacuo* resulting in the precipitation of  $[\text{Pt}\{6',6''\text{-Bis(2-pyridyl)-2,2':4',4'' :2 ',2'''-}$

quaterpyridineCl](SbF<sub>6</sub>)<sub>2</sub>. The product was washed on the frit with copious amounts of diethyl ether and then smaller amounts of cold acetonitrile. The purity of the complex was confirmed using <sup>1</sup>H NMR, <sup>195</sup>Pt NMR, elemental analysis and mass spectroscopy.

Yield: 37 mg, (65%), brown powder. <sup>1</sup>H NMR (400 MHz, DMSO-*d*<sub>6</sub>) δ/ ppm: 8.82 (4H, s, 3' 5'), 8.79 (4H, d, 3 3''), 8.08 (4H, s, 6 6''), 7.85 (4H, dt, 4 4''), 7.33 (4H, dt, 5 5''). <sup>195</sup>Pt NMR (DMSO-*d*<sub>6</sub>) ppm: -2710. TOF MS-ES<sup>+</sup>, m/z: 498.0071, (M<sup>2+</sup>) (C<sub>15</sub>H<sub>10</sub>Cl<sub>2</sub>N<sub>3</sub>Pt species). *Anal. Calc. for* C<sub>30</sub>H<sub>20</sub>Cl<sub>2</sub>N<sub>6</sub>Pt<sub>2</sub>Sb<sub>2</sub>F<sub>12</sub>·7H<sub>2</sub>O: C, 23.66; H, 2.25; N, 5.52; *Found*: C, 23.57; H, 2.65; N, 5.31.

### Synthesis of Ethyleneglycol ether Linked Dinuclear Platinum(II) Complexes

The synthesis of the complexes was carried out using the following literature procedure:<sup>10a</sup> To a stirred solution of [Pt(cod)Cl<sub>2</sub>] in dry methanol at room temperature, a suspension of the ligand in dry methanol was added at 65 °C drop wise. The reaction mixture was stirred for 24 hours at 45 °C, after which the solution was cooled and filtered. When the bright yellow filtrate was concentrated under *vacuo*, the desired compound precipitated. The compound was filtered, washed with chloroform (20 mL), cold methanol (1 x 5 mL), diethyl ether (2 x 15 mL) and dried and stored in a desiccator.

The identity and the purity of the final complexes were confirmed by using <sup>1</sup>H NMR, <sup>195</sup>Pt NMR, elemental analyses and mass spectroscopy. The <sup>1</sup>H NMR spectra obtained show similarity in the aromatic region. Presence of a peak at about -2500 to -2700 ppm on the <sup>195</sup>Pt NMR spectra confirms the coordination of the ligand to platinum metal.

**(Pt<sub>2</sub>dteg):** Yield: 35 mg, (45%), red brown powder. <sup>1</sup>H NMR (400 MHz, DMSO-*d*<sub>6</sub>) δ/ ppm: 8.97 (4H, s, 3' 5'), 8.94 (4H, d, 6 6''), 8.70 (4H, d, 3 3''), 8.55 (4H, dt, 4 4''), 7.99 (4H, dt, 5 5''), 4.71 (4H, t, CH<sub>2</sub>), <sup>195</sup>Pt NMR (DMSO-*d*<sub>6</sub>) ppm: -2714. TOF MS-ES<sup>+</sup>, m/z: (M<sup>2+</sup>), 464.1578 (C<sub>15</sub>H<sub>11</sub>ClN<sub>3</sub>Pt species). *Anal. Calc. for* C<sub>32</sub>H<sub>24</sub>Cl<sub>4</sub>N<sub>6</sub>O<sub>2</sub>Pt<sub>2</sub>: C, 36.38; H, 2.29; N, 7.95; *Found*: C, 35.89; H, 2.72; N, 7.51.

**(Pt<sub>2</sub>tdteg):** Yield: 47 mg, (51%), orange powder. <sup>1</sup>H NMR (400 MHz, DMSO-*d*<sub>6</sub>) δ/ ppm: 8.57 (4H, d, 6 6''), 8.43 (4H, d, 3 3''), 8.2 (4H, dt, 4 4''), 8.17 (4H, s, 3' 5'), 7.80 (4H, dt, 5 5''), 4.66 (4H, t, CH<sub>2</sub>), 4.01 (4H, t, CH<sub>2</sub>), <sup>195</sup>Pt NMR (DMSO-*d*<sub>6</sub>) ppm: -2699. TOF MS-ES<sup>+</sup>, m/z: 568.1068, (M<sup>2+</sup>) (C<sub>19</sub>H<sub>18</sub>ClN<sub>3</sub>O<sub>3</sub>Pt species). *Anal. Calc. for* C<sub>34</sub>H<sub>28</sub>Cl<sub>4</sub>N<sub>6</sub>O<sub>3</sub>Pt<sub>2</sub>: C, 37.10; H, 2.56; N, 7.64; *Found*: C, 36.78; H, 2.92; N, 7.17.

**(Ptddtteg):** Yield: 56 mg, (57%), orange powder.  $^1\text{H}$  NMR (400 MHz,  $\text{DMSO-}d_6$ )  $\delta$ / ppm: 8.71 (4H, d, 6 6''), 8.60 (4H, t, 4 4''), 8.18 (4H, br, 3 3''), 8.06 (4H, s, 3' 5'), 7.95 (4H, dt, 5 5''), 4.70 (4H, br, CH<sub>2</sub>), 4.22 (4H, br, CH<sub>2</sub>), 4.14 (4H, t, CH<sub>2</sub>),  $^{195}\text{Pt}$  NMR ( $\text{DMSO-}d_6$ ) ppm: -2683. TOF MS-ES<sup>+</sup>,  $m/z$ : 568.1073, ( $\text{M}^{2+}$ ) ( $\text{C}_{19}\text{H}_{18}\text{ClN}_3\text{O}_3\text{Pt}$  species). *Anal. Calc. for*  $\text{C}_{36}\text{H}_{32}\text{Cl}_4\text{N}_6\text{O}_4\text{Pt}_2$ : C, 37.77; H, 2.82; N, 7.34; *Found*: C, 37.38; H, 3.30; N, 6.91.

**(Ptddttteg):** Yield: 56 mg, (57%), orange powder.  $^1\text{H}$  NMR (400 MHz,  $\text{DMSO-}d_6$ )  $\delta$ / ppm: 8.71 (4H, d, 6 6''), 8.61 (4H, t, 4 4''), 8.38 (4H, br, 3 3''), 8.03 (4H, s, 3' 5'), 7.98 (4H, dt, 5 5''), 4.48 (4H, br, CH<sub>2</sub>), 4.06 (4H, br, CH<sub>2</sub>), 4.01 (4H, br, CH<sub>2</sub>), 4.00 (4H, br, CH<sub>2</sub>),  $^{195}\text{Pt}$  NMR ( $\text{DMSO-}d_6$ ) ppm: -2691. TOF MS-ES<sup>+</sup>,  $m/z$ : 887.2581, ( $\text{M}^{2+}$ ), ( $\text{C}_{38}\text{H}_{36}\text{ClN}_6\text{O}_5\text{Pt}$  species). *Anal. Calc. for*  $\text{C}_{38}\text{H}_{36}\text{Cl}_4\text{N}_6\text{O}_5 \cdot 7\text{H}_2\text{O}$ : C, 34.02; H, 3.64; N, 6.61; *Found*: C, 34.49; H, 3.41; N, 6.15.

Details of the characteristic data agree well with the proposed chemical structures of the complexes. Representative spectra for analysis are given under Supporting Information.

#### 6.2.4 Instrumentation and Physical Measurements

$^1\text{H}$  NMR were recorded on either a Bruker Avance DPX 400 or 500 MHz spectrometer, at 303 K (unless or otherwise stated) using  $\text{Si}(\text{CH}_3)_4$  as the reference for the chemical shifts.  $^{195}\text{Pt}$  NMR were done on a 500 MHz spectrometer ( $^{195}\text{Pt}$ , 107.5 MHz) chemical shifts externally referenced to  $\text{K}_2[\text{PtCl}_6]$ . Low resolution electron spray ionization (ESI<sup>+</sup>) mass spectra were recorded on a TOF Micromass spectrometer. Elemental analyses were performed by a Thermal Scientific Flash 2000. Kinetic analyses were studied on an Applier Photophysics SX 20 stopped-flow reaction analyser coupled with an online data acquisition system with controlled temperature within  $\pm 0.1$  °C. The wavelengths for the kinetic analysis were predetermined on Varian Cary 100 Bio UV/visible spectrophotometer with an attached Varian Peltier temperature-controller within  $\pm 0.1$  °C and an online kinetic application.

#### 6.2.5 Computational Modelling

Computational modelling for the complexes were performed at Density Functional Theoretical (DFT) level based on B3LYP/LanL2DZ<sup>18</sup> (Los Alamos National Laboratory 2 double  $\xi$ ) level theory, with inner core electrons of Pt atom replaced by relative Effective Core Potential (ECP). Due to low electronic spin of Pt(II), the DFT calculations of the complexes were done as singlet state. The complexes were computed in methanol solution taking into account the solvolysis effect by means of the Conductor

Polarizable Continuum Model (C-PCM).<sup>19</sup> The Gaussian09 suite of programs was used for all computations.<sup>20</sup>

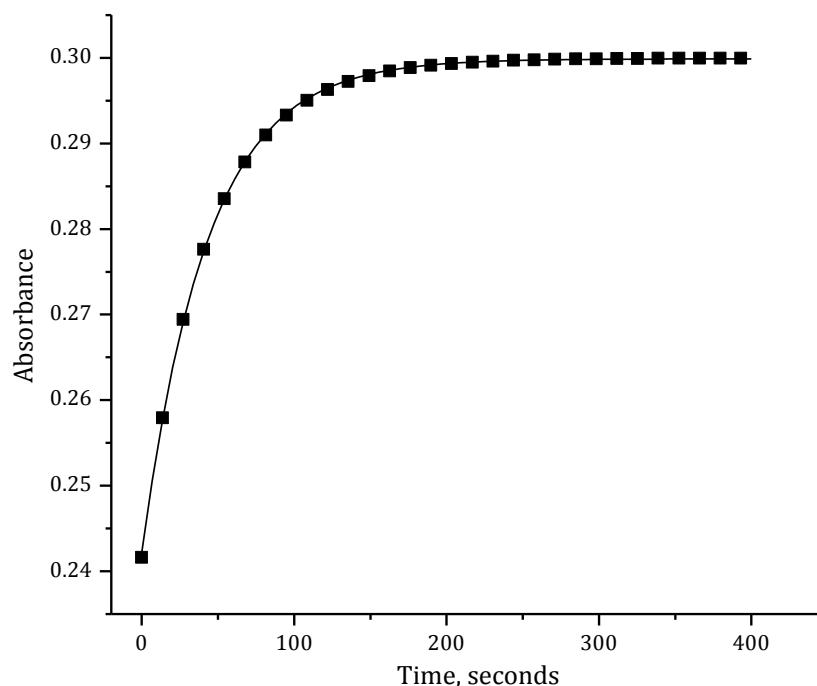
### 6.2.6 Kinetic Analyses

All kinetic measurements were performed under *pseudo* first-order conditions using at least 20-fold excess (a 10-fold excess of nucleophile at each Pt(II) centre) of the nucleophile in 0.02 M ionic solution, made by dissolving the required amount of LiCF<sub>3</sub>SO<sub>3</sub> (0.018 M) and LiCl (0.002 M) in dry methanol. LiCl was added to suppress any possibility of solvolysis reactions. Since CF<sub>3</sub>SO<sub>3</sub><sup>-</sup> does not coordinate with the Pt(II) metal centre,<sup>21</sup> all substitution kinetics were studied in this media. Nucleophiles were used in large excess in order to drive the reactions to completion.

Pt(II) complex solutions were prepared by dissolving the required amount of the complex in the ionic solution. Nucleophile solutions were prepared at 100 times the concentration of the Pt(II) complex. Subsequent dilutions of the nucleophile stock solution afforded solutions of 20, 40, 60 and 80 times the concentration of metal complex. The wavelengths chosen for the kinetic investigations were pre-determined by monitoring the change in absorbance of the mixture of the metal complex and the nucleophile as a function of time using UV/visible absorption spectra and are summarised in *Table S6.1* (Supporting Information). All data were graphically analysed using the software package, Origin 7.5<sup>®22</sup> to determine the observed rate constants,  $k_{\text{obs}}$ .

## 6.3 Results

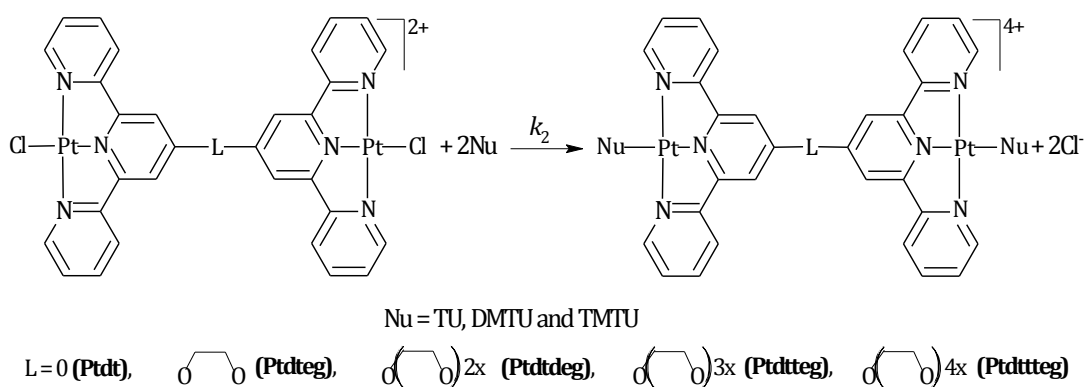
Substitution kinetics of coordinated chlorides from the Pt(II) complexes by thiourea nucleophiles, viz. TU, DMTU and TMTU were investigated under *pseudo* first-order conditions using conventional stopped-flow reaction analyzer. An example of a time resolved kinetic trace obtained from a stopped-flow analyzer for the simultaneous substitution of the chloride ligands in **Ptdtteg** ( $3.0 \times 10^{-5}$  mol dm<sup>-3</sup>) with DMTU (0.899 mol dm<sup>-3</sup>) at 298 K is given in *Figure 6.2*.



**Figure 6.2** Kinetic trace at 301 nm for the reaction of Ptdtteg ( $3.0 \times 10^{-5} \text{ mol dm}^{-3}$ ) with DMTU ( $8.99 \times 10^{-4} \text{ mol dm}^{-3}$ ) at 298 K,  $I = 0.02 \text{ M LiCF}_3\text{SO}_3$ , adjusted with LiCl.

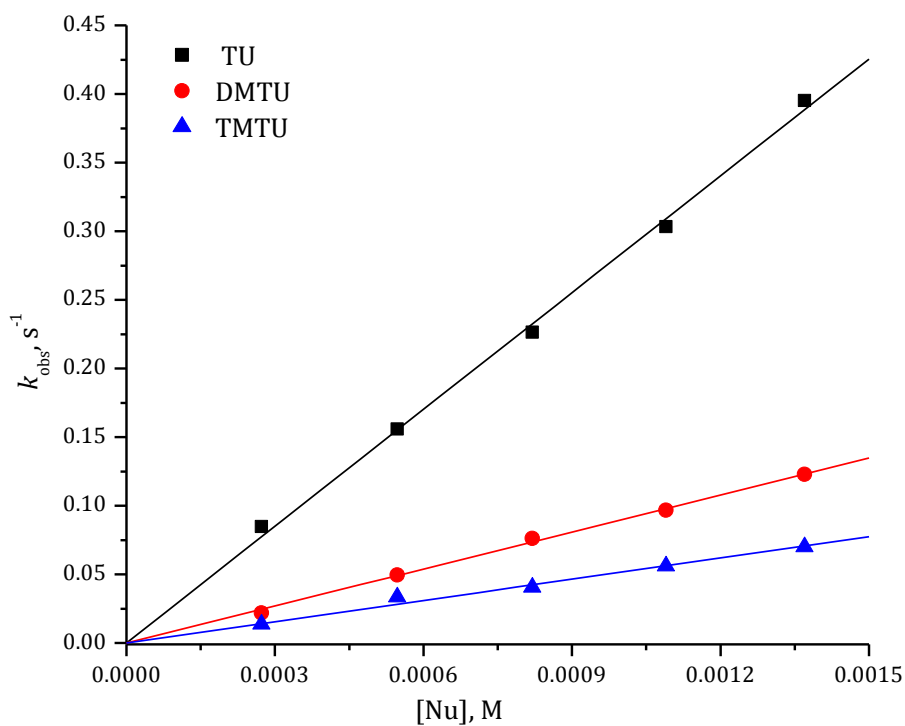
All kinetic data obtained were fitted to first-order exponential decay function to generate the observed *pseudo* first-order rate constants, ( $k_{\text{obs}}$ ), which were plotted against the concentration of the incoming nucleophiles. The values used represent an average of at least eight independent runs. Straight line graphs with zero intercepts were obtained for each of the nucleophile, indicating that the reactions were irreversible in nature and can be represented by *Scheme 6.1* and the corresponding rate law given by *Equation 6.1*.<sup>23</sup> Representative plots for **Ptdtteg**, shown in *Figure 6.3* clearly indicate that the substitution reactions were first-order with respect to the incoming nucleophile. Kinetic data obtained from the slope of the *Equation 6.1* are summarized in *Table 6.1*.





**Scheme 6.1** Proposed substitution mechanism for the dinuclear Pt(II) complex system with thiourea nucleophiles.

$$k_{\text{obs}} = k_2[\text{Nu}] \quad (6.1)$$

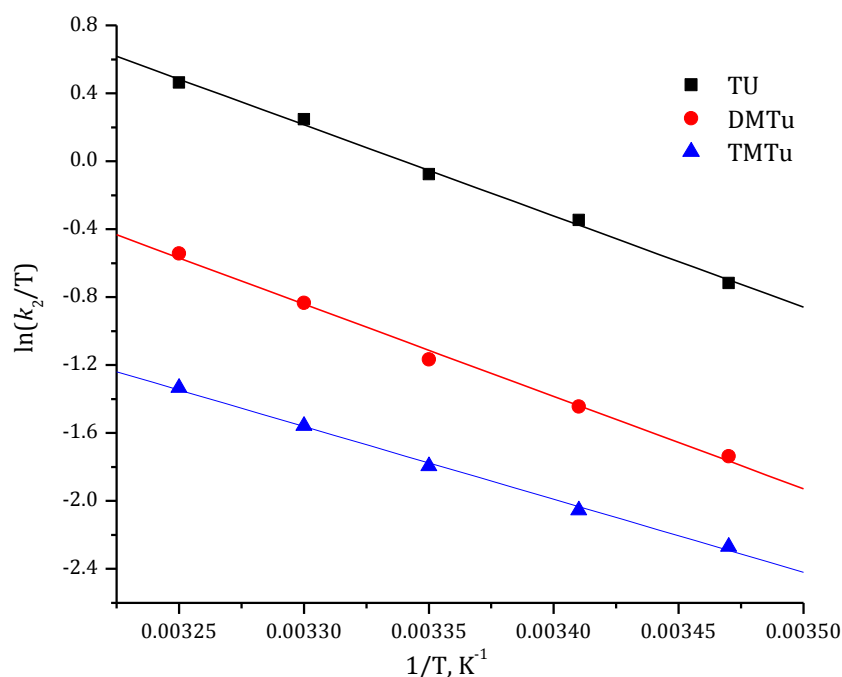


**Figure 6.3** Dependence of the *pseudo* first-order rate constants ( $k_{\text{obs}}$ ) on the concentrations of the nucleophiles for the chloride substitution from Ptdteg ( $2.65 \times 10^{-5}$  M) in methanol solution ( $I = 0.02$  M) at 298 K.

The temperature dependence studies were performed in a similar manner, using a single nucleophile concentration in the temperature range 15 - 40 °C in 5 °C intervals. The activation parameters, entropy of activation ( $\Delta S^\ddagger$ ) and enthalpy of activation ( $\Delta H^\ddagger$ ) were then obtained by using the Eyring equation.<sup>23</sup> Figure 6.4 shows the representative plots obtained for **Ptdteg** with the different nucleophiles for the forward reactions. The data obtained are summarized in Table 6.1. Representative graphs are given in Figures S6.1 to S6.8.

**Table 6.1** Summary of the second-order rate constants,  $k_2$  and activation parameters, with the corresponding standard deviations for the substitution of the chloro ligands by a series of thiourea nucleophiles at  $I = 0.02$  M  $\text{LiCF}_3\text{SO}_3$ , adjusted with  $\text{LiCl}$ . Data for **Ptpty** is taken from literature<sup>24</sup> and included for comparison.

Complex	Nu	$k_2/\text{M}^{-1}\text{s}^{-1}$	$\Delta S^\ddagger / \text{J K}^{-1}\text{mol}^{-1}$	$\Delta H^\ddagger / \text{kJ mol}^{-1}$
<b>Ptpty</b>	TU	$1494 \pm 10$	$-88 \pm 5$	$29 \pm 2$
	DMTU	$448 \pm 10$	$-73 \pm 4$	$36 \pm 1$
	TMTU	$82 \pm 4$	$-91 \pm 8$	$35 \pm 2$
<b>Ptdt</b>	TU	$1520 \pm 28$	$-85 \pm 6$	$30 \pm 2$
	DMTU	$838 \pm 14$	$-31 \pm 7$	$48 \pm 2$
	TMTU	$139 \pm 3$	$-50 \pm 8$	$46 \pm 3$
<b>Ptdteg</b>	TU	$281 \pm 2$	$-52 \pm 6$	$44 \pm 2$
	DMTU	$90 \pm 1$	$-59 \pm 3$	$54 \pm 1$
	TMTU	$52 \pm 1$	$-96 \pm 2$	$35 \pm 1$
<b>Ptdtdeg</b>	TU	$132 \pm 2$	$-50 \pm 3$	$46 \pm 1$
	DMTU	$43 \pm 0.6$	$-89 \pm 4$	$37 \pm 1$
	TMTU	$27 \pm 0.2$	$-88 \pm 3$	$39 \pm 1$
<b>Ptdtteg</b>	TU	$100 \pm 1$	$-96 \pm 5$	$33 \pm 2$
	DMTU	$40 \pm 0.6$	$-62 \pm 6$	$45 \pm 2$
	TMTU	$14 \pm 0.2$	$-49 \pm 12$	$51 \pm 4$
<b>Ptdttteg</b>	TU	$43 \pm 0.7$	$-49 \pm 5$	$49 \pm 2$
	DMTU	$28 \pm 0.4$	$-69 \pm 6$	$45 \pm 2$
	TMTU	$22 \pm 0.4$	$-78 \pm 8$	$42 \pm 3$



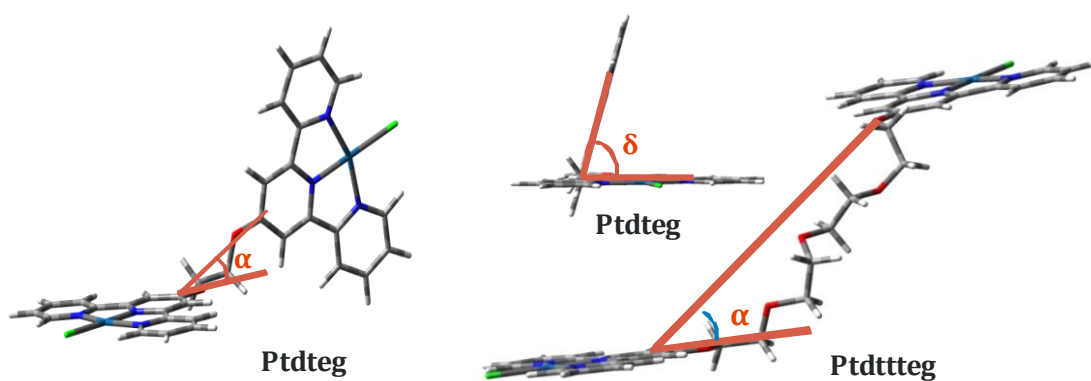
**Figure 6.4** Eyring plots obtained for Ptdteg with the nucleophiles for the forward reactions over the temperature range 15 - 35 °C.

### 6.3.1 Computational Modelling

The geometry optimized structures of the platinum complexes investigated are shown in Table 6.2 (also see Table S6.2) while the data obtained are summarized in Table 6.3 and Table S6.3 (Supporting Information). The geometry around the Pt(II) centre is slightly distorted square planar which is typical for Pt(II) terpyridine complexes.<sup>24-25</sup> The highest occupied molecular orbital (HOMO) electron density of the complexes are predominantly concentrated on the Pt(II) centre and the chloride ligands whereas the lowest unoccupied molecular orbital (LUMO) mainly lie on the terpyridine ligand backbone. The  $\pi$  systems of the two terpyridine moieties of the ligand interact with the Pt(II) metal centre through the metal  $d$  orbitals. This makes the two halves of the complex to orient at an angle to each other which decreases with increase in the length of the linker ( $\delta$  as represented in Figure 6.5 in **Ptdteg**, **Ptdtdeg** and **Ptdtteg**). This bonding orientation to the platinum metal centre prevents possibility of  $\pi$  interaction across the system.<sup>26</sup> As expected, in the back to back terpyridine complex, **Ptdt**, the HOMO and LUMO electron density span throughout the molecule due to the extended  $\pi$ -conjugation (Figure 6.6, Table 6.2). In the case of the shortest linker (**Ptdteg**), due to the interaction of the lone pair of electrons on O1 atoms with the electrons on the

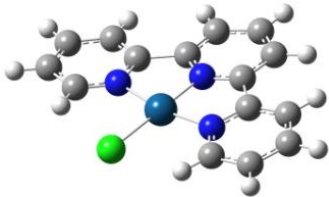
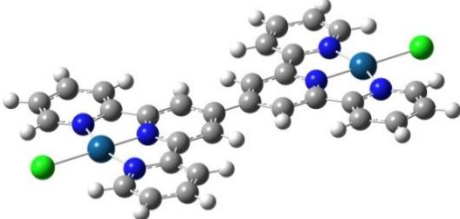
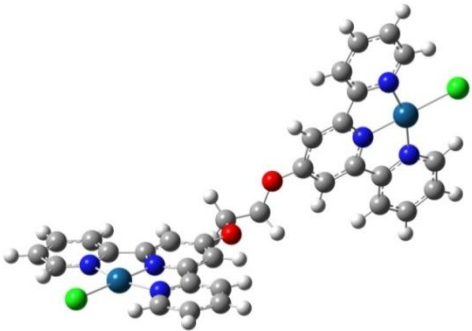
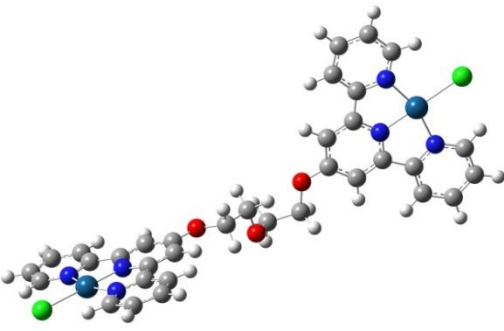
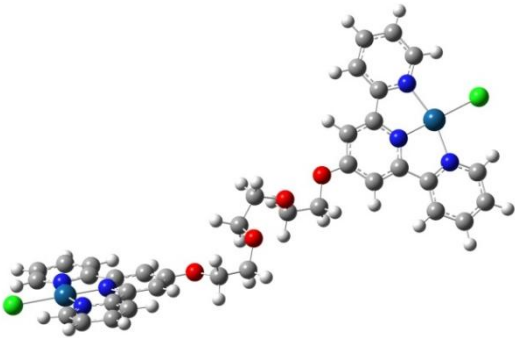
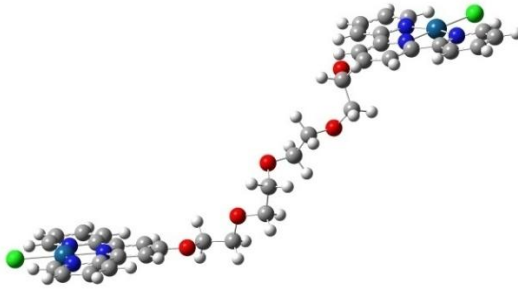
terpyridine ligands,<sup>27</sup> the  $\pi$  electron density spreads throughout the ligand system and hence the observed DFT calculated HOMO and LUMO electron density.<sup>28</sup> However, DFT calculations show that the HOMO and LUMO electrons are restricted on one side of the molecules as the length of the spacer between the two terpyridine ligands was increased (*Figure S6.9*, Supporting information). This is because the electronic charge distribution depends on the degree of metal-metal coupling and the perturbations in the molecular environment; such that, increase in the length of the linker decreases the metal-metal coupling leading to modest perturbations whereby localizing the charge on one metal centre of the complex.<sup>29</sup> Thus, it seems that the two Pt(II) terpyridine moieties become independent of each other with increase in the chain length. Furthermore, the two terpyridine moieties lie at an inclined angle,  $\alpha$ , which increases with increase in the chain length as exemplified in the *Figure 6.5*.

On comparing the DFT calculated natural bond orbital (NBO) charges on the platinum and  $N_{trans}$  atoms of **Ptppy** and back to back linked complex, **Ptdt**, the charge on Pt(II) centre increases from **Ptppy** to **Ptdt** while it decreases for  $N_{trans}$  from **Ptppy** to **Ptdt**. However, when **Ptdt** was compared with **Ptdteg**, the opposite was observed, *i.e.* the NBO charge on the platinum centre decreases from **Ptdt** to **Ptdteg** then remains constant, while the opposite is true for  $N_{trans}$  which becomes more negative and remains constant as the chain length increases. This observation for **Ptdt** and **Ptdteg** is due to the inductive  $\sigma$ -donation from the ethyleneglycol ether linker to the Pt(II) centre. Nevertheless, the fact that the values are roughly constant as the length of the polyethyleneglycol ether linker is increased indicates that the  $\sigma$ -inductive effect does not play a significant role on increasing the length of the linker beyond one unit of ethyleneglycol ether. Furthermore, since the DFT-based global electrophilicity index ( $\omega$ , related to the capacity of the molecule to accept electrons),<sup>30</sup> obtained by using the chemical hardness ( $\eta$ )<sup>31</sup> and electronic potential ( $\mu$ ),<sup>30c</sup> is a strong tool to determine the chemical reactivity, this parameter was calculated and the values show similar trend between **Ptppy**, **Ptdt** and **Ptdteg** as reported above.



**Figure 6.5** Aerial view showing the angles of inclination,  $\alpha$ , in the DFT calculated distorted slip-up stair case like linkers and the angle of twisting ( $\delta$ ) of the tpy moieties from each other.

Table 6.2 Geometry optimised structures of the complexes investigated.

Compound	Compound
 <b>Ptttpy</b>	 <b>Ptdt</b>
 <b>Ptdteg</b>	 <b>Ptdtdeg</b>
 <b>Ptdtteg</b>	 <b>Ptdttteg</b>

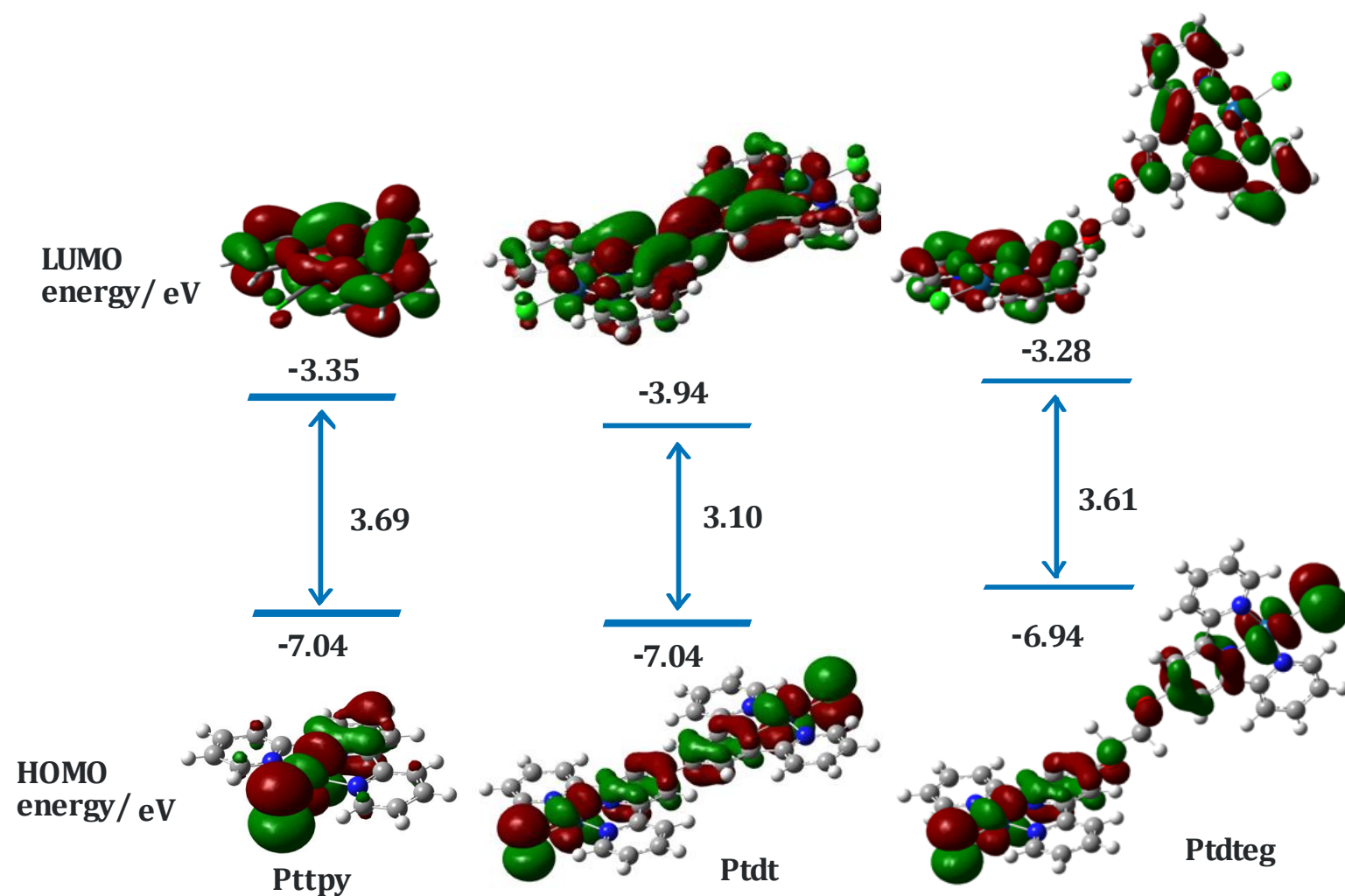


Figure 6.6 DFT calculated minimum energy structures, frontier molecular orbitals (HOMO and LUMO) of Pttpy, Ptdt and Ptdteg. Data for Pttpy is included for comparisons. Data for Ptdtdeg, Ptdtteg and Ptdttteg are included in *Figure S6.9* (Supporting Information).

**Table 6.3** Summary of DFT calculated data for the complexes investigated. Included is the data obtained for the DFT calculated Pttpty complex for comparisons.

Complex	Pttpty	Ptdt	Ptdteg	Ptdtdeg	Ptdtteg	Ptdttteg
<b>Bond Length (Å)</b>						
Pt—Cl	2.443	2.440	2.441	2.441	2.445	2.443
Pt—N1( <i>trans</i> )	1.961	1.954	1.960	1.960	1.961	2.961
Length of linker	-	-	2.926	5.040	8.316	11.65
Pt...Pt	-	10.95	14.34	16.99	19.95	21.87
<b>Bond angles (°)</b>						
Dihedral angle ( $\delta$ )	-	3.27	65.45	56.55	55.95	10.60
Inclination angle ( $\alpha$ )	-	0.01	20.44	25.79	26.00	45.14
<b>NBO charges</b>						
Pt1/Pt2	0.604	0.620	0.595	0.593	0.593	0.592
N1 ( <i>trans</i> )	-0.453	-0.446	-0.469	-0.471	-0.470	-0.471
Cl	-0.502	-0.496	-0.504	-0.504	-0.505	-0.505
$\Delta E$ / eV	3.69	3.10	3.61	3.64	3.64	3.64
$\eta$ / eV	1.85	1.55	1.83	1.82	1.82	1.82
$\mu$ / eV	-5.20	-5.49	-5.11	-5.09	-5.08	5.07
$\omega$ / eV	7.31	9.72	7.13	7.12	7.09	7.06
Symmetry	$C_2$	$C_1$	$C_1$	$C_1$	$C_1$	$C_1$

$\eta$  = chemical hardness,  $\mu$  = chemical potential and  $\omega$  = global electrophilicity index.<sup>30-31</sup>

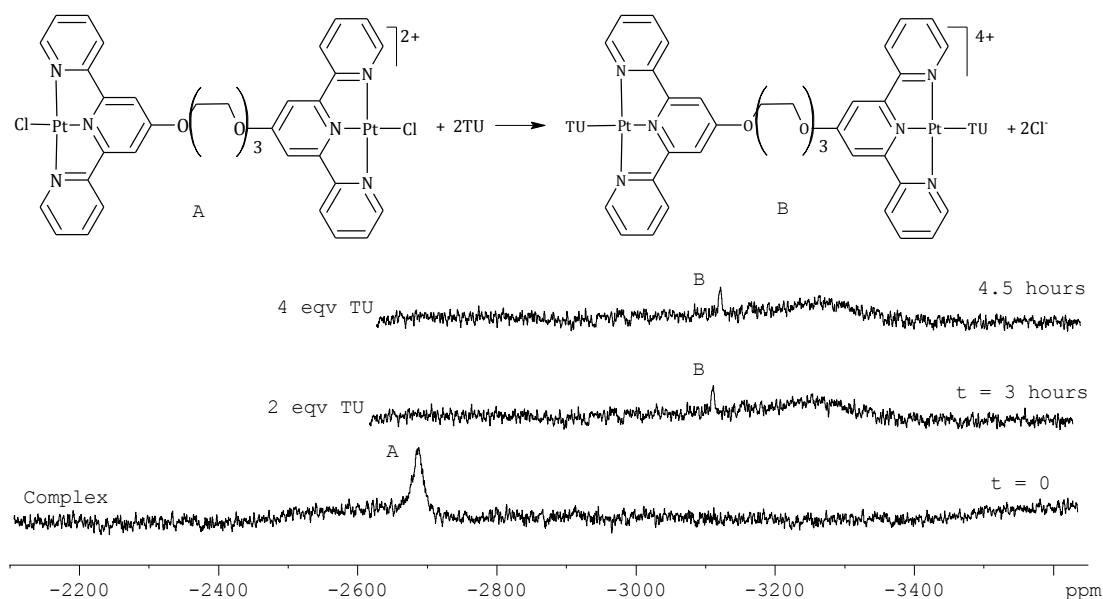
## 6.4 Discussion

The complexes were synthesized and characterized using  $^1\text{H}$  NMR,  $^{195}\text{Pt}$  NMR, MS and elemental analysis (See *Figures S6.10 to S6.29*). In the current study, substitution kinetics of chloride ligands from the dinuclear Pt(II) complexes by thiourea nucleophiles occurred simultaneously by a single step. Data summarized in *Tables 6.1 and 6.3* (also *Tables S6.4 to S6.13*) show that the Pt(II) complexes are somewhat symmetrical such that the nucleophiles cannot differentiate the two Pt(II) centres. The symmetrical nature of the Pt(II) centres is supported by the DFT calculated similar NBO charges on the Pt(II) centres (*Table 6.3*) indicating that the two Pt(II) centres are in similar chemical environments regardless of the distance between the two Pt(II) centres. Similar substitution behaviour has been reported previously by Jaganyi and co-workers<sup>32</sup> for dinuclear Pt(II) complexes containing flexible diamine linkers.

Simultaneous substitution of the chloride ligands is further confirmed using  $^{195}\text{Pt}$  NMR of **Ptdtteg** with TU (2 to 4 eqv) in DMF-  $d_6$  (*Figure 6.7*). At  $t = 0$ , a signal due to the starting complex (**Ptdtteg**) is observed at  $\delta = -2687$  ppm, represented as A. This



chemical shift at  $\delta = -2687$  ppm has moved to  $\delta = -3099$  ppm, (B) after 3 hours and is attributed to the formation of TU substituted product which exhibits a chemical shift due to Pt(NNN)TU centres as reported by Jaganyi *et al.*<sup>14e</sup> Unlike the previous findings for dinuclear Pt(II) complexes with flexible diamine,<sup>14a,14c</sup> rigid azine<sup>14e</sup> and cyclic<sup>10b</sup> linkers, the dinuclear complexes reported in this work are more stable showing no dechelation as can be seen from Figure 6.7.



**Figure 6.7** <sup>195</sup>Pt NMR the reaction mixture of Ptdtgeg ( $2 \times 10^{-2}$  M) with six equivalents of TU (2.0 M), showing a peak for pure dinuclear Pt(II) complex at  $\delta = -2687$  ppm before the reaction ( $t = 0$ ) and the final substituted product (B,  $\delta = -3099$  ppm) corresponding to [(TU)Pt(dtgeg)Pt(TU)]<sup>4+</sup>, over a period of 4.5 hours after the reaction begins.

When compared the mononuclear analogue, **Ptttpy** with the linker free back to back terpyridine complex, **Ptdt**, the reactivity increases slightly which can be attributed to the expansion of the  $\pi$ -conjugated electron system over the two Pt(II) centres. This increases the electronic communication within the terpyridine ligand system. Thus, decreases the electron density at the Pt(II) metal centre due to the enhanced  $\pi$ -backbonding ability of the ligand system.<sup>33</sup> As a result, the Pt(II) metal centres in **Ptdt** become more electrophilic thereby enhancing the binding of the incoming nucleophile. This is clearly seen from the DFT calculated NBO charges on the platinum centres which increases from **Ptttpy** to **Ptdt**. Further support for this comes from the remarkably higher DFT calculated global electrophilicity index of **Ptdt** compared to **Ptttpy**, a clear indication of the greater ability of **Ptdt** to accept electron density from

the incoming nucleophile to that of **Pttpy**.<sup>30b,c,34</sup> This, together with the increased overall charge, (2+)<sup>7b,14c</sup> attributes to the higher substitution reactivity of **Ptdt**. Compared to **Pttpy** and to the rest of the complexes, steric hindrance is an additional factor.

To understand the role of the linker on the rate of substitution of chloride ligands, the reactivity of **Ptdt** and **Ptdteg** are compared so as to explain the huge drop in the reactivity. The difference between them is the presence of the ethyleneglycol ether linker in the case of **Ptdteg**. The kinetic data shows that the reactivity of **Ptdt** is five times greater than **Ptdteg** which implies that, as reported in **Chapter 5**, the ethyleneglycol ether linker acts as a  $\sigma$ -donor using the two lone pair of electrons on the O1 atoms. This inductive  $\sigma$ -donation increases the charge on the N<sub>trans</sub> atom from **Ptdt** (-0.446) to **Ptdteg** (-0.469) which in turn decreases the NBO charge on the platinum centres from **Ptdt** (0.620) to **Ptdteg** (0.595). This is in line with the reported literatures,<sup>1c,24,35</sup> where electron donating groups on the ancillary position of terpyridine reduces the positive charge at the metal centre, thereby decreasing its electrophilicity. Further support for this comes from the significant decrease in the DFT calculated global electrophilicity index for **Ptdteg** (7.13 eV) to that of **Ptdt** (9.72 eV). Hence, **Ptdt** has a greater tendency to accept the incoming nucleophiles and thus, enhances the  $\pi$ -backbonding of electrons from the  $d_{xz}$  orbital of platinum into the antibonding  $\pi^*$  orbital of the ligand whereby stabilizing the transition state intermediate. In other words, the significantly slower reactivity of **Ptdteg** indicates that the nature of the bridging ligand in **Ptdteg** decreases the  $\pi$ -backbonding ability of the terpyridine moiety.<sup>33</sup> This can also be seen from the greater tilt angle,<sup>36</sup>  $\delta$ , obtained for **Ptdteg** (65.45 °) compared to that of **Ptdt** (3.27 °), despite the  $\pi$ -delocalization noticed with O1 atoms of the linker in **Ptdteg**. Together with the mentioned electronic effects, the decrease in rate of substitution reactions from the linker free **Ptdt** to **Ptdteg** is also due to the presence of the axially imposed steric influences on one side of the Pt(II) coordination sphere as illustrated in *Figure 6.5*.

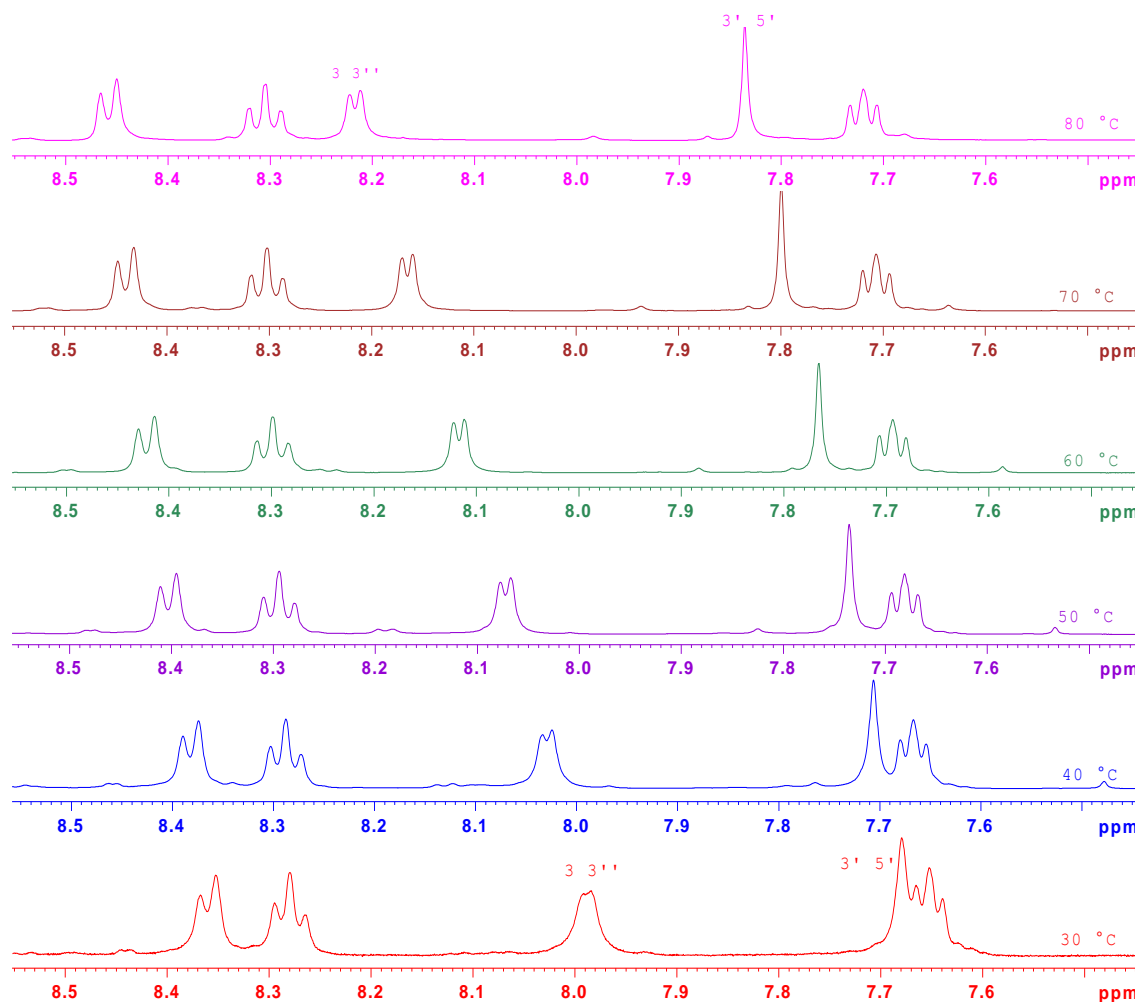
Further analysis of the reactivity of the polyethyleneglycol ether linked complexes show a decrease in the reactivity as the length of the linker is increased from **Ptdteg** (2.926 Å) to **Ptdettteg** (11.65 Å). When viewed along the axis perpendicular to the mean planes containing the platinum atoms, the DFT calculated minimum energy structures show that the complexes adopt twisted slip up staircase like geometry so that the second terpyridine moiety lie in an inclination angle,  $\alpha$  which is dependent on

the length of the linker. Relative to the plane containing one of the terpyridine moieties, the other chelate moiety projected by the linker increases from 20.44 ° in **Ptdteg** to 45.14 ° in **Ptdtteg**. Thus, the steric imposition on one side of the Pt(II) coordinated sphere increases with the increase in the length of the linker, whereby impeding the approach of the axially incoming nucleophile. This steric influence is the main factor responsible for the decreasing reactivity from **Ptdteg** to **Ptdtteg**. This deduction is also supported when one compares the trend at the reactivity of these dinuclear complexes to that of the mono nuclear complexes which shows the reactivity to be relatively constant as the linker is increased. The decrease in the reactivity is also due to the poor electronic transitions between the metal centres due to the longer spaces and large reorganizational energies caused by the highly twisted the systems as the length of the linker increases.<sup>36-37</sup> It is known that the reactivity increases with increase in the coupling between the metal centres, which decreases with increase in the distance between the metal centres.<sup>37-38</sup> This trend in the decrease in reactivity has been reported by van Eldik *et al.*<sup>9,14b</sup> and Jaganyi *et al.*<sup>32</sup> for dinuclear Pt(II) complexes with flexible linkers.

In addition to steric hindrance, the decrease in reactivity is also attributed to the fact that the charges on the metal centres do not affect each other<sup>9,39</sup> thus, reducing the overall electrophilicity of the molecule as supported by the DFT calculation.<sup>30c</sup> It can also be argued that the other factor contributing to the observed decrease in the reactivity from **Ptdteg** to **Ptdtteg** is the increase in electrostatic attraction induced between the ethyleneglycol ether polymer units as well as the platinum metal centres and the terpyridine moieties by the lone pair of electrons on the oxygen atoms in the linker.<sup>40</sup>

To further investigate the steric influence introduced by the linker, analysis of <sup>1</sup>H NMR study of **Ptdtteg** (0.02 M) at six different temperatures (30 °C to 80 °C, *Figure 6.8*, also see *Figure S6.30*, Supporting Information) shows more down fielded chemical shifts with improved multiplicity (in case of proton 3 3'' from broad to a doublet) as the temperature was increased. This is an indication of the disruption of the self-associated dimmers such as  $\pi$ -stacked molecules in solution at high temperature.<sup>41</sup> However, since the kinetic investigations are performed at the concentration levels of 10<sup>-5</sup> M, in such diluted solutions, the probability of formation of dimmers is unlikely.<sup>42</sup> Therefore, the improved multiplicity is due to the relief of intrinsic steric effect within the complex which is due to the increase in rotations about the flexible linker. This increases with

the increase in the length of the linker which imposes a greater degree of steric influence on the Pt(II) centre. This has a net effect of influencing the axial attack of the incoming nucleophile whereby slowing the reactivity.<sup>32</sup>



**Figure 6.8**  $^1\text{H}$  spectra of Ptdttteg (0.02 M) in  $\text{DMSO-}d_6$  at temperatures, 30 °C to 80 °C.

In general, when comparing the reactivity of the Pt(II) dinuclear complexes with their representative monomer (**Chapter 5**), the reactivity of the dinuclear complexes was slower than the reactivity of the mononuclear complexes. Unlike the mononuclear complexes, the reactivity of the dinuclear complexes decreases with increase in the length of the linker. However, one notes that the reactivity of the Pt(II) dinuclear complex with the shortest linker **Ptdteg** is slightly faster ( $281 \pm 2.0 \text{ M}^{-1} \text{ s}^{-1}$ ) than its monomer, **Pttpyeg** ( $257 \pm 5 \text{ M}^{-1} \text{ s}^{-1}$ ) (See **Chapter 5, Table 5.2**). This increase in reactivity is related to the increased overall charge of the molecule, as such when the

distance between the two Pt(II) centres is small, the molecule behaves more like a 2+ charge at each metal centre than 1+.<sup>9</sup>

The reactivity of the nucleophiles shows a clear dependence on the steric effects, which is typical of a mechanism involving bond making in the transition state.<sup>10b,14a</sup> In all cases TU has the highest reactivity and the rate decreases as the incoming nucleophile gets bulky, *i.e.* rate with TMTU is significantly slower. From the results obtained for activation parameters, the large entropies of activation, ( $\Delta S^\ddagger$ ) suggest a more ordered transition state. The relatively small enthalpies of activation, ( $\Delta H^\ddagger$ ) support an easy bond formation in the transition state which is typical for  $d^8$  square planar Pt(II) complexes during associative mode of substitution.<sup>14c,14e,24-25,35b,43</sup>

## 6.5 Conclusions

The lability of the dinuclear polyethyleneglycol ether linked complexes; **Ptdteg**, **Ptdtdeg**, **Ptdtteg** and **Ptdttteg** differ significantly from the corresponding linker free dinuclear complex, **Ptdt** and the monomeric complex, **Ptpty**. The differences in reactivity can be accounted for in terms of the electronic as well as steric effect due to structural differences. The introduction of the linker results in decreased electrophilicity of the platinum centre and the whole complex because of the ethyleneglycol ether acts as a  $\sigma$ -donor by using the lone pair of electrons on the oxygen atoms. In addition, the reactivity of the ethyleneglycol ether linked complexes decrease with increase in the distance between the Pt(II) metal centres. This is due to steric hindrance which increases with the length of the linker. Unlike the mono nuclear Pt(II) complexes whose reactivity remains relatively constant, the reactivity of these dinuclear complexes decrease with increase in the length of the linker.

The substitution reactions of these complexes have shown to be more stable with the S-donor nucleophiles compared to what has been reported in literature which showed dechelation of the ligand and linker.<sup>10b,14c,14e</sup> The substitution rates showed a positive dependence to the steric effects of the incoming nucleophiles, hence, the rate constants for TU are much faster than DMTU and TMTU. The activation parameters, enthalpy of activation and entropy of activation well support an associative mode of mechanism. This study clearly shows that the nature of the bridging ligand uniquely influences the rate of substitution reactions when compared to the similar studies reported in literature.<sup>9,14c</sup>

## 6.6 References

- (1) (a) Storr, T.; Thomson, K. H.; Orving, C. *Chem. Soc. Rev.* **2006**, *35*, 534(b) Reedijk, J. *Proc. Natl. Acad. Sci. U. S. A.* **2003**, *100*, 3611(c) Pantoja, E.; Gallipoli, A.; van Zutphen, S.; Komeda, S.; Reddy, D.; Jaganyi, D.; Lutz, M.; Tooke, D. M.; Spek, A. L.; Navarro-Ranninger, C.; Reedijk, J. *J. Inorg. Biochem.* **2006**, *100*, 1955(d) Wong, E.; Giandomenico, C. M. *Chem. Rev.* **1999**, *99*, 2451(e) Roy, S.; Westmaas, J. A.; Hagen, K. D.; van Wezel, G. P.; Reedijk, J. *J. Inorg. Biochem.* **2009**, *103*, 1288.
- (2) (a) Wheate, N. J.; Collins, J. G. *Coord. Chem. Rev.* **2003**, *241*, 133(b) Brabec, V.; Kasparková, J. *J. Drug Resist. Updates.* **2005**, *8*, 131(c) Bloemink, M. J.; Reedijk, J. *Met. Ions Biol. Syst.* **1996**, *32*, 641(d) Adams, M.; A'Hern, R. P.; Calvert, A. H.; Carmichael, J.; Clark, P. I.; Coleman, R. E. *Br. J. Cancer.* **1998**, *78*, 1404(e) Komeda, S.; Lutz, M.; Spek, A. L.; Chikuma, M.; Reedijk, J. *Inorg. Chem.* **2000**, *39*, 4230(f) Farrell, N.; De Almeida, S. G.; Skov, K. A. *J. Am. Chem. Soc.* **1988**, *110*, 5018(g) Farrell, N.; Qu, Y.; Hacker, M. P. *J Med Chem* **1990**, *33*, 2179(h) Komeda, S.; Lutz, M.; Spek, A. L.; Yamanaka, Y.; Sato, T.; Chikuma, M.; Reedijk, J. *J. Am Chem Soc.* **2002**, *124*, 4738(i) Summa, N.; Maigut, J.; Puchta, R.; van Eldik, R. *Inorg. Chem.* **2007**, *46*, 2094.
- (3) Liu, Q.; Qu, Y.; van Antwerpen, R.; Farrell, N. *Biochemistry.* **2006**, *45*, 4248.
- (4) (a) Farrell, M. *Comments Inorg. Chem.* **1995**, *16*(6), 373(b) Kasparkova, J.; Zehnulova, J.; Farrell, N.; Brabec, V. *J. Biol. Chem.* **2002**, *277*, 48076(c) Farrell, N. P.; De- Almedia, S. G.; Skov, K. A. *J. Am. Chem. Soc.* **1988**, *110*, 5018.
- (5) Qu, Y.; Scarsdale, N. J.; Tran, M. C.; Farrel, N. *J. Inorg. Biochem.* **2004**, *98*, 1585.
- (6) Johnson, S. W.; Ferry, K. V.; Hamilton, T. C. *Drug Resist. Updates.* **1998**, *1*, 243.
- (7) (a) Davies, M. S.; Cox, J. W.; Berners- Price, S.; Barklage, W.; Qu, Y.; Farrell, N. *Inorg. Chem.* **2000**, *39*, 1710(b) Davies, M. S.; Thomas, D. S.; Hegmans, A.; Berners-Price, S. J.; Farrell, N. *Inorg. Chem.* **2002**, *41*, 1101.
- (8) (a) Qu, Y.; Farrell, N. *J. Am. Chem. Soc.* **1991**, *113*, 4851(b) Kortés, R. A.; Geib, S. J.; Lin, F.-T.; Shepherd, R. E. *Inorg. Chem.* **1999**, *38*, 5045.
- (9) Hofmann, A.; van Eldik, R. *J. Chem. Soc., Dalton Trans.* **2003**, 2979.
- (10) (a) Roy, S. In *PhD Thesis*; University of Leiden, *Synergy of intercalation and coordination binding to design novel DNA-targeting antineoplastic metallodrugs*, 2008, 230 - 248(b) Mambanda, A.; Jaganyi, D. *Dalton Trans.* **2012**, *41*, 908.
- (11) Kalayda, G. V. In *PhD Thesis*; Natuurwetenschappen, F. d. W. e., Ed.; University of Leiden, 2006, 125 - 137.
- (12) Kasparková, J.; Vraná, O.; Farrell, N.; Brabec, V. *JBIC, J. Biol. Inorg. Chem.* **2004**, *98*, 1560.

- (13) McFadyen, W. D.; Wakelin, L. P. G.; Roos, I. A. G.; Leopold, V. A. *J. Med. Chem.* **1985**, *28*, 1113.
- (14) (a) Ertürk, H.; Maigut, J.; Puchta, R.; van Eldik, R. *J. Chem. Soc. Dalton Trans.* **2008**, 2759 (b) Ertürk, H.; Hofmann, A.; Puchta, R.; van Eldik, R. *Dalton Trans.* **2007**, 2295 (c) Jaganyi, D.; Mambanda, A.; Hochreuther, S.; van Eldik, R. *Dalton Trans.*, **2010**, *39*, 3595 (d) Reddy, D.; Jaganyi, D. *Int. J. Chem. Kinet.* **2011**, *43*, 161 (e) Ongoma, P. O.; Jaganyi, D. *Dalton Trans.*, **2013**, *42*, 2724.
- (15) Perrin, D. D.; Armarego, W. L. F.; Perrin, D. R. *Purification of Laboratory Chemicals*; 2<sup>nd</sup> ed.; Pergamon: Oxford, 1980.
- (16) Constable, E. C.; Ward, M. D. *J. Chem. Soc. Dalton Trans.* **1990**, 1405.
- (17) van der Schilden, K., Ph. D. Thesis, Laiden University, *The Development of Polynuclear Ruthenium and Platinum Polypyridyl Complexes in Search of New Anticancer Agents.*, 2006, 50- 106.
- (18) (a) Becke, A. G. *J. Chem. Phys.* **1993**, *98*, 5648 (b) Lee, C. T.; Yang, W. T.; Parr, R. G. *Phys. Rev. B* **1988**, *37*, 785 (c) Hay, P. J.; Wadt, W. R. *J. Chem. Phys.* **1985**, *82*, 299.
- (19) (a) Barone, V.; Cossi, M. *J. Phys. Chem. A* **1998**, *102*, 1995 (b) Cossi, M.; Rega, N.; Scalmani, G.; Barone, V. *J. Comput. Chem.* **2003**, *24*, 669.
- (20) Frisch, M. J.; Trucks, G. W.; Schlegel, H. B.; Scuseria, G. E.; Robb, M. A.; Cheeseman, J. R.; Scalmani, G.; Barone, V.; Mennucci, B.; Petersson, G. A.; Nakatsuji, H.; Caricato, M.; Hratchian, X. L.; H. P. ; Izmaylov, A. F.; Bloino, J.; Zheng, G.; Sonnenberg, J. L.; Hada, M.; Ehara, M.; Toyota, K.; Fukuda, R.; Hasegawa, J.; Ishida, M.; Nakajima, T.; Honda, Y.; Kitao, O.; Nakai, H.; Vreven, T.; Montgomery, J. A.; Peralta, J. J. E. ; Ogliaro, F.; Bearpark, M.; Heyd, J. J.; Brothers, E.; Kudin, K. N.; Staroverov, V. N.; Kobayashi, R.; Normand, J.; Raghavachari, K.; Rendell, A.; Burant, J. C.; Iyengar, S. S.; Tomasi, J.; Cossi, M.; Rega, N.; M. Millam, J.; Klene, M.; Knox, J. E.; Cross, J. B.; Bakken, V.; Adamo, C.; Jaramillo, J.; Gomperts, R.; Stratmann, R. E.; Yazyev, O.; Austin, A. J.; Cammi, R.; Pomelli, C.; Ochterski, J. W.; Martin, R. L.; Morokuma, K.; Zakrzewski, V. G.; Voth, G. A.; Salvador, P.; Dannenberg, J. J.; Dapprich, S.; Daniels, A. D.; Farkas, O.; Foresman, J. B.; Ortiz, J. V.; Cioslowski, J.; Fox, D. J.; Gaussian, I., Wallingford CT, 2009., Ed.; Gaussian, Inc., Wallingford CT., 2009.
- (21) Appleton, T. G.; Hall, J. R.; Ralph, S. F.; Thompson, C. S. M. *Inorg. Chem.* **1984**, *23*, 3521.
- (22) Microcal™ Origin™ Version 7.5; Microcal Software, Inc., Northampton, MA, 1991- 2003.

- (23) Atwood, J. D. *Inorganic and Organic Reaction Mechanisms*; 2nd ed.; Wiley- VCH Inc. New York, 1997, 32-34, 43-61.
- (24) Jaganyi, D.; Reddy, D.; Gertenbach, J. A.; Hofmann, A.; van Eldik, R. *Dalton Trans.* **2004**, 299.
- (25) Jaganyi, D.; De Boer, K. L.; Gertenbach, J.; Perils, J. *Int. J. Chem. Kinet.* **2008**, *40*, 808.
- (26) Perrine, T. M.; Dunietz, B. D. *J. Phys Chem. A.* **2008**, *112*, 2043.
- (27) Chow, H. S., PhD Thesis, University of Basel, *Metal Complexes of 4'-Substituted-2,2':6',2''-Terpyridines in Supramolecular Chemistry*, 2005, 33- 66.
- (28) MOE (Molecular Operating Environment).
- (29) Quardokus, R. C.; Lu, Y.; Wasio, N. A.; Lent, C. S.; Justaud, F.; Lapinte, C.; Kandel, S. A. *J. Am. Chem. Soc.* **2011**, *134*, 1710.
- (30) (a) Parr, R. G.; Szentpaly, L.; Liu, S. *J. Am. Chem. Soc.* **1999**, *121*, 1922(b) Elango, M.; Parthasarathi, R.; Narayanan, G. K.; Sabeelullah, A. M.; Sarkar, U.; Venkatasubramaniyan, N. S.; Subramanian, V.; Chattaraj, P. K. *J. Chem. Sci.* **2005**, *117*, 61(c) Mebi, C. A. *J. Chem. Sci.* **2011**, *123*, 727.
- (31) Chattaraj, P. K.; Sarkar, U. *arXiv:physics/0509089* **2005**, 1.
- (32) Jaganyi, D.; Munisamy, V. M.; Reddy, D. *Int. J. Chem. kinet.* **2006**, *38*, 202.
- (33) Soldatovic, T.; Jovanovic, S.; Bugarcic, Z. D.; van Eldik, R. *Dalton Trans.* **2012**, *41*, 876.
- (34) Chattaraj, P. K.; Giri, S.; Duley, S. *Chem. Rev.* **2011**, *111*, PR43.
- (35) (a) Hofmann, A.; Dahlenburg, L.; van Eldik, R. *Inorg. Chem.* **2003**, *42*, 6528(b) Reddy, D.; Jaganyi, D. *Dalton Trans* **2008**, 6724.
- (36) Indelli, M. T.; Scandola, F.; Collin, J.-P.; Sauvage, J.-P.; Sour, A. *Inorg. Chem.* **1996**, *35*, 303.
- (37) Indelli, M. T.; Bignozzi, C. A.; Harriman, A.; Schoonover, J. R.; Scandola, F. *J. Am. Chem. Soc.* **1994**, *116*, 3768.
- (38) (a) Grosshenny, V.; Harriman, A.; Hissler, M.; Ziessel, R. *J. Chem. Soc. Faraday Trans.* **1996**, *92*, 2223(b) Oevering, H.; Verhoeven, J. W.; Paddon-Row, M. N.; Cotsaris, E. *Chem. Phys. Lett.* **1988**, *143*, 488.
- (39) (a) Ruhayel, R. A.; Langner, J. S.; Oke, M.-J.; Berners-Price, S. J.; Zgani, I.; Farrell, N. P. *J. Amer. Chem. Soc.* **2012**, *134*, 7135(b) Davies, M. S.; Cox, J. W.; Berners-Price, S. J.; Barklage, W.; Qu, Y.; Farrell, N. *Inorg. Chem.* **2006**, *39*, 1710(c) Hochreuther, S.; Puchta, R.; van Eldik, R. *Inorg. Chem.* **2011**, *50*, 8984.
- (40) Yu, C.; Chan, K. H.-Y.; Wong, K. M.-C.; Yam, V. W.-W. *Chem. Eur. J.* **2008**, *14*, 4577.



- (41) Yam, V. W.-W.; Chan, K. H.-Y.; Wong, K. M.-C.; Chu, B. W.-K. *Angew. Chem. Int. Ed.* **2006**, *45*, 6169.
- (42) Barigelletti, F.; Flamigni, L.; Collin, J.-P.; Sauvage, J.-P. *Chem. Commun.* **1997**, 333.
- (43) (a) Mambanda, A.; Jaganyi, D. *Dalton Trans* **2011**, *40*, 79 (b) Asperger, S. *Chemical Kinetics and Inorganic Reaction Mechanisms*; 2nd ed.; Kluwer Academic/ Plenum Publisher: New York, 2003, 152-153(c) Romeo, R.; Plutino.M.R; Scolaro, L. M.; Stoccoro, S.; Minghetti, G. *Inorg. Chem.* **2000**, *39*, 4749.

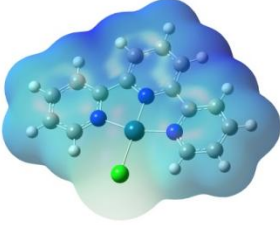
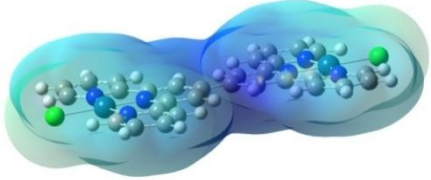
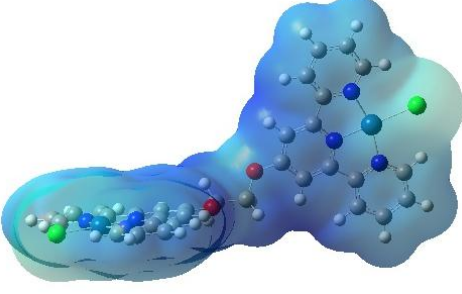
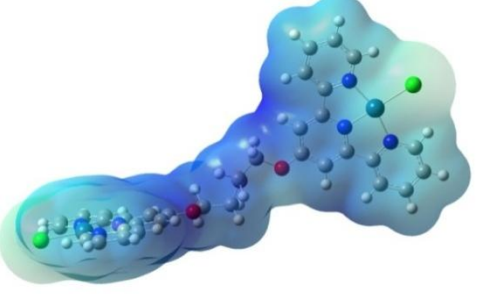
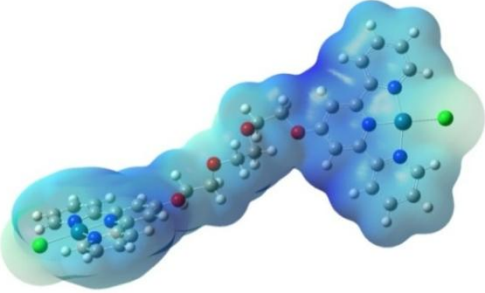
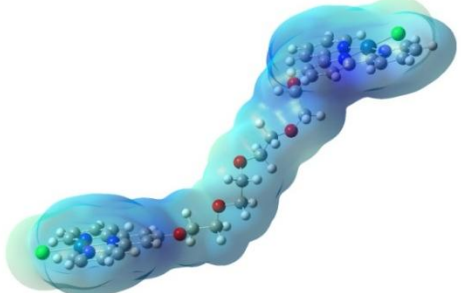
## 6.7 Supporting Information

A summary of wavelengths at which the kinetic studies were performed, plots of the dependence of  $k_{\text{obs}}$  against concentration of the nucleophiles and plots from temperature dependence studies along with tables of kinetic data, graphs of exemplary mass spectra and the representative spectra for  $^1\text{H}$  NMR and  $^{195}\text{Pt}$  NMR work reported in this study are given as electronic Supporting Information (ESI).

**Table S6.1** Summary of the wavelengths (nm) used to study the substitution reactions of the complexes with thiourea nucleophiles.

Complex	Nu	Wavelength ( $\lambda$ ), nm
<b>Ptdt</b>	TU	330
	DMTU	330
	TMTU	333
<b>Ptdteg</b>	TU	330
	DMTU	330
	TMTU	352
<b>Ptdtdeg</b>	TU	400
	DMTU	331
	TMTU	301
<b>Ptdtteg</b>	TU	356
	DMTU	301
	TMTU	330
<b>Ptdttteg</b>	TU	400
	DMTU	275
	TMTU	332

**Table S6.2** Geometry- optimised structures of the platinum complexes investigated and distribution of the electron density on the platinum complexes investigated. The blue area indicates the most electropositive areas and the orange region indicates the most electronegative areas.

Compound	Structure
 <b>Ptppy</b>	 <b>Ptdt</b>
 <b>Ptdteg</b>	 <b>Ptdtdeg</b>
 <b>Ptdtteg</b>	 <b>Ptdttteg</b>

**Table S6. 3** Summary of DFT calculated data for the complexes investigated. Included is the data obtained for the DFT calculated PtTpy for comparisons.

Complex	Ptttpy	Ptdt	Ptdteg	Ptdtdeg	Ptdtteg	Ptdttteg
<b>Bond Length (Å)</b>						
Pt1—N2(cis)	2.049	2.050	2.049	2.049	2.052	2.051
Pt—N3(cis)	2.049	2.050	2.049	2.049	2.051	2.051
Pt—N1(trans)	1.961	1.954	1.960	1.960	1.961	2.961
4'C—O1			1.371	1.370	1.368	1.368
O1—O2			2.926	3.071	2.949	2.945
O2—O3				3.071	3.014	3.013
O3—O4						3.705
O4—O5						3.002
Pt1—O1			6.070	6.071	6.070	6.071
Pt1---Pt2		10.952	14.344	16.993	19.948	21.874
Cl---Cl		15.833		21.691	24.722	26.296
4'C-4'C		1.495		7.998		13.769
<b>Bond angles (°)</b>						
N1—Pt—Cl	179.99	179.99	179.29	179.71	179.55	179.63
N2—Pt—Cl	99.05	99.20	99.03	98.92	99.25	99.36
N3—Pt—Cl	99.05	99.19	99.34	99.46	99.21	99.09
N3—Pt—N2	161.90	161.61	161.63	161.62	161.54	161.55
N2—Pt—N1	80.95	80.80	80.91	80.91	80.84	80.84
N1—Pt—N3	80.95	80.81	80.71	80.71	80.70	80.70
Dihedral -cl	0.007	0.157	0.97	0.233	0.674	1.065
<b>NBO charges</b>						
N2	-0.493	-0.492	-0.492	-0.492	-0.493	-0.492
N3	-0.493	-0.492	-0.469	-0.493	-0.492	-0.493
O1			-0.561	-0.566	-0.565	-0.558
O2			-0.561	-0.647	-0.650	-0.649
O3					-0.645	-0.645
O4					-0.559	-0.645
O5						-0.559
C 4	-0.134	0.013	0.406	0.408/0.408	0.408	0.408
EHOMO/ eV	-7.04	-7.04	-6.94	-6.91	-6.90	6.89
ELUMO/ eV	-3.35	-3.94	-3.28	-3.27	-3.26	3.25
Dipole moment	13.3	0.002	5.91	6.23	7.21	8.97

**Table S6. 4** Average observed rate constants,  $k_{\text{obs}}$ ,  $\text{s}^{-1}$ , for the displacement of the chloride ligands in Ptdt with the nucleophiles, at  $T = 298 \text{ K}$ ,  $I = 0.02 \text{ M LiCF}_3\text{SO}_3$ , adjusted with LiCl

TU		DMTU		TMTU	
Conc., mM	$k_{\text{obs}}$ , $\text{s}^{-1}$	Conc., mM	$k_{\text{obs}}$ , $\text{s}^{-1}$	Conc., mM	$k_{\text{obs}}$ , $\text{s}^{-1}$
0.321	0.56224	0.321	0.24	0.321	0.03699
0.642	1.03629	0.642	0.55002	0.642	0.08896
0.963	1.36725	0.963	0.7599	0.963	0.12844
1.280	1.96703	1.280	1.11151	1.280	0.18886
1.610	2.45658	1.610	1.35162	1.610	0.2194

**Table S6. 5** Temperature dependence of  $k_2 \text{ M}^{-1}\text{s}^{-1}$ , for the displacement of the chloride ligands in Ptdt by the nucleophiles at 60-fold excess over [dt], at  $T = 298 \text{ K}$ ,  $I = 0.02 \text{ M LiCF}_3\text{SO}_3$ , adjusted with LiCl.

TU		DMTU		TMTU	
$1/T$ , $\text{K}^{-1}$	$\ln(k_2/T)$	$1/T$ , $\text{K}^{-1}$	$1/T$ , $\text{K}^{-1}$	$\ln(k_2/T)$	$1/T$ , $\text{K}^{-1}$
0.00347	1.10512	0.00347	0.02413	0.00347	-1.52777
0.00341	1.35682	0.00341	0.45205	0.00341	-1.12132
0.00335	1.56066	0.00335	-	0.00335	-0.80445
0.0033	1.68841	0.0033	1.0636	0.0033	-
0.00325	1.95483	0.00325	1.33994	0.00325	-0.26244

**Table S6. 6** Average observed rate constants,  $k_{\text{obs}}$ ,  $\text{s}^{-1}$ , for the displacement of the chloride ligands in Ptdteg with the nucleophiles, at  $T = 298 \text{ K}$ ,  $I = 0.02 \text{ M LiCF}_3\text{SO}_3$ , adjusted with LiCl

TU		DMTU		TMTU	
Conc., mM	$k_{\text{obs}}$ , $\text{s}^{-1}$	Conc., mM	$k_{\text{obs}}$ , $\text{s}^{-1}$	Conc., mM	$k_{\text{obs}}$ , $\text{s}^{-1}$
0.273	0.08029	0.273	0.02191	0.273	0.01364
0.547	0.15586	0.547	0.04942	0.547	0.03339
0.820	0.22643	0.820	0.07608	0.820	0.04063
1.090	0.30329	1.090	0.09664	1.090	0.05598
1.370	0.38862	1.370	0.12295	1.370	0.07003

**Table S6. 7** Temperature dependence of  $k_2$   $\text{M}^{-1}\text{s}^{-1}$ , for the displacement of the chloride ligands in Ptdteg by the nucleophiles at 60-fold excess over [Ptdteg], at  $T = 298 \text{ K}$ ,  $I = 0.02 \text{ M LiCF}_3\text{SO}_3$ , adjusted with LiCl.

TU		DMTU		TMTU	
$1/T, \text{K}^{-1}$	$\ln(k_2/T)$	$1/T, \text{K}^{-1}$	$1/T, \text{K}^{-1}$	$\ln(k_2/T)$	$1/T, \text{K}^{-1}$
0.00347	-0.71663	0.00347	-1.73801	0.00347	-2.26834
0.00341	-0.34561	0.00341	-1.44339	0.00341	-2.05389
0.00335	-0.07635	0.00335	-1.16699	0.00335	-1.79427
0.0033	0.24629	0.0033	-0.8345	0.0033	-1.55744
0.00325	0.46319	0.00325	-0.54278	0.00325	-1.33352

**Table S6. 8** Average observed rate constants,  $k_{\text{obs}}$ ,  $\text{s}^{-1}$ , for the displacement of the chloride ligands in Ptdtdeg with the nucleophiles, at  $T = 298 \text{ K}$ ,  $I = 0.02 \text{ M LiCF}_3\text{SO}_3$ , adjusted with LiCl.

TU		DMTU		TMTU	
Conc., mM	$k_{\text{obs.}}, \text{s}^{-1}$	Conc., mM	$k_{\text{obs.}}, \text{s}^{-1}$	Conc., mM	$k_{\text{obs.}}, \text{s}^{-1}$
0.300	0.04376	0.300	0.0138		
0.599	0.0812	0.599	0.02517	0.599	0.01599
0.899	0.11215	0.899	0.0406	0.899	0.02409
1.200	0.15854	1.200	0.05333	1.200	0.03239
1.500	0.20028	1.500	0.06342	1.500	0.03922

**Table S6. 9** Temperature dependence of  $k_2$   $\text{M}^{-1}\text{s}^{-1}$ , for the displacement of the chloride ligands in Ptdtdeg by the nucleophiles at 60-fold excess over [Ptdtdeg], at  $T = 298 \text{ K}$ ,  $I = 0.02 \text{ M LiCF}_3\text{SO}_3$ , adjusted with LiCl.

TU		DMTU		TMTU	
$1/T, \text{K}^{-1}$	$\ln(k_2/T)$	$1/T, \text{K}^{-1}$	$1/T, \text{K}^{-1}$	$\ln(k_2/T)$	$1/T, \text{K}^{-1}$
0.00347	-1.52978	0.00347	-2.38665	0.00347	-2.95927
0.00341	-1.20269	0.00341	-2.07121	0.00341	-2.64596
0.00335	-0.87131	0.00335	-1.86044	0.00335	-2.40916
0.0033	-0.53935	0.0033	-1.60949	0.0033	-2.13455
0.00325	-0.2974	0.00325	-1.36041	0.00325	-1.90089

**Table S6. 10** Average observed rate constants,  $k_{\text{obs}}$ ,  $\text{s}^{-1}$ , for the displacement of the chloride ligands in Ptdtteg with the nucleophiles, at  $T = 298 \text{ K}$ ,  $I = 0.02 \text{ M LiCF}_3\text{SO}_3$ , adjusted with LiCl.

TU		DMTU		TMTU	
Conc., mM	$k_{\text{obs.}}, \text{s}^{-1}$	Conc., mM	$k_{\text{obs.}}, \text{s}^{-1}$	Conc., mM	$k_{\text{obs.}}, \text{s}^{-1}$
0.300	0.01937	0.300	0.01042	0.300	0.00165
0.599	0.0569	0.599	0.02305	0.599	0.00815
0.899	0.08797	0.899	0.03674	0.899	0.01289
1.200	0.12138	1.200	0.04958	1.200	0.01637
1.500	0.15091	1.500	0.05965	1.500	0.02175

**Table S6.11** Temperature dependence of  $k_2 \text{ M}^{-1}\text{s}^{-1}$ , for the displacement of the chloride ligands in Ptdtteg by the nucleophiles at 60-fold excess over [Ptdtteg], at  $T = 298 \text{ K}$ ,  $I = 0.02 \text{ M LiCF}_3\text{SO}_3$ , adjusted with LiCl.

TU		DMTU		TMTU	
$1/T, \text{K}^{-1}$	$\ln(k_2/T)$	$1/T, \text{K}^{-1}$	$1/T, \text{K}^{-1}$	$\ln(k_2/T)$	$1/T, \text{K}^{-1}$
0.00347	-1.56957	0.00347	-2.5684	0.00341	-3.51306
0.00341	-1.30861	0.00341	-2.22585	0.00335	-3.03487
0.00335	-1.11407	0.00335	-1.98735	0.0033	-2.83065
0.0033	-0.91965	0.0033	-1.65603	0.00325	-2.50241
0.00325	-0.63777	0.00325	-1.31503	0.00319	-2.07025

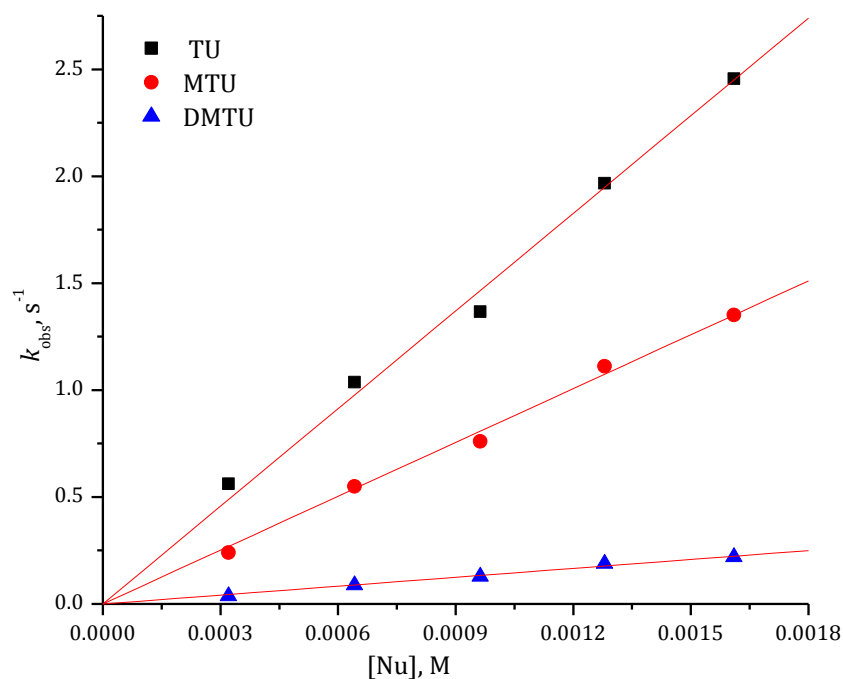
**Table S6. 12** Average observed rate constants,  $k_{\text{obs}}$ ,  $\text{s}^{-1}$ , for the displacement of the chloride ligands in Ptdttteg with the nucleophiles, at  $T = 298 \text{ K}$ ,  $I = 0.02 \text{ M LiCF}_3\text{SO}_3$ , adjusted with LiCl.

TU		DMTU		TMTU	
Conc., mM	$k_{\text{obs.}}, \text{s}^{-1}$	Conc., mM	$k_{\text{obs.}}, \text{s}^{-1}$	Conc., mM	$k_{\text{obs.}}, \text{s}^{-1}$
0.300	0.01435	0.274	0.00685		
0.599	0.0253	0.548	0.01407	0.548	0.01329
0.899	0.03679	0.821	0.02253	0.821	0.01801
1.200	0.05035	1.100	0.03109	1.100	0.02493
1.500	0.06627	1.370	0.03848	1.370	0.03001

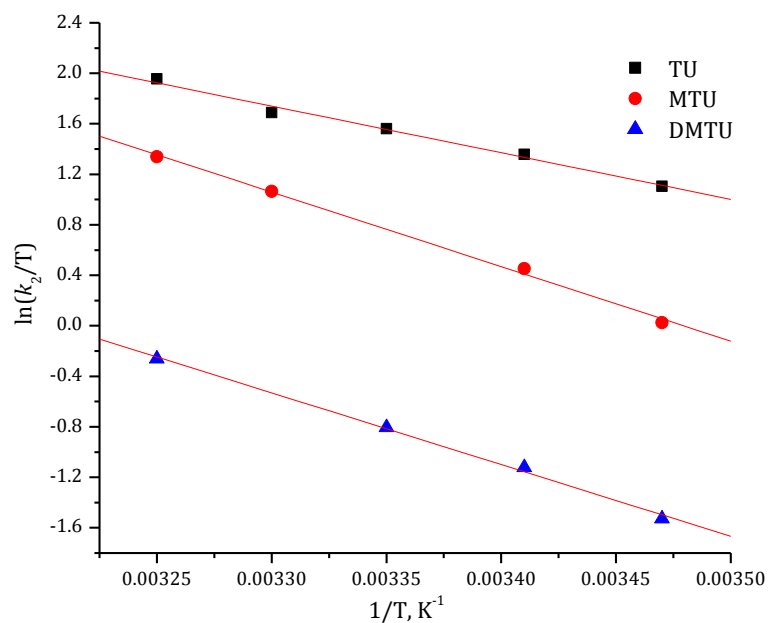
**Table S6. 13**      Temperature dependence of  $k_2$   $\text{M}^{-1}\text{s}^{-1}$ , for the displacement of the chloride ligands in  $\text{Pt}(\text{dttt})\text{eg}$  by the nucleophiles at 60-fold excess over  $[\text{Pt}(\text{dttt})\text{eg}]$ , at  $T = 298 \text{ K}$ ,  $I = 0.02 \text{ M LiCF}_3\text{SO}_3$ , adjusted with  $\text{LiCl}$ .

TU		DMTU		TMTU	
$1/T, \text{K}^{-1}$	$\ln(k_2/T)$	$1/T, \text{K}^{-1}$	$1/T, \text{K}^{-1}$	$\ln(k_2/T)$	$1/T, \text{K}^{-1}$
0.00347	-2.61068	0.00347	-3.1753	0.00347	-3.28899
0.00341	-2.28225	0.00341	-2.80547	0.00341	-2.92163
0.00335	-1.98584	0.00335	-2.47622	0.00335	-2.70047
0.0033	-1.59011	0.0033	-2.2582	0.0033	-2.4499
0.00325	-1.28713	0.00325	-1.94006	0.00325	-2.08984

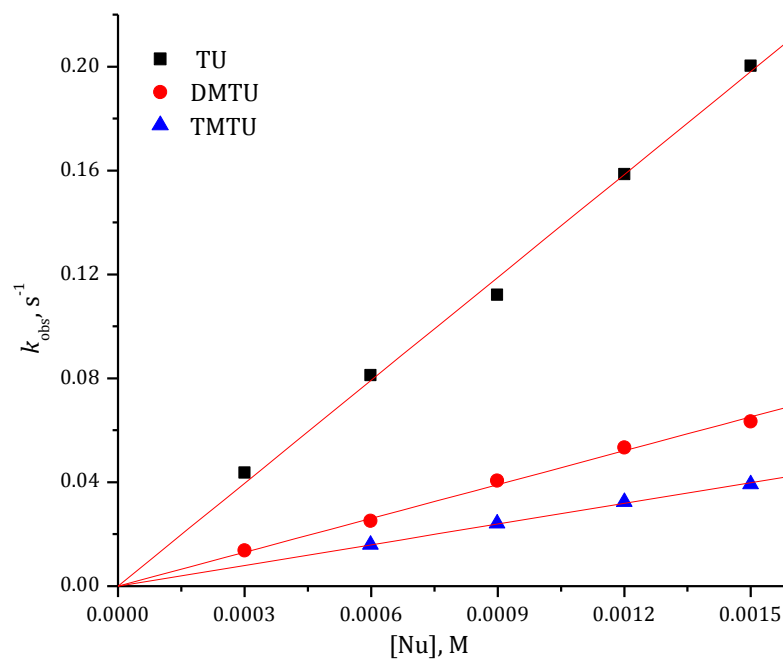




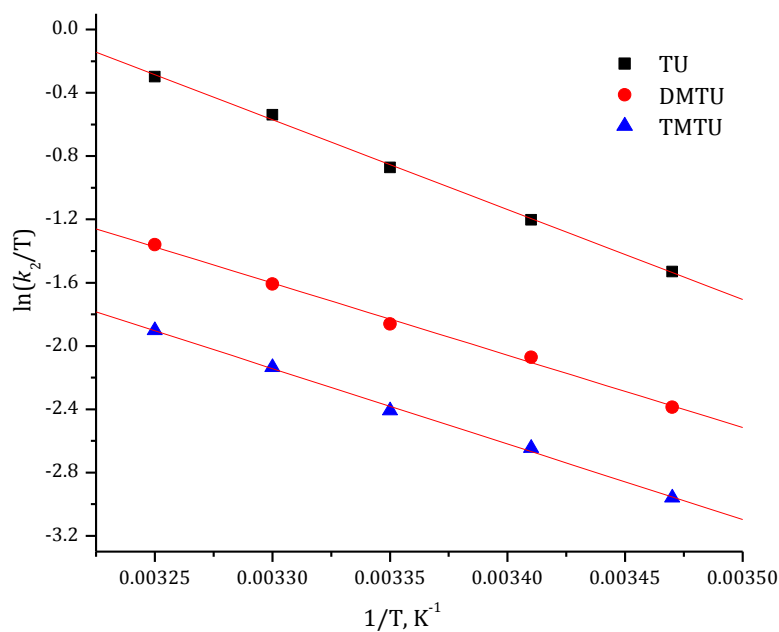
**Figure S6.1** Dependence of the *pseudo* first-order rate constants ( $k_{obs}$ ) on the concentrations of the nucleophiles for the chloride substitution from Ptdt ( $3.2 \times 10^{-5}$  M) in methanol solution ( $I = 0.02$  M) at 298 K.



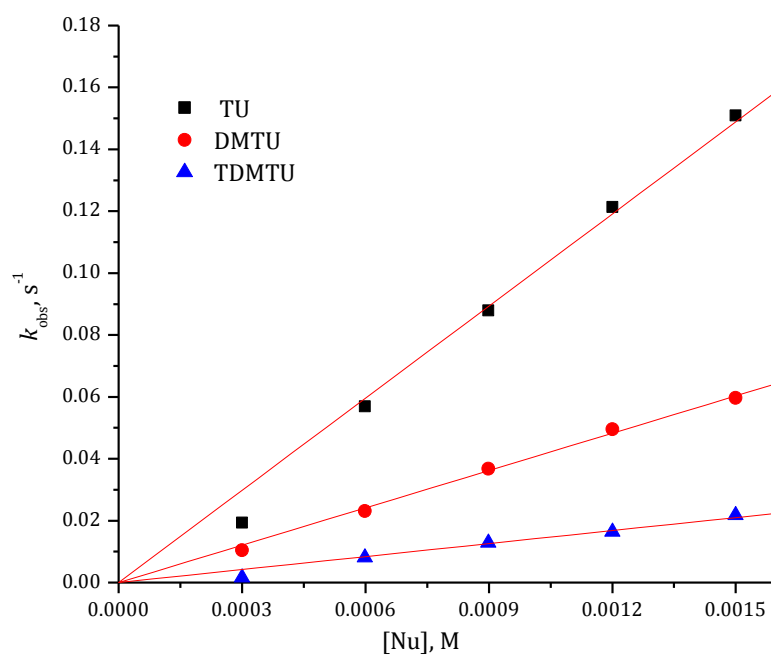
**Figure S6.2** Eyring plots obtained for Ptdt with the nucleophiles for the forward reactions over the temperature range 15 - 35 °C in methanol solution ( $I = 0.02$  M).



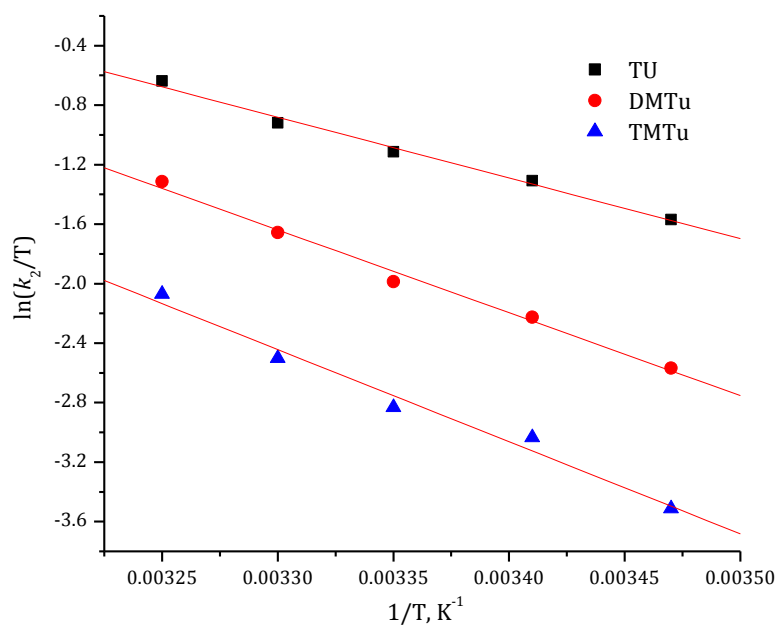
**Figure S6.3** Dependence of the *pseudo* first-order rate constants ( $k_{obs}$ ) on the concentrations of the nucleophiles for the chloride substitution from Ptdtdeg ( $3.0 \times 10^{-5}$  M) in methanol solution ( $I = 0.02$  M) at 298 K.



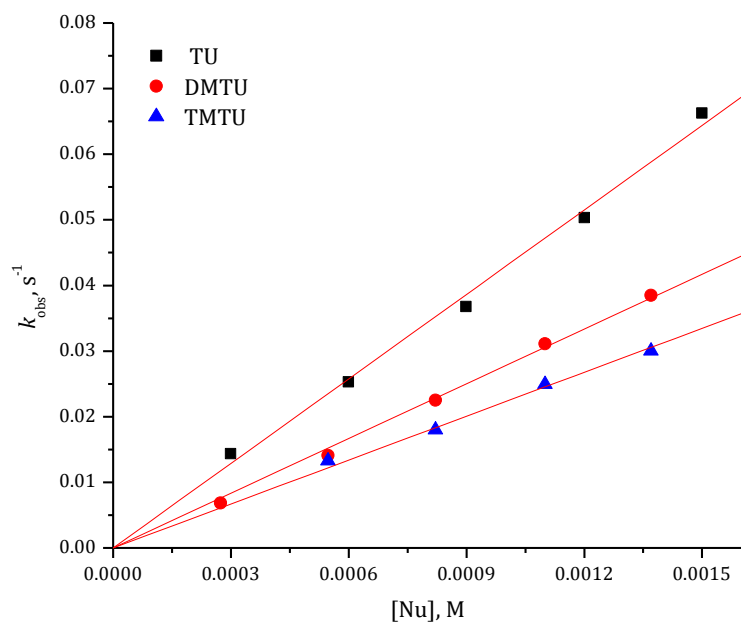
**Figure S6.4** Eyring plots obtained for Ptdtdeg with the nucleophiles for the forward reactions over the temperature range 15-35 °C in methanol solution ( $I = 0.02$  M).



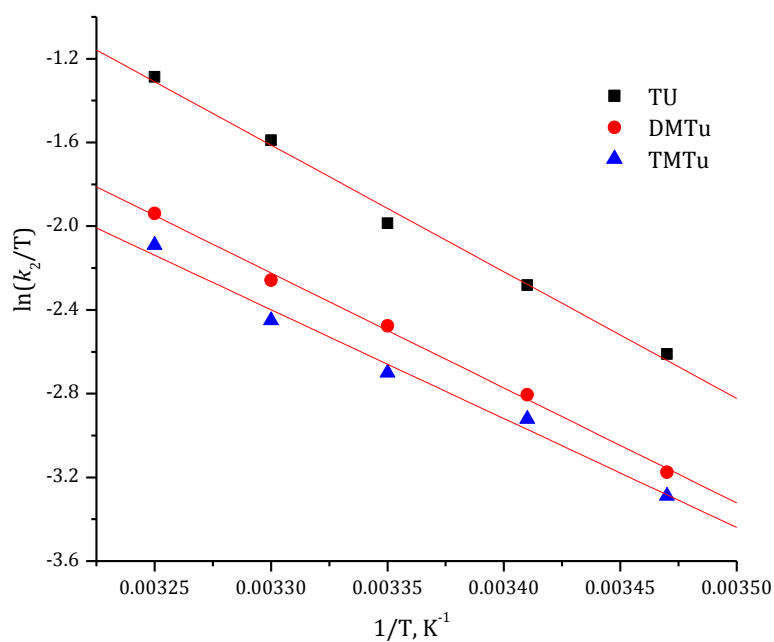
**Figure S6.5** Dependence of the *pseudo* first-order rate constants ( $k_{obs}$ ) on the concentrations of the nucleophiles for the chloride substitution from Ptdtgeg ( $3.0 \times 10^{-5}$  M) in methanol solution ( $I = 0.02$  M) at 298 K.



**Figure S6.6** Eyring plots obtained for Ptdtgeg with the nucleophiles for the forward reactions over the temperature range 15–35 °C in methanol solution ( $I = 0.02$  M).



**Figure S6.7** Dependence of the *pseudo* first-order rate constants ( $k_{\text{obs}}$ ) on the concentrations of the nucleophiles for the chloride substitution from Ptdttteg ( $3.0 \times 10^{-5}$  M) in methanol solution ( $I = 0.02$  M) at 298 K.



**Figure S6.8** Eyring plots obtained for Ptdttteg with the nucleophiles for the forward reactions over the temperature range 15–35 °C in methanol solution ( $I = 0.02$  M).

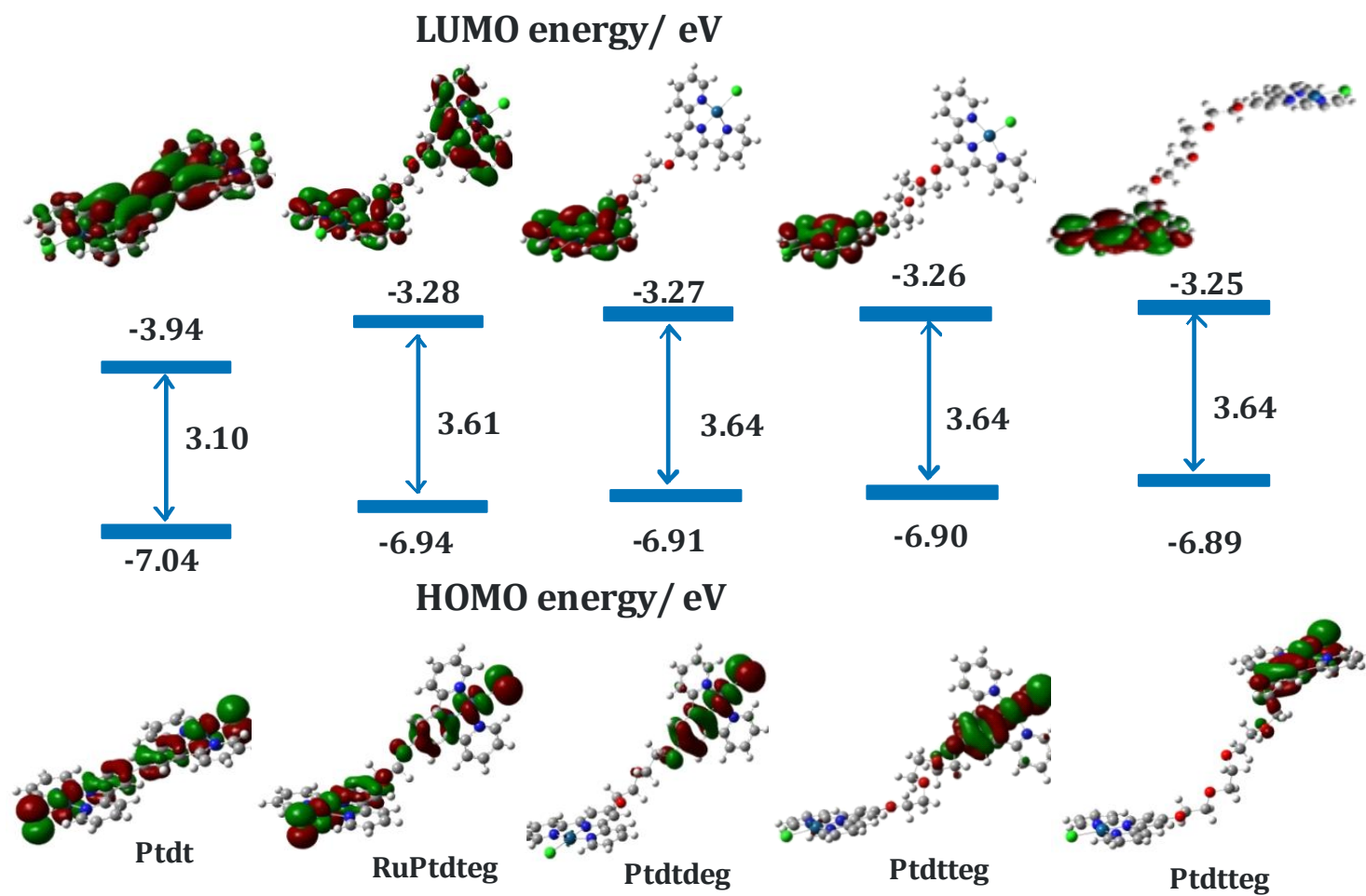


Figure S6.9 DFT calculated minimum energy structures, frontier molecular orbitals (HOMO and LUMO) of the complexes instigated.

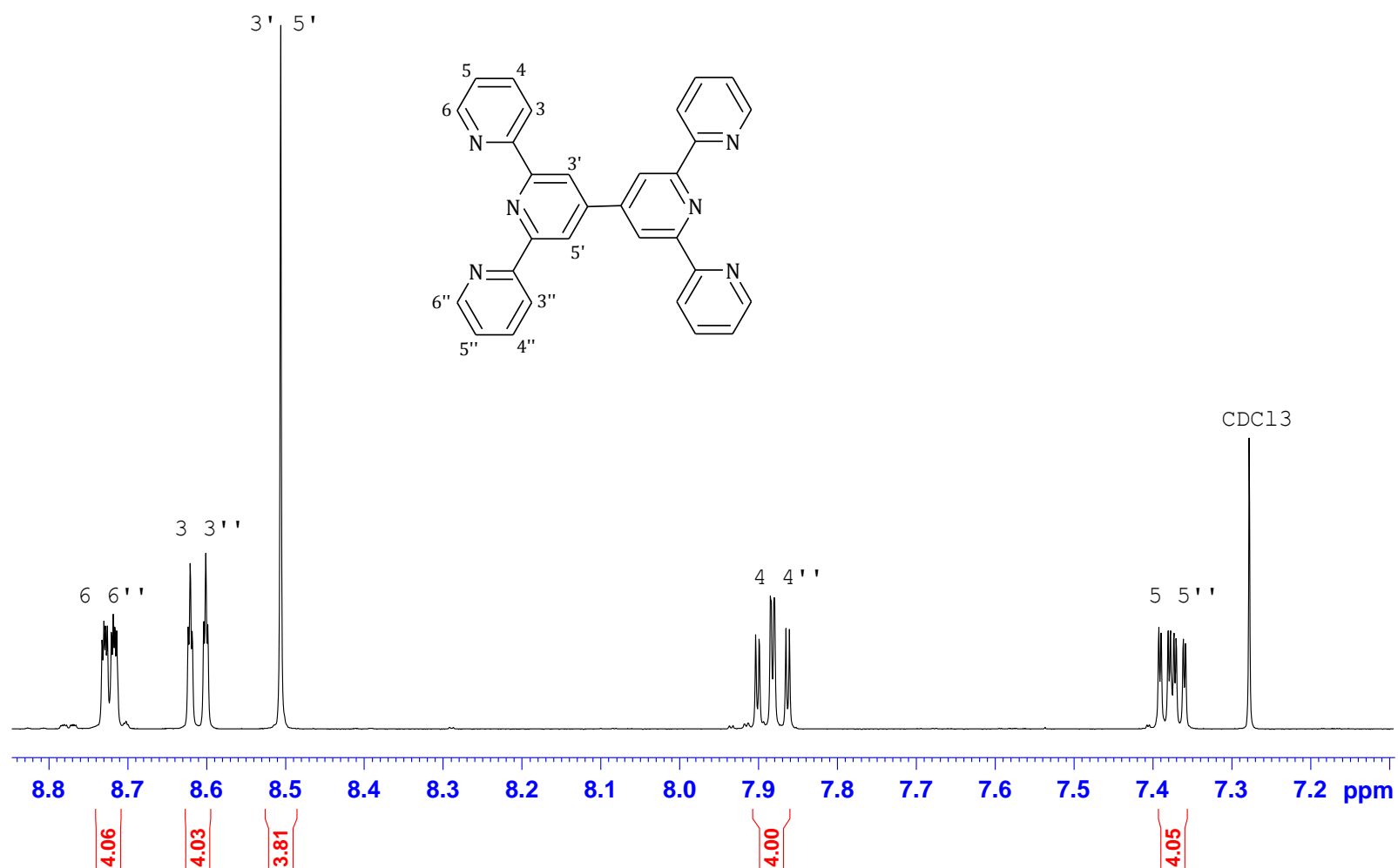


Figure S6.10  $^1\text{H}$ NMR spectrum of 2,2':6',2''-bisterpyridine in  $\text{CDCl}_3$ .

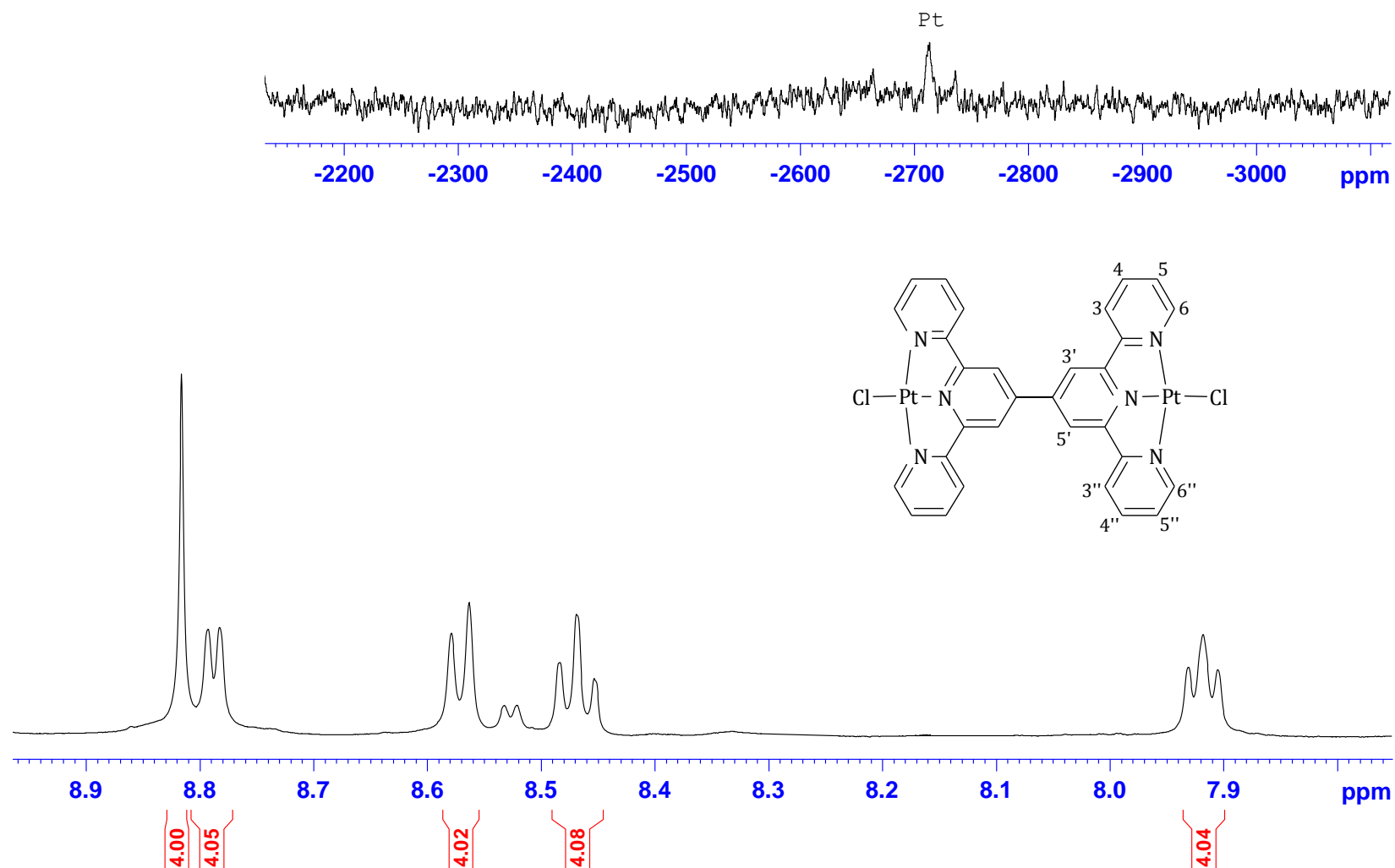


Figure S6.11  $^1\text{H}$  NMR spectrum of Ptdt in DMSO. Inset is the  $^{195}\text{Pt}$  NMR spectrum of the complex.

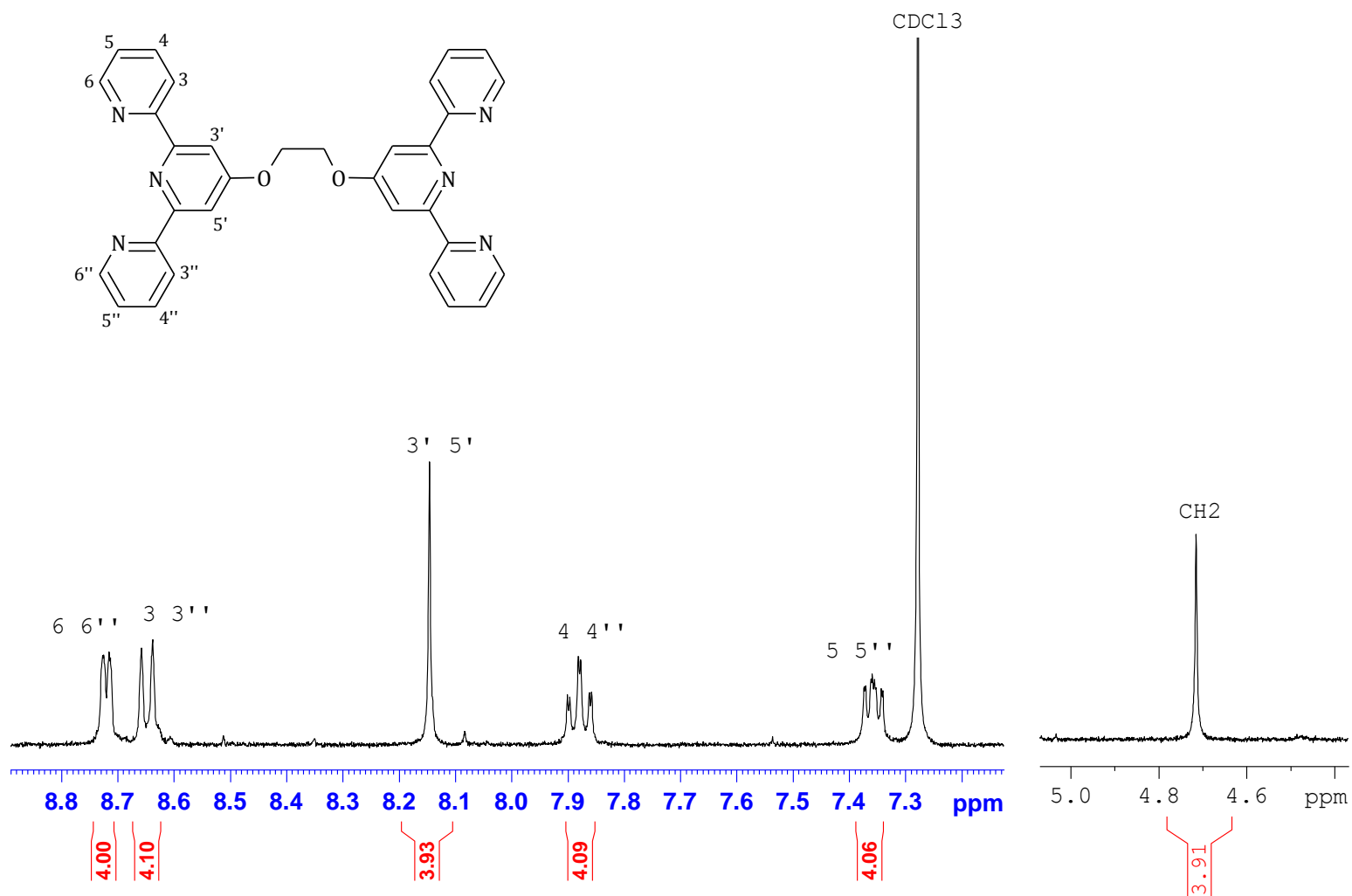


Figure S6.12  $^1\text{H}$ NMR spectrum dteq in  $\text{CDCl}_3$ .



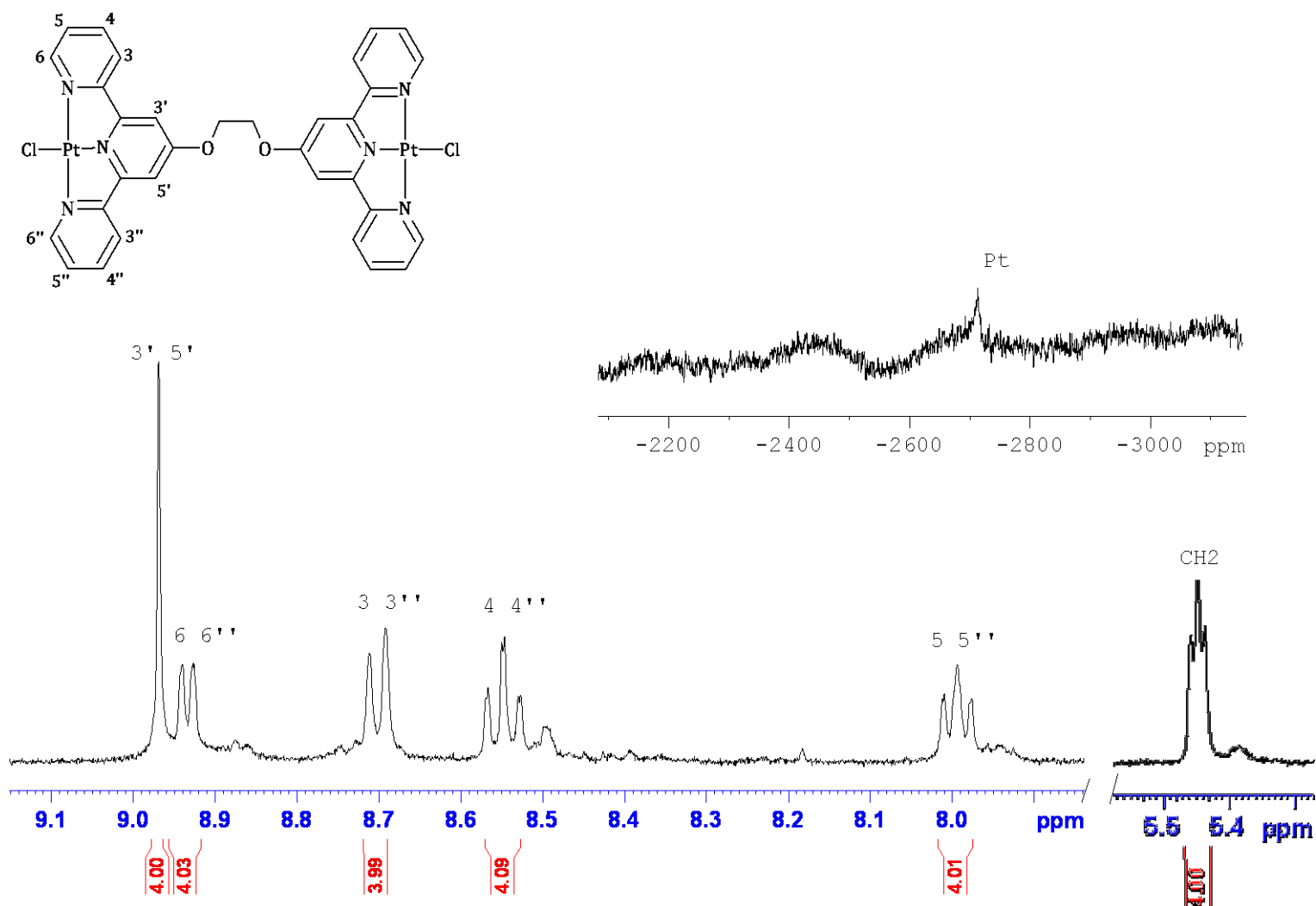


Figure S6.13  $^1\text{H}$ NMR spectrum of Pt dtegeg in DMSO. Inset is the  $^{195}\text{Pt}$  NMR spectrum of the complex.

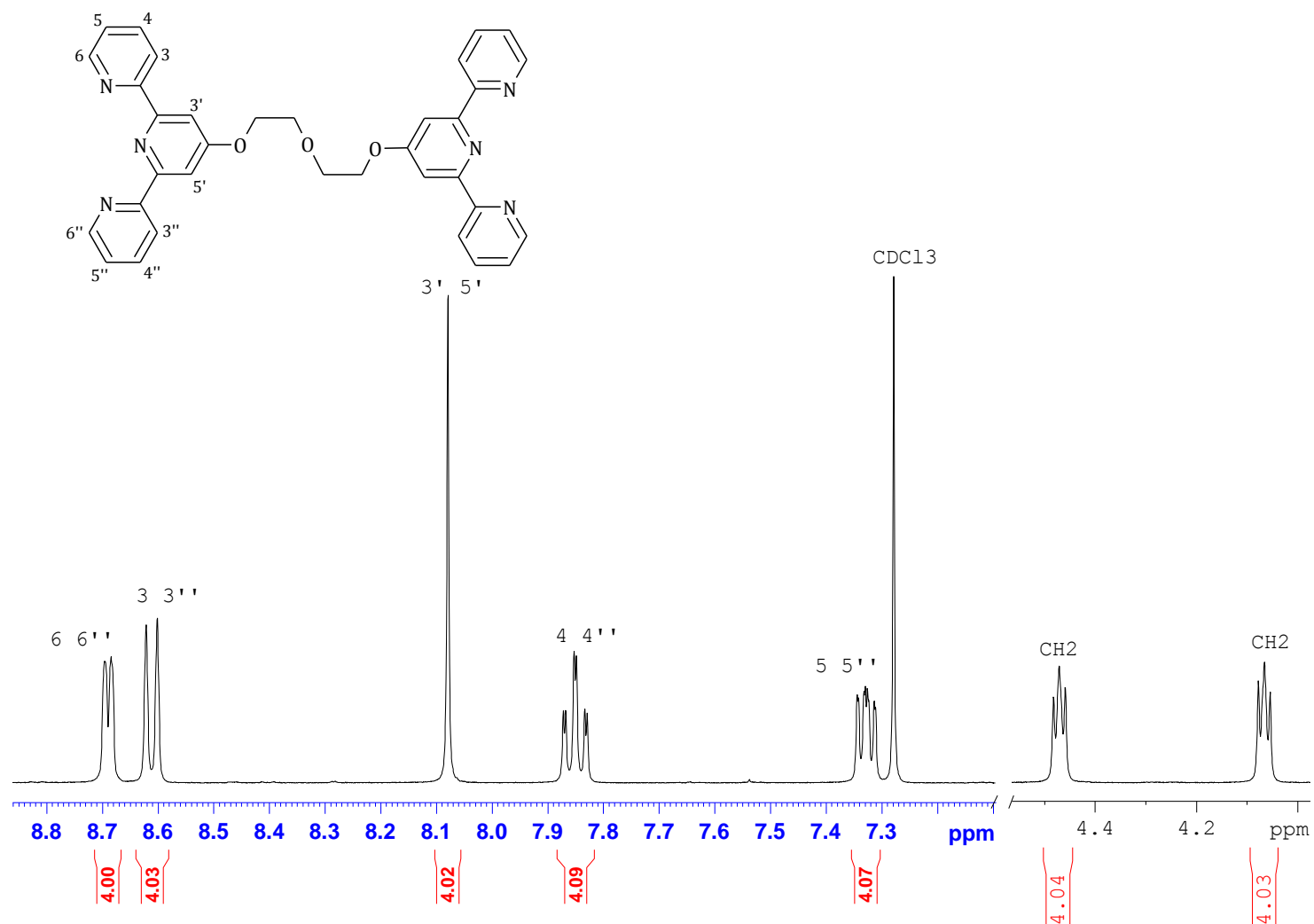


Figure S6.14 <sup>1</sup>H NMR spectrum dtdeg in CDCl<sub>3</sub>.

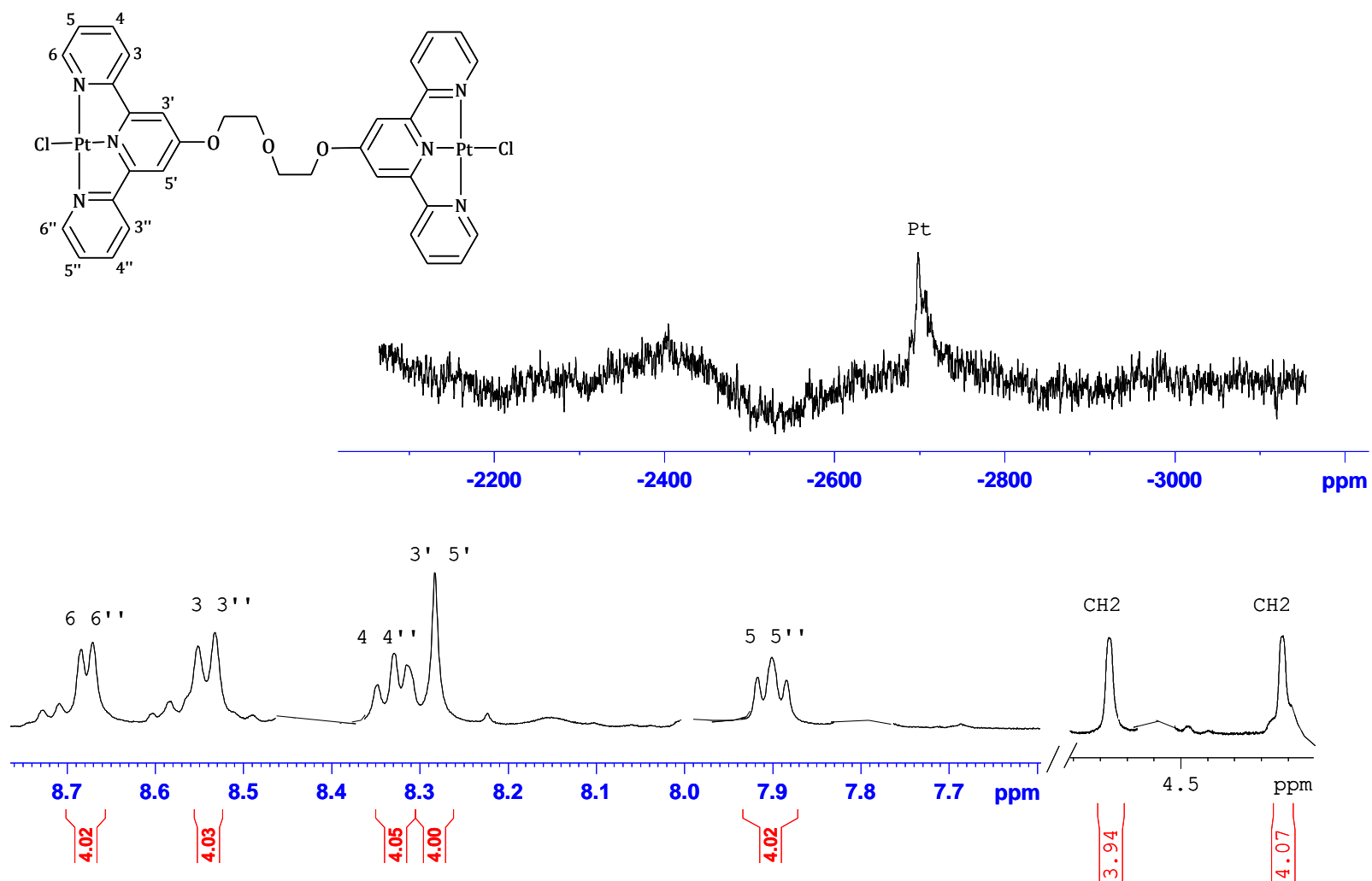
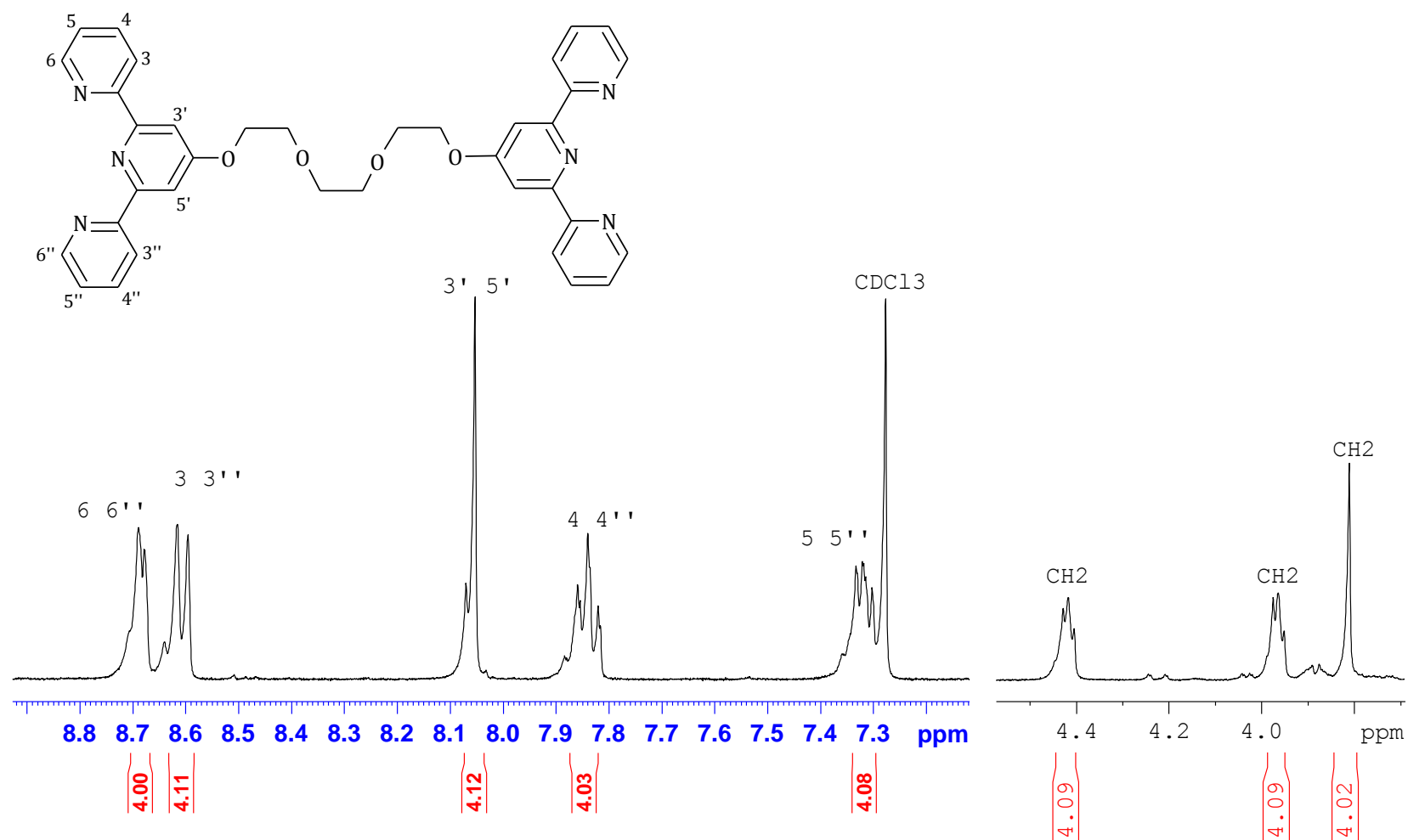


Figure S6.15  $^1\text{H}$ NMR spectrum of Ptdtdeg in DMSO. Inset is the  $^{195}\text{Pt}$  NMR spectrum of the complex.

Figure S6.16 <sup>1</sup>H NMR spectrum dtteg in CDCl<sub>3</sub>.

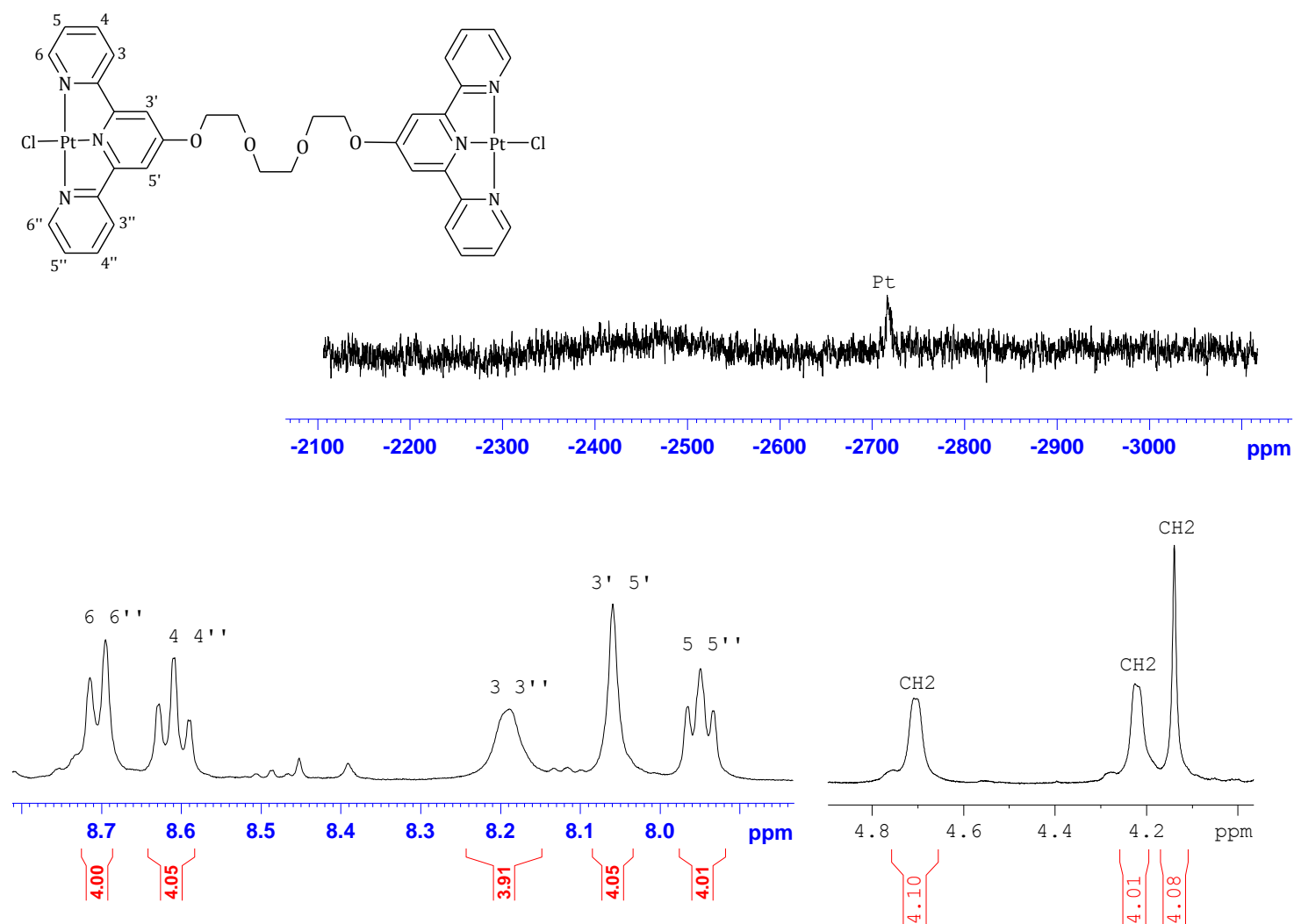
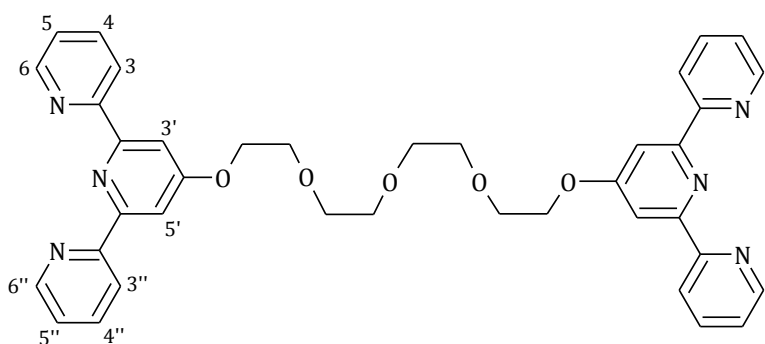


Figure S6.17  $^1\text{H}$ NMR spectrum of Ptdtteg in DMSO. Inset is the  $^{195}\text{Pt}$  NMR spectrum of the complex.



**Figure S6.18**  $^1\text{H}$ NMR spectrum dttteg in  $\text{CDCl}_3$ .

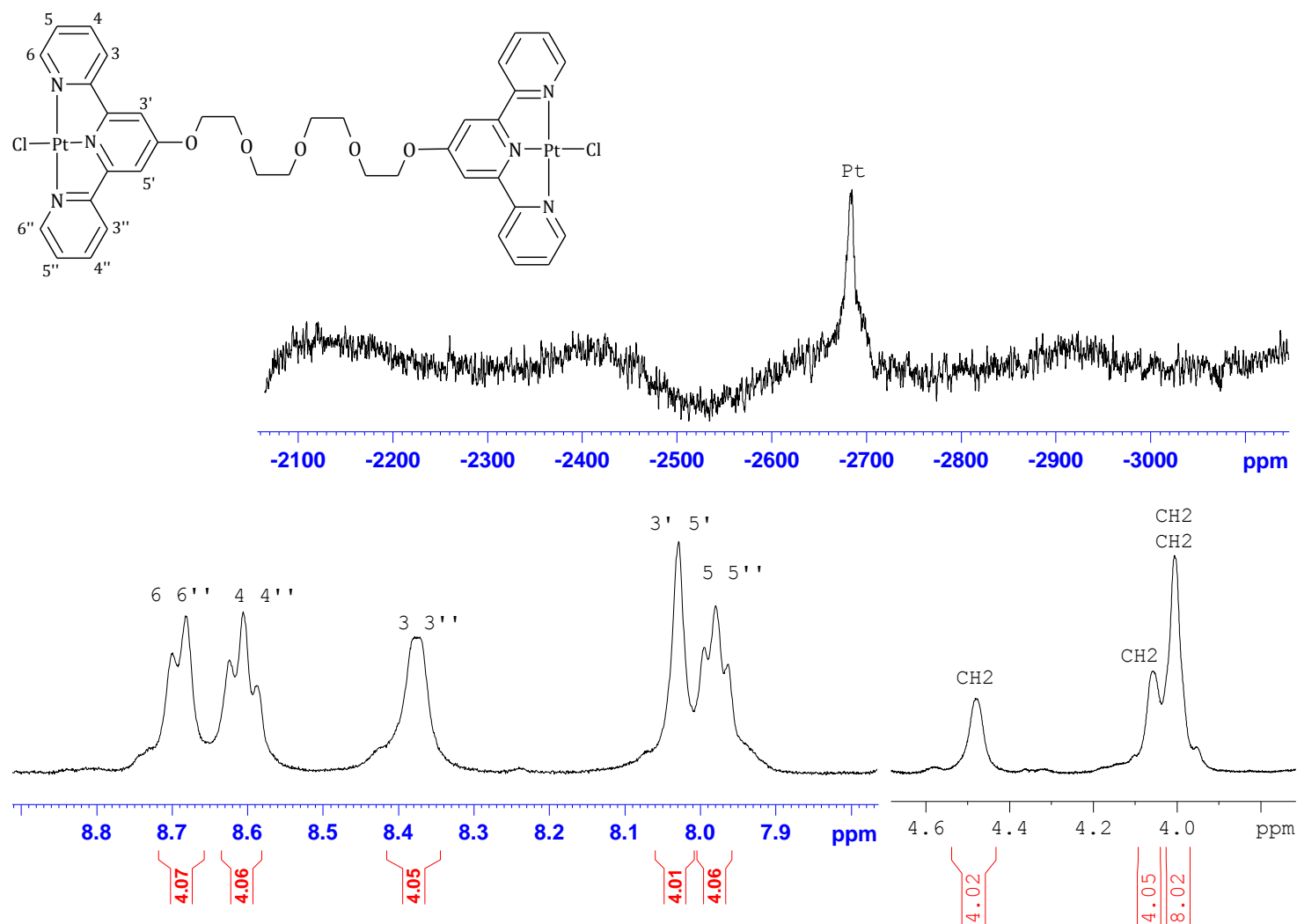


Figure S6.19  $^1\text{H}$ NMR spectrum of Pttdtttg in DMSO. Inset is the  $^{195}\text{Pt}$  NMR spectrum of the complex.

## Elemental Composition Report

Page 1

## Single Mass Analysis

Tolerance = 50.0 PPM / DBE: min = -1.5, max = 50.0

Element prediction: Off

Number of isotope peaks used for i-FIT = 3

Monoisotopic Mass, Even Electron Ions

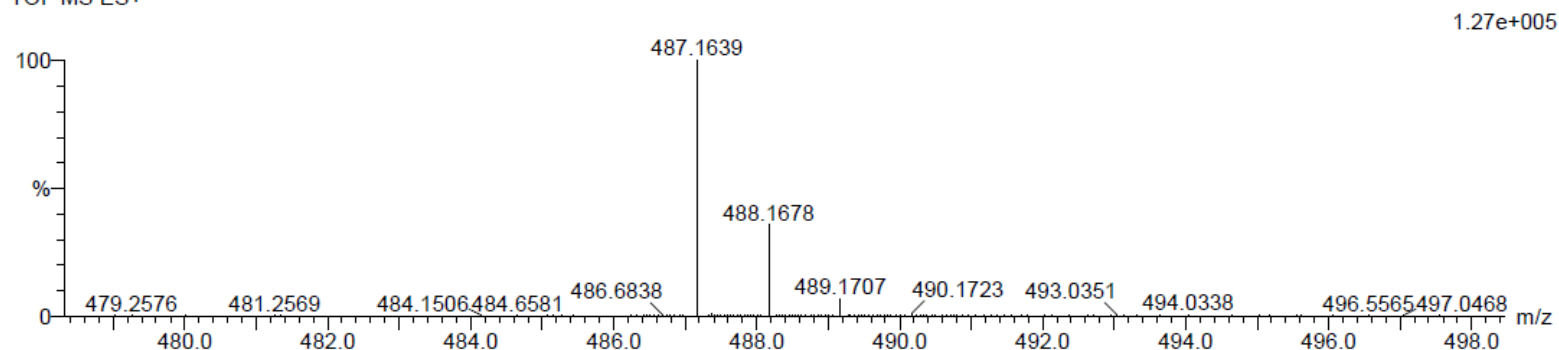
5 formula(e) evaluated with 1 results within limits (up to 50 best isotopic matches for each mass)

Elements Used:

C: 30-35 H: 20-25 N: 5-10 Na: 1-1

tpytpy 11 (0.188) Cm (1:29)

TOF MS ES+



Minimum: -1.5  
Maximum: 5.0 50.0 50.0

Mass	Calc. Mass	mDa	PPM	DBE	i-FIT	i-FIT (Norm)	Formula
487.1639	487.1647	-0.8	-1.6	23.5	566.6	0.0	C30 H20 N6 Na

Figure S6.20 High resolution ESI mass spectrum of 6',6''-Bis(2-pyridyl)-2,2':4',4'' :2'',2'''-quaterpyridine.



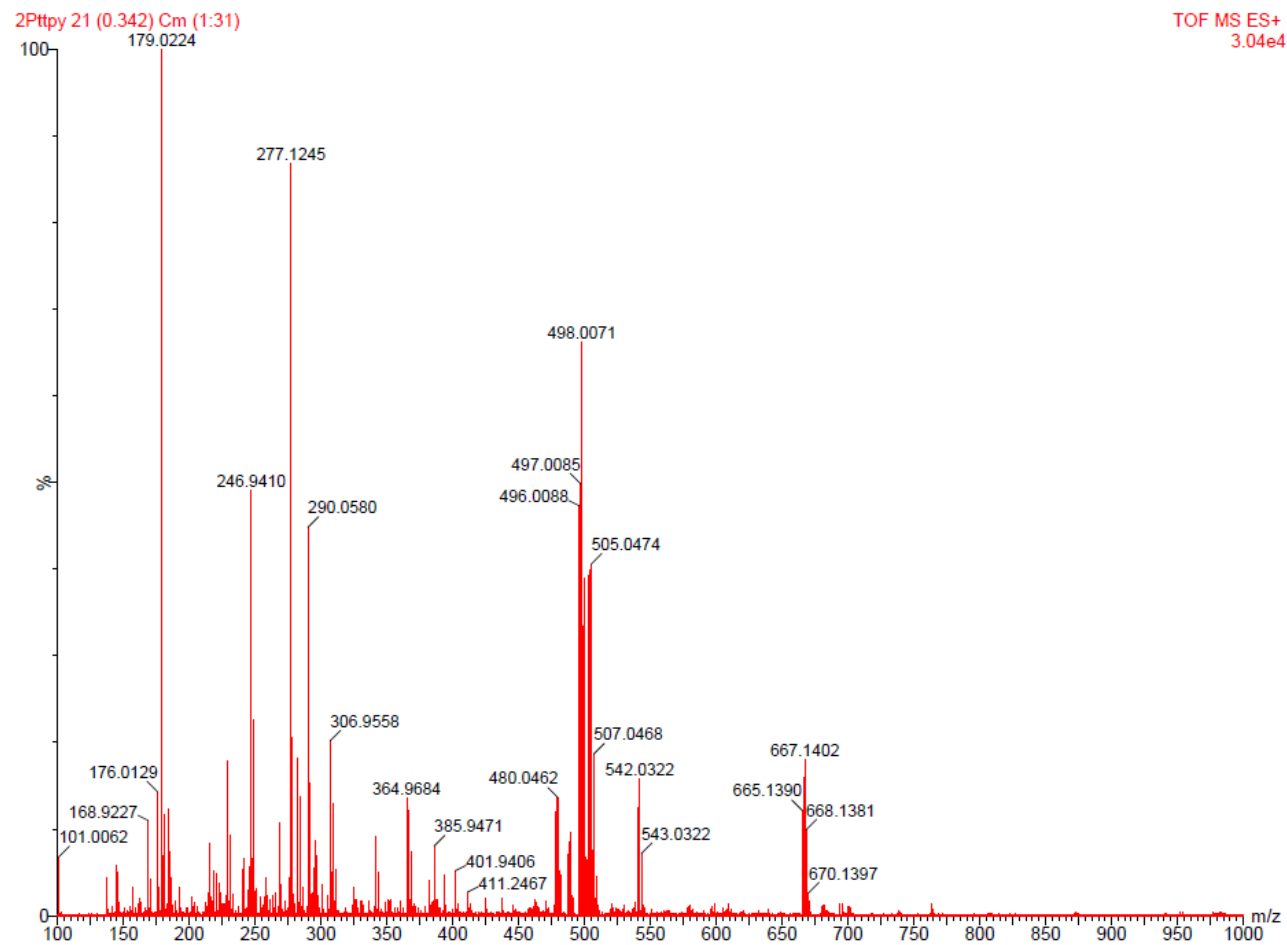


Figure S6.21 Low resolution ESI mass spectrum of Ptdt.

**Single Mass Analysis**

Tolerance = 5.0 PPM / DBE: min = -1.5, max = 50.0

Element prediction: Off

Number of isotope peaks used for i-FIT = 3

Monoisotopic Mass, Even Electron Ions

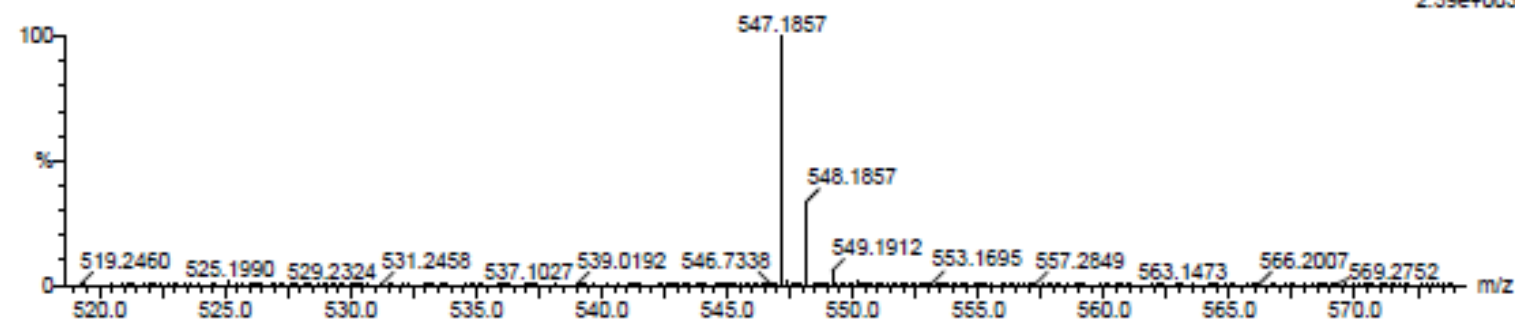
19 formula(e) evaluated with 1 results within limits (all results (up to 1000) for each mass)

Elements Used:

C: 30-35 H: 20-25 N: 5-10 O: 0-5 Na: 1-1

Alshath

Dteg 11 (0.187)

TOF MS ES+  
2.59e+003

Minimum: -1.5  
Maximum: 5.0 5.0 50.0

Mass	Calc. Mass	mDa	PPM	DBE	i-FIT	i-FIT (Norm)	Formula
547.1857	547.1858	-0.1	-0.2	23.5	88.1	0.0	C32 H24 N6 O2 Na

Figure S6.22 High resolution ESI mass spectrum of dteg.

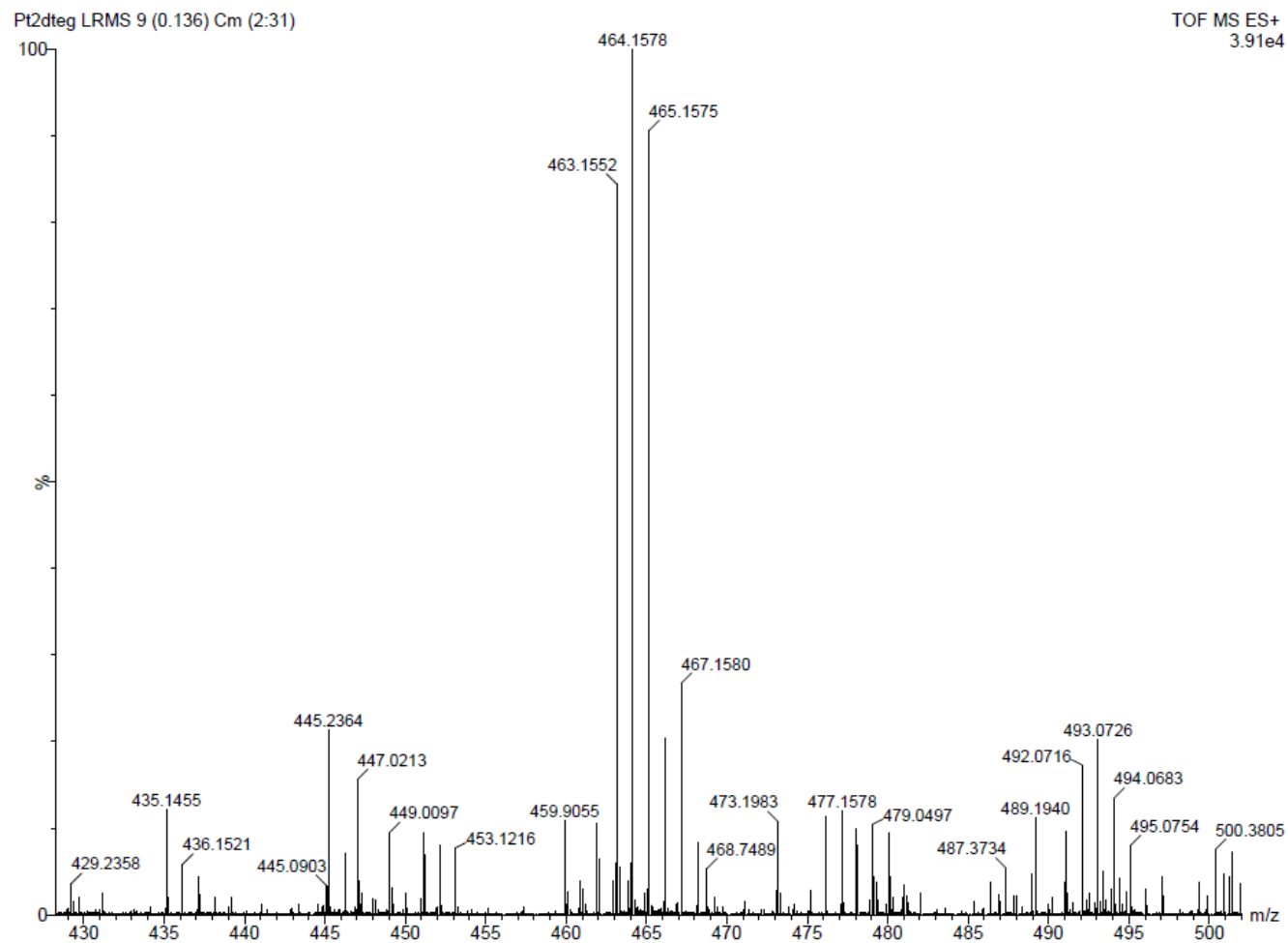


Figure S6.23 Low resolution ESI mass spectrum of Pt2dteg.

**Single Mass Analysis**

Tolerance = 5.0 PPM / DBE: min = -1.5, max = 50.0

Element prediction: Off

Number of isotope peaks used for i-FIT = 3

Monoisotopic Mass, Even Electron Ions

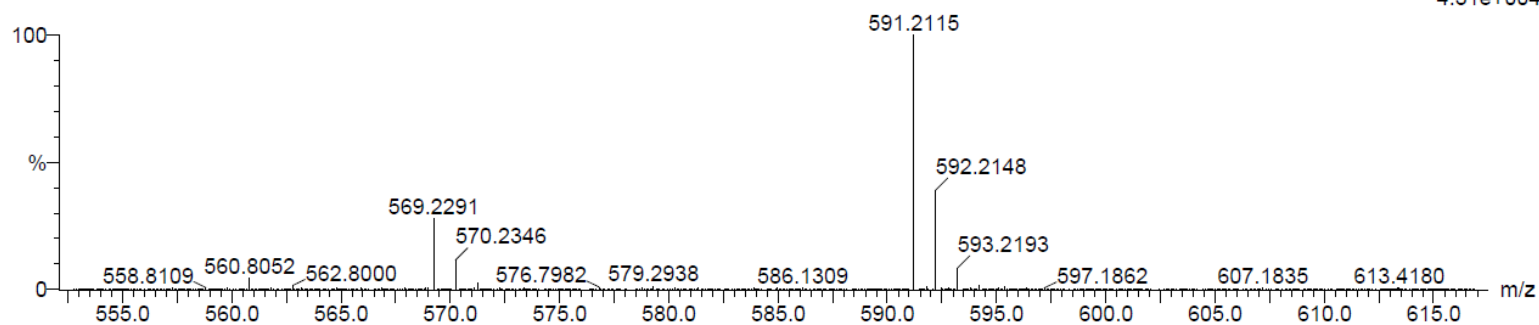
21 formula(e) evaluated with 1 results within limits (all results (up to 1000) for each mass)

Elements Used:

C: 30-35 H: 25-30 N: 0-10 O: 0-5 Na: 1-1

Aishath

dtdeg 4 (0.051) Cm (2:5)

TOF MS ES+  
4.31e+004

Minimum: -1.5  
Maximum: 5.0 5.0 50.0

Mass	Calc. Mass	mDa	PPM	DBE	i-FIT	i-FIT (Norm)	Formula
591.2115	591.2121	-0.6	-1.0	23.5	203.9	0.0	C34 H28 N6 O3 Na

**Figure S6.24** High resolution ESI mass spectrum of dtdeg.

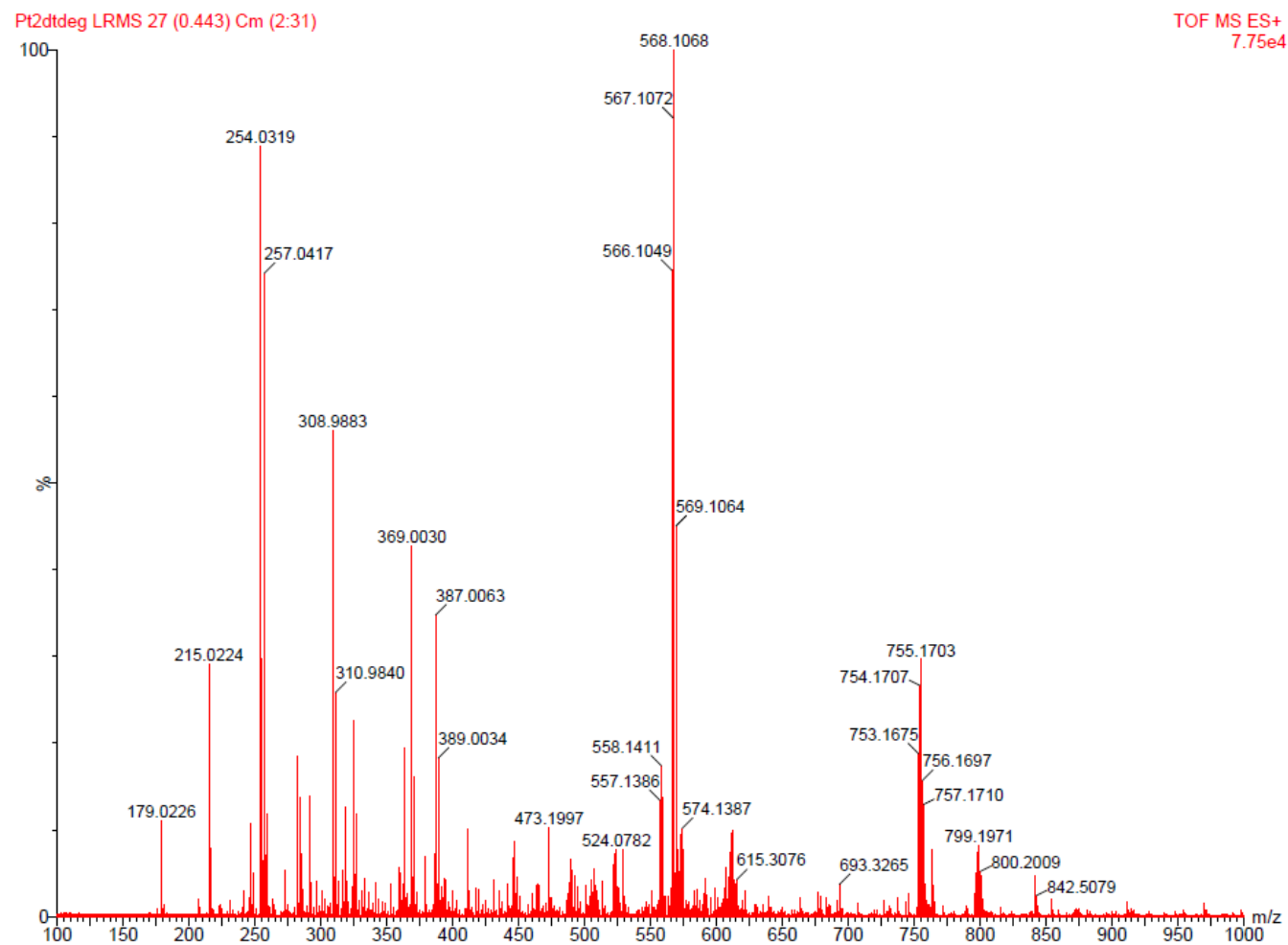


Figure S6.25 Low resolution ESI mass spectrum of Pt2dtddeg.

**Single Mass Analysis**

Tolerance = 5.0 PPM / DBE: min = -1.5, max = 50.0

Element prediction: Off

Number of isotope peaks used for i-FIT = 3

Monoisotopic Mass, Even Electron Ions

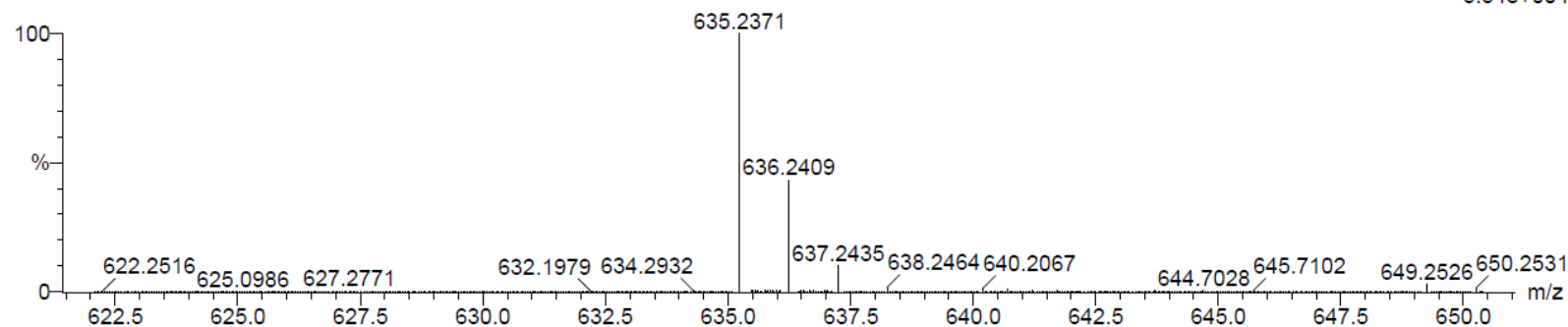
40 formula(e) evaluated with 1 results within limits (all results (up to 1000) for each mass)

Elements Used:

C: 35-40 H: 30-35 N: 5-10 O: 0-10 Na: 1-1

Aishath

dtteg 23 (0.376) Cm (1:31)

TOF MS ES+  
5.54e+004

Minimum: -1.5  
Maximum: 5.0 5.0 50.0

Mass	Calc. Mass	mDa	PPM	DBE	i-FIT	i-FIT (Norm)	Formula
635.2371	635.2383	-1.2	-1.9	23.5	377.3	0.0	C36 H32 N6 O4 Na

**Figure S6.26** High resolution ESI mass spectrum of dtteg.

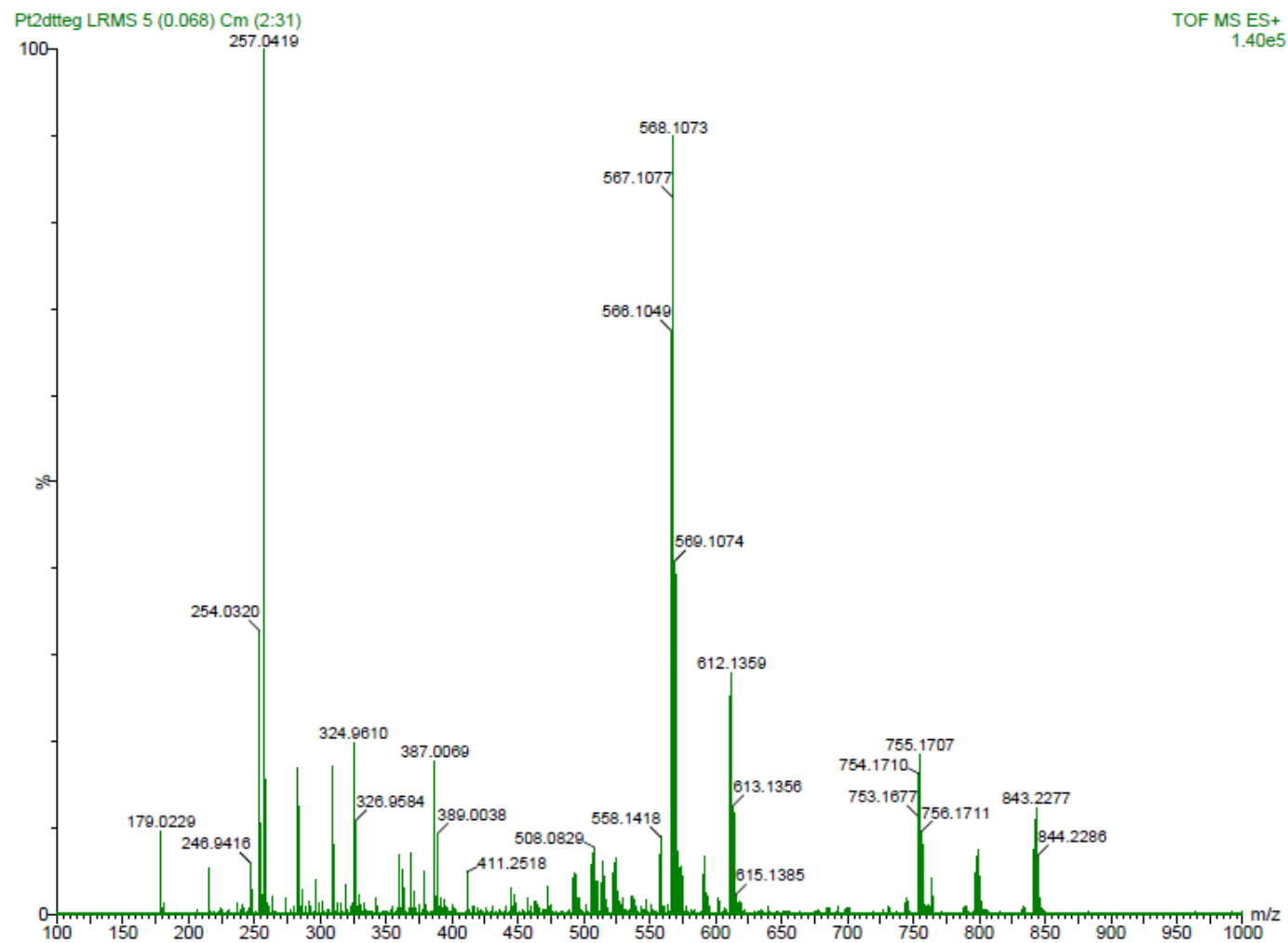


Figure S6.27 Low resolution ESI mass spectrum of Pt2dttg.

**Single Mass Analysis**

Tolerance = 5.0 PPM / DBE: min = -1.5, max = 50.0

Element prediction: Off

Number of isotope peaks used for i-FIT = 3

Monoisotopic Mass, Even Electron Ions

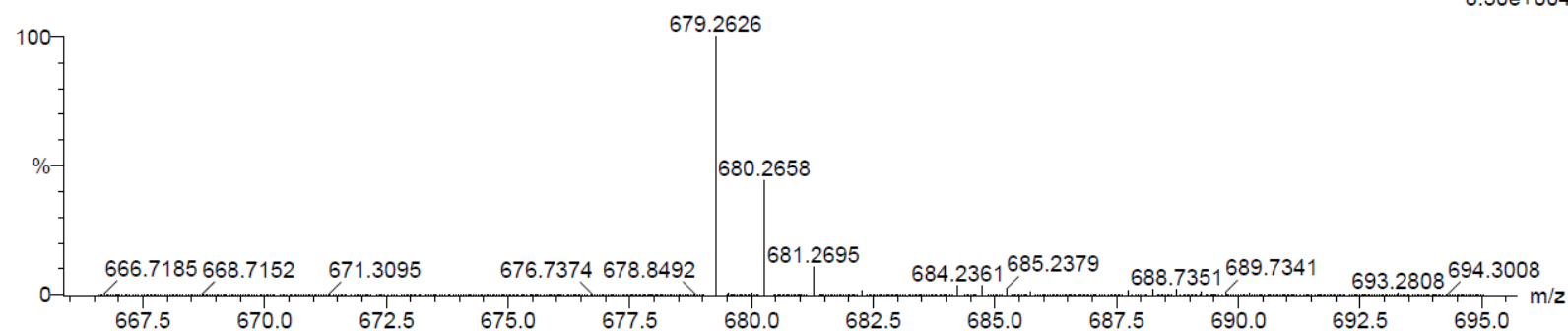
23 formula(e) evaluated with 1 results within limits (all results (up to 1000) for each mass)

Elements Used:

C: 35-40 H: 35-40 N: 5-10 O: 0-10 Na: 1-1

Aishath

dtteg LRMS 2 (0.017) Cm (1:31)

TOF MS ES+  
8.30e+004

Minimum: -1.5  
Maximum: 5.0 5.0 50.0

Mass	Calc. Mass	mDa	PPM	DBE	i-FIT	i-FIT (Norm)	Formula
679.2626	679.2645	-1.9	-2.8	23.5	422.8	0.0	C38 H36 N6 O5 Na

**Figure S6.28** High resolution ESI mass spectrum of dtteg.



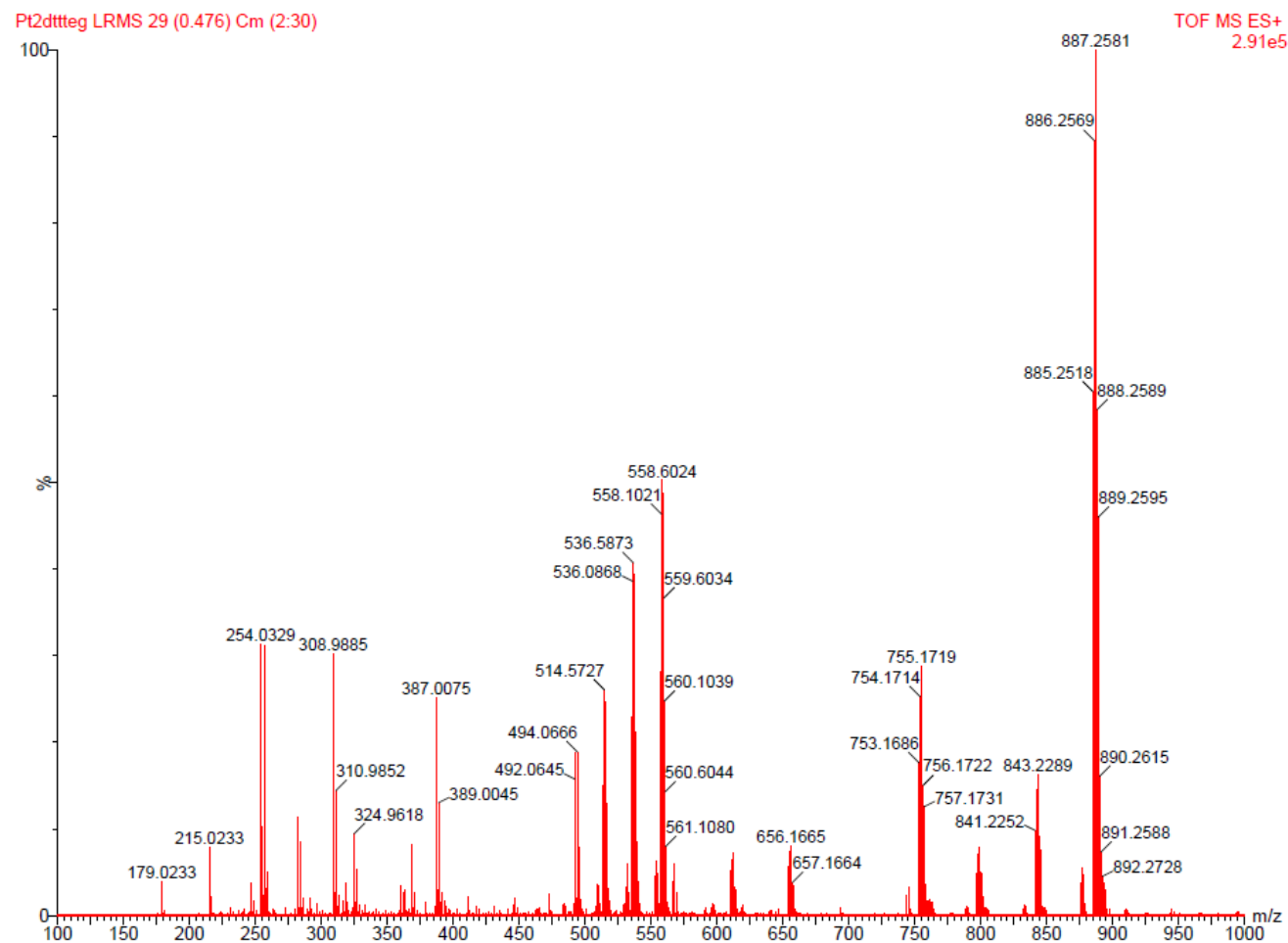
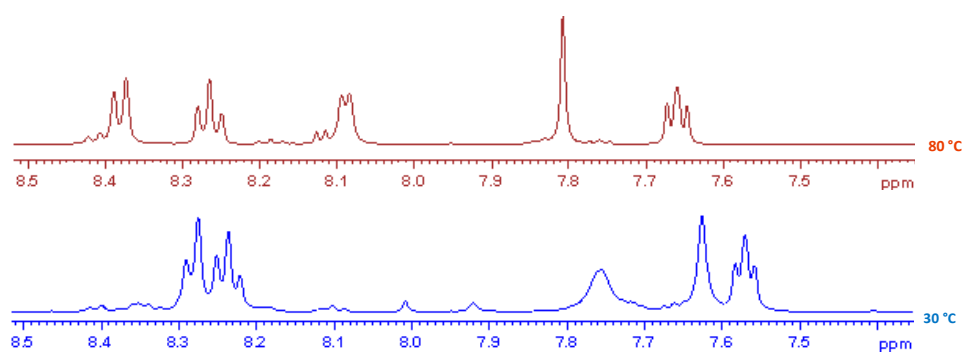


Figure S6.29 Low resolution ESI mass spectrum of Pt2dtttteg.



**Figure S6.30**  $^1\text{H}$  spectra of Ptdtteg (0.02 M) in  $\text{DMSO-}d_6$  at temperatures, 30 °C (bottom spectrum) and 80 °C (top spectrum).

**Table Contents- 7**

List of Figures.....	ii
List of Tables.....	ii
List of Schemes .....	iii
Chapter Seven .....	1
<b>Role of Bridging Polyethyleneglycol Ether Linkers on the Rate of Ligand Substitution of Heterometallic Ruthenium(II)-Platinum(II) Complexes .....</b>	<b>1</b>
7.0    Abstract .....	1
7.1    Introduction.....	1
7.2    Experimental.....	4
7.2.1    Materials.....	4
7.2.2    Synthesis .....	5
7.2.3    Synthesis of [(tpy)Ru(polyethyleneglycol ether)]Cl <sub>2</sub> Moieties.....	5
7.2.4    Synthesis of Platinum(II) Complexes .....	7
7.2.5    Instrumentation and Physical Measurements.....	8
7.2.6    Preparation of Solution for Kinetic Analysis .....	9
7.2.7    Computational Modelling.....	9
7.3    Results.....	12
7.3.1    Kinetic Studies on Substitution Reactions of Chloro Complexes .....	12
7.3.2    Discussion .....	16
7.4    Conclusions.....	20
7.5    References .....	21
7.6    Supporting Information.....	25

### List of Figures

Figure 7.1	Structure of heterometallic complexes investigated. Shown on the structure, RuPtdttteg is the numbering scheme employed for characterizations and DFT data. Rectangular inset shows the structures of additional mononuclear complexes, without the linker (Ptppy) and with the linker (Ptppyeg) for comparisons. The kinetic data for Ptppy is obtained from reference and Ptppyeg from our previous work ( <i>Chapter 5</i> ).....	4
Figure 7.2	DFT calculated minimum energy structures, frontier molecular orbitals (HOMO and LUMO) of RuPtdteg showing the V-shape geometry. Included is the data obtained for the DFT calculated complexes, Ptppy and Ptppyeg for comparisons. Calculations were performed at B3LYP/LanL2DZ level of theory in all the systems. Data for Ptdtdeg, Ptdtteg and Ptdttteg are included in Figure S7.1 (Supporting Information) .....	11
Figure 7.3	Kinetic trace for the substitution reaction of RuPtdtdeg ( $1.0 \times 10^{-5}$ M) with TU ( $3.0 \times 10^{-5}$ M) in methanol solution ( $I = 0.02$ M) at 330 nm at 298 K.....	12
Figure 7.4	Dependence of the <i>pseudo</i> first-order rate constants ( $k_{\text{obs}}$ ) on the concentrations of the nucleophiles for the chloride substitution from RuPtdtdeg ( $1.0 \times 10^{-5}$ M) in methanol solution ( $I = 0.02$ M) at 298 K.....	15
Figure 7.5	Eyring plots obtained for RuPtdtdeg with the nucleophiles for the forward reactions over the temperature range 15 - 35 °C.....	16
Figure 7.6	Aerial view showing the steric disposition of the pendant group on the 4'-position of the chelate ligand (tpy) bonded to the Pt(II) metal centre obtained from DFT calculations. ....	18

### List of Tables

Table 7.1	Summary of DFT calculated data for the complexes investigated. Included for comparison purposes is the data for Ptppy and Ptppyeg. Calculations were performed at B3LYP/LanL2DZ level of theory in all the systems. ..	10
Table 7.2	Summary of second-order rate constants, $k_2$ and activation parameters, with the corresponding standard deviations for the substitution of the chloro ligand by a series of thiourea nucleophiles and iodide at $I = 0.02$ M LiCF <sub>3</sub> SO <sub>3</sub> , adjusted with LiCl. Data for Ptppy is taken from literature and data on mononuclear complexes are from <i>Chapter 5</i> and are included for comparison.....	14

**List of Schemes**

Scheme 7.1	The general reaction scheme for the reactions between the complexes and the nucleophiles studied. ....	17
------------	--	----

# Chapter Seven

## Role of Bridging Polyethyleneglycol Ether Linkers on the Rate of Ligand Substitution of Heterometallic Ruthenium(II)-Platinum(II) Complexes

### 7.0 Abstract

The ligand substitution kinetics of heterometallic Ru(II)-Pt(II) complexes linked by polyethyleneglycol ether units *viz*; [(tpy)Ru(tpy)-O(CH<sub>2</sub>CH<sub>2</sub>O)<sub>n</sub>-(tpy)PtCl] (where tpy = 2,2':6',2''-terpyridine and n = 1 (**RuPtdtdeg**), 2 (**RuPtdtdeg**), 3 (**RuPtdtteg**) and 4 (**RuPtdttteg**)) with thiourea (TU), 1,3-dimethyl-2-thiourea (DMTU), 1,1,3,3-tetramethyl-2-thiourea (TMTU) and iodide (I<sup>-</sup>) were investigated under *pseudo* first-order conditions as a function of concentration and temperature by using UV/visible spectrophotometry and conventional stopped-flow technique. The observed first-order rate constants followed the simple associative rate law  $k_{\text{obs}} = k_2[\text{Nu}]$ . Density functional theory (DFT) calculations at LanL2DZ/ B3LYP level of theory demonstrate that the rate of substitution reactions of the heterometallic complexes is geometrically controlled. Increasing the length of the polyethyleneglycol ether linker increases the entrapment effect of the nucleophiles due to the V-shape geometry of the complexes which in turn decreases the steric influence by the Ru(tpy)<sub>2</sub> moiety on the reactive Pt(II) metal centre thereby increasing the reactivity. The electronic transitions between Ru(II) and Pt(II) is insignificant in the presence of a non-aromatic polyethyleneglycol ether linker. The activation parameters obtained support an associative mode of mechanism, where bond formation in the transition state is favoured.

### 7.1 Introduction

Cisplatin, *cis*-[PtCl<sub>2</sub>(NH<sub>3</sub>)<sub>2</sub>], is one of the most effective anticancer drugs available to date.<sup>1</sup> However, due to its significant side effects, tumour resistance and poor solubility in water has resulted in the development of many other complexes for cancer treatment.<sup>2</sup> Currently, the focus of research is on developing structurally new metal based complexes capable of cleaving DNA.<sup>1a-c,3</sup> As a result, many transition metal complexes have been reported with systems which are promising as structural probes and therapeutic agents.<sup>4</sup> In this regard, polypyridine Ru(II) complexes are considered as good candidates due to their light responsive properties<sup>5</sup> such as their ability to

control the reaction, conversion of light energy to chemical energy and being highly targeted.<sup>4m,6</sup>

Within this framework, Ru-based complexes have recently been reported as a new class of anticancer agents.<sup>2e,7</sup> For example, the mononuclear antimetastatic coordinated imidazolium complexes, [*trans*-RuCl<sub>4</sub> (1Himidazole)(DMSO-S)] (NAMI-A) and indazolium [*trans*-RuCl<sub>4</sub>(1H-indazole)<sub>2</sub>] (KP1019)<sup>7i</sup> were reported to exhibit potential toxicity and low levels of frequent side effects compared to cisplatin. The complexes were successful in phase-I clinical trials.<sup>8</sup> Ru-based complexes are also potential candidates for photodynamic therapy (PDT) due to their ability to absorb visible light and photo cleaves DNA,<sup>4k,9</sup> most likely due to their longer lived metal-to-ligand charge transfer transitions (MLCT).<sup>10</sup> Furthermore, multinuclear Ru(II) complexes have gained a special interest on assumption that the greater size and the high charge would increase the DNA binding capacity relative to their mononuclear complexes.<sup>11</sup> In this regard, Ru(II) complexes of polypyridyl ligand systems, especially, 2,2':6',2''-terpyridine (tpy) has been of interest in the area of multinuclear supramolecular chemistry.<sup>12</sup>

In multinuclear complexes, the bridging ligand (BL) plays an important role in controlling the biological and spectroscopic properties. For example, the high toxicity shown by the Pt(II) complexes linked by polynuclear  $\alpha,\omega$ -diaminoalkane is thought to be due to their ability to form long-ranged DNA adducts.<sup>13</sup> The complexes, **BBR3464** which contains two *trans*-[PtCl(NH<sub>3</sub>)<sub>2</sub>]<sup>+</sup> units connected by a tetraamine [Pt(NH<sub>3</sub>)<sub>2</sub>{H<sub>2</sub>N(CH<sub>2</sub>)<sub>6</sub>NH<sub>2</sub>}<sub>2</sub>]<sup>2+</sup> unit and the binuclear alkyldiamine complex [{*cis*-PtCl<sub>2</sub>(NH<sub>3</sub>)<sub>2</sub>}(diamine)] known as 2,2'/c,c'-bn are expected to form different DNA adducts.<sup>14</sup> Unfortunately, after the phase-II clinical trials, further evaluation of **BBR3464** was limited due to its low activity.<sup>15</sup> Apart from alkyldiamine bridged complexes, polyethyleneglycol linked complexes were also recently reported<sup>16</sup> as possible anticancer agents. Examples include, flexible bis[4'-(2,2':6',2''-terpyridyl)]-diethyleneglycol ether (dtdeg) and its coordinated metal complexes of platinum, ruthenium and copper which can modify calf thymas (CT) DNA.<sup>16</sup> This ligand system was reported to form both heterometallic and homometallic compounds.<sup>17</sup>

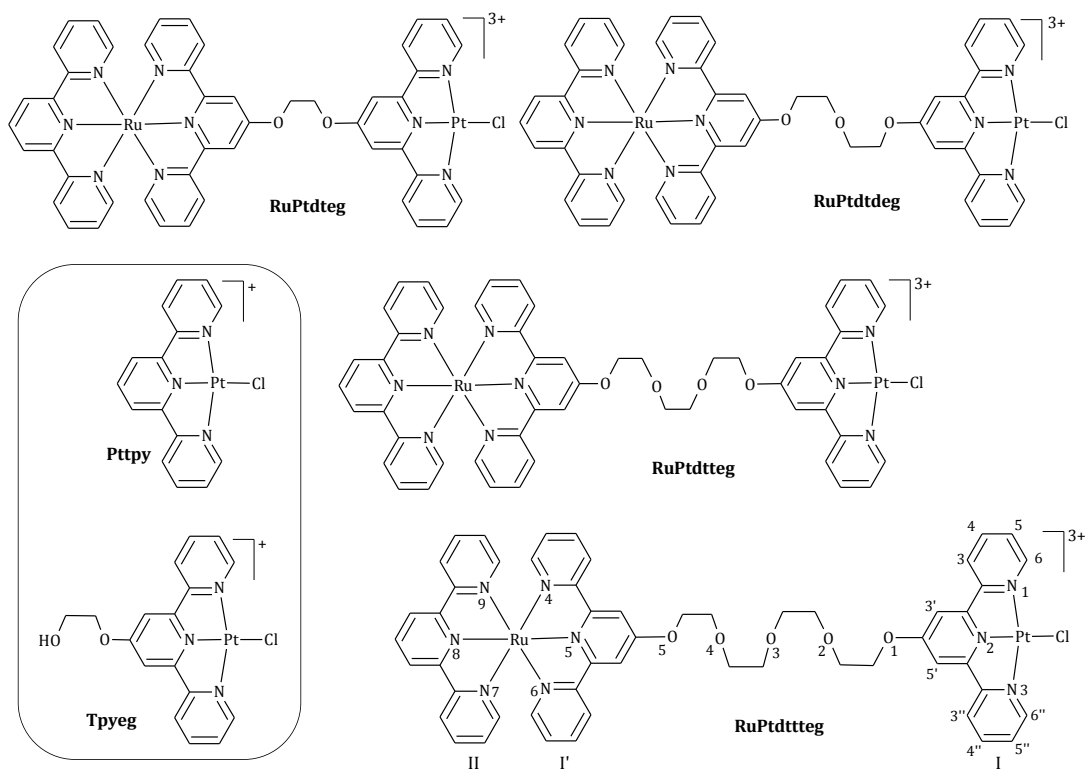
Incorporation of a labile Pt(II) complex coupled to a light absorbing Ru(II) moiety results in a group of Ru(II)-Pt(II) supramolecular complexes that could alter the targeted PDT and optical excitation into therapeutic window.<sup>1d,3a,10c</sup> Integration of a

light absorbing (LA) unit into the structural framework increases the possibility of photoactivation. This alternatively affects the photophysical properties of the complex.<sup>18</sup> The octahedral geometry of ruthenium metal centre, compared to that of square planar cisplatin, is also thought to impose unique interactions with DNA with a different anticancer profile.<sup>19</sup> The development of polynuclear with heteronuclearity comprising Ru-Pt centres is a remarkable challenge. Selective reactivity may be achieved depending on the geometry at the metal centres displaying different mechanisms of actions. This expansion of mixed-metal Ru-Pt complexes may overcome the limitations of platinum based complexes and provide an alternative for more targeting metal based PDT agents, while keeping the photocleavage and DNA binding properties.<sup>9a</sup>

Mixed metal complexes bridged with polyazine of the form  $[(bpy)_2Ru(dpp)PtCl_2]^{2+}$ ,<sup>18</sup>  $[(bpy)_2Ru(dpq)PtCl_2]^{2+}$  and  $[(bpy)_2Ru(dpb)PtCl_2]^{2+}$  (where bpy = 2,2'-bipyridine, dpp = 2,3-bis(2-pyridyl), dpq = 2,3-bis(2-pyridyl)quinoxaline and dpb = 2,3-bis(2-pyridyl)-benzoquinoxaline) have been reported where the latter two complexes exhibit DNA binding.<sup>20</sup> These complexes have several advantages such as high solubility compared to the well-known neutral cisplatin. Thus, information obtained on such varied molecular framework would be an important tool for designing effective anticancer drugs.

Based on the previous work on mono nuclear and dinuclear 4'-functionalised Pt(II) terpyridine complexes, this study aims to increase our understanding of the role of flexible ethyleneglycol ether linkers on the reactivity of the mixed metal Ru(II)-Pt(II) complexes when one end of the molecule is capped with Ru(II)terpyridine moiety. Keeping in mind that multinuclear Pt(II) complexes linked by flexible alkyldiamine bridged complexes show high activity against tumour cells which are cisplatin resistant,<sup>21</sup> the complexes reported here are also dinuclear and comprise of different metal centres, which result in a vacant Pt(II) coordination site for DNA binding and a substitutionally inert but photodynamically active Ru(tpy)<sub>2</sub> site. In this study, the two metal centres are connected by a flexible bis[4'-(2,2':6',2''-terpyridyl)]- ethyleneglycol ether ligands of different chain lengths. Our motivation for incorporating the Pt(II) moiety to the Ru(II) moiety is to investigate the effect of Ru(tpy)<sub>2</sub> on the substitution reactivity at the Pt(II) centre. The complexes used in this investigation are shown in *Figure 7.1*.





**Figure 7.1** Structure of heterometallic complexes investigated. Shown on the structure, **RuPtdttteg** is the numbering scheme employed for characterizations and DFT data. Rectangular inset shows the structures of additional mononuclear complexes, without the linker (**Ptpy**) and with the linker (**Ptpyeg**) for comparisons. The kinetic data for **Ptpy** is obtained from reference<sup>22</sup> and **Ptpyeg** from our previous work (*Chapter 5*).

## 7.2 Experimental

### 7.2.1 Materials

Methanol (Merck, South Africa) was distilled over magnesium prior to use for kinetic analysis.<sup>23</sup> Dimethylformamide (99.9%) (Sigma-Aldrich) was used without further purification. 4'-chloro-2,2':6',2''-terpyridine (99%), the platinum salt, potassium tetrachloroplatinate (II) (99.9%) and ruthenium salt,  $\text{RuCl}_3 \cdot 3\text{H}_2\text{O}$  (99%) were purchased from Aldrich. All other chemicals were bought from Sigma Aldrich and were of analytical grade hence, used as received.

### 7.2.2 Synthesis

The ligands linked by ethyleneglycol ether viz. bis[4'-(2,2':6',2''-terpyridyl)]-ethyleneglycol ether (**dteg**), bis[4'-(2,2':6',2''-terpyridyl)]-diethyleneglycolether (**dtdeg**), bis[4'-(2,2':6',2''-terpyridyl)]-triethyleneglycolether (**dtteg**) and bis[4'-(2,2':6',2''-terpyridyl)]-tetraethyleneglycolether (**dtteg**) were synthesized and characterized as reported in the previous chapter. The ruthenium precursor **[Ru(tpy)Cl<sub>3</sub>]** was synthesized according to the literature procedure.<sup>24</sup>

### 7.2.3 Synthesis of [(tpy)Ru(polyethyleneglycol ether)]Cl<sub>2</sub> Moieties

The polyethyleneglycol ether linked Ru(II)tpy moieties (**[(tpy)Ru(dteg)]Cl<sub>2</sub>**), **[(tpy)Ru(dtdeg)]Cl<sub>2</sub>**, **[(tpy)Ru(dtteg)]Cl<sub>2</sub>** and **[(tpy)Ru(dttteg)]Cl<sub>2</sub>**) (where tpy, **dteg**, **dtdeg**, **dtteg** and **dttteg** have the same meaning as stated previously) were synthesized following the literature procedure.<sup>25</sup> To a filtered solution of excess silver tetrafluoroborate (AgBF<sub>4</sub>) in acetone, was added Ru(tpy)Cl<sub>3</sub> and the reaction mixture was refluxed in dark for 18 hours. The reaction mixture was then cooled to room temperature and the resulting silver chloride (AgCl) precipitate filtered. The filtrate was evaporated in *vacuo* resulting into a dark green oil. The diterpyridine ethyleneglycol ether linked ligand (**dteg**, **dtdeg**, **dtteg** and **dttteg**) was added and the mixture refluxed in DMF for 1.5 hours. The solvent DMF reduces Ru(III) to Ru(II). The reaction mixture was filtered, concentrated under *vacuo* resulting into a red oil. The oil was then added to a saturated solution of lithium chloride (LiCl) in ethanol to obtain the chloride salt. The crude product was obtained by precipitation with a large amount of acetone. The precipitate was column chromatographed on neutral alumina with acetone: methanol: ethanol (8 : 1 : 1). The pure product was obtained from the first red band and precipitated with diethyl ether.

The purity of the products was confirmed by <sup>1</sup>H NMR and mass spectroscopy. The <sup>1</sup>H NMR spectra obtained show similarity in the aromatic region for all the Ru(tpy) linked ligands. The mass spectra for all the complexes show characteristic fragmentations.

**[(tpy)Ru(dteg)]Cl<sub>2</sub>**

Yield: 0.031 g, (30 %), dark red powder. <sup>1</sup>H NMR (400 MHz, DMSO-*d*<sub>6</sub>)  $\delta$ / ppm: 9.03 (2H, d, II3' 5'), 8.96 (2H, d, I'3 3''), 8.90 (2H, d, II3 3''), 8.89 (2H, d, I6 6''), 8.89 (2H, d, I3 3'), 8.79 (2H, s, I' 3' 5'), 8.56 (1H, t, II4'), 8.55 (2H, m, I3' 5'), 8.49 (2H, m, I4 4''), 8.04 (2H, m, I'4 4''), 8.03 (2H, m, II6 6''), 7.55 (2H, d, I5 5''), 7.52 (2H, d, I'6 6''), 7.31 (2H, t, II5 5''), 7.28 (2H, t, I'5 5''), 5.10 (2H, t, 1'), 5.10 (2H, t, 1).

**[(tpy)Ru(dtdeg)]Cl<sub>2</sub>**

Yield: 55 mg, (49%), Dark red powder. <sup>1</sup>H NMR (400 MHz, DMSO-*d*<sub>6</sub>)  $\delta$ / ppm: 9.08 (2H, d, II3' 5'), 8.87 (2H, d, I'3 3''), 8.86 (2H, s, I' 3' 5'), 8.83 (2H, d, II3 3''), 8.67 (2H, d, I6 6''), 8.62 (2H, d, I3 3'), 8.45 (1H, t, II4'), 8.03 (2H, s, I3' 5'), 7.99 (2H, t, I4 4''), 7.97 (2H, t, I'4 4''), 7.51 (2H, d, II6 6''), 7.47 (2H, t, I5 5''), 7.37 (2H, d, I'6 6''), 7.25 (2H, t, II5 5''), 7.22 (2H, t, I'5 5''), 4.77 (2H, t, 1'), 4.51 (2H, t, 1), 4.15 (2H, t, 2'), 4.07 (2H, t, 2). TOF MS-ES<sup>+</sup>, *m/z*: 451.6112, (M<sup>2+</sup>).

**[(tpy)Ru(dtteg)]Cl<sub>2</sub>**

Yield: 41 mg, (46%), Dark red powder. <sup>1</sup>H NMR (400 MHz, DMSO-*d*<sub>6</sub>)  $\delta$ / ppm: 9.06 (2H, d, II3' 5'), 8.85 (2H, d, I'3 3''), 8.83 (2H, d, II3 3''), 8.80 (2H, s, I' 3' 5'), 8.67 (2H, d, I6 6''), 8.60 (2H, d, I3 3'), 8.47 (1H, t, II4'), 7.99 (2H, br, I4 4''), 7.98 (2H, b, I'4 4''), 7.96 (2H, s, I3' 5'), 7.52 (2H, d, II6 6''), 7.47 (2H, t, I5 5''), 7.36 (2H, d, I'6 6''), 7.26 (2H, t, II5 5''), 7.21 (2H, t, I'5 5''), 4.71 (2H, t, 1'), 4.41 (2H, t, 1), 4.03 (2H, t, 2'), 3.91 (2H, t, 2) 3.78 (2H, br, 3'), 3.77 (2H, br, 3). TOF MS-ES<sup>+</sup>, *m/z*: 473.6598, (M<sup>2+</sup>).

**[(tpy)Ru(dttteg)]Cl<sub>2</sub>**

Yield: 35 mg, (44%), Dark red powder. <sup>1</sup>H NMR (400 MHz, DMSO-*d*<sub>6</sub>)  $\delta$ / ppm: 9.05 (2H, d, II3' 5'), 8.85 (2H, d, I'3 3''), 8.81 (2H, s, I' 3' 5'), 8.80 (2H, d, II3 3''), 8.68 (2H, d, I6 6''), 8.60 (2H, d, I3 3'), 8.46 (1H, t, II4'), 7.93 (2H, s, I3' 5'), 8.00 (2H, br, I4 4''), 7.97 (2H, b, I'4 4''), 7.52 (2H, d, II6 6''), 7.46 (2H, t, I5 5''), 7.36 (2H, d, I'6 6''), 7.26 (2H, t, II5 5''), 7.21 (2H, t, I'5 5''), 4.68 (2H, t, 1'), 4.37 (2H, t, 1), 4.01 (2H, t, 2'), 3.85 (2H, t, 2) 3.73 (2H, t, 3'), 3.67 (2H, t, 3), 3.66 (2H, t, 4'), 3.64 (2H, t, 4). TOF MS-ES<sup>+</sup>, *m/z*: 495.6725, (M<sup>2+</sup>).

---

<sup>+</sup>  $\delta$  ppm, s = singlet, d = doublet, m = multiplet, dd = doublet of doublet, dt = doublet of triplets, t = triplet, br = broad (the same applies for all the ligands and complexes)

### 7.2.4 Synthesis of Platinum(II) Complexes

The mixed metal complexes were synthesized following the literature procedure.<sup>25</sup> The ditpyeneglycol ether linked Ru(II) moiety and Pt(cod)Cl<sub>2</sub><sup>26</sup> were refluxed in dry methanol under nitrogen for six hours. The reaction mixture was cooled to room temperature, filtered and volume reduced to half. The required compound was precipitated with slow diffusion of diethyl ether, filtered and dried in desiccators.

The purity of the final complexes was confirmed by <sup>1</sup>H NMR, <sup>195</sup>Pt NMR, elemental analyses and mass spectroscopy. The <sup>1</sup>H NMR spectra obtained show similarity in the aromatic region for the heterometallic complexes. The <sup>195</sup>Pt NMR of all the complexes exhibited a characteristic signal at about -2700 ppm which confirms the coordination of platinum to the ligand. The mass spectra obtained show characteristic fragmentation of the molecules.

#### RuPtdteg

Yield: 0.035 g, (78 %), dark red powder. <sup>1</sup>H NMR (400 MHz, DMSO-*d*<sub>6</sub>) δ/ ppm: 9.04 (2H, d, II3' 5'), 8.96 (2H, d, I3 3''), 8.91 (6H, m, I'6 6', I3' 5', , II3 3''), 8.80 (2H, d, I'3 3''), 8.54 (2H, m, I' 3' 5', I'4 4''), 8.78 (1H, t, II4 4''), 8.01 (2H, t, II4 4''), 8.00 (2H, t, I4 4'), 7.99 (2H, t, I'5 5''), 7.55 (2H, d, II6 6''), 7.51 (2H, d, I6 6''), 7.31 (2H, m, II5 5''), 7.29 (2H, m, I5 5''), 5.09 (4H, m, 1,1'), <sup>195</sup>Pt NMR (500 MHz, DMSO- *d*<sub>6</sub>) δ/ ppm: -2706. *Anal. Calc. for* C<sub>47</sub>H<sub>35</sub>Cl<sub>4</sub>N<sub>9</sub>O<sub>2</sub>PtRu·5H<sub>2</sub>O: C, 43.90; H, 3.53; N, 9.80; *Found*: C, 43.41; H, 3.91; N, 9.32. TOF MS-ES+, *m/z*: 385.9565, (M<sup>3+</sup>+Na)

#### RuPtdtdeg

Yield: 0.035 g, (78 %), dark red powder. <sup>1</sup>H NMR (400 MHz, DMSO-*d*<sub>6</sub>) δ/ ppm: 9.08 (2H, d, II3' 5'), 8.95 (2H, d, I3 3''), 8.92 (2H, d, I'6 6'), 8.89 (2H, s, I3' 5'), 8.84 (2H, d, II3 3''), 8.83 (2H, d, I'3 3''), 8.55 (2H, s, I' 3' 5'), 8.49 (1H, t, II4 4''), 8.46 (2H, t, I'4 4''), 8.01 (2H, t, II4 4''), 7.99 (2H, t, I4 4'), 7.93 (2H, t, I'5 5''), 7.52 (2H, d, II6 6''), 7.36 (2H, d, I6 6''), 7.28 (2H, t, II5 5''), 7.22 (2H, t, I5 5''), 4.77 (2H, t, 1), 4.73 (2H, t, 1'), 4.14 (2H, t, 2), 4.11 (2H, t, 2'), <sup>195</sup>Pt NMR (500 MHz, DMSO- *d*<sub>6</sub>) δ/ ppm: -2706. *Anal. Calc. for* C<sub>49</sub>H<sub>39</sub>Cl<sub>4</sub>N<sub>9</sub>O<sub>3</sub>PtRu·10 H<sub>2</sub>O: C, 41.44; H, 4.19; N, 8.91; *Found*: C, 41.65; H, 4.02; N, 8.59. TOF MS-ES+, *m/z*: 378.0520, (M<sup>3+</sup> + 1).

**RuPtdtteg**

Yield: 0.030 g, (75 %), dark red powder.  $^1\text{H}$  NMR (400 MHz,  $\text{DMSO-}d_6$ )  $\delta$ / ppm: 9.07 (2H, d, II3' 5'), 8.92 (2H, d, I'3 3''), 8.87 (2H, d, II3 3''), 8.84 (2H, d, I6 6''), 8.81 (2H, s, I' 3' 5'), 8.71 (2H, d, I3 3'), 8.49 (1H, t, II4'), 8.49 (2H, t, I'4 4''), 8.41 (2H, s, I3' 5'), 8.01 (2H, br, I4 4''), 8.01 (2H, t, II4 4''), 7.94 (2H, t, I5 5''), 7.52 (2H, d, II6 6''), 7.37 (2H, d, I'6 6''), 7.27 (2H, t, II5 5''), 7.212 (2H, t, I'5 5''), 4.71 (2H, t, 1'), 4.41 (2H, t, 1), 4.03 (2H, t, 2'), 3.91 (2H, t, 2), 3.78 (2H, br, 3'), 3.77 (2H, br, 3),  $^{195}\text{Pt}$  NMR (500 MHz,  $\text{DMSO-}d_6$ )  $\delta$ / ppm: -2715. *Anal. Calc. for  $\text{C}_{51}\text{H}_{43}\text{ClN}_9\text{O}_4\text{PtRu}\cdot 2\text{H}_2\text{O}$* : C, 37.16; H, 2.87; N, 7.65; *Found*: C, 37.21; H, 3.00; N, 7.63. TOF MS-ES+,  $m/z$ : 392.7272, ( $\text{M}^{3+}$ ).

**RuPtdttteg**

Yield: 0.031 g, (76 %), dark red powder.  $^1\text{H}$  NMR (400 MHz,  $\text{DMSO-}d_6$ )  $\delta$ / ppm: 9.07 (2H, d, II3' 5'), 8.95 (2H, d, I3 3''), 8.87 (2H, d, I'6 6'), 8.84 (2H, d, II3 3''), 8.82 (2H, s, I3' 5'), 8.71 (2H, d, I'3 3''), 8.51 (2H, t, I' 3' 5'), 8.49 (1H, t, II4 4''), 8.41 (2H, s, I'4 4''), 8.01 (2H, t, II4 4''), 7.99 (2H, t, I4 4'), 7.93 (2H, t, I'5 5''), 7.51 (2H, d, II6 6''), 7.38 (2H, d, I6 6''), 7.27 (2H, t, II5 5''), 7.22 (2H, t, I5 5''), 4.68 (2H, t, 1), 4.59 (2H, t, 1'), 4.00 (2H, t, 2), 3.92 (2H, t, 2') 3.73 (2H, t, 3'), 3.69 (2H, t, 3), 3.66 (2H, t, 4'), 3.64 (2H, t, 4),  $^{195}\text{Pt}$  NMR (500 MHz,  $\text{DMSO-}d_6$ )  $\delta$ / ppm: -2717. *Anal. Calc. for  $\text{C}_{53}\text{H}_{47}\text{Cl}_4\text{N}_9\text{O}_5\text{PtRu}\cdot 5\text{H}_2\text{O}$* : C, 44.89; H, 4.05; N, 8.89; *Found*: C, 44.43; H, 4.25; N, 9.34. TOF MS-ES+,  $m/z$ : 407.4033, ( $\text{M}^{3+}$ ).

**7.2.5 Instrumentation and Physical Measurements**

$^1\text{H}$  NMR were recorded on either a Bruker Avance DPX 400 or 500 MHz spectrometer, at 303 K using  $\text{Si}(\text{CH}_3)_4$  as the reference for the chemical shifts.  $^{195}\text{Pt}$  NMR were done on a 500 MHz spectrometer ( $^{195}\text{Pt}$ , 107.5 MHz) chemical shifts externally referenced to  $\text{K}_2[\text{PtCl}_6]$ . Low resolution electron spray ionization (ESI<sup>+</sup>) mass spectra were recorded on a TOF Micromass spectrometer. Elemental analyses were performed by a Thermal Scientific Flash 2000. Kinetic analyses were studied on an Applied Photophysics SX 20 stopped-flow reaction analyser coupled with an online data acquisition system with controlled temperature within  $\pm 0.1$  °C. The wavelengths for the kinetic analysis were predetermined on Varian Cary 100 Bio UV/visible spectrophotometer with an attached Varian Peltier temperature-controller within  $\pm 0.1$  °C coupled with kinetic application.

### 7.2.6 Preparation of Solution for Kinetic Analysis

All kinetic measurements were performed under *pseudo* first-order conditions using at least 10-fold excess of the nucleophile in 0.02 M ionic solution, made by dissolving the required amount of lithium triflate ( $\text{LiCF}_3\text{SO}_3$ ) (0.018 M) and LiCl (0.002 M) in dry methanol. LiCl was added to suppress the solvolysis reactions. Since  $\text{CF}_3\text{SO}_3^-$  does not coordinate to Pt(II) metal centre,<sup>27</sup> all substitution kinetics were studied in this media. Nucleophiles were used in large excess in order to drive the reactions to completion. Ru(II)-Pt(II) complex solutions were prepared by dissolving the required amount of the complex in the ionic solution. Nucleophile solutions were prepared at 50 times the concentration of the Pt(II) complex. Subsequent dilutions of the nucleophile stock solution afforded solutions of 10, 20, 30 and 40 times the concentration of metal complex. The selected wavelengths for the kinetic runs are given in *Table S7.1*.

### 7.2.7 Computational Modelling

Computational modelling for the complexes were performed at Density Functional Theoretical (DFT) level based on B3LYP/LanL2DZ<sup>28</sup> (Los Alamos National Laboratory 2 double  $\xi$ ) level theory, with inner core electrons of Pt atom replaced by relative Effective Core Potential (ECP). Due to low electronic spin of Pt(II), the DFT calculations of the complexes were done at singlet state. The complexes were computed in methanol solution taking into account the solvolysis effect by means of the Conductor Polarizable Continuum Model (C-PCM).<sup>29</sup> The Gaussian09 suite of programs was used for all computational calculations.<sup>30</sup> A summary of respective bond lengths, bond angles and DFT calculated natural bond orbital (NBO) charges, highest occupied molecular orbital (HOMO) and lowest unoccupied molecular orbital (LUMO) energies obtained from the modelled structures of the platinum complexes are given in *Table 7.1* and *Figure 7.2* (also Supporting Information *Tables S7.2* and *S7.3*). The numbering scheme used is as given in *Figure 7.1*.

**Table 7.1** Summary of DFT calculated data for the complexes investigated. Included for comparison purposes is the data for Pttpy and Pttpyeg. Calculations were performed at B3LYP/LanL2DZ level of theory in all the systems.

Complex	Pttpy	Pttpyeg	RuPtdteg	RuPtdtdeg	RuPtdtteg	RuPtdttteg
<b>Bond Length (Å)</b>						
Pt1/—Cl	2.443	2.445	2.440	2.442	2.443	2.443
Pt—N1( <i>trans</i> )	1.961	1.961	1.961	1.961	1.961	1.960
Ru...Pt	-	-	11.48	13.96	16.60	19.59
X	-	9	13	15	16	19
<b>Bond angles (°)</b>						
Ru-Pt cavity, $\delta$			138	119	100	95
<b>NBO charges</b>						
Pt	0.604	0.592	0.595	0.594	0.593	0.593
Ru			0.307	0.307	0.307	0.307
N1( <i>trans</i> )	-0.453	-0.471	-0.469	-0.470	-0.470	-0.471
$E_{\text{HOMO/eV}}$	-7.04	-6.87	-6.28	-6.25	-6.24	-6.25
$E_{\text{LUMO/eV}}$	-3.35	-3.21	-3.34	-3.29	-3.28	-3.27
$\Delta E$	3.69	3.66	2.94	2.96	2.96	2.98
$\eta$ / eV	1.85	1.83	1.47	1.48	1.48	1.49
$\mu$ / eV	-5.20	-5.04	-4.81	-4.77	-4.76	-4.76
$\omega$ / eV	7.31	6.94	7.87	7.69	7.65	7.60
Point Group	$C_2$	$C_1$	$C_1$	$C_1$	$C_1$	$C_1$
Dipole moment	13.30	11.21	26.00	37.27	45.50	43.16

$\eta$  = chemical hardness,  $\mu$  = chemical potential and  $\omega$  = global electrophilicity index<sup>31</sup> and X = Aerial distance between the Pt(II) centre and the capped terpyridine ligand.

The mappings of the HOMO and LUMO orbitals are similar for all the ethyleneglycol ether linked complexes, where the HOMO orbitals are predominantly concentrated on the Ru(II) centre and terpyridine moiety connected to the Ru(II) while the LUMO electron density purely lies on the **Pttpy** fragment. The HOMO-LUMO energy gap is somewhat the same along the series which is similar to what was reported previously for dinuclear Pt(II) complexes with alkyldiammine flexible linkers.<sup>32</sup> The NBO charges on the Pt(II) centers of the dinuclear complexes of ethyleneglycol ether linker are practically constant indicating that there is no significant change in the Pt(II) environment with changing the length of the polyethylene glycol ether linker.

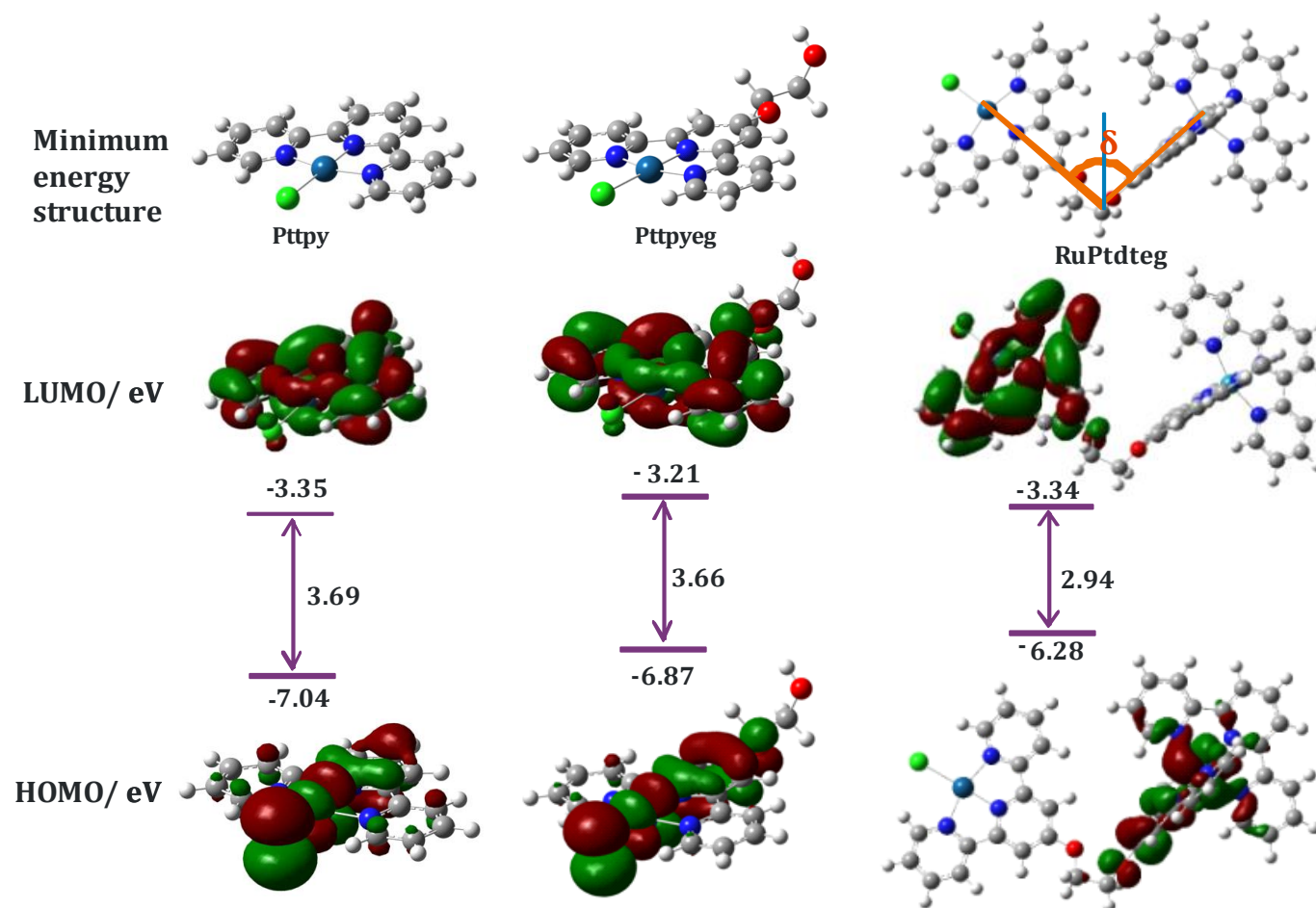


Figure 7.2

DFT calculated minimum energy structures, frontier molecular orbitals (HOMO and LUMO) of RuPttdte showing the V-shape geometry. Included is the data obtained for the DFT calculated complexes, Pttdte and Pttdte for comparisons. Calculations were performed at B3LYP/LanL2DZ level of theory in all the systems. Data for Pttdte, Pttdte and Pttdte are included in Figure S7.1 (Supporting Information *Figure S7.1*)

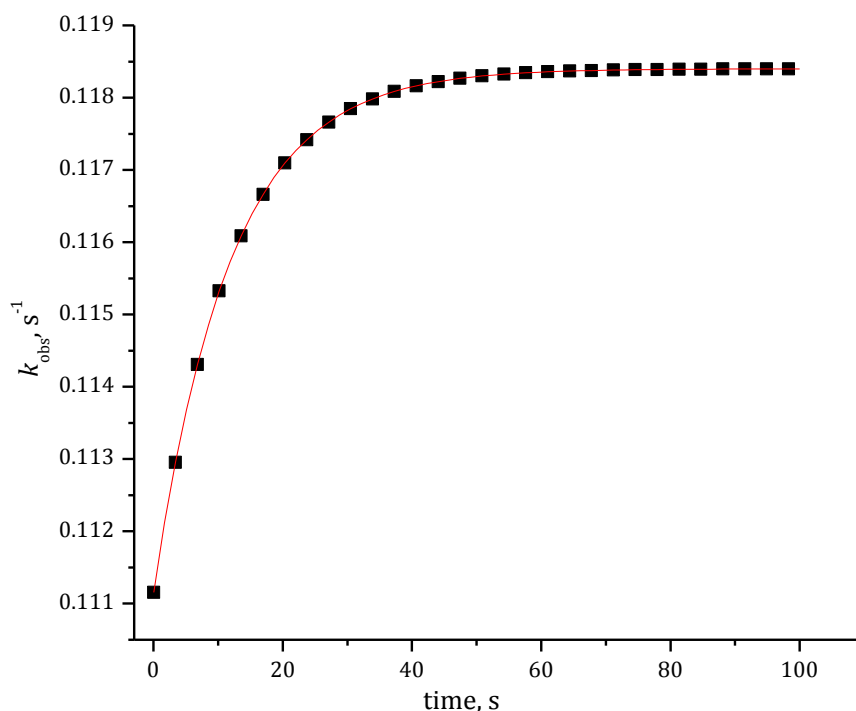


### 7.3 Results

Substitution kinetics of coordinated chlorides from the Pt(II) complexes by thiourea nucleophiles, *viz.* TU, DMTU and TMTU and an ionic nucleophile,  $I^-$  were investigated under *pseudo* first-order conditions using conventional stopped-flow reaction analyzer. The data obtained is supported by DFT calculations.

#### 7.3.1 Kinetic Studies on Substitution Reactions of Chloro Complexes

The wavelengths chosen for the kinetic investigations were pre-determined by monitoring the change in absorbance of the mixture of the metal complex and the nucleophile as a function of time using UV/visible absorption spectra and are summarised in 7.1. All data were mathematically analysed using the software package, Origin 7.5<sup>®33</sup> to determine the observed rate constants,  $k_{\text{obs}}$ . An example of a time resolved kinetic trace obtained from a stopped-flow analyser for the substitution of the chloride ligand in **RuPtdtdeg** ( $1.0 \times 10^{-5}$  M) with TU ( $3.0 \times 10^{-5}$  M) at 298 K is given in Figure 7.3.



**Figure 7.3** Kinetic trace for the substitution reaction of **RuPtdtdeg** ( $1.0 \times 10^{-5}$  M) with TU ( $3.0 \times 10^{-5}$  M) in methanol solution ( $I = 0.02$  M) at 330 nm at 298 K.

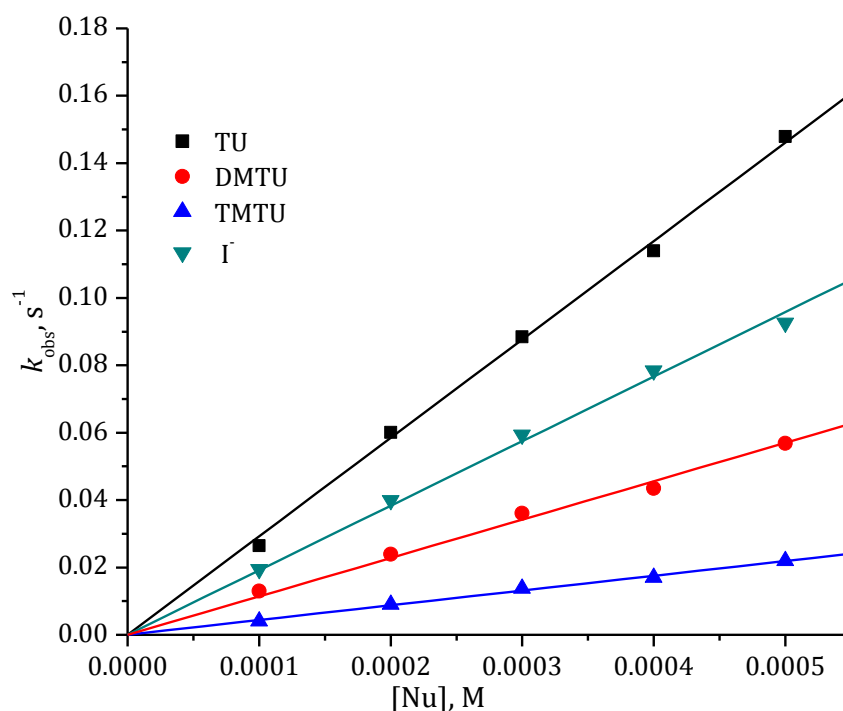
All kinetic data obtained were fitted to first-order exponential decay function to generate the observed *pseudo* first-order rate constants, ( $k_{\text{obs}}$ ), and were plotted against the concentration of the incoming nucleophiles. The values used represent an average of at least eight independent runs. Straight line graphs with zero intercepts were obtained indicating that the reactions were irreversible in nature and can therefore be represented by the corresponding associative rate law given by *Equation 7.1*.<sup>34</sup> Representative plots for **RuPtdtdeg**, shown in *Figure 7.4* clearly indicate that the substitution reactions were first-order with respect to the incoming nucleophile. Data obtained from the slope of *Equation 7.1* at 298 K is summarized in *Table 7.2*.

$$k_{\text{obs}} = k_2[\text{Nu}] \quad (7.1)$$

**Table 7.2** Summary of second-order rate constants,  $k_2$  and activation parameters, with the corresponding standard deviations for the substitution of the chloro ligand by a series of thiourea nucleophiles and iodide at  $I = 0.02 \text{ M LiCF}_3\text{SO}_3$ , adjusted with LiCl. Data for Pttpy is taken from literature<sup>22</sup> and data on mononuclear complexes are from *Chapter 5* and are included for comparison.

Complex	Nu	$k_2/\text{M}^{-1} \text{ s}^{-1}$	$\Delta S^\ddagger / \text{J K}^{-1} \text{ mol}^{-1}$	$\Delta H^\ddagger / \text{kJ mol}^{-1}$	$*k_2/\text{M}^{-1} \text{ s}^{-1}$
<b>Pttpy</b>	TU	$1494 \pm 10$	$-88 \pm 5$	$29 \pm 2$	
	DMTU	$448 \pm 10$	$-73 \pm 4$	$36 \pm 1$	
	TMTU	$82 \pm 4$	$-91 \pm 8$	$35 \pm 2$	
	I <sup>-</sup>	$243 \pm 4$	$-42 \pm 11$	$47 \pm 3$	
<b>Ptptyeg</b>	TU	$257 \pm 5$	$-56 \pm 6$	$43 \pm 2$	
	DMTU	$81 \pm 1$	$-98 \pm 7$	$33 \pm 2$	
	TMTU	$22 \pm 1$	$-57 \pm 7$	$40 \pm 2$	
	I <sup>-</sup>	$95 \pm 2$	$-32 \pm 8$	$53 \pm 3$	
<b>RuPtdteg</b>	TU	$288 \pm 3$	$-115 \pm 5$	$24 \pm 2$	
	DMTU	$104 \pm 1$	$-99 \pm 3$	$32 \pm 1$	
	TMTU	$33 \pm 1$	$-111 \pm 6$	$31 \pm 2$	
	I <sup>-</sup>	$238 \pm 3$	$-85 \pm 6$	$35 \pm 2$	
<b>RuPtdtdeg</b>	TU	$298 \pm 5$	$-112 \pm 3$	$25 \pm 1$	$265 \pm 1$
	DMTU	$114 \pm 2$	$-69 \pm 1$	$41 \pm 0.3$	$83 \pm 1$
	TMTU	$44 \pm 1$	$-90 \pm 4$	$37 \pm 1$	$23 \pm 1$
	I <sup>-</sup>	$192 \pm 3$	$-80 \pm 5$	$36 \pm 2$	$91 \pm 2$
<b>RuPtdtteg</b>	TU	$309 \pm 5$	$-78 \pm 7$	$38 \pm 2$	$277 \pm 1$
	DMTU	$175 \pm 2$	$-121 \pm 1$	$21 \pm 0.3$	$93 \pm 1$
	TMTU	$32 \pm 1$	$-105 \pm 1$	$33 \pm 0.3$	$19 \pm 0.3$
	I <sup>-</sup>	$206 \pm 2$	$-89 \pm 5$	$33 \pm 2$	$91 \pm 1$
<b>RuPtdttteg</b>	TU	$330 \pm 5$	$-98 \pm 4$	$30 \pm 12$	$321 \pm 4$
	DMTU	$108 \pm 1$	$-119 \pm 4$	$26 \pm 12$	$102 \pm 1$
	TMTU	$37 \pm 1$	$-114 \pm 5$	$30 \pm 2$	$13 \pm 1$
	I <sup>-</sup>	$228 \pm 2$	$-14 \pm 5$	$55 \pm 2$	$156 \pm 2$

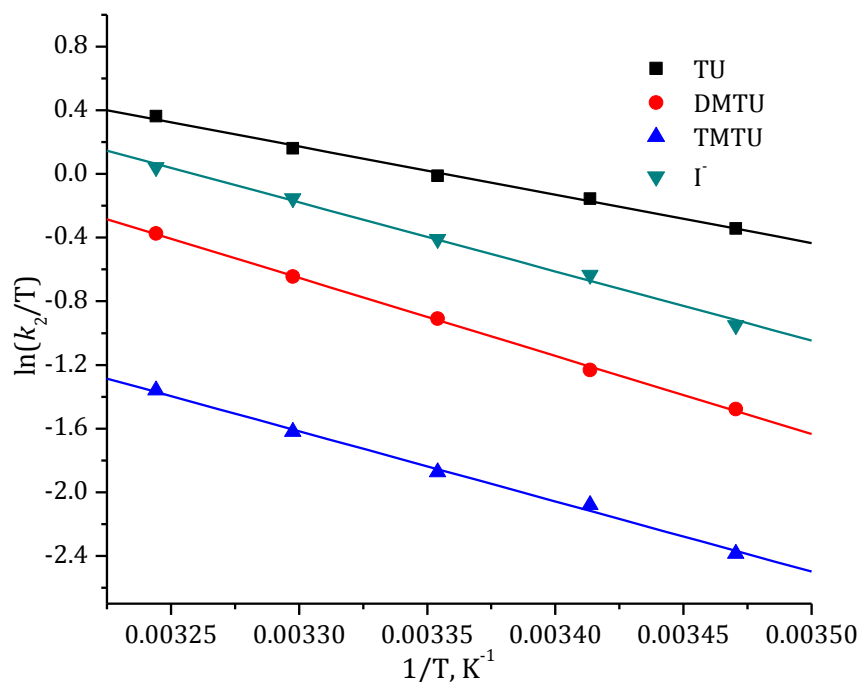
\* = rate constants of the corresponding mononuclear complexes from *Chapter 5*.



**Figure 7.4** Dependence of the *pseudo* first-order rate constants ( $k_{obs}$ ) on the concentrations of the nucleophiles for the chloride substitution from RuPtdtdeg ( $1.0 \times 10^{-5}$  M) in methanol solution ( $I = 0.02$  M) at 298 K.

The temperature dependence studies were performed using a single nucleophile concentration in the temperature range 15 - 35 °C in 5 °C intervals. The entropy of activation ( $\Delta S^\ddagger$ ) and enthalpy of activation ( $\Delta H^\ddagger$ ) were then obtained from the slopes and intercepts of the Eyring equation<sup>34</sup> respectively as given in Equation 7.2. Figure 7.5 shows the representative plots obtained for **RuPtdtdeg** with the nucleophiles for the forward reactions with the nucleophiles and the data obtained are summarized in Table 7.2. Representative data and graphs are also given in Tables S7.4 to S7.11 and Figure S7.2 to S7.7 respectively.

$$\ln(k_2/T) = -\Delta H^\ddagger / RT + (23.8 + \Delta S^\ddagger / R) \quad (7.2)$$

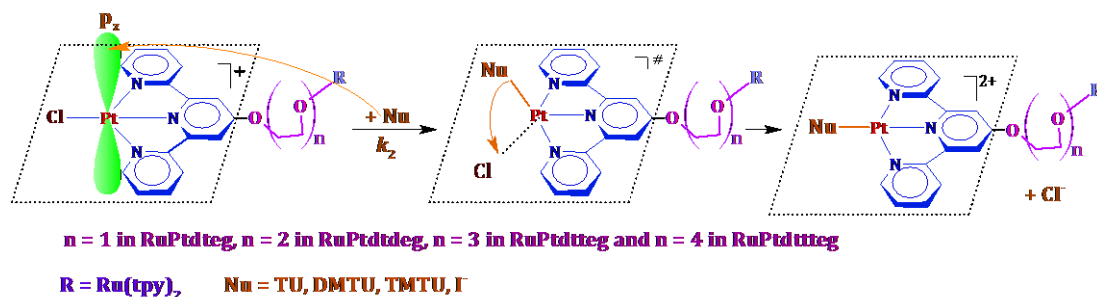


**Figure 7.5** Eyring plots obtained for RuPtdddeg with the nucleophiles for the forward reactions over the temperature range 15 - 35 °C.

### 7.3.2 Discussion

In this study, four heterometallic Ru(II)-Pt(II) tpy complexes linked by polyethyleneglycol ether units of different lengths were synthesized and characterized following the literature procedure.<sup>25</sup> The spectroscopic data obtained is in good agreement with those reported in literature<sup>25</sup> and the structural formulae (Figures S7.8 to S7.23).

Substitution kinetics of coordinated chloride from the Ru(II)-Pt(II) complexes (Figure 7.1) by four different nucleophiles (Nu), *i.e.* TU, DMTU, TMTU and an ionic nucleophile,  $I^-$  were studied under *pseudo* first-order conditions using the conventional stopped-flow analyzer. Only one step, taken to be the substitution of the chloride ligand was observed which is typical for square planar **Ptpty** type complexes.<sup>22,35</sup> Thus, the proposed substitution mechanism for the complexes studied can be represented as shown by Scheme 7.1. The data obtained is summarized in Table 7.2.



Scheme 7.1      The general reaction scheme for the reactions between the complexes and the nucleophiles studied.

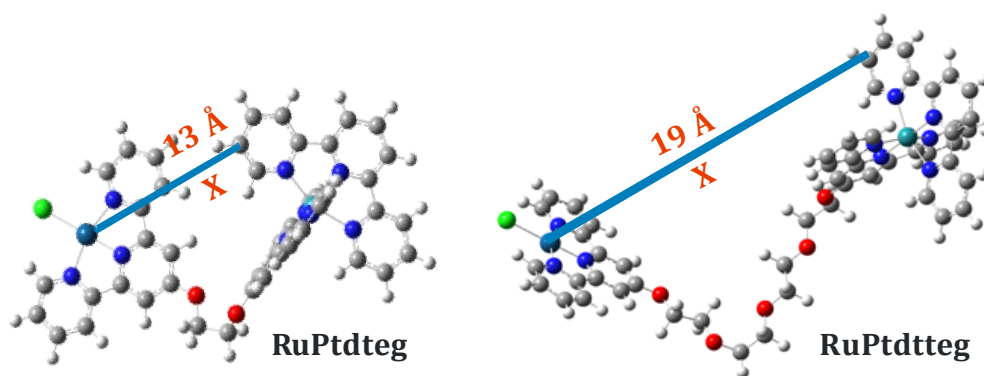
In **Chapter 5**, it is reported that the ethylene glycoxy pendant groups act as  $\sigma$ -donors decreasing the  $\pi$ -backbonding ability of the parent **Ptpty** by incorporating the lone pair electrons of the oxygen (O1) atom into the terpyridine moiety resulting in a decreased reactivity. A similar observation is made in this study as well. A glance at the rate constants for the displacement of the coordinated chloride ligand shows a drop from **Ptpty** to **Ptptyeg** followed by a slight increase as the length of the polyethyleneglycol ether bridging linker between Ru(II) and Pt(II) moieties is increased. This is an indication that the increase in the number of polyethyleneglycol ether units has a minor influence on the rate of substitution reactions (*Table 7.2*).

DFT calculations show an increase in the global electrophilicity index,  $\omega$ , of the complex when the  $Ru(tpy)_2$  moiety is attached to the **Ptptyeg**, an indication of the presence of  $\pi$ -back donation. This remains constant as the chain length is increased. Therefore, the increase is due to the two terpyridine moieties attached to the Ru(II) and not an increase in the  $\pi$ -backbonding on the Pt(II) centre whose NBO charge remains constant. This is also true with respect to the other changes such as the chemical potential ( $\mu$ ) and hardness ( $\eta$ ). General analysis of the DFT calculated data for the investigated heterometallic complexes are very similar, which indicates that the change in reactivity is not due to an electronic effect.<sup>36</sup>

To understand the effect of  $Ru(tpy)_2$  moiety on the reactivity of the ethyleneglycol ether linked Ru(II)-Pt(II) complexes, the reactivity of the **Ptptyeg** (from **Chapter 5**) and **RuPtdeg** are compared. From the second order rate constants, it is noticeable that the reactivity increases slightly from **Ptptyeg** ( $257 \pm 5 \text{ M}^{-1} \text{ s}^{-1}$ ) to **RuPtdeg** ( $288 \pm 3 \text{ M}^{-1} \text{ s}^{-1}$ ). A similar increase is observed for the other heterometallic complexes when compared to their corresponding mono nuclear complexes having the same size of the polyethyleneglycol ether unit. One of the factors responsible for this slight increase in

the reactivity is the overall increase in the charge of the molecule on attaching Ru(tpy)<sub>2</sub> moiety to the mono nuclear Pt(II) complexes.

The other factor influencing the reactivity of these heterometallic complexes is the steric hindrance imposed by the geometry adopted by the capped Ru(tpy)<sub>2</sub> moiety as depicted in *Figure 7.6*. DFT calculated optimized geometries show that there is no extended  $\pi$ -electronic communication between the terpyridine ligand systems at the two metal centres. Also, the  $\pi$ -extended molecular orbital in each terpyridine ligand system in **RuPtdteg** are mutually orthogonal at the Ru(II) metal centre. Thus, this geometry breaks the flow of delocalized electron density across the entire heterometallic system but introduces steric hindrance on one side of the **Pttpty** moiety. This factor should have a decreasing effect on the rate.



**Figure 7.6** Aerial view showing the steric disposition of the pendant group on the 4'-position of the chelate ligand (tpy) bonded to the Pt(II) metal centre obtained from DFT calculations.

The DFT calculated optimized structures shown in *Figure 7.2* and *Figure S7.1* show that the polyethyleneglycol ether bridging linkers are twisted such that the coordination sphere of the capped Ru(tpy)<sub>2</sub> moieties effectively 'shadows' the Pt(II) centre from one of the directions of the approach of the nucleophile. When the chain length is increased, both the twisting as well as the distance between the two metal centres carrying the terpyridine ligands also increases. For example, the Ru(tpy)<sub>2</sub> moiety in **RuPtdteg** shows a greater degree of aerial steric overlapping on the Pt(II) metal centre by the capped terpyridine system (a distance of 13 Å) while those in **RuPtdtteg**, the distance between the Pt(II) metal centre and the capped terpyridine ligand is 19 Å (*Figure 7.6*). Thus, it is evident that the length of the linker influences the degree of steric disposition.<sup>32</sup> When the chain length is short, the steric influence to the axially incoming

nucleophile is greater and decreases proportionally as the chain length of the linker increases. This should result in gradual increase in reactivity from **RuPtdteg** to **RuPtdttteg** as observed.

Furthermore, the two metal centres form a V-shape structure of angle  $\delta$ .<sup>32,37</sup> As reported by Jaganyi *et al.*,<sup>32</sup> this geometry enhances the entrapment of the incoming nucleophiles, thereby increasing the successful collision frequencies between the nucleophiles and the reactive Pt(II) centre, leading to a greater number of nucleophile-metal encounter pairs possessing greater energy than the required activation energy.<sup>32</sup> DFT calculations show that the depth of the cage increases with increase in the length of the linker as angle,  $\delta$  decreases. The deeper the depth, the greater the successful collisions and hence, the reactivity.<sup>32</sup> This elucidation, along with the steric influence affirms the observed slight increase in the reactivity with the increase in the polyethyleneglycol ether units. Thus, the increase in the rate of substitution reactions of the heterometallic complexes investigated in this work is mainly due to the structural architecture of the system which entraps the nucleophile. Furthermore, for heterometallic complexes bridged by non-aromatic flexible spaces, apart from their weak electronic transitions due to the rotational isomers and larger reorganizational energies, changes in electronic effect due to the changes in the length of the linker are difficult to investigation as they are spectroscopically almost indistinguishable.<sup>38</sup> When compared the results of in this study with what has been obtained for the heterometallic Ru(II)-Pt(II) complexes in **Chapter 3** (with a rigid aromatic linker) and **Chapter 4** (with semi-rigid aromatic linker), one notices that the presence of a non-aromatic flexible linker decreases the metal-metal interactions and the electronic effects<sup>39</sup> due to the Ru(II) metal centre on the overall reactivity of the complex.

Substitution reactions of the complexes show clear dependence on the steric hindrance of the incoming nucleophiles which is typical for square planar Pt(II) complexes.<sup>40</sup> The sterically hindered nucleophiles, TMTU and DMTU show much slower reactivity than that of TU. Due to the high electrostatic force induced by high polarizability of the anionic  $\Gamma^-$  on the positively charge metal centre,<sup>32</sup> the reactivity of  $\Gamma^-$  is comparable to TU.

The activation parameters obtained for the substitution reactions support an associative mode of mechanism. The large and negative entropy of activation ( $\Delta S^\ddagger$ )



support along with the small enthalpy of activation ( $\Delta H^\ddagger$ ) support an associative mode of substitution as reported for square planar Pt(II) complexes.<sup>22,26,32,35a,b,41</sup>

## 7.4 Conclusions

DFT calculated data shows electronic change from **Pttpy** to **Pttpyeg** as reported before. But after the introduction of the Ru(tpy)<sub>2</sub> moiety, no significant electronic change is observed as the length of the linker is increased. The substitution reactivity of the heterometallic Ru(II)-Pt(II) dinuclear complexes investigated in this study are geometrically controlled. The increase in the length of the polyethyleneglycol ether linker decreases the steric hindrance imposed on the Pt(II) centre by the Ru(tpy)<sub>2</sub> moiety resulting in increased reactivity. This is further driven by the entrapment effect of the nucleophile due to the V-shape geometry adopted by the heterometallic complexes. It can be concluded that, presence of Ru(tpy)<sub>2</sub> moiety influences the structural geometry of the complex system which in turn controls the reactivity of the Pt(II) centre. Unlike the work reported in **Chapter 3** and **Chapter 4**, it is noticeable that the electronic transitions between Ru(II) and Pt(II) is insignificant in the presence of a non-aromatic flexible linker.<sup>39</sup> In all cases the reactivity of the complexes are sensitive to the steric nature of the incoming nucleophiles which decreases with increase in the size of the nucleophile. The mode of activation remains associative in nature.

## 7.5 References

- (1) (a) Sherman, S. E.; Gibson, D.; Wang, A. H. J.; Lippard, S. J. *J. Am. Chem. Soc.* **1988**, *110*, 7368(b) Abu-Surrah, A. S.; Kethunen, M. *Curr. Med. Chem.* **2006**, *13*, 1337(c) Jung, Y. W.; Lippard, S. J. *J. Chem. Rev.* **2007**, *107*, 1387(d) Milkevitch, M.; Storrie, H.; Brauns, E.; Brewer, K. J.; Shirley, B. W. *Inorg. Chem.* **1997**, *36*, 4534.
- (2) (a) Di Blasi, P.; Bernareggi, A.; Beggiolin, L.; Piazzoni, L.; Menta, E. *Anticancer Res.* **1998**, *18*, 3113(b) Huq, F.; Daghriri, H.; Yu, J. Q.; Tayyem, H.; Beale, P.; Zhang, M. *Eur. J. Med. Chem.* **2004**, *39*, 947(c) Loehrer, P. J.; Einhorn, L. H. *Ann. Intern. Med.* **1984**, *100*, 704(d) Clarke, M. J. *Coord. Chem. Rev.* **2003**, *236*, 209(e) Jakupec, M. A.; Galanski, M.; Arion, V. B.; Hartinger, C. G.; Keppler, B. K. *Dalton Trans.* **2008**, 183.
- (3) (a) Williams, R. L.; Toft, H. N.; Winkel, B. S. J.; Brewer, K. J. *Inorg. Chem.* **2003**, *42*, 4394(b) Burnner, J.; Barton, J. K. *J. Am. Chem. Soc.* **2006**, *128*, 6772.
- (4) (a) Absalon, M. J.; Wu, W.; Stubbe, J. *Biochemistry.* **1995**, *34*, 2076(b) Tullius, T. D. *Nature* **1988**, *332*, 663(c) Sardesai, N. Y.; Zimmermann, K.; Barton, J. K. *J. Am. Chem. Soc.* **1994**, *116*, 7502(d) Mrksich, M.; Dervan, P. B. *J. Am. Chem. Soc.* **1995**, *117*, 3325(e) Hergueta-Bravo, A.; Jimenez-Hernandez, M. E.; Montero, F.; Oliveros, E.; Orellana, G. *J. Phys. Chem. B* **2002**, *106*, 4010(f) Juskowiak, B.; Dominiak, A.; Takenaka, S.; Takagi, M. *Photochem. Photobiol.* **2001**, *74*, 391(g) Moucheron, C.; Kirsch-DeMesmaeker, A.; Kelly, J. M. *J. Photochem. Photobiol. B* **1997**, *40*, 91(h) Tossi, A. B.; Kelly, J. M. *Photochem. Photobiol.* **1989**, *49*, 545(i) Barton, J. K.; Raphael, A. L. *Proc. Natl. Acad. Sci. U.S.A.* **1985**, *82*, 6460(j) Barton, J. K.; Holmlin, R. E. *Inorg. Chem.* **1995**, *34*, 7(k) Fleisher, M. B.; Waterman, K. C.; Turro, N. J.; Barton, J. K. *Inorg. Chem.* **1986**, *25*, 3549(l) Bhattacharya, S.; Mandal, S. S. *Chem. Commun.* **1996**, 1515(m) Farinas, E.; Tan, J. D.; Baidya, N.; Mascharak, P. K. *J. Am. Chem. Soc.* **1993**, *115*, 2996(n) Paillous, N.; Vincendo, P. *J. Photochem. Photobiol. B* **1993**, *20*, 203(o) Armitage, B. *Chem. Rev.* **1998**, *98*, 1171.
- (5) D'Aléo, A.; Williams, R. M.; Chriqui, Y.; Iyer, V. M.; Belser, P.; Vergeer, F.; Ruiz, V.; Unwin, P. R.; De Cola, L. *Open J. Inorg. Chem.* **2007**, *1*, 26.
- (6) (a) Fu, P. K. L.; Bradley, P. M.; Turro, C. *Inorg. Chem.* **2001**, *40*, 2476(b) Holder, A. A.; Swavey, S.; Brewer, K. J. *Inorg. Chem.* **2003**, *43*, 303.
- (7) (a) Hannon, M. *Chem. Soc. Rev.* **2007**, *36*, 280(b) Richards, A. D.; Rodger, A. *Chem. Soc. Rev.* **2007**, *36*, 471(c) Clarke, M. J. *Coord. Chem. Rev.* **2003**, *236*, 209(d) Alessio, E.; Mestroni, G.; Bergamo, A.; Sava, G. *Met Ions Biol Syst.* **2004**, *42*,

- 323(e) Galanski, M.; Arion, V. B.; Jakupec, M. A.; Keppler, B. K. *Curr. Pharm. Design.* **2003**, *9*, 2078(f) Clarke, M. J. *Coord. Chem. Rev.* **2002**, *232*, 69(g) Dyson, P. J.; Sava, G. *Dalton Trans.* **2006**, 1929(h) Kennedy, D. C.; Patrick, B. O.; James, B. R. *Can. J. Chem.* **2011**, *89*, 948(i) Webb, M. I.; Chard, R. A.; Al-Jobory, Y. M.; Jones, M. R.; Wong, E. W. Y.; Walsby, C. J. *Inorg. Chem.* **2011**, *51*, 954.
- (8) (a) Hartinger, C. G.; Zorbas-Seifried, S.; Jakupec, M. A.; Kynast, B.; Zorbas, H.; Keppler, B. K. *J. Inorg. Biochem.* **2006**, *100*, 891(b) Hartinger, C. G.; Jakupec, M. A.; Zorbas-Seifried, S.; Groessl, M.; Egger, A.; Berger, W.; Zorbas, H.; Dyson, P. J.; Keppler, B. K. *Chem. Biodiversity.* **2008**, *5*, 2140(c) Lentz, F.; Drescher, A.; Lindauer, A.; Henke, M.; Hilger, R. A.; Hartinger, C. G.; Scheulen, M. E.; Dittrich, C.; Keppler, B. K.; Jaehde, U. *Anti-Cancer Drugs.* **2009**, *20*, 97.
- (9) (a) Higgins, S. L. H.; White, T. A.; Winkel, B. S. J.; Brewer, K. J. *Inorg. Chem.* **2011**, *50*, 463(b) Sharman, W. M.; Allen, C. M.; van Lier, J. E. *Drug Disc. Today.* **1999**, *4*, 507.
- (10) (a) Barton, J. K.; Basile, L. A.; Danishefsky, A.; Alexandrescu, A. *Proc. Natl. Acad. Sci. U.S.A.* **1984**, *81*, 1961(b) Kumar, C. V.; Barton, J. K.; Turro, N. J. *J. Am. Chem. Soc.* **1985**, *107*, 5518(c) Miao, R.; Mongelli, M. T.; Zigler, D. F.; Winkel, B. S. J.; Brewer, K. J. *Inorg. Chem.* **2006**, *45*, 10413(d) Swavey, S.; Fang, Z. L.; Brewer, K. J. *Inorg. Chem.* **2002**, *41*, 2598.
- (11) Cox, J. W.; Berners-Price, S.; Davies, M. S.; Qu, Y.; Farrell, N. *J. Am. Chem. Soc.* **2001**, *123*, 1316.
- (12) (a) Balzani, V.; Credi, A.; Raymo, F. M.; Stoddart, J. F. *Angew. Chem. Int. Ed.* **2000**, *39*, 3348(b) Balzani, V.; Juris, A. *Coord. Chem. Rev.* **2001**, *211*, 97.
- (13) Farrell, N.; Qu, Y.; Bierbach, U.; Valsecchi, M.; Menta, E. *Cisplatin. Chemistry and Biochemistry of a Leading Anticancer Drug*; Lippert, B. ed.: Verlag Helvetica Chimica Acta, Zurich, Wiley-VCH, Weinheim., 1999, 479- 496.
- (14) Hochreuther, S.; Puchta, R.; van Eldik, R. *Inorg. Chem.* **2011**, *50*, 8984.
- (15) Shah, N.; Dizon, D. S. *Future Oncology.* **2009**, *5*, 33.
- (16) Roy, S. PhD Thesis, PhD Thesis. *Synergy of intercalation and coordination binding to design novel DNA-targeting antineoplastic metallodrugs*, University of Leiden., 2008, 230- 248.
- (17) van der Schilden, K.; Garcia, F.; Kooijman, H.; Spec, A. L.; Haanoot, J. G.; Reedijk, J. *Angew. Chem. Int. Ed.* **2004**, *43*, 5668.
- (18) Yam, V. W.-W.; Lee, V. W.-M.; Cheung, K.-K. *Organometallics.* **1997**, *16*, 2833.
- (19) Hegmans, A.; Berners-Price, S. J.; Davies, M. S.; Thomas, D. S.; Humphreys, A. S.; Farrell, N. *J. Am. Chem. Soc.* **2004**, *126*, 2166.

- (20) Milkevitch, M.; Brauns, E.; Brewer, K. J. *Inorg. Chem.* **1996**, *35*, 1737.
- (21) (a) Farrell, N.; Qu, Y. *Inorg. Chem.* **1989**, *28*, 3416(b) Farrell, M.; De Almeida, S. G.; Skov, K. A. *J. Am. Chem. Soc.* **1988**, *110*, 5018(c) Farrell, N.; Qu, Y.; Hacker, M. P. *J Med Chem* **1990**, *33*, 2179(d) Kraker, A.; Elliott, W.; Van Houten, B.; Farrell, N.; Hoeschele, J.; Roberts, J. J. *Inorg. Biochem.* **1989**, *36*, 160.
- (22) Jaganyi, D.; Reddy, D.; Gertenbach, J. A.; Hofmann, A.; van Eldik, R. *Dalton Trans.* **2004**, 299.
- (23) Perrin, D. D.; Armarego, W. L. F.; Perrin, D. R. *Purification of Laboratory Chemicals*; 2<sup>nd</sup> ed.; Pergamon: Oxford, 1980.
- (24) Takeuchi, K. J.; Thompson, M. S.; Pipes, D. W.; Meyer, T. J. *Inorg. Chem.* **1984**, *23*, 1845.
- (25) van der Schilden, K., Ph. D. Thesis, *The Development of Polynuclear Ruthenium and Platinum Polypyridyl Complexes in Search of New Anticancer Agents*, Laiden University, 50- 106., 2006.
- (26) Reddy, D.; Jaganyi, D. *Dalton Trans.* **2008**, 6724.
- (27) Appleton, T. G.; Hall, J. R.; Ralph, S. F.; Thompson, C. S. M. *Inorg. Chem.* **1984**, *23*, 3521.
- (28) (a) Becke, A. G. *J. Chem. Phys.* **1993**, *98*, 5648(b) Lee, C. T.; Yang, W. T.; Parr, R. G. *Phys. Rev. B* **1988**, *37*, 785(c) Hay, P. J.; Wadt, W. R. *J. Chem. Phys.* **1985**, *82*, 299.
- (29) (a) Barone, V.; Cossi, M. *J. Phys Chem. A* **1998**, *102*, 1995(b) Cossi, M.; Rega, N.; Scalmani, G.; Barone, V. *J. Comput. Chem.* **2003**, *24*, 669.
- (30) Frisch, M. J.; Trucks, G. W.; Schlegel, H. B.; Scuseria, G. E.; Robb, M. A.; Cheeseman, J. R.; Scalmani, G.; Barone, V.; Mennucci, B.; Petersson, G. A.; Nakatsuji, H.; Caricato, M.; Hratchian, X. L.; H. P. ; Izmaylov, A. F.; Bloino, J.; Zheng, G.; Sonnenberg, J. L.; Hada, M.; Ehara, M.; Toyota, K.; Fukuda, R.; Hasegawa, J.; Ishida, M.; Nakajima, T.; Honda, Y.; Kitao, O.; Nakai, H.; Vreven, T.; Montgomery, J. A.; Peralta, J., J. E. ; Ogliaro, F.; Bearpark, M.; Heyd, J. J.; Brothers, E.; Kudin, K. N.; Staroverov, V. N.; Kobayashi, R.; Normand, J.; Raghavachari, K.; Rendell, A.; Burant, J. C.; Iyengar, S. S.; Tomasi, J.; Cossi, M.; Rega, N.; M. Millam, J.; Klene, M.; Knox, J. E.; Cross, J. B.; Bakken, V.; Adamo, C.; Jaramillo, J.; Gomperts, R.; Stratmann, R. E.; Yazyev, O.; Austin, A. J.; Cammi, R.; Pomelli, C.; Ochterski, J. W.; Martin, R. L.; Morokuma, K.; Zakrzewski, V. G.; Voth, G. A.; Salvador, P.; Dannenberg, J. J.; Dapprich, S.; Daniels, A. D.; Farkas, O.; Foresman, J. B.; Ortiz, J. V.; Cioslowski, J.; Fox, D. J.; Gaussian, I., Wallingford CT, 2009., Ed.; Gaussian, Inc., Wallingford CT., 2009.

- (31) (a) Parr, P. G.; Donnelly, R. A.; Levy, M.; Palke, W. E. *J. Chem Phys.* **1978**, *68*, 3801 (b) Parr, P. G.; Yang, W. *Density Dunctional Theory of Atoms and Molecules*; Oxford University: New York, 1989 (c) Parr, P. G.; Pearson, R. G. *J. Am. Chem. Soc.* **1983**, *105*, 7512 (d) Parr, R. G.; Szentpaly, L.; Liu, S. *J. Am. Chem. Soc.* **1999**, *121*, 1922 (e) Boyd, D. B.; J., O. *Chem.* **1985**, *50*, 885 (f) Chattaraj, P. K.; Giri, S.; Duley, S. *Chem. Rev.* **2011**, *111*, PR43.
- (32) Jaganyi, D.; Mambanda, A.; Hochreuther, S.; van Eldik, R. *Dalton Trans.* **2010**, *39*, 3595.
- (33) Microcal™ Origin™ Version 7.5; Microcal Software, Inc., Northampton, MA, 1991- 2003.
- (34) Atwood, J. D. *Inorganic and Organic Reaction Mechanisms*; 2nd ed.; Wiley- VCH Inc. New York, 1997, 32-34, 43-61.
- (35) (a) Jaganyi, D.; De Boer, K. L.; Gertenbach, J.; Perils, J. *Int. J. Chem. Kinet.* **2008**, *40*, 808 (b) Ongoma, P. O.; Jaganyi, D. *Dalton Trans.* **2012**, *41*, 10724 (c) Reddy, D.; Akerman, K.; Akerman, M.; Jaganyi, D. *Transition Met. Chem.* **2011**, *36*, 593.
- (36) Campodónico, P. R.; Fuentealba, P.; Castro, E. A.; Santos, J. G.; Contreras, R. *J. Org. Chem.* **2005**, *70*, 1754.
- (37) Hofmann, A.; van Eldik, R. *J. Chem. Soc., Dalton Trans.* **2003**, 2979.
- (38) (a) Indelli, M. T.; Scandola, F.; Collin, J.-P.; Sauvage, J.-P.; Sour, A. *Inorg. Chem.* **1996**, *35*, 303 (b) Indelli, M. T.; Bignozzi, C. A.; Harriman, A.; Schoonover, J. R.; Scandola, F. *J. Am. Chem. Soc.* **1994**, *116*, 3768.
- (39) (a) Barigelletti, F.; Flamigni, L.; Collin, J.-P.; Sauvage, J.-P. *Chem. Commun.* **1997**, 333 (b) Sauvage, J. P.; Collin, J. P.; Chambron, J. C.; Guillerez, S.; Couret, C.; Balzani, V.; Barigelletti, F.; De Cola, L.; Flamigni, L. *Chem. Rev.* **1994**, *94*, 993 (c) Grosshenny, V.; Harriman, A.; Hissler, M.; Ziessel, R. *J. Chem. Soc., Faraday Trans.* **1996**, *92*, 2223.
- (40) (a) Mambanda, A.; Jaganyi, D. *Dalton Trans.* **2012**, *41*, 908 (b) Ertürk, H.; Maigut, J.; Puchta, R.; van Eldik, R. *J. Chem. Soc. Dalton Trans.* **2008**, 2759.
- (41) (a) Ongoma, P. O.; Jaganyi, D. *Dalton Trans.* **2013**, *42*, 2724 (b) Romeo, R.; Plutino, M. R.; Scolaro, L. M.; Stoccoro, S.; Minghetti, G. *Inorg. Chem.* **2000**, *39*, 4749.

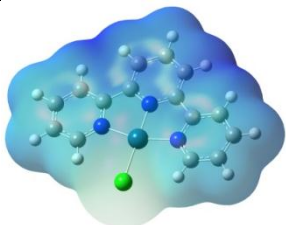
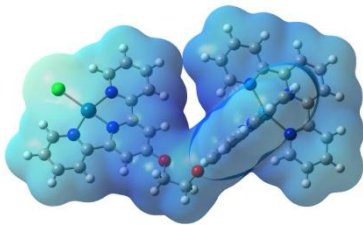
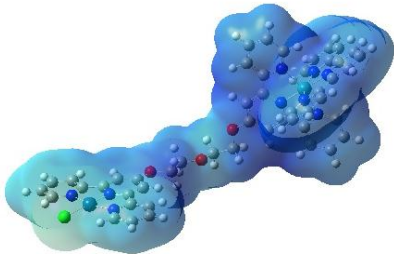
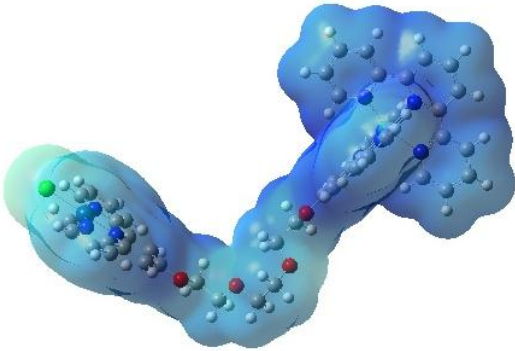
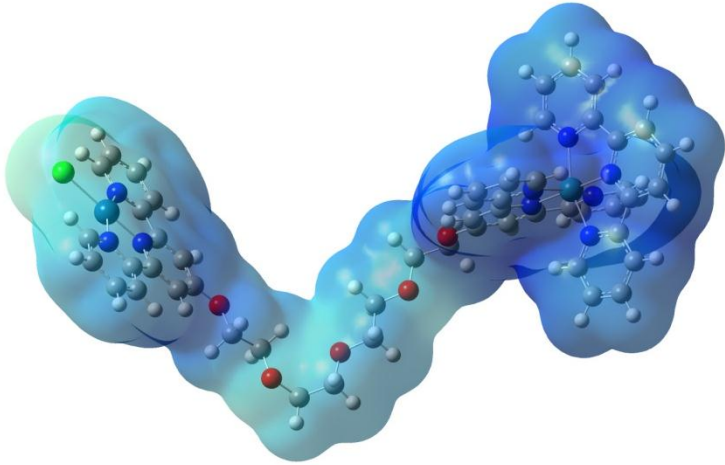
## 7.6 Supporting Information

A summary of wavelengths at which the kinetic studies were performed, plots of the dependence of  $k_{\text{obs}}$  against concentration of the nucleophiles and plots from temperature dependence studies along with tables of kinetic data, graphs of exemplary mass spectra and the representative spectra for  $^1\text{H}$  NMR and  $^{195}\text{Pt}$  NMR work reported in this study are given as electronic supporting information (ESI).

**Table S7.1** Summary of the wavelengths (nm) used to study the substitution reactions of the complexes with thiourea nucleophile

Complex	Nu	Wavelength ( $\lambda$ ), nm
<b>RuPtdteg</b>	TU	292
	DMTU	291
	TMTU	292
	I <sup>-</sup>	292
<b>RuPtdtdeg</b>	TU	291
	DMTU	291
	TMTU	290
	I <sup>-</sup>	290
<b>RuPtdtteg</b>	TU	279
	DMTU	279
	TMTU	292
	I <sup>-</sup>	290
<b>RuPtdttteg</b>	TU	291
	DMTU	291
	TMTU	291
	I <sup>-</sup>	291

**Table S7.2**      Geometry optimised structures of the platinum complexes investigated and distribution of the electron density on the platinum complexes investigated. The blue area indicates the most electropositive areas and the orange region indicates the most electronegative areas.

Compound	Structure
 <b>Pttpy</b>	 <b>RuPtdteg</b>
 <b>RuPtdtdeg</b>	 <b>RuPtdtteg</b>
 <b>RuPtdttteg</b>	

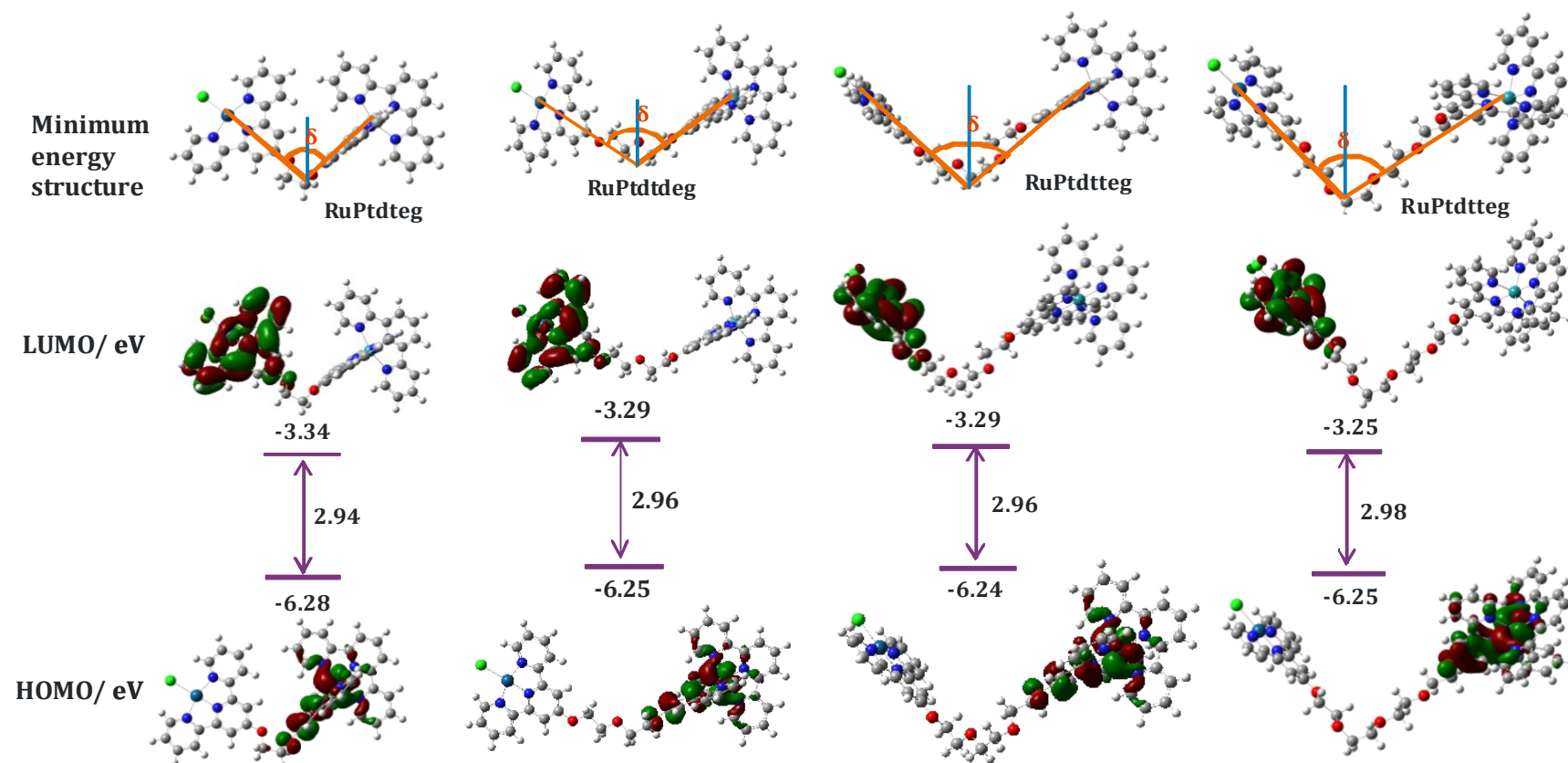


Figure S7.1 DFT calculated minimum energy structures, frontier molecular orbitals (HOMO and LUMO) of the complexes showing the V-shape geometry. Calculations were performed at B3LYP/LanL2DZ level of theory in all the systems.



**Table S7.3** Summary of DFT calculated data for the heterometallic RuPtpy complexes investigated. Included is the data obtained for the DFT calculated Ptpy complex for comparisons.

Complex	Ptpy	Ru(tpy) <sub>2</sub>	RuPtdteg	RuPtdtdeg	RuPtdtteg	RuPtdttteg
<b>Bond Length/ (Å)</b>						
Pt1/—Cl	2.443		2.440	2.442	2.443	2.443
Pt—N1 <sub>trans</sub>	1.961		1.961	1.961	1.961	1.960
4'C—O1			1.373	1.370	1.368	1.368
Length of the linkekr			2.958	5.616	7.5586	9.967
Ru...Pt			11.475	13.962	16.599	19.589
O1-O2				3.653	2.9331	3.0501
O2-O3				2.2.962	3.0859	3.0302
O3-O4					2.9452	3.7652
O4-O5						2.9877
Ru-N <sub>trans</sub>		2.009	2.014	2.018	2.014	2.014
<b>Bond angles/ (°)</b>						
N1PtN2			80.87	80.40	80.86	80.88
N2PtN3			80.77	81.03	80.73	80.73
N1PtCl			99.2	99.61	99.39	99.09
N2PtCl			178.73	176.98	179.65	179.98
N3PtCl			99.05	99.00	99.01	98.28
N1PtN3			161.63	161.38	161.59	161.62
N4RuN5		78.90	78.60	78.80	78.59	78.56
N5RuN6		78.90	78.70	78.37	78.74	78.76
N4RuN6		157.80	157.30	157.16	157.32	157.32
N5RuN8		179.995	179.30	179.56	179.77	179.86
N7RuN8			78.95	79.02	78.96	79.00
N8RuN9			78.98	78.88	78.98	78.94
N7RuN9			157.93	157.89	157.94	157.94
Ru-N <sub>trans</sub>		2.009	2.014	2.018	2.014	2.014
Dihed- Cl			2.126	0.304	0.677	0.869
<b>NBO charges</b>						
Pt	0.604		0.595	0.594	0.592	0.592
Ru		0.309	0.307	0.307	0.307	0.307
N1( <i>trans</i> )	-0.453		-0.469	-0.470	-0.470	-0.471
O1			-0.568	-0.561	-0.558	-0.564
O2			-0.572	-0.646	-0.653	-0.657
O3				-0.571	-0.652	-0.655
O4					-0.571	-0.651
O5						-0.575
C 4'	-0.134		0.406	0.408	0.408	0.409
C 4' to Ru		-0.156	0.388	0.389	0.390	0.390
Cl	-0.502		-0.503	-0.504	-0.505	-0.505
N1			-0.492	-0.493	-0.492	-0.493
N2			-0.469	-0.470	-0.471	-0.471
N3			-0.493	-0.493	-0.493	-0.493
N4		-4.21	-0.420	-0.420	-0.420	-0.419

.....Continuation of Table S7.3

N5	-4.10	-0.427	-0.429	-0.429	-0.428
N6	-4.21	-0.420	-0.419	-0.419	-0.420
N7	-4.21	-0.421	-0.421	-0.421	-0.421
N8	-4.10	-0.410	-0.409	-0.410	-0.409
N9	-4.21	-0.421	-0.421	-0.421	-0.421
$E_{\text{HOMO}}/\text{eV}$	-7.04	-6.28	-6.28	-6.25	-6.25
$E_{\text{LUMO}}/\text{eV}$	-3.35	-2.87	-3.34	-3.29	-3.27
$\Delta E/\text{eV}$	3.69	3.41	2.94	2.96	2.98
Point Group	C2	C2	C1	C1	C1

**Table S7.4** Average observed rate constants,  $k_{\text{obs}}$ ,  $\text{s}^{-1}$ , for the displacement of the chloride ligand in RuPtdteg with the nucleophiles, at  $T = 298 \text{ K}$ ,  $I = 0.02 \text{ M LiCF}_3\text{SO}_3$ , adjusted with LiCl.

TU		DMTU		TMTU		I	
Conc., M	$k_{\text{obs.}}, \text{s}^{-1}$	Conc., M	$k_{\text{obs.}}, \text{s}^{-1}$	Conc., M	$k_{\text{obs.}}, \text{s}^{-1}$	Conc., M	$k_{\text{obs.}}, \text{s}^{-1}$
0.0001	0.02645	0.0001	0.01049	0.0001	0.00325	0.0001	0.02351
0.0002	0.06005	0.0002	0.01921	0.0002	0.00677	0.0002	0.0530
0.0003	0.08845	0.0003	0.0293	0.0003	0.0105	0.0003	0.08209
0.0004	0.1140	0.0004	0.03851	0.0004	0.01340	0.0004	0.11434
0.0005	0.14303	0.0005	0.05041	0.0005	0.01573	0.0005	0.13969

**Table S7.5** Average observed rate constants,  $k_{\text{obs}}$ ,  $\text{s}^{-1}$ , for the displacement of the chloride ligand in RuPtdtdeg with the nucleophiles, at  $T = 298 \text{ K}$ ,  $I = 0.02 \text{ M LiCF}_3\text{SO}_3$ , adjusted with LiCl.

TU		DMTU		TMTU		I	
Conc., M	$k_{\text{obs.}}, \text{s}^{-1}$	Conc., M	$k_{\text{obs.}}, \text{s}^{-1}$	Conc., M	$k_{\text{obs.}}, \text{s}^{-1}$	Conc., M	$k_{\text{obs.}}, \text{s}^{-1}$
0.0001	0.02364	0.0001	0.01294	0.0001	0.00403	0.0001	0.0194
0.0002	0.05582	0.0002	0.0239	0.0002	0.009	0.0002	0.03995
0.0003	0.08845	0.0003	0.03605	0.0003	0.01375	0.0003	0.05937
0.0004	0.11821	0.0004	0.04349	0.0004	0.01703	0.0004	0.0784
0.0005	0.15223	0.0005	0.05681	0.0005	0.0220	0.0005	0.09259

**Table S7.6** Average observed rate constants,  $k_{\text{obs}}$ ,  $\text{s}^{-1}$ , for the displacement of the chloride ligand in RuPtdtteg with the nucleophiles, at  $T = 298 \text{ K}$ ,  $I = 0.02 \text{ M LiCF}_3\text{SO}_3$ , adjusted with LiCl.

TU		DMTU		TMTU		$\Gamma$	
Conc., M	$k_{\text{obs.}}, \text{s}^{-1}$	Conc., M	$k_{\text{obs.}}, \text{s}^{-1}$	Conc., M	$k_{\text{obs.}}, \text{s}^{-1}$	Conc., M	$k_{\text{obs.}}, \text{s}^{-1}$
0.0001	0.02785	0.0001	0.01503	0.0001	0.00317	0.0001	0.02092
0.0002	0.05957	0.0002	0.03313	0.0002	0.0064	0.0002	0.04301
0.0003	0.08592	0.0003	0.05378	0.0003	0.0102	0.0003	0.06445
0.0004	0.1273	0.0004	0.07055	0.0004	0.01268	0.0004	0.08215
0.0005	0.1564	0.0005	0.08798	0.0005	0.01569	0.0005	0.1012

**Table S7.7** Average observed rate constants,  $k_{\text{obs}}$ ,  $\text{s}^{-1}$ , for the displacement of the chloride ligand in RuPtdtteg with the nucleophiles, at  $T = 298 \text{ K}$ ,  $I = 0.02 \text{ M LiCF}_3\text{SO}_3$ , adjusted with LiCl.

TU		DMTU		TMTU		$\Gamma$	
Conc., M	$k_{\text{obs.}}, \text{s}^{-1}$	Conc., M	$k_{\text{obs.}}, \text{s}^{-1}$	Conc., M	$k_{\text{obs.}}, \text{s}^{-1}$	Conc., M	$k_{\text{obs.}}, \text{s}^{-1}$
0.0001	0.02855	0.0001	0.00992	0.0001	0.00383	0.0001	0.02129
0.0002	0.06756	0.0002	0.02193	0.0002	0.00856	0.0002	0.04449
0.0003	0.09465	0.0003	0.03241	0.0003	0.01093	0.0003	0.06845
0.0004	0.13498	0.0004	0.04224	0.0004	0.01487	0.0004	0.09023
0.0005	0.16538	0.0005	0.0515	0.0005	0.01852	0.0005	0.11523

**Table S7.8** Temperature dependence of  $k_2 \text{ M}^{-1}\text{s}^{-1}$ , for the displacement of the chloride ligand in RuPtdteg by the nucleophiles at 30-fold excess over [RuPtdteg], at  $T = 298 \text{ K}$ ,  $I = 0.02 \text{ M LiCF}_3\text{SO}_3$ , adjusted with LiCl.

TU		DMTU		TMTU		$\Gamma$	
$1/T, \text{K}^{-1}$	$\ln(k_2/T)$	$1/T, \text{K}^{-1}$	$\ln(k_2/T)$	$1/T, \text{K}^{-1}$	$\ln(k_2/T)$	$1/T, \text{K}^{-1}$	$\ln(k_2/T)$
0.00347	-0.29331	0.00347	-1.5313	0.00347	-2.58986	0.00347	-0.655
0.00341	-0.16154	0.00341	-1.3484	0.00341	-2.3264	0.00341	-0.4338
0.00335	-0.01119	0.00335	-1.1160	0.00335	-2.14416	0.00335	-0.23417
0.0033	0.17209	0.0033	-0.8985	0.0033	-1.98934	0.0033	-0.04125
0.00325	0.37532	0.00325	-0.6576	0.00325	-1.70274	0.00325	0.28088
						0.00319	0.52478

**Table S7.9** Temperature dependence of  $k_2$  M<sup>-1</sup>s<sup>-1</sup>, for the displacement of the chloride ligand in RuPtdtdeg by the nucleophiles at 30-fold excess over [RuPtdtdeg], at T = 298 K,  $I = 0.02$  M LiCF<sub>3</sub>SO<sub>3</sub>, adjusted with LiCl.

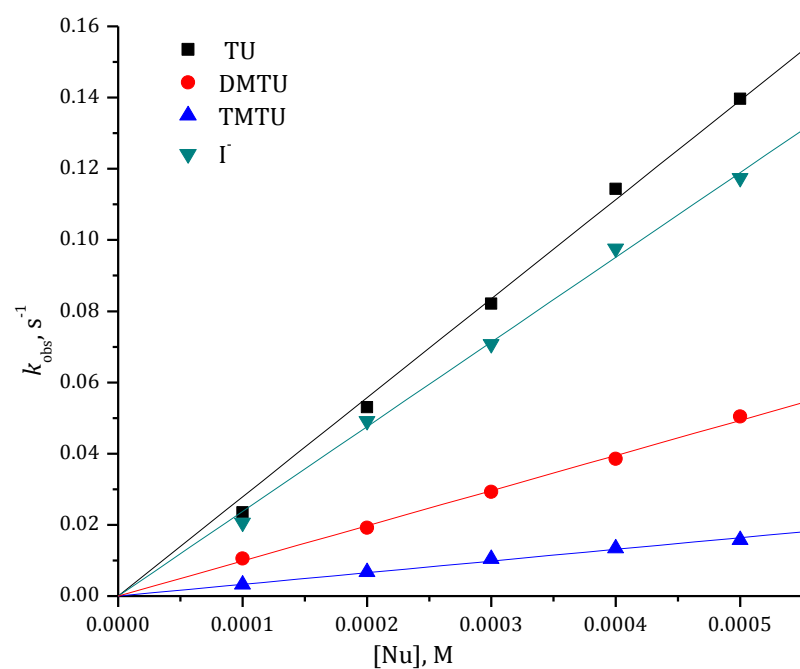
TU		DMTU		TMTU		Γ	
1/T, K <sup>-1</sup>	ln( $k_2$ /T)	1/T, K <sup>-1</sup>	ln( $k_2$ /T)	1/T, K <sup>-1</sup>	ln( $k_2$ /T)	1/T, K <sup>-1</sup>	ln( $k_2$ /T)
0.00347	-0.3421	0.00347	-1.47737	0.00347	-2.3850	0.00347	-0.9502
0.00341	-0.1550	0.00341	-1.23105	0.00341	-2.0790	0.00341	-0.6341
0.00335	-0.0112	0.00335	-0.90872	0.00335	-1.8726	0.00335	-0.4098
0.0033	0.1619	0.0033	-0.64428	0.0033	-1.6194	0.0033	-0.1539
0.00325	0.3624	0.00325	-0.37498	0.00325	-1.3598	0.00325	0.0427

**Table S7.10** Temperature dependence of  $k_2$  M<sup>-1</sup>s<sup>-1</sup>, for the displacement of the chloride ligand in RuPtdtteg by the nucleophiles at 30-fold excess over [RuPtdtteg], at T = 298 K,  $I = 0.02$  M LiCF<sub>3</sub>SO<sub>3</sub>, adjusted with LiCl.

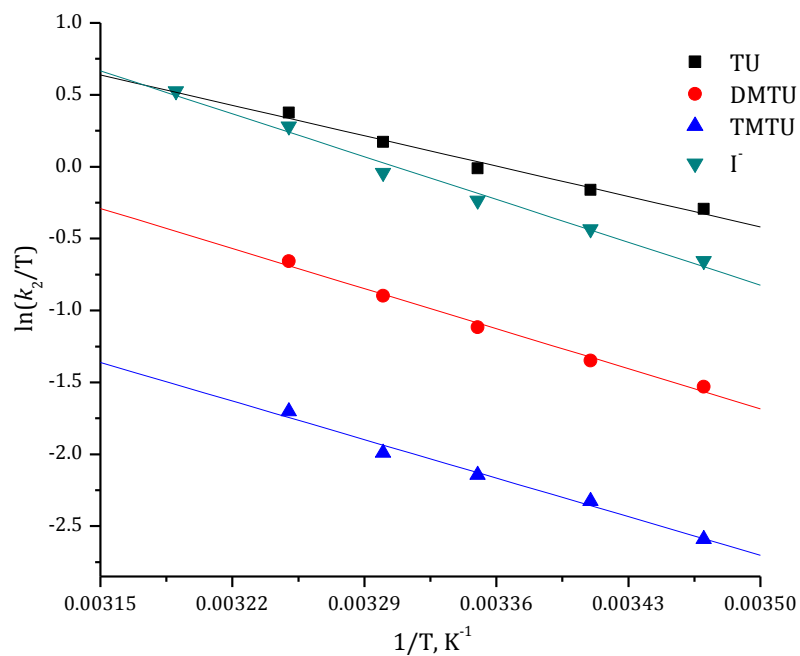
TU		DMTU		TMTU		Γ	
1/T, K <sup>-1</sup>	ln( $k_2$ /T)	1/T, K <sup>-1</sup>	ln( $k_2$ /T)	1/T, K <sup>-1</sup>	ln( $k_2$ /T)	1/T, K <sup>-1</sup>	ln( $k_2$ /T)
0.00347	-0.6281	0.00347	-0.85037	0.00347	-2.62875	0.00347	-0.74192
0.00341	-0.38894	0.00341	-0.68516	0.00341	-2.3944	0.00341	-0.50056
0.00335	-0.06947	0.00335	-0.50869	0.00335	-2.17168	0.00335	-0.32769
0.0033	0.1418	0.0033	-0.36284	0.0033	-1.95529	0.0033	-0.07531
0.00325	0.38179	0.00325	-0.19512	0.00325	-1.72447	0.00325	0.18349

**Table S7.11** Temperature dependence of  $k_2$  M<sup>-1</sup>s<sup>-1</sup>, for the displacement of the chloride ligand in RuPtdttteg by the nucleophiles at 30-fold excess over [RuPtdttteg], at T = 298 K,  $I = 0.02$  M LiCF<sub>3</sub>SO<sub>3</sub>, adjusted with LiCl.

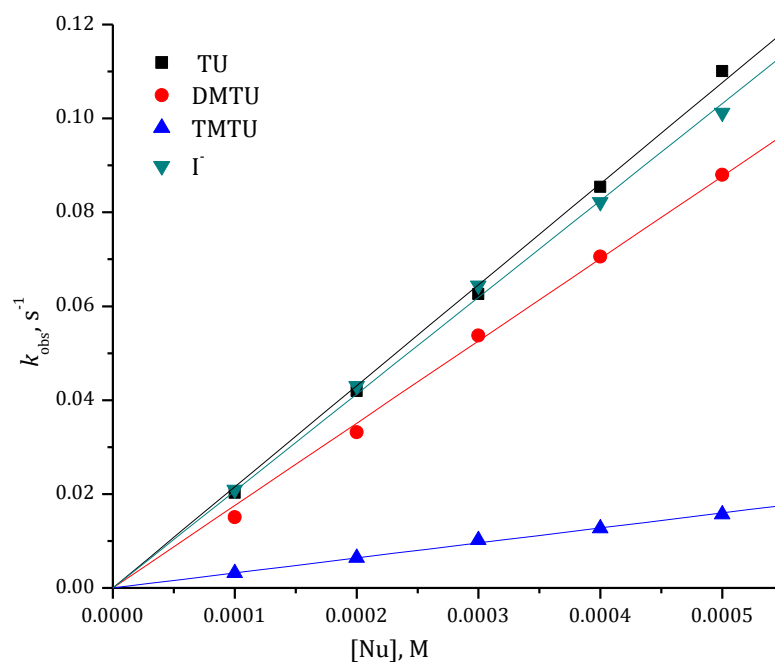
Tu		DMTu		TMTu		Γ	
1/T, K <sup>-1</sup>	ln( $k_2$ /T)	1/T, K <sup>-1</sup>	ln( $k_2$ /T)	1/T, K <sup>-1</sup>	ln( $k_2$ /T)	1/T, K <sup>-1</sup>	ln( $k_2$ /T)
0.00347	-0.34161	0.00347	-1.34703	0.00347	-2.50826	0.00347	-0.99346
0.00341	-0.09007	0.00341	-1.15574	0.00341	-2.23338	0.00341	-0.59206
0.00335	0.05659	0.00335	-1.01523	0.00335	-2.10202	0.00335	-0.26749
0.0033	0.26719	0.0033	-0.84209	0.0033	-1.88251	0.0033	0.18369
0.00325	0.48535	0.00325	-0.62498	0.00325	-1.66346	0.00324	0.50428



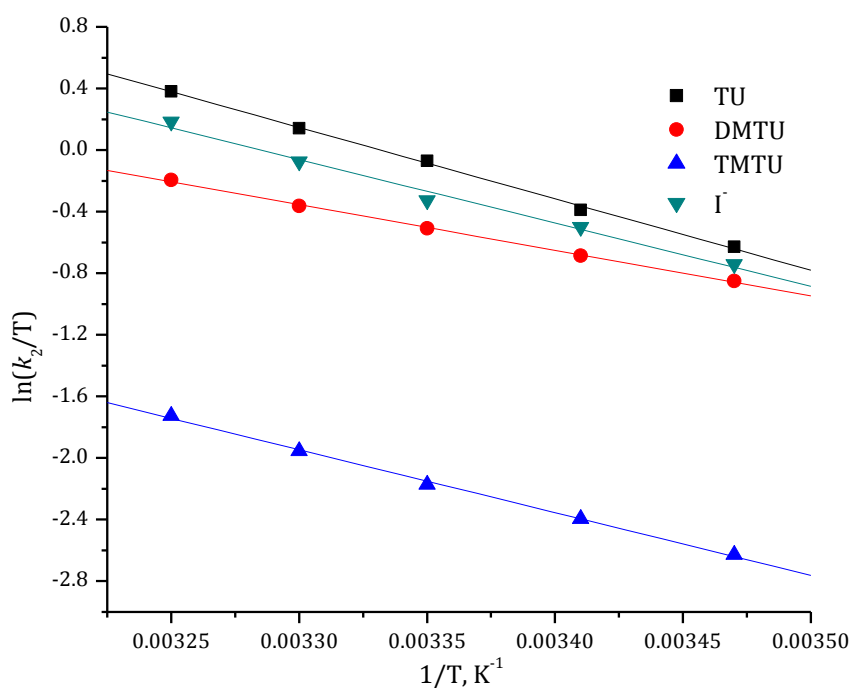
**Figure S7.2** Dependence of the *pseudo* first-order rate constants ( $k_{obs}$ ) on the concentrations of the nucleophiles for the chloride substitution from RuPtdteg ( $2.0 \times 10^{-5}$  M) in methanol solution ( $I = 0.02$  M) at 298 K.



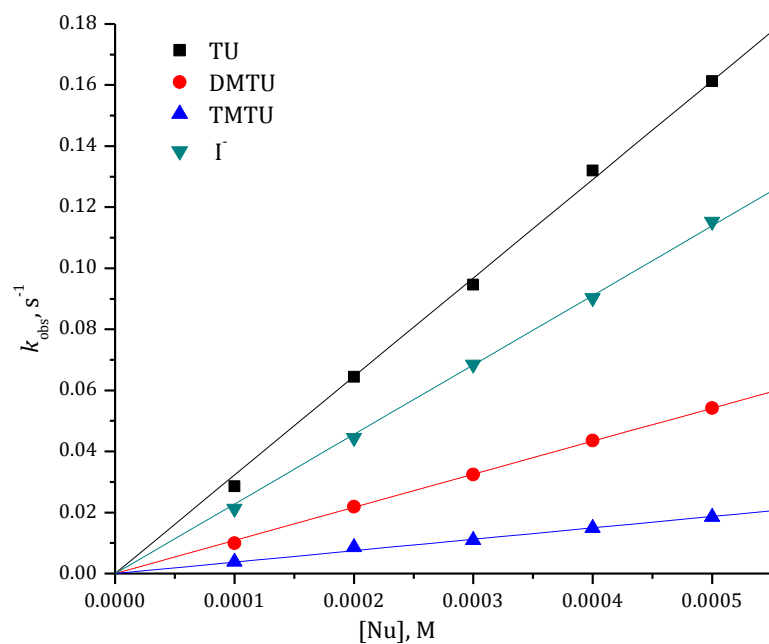
**Figure S7.3** Eyring plots obtained for RuPtdteg with the nucleophiles for the forward reactions over the temperature range 15-40 °C in methanol solution ( $I = 0.02$  M).



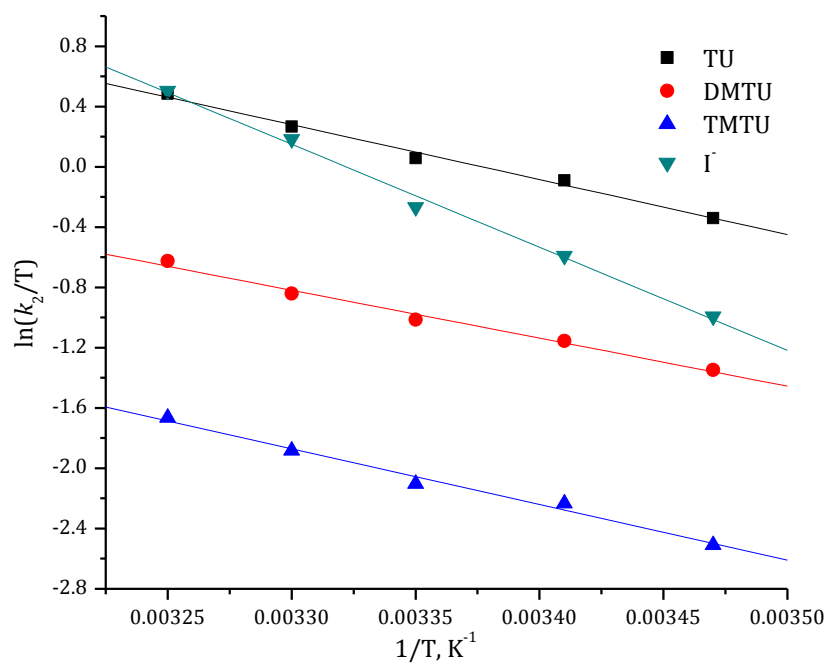
**Figure S7.4** Dependence of the *pseudo* first-order rate constants ( $k_{obs}$ ) on the concentrations of the nucleophiles for the chloride substitution from RuPtddteg ( $2.0 \times 10^{-5}$  M) in methanol solution ( $I = 0.02$  M) at 298 K.



**Figure S7.5** Eyring plots obtained for RuPtddteg with the nucleophiles for the forward reactions over the temperature range 15-35 °C in methanol solution ( $I = 0.02$  M).



**Figure S7.6** Dependence of the *pseudo* first-order rate constants ( $k_{obs}$ ) on the concentrations of the nucleophiles for the chloride substitution from RuPtdttteg ( $2.0 \times 10^{-5}$  M) in methanol solution ( $I = 0.02$  M) at 298 K.



**Figure S7.7** Eyring plots obtained for RuPtdttteg with the nucleophiles for the forward reactions over the temperature range 15-35 °C in methanol solution ( $I = 0.02$  M).

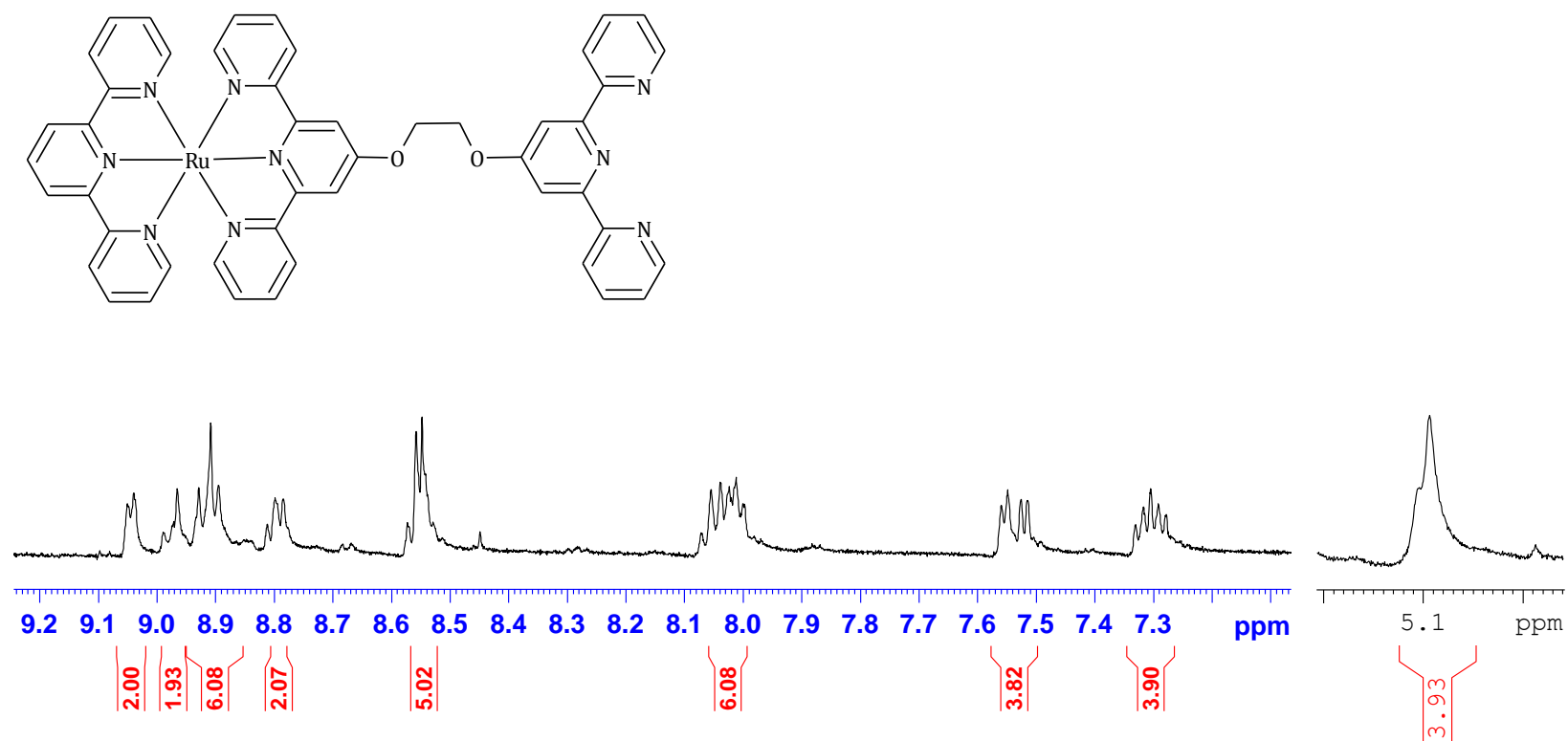


Figure S7.8  $^1\text{H}$  NMR spectrum of  $[(\text{tpy})\text{Ru}(\text{dteg})\text{Cl}_2]$  in  $\text{DMSO-}d_6$ .



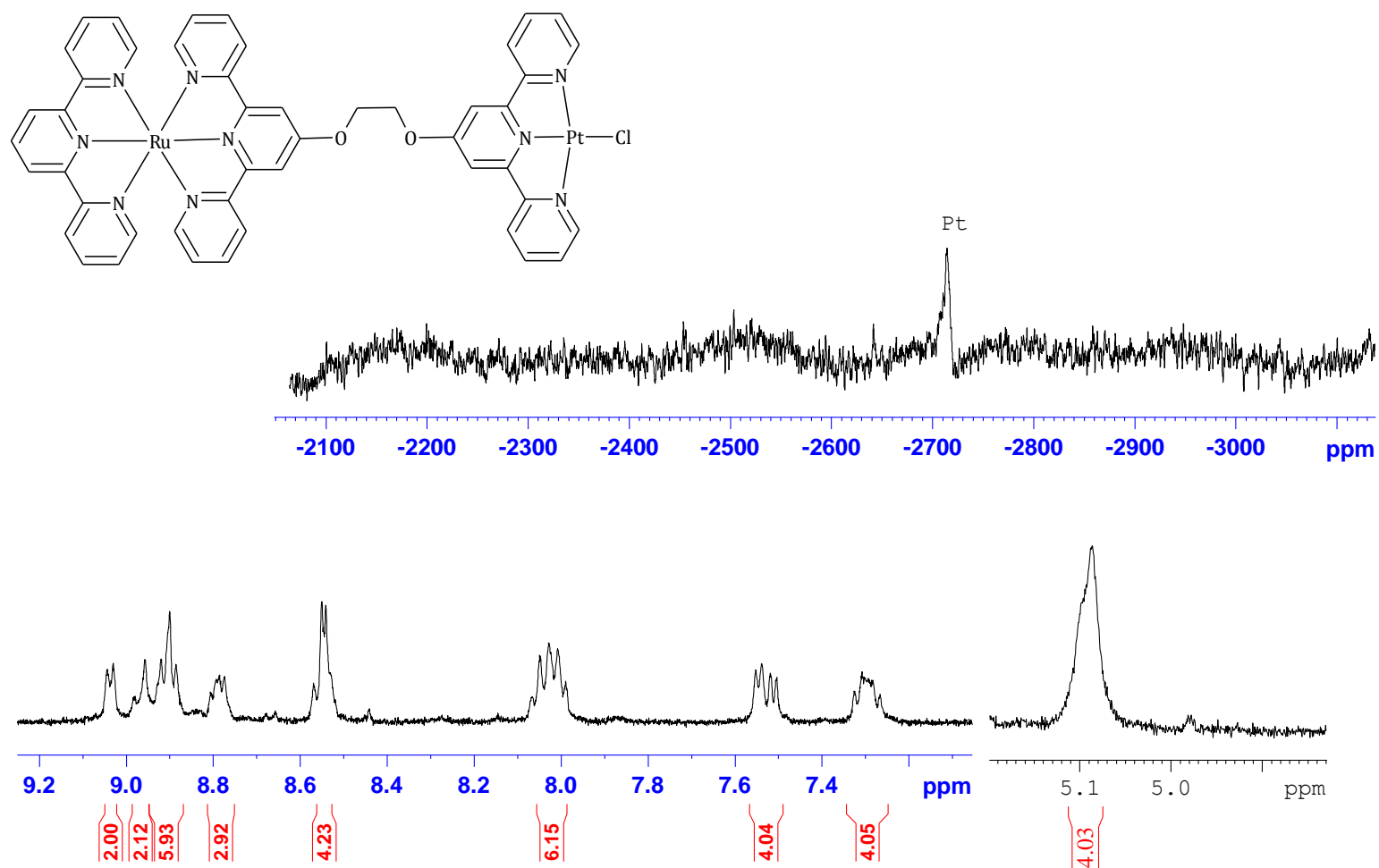


Figure S7.9  $^1\text{H}$  NMR spectrum of RuPtdeg in  $\text{DMSO}-d_6$ .

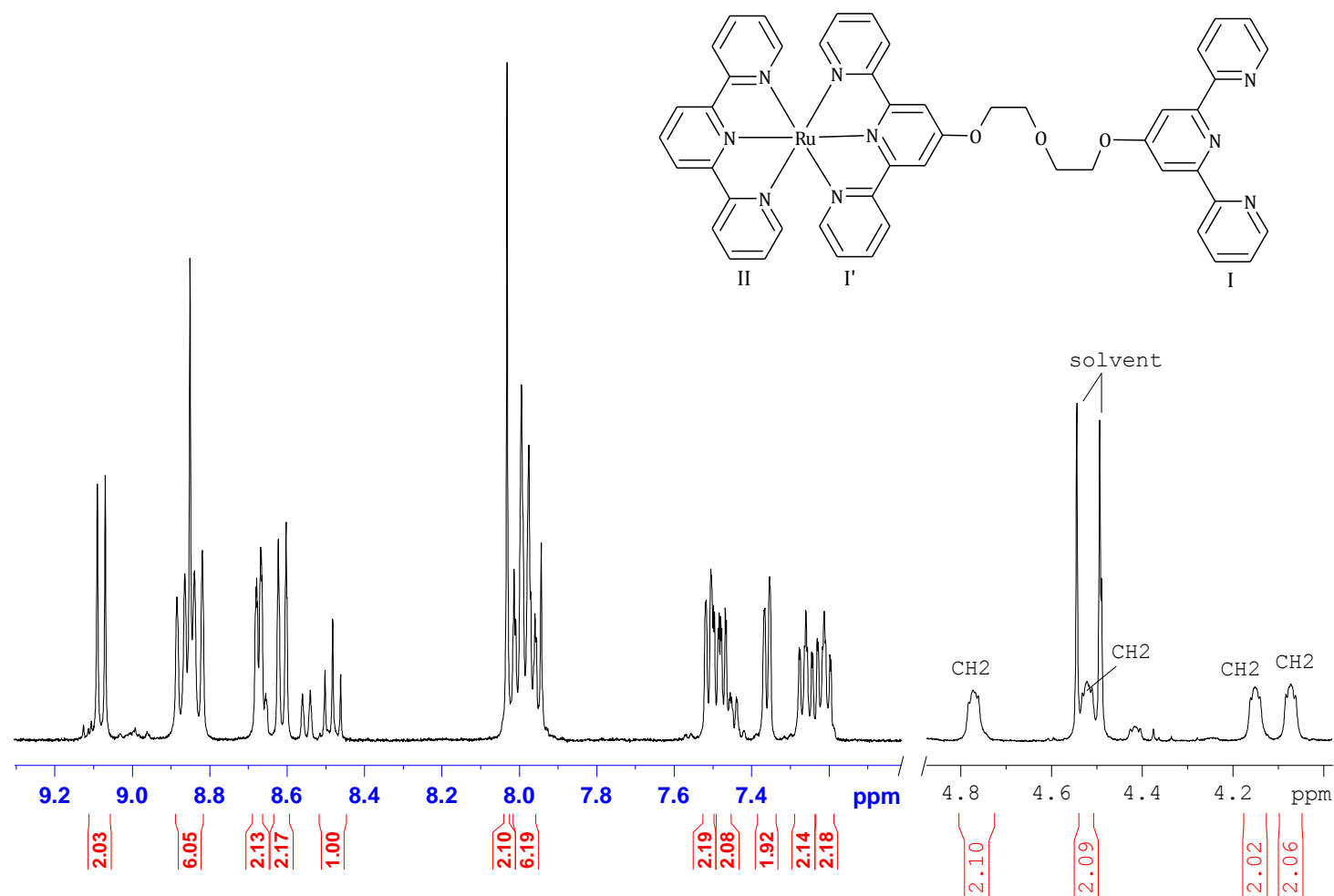


Figure S7.10  $^1\text{H}$  NMR spectrum of  $[(\text{tpy})\text{Ru}(\text{dtdeg})\text{Cl}_2]$  in  $\text{DMSO-}d_6$ .

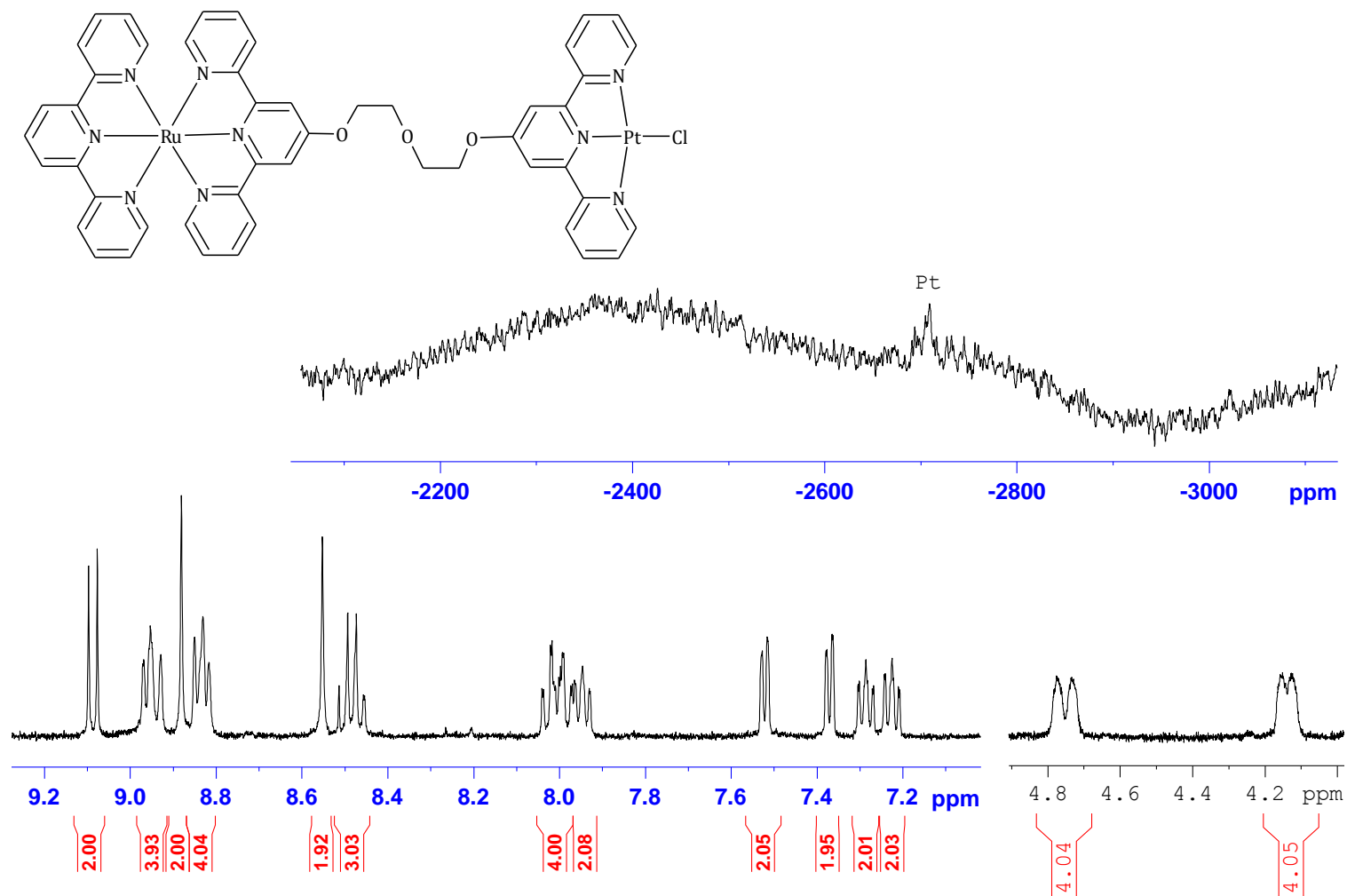


Figure S7.11  $^1\text{H}$  NMR spectrum of RuPtdddeg in  $\text{DMSO-}d_6$ .

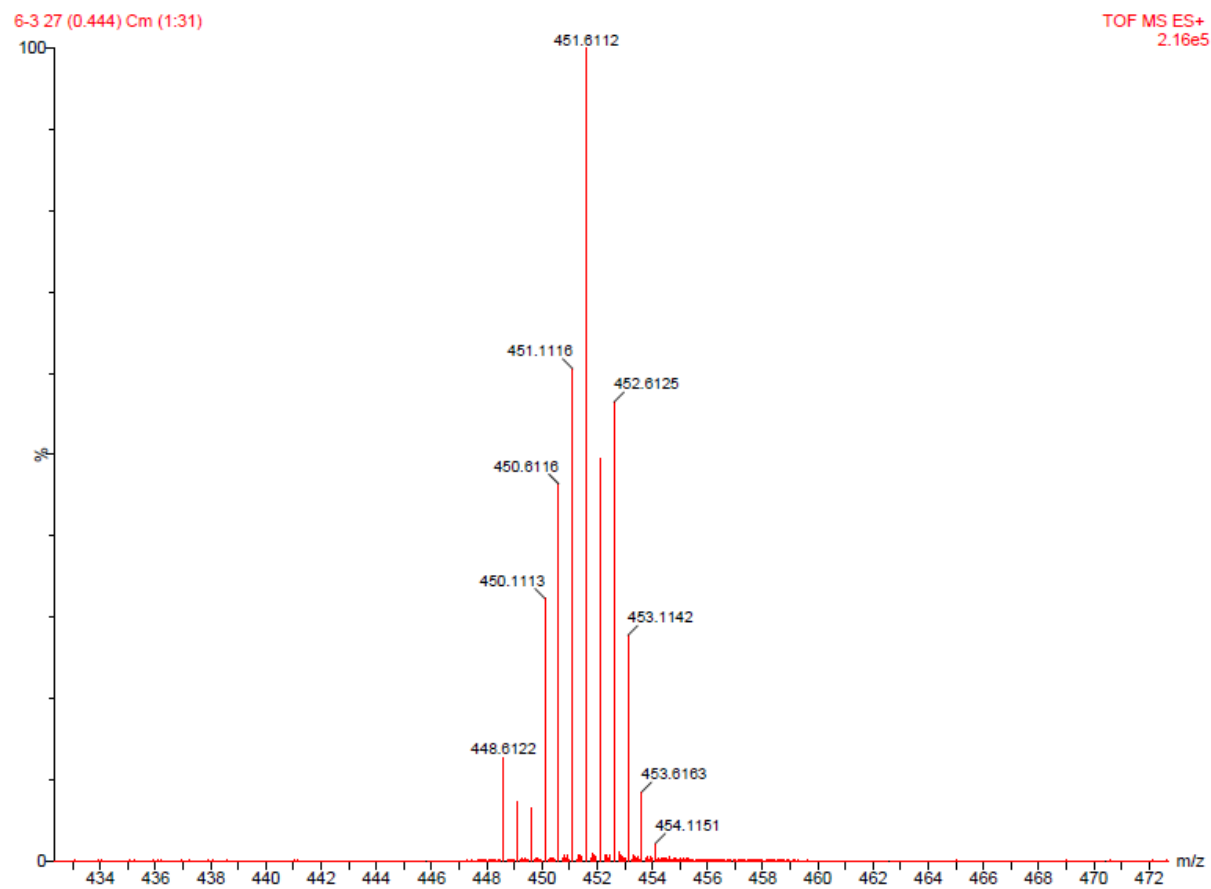


Figure S7.12 Low resolution ESI mass spectrum of Ru(tpy)dtdeg.

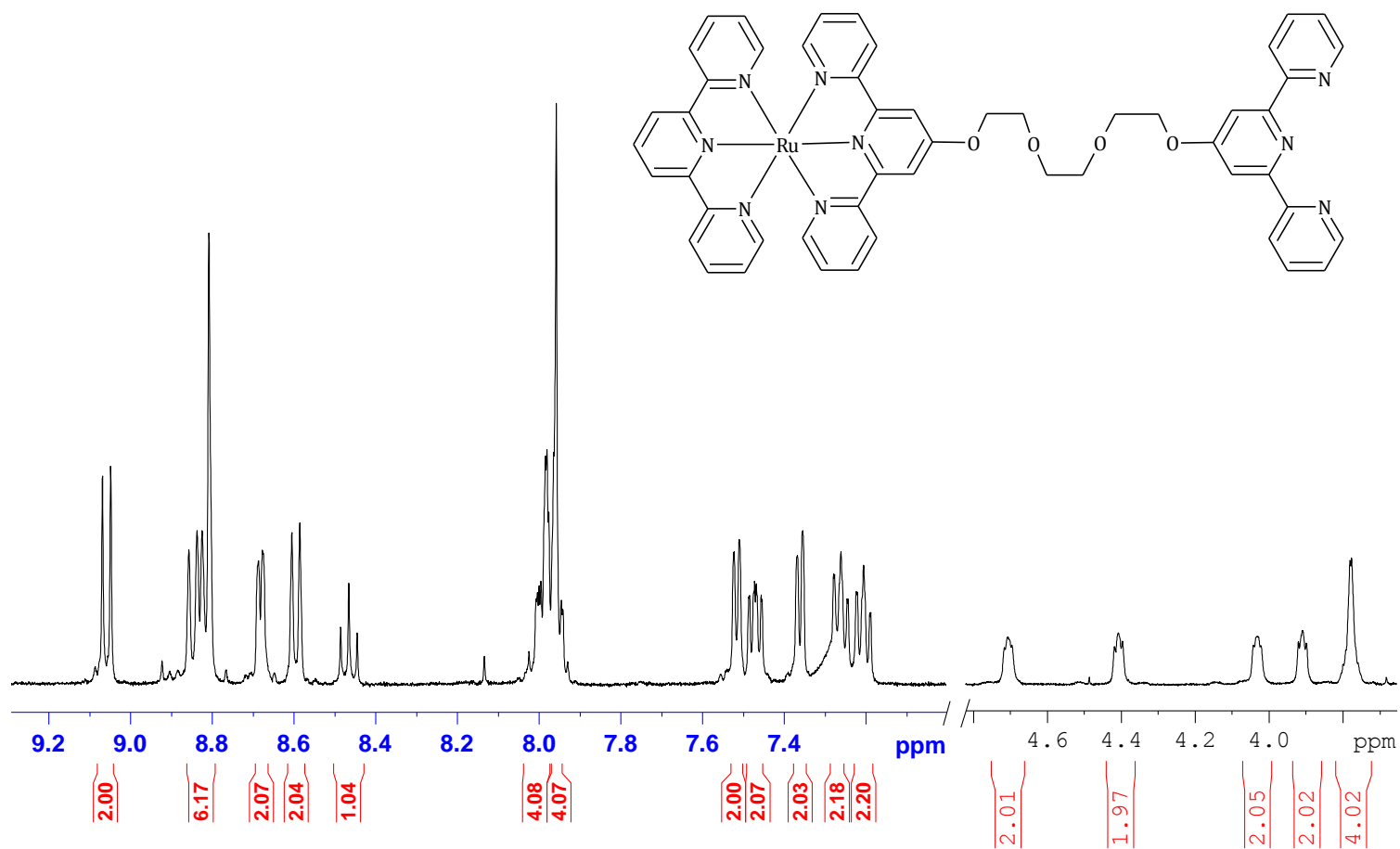


Figure S7.13  $^1\text{H}$  NMR spectrum of  $[(\text{tpy})\text{Ru}(\text{dtteg})\text{Cl}_2]$  in  $\text{DMSO-}d_6$ .

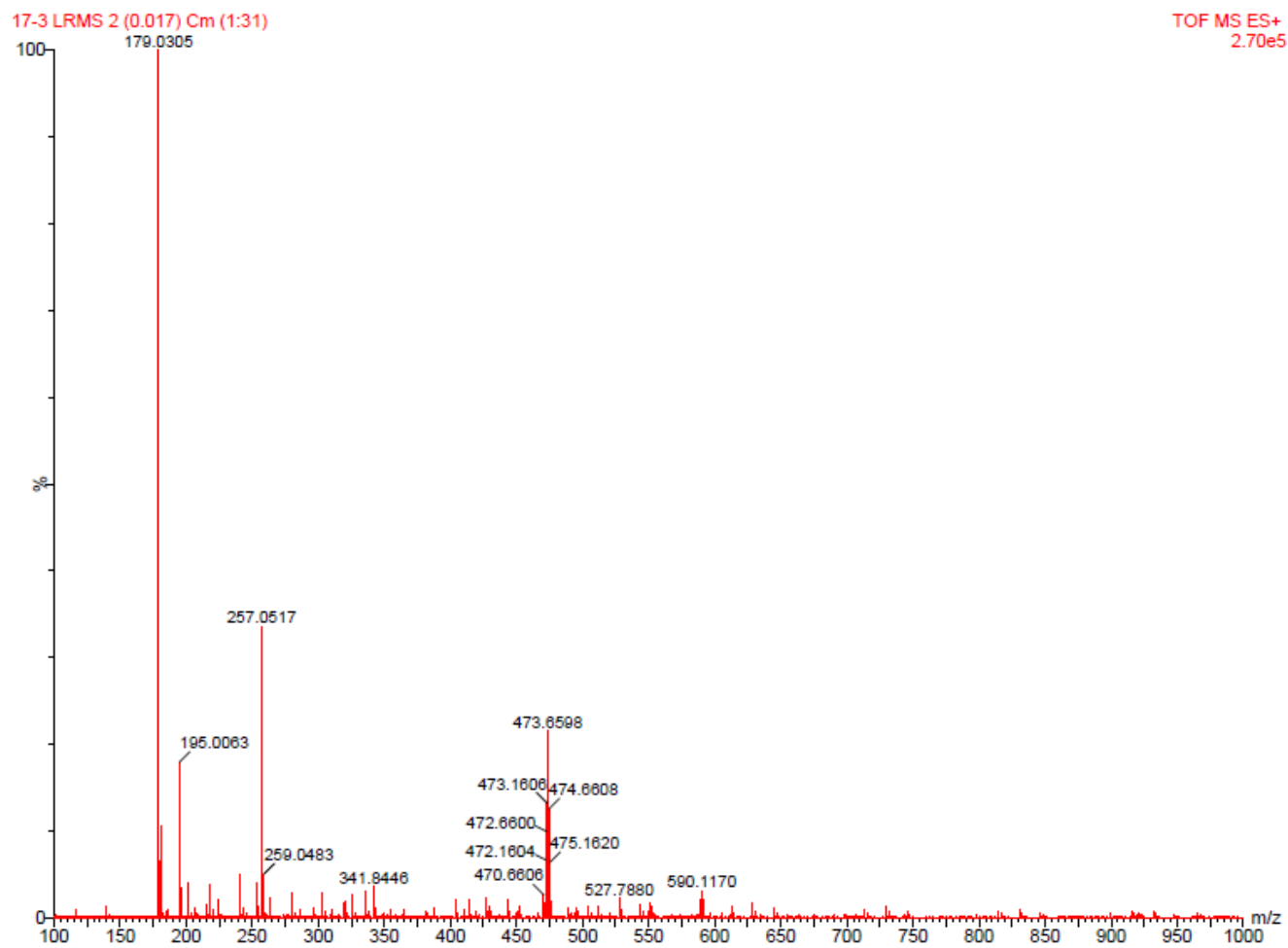


Figure S7.14 Low resolution ESI mass spectrum of Ru(tpy)dtteg.

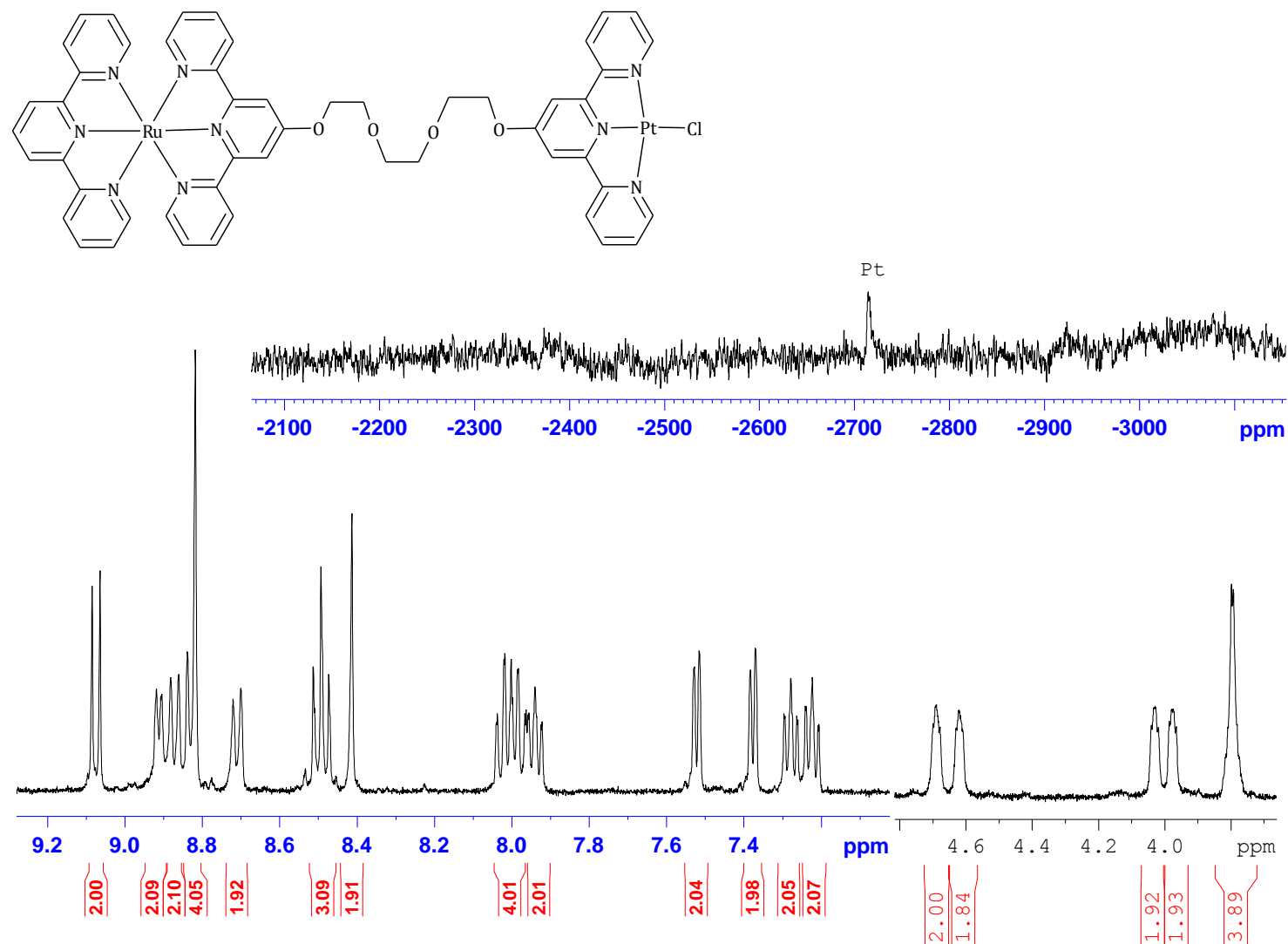


Figure S7.15  $^1\text{H}$  NMR spectrum of RuPttdtgeg in  $\text{DMSO-}d_6$ .

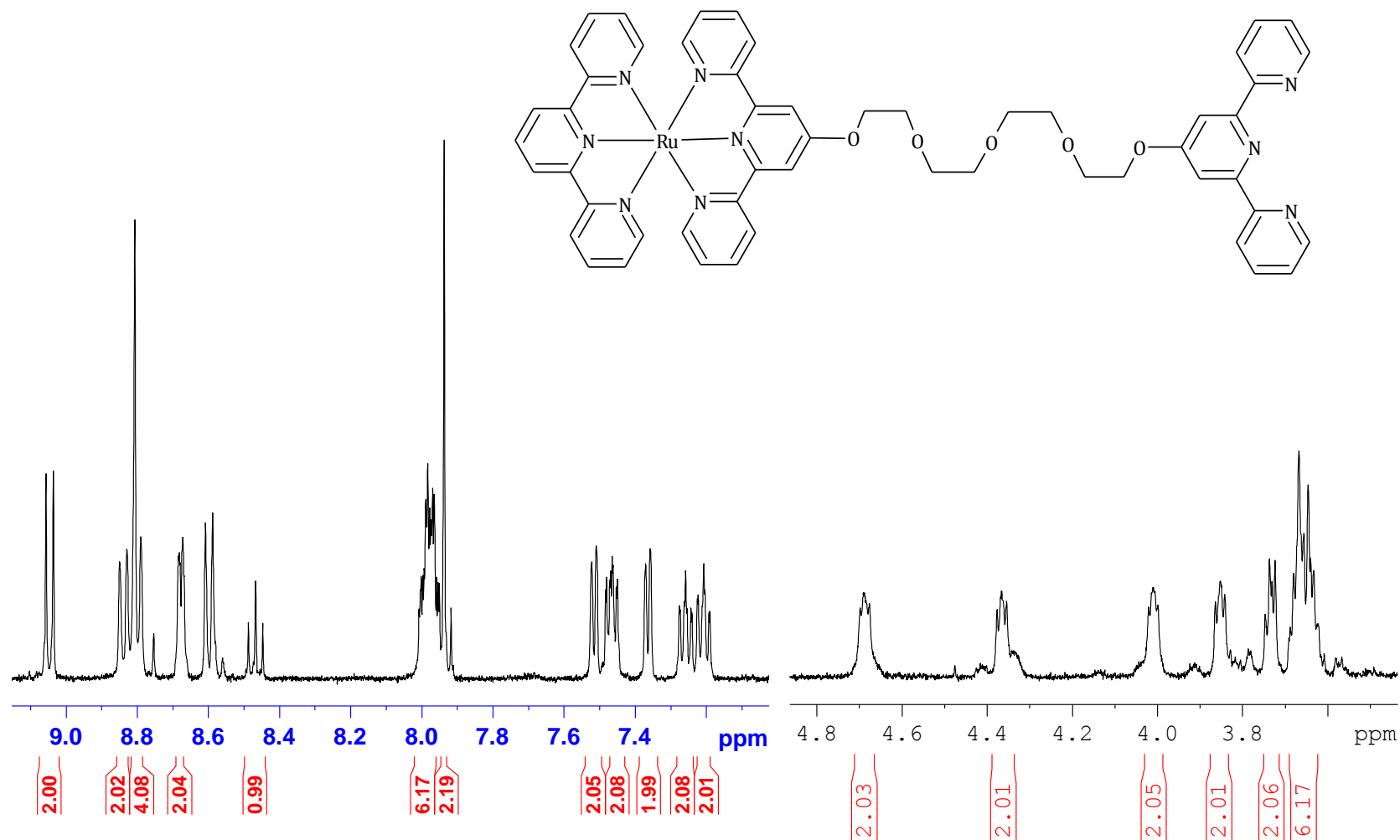


Figure S7.16  $^1\text{H}$  NMR spectrum of  $[(\text{tpy})\text{Ru}(\text{dttteg})\text{Cl}_2]$  in  $\text{DMSO-}d_6$ .



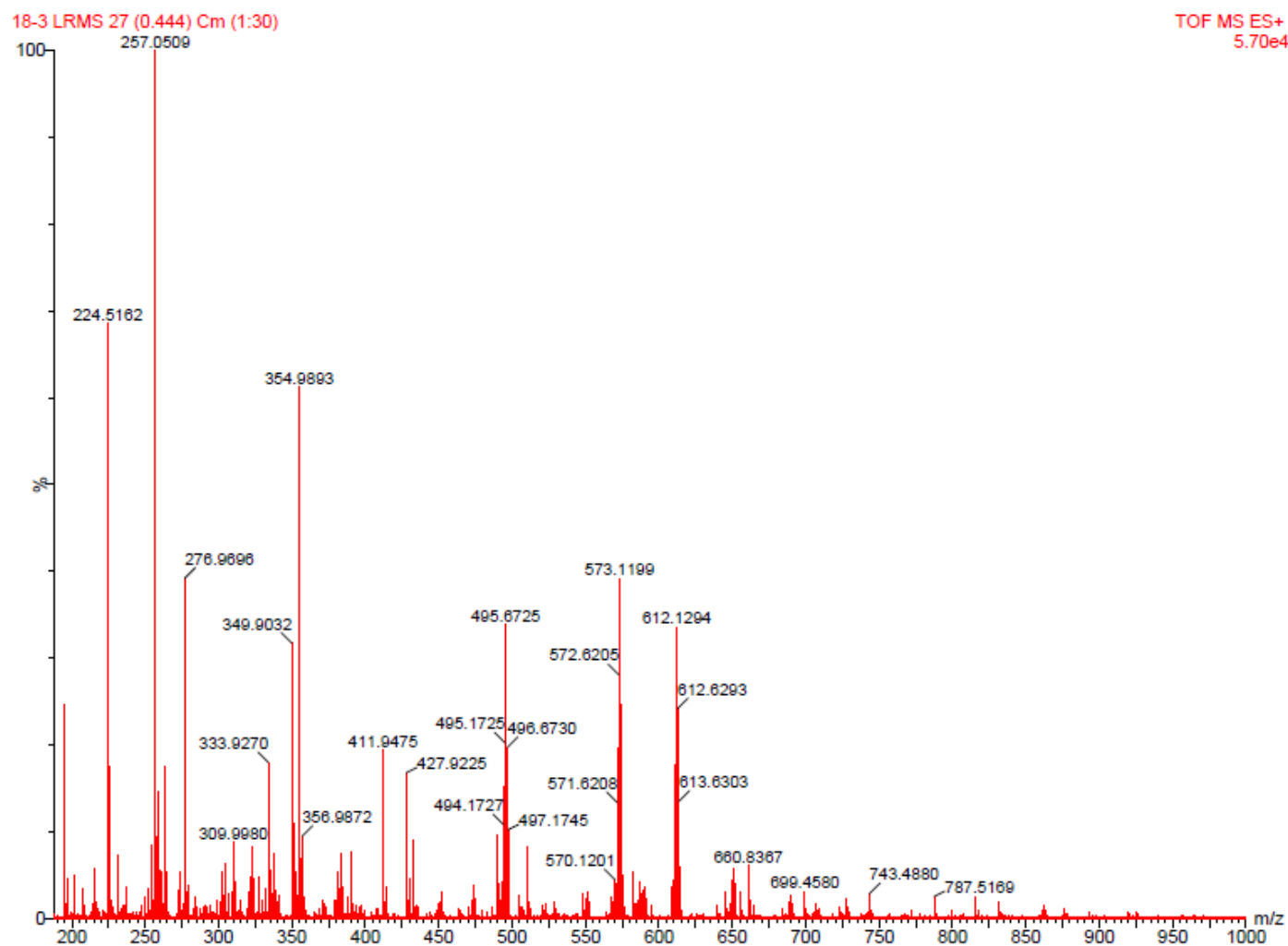


Figure S7.17 Low resolution ESI mass spectrum of Ru(tpy)dtteg.

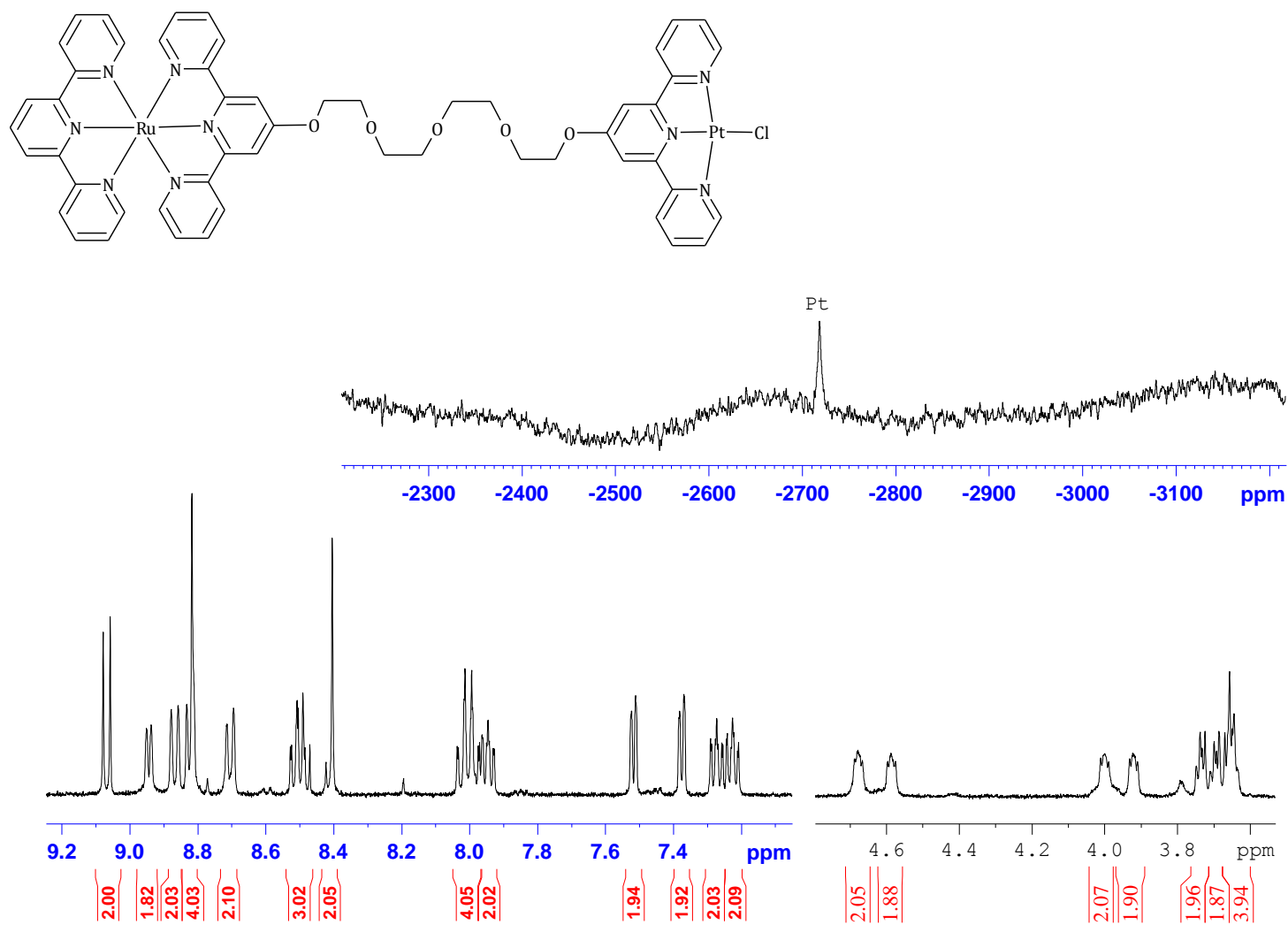


Figure S7.18  $^1\text{H}$  NMR spectrum of RuPttdtteg in  $\text{DMSO-}d_6$ .

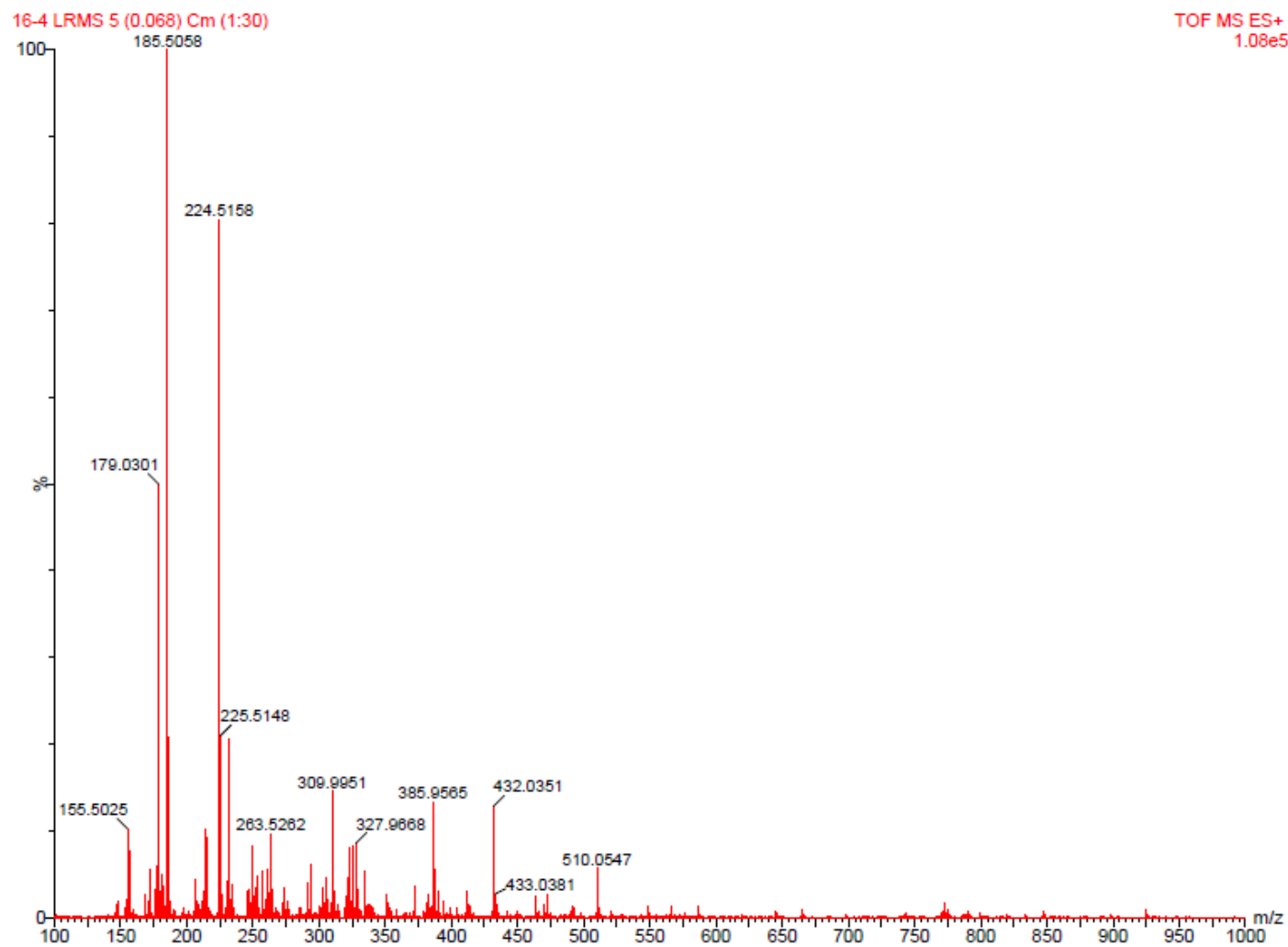


Figure S7.19 Low resolution ESI mass spectrum of RuPtdteg.

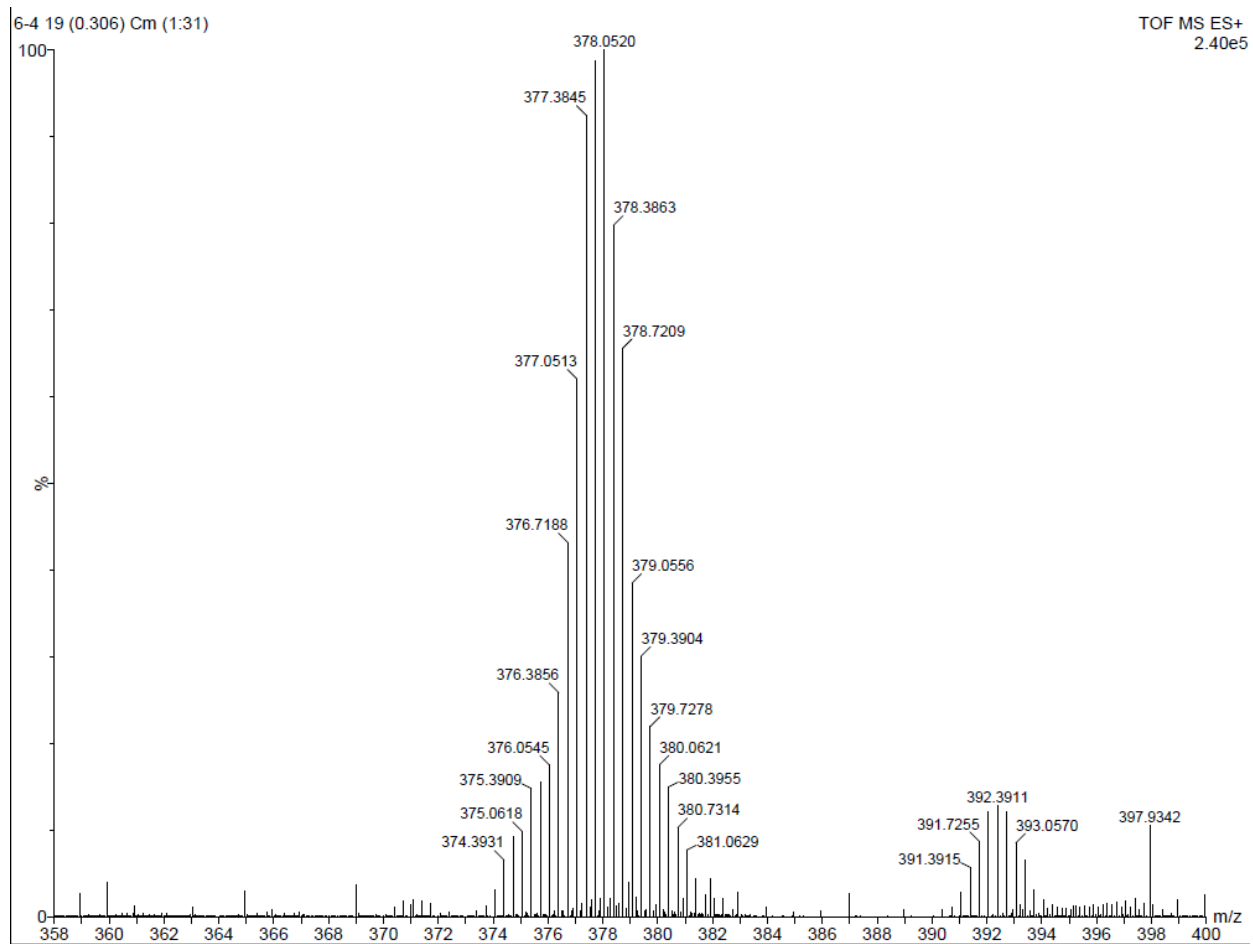


Figure S7.20 Low resolution ESI mass spectrum of RuPtdtdeg.

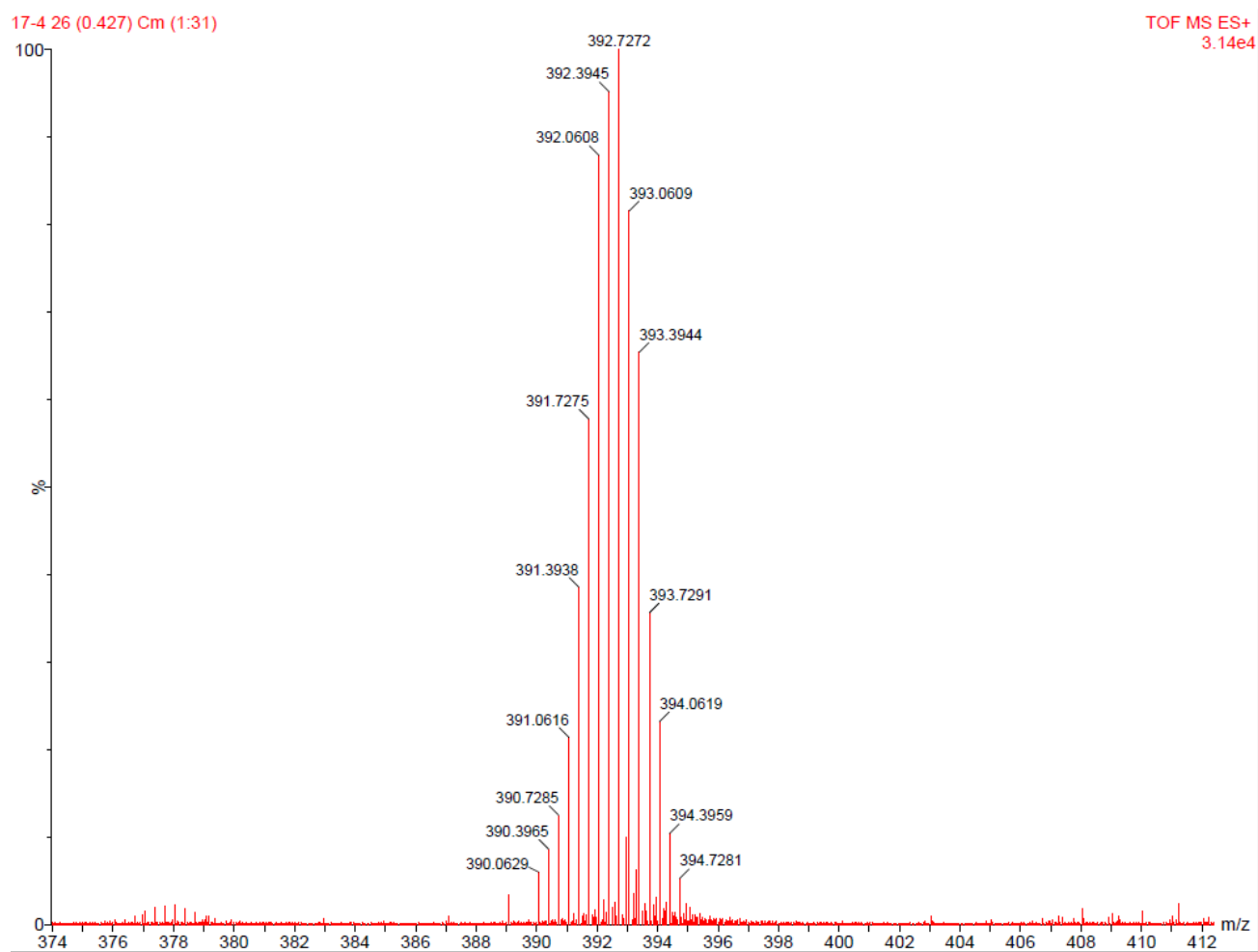


Figure S7.21 Low resolution ESI mass spectrum of RuPtdtgeg.

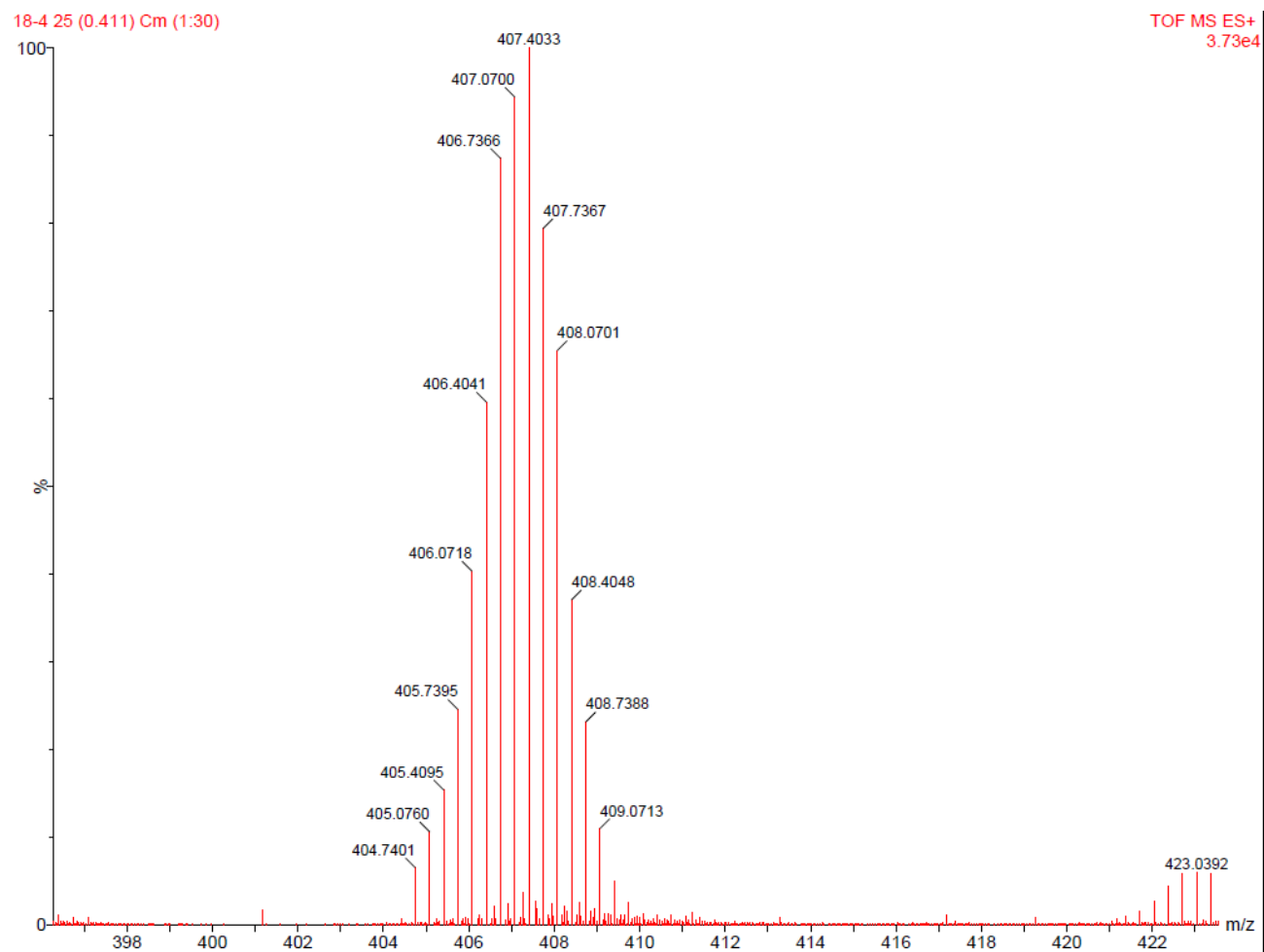
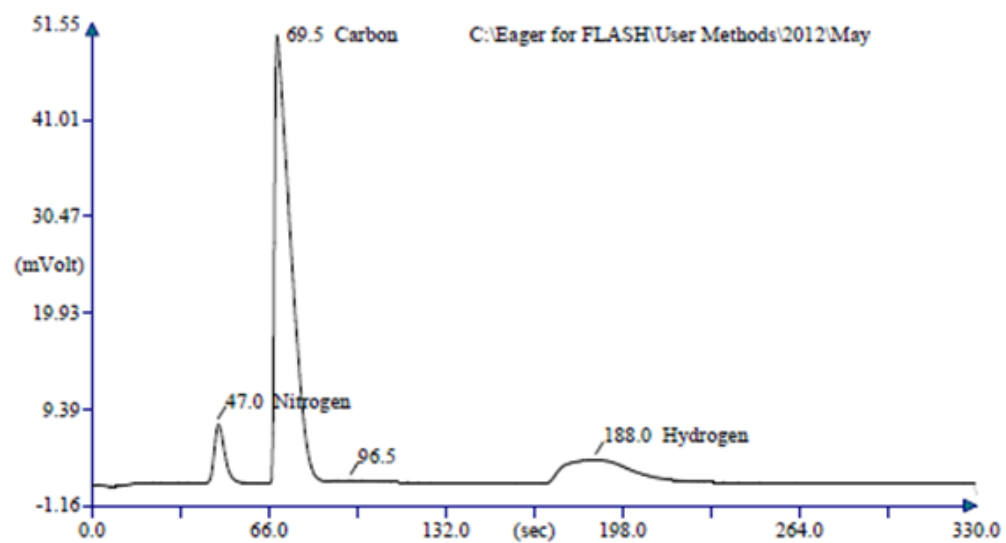


Figure S7.22 Low resolution ESI mass spectrum of RuPtdttteg.



Retention Time (min)	Element Name	Element %
0.783	Nitrogen	7.631
1.158	Carbon	37.210
1.608		0.000
3.133	Hydrogen	3.003
		47.844

Figure S7.23 Exemplary elemental analysis spectrum for RuPtdtteg.

**Experimental****[Ru(tpy)Cl<sub>3</sub>]**

Equal amounts of RuCl<sub>3</sub> · 3H<sub>2</sub>O (~150 mg) and tpy were refluxed in absolute EtOH (125 mL) for 3 hours. The resulting reaction mixture was cooled to room temperature and the precipitate was filtered, washed with cold absolute EtOH (5 mL) followed by copious amount of ethylether and dried under *vacuo*. Yield: 191 mg, 433 μmol, (76 %), brown precipitate.



**Table of Contents- 8**

List of Figures.....	i
List of Tables.....	i
Chapter Eight.....	1
<b>Summary and Future Prospects .....</b>	<b>1</b>
8.1    Summary.....	1
8.2    Work Completed but Not Included in This Thesis.....	7
8.3    Future Prospects.....	10
8.4    References.....	12

**List of Figures**

Figure 8.1	Structure of complexes reported in <i>Chapter 3</i> .....	3
Figure 8.2	Structure of complexes reported in <i>Chapter 4</i> .....	4
Figure 8.3	Structure of complexes reported in <i>Chapter 5</i> .....	5
Figure 8.4	Structure of complexes reported in <i>Chapter 6</i> .....	6
Figure 8.5	Structure of complexes reported in <i>Chapter 7</i> .....	7
Figure 8.6	Structure of the two heterometallic complexes; Ru(Ptdeg) <sub>2</sub> and (RuPt) <sub>2</sub> (deg) <sub>3</sub> investigated. Complexes, Ptptydeg and RuPtdeg are already reported in this thesis and Ptpty reported from literature are included for comparisons. ....	8
Figure 8.7	Structure of complexes synthesized and characterized. ....	10

**List of Tables**

Table 8.1	Summary of second-order rate constants, $k_2$ and activation parameters, with the corresponding standard deviations for the substitution of the chloro ligands by a series of thiourea nucleophiles and iodide ion at $I = 0.02$ M LiCF <sub>3</sub> SO <sub>3</sub> , adjusted with LiCl. Data for Ptptydeg and RuPtdtdeg are taken from <i>Chapter 5</i> and <i>Chapter 6</i> and data for Ptpty are included for comparison.....	9
-----------	---	---

# Chapter Eight

## Summary and Future Prospects

### 8.1 Summary

The main aim of this project was to investigate the thermodynamic and kinetic properties of heterometallic Ru(II)-Pt(II) complexes with N-donor chelate ligands that exhibit anticancer activity, with the focus on how the electronic and steric properties of a biologically active Ru(II) fragment influences the substitution reactivity of a Pt(II) metal centre. This was done by studying the rates of substitution as a function of concentration and temperature under *pseudo* first-order conditions. Knowledge on substitution kinetics is a vital aspect for the design of effective and improved antitumour drugs since it provides the basis for the rational mechanisms of interactions. Therefore, the rationale of this study was to provide meaningful information on the design and development of effective anticancer drugs, with reduced toxicity and improved uptake.

The structures of complexes enabled a systematic investigation into how the different linkers influence the reactivity of the mono- di and heteronuclear complexes as well as how the different metal centers (Ru(II) and Co(II)) influence the reactivity of the Pt(II) metal centre. A series of neutral biologically relevant thiourea nucleophiles (TU, MTU, DMTU and TMTU) along with some ionic nucleophiles ( $I^-$  and  $SCN^-$ ) were used for the substitution reactions. The results and the discussions are reported in **Chapter 3** to **Chapter 7** of this Thesis. The structures of the complexes studied (*Figures 8.1, 8.2, 8.3, 8.4 and 8.5*) are reported in the chapter summary for clarity.

**Chapter 1** presented an introduction to the development of the platinum and ruthenium anticancer complexes. The clinical success of cisplatin, its mechanism of actions, its cellular resistance and the development of other platinum based anticancer drugs along with the current focus on the development of platinum drugs. This chapter also summarizes the theory on ligand substitution reactivity of Pt(II) complexes focusing on relevant and current research work on the subject. The second part of this chapter presents a short summary of development of anticancer ruthenium complexes with an insight into the biological features of ruthenium that make its complexes as potential biological probes as therapeutic agents. It also deals with applications in

photodynamic therapy, DNA binding including postulated mechanism of action of ruthenium anticancer agents and the substitution reactions. The last part of this chapter focuses on a short summary of some of the heterometallic Ru(II)-Pt(II) complexes reported and their biological activities.

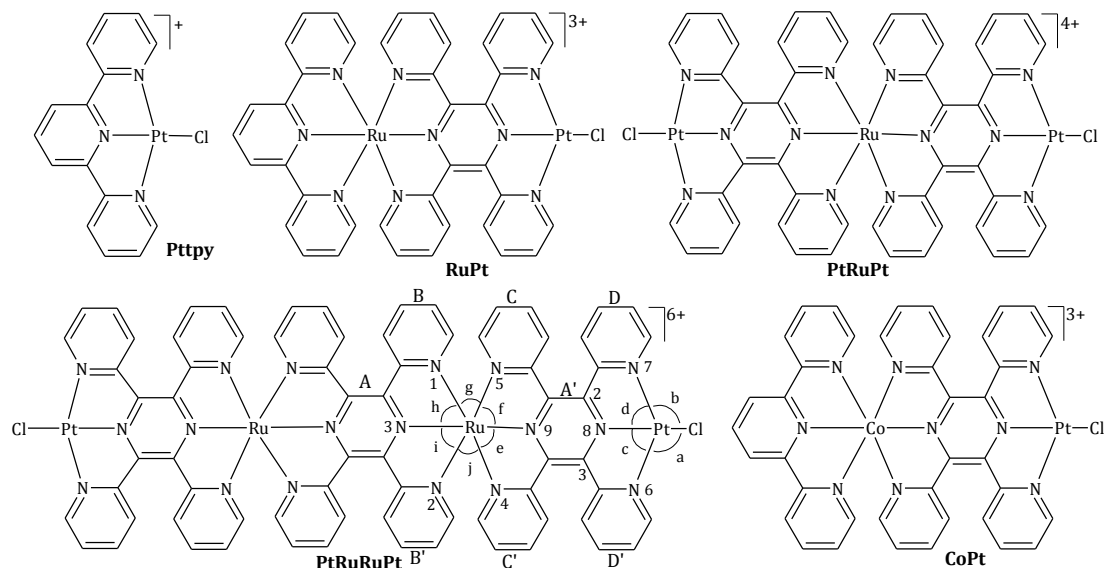
**Chapter 2** presented an introduction to the substitution reactions of Pt(II) complexes and the relevant kinetic theory including the techniques employed in investigating the ligand substitution reactions. It also reviewed on the factors influencing the ligand substitution reactions and links these to current mechanistic investigations reported into the ligand substitution reactions of Pt(II) complexes.

In **Chapter 3**, the substitution kinetics of heterometallic Ru(II)-Pt(II) complexes linked by tppz (where tppz = tetra-2-pyridyl-1,4-pyrazine) ligands is reported. In this study it was found that incorporation of Ru(tppz) increases the reactivity of Pt(II) metal centre in [Pt(tpy)Cl]Cl (**Pttpy**) (where tpy = 2,2':6',2''-terpyridine) and is ascribed to the increased  $\pi$ -back donation from the tppz ligand which increases the electrophilicity of the metal centre, overall charge and the global electrophilicity index of the complex. Additionally, it also increases the metal-metal interactions and electronic transitions within the complex. The increase in the number of tppz ligands further stabilises the anti-bonding lowest unoccupied molecular orbital (LUMO) ( $\pi^*$ ). Presence of two Ru(II) metal centres in [ClPtRu<sub>2</sub>(tppz)<sub>3</sub>PtCl](PF<sub>6</sub>)<sub>6</sub> (**PtRuRuPt**) further enhances intermetallic communication within the complex.

An interesting aspect of this work is the considerable decrease in the rate of substitution reactions by changing the metal centre from Ru(II) to a Co(II). The rate of substitution decreased by a factor of four due to the weaker  $\pi$ -back donation of electron density in [(tpy)Co(tppz)PtCl](PF<sub>6</sub>)<sub>3</sub> (**CoPt**) complex. UV/visible spectrophotometric analysis along with the density functional theory (DFT) calculations indicate that (Pt( $d\pi$ ) $\rightarrow$ tppz( $\pi^*$ )) electronic transitions are weaker for **CoPt** which is an indication of weak  $\pi$ -backbonding from the Pt(II)  $d$  orbitals to the tppz ligand. Based on the facts it was concluded that the Ru(II) is better at accepting the electron density than Co(II). Furthermore, the reactivity of the complexes is also driven by the increase in the global electrophilicity index of the complexes.

<sup>1</sup>H NMR and <sup>195</sup>Pt NMR spectroscopic techniques were used to demonstrate the stepwise substitution observed when thiourea was the incoming nucleophile. From the

NMR study it was shown that second step observed was due to the degradation of the coordinated ligand from the Pt(II) metal centre forming  $\text{Pt}(\text{TU})_4$  which was achieved in the presence of excess thiourea and its derivatives.

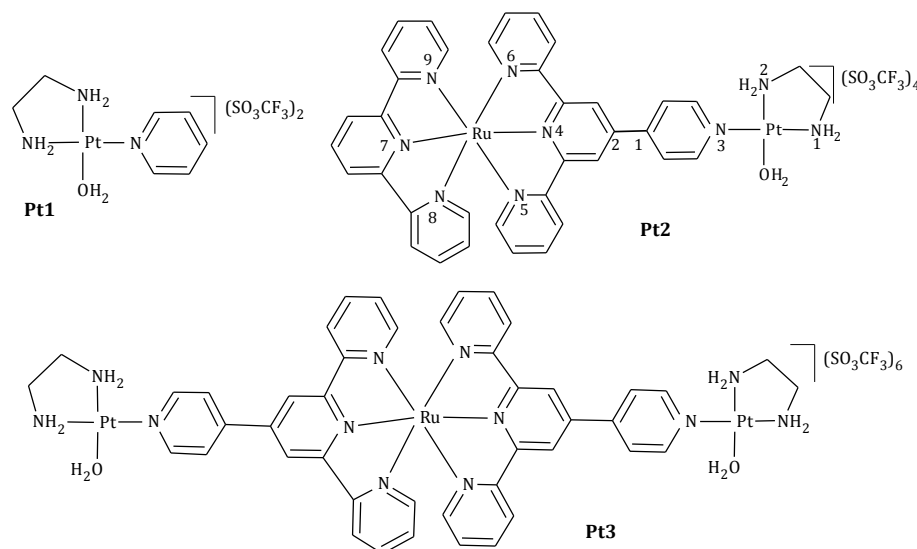


**Figure 8.1** Structure of complexes reported in *Chapter 3*.

The rates of substitution of a series of heterometallic Ru(II)-Pt(II) complexes of *cis* geometry with a semi-rigid linker (qpy = 4'-pyridyl-2,2':6',2''-terpyridine) are reported in **Chapter 4**. The reactivity increases from the mononuclear, *cis*-[Pt(en)(py)H<sub>2</sub>O](CF<sub>3</sub>SO<sub>3</sub>)<sub>2</sub>, **Pt1** to heterometallic *cis*-[(tpy)Ru(qpy)Pt(en)H<sub>2</sub>O](CF<sub>3</sub>SO<sub>3</sub>)<sub>4</sub>, **Pt2** and *cis*-[H<sub>2</sub>O(en)Pt(qpy)Ru(qpy)Pt(en)H<sub>2</sub>O](CF<sub>3</sub>SO<sub>3</sub>)<sub>6</sub>, **Pt3** (where en = 1,2-ethylenediamine, py = pyridine). Substitution reactions proceeded *via* a single step. <sup>195</sup>Pt NMR spectroscopic analysis of **Pt3-Cl** with TU showed simultaneous substitution of the aqua ligands in **Pt3** with no dechelation. This reaffirms that the *cis* geometry at the Pt(II) centre confers stability which precludes labilization of the Ru(qpy) linker.

Apart from the increased overall charge and the electrophilicity, the octahedrally coordinated Ru(II) moiety lowers the LUMO energy of the complexes thereby enhancing the transfer of electrons from the highest occupied molecular orbital (HOMO) the empty LUMO energy level of the ligand systems. Furthermore, presence of Ru(II) moiety increases the metal-metal coupling and electronic transitions within the complex. The effect of increasing or decreasing the electron density of the Pt(II) centre is also noted in the  $\text{p}K_{\text{a}}$  values, which decreases with increasing overall charge of the complex.

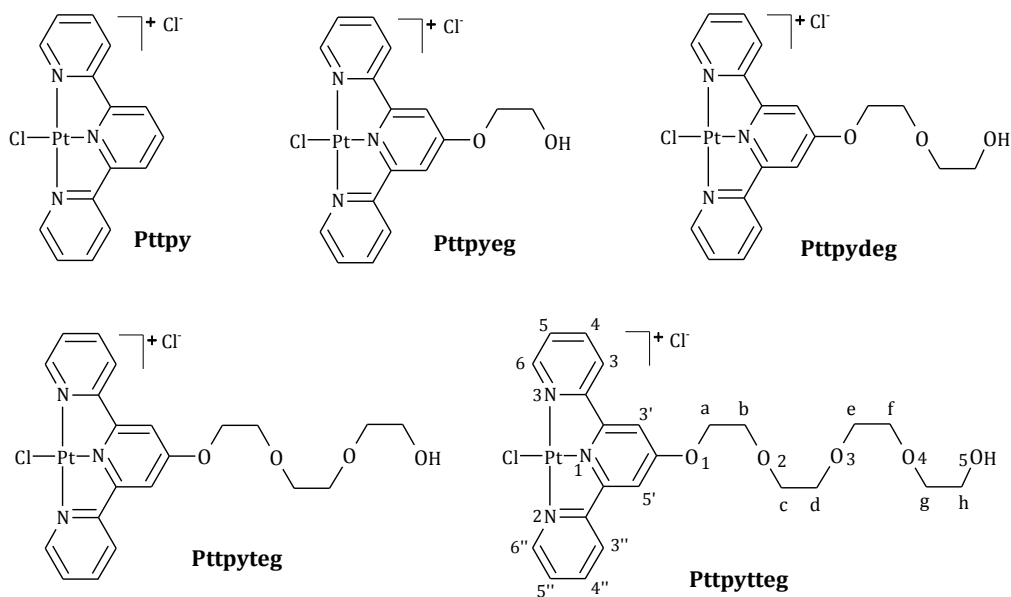
The reactivity of **Pt2** and **Pt3** are not of much difference. The Ru(II) metal centre prevents the flow of electron density through the three metal centres since the two qpy ligands lie orthogonal to each other at the central Ru(II) centre.



**Figure 8.2** Structure of complexes reported in *Chapter 4*.

The substitution kinetics of Pt(II) terpyridine (**Pttpy**) complexes possessing polyethylene glyoxy pendant unit attached *trans* to the leaving group of **Pttpy** is reported in *Chapter 5*. The polyethylene glyoxy pendant unit acts as a  $\sigma$ -donor towards the Pt(II) centre, thereby decreasing the reactivity compared to the parent **Pttpy** molecule. The  $\sigma$ -donation due to the pendant unit and the  $\pi$ -electronic contribution due to O1 was found to be effective only up to one unit of the ethylene glyoxy pendant, beyond which there is no significant electronic effect on the Pt(II) metal centre.

The reactivity is retarded from **Pttpy** to Pt(II)-4'-(ethylene glyoxy)-2,2':6,2''-terpyridine (**Pttpyeg**). This is attributed to both steric and electronic effects caused by the appended ethylene glyoxy pendant. However, the slight increase in substitution reactivity from **Pttpyeg** to Pt(II)-4'-(tetraethyleneglyoxy)-2,2':6,2''-terpyridine (**Pttpytteg**) was controlled mainly by steric effects which decrease as the angle of inclination of the appended ethylene glyoxy pendant decreases relative to the Pt(II) plane. The complexes are sensitive to steric size of the incoming nucleophiles as demonstrated by the decrease in rate constant depending on the size.

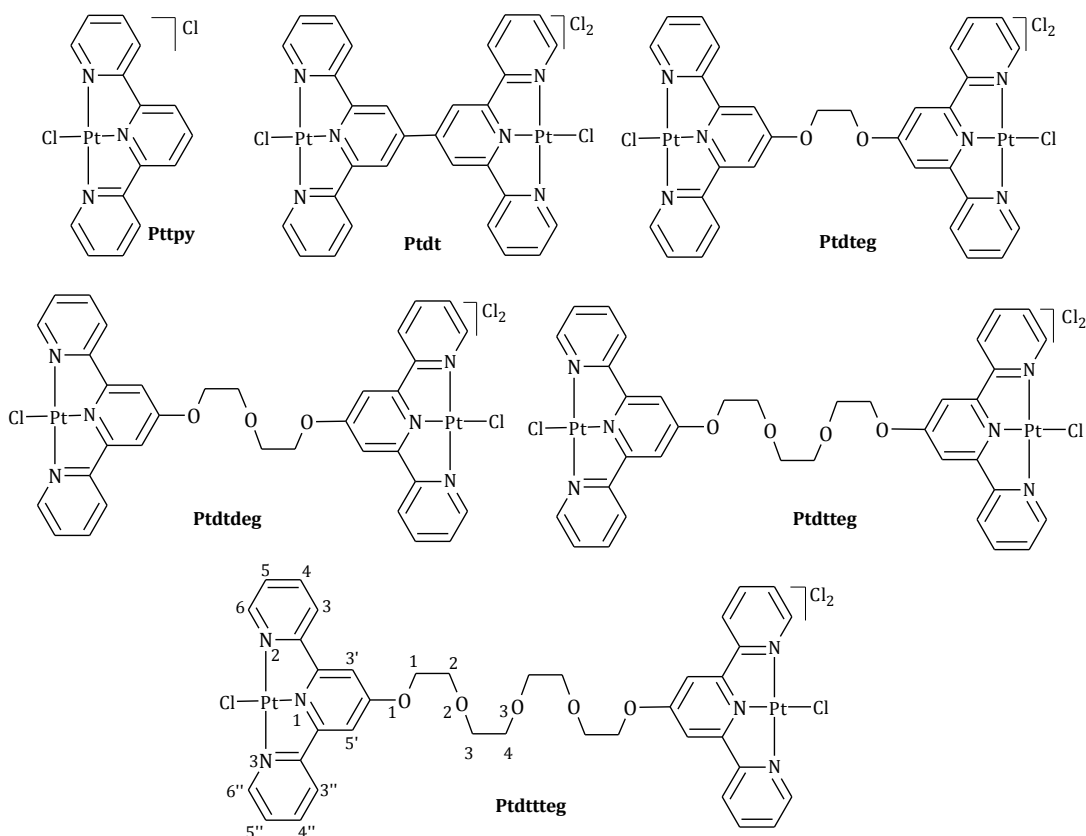


**Figure 8.3**                      **Structure of complexes reported in Chapter 5.**

In **Chapter 6**, the work from **Chapter 5** is extended to investigate the substitution reactivity of dinuclear Pt(II) complexes bridged with polyethyleneglycol ether of the type  $[\text{ClPt}(\text{tpy})-\text{O}(\text{CH}_2\text{CH}_2\text{O})_n(\text{tpy})\text{PtCl}]\text{Cl}_2$  where  $n = 1$  (**Ptdteg**), 2 (**Ptddeg**), 3 (**Ptdtteg**), 4 (**Ptdttteg**). A linker free complex,  $\text{ClPt}(\text{tpy})-(\text{tpy})\text{PtCl}]\text{Cl}_2$ , (**Ptdt**) was also investigated.

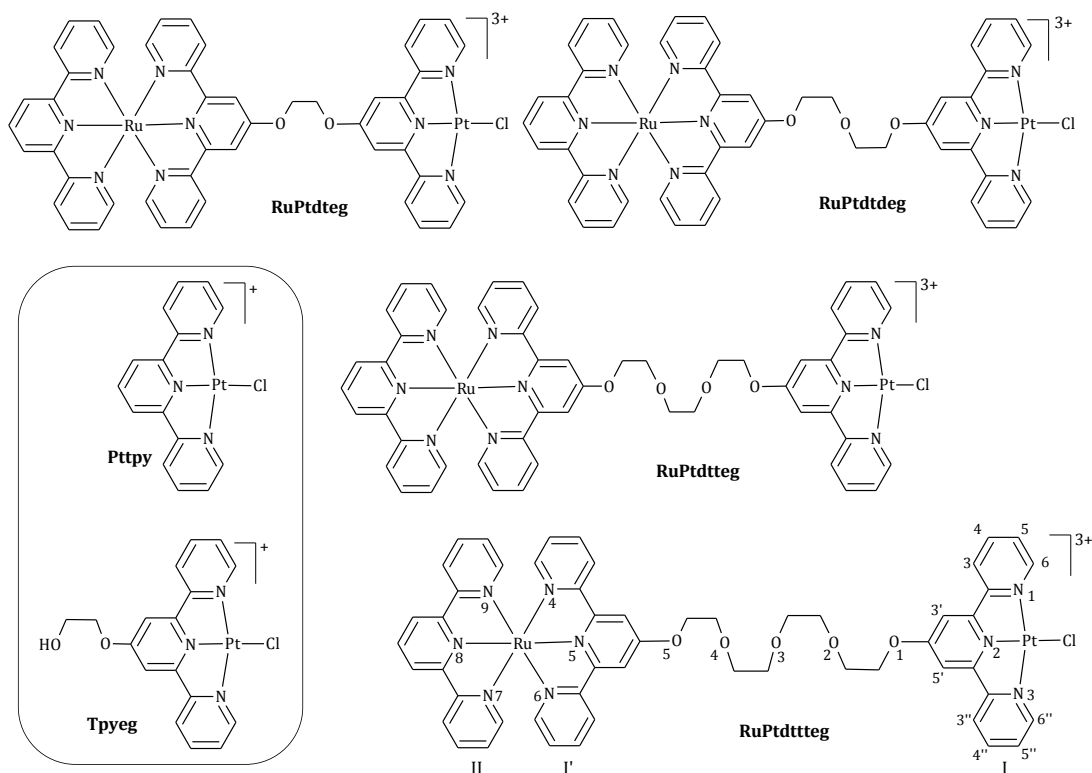
The lability of the dinuclear polyethyleneglycol ether linked complexes differs significantly from the corresponding linker free dinuclear complex, **Ptdt** and the monomeric complex, **Pttpy**. The difference in reactivity was accounted for in terms of the electronic as well as steric effects. Introduction of the linker decreases the electrophilicity of the platinum centre as well as the overall electrophilicity of the whole complex. The ethyleneglycol ether units donate electrons to the Pt(II) centre including the lone pair of electrons on the O1 oxygen atoms. The reactivity of the glycolether linked complexes decrease with increase in the distance between the Pt...Pt metal centres. This decrease in reactivity is also accounted for the increase in the steric hindrance at the Pt(II) centres by the terpyridine ligands due to the geometry imposed by the linker.

The results from this study clearly show that the nature of the bridging ligand uniquely influences the rate of substitution reactions. The complexes showed coordination stability for the substitution of the S-donor nucleophiles.



**Figure 8.4** Structure of complexes reported in Chapter 6.

In **Chapter 7**, the work reported in **Chapter 5** and **Chapter 6** is extended to investigate the substitution reactivity of heterometallic Ru(II)-Pt(II) complexes bridged by polyethyleneglycol ether units *viz*;  $[(\text{tpy})\text{Ru}(\text{tpy})-\text{O}(\text{CH}_2\text{CH}_2\text{O})_n-(\text{tpy})\text{PtCl}]$  (where tpy = 2,2':6',2''-terpyridine and  $n = 1$  (**RuPtdteg**), 2 (**RuPtdtdeg**), 3 (**RuPtdttteg**) and 4 (**RuPtdtttteg**)). The measured rate constants show that the increase in the length of the polyethyleneglycol ether linker increases the entrapment effect of the nucleophiles due to the V-shape geometry of the complexes. The reactivity is also influenced by the steric hindrance imposed by the  $\text{Ru}(\text{tpy})_2$  moiety at the reactive Pt(II) metal centre. The electronic transitions between Ru(II) and Pt(II) is insignificant in the presence of a non-aromatic polyethyleneglycol ether linker. Density functional theory (DFT) calculated data for the complexes show that the rate of substitution reactions of the heterometallic complexes is geometrically controlled.



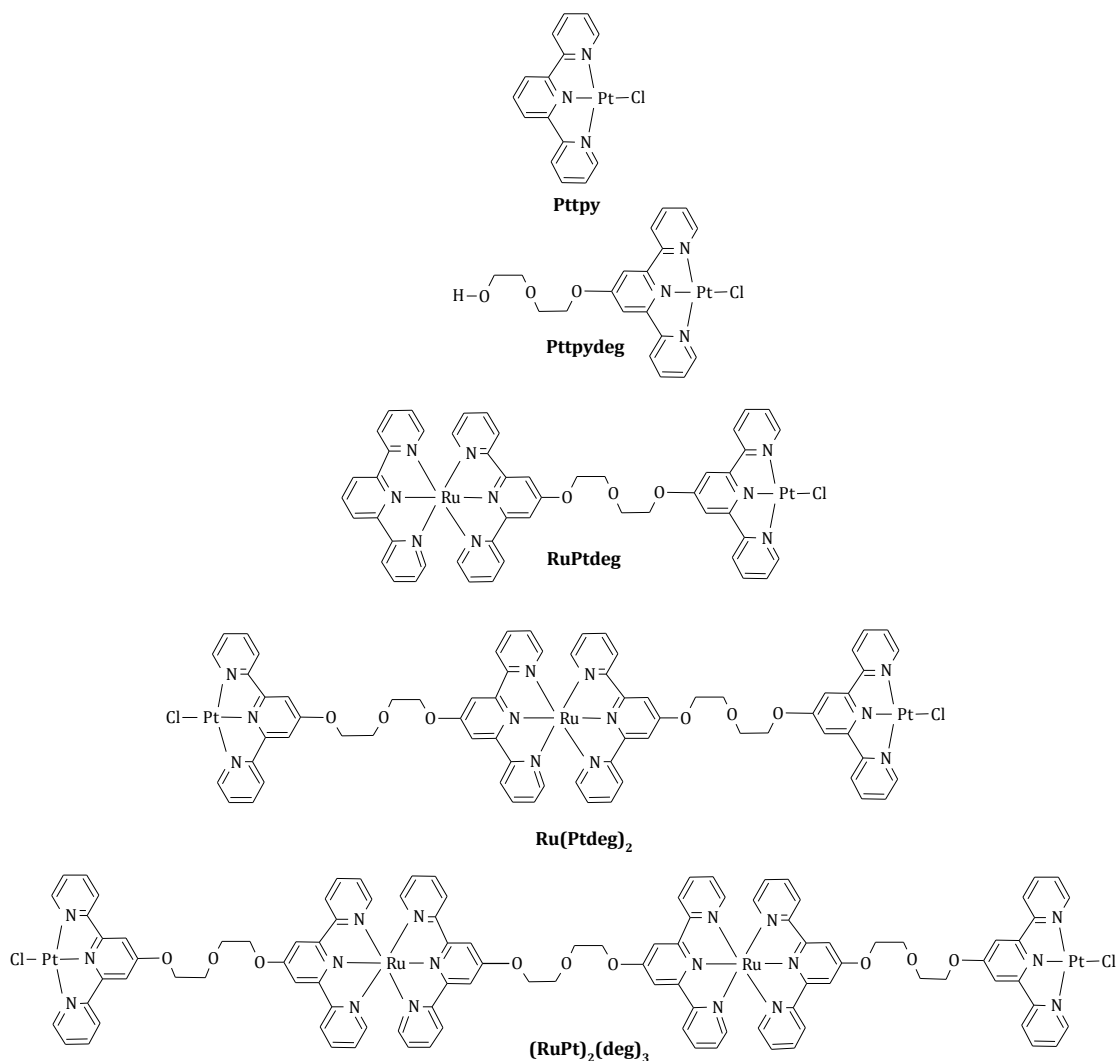
**Figure 8.5** Structure of complexes reported in Chapter 7.

In the work reported in *Chapters 3* to *Chapter 7*, large and negative entropy of activation and the positive enthalpy of activation support an associative mode of activation. In all cases the reactivity of the complexes is sensitive to the steric nature of the incoming nucleophiles which decreases with increase in the size of the nucleophile.

## 8.2 Work Completed but Not Included in This Thesis

The work reported in this thesis can be extended further to investigate new analogues of heterometallic Ru(II)-Pt(II) systems. As an extension of the current study, the two heterometallic Ru(II)-Pt(II) complexes<sup>1</sup> bridged by diethyleneglycol ether units *viz*; [ClPt(tpy)-O(CH<sub>2</sub>CH<sub>2</sub>O)<sub>2</sub>(tpy)Ru(tpy)O(CH<sub>2</sub>CH<sub>2</sub>O)<sub>2</sub>(tpy)PtCl], **Ru(Ptdeg)<sub>2</sub>** and [ClPt(tpy)-O(CH<sub>2</sub>CH<sub>2</sub>O)<sub>2</sub>(tpy)Ru(tpy)-O(CH<sub>2</sub>CH<sub>2</sub>O)<sub>2</sub>(tpy)Ru(tpy)O(CH<sub>2</sub>CH<sub>2</sub>O)<sub>2</sub>(tpy)PtCl], **(RuPt)<sub>2</sub>(deg)<sub>3</sub>** (*Figure 8.6*) were synthesized and characterized. Their substitution kinetics has also been investigated as chloro complexes with thiourea and I<sup>-</sup> nucleophiles in methanol.





**Figure 8.6** Structure of the two heterometallic complexes; **Ru(Ptdeg)<sub>2</sub>** and **(RuPt)<sub>2</sub>(deg)<sub>3</sub>** investigated. Complexes, **Ptptydeg** and **RuPtdeg** are already reported in this thesis and **Ptppy** reported from literature are included for comparisons.

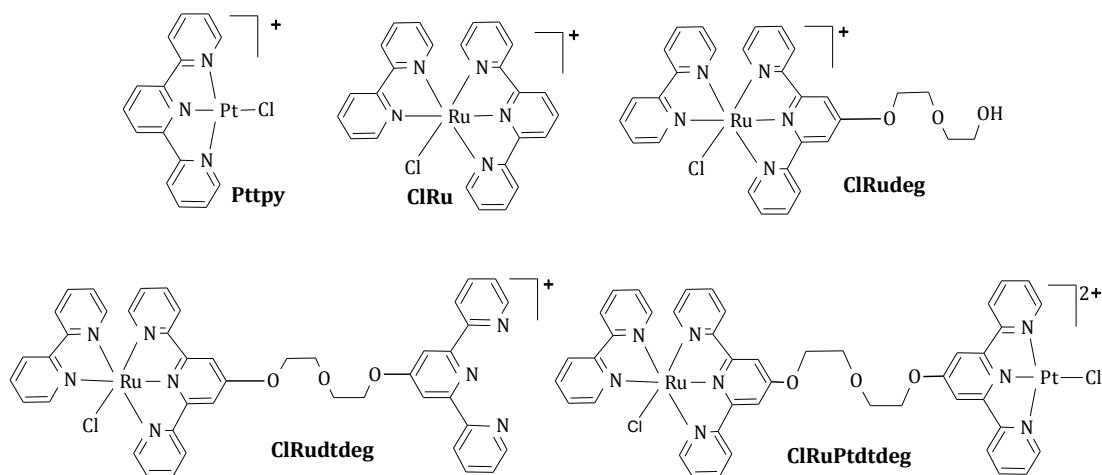
This is an extension of the work on the heterometallic complexes with the flexible linkers reported in this Thesis. The main aim of this work is to understand the effect on the substitution kinetics when the number of metal centres and the diethyleneglycol ether linkers are increased. The complexes were selected due to their comparable cytotoxic activity to cisplatin. The heterometallic complex **Ru(Ptdeg)<sub>2</sub>** inhibit cell growth of A2780cis cells for 50% at a concentration of 20  $\mu\text{M}$ .<sup>1</sup> The complex **(RuPt)<sub>2</sub>(deg)<sub>3</sub>** was reported to show moderate cytotoxicity against A2780cis and A2780R cells-lines.<sup>1</sup> Since the complexes are able to bind with DNA, they may play an important role in medicinal chemistry and molecular biology. The heterometallic complexes mentioned are potentially bifunctional, where Ru(II) bridging ligand provides a possible intercalation site while the Pt(II)Cl site can covalently bind to DNA.

The substitution kinetics of the complexes were fast and were followed on stopped-flow reaction analyzer *via* a single step. The kinetics data obtained are given in *Table 8.1*. The substitution reactions gave single exponential fits following the rate law,  $k_{\text{obs}} = k_2[\text{Nu}]$ . The activation parameters, enthalpy of activation and entropy of activation well support an associative mode of mechanism. The manuscript for this work is under preparation.

**Table 8.1** Summary of second-order rate constants,  $k_2$  and activation parameters, with the corresponding standard deviations for the substitution of the chloro ligands by a series of thiourea nucleophiles and iodide ion at  $I = 0.02 \text{ M LiCF}_3\text{SO}_3$ , adjusted with LiCl. Data for Ptppydeg and RuPtdtdeg are taken from *Chapter 5* and *Chapter 6* and data for Ptppy<sup>2</sup> are included for comparison.

Complex	Nu	$k_1/\text{M}^{-1}\text{s}^{-1}$	$\Delta S^\ddagger / \text{JK}^{-1} \text{mol}^{-1}$	$\Delta H^\ddagger / \text{kJ mol}^{-1}$
<b>Ptppy</b>	TU	$1494 \pm 10$	$-88 \pm 5$	$29 \pm 2$
	DMTU	$448 \pm 10$	$-73 \pm 4$	$36 \pm 1$
	TMTU	$82 \pm 4$	$-91 \pm 8$	$35 \pm 2$
	I <sup>-</sup>	$243 \pm 4$	$-42 \pm 11$	$47 \pm 3$
<b>Ptppydeg</b>	TU	$265 \pm 1$	$-66 \pm 5$	$40 \pm 1$
	DMTU	$83 \pm 0.8$	$-54 \pm 9$	$46 \pm 3$
	TMTU	$23 \pm 0.5$	$-83 \pm 7$	$41 \pm 2$
	I <sup>-</sup>	$91 \pm 2$	$-44 \pm 9$	$48 \pm 3$
<b>RuPtdtdeg</b>	TU	$298 \pm 5$	$-112 \pm 3$	$25 \pm 1$
	DMTU	$114 \pm 2$	$-69 \pm 0.7$	$41 \pm 0.2$
	TMTU	$44 \pm 0.9$	$-90 \pm 4$	$37 \pm 1$
	I <sup>-</sup>	$192 \pm 3$	$-80 \pm 5$	$36 \pm 2$
<b>Ru(Ptdeg)<sub>2</sub></b>	TU	$306 \pm 3$	$-93 \pm 3$	$31 \pm 1$
	DMTU	$96 \pm 0.4$	$-114 \pm 1$	$28 \pm 0.4$
	TMTU	$30 \pm 0.8$	$-36 \pm 6$	$54 \pm 2$
	I <sup>-</sup>	$252 \pm 2$	$-113 \pm 4$	$26 \pm 1$
<b>(RuPt)<sub>2</sub>(deg)<sub>3</sub></b>	TU	$166 \pm 2$	$-47 \pm 7$	$46 \pm 2$
	DMTU	$45 \pm 0.4$	$-43 \pm 9$	$50 \pm 3$
	TMTU	$17 \pm 0.6$	$-20 \pm 6$	$60 \pm 2$
	I <sup>-</sup>	$205 \pm 3$	$-73 \pm 7$	$38 \pm 2$

Another interesting series of heterometallic Ru(II)-Pt(II) complexes synthesized during this work is given in *Figure 8.7*. The complexes are synthesized and fully characterized.



**Figure 8.7** Structure of complexes synthesized and characterized.

Kinetics of **ClRu** was followed in aqua form at pH = 2, T = 298 K, I = 0.02 M HCF<sub>3</sub>SO<sub>3</sub>, adjusted with LiCF<sub>3</sub>SO<sub>3</sub> with TU and DMTU (data obtained is not presented here). Investigations on substitution kinetics of the other complexes are under progress. The complexes are chosen to study their substitution kinetics in order to understand how the substitution reactivity at the Ru(II) metal differs from that of the Pt(II) metal centre. The effect of the diethyleneglycol ether linker on the Pt(II) centre is reported in this thesis. The design of the complexes in this set of complexes however, would allow to understand the influence of the diethyleneglycol ether linker on the Ru(II) metal centre. Furthermore, the work would also investigate how the substitution behaviour at the Ru(II) metal centre is affected when a Pt(II) metal centre is attached to the Ru(II) molecule.

### 8.3 Future Prospects

It would be interesting to investigate the biological activity of the novel complexes reported in this thesis. Moreover, further study should be done probably by using DNA substrates to mimic the interactions of platinum complexes with DNA. Most of the complexes investigated in this study are expected to interact with DNA in a different way compared to the known mechanisms of cisplatin. Ongoing studies<sup>1,3</sup> have shown that the type of Ru(II)-Pt(II) complexes investigated in this study have prominent DNA binding properties.

Another approach in the extension of this work is to use other bioactive metals such as gold(III),<sup>4</sup> iron(II) or iron (III) in place of Pt(II) and Ru(II). Research has shown that gold complexes show high anticancer activity.<sup>5</sup> Furthermore, it would also be interesting to understand how the substitution reactivity of the Pt(II) centres is effected by the use of alkydiamine linkers instead of polyethyleneglycol ether bridges. Alkydiamine linked Pt(II) complexes such as **BBR3464** were reported as potential anticancer agents.<sup>6</sup> Other flexible linkers containing different atoms such as sulphur and nitrogen can also be used.<sup>7</sup>

It would be interesting to study the substitution kinetics of the complexes presented in **Chapter 4** by changing the ligand system around the Pt(II) metal centre from ethylenediamine (en) to *cis* and *trans* platin analogues.<sup>1</sup> Tethering of Ru(II) moiety to known drugs may undergo different modes of actions than cisplatin which may produce interesting results. This might also improve the anticancer activity of the complexes. Another different strategy that can be employed is to reverse the coordination sites of the metals with qpy linker, *i.e.* Pt(II) coordinating to the tridentate terpyridine part and Ru(II) coordinating to the monodentate fourth pyridine.<sup>1</sup> This could produce interesting polynuclear heterometallic Ru(II)-Pt(II) complexes which can resemble the Keppler type molecule.<sup>1,8</sup>

In short, research on heterometallic antitumour drugs is an area of interest. Substitution kinetics of such complexes is novel and therefore full of prospects. Clinical investigations of heterometallic anticancer drugs are under process. There is room for further development of effective heterometallic Ru(II)-Pt(II) anticancer drugs with more promising cytotoxicity. However, more research needs to be done to further development of the complexes and the concept.

## 8.4 References

- (1) van der Schilden, K., University of Leiden, PhD Thesis, The Development of Polynuclear Ruthenium and Platinum Polypyridyl Complexes. 13- 35, 109- 129, 132- 147., 2006.
- (2) Jaganyi, D.; Reddy, D.; Gertenbach, J. A.; Hofmann, A.; van Eldik, R. *Dalton Trans.* **2004**, 299.
- (3) (a) Swavey, S.; Fang, Z. L.; Brewer, K. J. *Inorg. Chem.* **2002**, *41*, 2598(b) Holder, A. A.; Swavey, S.; Brewer, K. J. *Inorg. Chem.* **2003**, *43*, 303(c) Miao, R.; Mongelli, M. T.; Zigler, D. F.; Winkel, B. S. J.; Brewer, K. J. *Inorg. Chem.* **2006**, *45*, 10413(d) Higgins, S. L. H.; White, T. A.; Winkel, B. S. J.; Brewer, K. J. *Inorg. Chem.* **2011**, *50*, 463(e) Jain, A.; Wang, J.; Mashack, E. R.; Winkel, B. S. J.; Brewer, K. J. *Inorg. Chem.* **2009**, *48*, 9077(f) Sun, D.; Liu, Y.; Liu, D.; Zhang, R.; Yang, X.; Liu, J. *Chem. Eur. J.* **2012**, *18*, 4285.
- (4) (a) Janković, S. M.; Djeković, A.; Bugarčić, Ž.; Janković, S. V.; Lukić, G.; Folić, M.; Čanović, D. *Biomaterials* **2012**, *25*, 919(b) Giovagnini, L.; Ronconi, L.; Aldinucci, D.; Lorenzon, D.; Sitran, S.; Fregoni, D. *J. Med. Chem.* **2005**, *48*, 1588.
- (5) Desoize, B. *Anticancer Res.* **2004**, *24*, 1529.
- (6) (a) Farrell, N. *Comments Inorg. Chem.* **1995**, *16*(6), 373(b) Farrell, N. *Met. Ions Biol. Syst.* **2004**, *42*, 251(c) Farrell, M.; De Almeida, S. G.; Skov, K. A. *J. Am. Chem. Soc.* **1988**, *110*, 5018(d) Farrell, N.; Qu, Y.; Feng, L.; Van Houten, B. *Biochemistry.* **1990**, *29*, 9522.
- (7) Schubert, U. S.; Eschbaumer, C.; Hien, O.; Andres, P. R. *Tetrahedron Lett.* **2001**, *42*, 4705.
- (8) (a) Smith, C. A.; Sutherland-Smith, A. J.; Kratz, F.; Baker, E. N.; Keppler, B. H. *J. Biol. Inorg. Chem.* **1996**, *1*, 424(b) Hartinger, C. G.; Jakupec, M. A.; Zorbas-Srified, S.; Groessl, M.; Egger, A.; Berger, W.; Zorbas, H.; Dyson, P. J.; Keppler, B. *K. Chem. Biodiversity.* **2008**, *5*, 2140.